BULLETIN OF RUSSIAN STATE MEDICAL UNIVERSITY

BIOMEDICAL JOURNAL OF PIROGOV RUSSIAN NATIONAL RESEARCH MEDICAL UNIVERSITY

Indexed in Scopus. CiteScore 2023: 0,8

Indexed in WoS. JCR 2021: 0.5

Five-year h-index is 10

Scopus®

WEB OF SCIENCE™

Google scholar

SCImago Journal & Country Rank 2020: 0.14

Listed in HAC 31.01.2020 (№ 507)

Open access to archive

SJR
Scimago Journal & Country Rank

ВЫСШАЯ АТТЕСТАЦИОННАЯ КОМИССИЯ (ВАК)

CYBERLENINKA

ВЕСТНИК РОССИЙСКОГО ГОСУДАРСТВЕННОГО МЕДИЦИНСКОГО УНИВЕРСИТЕТА

НАУЧНЫЙ МЕДИЦИНСКИЙ ЖУРНАЛ РНИМУ ИМ. Н. И. ПИРОГОВА

Scopus®

WEB OF SCIENCE™

Google scholar

SJR
Scimago Journal & Country Rank

ВЫСШАЯ АТТЕСТАЦИОННАЯ КОМИССИЯ (ВАК)

CYBERLENINKA

Contents
Содержание

APPROACHES TO THERAPY OF CRIGLER–NAJJAR SYNDROME TYPE 1 IN CHILDREN

Gautier MS ✉, Degtyareva AV, Degtyarev DN, Ushakova LV, Filippova EA, Albegova MB, Bavykin AS, Savilova AM, Zhdanova SI

Kulakov National Medical Research Center for Obstetrics, Gynecology and Perinatology, Moscow, Russia

The review is focused on exploring the etiology, pathogenesis, clinical manifestations, and primarily the contemporary treatment methods for Crigler–Najjar syndrome type 1. It considers relevant data regarding the efficacy and safety of the currently existing therapeutic strategies. Effective management of this condition relies on early diagnosis and prompt initiation of treatment, which are crucial for preventing disabling neurological complications associated with bilirubin encephalopathy in patients with Crigler–Najjar syndrome type 1. Prolonged phototherapy is the key treatment method, while liver transplantation represents a radical approach. Recent advances in gene therapy and the use of mesenchymal multipotent stromal cells present novel opportunities for developing alternative, less invasive treatment modalities aimed at improving the quality of life in such patients and reducing their dependence on long-term phototherapy, along with post-transplantation risk.

ПОДХОДЫ К ТЕРАПИИ СИНДРОМА КРИГЛЕРА–НАЙЯРА 1-ГО ТИПА У ДЕТЕЙ

М. С. Готье ✉, А. В. Дегтярева, Д. Н. Дегтярев, Л. В. Ушакова, Е. А. Филиппова, М. Б. Албегова, А. С. Бавыкин, А. М. Савилова, С. И. Жданова

Национальный медицинский исследовательский центр акушерства, гинекологии и перинатологии имени В. И. Кулакова Министерства здравоохранения России, Москва, Россия

Обзор посвящен изучению этиологии, патогенеза, клинической картины и, прежде всего, современных методов лечения синдрома Криглера–Найяра (СКН) 1-го типа. Рассмотрены актуальные данные об эффективности и безопасности существующих терапевтических стратегий. Эффективная терапия данного заболевания основана на ранней диагностике и незамедлительном начале лечения, что критически важно для предотвращения инвалидизирующих неврологических осложнений, связанных с билирубиновой энцефалопатией у пациентов с СКН 1-го типа. Ключевым методом лечения является продолжительная фототерапия, а радикальной мерой — трансплантация печени. Последние достижения в области генной терапии и использования мезенхимальных мультипотентных стромальных клеток открывают новые возможности для разработки альтернативных, менее инвазивных методов лечения, направленных на улучшение качества жизни пациентов с этим заболеванием и снижение их зависимости от длительной фототерапии и послеоперационных рисков, связанных с трансплантацией печени.

Crigler–Najjar syndrome (CNS) is a rare autosomal recessive inherited disorder characterized by impaired conjugation of bilirubin in the liver caused by lack or low level of the uridine diphosphate glucuronosyltransferase (UGT) enzyme, which leads to the development of nonhemolytic jaundice.

Etiology

The *UGT1A1* gene encoding the UGT enzyme plays a key role in conjugation of indirect bilirubin. Mutations in the *UGT1A1* gene can completely arrest or hamper the activity of this enzyme, which translates into hyperbilirubinemia. Depending on the degree of decrease in enzyme activity, CNS is classified into types 1 and 2 (CNS1 and CNS2). In CNS1 cases, there is no enzyme activity, and therefore, without treatment, the disease causes severe neurological disorders due to bilirubin encephalopathy. In CNS2 cases, the level of bilirubin in the blood serum is high, but, as a rule, there is no progression to neurological disorders.

CNS1 is extremely rare: its incidence is about 0.6–1 case per 1 million live newborns worldwide, and less than one per 100,000 newborns in Europe [1, 2]. There are no prevalence specifics in terms of sex and ethnicity, but it is known that CNS1 is diagnosed more often in genetically isolated populations, such as communities of Old Believers and Mennonites, as well as among children born to parents in a related marriage [3, 4].

The CNS1 phenotype can occur due to various changes in the coding sequences of the bilirubin uridine diphosphate glucuronosyltransferase (*UGT1A1*) gene, such changes conditioning formation of an abnormal protein that fully arrests or disrupts the activity of the enzyme. This cause-effect relationship makes CNS1 different from the Gilbert's syndrome, when the triggering defect is in the promoter region rather than in the gene itself, and the result thereof is a smaller amount of synthesized normal enzyme [5]. The *UGT* gene is expressed in many isoforms, but UGT1A1 is the only one that significantly contributes to bilirubin conjugation in humans. Deletions, insertions, missense mutations, or premature stop codons

in the *UGT1A1* gene can be located in any of the five exons that make up the *UGT1A1* mRNA. Genetic changes in exon 1 affect only the activity of bilirubin UGT isoform (*UGT1A1*), while mutations in exons 2-5, contrarily, affect all isoforms expressed from the UGT1A locus [6].

Clinical picture

The manifestation of the CNS1 syndrome is jaundice caused by a high level of unconjugated bilirubin. It usually appears on the second or third day of life, when the bilirubin level exceeds 85 μmol/l. Subsequently, it progressively increases and reaches 340–500 μmol/l in the first 10 days of life, and in severe cases the said level rises to 850 μmol/l. The probability of development of bilirubin encephalopathy is the highest in the early neonatal period, when the blood-brain barrier is more permeable. Total serum bilirubin and the bilirubin/albumin ratio are the indicators used to assess the risk of neurological complications. For children older than 1 month, the total serum bilirubin level above 510 μmol/l and the bilirubin/albumin ratio exceeding 1.0 mol/mol are considered the absolute thresholds of neurotoxicity [3, 7]. In the neonatal period, the threshold level of bilirubin depends on a combination of factors: gestational and postnatal age and the condition of the child. Untreated, CSN1 leads to acute bilirubin encephalopathy, kernicterus, and persistent cognitive disorders. The symptoms of CNS damage associated with CNS1 include altered state of consciousness, changes in muscle tone, hearing loss, etc. There is a report describing a case of late diagnosing of CNS1 that progressed into severe neurological disorders in the form of spastic tetraparesis [8]. In another clinical case, neurological disorders were detected in a 4-month-old child suffering from CNS1; they manifested as neurodevelopmental delay and focal structural epilepsy [9]. Kernicterus is a consequence of deposition of bilirubin in brain cells, mainly in the basal ganglia, globus pallidus, hippocampus, subthalamic nucleus, horn of Ammon, cranial nerve nuclei, and cerebellum. Choreoathetoid cerebral palsy, high-frequency central sensorineural hearing loss, vertical gaze palsy, and enamel hypoplasia are the main markers of kernicterus [10]. It is important to note that bilirubin encephalopathy can also occur in adolescents or adults, so a broader term, kernicterus spectrum disorder, was coined, and it combines the diagnoses based on clinical and pathophysiological criteria [4, 11, 12]. There is a report covering 239 cases of CNS1 and describing the various outcomes of the disease, including the high risk of bilirubin encephalopathy and other serious complications. The authors note that in 45% of patients, the disease progresses into brain damage, 27% require liver transplantation, and in 19% of cases the treatment involved exchange transfusion or plasmapheresis [3].

Historically, CNS1 was regarded as indirect hyperbilirubinemia without damage to liver tissue. However, recent reports indicate that liver fibrosis is registered in 40–60% of patients that need liver transplantation because of this disease, and the degree of fibrosis correlates with bilirubin concentration and age. Liver biopsies sampled during liver transplantation in 22 patients with CNS1 showed varying degrees of fibrosis in 41% of them in the absence of clinical and laboratory findings suggestive of liver cirrhosis and portal hypertension [13].

The quality of life in CNS1 cases can be significantly low both for the patients and for the caregivers. Patients require 10–12 hours of phototherapy per day from the first days of life [14]. Although it is a non-invasive and simple treatment method, phototherapy has a noticeable effect on the lifestyle of the family, imposing social restrictions and a heavy burden on patients and their caregivers [15]. Liver transplantation is a radical treatment method, but it carries the risks associated with donor selection, potential transplant rejection, and the need for lifelong immunosuppressive therapy.

A special problem is that of pregnancy hyperbilirubinemia with CNS1 in the background. This condition implies a risk of kernicterus in the fetus due to a high level of bilirubin in the mother. Unconjugated bilirubin passes through the placenta by passive diffusion [15]. The recommended treatment protocol prescribes monitoring and phototherapy the duration of which ensures a maternal bilirubin level below 200 μmol/l and a bilirubin/albumin ratio less than 0.5 mol/mol [16]. There is evidence of successful phototherapy in the first trimester and phenobarbital in subsequent trimesters given with the aim to maintain safe bilirubin levels in pregnant women with type CNS2 [17]. There is also experience of management of newborns from women with CNS1 who required blood transfusions after birth; one of them was diagnosed with sensorineural hearing loss at 7 months, despite phototherapy and albumin infusion the mother underwent during pregnancy [18].

Diagnostics

Prevention of neurological complications of kernicterus requires diagnosing CNS1 at early stages. Differential diagnosis involves other causes of unconjugated hyperbilirubinemia, such as jaundice caused by breast milk composition, polycythemia, systemic diseases, and other hereditary disorders of bilirubin metabolism. The key difference between CNS1 and CNS2 is the ultimate level of bilirubin, although in the first weeks of life, the respective thresholds that mark brain damage may coincide for these two conditions. A phenobarbital test helps to diagnose the disease: in CNS2 cases, this drug pushes blood bilirubin down by about 25%, but has no such effect in patients with CNS1.

Molecular genetic study can confirm or disprove a CNS diagnosis; it is designed to seek pathogenic variants in the *UGT1A1* gene encoding the enzyme enabling bilirubin conjugation. CNS1 can stem from various genetic defects, including missense and nonsense mutations, insertions, deletions, and splicing disorders affecting any of the five exons of the *UGT1A1* coding region. Therefore, it is important to sequence not only all exons, but also flanking introns, using targeted Sanger sequencing or next generation sequencing [19]. CNS1 is associated with more severe mutations, including premature stop codons, frameshift or missense mutations (substitution of one amino acid), which stop the activity of the UGT enzyme completely. CNS2, on the contrary, is typically linked to missense mutations that reduce the catalytic activity of the enzyme, but do not fully arrest it. If a patient with CNS2 also has a *UGT1A128* type promoter mutation, characteristic of Gilbert's syndrome, decreased enzyme expression can make hyperbilirubinemia even more pronounced [15, 20, 21].

Treatment

Currently, there are various approaches to the treatment of CNS1. Below, we are describing the most common and best studied of them.

The approaches to treatment of unconjugated bilirubinemia in the neonatal period with CNS1 in the background are similar to those practiced for other causes of indirect hyperbilirubinemia. Under the current clinical recommendations, phototherapy and/or exchange transfusion are prescribed when the total serum bilirubin level reaches certain threshold values.

Phototherapy

Phototherapy (PT) is the first choice against CNS1, especially for babies and children. It can significantly alter the course of the disease. PT works by converting bilirubin IX-alpha-ZZ into its configuration isomers (for example, lumirubin), which can then be excreted in bile without conjugation [22]. Although PT has been used in the treatment of indirect hyperbilirubinemia for many decades, it should be noted that the first recommendations describing how to apply it effectively in CNS cases were published only in June 2020. They detail what light source should be used, what is the optimal distance between the said source and the skin, how much of the skin should be exposed to the light, and for how long [3]. Whenever a newborn exhibits high serum bilirubin content, it is best to initiate treatment as soon as possible. If exchange transfusion is necessary, PT should be started thereafter. The average duration of the PT sessions is 12.4 ± 0.8 hours per day, including nighttime. Various PT systems deliver high-intensity radiation to large areas of the body, but their effectiveness decreases during puberty due to a number of factors (skin thickening, increased pigmentation, decreasing body surface area to body weight ratio). At the same time, adolescent patients are at a high risk of bilirubin levels spiking to critical values that imply the possibility of development of neurological disorders. For them, it is necessary to consider alternative or auxiliary treatments [3, 23].

Although PT is effective against bilirubin level abnormalities, it has its side effects. One review discusses PT as a treatment for hyperbilirubinemia in neonates, evaluating its effectiveness and potential risks, including impacts on the immune system, and the development of tumors, nevi, and allergies. [24]. There is reported evidence confirming the PT's capability to change the levels of cytokines in the blood of newborns. There is also data showing that with 24-hour sessions of PT in the background, the level of interleukin 6 (IL6) drops [25]. Other studies report growing levels of IL2 and IL10, and decreasing level of IL1b. PT was also shown to affect the amount and activity of leukocytes. A number of studies indicate a temporary growth of leukocyte levels, but these changes fade over time and have no clinical significance. The authors present evidence that PT can affect the level of antibodies and immunoglobulins in the newborn's body. Light waves of a certain length can cause structural changes in bilirubin molecules, turning them into more soluble forms that are easier to eliminate from the body. This can have an indirect effect on the metabolism of proteins, including antibodies and immunoglobulins. PT can also alter cellular metabolism, which entails modification of the processes of proliferation and differentiation of cells, including those involved in the production of antibodies and immunoglobulins [26, 27].

There is also evidence that PT may be associated with an increased risk of neoplasms in children. Two large cohort studies were conducted in California, and they found a link between PT in infancy and subsequent acute myeloid leukemia (AML) in children: this therapy raised the risk of the disease [28]. Other studies, however, have not confirmed the association of PT with a high risk of cancer. For example, there is no established connection between PT and the development of melanoma or other skin cancers, same as there is no convincing evidence of PT increasing the risk of basal cell carcinoma or squamous cell carcinoma [29]. Thus, the effect of PT on tumor development remains a controversial issue that requires further investigation.

There are studies showing that children who received PT in the neonatal period may be at a higher risk of developing allergies, including bronchial asthma and pollinosis [30, 31].

The high risk of gallstone formation associated with CNS deserves a special note. There are no published papers pointing to a connection between PT and cholelithiasis, however, it can be assumed that such a connection is possible, and it is caused by the active conjugation of bilirubin under the influence of PT, dehydration, and, as a result, a high probability of bile sludge. Normally, the level of urobilin in bile is very low, however, with PT in the background, water-soluble isomers of urobilinogen are released into the bile, and some of them can be converted back into urobilin, which forms crystals participating in the aggregation of gallstones. A worldwide cohort study claims the incidence of gallstone disease among CNS patients is at least 15% [2], and other authors report its occurrence in up to 41% of cases [3].

Gene therapy

In CNS cases, gene therapy is aimed at correcting the function of the mutated gene by achieving stable expression of the functional copy thereof. Currently, this form of treatment is enabled by viral vectors, with adeno-associated virus (AAV) vectors being best for intracellular gene therapy. The efficacy of AAV-mediated gene therapy was confirmed in preclinical models and in clinical settings involving treatment of hemophilia type A and B. Consequently, FDA has approved Valoctocogene roxaparvovec as a drug for hemophilia A [32]. One study has shown that vectors based on the adeno-associated virus effectively transduce liver cells in cell culture as well as in animal models, including mice and rats. Moreover, introduction of these vectors was demonstrated to lead to normalization of bilirubin levels in the blood of animals with CNS. Preclinical studies dedicated to the safety and effectiveness of AAV vectors included an analysis of the immune response and biodistribution, which has shown that such vectors mainly accumulate in the liver, spleen, and lymph nodes, as per their tropism towards these organs following an intravenous administration. Several months after the injection, some vector particles were found in the gonads. These data signal the need for careful monitoring of the potential risk of gene transmission through reproductive cells. Overall, the findings confirm that AAV vectors are a safe and effective CNS therapy component, and their practical application requires clinical trials [33]. There have been published data on the efficacy of gene therapy in adult patients with CNS1, which confirm it can decrease the level of bilirubin to the values below the neurotoxic threshold; the effect is persistent, and allows partial or even complete cancellation of PT. The study also investigated safety and efficacy of a single intravenous infusion of an AAV vector. The participants of the experiment were five adults with CNS1; three of them received a higher dose, and the level of bilirubin in them dropped below 300 µmol/l (17.5 mg/dl), which allowed canceling PT for the follow-up period of 18 months. However, no subject had the bilirubin level completely returned to normal [34]. Although gene therapy is promising against CNS1, there are doubts about its long-term efficacy and safety. Indeed, it is yet unclear how long does the effect of a single administration of an AAV-transgenic vector persists [35]. The effectiveness of a vector drug is mainly hampered by the produced antibodies that neutralize AAV and, consequently, impose limitations on further introduction of vectors [36]. In the preclinical rat and mice studies, all animals developed a significant immune response to the AAV capsid, and some of them produced antibodies to the *UGT1A1* protein. Searching for the source of this immune response, the researchers have set up experiments using vectors carrying the *UGT1A1* transcripts from different species (mouse and rat

variants), and have thus learned that antibodies against the human *UGT1A1* variant are formed less frequently when using species-specific variants. It is possible that species-specific transcripts decrease the immunogenicity of vectors [33]. In addition to the above, multiple infusions of AAV vectors pose a potential genotoxicity threat [37]. A study that investigated how antibodies to the AAV vector affect the effectiveness of gene therapy against CNS1 has shown that about a third of patients have these antibodies, and that when their level is low, the barrier set b them can be overcome by using the vectors with both full and empty capsids [38]. The issue of suppression of the humoral immune response remains extremely relevant for vector-based medicines. Currently, there is no generally accepted approach to preventing the production of neutralizing antibodies to the injected vector. One option suggests using corticosteroids such as prednisone or methylprednisolone to suppress the activity of the immune system. Other immunosuppressants are also used, including cytostatics such as azathioprine, cyclosporine A, mycophenolate mofetil, and tacrolimus [34].

Gene therapy using AAV vectors is particularly promising for adult patients, but not so much for children and adolescents, whose liver is growing, and the body actively produces hepatocytes, which may reduce the efficacy of such treatment [39]. A 2006 rat study compared the effectiveness of various AAV serovars in the context of creation of vectors. It was shown in vivo that AAV vectors are most effective in correcting *UGT1A1* deficiency. However, large inclusions of fat of indeterminate origin were found in the livers of all the involved animals, raising concerns about possible side effects [40].

The deontological problem associated with gene therapy is the risk of patients developing illusory hopes about the effectiveness of conservative therapy, and consequently neglecting other treatment methods, including PT and liver transplantation.

Liver transplantation

Liver transplantation (LT) is the only definitive treatment option for CNS1 [41, 42]. Currently, there are no well-founded recommendations telling why and, in particular, when a CNS1 patient should undergo LT. It is still unclear at what stage of the disease's progression LT should be considered, and which clinical and laboratory indicators are to be taken as signals the patient should be referred to the transplantologist [43] in cases when liver function is preserved and there are no life-threatening conditions that unequivocally call for LT. At the same time, deterioration of the patient's quality of life due to the daily PT sessions, and loss of the effectiveness of this procedure with age can be valid indications for LT. Development of the gene therapy methods raises new questions about the feasibility of LT. The possibility of recovery without surgery is appealing to the patients and their parents, which translates into a long follow-up period that can have episodic spikes of the bilirubin levels to neurotoxic values. Thus, determining the optimal time for LT is a crucial task: performing it too late can lead to irreversible damage to the brain, while opting for the operation at an early age increases the risk of complications. In addition, LT undoubtedly implies intraoperative and postoperative risks, and requires lifelong immunosuppression. There is a case description covering LT from living related donors to four children with CNS1 aged 2, 8.5, 15 months and 13 years. All children exhibited high levels of unconjugated bilirubin against the background of continuous PT. One patient had neurological disorders as a consequence of bilirubin

encephalopathy. After transplantation, the bilirubin levels in all children returned to normal, but the patient with neurological deficits and spastic disorders died 10 months later due to chronic aspiration syndrome. The authors of this case highlight the importance of performing LT before the development of neurological disorders [44]. It is important to start therapy (exchange transfusion/plasmapheresis/PT) at the first signs of bilirubin encephalopathy and consider LT at the early stage to prevent neurological complications. There are other studies that confirm the need for early LT, one of them is a clinical case involving a transplantation to an 18-months-old child with CNS1 performed when the growing level of bilirubin triggered development of kernicterus accompanied by neurological complications in the form of depression syndrome, increased muscle tone, and, subsequently, athetoid motor disorders. The patient received a left lobe of the liver from a deceased donor, and the neurological disorders began to subside after that [45]. Other authors have described cases of LT to three patients with CNS1 aged 7, 12, and 3 years. The seven-year-old child had a mental retardation. The twelve-year-old patient had a more severe brain damage: impaired motor coordination, delayed speech, mental and physical development caused by bilirubin encephalopathy. The three-year-old child did not exhibit any signs of a neurological deficit. All of them needed intensive PT, and none had complications connected therewith. Moreover, the two patients with neurological disorders enjoyed better mental and motor development indicator values after PT. These results confirm the opinion that early LT can be an effective treatment method allowing to prevent irreversible brain damage in patients with the disease in question [46].

Multipotent mesenchymal stromal cells

In the last decade, stem cells have been studied intensively as components of treatment of several metabolic disorders, and CNS1. Multipotent mesenchymal stromal cells (MMSCs) have also been used in CNS1 therapy. Such cells can be safely obtained from the fetal membranes or the remaining placental part of the navel cord after natural childbirth. The current experience of using MMSCs in clinical practice confirms their safety and lack of the need for immunosuppressive therapy. Administered intravenously, these cells have been shown to selectively accumulate in the liver; they can then differentiate into hepatocytes, and participate in liver regeneration [47]. Stem cells derived from bone and adipose tissues can restore liver function by differentiating into hepatocytes, and cells derived from the umbilical cord blood differentiate into cellular structures similar to hepatocytes, which express markers specific to hepatocytes and retain the potential for hepatogenesis required in cell therapy. Cells derived from the placenta also have great potential for multilinear differentiation [48–50]. Administration of MMSCs obtained from human umbilical cord blood directly into the liver of mice has shown a high potential for the restoration of liver tissue and its functions [51, 52]. The data from these studies indicate that cells isolated from the umbilical cord have characteristics similar to those of bone marrow stem cells. In a mice model of damaged liver, MMSCs cells distributed throughout the body 7 days after transplantation, including the liver. Fourteen days after transplantation, the liver of mice saw expression of genes specific to hepatocytes. There is a described case of transplanting MMSCs to a child with CNS1 [53]. With six injections of the cells in the background, the duration of PT has decreased to 2 hours a day within 2 years. The positive effect developed within 4–7 days after administration and persisted for 2–3 months. There were no

side effects or complications registered during and after the transplantation. Thus, intravenous transplantation of MMSCs is an effective treatment CNS1 that eases the need for PT, significantly improves the quality of life of patients, and prolongs the use of their own liver [53].

CONCLUSION

CNS is a serious disease with potentially disabling neurological consequences and a possible lethal outcome. To date, no clear protocol for the management of patients with CNS1 has been developed. Phototherapy is the main method of controlling the level of bilirubin in children with this disease; it is applicable from the first days of life, but the quality of life of the patients receiving PT is low because of the need for continuous sessions. Liver transplantation is a radical CNS1 treatment method that implies postoperative risks and the need for lifelong immunosuppression. Moreover, currently, there is no consensus regarding the optimal timing of LT in CNS cases. Gene therapy's safety and effectiveness in CNS patients is being investigated. Although it remains a promising treatment for this disease, doubts remain about its long-term effect and potential harm.

References

1. Ebrahimi A, Rahim F. Crigler–Najjar Syndrome: Current Perspectives and the Application of Clinical Genetics. Endocr Metab Immune Disord Drug Targets. 2018; 18 (3): 201–11.
2. Aronson SJ, et al. Disease burden and management of Crigler–Najjar syndrome: Report of a world registry. Liver International. 2022; 42 (7): 1593–604.
3. Strauss KA, et al. Crigler–Najjar Syndrome Type 1: Pathophysiology, Natural History, and Therapeutic Frontier. Hepatology. 2020; 71 (6): 1923–39.
4. Kovačić Perica M, et al. Case report: Crigler–Najjar syndrome type 1 in Croatia—more than a one in a million: a case series. Front Pediatr. 2023; 11.
5. Ilchenko Lyu, et al. Nasledstvennaja nekon#jugirovannaja giperbilirubinemija (sochetanie sindroma Kriglera–Najjara II tipa i sindroma Zhil'bera). Hepatology and Gastroenterology. 2021; 5 (1): 79–84. Russian.
6. Ivanova AA, Maksimov VN. Molekuljarno-geneticheskie aspekty sindroma Zhil'bera, sindromov Kriglera–Najjara I i II tipov. Jeksperimental'naja i klinicheskaja gastrojenterologija. 2023; 8: 56–62. Russian.
7. Iskander I, et al. Serum Bilirubin and Bilirubin/Albumin Ratio as Predictors of Bilirubin Encephalopathy. Pediatrics. 2014; 134 (5): e1330–e1339.
8. Voronchihina AS, Spivakovskij YuM. Klinicheskij sluchaj pozdnej diagnostiki sindroma Kriglera–Najjara u rebenka 5 let. 2024; s. 950–2. Russian.
9. Karzhavina LI, Efishova SG, Tamahina NV. Klinicheskij sluchaj sindroma Kriglera–Najjara 1-go tipa u rebenka pervogo goda zhizni. 2022; s. 85–89. Russian.
10. Degtyareva AV. Sindrom Kriglera–Najara. Rossijskij vestnik perinatologii i pediatrii. 1999; 44 (4): 44–48. Russian.
11. Shapiro SM, Riordan SM. Review of bilirubin neurotoxicity II: preventing and treating acute bilirubin encephalopathy and kernicterus spectrum disorders. Pediatr Res. 2020; 87 (2): 332–7.
12. Shapiro S, et al. The Neurological Sequelae of Neonatal Hyperbilirubinemia: Definitions, Diagnosis and Treatment of the Kernicterus Spectrum Disorders (KSDs). Curr Pediatr Rev. 2017; 13.
13. Mitchell E, et al. Hepatic Parenchymal Injury in Crigler–Najjar Type I. J Pediatr Gastroenterol Nutr. 2018; 66 (4): 588–94.
14. Bortolussi G, Muro AF. Advances in understanding disease mechanisms and potential treatments for Crigler–Najjar syndrome. Expert Opin Orphan Drugs. 2018; 6 (7): 425–39.
15. Dhawan A, et al. Disease burden of Crigler–Najjar syndrome: Systematic review and future perspectives. J Gastroenterol Hepatol. 2020; 35 (4): 530–43.
16. Wilson JHP, et al. Recommendations for Pregnancies in Patients with Crigler–Najjar Syndrome. 2012; c. 59–62.
17. Bansal S, et al. Effects of high bilirubin level in pregnancy in Crigler–Najjar syndrome type 2: An extremely rare but important clinical entity to recognize. Med J Armed Forces India. 2023; 79 (5): 597–600.
18. Hannam S, et al. Normal neurological outcome in two infants treated with exchange transfusions born to mothers with Crigler–Najjar Type 1 disorder. Eur J Pediatr. 2009; 168 (4): 427–9.
19. Kadakol A, et al. Genetic lesions of bilirubin uridine-diphosphoglucuronate glucuronosyltransferase (UGT1A1) causing Crigler–Najjar and Gilbert syndromes: Correlation of genotype to phenotype. Hum Mutat. 2000; 16 (4): 297–306.
20. Ebrahimi A, Rahim F. Crigler–Najjar Syndrome: Current Perspectives and the Application of Clinical Genetics. Endocr Metab Immune Disord Drug Targets. 2018; 18 (3): 201–11.
21. Canu G, et al. Gilbert and Crigler Najjar syndromes: An update of the UDP-glucuronosyltransferase 1A1 (UGT1A1) gene mutation database. Blood Cells Mol Dis. 2013; 50 (4): 273–80.
22. Tcaciuc E, Podurean M, Tcaciuc A. Management of Crigler–Najjar syndrome. Med Pharm Rep. 2021; 94 (1): S64–S67.
23. Itoh S, Onishi S. Kinetic study of the photochemical changes of (ZZ) -bilirubin IX α bound to human serum albumin. Demonstration of (EZ) -bilirubin IX α as an intermediate in photochemical changes from (ZZ) -bilirubin IX α to (EZ) -cyclobilirubin IX α. Biochemical Journal. 1985; 226 (1): 251–8.
24. Faulhaber FRS, Procianoy RS, Silveira RC. Side Effects of Phototherapy on Neonates. American Journal of Perinatology. 2019; 36 (3): 252–7.
25. Zarkesh M, et al. The effect of neonatal phototherapy on serum level of interlukin-6 and white blood cells' count. J Clin Neonatol. 2016; 5 (3): 189.
26. Sirota L, et al. Phototherapy for neonatal hyperbilirubinemia affects cytokine production by peripheral blood mononuclear cells. Eur J Pediatr. 1999; 158 (11): 910–3.
27. Procianoy R, et al. The Influence of Phototherapy on Serum Cytokine Concentrations in Newborn Infants. Am J Perinatol. 2010; 27 (05): 375–9.
28. Newman TB, et al. Retrospective Cohort Study of Phototherapy and Childhood Cancer in Northern California. Pediatrics. 2016; 137 (6).
29. Berg P. Is Phototherapy in Neonates a Risk Factor for Malignant Melanoma Development? Arch Pediatr Adolesc Med. 1997; 151 (12): 1185.
30. Tham EH, et al. Phototherapy for neonatal hyperbilirubinemia and childhood eczema, rhinitis and wheeze. Pediatr Neonatol. 2019; 60 (1): 28–34.
31. Kuzniewicz MW, et al. Hyperbilirubinemia, Phototherapy, and Childhood Asthma. Pediatrics. 2018; 142 (4).
32. Fda. Package Insert — HEMGENIX.
33. Collaud F, et al. Preclinical Development of an AAV8-hUGT1A1 Vector for the Treatment of Crigler–Najjar Syndrome. Mol Ther Methods Clin Dev. 2019; 12: 157–74.
34. D'Antiga L, et al. Gene Therapy in Patients with the Crigler–Najjar Syndrome. New England Journal of Medicine. 2023; 389 (7): 620–31.
35. Aronson SJ, Ronzitti G, Bosma PJ. What's next in gene therapy for Crigler–Najjar syndrome? Expert Opinion on Biological Therapy. 2023; 23 (2): 119–21.
36. George LA, et al. Long-Term Follow-Up of the First in Human Intravascular Delivery of AAV for Gene Transfer: AAV2-hFIX16 for Severe Hemophilia B. Molecular Therapy. 2020; 28 (9): 2073–82.
37. Sabatino DE, et al. Evaluating the state of the science for adeno-

associated virus integration: An integrated perspective. Molecular Therapy. 2022; 30 (8): 2646–63.

38. Aronson SJ, et al. Prevalence and Relevance of Pre-Existing Anti-Adeno-Associated Virus Immunity in the Context of Gene Therapy for Crigler–Najjar Syndrome. Hum Gene Ther. 2019; 30 (10): 1297–305.

39. Bortolussi G, Muro AF. Advances in understanding disease mechanisms and potential treatments for Crigler–Najjar syndrome. Expert Opin Orphan Drugs. 2018; 6 (7): 425–39.

40. Seppen J, et al. Adeno-associated Virus Vector Serotypes Mediate Sustained Correction of Bilirubin UDP Glucuronosyltransferase Deficiency in Rats. Molecular Therapy. 2006; 13 (6): 1085–92.

41. Bortolussi G, Muro AF. Advances in understanding disease mechanisms and potential treatments for Crigler–Najjar syndrome. Expert Opin Orphan Drugs. 2018; 6 (7): 425–439.

42. Fagiuoli S, et al. Monogenic diseases that can be cured by liver transplantation. J Hepatol. 2013; 59 (3): 595–612.

43. Di Dato F, D'Uonno G, Iorio R. Crigler–Najjar syndrome: looking to the future does not make us forget the present. Orphanet Journal of Rare Diseases. 2024; 19 (1).

44. Özçay F, et al. Living Related Liver Transplantation in Crigler–Najjar Syndrome Type 1. Transplant Proc. 2009; 41 (7): 2875–7.

45. Tu Z-H, et al. Liver transplantation in Crigler–Najjar syndrome type I disease. Hepatobiliary & Pancreatic Diseases International. 2012; 11 (5): 545–8.

46. Schauer R, et al. Treatment of Crigler–Najjar type 1 disease: relevance of early liver transplantation. J Pediatr Surg. 2003; 38 (8): 1227–31.

47. Graffmann N, et al. Generation of a Crigler–Najjar Syndrome Type I patient-derived induced pluripotent stem cell line CNS705 (HHUUKDi005-A). Stem Cell Res. 2021; 51.

48. Martin–Rendon E, et al. 5–Azacytidine–treated human mesenchymal stem/progenitor cells derived from umbilical cord, cord blood and bone marrow do not generate cardiomyocytes in vitro at high frequencies. Vox Sang. 2008; 95 (2): 137–48.

49. Fukuchi Y, et al. Human Placenta–Derived Cells Have Mesenchymal Stem/Progenitor Cell Potential. Stem Cells. 2004; 22 (5): 649–58.

50. Kakinuma S, et al. Human Cord Blood Cells Transplanted Into Chronically Damaged Liver Exhibit Similar Characteristics to Functional Hepatocytes. Transplant Proc. 2007; 39 (1): 240–3.

51. Yan Y, et al. Mesenchymal stem cells from human umbilical cords ameliorate mouse hepatic injury in vivo. Liver International. 2009; 29 (3): 356–65.

52. Campard D, et al. Native Umbilical Cord Matrix Stem Cells Express Hepatic Markers and Differentiate Into Hepatocyte-like Cells. Gastroenterology. 2008; 134 (3): 833–48.

53. Suhih GT, et al. Terapevticheskij jeffekt mul'tipotentnyh mezenhimal'nyh stromal'nyh kletok, poluchennyh iz pupoviny cheloveka, u pacienta s sindromom Kriglera–Najjara I tipa. Rossijskij Vestnik perinatologii i pediatrii. 2019; 64 (4): 26–34. Russian.

Литература

1. Ebrahimi A, Rahim F. Crigler–Najjar Syndrome: Current Perspectives and the Application of Clinical Genetics. Endocr Metab Immune Disord Drug Targets. 2018; 18 (3): 201–11.

2. Aronson SJ, et al. Disease burden and management of Crigler–Najjar syndrome: Report of a world registry. Liver International. 2022; 42 (7): 1593–604.

3. Strauss KA, et al. Crigler–Najjar Syndrome Type 1: Pathophysiology, Natural History, and Therapeutic Frontier. Hepatology. 2020; 71 (6): 1923–39.

4. Kovačić Perica M, et al. Case report: Crigler–Najjar syndrome type 1 in Croatia—more than a one in a million: a case series. Front Pediatr. 2023; 11.

5. Ильченко Л. Ю. и др. Наследственная неконъюгированная гипербилирубинемия (сочетание синдрома Криглера–Найяра II типа и синдрома Жильбера). Hepatology and Gastroenterology. 2021; 5 (1): 79–84.

6. Иванова А. А., Максимов В. Н. Молекулярно-генетические аспекты синдрома Жильбера, синдромов Криглера–Найяра I и II типов. Экспериментальная и клиническая гастроэнтерология. 2023; 8: 56–62.

7. Iskander I, et al. Serum Bilirubin and Bilirubin/Albumin Ratio as Predictors of Bilirubin Encephalopathy. Pediatrics. 2014; 134 (5): e1330–e1339.

8. Ворончихина А. С., Спиваковский Ю. М. Клинический случай поздней диагностики синдрома Криглера–Найяра у ребенка 5 лет. 2024; с. 950–2.

9. Каржавина Л. И., Ефишова С. Г., Тамахина Н. В. Клинический случай синдрома Криглера–Найяра 1-го типа у ребенка первого года жизни. 2022; с. 85–89.

10. Дегтярева А. В. Синдром Криглера–Найяра. Российский вестник перинатологии и педиатрии. 1999; 44 (4): 44–48.

11. Shapiro SM, Riordan SM. Review of bilirubin neurotoxicity II: preventing and treating acute bilirubin encephalopathy and kernicterus spectrum disorders. Pediatr Res. 2020; 87 (2): 332–7.

12. Shapiro S, et al. The Neurological Sequelae of Neonatal Hyperbilirubinemia: Definitions, Diagnosis and Treatment of the Kernicterus Spectrum Disorders (KSDs). Curr Pediatr Rev. 2017; 13.

13. Mitchell E, et al. Hepatic Parenchymal Injury in Crigler–Najjar Type I. J Pediatr Gastroenterol Nutr. 2018; 66 (4): 588–94.

14. Bortolussi G, Muro AF. Advances in understanding disease mechanisms and potential treatments for Crigler–Najjar syndrome. Expert Opin Orphan Drugs. 2018; 6 (7): 425–39.

15. Dhawan A, et al. Disease burden of Crigler–Najjar syndrome: Systematic review and future perspectives. J Gastroenterol Hepatol. 2020; 35 (4): 530–43.

16. Wilson JHP, et al. Recommendations for Pregnancies in Patients with Crigler–Najjar Syndrome. 2012; c. 59–62.

17. Bansal S, et al. Effects of high bilirubin level in pregnancy in Crigler–Najjar syndrome type 2: An extremely rare but important clinical entity to recognize. Med J Armed Forces India. 2023; 79 (5): 597–600.

18. Hannam S, et al. Normal neurological outcome in two infants treated with exchange transfusions born to mothers with Crigler–Najjar Type 1 disorder. Eur J Pediatr. 2009; 168 (4): 427–9.

19. Kadakol A, et al. Genetic lesions of bilirubin uridine-diphosphoglucuronate glucuronosyltransferase (UGT1A1) causing Crigler–Najjar and Gilbert syndromes: Correlation of genotype to phenotype. Hum Mutat. 2000; 16 (4): 297–306.

20. Ebrahimi A, Rahim F. Crigler–Najjar Syndrome: Current Perspectives and the Application of Clinical Genetics. Endocr Metab Immune Disord Drug Targets. 2018; 18 (3): 201–11.

21. Canu G, et al. Gilbert and Crigler Najjar syndromes: An update of the UDP-glucuronosyltransferase 1A1 (UGT1A1) gene mutation database. Blood Cells Mol Dis. 2013; 50 (4): 273–80.

22. Tcaciuc E, Podurean M, Tcaciuc A. Management of Crigler–Najjar syndrome. Med Pharm Rep. 2021; 94 (1): S64–S67.

23. Itoh S, Onishi S. Kinetic study of the photochemical changes of (ZZ) -bilirubin IX α bound to human serum albumin. Demonstration of (EZ) -bilirubin IX α as an intermediate in photochemical changes from (ZZ) -bilirubin IX α to (EZ) -cyclobilirubin IX α. Biochemical Journal. 1985; 226 (1): 251–8.

24. Faulhaber FRS, Procianoy RS, Silveira RC. Side Effects of Phototherapy on Neonates. American Journal of Perinatology. 2019; 36 (3): 252–7.

25. Zarkesh M, et al. The effect of neonatal phototherapy on serum level of interlukin-6 and white blood cells′ count. J Clin Neonatol. 2016; 5 (3): 189.

26. Sirota L, et al. Phototherapy for neonatal hyperbilirubinemia affects cytokine production by peripheral blood mononuclear cells. Eur J Pediatr. 1999; 158 (11): 910–3.

27. Procianoy R, et al. The Influence of Phototherapy on Serum Cytokine Concentrations in Newborn Infants. Am J Perinatol. 2010; 27 (05): 375–9.

28. Newman TB, et al. Retrospective Cohort Study of Phototherapy and Childhood Cancer in Northern California. Pediatrics. 2016; 137 (6).

29. Berg P. Is Phototherapy in Neonates a Risk Factor for Malignant Melanoma Development? Arch Pediatr Adolesc Med. 1997; 151 (12): 1185.

30. Tham EH, et al. Phototherapy for neonatal hyperbilirubinemia and childhood eczema, rhinitis and wheeze. Pediatr Neonatol. 2019; 60 (1): 28–34.

31. Kuzniewicz MW, et al. Hyperbilirubinemia, Phototherapy, and Childhood Asthma. Pediatrics. 2018; 142 (4).

32. Fda. Package Insert — HEMGENIX.

33. Collaud F, et al. Preclinical Development of an AAV8-hUGT1A1 Vector for the Treatment of Crigler–Najjar Syndrome. Mol Ther Methods Clin Dev. 2019; 12: 157–74.

34. D'Antiga L, et al. Gene Therapy in Patients with the Crigler–Najjar Syndrome. New England Journal of Medicine. 2023; 389 (7): 620–31.

35. Aronson SJ, Ronzitti G, Bosma PJ. What's next in gene therapy for Crigler–Najjar syndrome? Expert Opinion on Biological Therapy. 2023; 23 (2): 119–21.

36. George LA, et al. Long-Term Follow-Up of the First in Human Intravascular Delivery of AAV for Gene Transfer: AAV2-hFIX16 for Severe Hemophilia B. Molecular Therapy. 2020; 28 (9): 2073–82.

37. Sabatino DE, et al. Evaluating the state of the science for adeno-associated virus integration: An integrated perspective. Molecular Therapy. 2022; 30 (8): 2646–63.

38. Aronson SJ, et al. Prevalence and Relevance of Pre-Existing Anti-Adeno-Associated Virus Immunity in the Context of Gene Therapy for Crigler–Najjar Syndrome. Hum Gene Ther. 2019; 30 (10): 1297–305.

39. Bortolussi G, Muro AF. Advances in understanding disease mechanisms and potential treatments for Crigler–Najjar syndrome. Expert Opin Orphan Drugs. 2018; 6 (7): 425–39.

40. Seppen J, et al. Adeno-associated Virus Vector Serotypes Mediate Sustained Correction of Bilirubin UDP Glucuronosyltransferase Deficiency in Rats. Molecular Therapy. 2006; 13 (6): 1085–92.

41. Bortolussi G, Muro AF. Advances in understanding disease mechanisms and potential treatments for Crigler–Najjar syndrome.

42. Fagiuoli S, et al. Monogenic diseases that can be cured by liver transplantation. J Hepatol. 2013; 59 (3): 595–612.

43. Di Dato F, D'Uonno G, Iorio R. Crigler–Najjar syndrome: looking to the future does not make us forget the present. Orphanet Journal of Rare Diseases. 2024; 19 (1).

44. Özçay F, et al. Living Related Liver Transplantation in Crigler–Najjar Syndrome Type 1. Transplant Proc. 2009; 41 (7): 2875–7.

45. Tu Z-H, et al. Liver transplantation in Crigler–Najjar syndrome type I disease. Hepatobiliary & Pancreatic Diseases International. 2012; 11 (5): 545–8.

46. Schauer R, et al. Treatment of Crigler–Najjar type 1 disease: relevance of early liver transplantation. J Pediatr Surg. 2003; 38 (8): 1227–31.

47. Graffmann N, et al. Generation of a Crigler–Najjar Syndrome Type I patient-derived induced pluripotent stem cell line CNS705 (HHUUKDi005-A). Stem Cell Res. 2021; 51.

48. Martin–Rendon E, et al. 5–Azacytidine–treated human mesenchymal stem/progenitor cells derived from umbilical cord, cord blood and bone marrow do not generate cardiomyocytes in vitro at high frequencies. Vox Sang. 2008; 95 (2): 137–48.

49. Fukuchi Y, et al. Human Placenta–Derived Cells Have Mesenchymal Stem/Progenitor Cell Potential. Stem Cells. 2004; 22 (5): 649–58.

50. Kakinuma S, et al. Human Cord Blood Cells Transplanted Into Chronically Damaged Liver Exhibit Similar Characteristics to Functional Hepatocytes. Transplant Proc. 2007; 39 (1): 240–3.

51. Yan Y, et al. Mesenchymal stem cells from human umbilical cords ameliorate mouse hepatic injury in vivo. Liver International. 2009; 29 (3): 356–65.

52. Campard D, et al. Native Umbilical Cord Matrix Stem Cells Express Hepatic Markers and Differentiate Into Hepatocyte-like Cells. Gastroenterology. 2008; 134 (3): 833–48.

53. Сухих Г. Т., et al. Терапевтический эффект мультипотентных мезенхимальных стромальных клеток, полученных из пуповины человека, у пациента с синдромом Криглера–Найяра I типа. Российский Вестник перинатологии и педиатрии. 2019; 64 (4): 26–34.

INCREASED PHYSICAL ACTIVITY UNDER CONDITIONS OF NORMOXIA CAUSES IDIOPATHIC CACHEXIA IN *HETEROCEPHALUS GLABER*

Adrianov MA[1] ✉, Bobrov M[2], Mamedov I[3], Manskih V[1], Rachkova AA[1,4], Shelekhova AM[1], Eldarov CM[1,4], Averina OA[1], Vyssokikh MYu[1,4]

[1] Belozersky Institute of Physico-Chemical Biology, Lomonosov Moscow State University, Moscow, Russia
[2] Sirius University of Science and Technology, Sirius, Russia
[3] Shemyakin–Ovchinnikov Institute of Bioorganic Chemistry, Russian Academy of Sciences, Moscow, Russia
[4] Kulakov National Medical Research Center for Obstetrics, Gynecology and Perinatology, Moscow, Russia

Enrichment of habitat of the captive rodents *Heterocephalus glaber* (naked mole rats) allowing them to implement the innate behavioral pattern of digging through hard soil somehow led to the emergence of unusual animals showing signs of cachexia in the colony; these differed from other animals by the reduced body mass index associated with subcutaneous fat reduction. Furthermore, the animals itself showed aggressive eating behavior, but showed no weight gain even after stopping digging due to detachment of the camera with soil. The study aimed to clarify the pathogenetic mechanism underlying the reported phenomenon. For that animals showing signs of cachexia (one female and two males aged 4–5 years) were withdrawn from the colony, along with the animals showing no such signs (two females and one male aged 4–5 years) as controls. Histologic assessment of tissues revealed cardiac hypertrophy and hyperlipofuscinosis of the liver. Cardiac hypertrophy was also suggested by the results of the animal heart microRNA sequencing bioinformatics analysis that revealed elevated levels of microRNA responsible for the increased cell division activity and reduced apoptotic activity in the heart. These data suggest that the animals living in the habitat with the increased oxygen content (21% vs. 8% in the natural habitat, underground) experienced severe oxidative stress during physical activity, which resulted in dysfunction of body's regulatory systems, increased metabolism at rest, cardiovascular system overload, and damage to organs and tissues. Thus, naked mole rats can have normal physical activity only under conditions of low oxygen content.

Keywords: naked mole rat, cachexia, physical burden, oxidative stress, lipofuscinosis, basal metabolic rate, hyperoxia

ПОВЫШЕННАЯ ФИЗИЧЕСКАЯ НАГРУЗКА В УСЛОВИЯХ НОРМОКСИИ ВЫЗЫВАЕТ ИДИОПАТИЧЕСКУЮ КАХЕКСИЮ У *HETEROCEPHALUS GLABER*

М. А. Адрианов[1] ✉, М. Ю. Бобров[2], И. З. Мамедов[3], В. Н. Манских[1], А. А. Рачкова[1,4], А. М. Шелехова[1], Ч. М. Эльдаров[1,4], О. А. Аверина[1], М. Ю. Высоких[1,4]

[1] Научно-исследовательский институт физико-химической биологии имени А. Н. Белозерского, Московский государственный университет имени М. В. Ломоносова, Москва, Россия
[2] Научно-технологический университет «Сириус», Сириус, Россия
[3] Институт биоорганической химии имени М. М. Шемякина и Ю. А. Овчинникова Российской академии наук, Москва, Россия
[4] Национальный медицинский исследовательский центр акушерства, гинекологии и перинатологии имени В. И. Кулакова, Москва, Россия

Обогащение среды обитания живущих в неволе грызунов *Heterocephalus glaber* (голых землекопов), позволившее им реализовать врожденный поведенческий паттерн рытья плотного грунта, неизвестным образом привело к появлению в колонии необычных животных с признаками кахексии, отличавшихся от остальных животных сниженным индексом массы тела на фоне уменьшения доли подкожного жира. Сами животные демонстрировали при этом агрессивное пищевое поведение, но не набирали веса даже после прекращения рытья при отсоединении камеры с грунтом. Целью работы было выяснить патогенетический механизм наблюдаемого явления. Для этого из колонии изъяли животных с признаками кахексии (одна самка и два самца возрастом 4–5 лет), а также животных, не имеющих данных признаков (две самки и один самец возрастом 4–5 лет) в качестве контрольных. При гистологическом анализе тканей были выявлены гипертрофия сердца и гиперлипофусциноз печени. На гипетрофию сердца также указывали результаты биоинформатического анализа секвенирования микроРНК сердца животных, который показал повышенный уровень микроРНК, ответственных за повышение активности деления клеток, и снижение активности апоптоза в сердце. Эти данные свидетельствуют о том, что животные, находясь в среде обитания с повышенным для них содержанием кислорода (21% против 8% в естественной среде обитания под землей), при выполнении физических нагрузок испытали сильный окислительный стресс, что привело к нарушению работы регуляторных систем организма, подъему метаболизма в покое, перегрузке работы сердечно-сосудистой системы и повреждению органов и тканей. Таким образом, голые землекопы могут вести нормальную для них физическую активность только в условиях низкого содержания кислорода.

Ключевые слова: голый землекоп, кахексия, физическая нагрузка, окислительный стресс, липофусциноз, метаболизм в состоянии покоя, гипероксия

Naked mole rats (Heterocephalus glaber), the subterranean rodents inhabiting the Horn of Africa (Somali, Ethiopia), are incredibly interesting to study. One of their distinguishing features is eusociality, while the other is abnormally high life expectancy. Thus, naked mole rats having the relatively low body weight (30–80 g) can live up to 37 years under laboratory conditions [1], while the rodent with the same weight, such as house mouse (Mus musculus), lives up to 3 years under laboratory conditions and up to 1.5 years in the wild [2].

Creating housing conditions for laboratory animals similar to that in the animals' natural range is an essential component of the studies using animals for assessment of various biological processes. When dealing with naked mole rats, it is necessary to maintain high temperature and humidity. However, creating imitation of the underground labyrinth, which naked mole rats would inhabit while staying at the laboratory, is the most time-consuming process related to the naked mole rat housing [3]. The labyrinth itself consists of cylinders and connecting tunnels made of acrylic glass. However, such a housing system does not allow the animals to fully demonstrate their physical activity, since the cylinders are partially filled with the substrate, the animals could burrow. It is well known that low physical activity sometimes results in alteration of the skeletal muscle structure, which can lead to incorrect interpretation of the research results when comparing with other model objects [4]. In this regard, the laboratory staff decided to install a supplementary compartment filled with clay with the density close to that of the Horn of Africa soil in order to enrich the naked mole rats' environment.

Naked mole rats almost immediately began to dig tunnels in the soil, which was considered a normal animals' response. However, half a year later we started noticing exterior changes in some animals. These began to lose weight, their facial features became sharper, which resembled the state of other animals suffering from cachexia [5]. We believed that the reason was loss of the animal's subcutaneous fat. Furthermore, it should be noted that these animals were the first to approach to food, which they did not transfer to the nest, instead of what should have been done if these were workers, but eat it immediately, which suggested their increased need for food. It was decided to remove the compartment with clay and monitor the animals' body mass index throughout three years, with subsequent assessment of microRNAs in the organs that could be damaged: heart, kidney, liver, skeletal muscle. Moreover, to determine the cause of such abnormal animals' condition, histological specimens of the studied tissues and organs were prepared.

It was decided to study microRNA, because the naked mole rats' transcriptome is currently poorly understood, and microRNA is an evolutionarily highly conserved structure involved in regulation of expression of similar genes in different species [6]. The study aimed to determine the cause of such animals' condition.

METHODS

Maintenance and care of animals

The colony of naked mole rats ($n = 11$) obtained from the Leibniz Institute for Zoo and Wildlife Research (IZW) (Berlin, Germany) was reproduced in the Belozersky Institute of Physico-Chemical Biology, Lomonosov Moscow State University, to 54 animals before the study. Each animal had an individual RFID chip implanted subcutaneously for identification in the colony. The colony was kept in cylindrical plastic containers connected to each other with plastic tubes at a temperature of 27 ± 1 °C, humidity $50 \pm 10\%$, and the 12 : 12 h light/dark cycle (10:00–22:00 — light). The diet consisted of apples, sweet potatoes, carrots, cereals provided every day. The animals did not need water, since, due to their physiology, these can get water from solid foods only. To enrich the naked mole rats' environment, a rectangular container with high-density clay mimicking the soil typical for the animals' natural habitat was installed in the colony. The container was removed immediately after the emergence of the signs of cachexia in 9 animals (3 females and 6 males aged 2–6 years) out of 54. To control the condition of these animals, their body mass index was monitored every 4–5 months and compared with that of the control animals of the same age ($n = 9$; 4 females and 5 males). The animals were euthanized by decapitation after being anesthesized using inhalatory 5% isoflurane (Laboratorios Karizoo. S.A., Spain) with the flow rate of 0.4 L/min in the R500 unit (RWD, China).

Experimental groups of animals for histological assessment and microRNA sequencing

Two groups of naked mole rats were selected for the study: healthy animals ($n = 3$, one female and two males) with body temperature of 30 °C, body mass index of 0.33, and animals having an asthenic type ($n = 3$, two females and one male) with body temperature of 27 °C, body mass index of 0.25.

Animals' body mass index calculation

Body mass index (BMI, g/cm^2) was calculated using the following formula: BMI = animal's body weight, g / (animal's body length, cm)^2.

Histological assessment

The animals' liver specimens were fixed with the 10% formalin in 0.1M phosphate buffer (pH = 7.4); dehydrated in five portions of isopropyl alcohol (BioVitrum, Russia), 2 h per portion; soaked in two portions of the Histomix paraffin medium (BioVitrum, Russia), 2 h per portion, and embedded in paraffin blocks. The 3 µm slices were cut using the rotary microtome (Leika, Germany) and stained with Carazzi's hematoxylin and eosin in accordance with the routine protocol. The slides were examined using the AxioScope A1 microscope (Karl Zeiss, Germany). The MRc.5 digital camera (Karl Zeiss, Germany) was used for imaging.

MicroRNA extraction and sequencing

After euthanasia, liver, kidney, heart, skeletal muscle specimens were collected from each animal. RNA fractions containing microRNA were extracted from the tissue specimens using the miRNEasy kits (Qiagen, USA). The samples obtained were later used to create cDNA libraries and for further sequencing. The extracted fraction quality was assessed by microelectrophoresis on Bioanalyzer chips (Agilent, USA). Samples with the RNA integrity number (RIN) of at least 8 were selected for sequencing.

Sequencing involved the use of the NextSeq platform (Illumina, USA) and reagents and disposables from the NextSeq 500/550 High Output v2 kit (Illumina, USA). The cDNA libraries were prepared from the extracted RNA samples using the NEBnext kits (NEB, USA) in accordance with the methods recommended by the manufacturer. Qualitative and quantitative analysis of the libraries was conducted by Bioanalyzer microelectrophoresis (Agilent, USA) and fluorometry in Qubit

Dynamic changes in the animals' BMI
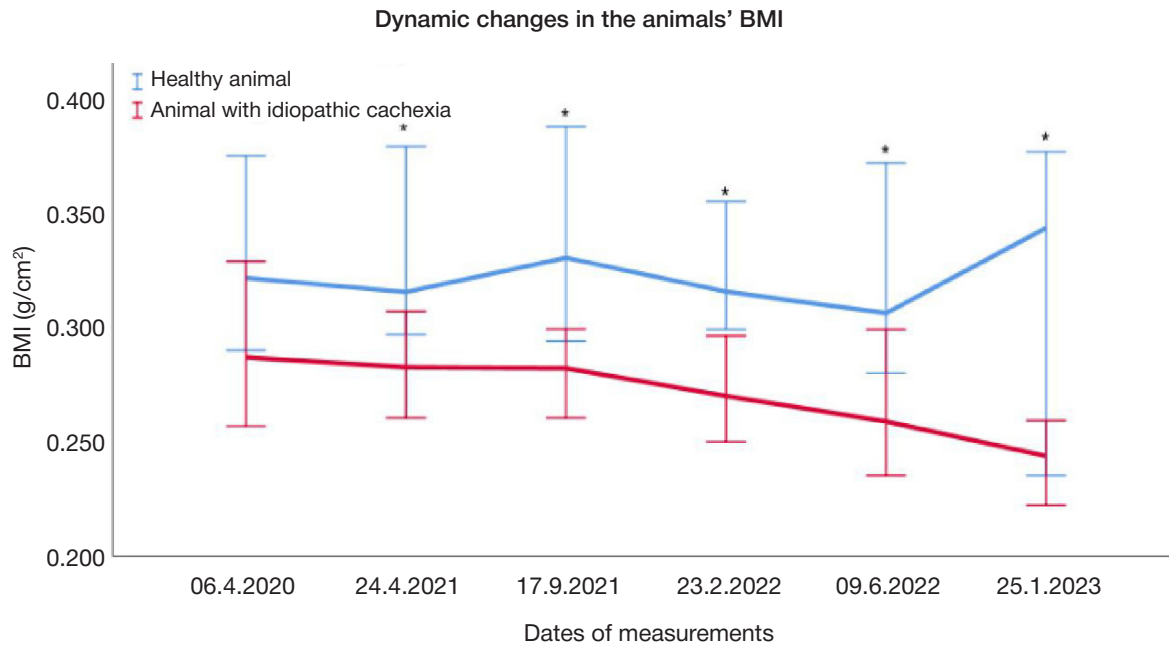
Fig. 1. Curve of the dynamic changes in the animals' BMI. * — $p < 0.05$

(ThermoFisher, USA). The sequencing quality was estimated using the BaseSpace service (Illumina, USA) based on the following parameters: cluster density, signal intensities in detection channels, percentage of clusters passing filter based on the aligned reads output. All the parameters were within the permissible range.

Bioinformatics analysis of microRNA sequencing data

The nucleotide sequences (reads) obtained by sequencing were subjected to mandatory quality control involving the use of the fastqc software tool; high-quality reads were selected for further testing (>30). Adapters were removed using the cutadapt software tool. After adapter removal, only sequences of 18–31 nucleotides corresponding to small RNAs were selected for further assessment.

The search for microRNA was performed using the mirDeep2 algorithm based on the naked mole rat genome and using information about the related genome (Mus musculus). Then random and/or non-specific sequences were deleted from the general list of sequences. Only sequences found in more than 60% of samples of the subgroup (experimental or control group for appropriate tissue or organ) that had passed all quality filters were selected for further assessment.

MicroRNA annotation and analysis

The search for human orthologs was performed for all microRNAs that had passed all filters using the blastn software tool; the human microRNA Mirbase v.22 database (https://mirbase.org/) was used as a database for comparison.

The microRNA-target interactions database Mirtarbase v 9.0 (https://mirtarbase.cuhk.edu.cn/~miRTarBase) and miRDB (https://mirdb.org/mirdb) were used to search for possible microRNA targets. Only interactions confirmed by the so-called "strong" evidence (by quantitative PCR, blotting or the use of reporter gene) were selected in Mirtarbase. The microRNA targets having the target score above 80 were selected in the miRDB database.

Enrichment based on various databases, such as GO, KEGG, Reactome, Wikipathways, using the STRING platform (https://string-db.org/) was performed for the microRNA–target pairs selected by this method in order to identify the most involved metabolic pathways and processes.

Statistical data processing

The data were processed in IBM® SPSS® 24 (IBM, USA) using the Mann–Whitney U test. The differences were considered significant at $p < 0.05$.

RESULTS

Animals' exterior

In the end of the study the animals with signs of cachexia had a significantly decreased BMI (by 15%) compared to the control animals from the same colony (Fig. 1). Exterior of the animals suffering from cachexia was dramatically different from that of the control animals. These animals had sunken flanks, sharp facial features (Fig. 2).

Histological assessment of the liver

After retrieval of the liver following euthanasia of the animals suffering from cachexia, the liver was deep brown, in contrast to that of the control animals (Fig. 3). Histological assessment of the liver revealed a complex of unique alterations not previously reported for mole rats. All the animals with spontaneous idiopathic cachexia showed accumulation of the large amount of light brown pigment, lipofuscin, in hepatocytes. In some animals, this pigment was more or less evenly distributed across hepatocytes of the liver lobule. In other animals, pigment deposition mainly in pericentral zones with the development of the clearly visible fatty degeneration of hepatocytes was observed. Furthermore, hepatocellular hypertrophy with dramatic enlargement of the cells and nuclei and the emergence of numerous eosinophilic granules (mitochondria) in the cytoplasm was found in periportal areas. In certain animals, the extramedullary hematopoiesis and erythrophagocytosis by hepatocytes phenomena were observed. In healthy animals, there were no lipofuscin or dystrophic changes in hepatocytes (Fig. 4).

Fig. 2. A. Exterior of the healthy animal. **B**. Exterior of the animal with idiopathic cachexia

Fig. 3. View of the liver of the animal with idiopathic cachexia

As is well known, lipofuscin is produced from the remnants of the membranes of intracellular organelles after their degradation in autophagosomes. That is why lipofuscin deposition in hepatocytes is a morphological sign of autophagy intensification and liver cell ageing.

Annotation of naked mole rat microRNA

After filtration of the sequences obtained by sequencing based on the length and quality, microRNA sequences from the naked mole rat liver, kidney, heart, and skeletal muscle were obtained. The overall pool of all the sequences identified was annotated similarly to human orthologs in Mirbase. The naked mole rat microRNA base was created for the first time (Table 1). A total of 162 sequences were reported 90–100% identical to human analogues. Moreover, no human analogues were identified for 22 naked mole rat small RNA sequences. Therefore, it is

reasonable to suppose that additional specific regulation of gene expression is typical for naked mole rats. Its adaptive value can be explored in the future by studying the range of microRNAs of the species genetically and environmentally close to naked mole rats (Mus musculus, Cavia porcellus, Ellobius talpinus, Cryptomys damarensis).

Potential targets were analyzed and enrichment based on GO, KEGG, Reactome, Wikipathways was performed for microRNAs identified in the liver, kidney, heart, and skeletal muscle (Table 2–5). The analysis of the signaling pathways and processes related to the microRNAs identified and their target genes has shown that there are numerous multidirectional ones determining a large number of cellular and even extracellular functions that are involved in normal physiology and spontaneous idiopathic cachexia of naked mole rats. In particular, such distant processes are dealt with, as anatomical structure development and double-stranded DNA binding.
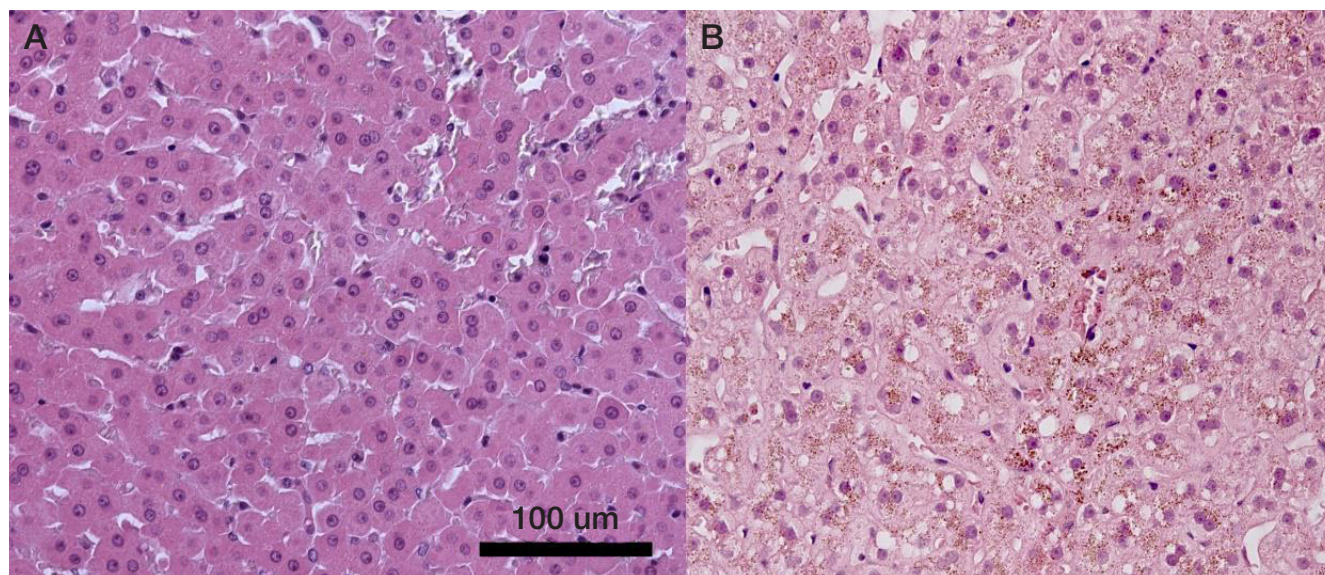
Fig. 4. A. Liver of the healthy animal. **B**. Liver of the animal with idiopathic cachexia. Brown inclusions in the cytoplasm are the lipofuscin deposits. H&E stain, 400x.

Especially noteworthy is the presence of microRNAs responsible for regulation of expression of the genes suppressing apoptosis, but inducing cell division in the naked mole rat heart.

DISCUSSION

The exterior and altered BMI of the animals suffering from cachexia suggest thet these animals failed to gain weight for some unknown reason, but demonstrated the same eating behavior, as other members of the colony, and were even more aggressive with food, since being workers the animals did not carry food to the nesting compartment, but eat it immediately in the feeding compartment.

Perhaps this is because these animals show much higher energy expenditure at rest, than the control animals, for example, as the hyperthyroid induced rats [7]. This is consistent with the data derived from the microRNA sequencing results. The animals suffering from cachexia have the increased share of microRNAs responsible for elevated cell division activity and the decrease in activity of programmed cell death and apoptosis in the heart, which suggests increased cell proliferation in the myocardium followed by its hypertrophy and is also associated with induced hyperthyroidism in mice [8]. Such hypertrophy is essential for the cardiac output increase; when the heart rate is increased, this leads to acceleration of metabolism, which was likely to be demonstrated by the animals unable to gain weight while maintaining the same diet. Such alterations in the heart can result in its failure observed in humans also suffering from hyperthyroidism, which will result in lower life expectancy of the animals suffering from cachexia compared to healthy animals [9].

The reported cachexic condition of the animals was also reflected by the animals' liver. The liver itself was bright brown, almost black. This can be associated with large deposits of lipofuscin in the liver tissue demonstrated by histological assessment. Perhaps, intense mitochondrial remodeling involving the autophagy processes took place in the liver tissue, which resulted from intense oxidative stress [10], since these animals are exposed to low oxygen levels (8–15%) in their natural habitat [11], while in laboratory settings these are kept at 21%, i.e. in hyperoxic environment. In the animals suffering from cachexia, an aggravating factor is increased metabolic rate at rest against the background of cardiovascular system hyperactivation, which entails active functioning of the respiratory system, thereby further loading the cachexic naked mole rat's body with excess blood oxygen levels capable of causing the reported manifestations in the liver [12] and heart.

CONCLUSIONS

Considering the facts, it can be assumed that such a condition of naked mole rats was caused by increased physical exertion in hyperoxic state, which could result in liver damage due to chronic oxidative stress resulting in reduced life expectancy and the development of the disorder in such animals. Such an effect demonstrates possible naked mole rats' vulnerability to increased atmospheric oxygen, which confirms that these are physiologically predisposed to living precisely at low oxygen levels. However, the cause of the animals' metabolic rate increase at rest even after removal of the provoking factor is poorly understood. Maybe this is associated with irreversible effects of the long-term oxidative stress, disturbing regulation of cells and integrative systems, on the body. To find out, it is necessary to conduct further studies of these animals, specifically to carry out transcriptome analysis and assess the expression of the differentially expressed microRNA targets.

References

1. Lee BP, Smith M, Buffenstein R, Harries LW. Negligible senescence in naked mole rats may be a consequence of well-maintained splicing regulation. GeroScience. 2020; 42: 633–51. Available from: https://doi.org/10.1007/s11357-019-00150-7.
2. Gorbunova V, Bozzella MJ, Seluanov A. Rodents for comparative aging studies: from mice to beavers. AGE. 2008; 30: 111–9. Available from: https://doi.org/10.1007/s11357-008-9053-4.
3. Smith M, Buffenstein R. Managed Care of Naked Mole-Rats. In: Buffenstein R, Park TJ, Holmes MM, editors. The Extraordinary Biology of the Naked Mole-Rat, vol. 1319. Cham: Springer International Publishing, 2021; p. 381–407.
4. Holloway GP, Holwerda AM, Miotto PM, Dirks ML, Verdijk LB, Van Loon LJC. Age-Associated Impairments in Mitochondrial ADP Sensitivity Contribute to Redox Stress in Senescent Human Skeletal Muscle. Cell Reports. 2018; 22: 2837–48. Available from: https://doi.org/10.1016/j.celrep.2018.02.069.
5. DeBoer MD. Animal models of anorexia and cachexia. Expert Opinion on Drug Discovery. 2009; 4: 1145–55. Available from: https://doi.org/10.1517/17460440903300842.
6. Bartel DP. MicroRNAs. Cell. 2004; 116: 281–97. Available from: https://doi.org/10.1016/S0092-8674(04)00045-5.
7. Iossa S, Liverini G, Barletta A. Relationship between the resting metabolic rate and hepatic metabolism in rats: effect of hyperthyroidism and fasting for 24 hours. Journal of Endocrinology. 1992; 135: 45–51. Available from: https://doi.org/10.1677/joe.0.1350045.
8. Parletta AC, Cerri GC, Gasparini CRB, Panico K, Vieira-Junior DN, Zacarias-Rodrigues LM, et al. Cardiac hypertrophy that affects hyperthyroidism occurs independently of the NLRP3 inflammasome. Pflugers Arch — Eur J Physiol. 2024; 476: 1065–75. Available from: https://doi.org/10.1007/s00424-024-02965-6.
9. Osuna PM, Udovcic M, Sharma MD. Hypothyroidism and the Heart. Methodist DeBakey Cardiovascular Journal. 2017; 13: 60. Available from: https://doi.org/10.14797/mdcj-13-2-60.
10. Wang X, Song X, Si Y, Xia J, Wang B, Wang P. Effect of autophagy-associated proteins on the arecoline-induced liver injury in mice. Exp Ther Med. 2018. Available from: https://doi.org/10.3892/etm.2018.6564.
11. McNab BK. The Metabolism of Fossorial Rodents: A Study of Convergence. Ecology. 1966; 47: 712–33. Available from: https://doi.org/10.2307/1934259.
12. Rogers LK, Tipple TE, Britt RD, Welty SE. Hyperoxia exposure alters hepatic eicosanoid metabolism in newborn mice. Pediatr Res. 2010; 67: 144–9. Available from: https://doi.org/10.1203/PDR.0b013e3181c2df4f.

Литература

1. Lee BP, Smith M, Buffenstein R, Harries LW. Negligible senescence in naked mole rats may be a consequence of well-maintained splicing regulation. GeroScience. 2020; 42: 633–51. Available from: https://doi.org/10.1007/s11357-019-00150-7.
2. Gorbunova V, Bozzella MJ, Seluanov A. Rodents for comparative aging studies: from mice to beavers. AGE. 2008; 30: 111–9. Available from: https://doi.org/10.1007/s11357-008-9053-4.
3. Smith M, Buffenstein R. Managed Care of Naked Mole-Rats. In:

Buffenstein R, Park TJ, Holmes MM, editors. The Extraordinary Biology of the Naked Mole-Rat, vol. 1319. Cham: Springer International Publishing, 2021; p. 381–407.

4. Holloway GP, Holwerda AM, Miotto PM, Dirks ML, Verdijk LB, Van Loon LJC. Age-Associated Impairments in Mitochondrial ADP Sensitivity Contribute to Redox Stress in Senescent Human Skeletal Muscle. Cell Reports. 2018; 22: 2837–48. Available from: https://doi.org/10.1016/j.celrep.2018.02.069.

5. DeBoer MD. Animal models of anorexia and cachexia. Expert Opinion on Drug Discovery. 2009; 4: 1145–55. Available from: https://doi.org/10.1517/17460440903300842.

6. Bartel DP. MicroRNAs. Cell. 2004; 116: 281–97. Available from: https://doi.org/10.1016/S0092-8674(04)00045-5.

7. Iossa S, Liverini G, Barletta A. Relationship between the resting metabolic rate and hepatic metabolism in rats: effect of hyperthyroidism and fasting for 24 hours. Journal of Endocrinology. 1992; 135: 45–51. Available from: https://doi.org/10.1677/joe.0.1350045.

8. Parletta AC, Cerri GC, Gasparini CRB, Panico K, Vieira-Junior DN, Zacarias-Rodrigues LM, et al. Cardiac hypertrophy that affects hyperthyroidism occurs independently of the NLRP3 inflammasome. Pflugers Arch — Eur J Physiol. 2024; 476: 1065–75. Available from: https://doi.org/10.1007/s00424-024-02965-6.

9. Osuna PM, Udovcic M, Sharma MD. Hypothyroidism and the Heart. Methodist DeBakey Cardiovascular Journal. 2017; 13: 60. Available from: https://doi.org/10.14797/mdcj-13-2-60.

10. Wang X, Song X, Si Y, Xia J, Wang B, Wang P. Effect of autophagy-associated proteins on the arecoline-induced liver injury in mice. Exp Ther Med. 2018. Available from: https://doi.org/10.3892/etm.2018.6564.

11. McNab BK. The Metabolism of Fossorial Rodents: A Study of Convergence. Ecology. 1966; 47: 712–33. Available from: https://doi.org/10.2307/1934259.

12. Rogers LK, Tipple TE, Britt RD, Welty SE. Hyperoxia exposure alters hepatic eicosanoid metabolism in newborn mice. Pediatr Res. 2010; 67: 144–9. Available from: https://doi.org/10.1203/PDR.0b013e3181c2df4f.

INTERFERON TYPE I-EXPRESSING RECOMBINANT VACCINIA VIRUS AS A PLATFORM FOR SELECTIVE IMMUNOTHERAPY OF GLIOBLASTOMA AND MELANOMA

Naberezhnaya ER[1], Soboleva AV[1], Vorobyev PO[1], Vadekhina VV[1], Yusubalieva GM[1,2,3], Isaeva IV[2], Baklaushev VP[1,2,3,4], Chumakov PM[1], Lipatova AV[1]✉

[1] Engelhardt Institute of Molecular Biology, Russian Academy of Science, Moscow, Russia,
[2] Federal Scientific and Clinical Center of Specialized Types of Medical Care and Medical Technologies of the Federal Medical Biological Agency, Moscow, Russia
[3] Federal Center of Brain Research and Neurotechnologies of the Federal Medical Biological Agency, Moscow, Russia
[4] Research Institute of Pulmonology of the Federal Medical Biological Agency, Moscow, Russia

Immunotherapy with oncolytic viruses (OVs) becomes a full-fledged neoadjuvant therapy method in the paradigm of evidence-based medicine for the growing number of cancers. The use of OVs for immunologically "cold" tumors causing minimal immune response and having the clearly immunosuppressive tumor microenvironment is especially relevant. Recombinant OVs carrying the sequences of proteins activating the immune system can be used to stimulate antitumor response. The study aimed to assess oncoselectivity and antitumor activity of the recombinant OV designed based on the LIVP vaccinia virus strain showing expression of human and murine interpheron alpha sequences (hIFNα and mIFNα, respectively). The in vitro experiments showed that the recombinant OVs designed showed oncoselectivity in relation to tumor cell lines of appropriate species. The ability to effectively infect human adenocarcinoma and glioblastoma cell lines was reported for LIVP-hIFNα. LIVP-mIFNα showed selectivity in relation to glioma Gl261 and melanoma B16 in vitro. The in vivo experiment involving the C57Bl/6 mice with subcutaneous melanoma B16 showed the ability of the intravenously administered LIVP-mIFNα to reduce the size of the subcutaneous tumor allograft and increase tumor infiltration with the CD8+ and NK cells. The recombinant virus designed can be a potential platform for the development of oncolytic virotherapy of human melanoma and glioblastoma.

Keywords: oncolytic viruses, interferon, viral oncolysis, recombinant vaccinia virus strains

РЕКОМБИНАНТНЫЙ ВИРУС ОСПОВАКЦИНЫ, ЭКСПРЕССИРУЮЩИЙ ИНТЕРФЕРОН ТИПА 1, КАК ПЛАТФОРМА ДЛЯ СЕЛЕКТИВНОЙ ИММУНОТЕРАПИИ ГЛИОБЛАСТОМЫ И МЕЛАНОМЫ

Е. Р. Набережная[1], А. В. Соболева[1], П. О. Воробьёв[1], В. В. Вадехина[1], Г. М. Юсубалиева[1,2,3], И. В. Исаева[2], В. П. Баклаушев[1,2,3,4], П. М. Чумаков[1], А. В. Липатова[1]✉

[1] Институт молекулярной биологии имени Энгельгардта Российской академии наук, Москва, Россия
[2] Федеральный научно-клинический центр специализированных видов медицинской помощи и медицинских технологий Федерального медико-биологического агентства, Москва, Россия
[3] Федеральный центр мозга и нейротехнологий Федерального медико-биологического агентства, Москва, Россия
[4] Научно-исследовательский институт пульмонологии Федерального медико-биологического агентства, Москва, Россия

Иммунотерапия онколитическими вирусами (ОВ) становится полноценным методом неоадъювантной терапии в парадигме доказательной медицины для все большего числа онкологических заболеваний. Особенно актуально применение ОВ для иммунологически «холодных» опухолей, вызывающих минимальный иммунный ответ и обладающих выраженным иммуносупрессивным опухолевым микроокружением. Для стимуляции противоопухолевого ответа применимы рекомбинантные ОВ, несущие последовательности иммуноактивирующих белков. Целью работы было исследовать онкоселективность и противоопухолевую активность рекомбинантного ОВ, созданного на базе штамма LIVP вируса осповакцины, экспрессирующего последовательности интерферона-альфа человека и мыши (hIFNα и mIFNα соответственно). В экспериментах с помощью метода Рида и Менча было показано, что созданные рекомбинантные ОВ проявляют онкоселективность в отношении опухолевых линий соответствующего вида. Для LIVP-hIFNα показана способность эффективно заражать линии аденокарциномы и глиобластомы человека. Для LIVP-mIFNα in vitro продемонстрирована селективность в отношении глиомы Gl261 и меланомы B16. В эксперименте in vivo на мышах линии C57Bl/6 с подкожной меланомой B16 показана способность LIVP-mIFNα после внутривенного введения уменьшать объем подкожного аллографта опухоли и увеличивать инфильтрацию опухоли CD8+- и NK-клетками. Созданный рекомбинантный вирус может быть потенциальной платформой для разработки онколитической виротерапии меланомы и глиобластомы человека.

Ключевые слова: онколитические вирусы, интерферон, вирусный онколиз, рекомбинантные штаммы вируса осповакцины

Though many therapeutic approaches are now available including modern surgery with intraoperative navigation, radiotherapy, neoadjuvant therapy with targeted drugs, immune checkpoint inhibitors, the survival rates for patients with some cancers such as glioblastoma, metastatic melanoma and a number of carcinomas with primary metastasis remain extremely low. Development of new therapeutic approaches aimed at elimination or prevention of distant metastases is therefore of high significance.

An important requirement for developing new antitumor agents is a highly selective oncolytic action, the ability to detect and destroy malignant/metastatic tumor cells only. Non-pathogenic or attenuated viruses are ideal candidates for the development of tumor-selective agents. Tumor selective therapeutic strains are capable of destroying tumor cells by replicating efficiently in the cells without damaging normal tissues [1].

Currently, using Poxviridae viruses as prototypes of oncolytic viruses for the treatment of metastatic carcinomas and melanoma is of particular attention. A promising oncolytic virus belonging to the *poxvirus* family is vaccinia virus (VV) [2], in particular, the Russian variant of the Lister VV strain (LIVP VV). The strain was widely used in the Smallpox Eradication Campaign (SEC); it is highly tumor selective [3, 4], in particular, the thymidine kinase (TK) knockout leads to selective replication of the virus in tumor cells where TK is usually overexpressed [5].

To improve the antitumor properties of attenuated VV strains, recombinant VV strains expressing different transgenes are costructed [6]. To date, many transgenes are known to be effectively expressed in VV including genes encoding cytokines and their receptors [7], immunostimulators [8–10], oncotoxic proteins [11], and angiogenesis inhibitors [12].

In this study, we constructed highly tumor selective poxvirus strains expressing human or mouse IFNα and tagRFP in a bicistronic cassette. The expression of IFNα by a recombinant oncolytic strain can enhance indirect immune-mediated oncolytic action through inducing the expression of the major histocompatibility complex class I molecules, increased activity of cytotoxic T lymphocytes, activation of T helper cells, macrophages, and NK cells [13].

In normal cells, interferon secretion stops protein translation and cell cycle processes and slows down cell metabolism [14]; protecting cells from viruses interferon mechanisms are therefore interfere with tumor cell proliferation. Microevolution results in accumulating errors in the signaling pathways of interferon induction and interferon response in tumor cells and as a consequence, cells may lose their antiviral defense abilities [15, 16]. The loss of protective interferon response mechanisms is one of the factors responsible for the uncontrolled proliferation of tumor cells [17].

Another thing making the oncolytic virotherapy so promising is the ability of OVs to induce a long-lasting cancer-specific immune activation [18]. Viruses kill tumor cells releasing various molecules such as tumor-associated antigens, pathogen-associated molecular patterns, damage-associated molecular patterns and cytokines [19]. The molecules promote activation of immune antigen-presenting cells and T cells developing an effective adaptive immune response against the tumor [20, 21].

Type I interferons inhibit virus replication in normal cells however, in tumor cells the inhibition is less effective [8, 17]. Type I interferons therefore have antitumor effect and are able to induce tumor specific cytotoxic T-lymphocytes and activate antiangiogenic factors [22]. Furthermore, vaccinia virus inhibits the interferon response system through the expression of certain genes [22]. The aim of the study was to evaluate the significance of interferon expression by vaccinia virus for the oncolytic activity of the virus.

METHODS

Vaccinia virus strains

LIVP-hIFNα, vaccinia virus expressing human IFNα and tagRFP; LIVP-mIFNα, vaccinia virus expressing mouse IFNα and tagRFP; LIVP-RFP, vaccinia virus expressing tagRFP.

Cell cultures

BHK-21 — baby hamster kidney cell line; HEK293T — transformed human embryonic kidney cell line containing SV40-antigen; U-87 MG, DBTRG-05MG, U251-MG, PrGlioma 3821, PrGlioma 6067, PrGlioma 6138 — human glioblastoma cell lines; HeLa — human cervical carcinoma cell line; HEF — human embryonic fibroblast cell line; Embr.astro — human embryonic astrocyte cell line; B16 — murine melanoma cell line; 4T1 — murine breast cancer cell line.

Cell lines were cultured on DMEM medium (PanEco, Russia) with addition of 10% fetal bovine serum (FBS) (HyClone, USA), penicillin-streptomycin (PanEco, Russia) and 2 mM L-glutamine. The cells were cultured at 37 °C and 5% CO_2, and the medium changed every 3–5 days.

Construction of recombinant vaccinia virus strains expressing mouse and human IFNα

Preparation of plasmid constructs for recombination

To obtain mouse IFNα cDNA fragment, Balb/c female was infected with Sendai virus (Moscow strain), 1×10^9 infectious particles. After 24 h, the mouse was euthanized. mRNA was extracted from spleen (Total RNA Isolation Kit, Evrogen, Russia) according to manufacturer's recommendations. cDNA was prepared by reverse transcription using Superscript III cDNA synthesis kit according to the manufacturer's instructions. Fragments were amplified by PCR using specific primers:

Forward: 5'-ATGGGGCTAGGCTCTGTGTG-3'

Reverse: 5'-TTTCTCTCTTCTCTCTCTCAGTCTTCCCA-3'

Human IFNa cDNA was obtained by reverse transcription of total RNA from peripheral blood mononuclear cells of a healthy donor. Primer sequences used for amplification:

Direct 5'-ATGGCCCCTCGCCCTTTGC-3'

Reverse: 5'-TTCCTTCCTCCTCCTCCTTAATCTTTCTTTCTTGCAAG-3'

After obtaining the amplicon, one more PCR was performed with primers containing restriction sites. The fragments were cloned using sticky ends into a shuttle vector developed previously in the Cell Proliferation Laboratory. The constructs were sequenced using Sanger method.

The constructs were transfected into the HEK293T cells using PEI [23] followed by infection with LIVP variant of the Lister strain of vaccinia virus. Using the plaque method, recombinant strains were selected on the BHK-21 line [7] and amplified as described previously [24].

Assessment of sensitivity of tumor cell lines to vaccinia virus strains

The sensitivity of tumor cell lines to vaccinia virus strains was assessed using resazurin staining. For this purpose, cells were spread on 96-well plates and infected with 10-fold serial

LIVP-RFP

LIVP-IFNα-RFP
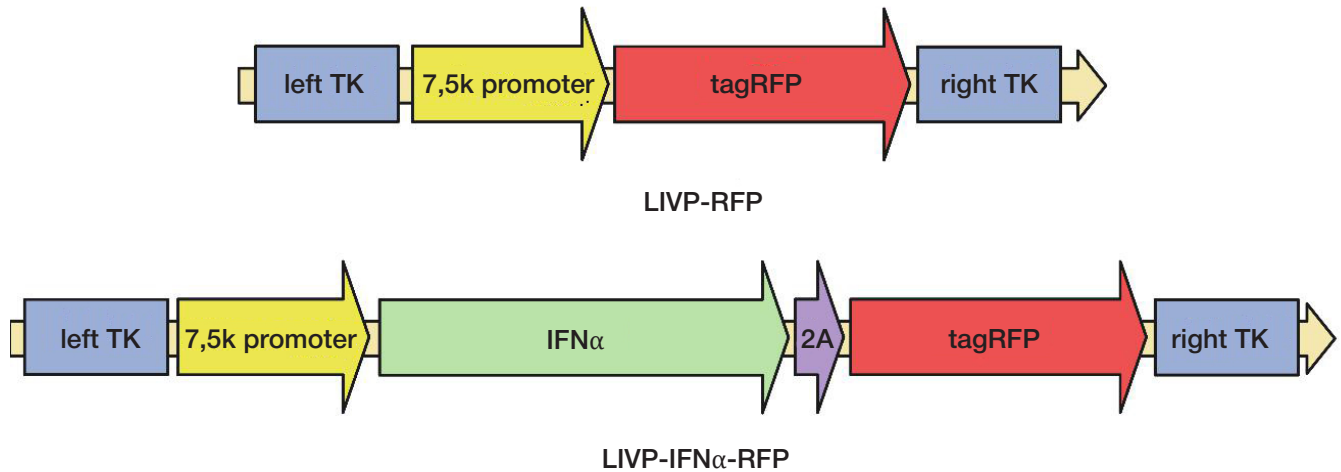
Fig. 1. Schematic illustration of the plasmid design

dilutions of the virus. Virus-free medium was used as a control. The cells were incubated at 37 °C, 5% CO_2. Cytotoxicity was assessed 72 h after infection. The test is based on the ability of viable cells to convert resazurin to resorufin by redox reactions. Cells were incubated with the dye for 4 h. The fluorescence level was measured at 590 nm using an excitation wavelength of 560 nm on a CLARIOstar microplate reader (BMG Labtech, Germany). Based on obtained data, the number of live cells was counted as a percentage relative to control, with $TCID_{50}$ values calculated.

Assessment of viral kinetics by flow cytometry

RFP expression in infected cells correlated with virus replication. Cell lines were seeded into 24-well plates ($1x\ 10^5$ /well). Cells were infected with LIVP-hIFNα (MOI of 1, 0.1). Cells were collected 24, 48, 72, 96 h after infection for analysis by flow cytometry. Samples were analyzed by red fluorescence detection in PE channel using a BD LSR Fortessa cytofluorimeter (Beckman Dickinson, Franklin Lakes, NJ, USA) with 10,000 events per sample.

Evaluation of the functional activity of interferon expressed by viruses

Vesicular stomatitis virus (Indiana strain) is a strain sensitive to the antiviral state of cells having no cytopathic effect (CPE) on cells with a functional interferon response system after treatment with interferon. IFNα-containing supernatant was obtained from virus-containing medium taken from BHK-21 cells infected with LIVP-hIFNα strain or HEK293T line in case of the LIVP-mIFNα strain. Virus-containing medium was collected after 48 h, centrifugated at 4 °C 4000 rpm for 20 min, filtered through 0.22 µm filter, and a supernatant containing IFNα was obtained. Only trace amounts of vaccinia virus remained in the filtered supernatant. The tumor cell line was treated in three repeats with recombinant human IFNα2β (Pharmaclone, Russia) or mouse recombinant interferon alpha (752802, Biolegend, USA) at different concentrations, and the supernatant with IFNα interferons at different concentrations. Supernatant from cells infected with LIVP-RFP and cells without interferon treatment were used as control. One day after interferon treatment, the absence of viral infection was checked using fluorescence
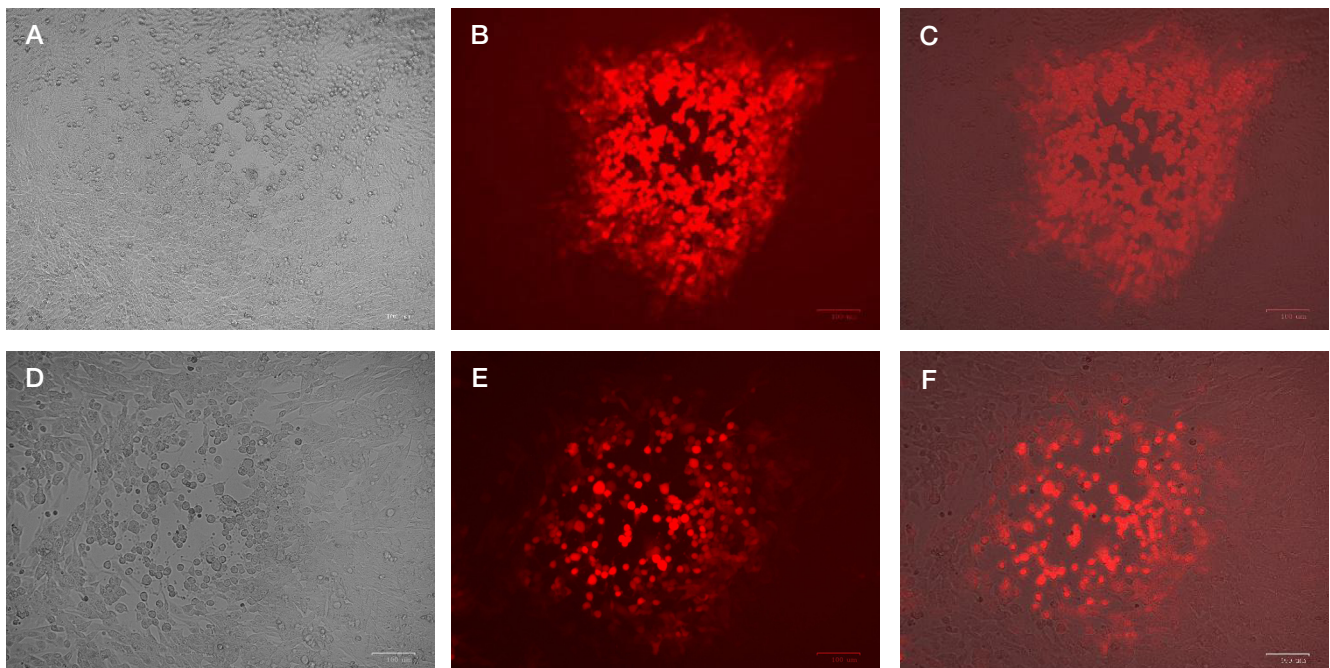
Fig. 2. Photographs of BHK-21 cells 24 h after infection with LIVP-mIFNα (**A–C**) and LIVP-hIFNα (**D–F**) (**A** and **D** — light field; **B** and **E** — red fluorescent channel; **C** and **F** — combined image). 200x magnification; scale bar = 100 µm
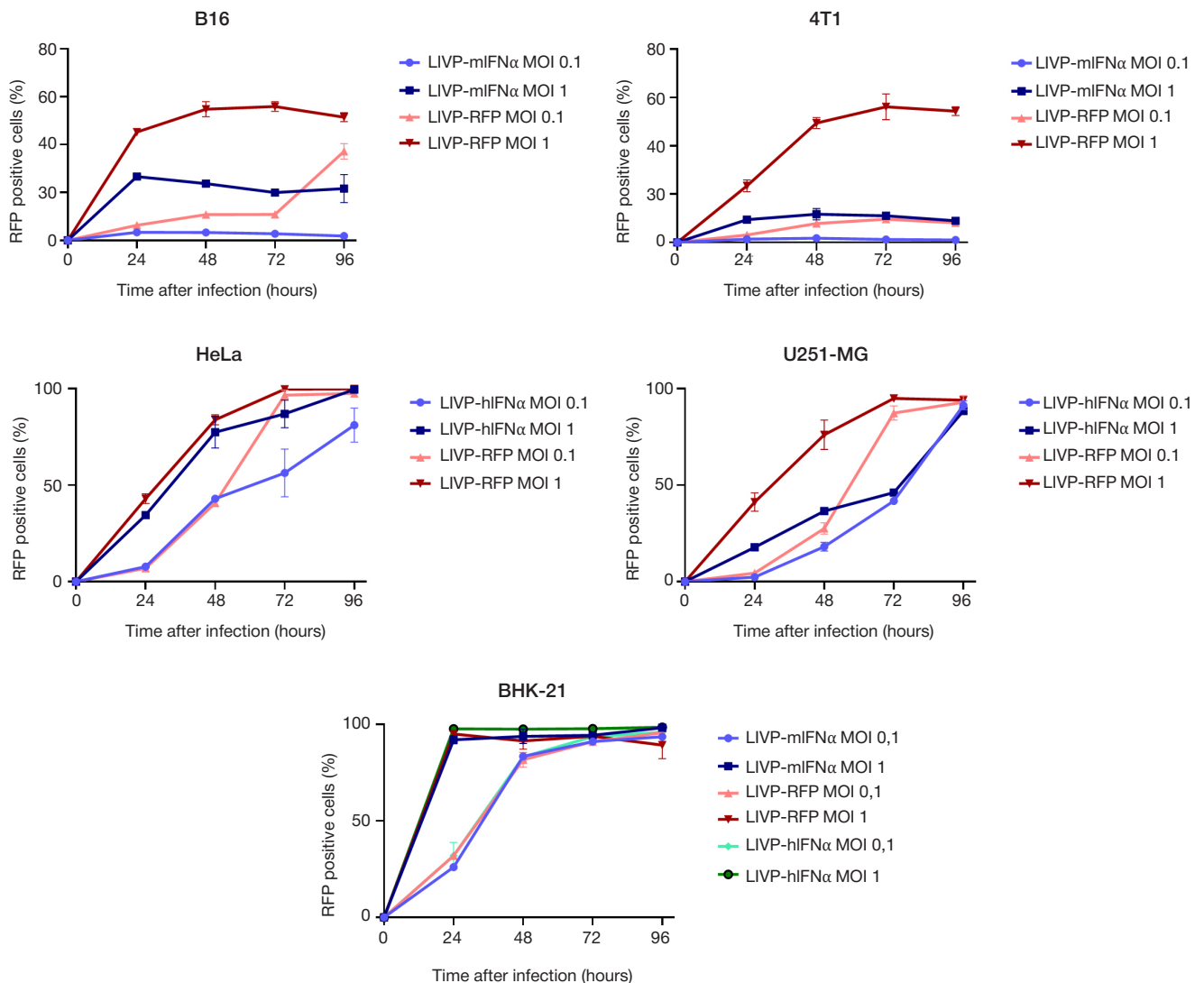
Fig. 3. Evaluation of virus replication kinetics 24, 48, 72 and 96 h after infection with recombinant VV strain on different cell lines

microscope. 24h after supernatant/interferon treatment, cells were infected with VSV in different multiplicities (100, 10, 1, 0.1, 0.01, 0.001). After 24 h, the cytopathic effect was assessed relative to the uninfected VSV control. And TCID$_{50}$ was calculated using the Reed–Muench method.

Modeling of subcutaneous melanoma in C57Bl/6 mice, virus administration

Female ($n = 12$) and male ($n = 12$) C57Bl/6 mice at 6-8 weeks of age were injected subcutaneously, above the posterior thigh, with 1x106 B16 cells to model the melanoma. Each day, tumor growth and development were assessed by visual inspection and measurement of tumor nodule size using a caliper. On the seventh day, mice with confirmed growth of subcutaneous tumor allografts were randomly assigned into three groups, LIVP-mIFNα ($n = 8$), LIVP-RFP ($n = 8$), and control ($n = 8$), with 4 females and 4 males in each group. LIVP-mIFNα and LIVP-RFP virus-containing solutions of 5×10^6 BOU/mL were dissolved in 100 µL PBS and injected intravenously into mice of the respective groups on day 7 and day 10 after tumor implantation. Animals in the control group were injected with saline at the same time points. The animals were observed during 24 days, and tumor size was measured to assess the dynamics of tumor growth or regression before treatment and

every 2 days thereafter. Tumor volume was calculated using the formula:

$$V = \frac{a \times b^2}{2}, \qquad (3)$$

where a is the smaller of the two orthogonal tumor measurements, b is the second orthogonal measurement. The average tumor volume (Vcp) was calculated in each group.

Histologic and immunohistochemical analysis

Histologic analysis was performed using three additional groups of C57Bl/6 mice that were injected with LIVP-mIFNα ($n = 3$), LIVP-RFP ($n = 3$), and saline ($n = 3$) in the same manner. On the 24th day after tumor implantation (14th day after the last virus injection), the animals were deeply anesthetized by intraperitoneal injection of a prohibitive dose of propofol; after apnea occurred, the mice were euthanized by dislocation of the cervical vertebrae; subcutaneous tumor allografts were carefully isolated together with the surrounding tissue to avoid damage to cystic cavities and placed in a tenfold volume of 10% neutral buffered formalin for 72 hours. Fixed tissues were dehydrated in ethanol solutions of ascending concentration (70%, 80%, 96%), then in isopropanol and O-xylene, and then embedded in paraffin. Paraffin sections 3–5 µm thick were

A

B
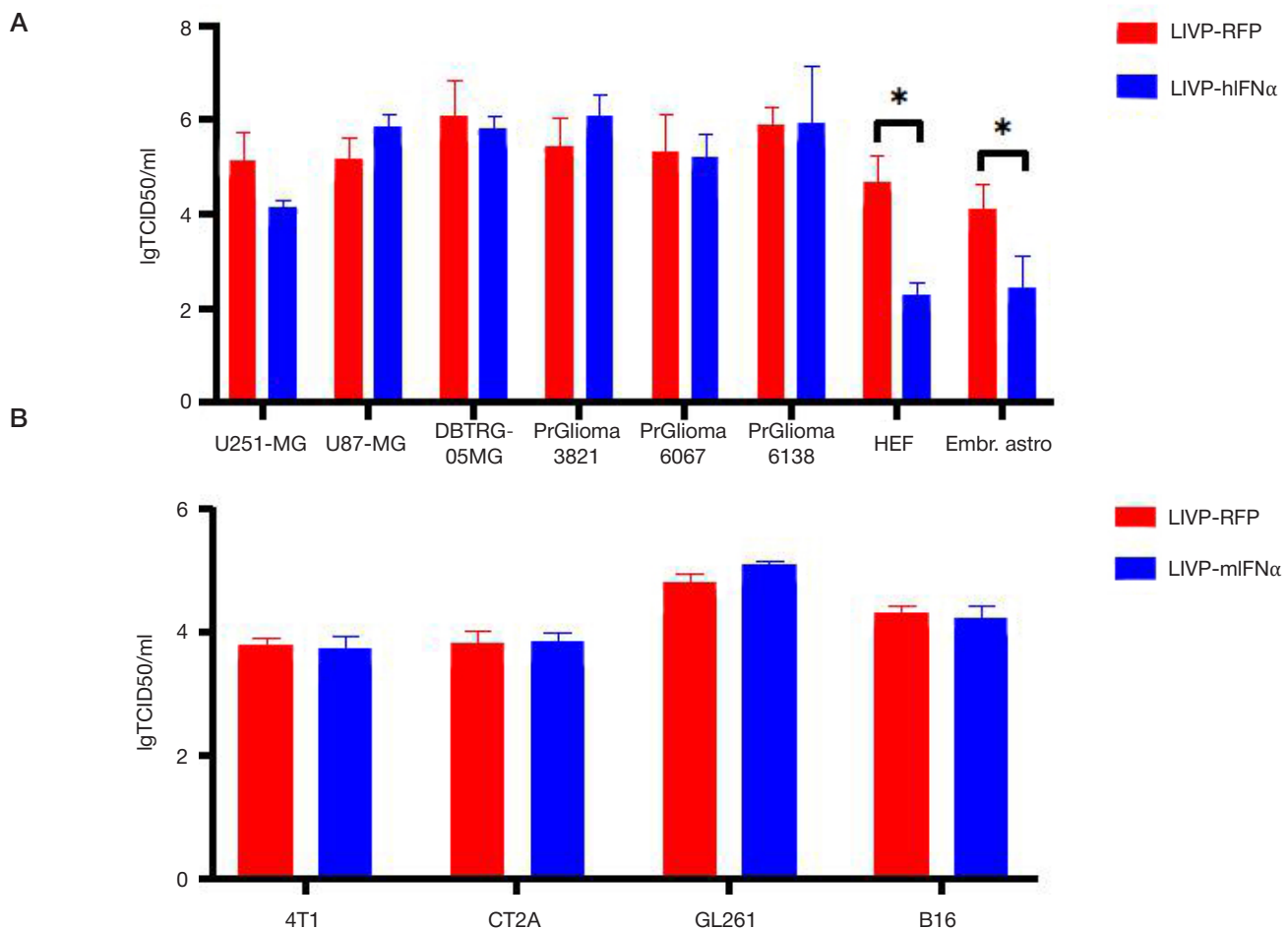
Fig. 4. Sensitivity of tumor and normal cell lines to vaccinia virus expressing tagRFP and a) human IFNα and b) mouse IFNα. X-axis: tumor cell lines, Y-axis: lgTCID$_{50}$/ml

prepared using a rotary microtome and mounted on slides. The sections were deparaffinized in O-xylene, isopropanol and ethanol before staining. For histologic examination, slices were stained with hematoxylin for 10 min, washed with distilled water, then with running tap water and stained with eosin for 30 s. Slices were rehydrated in 96% ethanol, isopropanol, and O-xylene and mounted using Vitrogel medium and 0.15 mm coverslips. Immunoperoxidase staining of paraffin sections for immune cell markers was performed using Benchmark Ultra Immunostainer (Ventana, USA) with primary antibodies to CD4, CD8, CD56 (Roche, USA) and OptiView DAB IHC Detection Kit (Roche, USA) according to the manufacturer's protocols. The stained and coverslipped preparations were scanned using Leica Aperio GT450 DX scanner (Leica Biosystems, USA) and processed at 20x magnification using Aperio ImageScope software.

RESULTS

Construction of recombinant strains

The IFNα gene is one of the promising transgenes that can enhance virus tumor selectivity due to its immunostimulatory properties and inhibition of viral replication in normal tissues. In our work, we constructed recombinant strains of the LIVP biovariety expressing under the control of the p7.5k VV IFNα promoter (human or mouse) as part of a bicistronic cassette with the red fluorescent protein RFP (Fig. 1). The use of this early promoter allowed to achieve a high level of interferon expression in tumor cells.

For further cultivation of the recombinant vaccinia virus strain, BHK-21 cell culture was used due to its high sensitivity to vaccinia virus. The recombinant variants expressed fluorescent protein (Fig. 2). The correctness of transgene expression was confirmed by Sanger sequencing of the amplicons of transcripts flanked by regions of the thymidine kinase gene of the vaccinia virus.

The efficiency of virus replication in different tumor lines was determined by flow cytometry 24, 48, 72, and 96 h after infection. Human HeLa adenocarcinoma and U251-MG glioblastoma, mouse B16 melanoma and 4T1 adenocarcinoma tumor cell lines were tested. BHK-21 cell line was used as a reference cell line. HeLa and U251-MG cell cultures were infected at MOI 1 and 0.1 with LIVP-hIFNα, LIVP-RFP strains. B16 and 4T1 cell cultures were infected in the same multiplicities with LIVP-mIFNα, LIVP-RFP strains. At 24, 48, 72, and 96 h after infection, the percentage of RFP-positive cells was determined.

The recombinant LIVP-mIFNα strain was found to replicate poorly in 4T1 adenocarcinoma however, more than 20% replication was observed in B16 melanoma at MOI 1 (Figure 3). LIVP-hIFNα showed efficient replication in human tumor cell cultures. After 24 h, the HeLa line infected with different multiplicities showed the maximum infectivity among the lines tested: 34.44 ± 1.38% for MOI 1 and 7.82 ± 0.96% for MOI 0.1. In human glioblastoma culture LIVP-hIFNα virus replication in case of MOI 1 was almost 100% 96 h after infection. To confirm the hypothesis of tumor selectivity of LIVP-hIFNα against glioblastoma, we tested its cytopathic effect on expanded panel of the tumor lines.
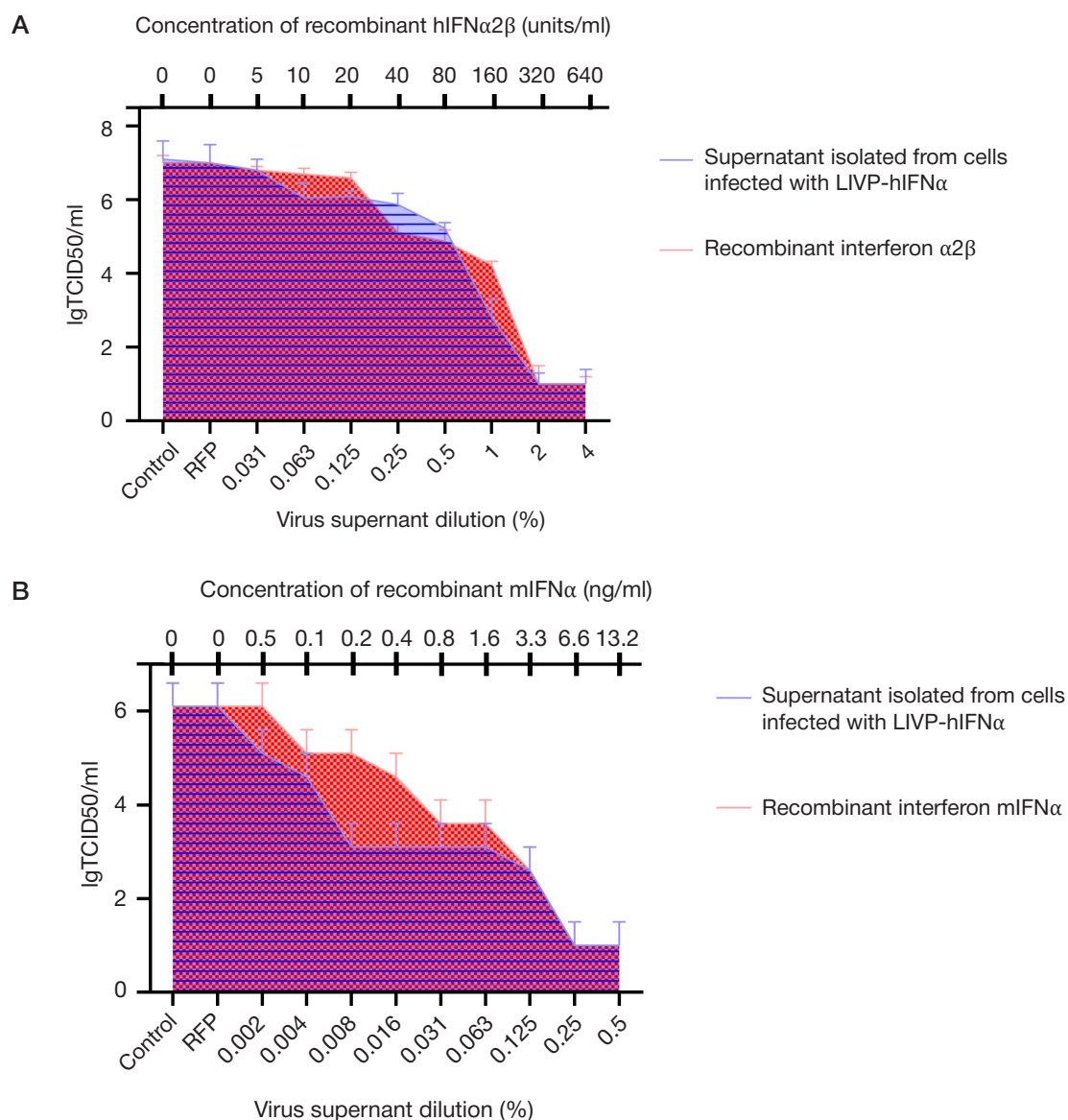
Fig. 5. Evaluation of functional activity of interferons expressed by LIVP-hIFNα strains on U87-MG cell line (**A**) and LIVP-mIFNα on the B16 cell line (**B**)

Evaluation of the cytopathogenic action of recombinant strains on a panel of tumor and normal cell lines

The oncolytic activity of vaccinia viruses expressing interferon alpha was examined in comparison with the tagRFP expressing strain on a panel of human and mouse tumor and normal cells. By titrating LIVP-hIFNα virus using Reed–Muench method and determining $TCID_{50}$ value, the sensitivity of glioblastoma cell lines U-87 MG, DBTRG-05MG, U251-MG, PrGlioma 3821, PrGlioma 6067, PrGlioma 6138 was evaluated (Fig. 4A) as well as of the two normal cell lines: human embryonic fibroblast line HEF, human embryonic astrocyte line Embr.astro. A strain expressing mouse interferon was tested on murine glioma cell lines CT2A and GL261 as well as on adenocarcinoma 4T1 and melanoma B16 (Fig. 4B).

Human glioblastoma lines were shown to be highly sensitivite to LIVP-hIFNα comparable to sensitivity of glioblastoma cells to the control virus expressing tagRFP (Fig. 4). Normal fibroblasts and astrocytes were found to have a lower sensitivity to vaccinia virus expressing hIFNα than to virus expressing tagRFP. The data suggest that the recombinant strain is more tumor selective compared to the control strain LIVP-RFP. Similar sensitivity levels of the cell lines to IFNα-expressing and tagRFP-expressing

viruses are in turn an evidence of the persisting direct cytopathic activity of the interferon-expressing virus against tumor cells.

Assessment of the functional activity of interferons expressed by vaccinia virus

The functional activity of interferons expressed by vaccinia virus was tested in the common way using vesicular stomatitis virus (VSV). Vesicular stomatitis virus is sensitive to the antiviral state of cells having no cytopathic effect (CPE) on cells with a functional interferon response system after treatment with interferon. Tumor cell lines U87-MG and B16 were shown to have a functional interferon response system [25]. Cell cultures were treated with filtered supernatant taken from cells infected with LIVP-hIFNα or LIVP-mIFNα as well as manufactured recombinant IFNαs (Fig. 5). Cells without interferon treatment and cells treated with filtered supernatant isolated from LIVP-RFP-infected cells were used as controls.

For the human interferon experiment, we used supernatant isolated from the BHK-21 cell line infected with LIVP-hIFNα. For the experiment with LIVP-mIFNα strain, we used supernatant from the HEK293T cell line, since mouse and hamster interferons are cross-reactive.
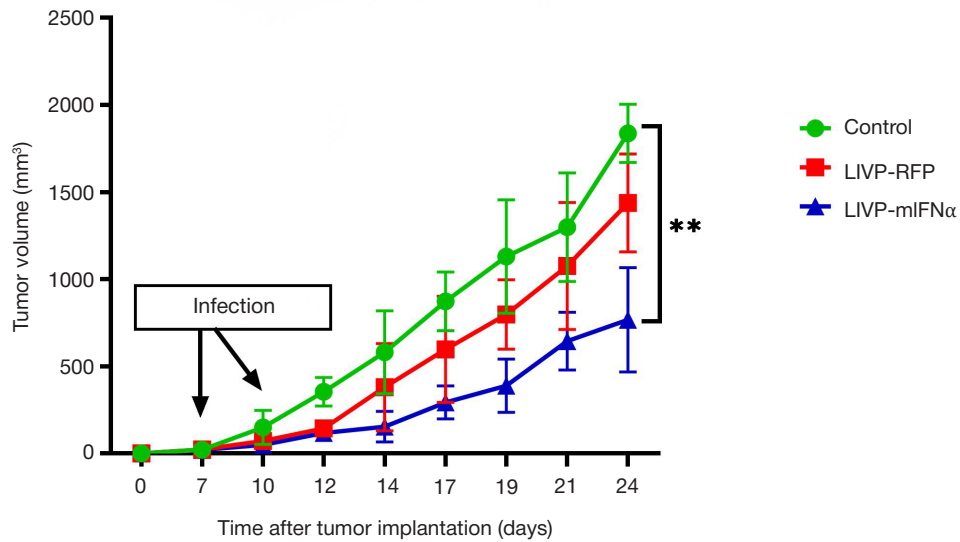
Fig. 6. Dynamics of tumor growth after LIVP-mIFNα injection

One day after interferon treatment, an absence of viral infection was checked using fluorescence microscope. 24 hafter interferon treatment, cells were infected with VSV in different multiplicities of infection.

Cytopathic effect (CPE) of vesicular stomatitis virus was not observed in cells treated with 320 units/ml recombinant interferon and for cells treated with 2% dilution of conditioned medium in the case of human interferon. For mouse interferon, CPE was not observed in cells treated with 6.6 ng/ml recombinant interferon or 0.25% dilution of conditioned medium.

Antitumor activity of LIVP-mIFNα *in vivo*

The oncolytic activity of LIVP-mIFNα vaccinia virus was investigated in C57Bl/6 mice with murine melanoma B16 (Fig. 6). Intravenous injections of virus were performed on day 7 and day 10 after tumor implantation. The control group of mice was injected with saline solution.

Tumor volumes were measured once every 2 days. Smaller tumor volumes were observed during treatment with vaccinia virus compared to the control group, especially when treated with virus expressing murine interferon alpha. The mean tumor volume was 1800 mm³ in the control group, 1450 mm³ in the group receiving LIVP-RFP, and 650 mm³ in the group receiving virus with murine interferon alfa (*p*-value < 0.01). Tumor volume reduction was 64% as compared to the control group (Fig. 6).

Summarizing the results, we can conclude that the developed tumor-selective strain of vaccinia virus expressing functionally active murine interferon alpha has significant antitumor activity in the murine melanoma B16 model.

DISCUSSION

DNA-containing vaccinia virus is a promising platform for construction of selective recombinant oncolytic strains as up to 25 kb fragments can be inserted into the virus genome [6]. To date, recombinant VV strains containing sequences of cytokines, chemokines, oncotoxic proteins [11], bacterial immune attractants (e.g., the ligand of the innate immune system receptor TLR5 flagellin [10]), and other proteins
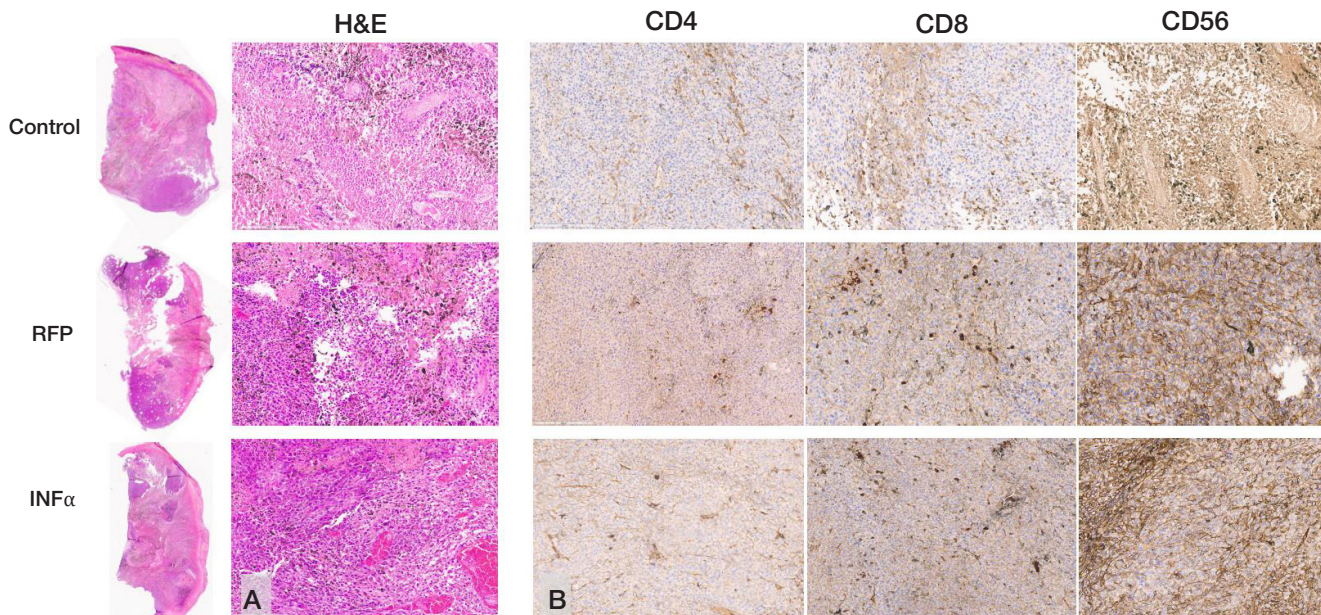
Fig. 7. Histological and immunohistochemical examination of tumor preparations 24 days after inoculation. **A**. Hematoxylin and eosin staining (general view of the tumor on the left side images and fragments at ×200 magnification on the right side images). **B**. Immunohistochemical staining for differentiation clusters: CD4, CD8, CD56. Representative preparations of animals from the control group, the group with LIVP-RFP, and the LIVP-mIFNα group, respectively, are shown from top to bottom.

activating antitumor immune response and recruiting cytotoxic immune cells to tumor have been created and successfully tested in preclinical and clinical studies [7, 26, 27].

A recombinant JX-594 virus strain with a deletion in the thymidine kinase (TK) gene containing the granulocyte-macrophage colony-stimulating factor (GM-CSF) sequence and lac-Z transgenes showed very encouraging results in phase II clinical trials of oncolytic therapy of colorectal cancer and melanoma liver metastases. JX-594 virus injected intravenously was detected in tumor tissue which was accompanied by IFNα secretion, induction of chemokines and activation of antitumor immune response [26].

In our study, in order to enhance tumor selectivity, we used a LIVP strain with a defective gene encoding thymidine kinase (TK), an enzyme essential for virus DNA synthesis which is hardly expressed during the normal cell cycle but is highly expressed in low-differentiated tumor cells [28]. We hypothesized that insertion of IFNα sequence into recombinant vaccinia virus could enhance the selectivity of virus replication in tumor cells where interferon signaling is often defective, and would also promote the activation of NK cells, macrophages, and cytotoxic T cells in response to tumor-specific virus replication and thus contribute to effective tumor eradication.

$TCID_{50}$ experiments with tumor and normal cell lines confirmed the enhanced tumor selectivity of LIVP-hIFNα and showed that normal cells have less sensitivity to vaccinia virus expressing IFNα than to virus expressing tagRFP. Decreased CPE of vesicular stomatitis virus after treatment of human glioblastoma and mouse adenocarcinoma cells with supernatants from LIVP-hIFNα and LIVP-mIFNα-infected cells, respectively, confirmed that IFNα expressed by infected cells is functionally active. HeLa cell line was shown to be the most sensitive to LIVP-hIFNα assuming the potential applicability of the recombinant virus for the therapy of adenocarcinomas. The observed sensitivity of U251-MG glioblastoma cells to LIVP-hIFNα seemed to be interesting as regards possible practical application of this virus in the therapy of glial tumors. The assumption was confirmed for five other lines of the tumor including primary glioblastoma cultures available. The data suggest that LIVP-hIFNα may be a promising oncolytic virus for glioblastoma therapy.

The results of *in vivo* experiments using a murine model of melanoma B16 confirmed our assumption of high tumor selectivity and enhanced oncolytic activity of LIVP-mIFNα. Decreased tumor volumes in animals administered intravenously with LIVP-mIFNα by 64% compared to control animals demonstrated the advantages of the recombinant VV inducing the secretion of functionally active IFNα by infected cells. Immunohistochemical assays showed a high level of infiltration of tumors treated with LIVP-mIFNα by CD8+ T cells and NK cells. The mechanisms of the increased oncolytic activity of LIVP-mIFNα need to be further investigated however, according to the up-to-date publications and our own data related to other recombinant strains [7, 10] containing cytokine sequences, it can be assumed that there is an increased activation of NK cells and cytotoxic T cells around IFNα-secreting tumors.

CONCLUSIONS

We constructed new recombinant strains of vaccinia virus expressing mouse and human IFNα having oncolytic activity similar to the parent strain, with significant tumor selectivity shown for LIVP-hIFNα due to decreased sensitivity of normal cells to the virus. The functional activity of interferons expressed by recombinant LIVP-hIFNα and LIVP-mIFNα strains was confirmed *in vitro*. A significantly higher oncolytic activity of LIVP-mIFNα *in vivo* was demonstrated in a murine model of melanoma B16.

References

1. Fukuhara H, Ino Y, Todo T. Oncolytic virus therapy: A new era of cancer treatment at dawn. Cancer Sci. 2016; 107 (10): 1373–9.
2. Shakiba Y, et al., Recombinant Strains of Oncolytic Vaccinia Virus for Cancer Immunotherapy. Biochemistry (Mosc). 2023; 88 (6): 823–41.
3. Shvalov AN, et al. Complete Genome Sequence of Vaccinia Virus Strain L-IVP. Genome Announc. 2016; 4 (3).
4. Zonov E, et al. Features of the Antitumor Effect of Vaccinia Virus Lister Strain. Viruses. 2016; 8 (1).
5. Hamad A, et al. Recent Developments in Glioblastoma Therapy: Oncolytic Viruses and Emerging Future Strategies. Viruses. 2023; 15 (2).
6. Naik S, Russell SJ. Engineering oncolytic viruses to exploit tumor specific defects in innate immune signaling pathways. Expert Opin Biol Ther. 2009; 9 (9): 1163–76.
7. Shakiba Y, et al. Oncolytic therapy with recombinant vaccinia viruses targeting the interleukin-15 pathway elicits a synergistic response. Mol Ther Oncolytics. 2023; 29: 158–68.
8. Kirn DH, et al. Targeting of interferon-beta to produce a specific, multi-mechanistic oncolytic vaccinia virus. PLoS Med. 2007; 4 (12): e353.
9. Park BH, et al. Use of a targeted oncolytic poxvirus, JX-594, in patients with refractory primary or metastatic liver cancer: a phase I trial. Lancet Oncol. 2008; 9 (6): 533–42.
10. Shakiba Y, et al. Oncolytic Efficacy of a Recombinant Vaccinia Virus Strain Expressing Bacterial Flagellin in Solid Tumor Models. Viruses. 2023; 15 (4).
11. Kochneva G, et al. Apoptin enhances the oncolytic properties of vaccinia virus and modifies mechanisms of tumor regression. Oncotarget. 2014; 5 (22): 11269–82.
12. Tysome JR, et al. Lister vaccine strain of vaccinia virus armed with the endostatin-angiostatin fusion gene: an oncolytic virus superior to dl1520 (ONYX-015) for human head and neck cancer. Hum Gene Ther. 2011; 22 (9): 1101–8.
13. Crouse J, Kalinke U, Oxenius A. Regulation of antiviral T cell responses by type I interferons. Nat Rev Immunol. 2015; 15 (4): 231–42.
14. Gastl G, Huber C. The biology of interferon actions. Blut. 1988; 56 (5): 193–9.
15. Matveeva OV, Chumakov PM. Defects in interferon pathways as potential biomarkers of sensitivity to oncolytic viruses. Rev Med Virol. 2018; 28 (6): e2008.
16. Pikor LA, Bell JC, Diallo JS. Oncolytic Viruses: Exploiting Cancer's Deal with the Devil. Trends Cancer. 2015; 1 (4): 266–77.
17. Stojdl DF, et al. Exploiting tumor-specific defects in the interferon pathway with a previously unknown oncolytic virus. Nat Med. 2000; 6 (7): 821–5.
18. Feola S, et al. Oncolytic ImmunoViroTherapy: A long history of crosstalk between viruses and immune system for cancer treatment. Pharmacol Ther. 2022; 236: 108103.
19. Li R, et al. Using oncolytic viruses to ignite the tumour immune microenvironment in bladder cancer. Nat Rev Urol. 2021; 18 (9): 543–55.
20. Kaufman HL, Kohlhapp FJ, Zloza A. Oncolytic viruses: a new class of immunotherapy drugs. Nat Rev Drug Discov. 2015; 14 (9): 642–62.
21. Davola ME, Mossman KL. Oncolytic viruses: how "lytic" must they be for therapeutic efficacy? Oncoimmunology. 2019; 8 (6): e1581528.

22. Kirn DH, Thorne SH, Targeted and armed oncolytic poxviruses: a novel multi-mechanistic therapeutic class for cancer. Nat Rev Cancer. 2009; 9 (1): 64–71.
23. Vorobyev PO, et al. Comparative Efficiency of Accessible Transfection Methods in Model Cell Lines for Biotechnological Applications. Bulletin of RSMU. 2022; 3: 11–18.
24. Kochneva G, et al. Engineering of double recombinant vaccinia virus with enhanced oncolytic potential for solid tumor virotherapy. Oncotarget. 2016; 7 (45): 74171–88.
25. Lin AH, et al. Blockade of type I interferon (IFN) production by retroviral replicating vectors and reduced tumor cell responses to IFN likely contribute to tumor selectivity. J Virol. 2014; 88 (17): 10066–77.
26. Samson A, et al. Neoadjuvant Intravenous Oncolytic Vaccinia Virus Therapy Promotes Anticancer Immunity in Patients. Cancer Immunol Res. 2022; 10 (6): 745–56.
27. Vasileva N, et al. The Recombinant Oncolytic Virus VV-GMCSF-Lact and Chemotherapy Drugs against Human Glioma. Int J Mol Sci. 2024; 25 (8).
28. Shakiba Y, et al. Comparison of the oncolytic activity of recombinant vaccinia virus strains LIVP-RFP and MVA-RFP against solid tumors. Bulletin of RSMU. 2023; 2: 4–11.

Литература

1. Fukuhara H, Ino Y, Todo T. Oncolytic virus therapy: A new era of cancer treatment at dawn. Cancer Sci. 2016; 107 (10): 1373–9.
2. Shakiba Y, et al., Recombinant Strains of Oncolytic Vaccinia Virus for Cancer Immunotherapy. Biochemistry (Mosc). 2023; 88 (6): 823–41.
3. Shvalov AN, et al. Complete Genome Sequence of Vaccinia Virus Strain L-IVP. Genome Announc. 2016; 4 (3).
4. Zonov E, et al. Features of the Antitumor Effect of Vaccinia Virus Lister Strain. Viruses. 2016; 8 (1).
5. Hamad A, et al. Recent Developments in Glioblastoma Therapy: Oncolytic Viruses and Emerging Future Strategies. Viruses. 2023; 15 (2).
6. Naik S, Russell SJ. Engineering oncolytic viruses to exploit tumor specific defects in innate immune signaling pathways. Expert Opin Biol Ther. 2009; 9 (9): 1163–76.
7. Shakiba Y, et al. Oncolytic therapy with recombinant vaccinia viruses targeting the interleukin-15 pathway elicits a synergistic response. Mol Ther Oncolytics. 2023; 29: 158–68.
8. Kirn DH, et al. Targeting of interferon-beta to produce a specific, multi-mechanistic oncolytic vaccinia virus. PLoS Med. 2007; 4 (12): e353.
9. Park BH, et al. Use of a targeted oncolytic poxvirus, JX-594, in patients with refractory primary or metastatic liver cancer: a phase I trial. Lancet Oncol. 2008; 9 (6): 533–42.
10. Shakiba Y, et al. Oncolytic Efficacy of a Recombinant Vaccinia Virus Strain Expressing Bacterial Flagellin in Solid Tumor Models. Viruses. 2023; 15 (4).
11. Kochneva G, et al. Apoptin enhances the oncolytic properties of vaccinia virus and modifies mechanisms of tumor regression. Oncotarget. 2014; 5 (22): 11269–82.
12. Tysome JR, et al. Lister vaccine strain of vaccinia virus armed with the endostatin-angiostatin fusion gene: an oncolytic virus superior to dl1520 (ONYX-015) for human head and neck cancer. Hum Gene Ther. 2011; 22 (9): 1101–8.
13. Crouse J, Kalinke U, Oxenius A. Regulation of antiviral T cell responses by type I interferons. Nat Rev Immunol. 2015; 15 (4): 231–42.
14. Gastl G, Huber C. The biology of interferon actions. Blut. 1988; 56 (5): 193–9.
15. Matveeva OV, Chumakov PM. Defects in interferon pathways as potential biomarkers of sensitivity to oncolytic viruses. Rev Med Virol. 2018; 28 (6): e2008.
16. Pikor LA, Bell JC, Diallo JS. Oncolytic Viruses: Exploiting Cancer's Deal with the Devil. Trends Cancer. 2015; 1 (4): 266–77.
17. Stojdl DF, et al. Exploiting tumor-specific defects in the interferon pathway with a previously unknown oncolytic virus. Nat Med. 2000; 6 (7): 821–5.
18. Feola S, et al. Oncolytic ImmunoViroTherapy: A long history of crosstalk between viruses and immune system for cancer treatment. Pharmacol Ther. 2022; 236: 108103.
19. Li R, et al. Using oncolytic viruses to ignite the tumour immune microenvironment in bladder cancer. Nat Rev Urol. 2021; 18 (9): 543–55.
20. Kaufman HL, Kohlhapp FJ, Zloza A. Oncolytic viruses: a new class of immunotherapy drugs. Nat Rev Drug Discov. 2015; 14 (9): 642–62.
21. Davola ME, Mossman KL. Oncolytic viruses: how "lytic" must they be for therapeutic efficacy? Oncoimmunology. 2019; 8 (6): e1581528.
22. Kirn DH, Thorne SH, Targeted and armed oncolytic poxviruses: a novel multi-mechanistic therapeutic class for cancer. Nat Rev Cancer. 2009; 9 (1): 64–71.
23. Vorobyev PO, et al. Comparative Efficiency of Accessible Transfection Methods in Model Cell Lines for Biotechnological Applications. Bulletin of RSMU. 2022; 3: 11–18.
24. Kochneva G, et al. Engineering of double recombinant vaccinia virus with enhanced oncolytic potential for solid tumor virotherapy. Oncotarget. 2016; 7 (45): 74171–88.
25. Lin AH, et al. Blockade of type I interferon (IFN) production by retroviral replicating vectors and reduced tumor cell responses to IFN likely contribute to tumor selectivity. J Virol. 2014; 88 (17): 10066–77.
26. Samson A, et al. Neoadjuvant Intravenous Oncolytic Vaccinia Virus Therapy Promotes Anticancer Immunity in Patients. Cancer Immunol Res. 2022; 10 (6): 745–56.
27. Vasileva N, et al. The Recombinant Oncolytic Virus VV-GMCSF-Lact and Chemotherapy Drugs against Human Glioma. Int J Mol Sci. 2024; 25 (8).
28. Shakiba Y, et al. Comparison of the oncolytic activity of recombinant vaccinia virus strains LIVP-RFP and MVA-RFP against solid tumors. Bulletin of RSMU. 2023; 2: 4–11.

IMPACT OF TUMOR ON THE CELL CYCLE AND DIFFERENTIATION OF HEMATOPOIETIC STEM CELLS

Aktanova AA[1,2] ✉, Bykova MV[1], Skachkov IP[1,2], Denisova VV[3], Pashkina EA[1,2]

[1] Research Institute of Fundamental and Clinical Immunology, Novosibirsk, Russia

[2] Novosibirsk State Medical University, Novosibirsk, Russia

[3] Immunopathology Clinic, Research Institute of Fundamental and Clinical Immunology, Novosibirsk, Russia

Today, there is a theory that proliferative potential of hematopoietic stem cells is depleted, and the balance of committed precursor cells shifts towards suppressors during the development of cancer. However, differentiation of hematopoietic stem cells can vary depending on the tumor type, localization, and microenvironment specifics. The study aimed to assess the impact of tumors of various origins on the CD34+ hematopoietic stem cells ($n = 10$). Assessment of the cell cycle and cell differentiation via both direct contact with the tumor and exchanging humoral factors only in transwells was conducted by flow cytometry. In the co-culture with K562, the number of hematopoietic stem cells being in their synthesis phase was 2.1%, while in the control it was 11.2% ($p = 0.01$); in the co-culture with SK-mel37, the number of hematopoietic stem cells being in the G_2–M cell cycle phase was reduced to 0.3% ($p < 0.05$). 1301 and K562 directed the hematopoietic stem cell differentiation towards granulocyte-macrophage precursor cells ($p < 0.05$), while 1301 and SK-mel37 directed it towards common multipotent progenitor cells. It is interesting that the number of pluripotent hematopoietic stem cells significantly increased (2-fold) compared to control after incubation with K562 in transwells (24.17% and 10.19%, respectively). Thus, properties of hematopoietic stem cells can vary depending on both tumor type and the way of interacting with these cells.

Keywords: hematopoietic stem cell, cell differentiation, committed precursor cells, proliferation, flow cytometry, T-cell leukemia, chronic myelogenous leukemia, melanoma

✉ **Correspondence should be addressed:** Alina A. Aktanova
Yadrintsevskaya, 14, Novosibirsk, 630099, Russia; aktanova_al@mail.ru

ВЛИЯНИЕ ОПУХОЛИ НА КЛЕТОЧНЫЙ ЦИКЛ И ДИФФЕРЕНЦИРОВКУ ГЕМОПОЭТИЧЕСКИХ СТВОЛОВЫХ КЛЕТОК

А. А. Актанова[1,2] ✉, М. В. Быкова[1], И. П. Скачков[1,2], В. В. Денисова[3], Е. А. Пашкина[1,2]

[1] Научно-исследовательский институт фундаментальной и клинической иммунологии, Новосибирск, Россия

[2] Новосибирский государственный медицинский университет Министерства здравоохранения, Новосибирск, Россия

[3] Клиника иммунопатологии Научно-исследовательского института фундаментальной и клинической иммунологии, Новосибирск, Россия

На сегодняшний день существует теория о том, что пролиферативный потенциал гемопоэтических стволовых клеток истощается, а баланс коммитированных предшественников смещается в сторону супрессоров в ходе развития онкологии, однако дифференцировка гемопоэтических стволовых клеток может варьироваться в зависимости от типа, локализации и специфики микроокружения опухоли. Целью исследования было оценить влияние опухолей различного генеза на CD34+-гемопоэтические стволовые клетки ($n = 10$). С помощью метода проточной цитометрии проводили анализ клеточного цикла и дифференцировки клеток как через прямой контакт с опухолью, так и через обмен только гуморальными факторами в трансвеллах. В ко-культуре с К562 количество ГСК, находящихся в синтетической фазе, составило 2,1%, в контроле — 11,2% ($p = 0,01$); в ко-культуре с SK-mel37 количество клеток, находящихся в фазе G_2–M клеточного цикла, снижалось до 0,3% ($p < 0,05$). 1301 и К562 направляли дифференцировку ГСК в сторону гранулоцитарно-макрофагальных предшественников ($p < 0,05$), а 1301 и SK-mel37 в сторону общих мультипотентных предшественников. Интересно, что после инкубации с К562 в трансвеллах статистически значимо увеличивалось количество плюрипотентных гемопоэтических стволовых клеток в два раза по сравнению с контролем (24,17% и 10,19% соответственно). Таким образом, свойства гемопоэтических клеток могут меняться как от вида опухоли, так и от способа взаимодействия с ними.

Ключевые слова: гемопоэтическая стволовая клетка, дифференцировка клеток, коммитированные предшественники, пролиферация, проточная цитометрия, Т-клеточный лейкоз, хроническая миелогенная лейкемия, меланома

✉ **Для корреспонденции:** Алина Александровна Актанова
ул. Ядринцевская, д. 14, г. Новосибирск, 630099, Россия; aktanova_al@mail.ru

It is well known that hematopoietic stem cells (HSCs) that form the pool of blood cells after maturation and differentiation throughout the life are an important component of the bone marrow niche. The niche represents specific microenvironment with humoral factors and specific cell contacts for HSCs, ensuring the strictly regulated processes of self-maintenance or self-renewal and cell differentiation. HSCs have a unique cell cycle with asymmetric division for maintenance and renewal of the pool of pluripotent HSCs and, at the same time, for generation of the essential common or more differentiated progenitor cells. The HSC activity depends directly on the cell cycle, on its duration or time before entering the cell cycle, as well as on the cell division rate. It is important to note that under homeostatic conditions the majority of HSCs should be through the G_0 phase of the cell cycle or the resting phase (up to 95%) to prevent premature depletion of cells, while self-renewal and differentiation of cells occur in phase G2 [1]. Since under conditions of the niche HSCs are usually in the resting state mediated by the intra- and extracellular mechanisms, including some proliferation inhibitors, such as CXCL4 and TGFβ, secreted by megakaryocytes [2], alterations of cell-to-cell contact or concentration, as well as the emergence of new humoral factors can bring HSCs out of the resting state, induce their proliferation and differentiation, similar to HSC proliferation associated with blood loss, irradiation or effects of pro-inflammatory cytokines [3]. In turn, this will lead to the decrease in HSC function, aberrant cell cycle regulation and even malignancy [4, 5]. It is interesting that cell division is not an essential phase preceding differentiation into common myeloid, megakaryocyte-erythroid and pre-megakaryocytic progenitors [6]. Along with these progenitors, common multipotent and lymphoid progenitors are distinguised in the hematopoietic process. Cells can be distinguished by differentiation markers acquired by HSC during specialization under exposure to various stimuli, including the combination of colony-stimulating factors. Cytokines also represent conventional stimuli, but these can have both negative and positive effects on differentiation. Thus, GM-CSF, G-CSF, M-CSF, EPO, TPO, SCF/KL, FL, TNF, LIF, IL12, IL11, IL6, IL5, IL4, IL3, IL1, SDF-1, FGF-4 can induce myelopoiesis, while TNF, IL4, TGFβ, IFN, MIP-1, IL10, IL13 can suppress myelopoiesis; IL2, IL4, IL7 are essential for activation of lymphopoiesis, and TGFβ, IL4 are essential for suppression of lymphopoiesis [7]. A broad range of factors potentially capable of directing HSC differentiation into these or other common or more specialized progenitors is synthesized in the tumor microenvironment due to the presence of a large number of tumor-associated cells. Thus, under certain conditions, it is possible to expand the pool of HSCs, HSC progenitors and, therefore, alter their functional activity, which can result in the disease process development in the body or worsening of the course of the existing disease process. For example, tumor process is associated with formation of specific microenvironment, in which, according to the latest data, an important role is played by hematopoietic stem cells. It is well known that the tumor can recruit cells during carcinogenesis, and HSCs are no exception. Furthermore, all the cells derived from HSCs in the solid tumor microenvironment are involved in tumor invasion, growth, progression, and chemoresistance [8]. HSCs or the so-called tumor-associated HSCs often represent tumor-initiating cells capable of causing differentiation of other cells into fibroblasts, macrophages and endothelial cells, which support tumor growth and recurrence via production and secretion of growth factors and extracellular matrix components, in addition to triggering angiogenesis [9]. Thus, along with other tumor-associated cells, hematopoietic stem cells contribute actively to the tumor process maintenance and progression. However, aspects of the interplay between hematopoietic stem cells and tumor cells are poorly understood. That is why it is necessary to assess the influence of both cell-to-cell contact and humoral factors on the key components of the HSC vital activity, such as proliferative capacity, cell cycle, and differentiation, which constituted the aim of our study.

METHODS

The CD34^{+}-separated hematopoietic stem cells (HSCs) of the donors ($n = 10$, average age 38.1 ± 3.4 years) were obtained at the Immunopathology Clinic of the Research Institute of Fundamental and Clinical Immunology. The study also involved the use of human T-cell leukemia 1301 cell line, human chronic myelogenous leukemia K562 cell line (European Collection of Authenticated Cell Cultures, Sigma Aldrich, Merck KGaA, Germany), and human melanima Sk-mel-37 cell line kindly provided by the Laboratory of Cellular Technologies of the Research Institute of Fundamental and Clinical Immunology (Novosibirsk, Russia).

HSC culture

The cryopreserved CD34-positive HSC samples were thawed and washed in accordance with the standard guidelines for frozen precursor cells [10, 11]. HSCs were enumerated in the 0.01% (10 mg/mL) methylene blue solution (Biolot, Russia) to determine cell viability using the Goryaev chamber. The cells obtained were cultured in different quantities (from 100,000 to 1,000,000 cells/mL) with appropriate RPMI-1640 medium (PanEco, Russia) or Stemline II (STEM) medium for hematopoietic stem cell reproduction (Sigma Aldrich Co. LLC, USA) used as positive control, supplemented with 50 mg/mL gentamicin (Dalfarma, Russia), 25 mg/mL tienam (Merck Sharp & Dohme Corp., Kenilworth, New Jersey, USA) within different time depending on the series of experiments at 37 °C, 5% CO_2 in the humidified atmosphere.

Tumor cell line culture

The suspension tumor cell lines K562 and 1301 and the adherent cell line SK-mel37 were cultured under standard conditions using the complete culture medium RPMI-1640 + 2 mM glutamine + 10% fetal bovine serum (HyClone, USA). The cultures were maintained within 100,000–1,000,000 cells/mL at 5% CO_2 and 37 °C. The conditioned culture media were selected taking into account the series of the experiment in the tumor cell line exponential growth phase and frozen for future use.

HSC viability and proliferation

HSCs (1×10^5 cells/250 mL) were incubated with the conditioned media from the 1301, K562, Sk-mel 37 tumor cell lines in different dilutions (100%, 50%, 10%) added the complete culture medium RPMI-60 with the 10% human albumin (Octapharma Pharmazeutika Produktionsgesellschaft, m.b.H., Austria) to the specified volume in the 96-well flat bottom plate (TPP, Switzerland) in triplets for 3, 5, and 7 days. The STEM specialized culture medium was used as positive control. DMSO was used as negative control. HSCs were cultured under standard conditions: at 37 °C, 5% CO_2, 90% relative humidity.

Furthermore, HSCs (1×10^5 cells/250 mL) were incubated with the tumor cell lines in specific plates to completely avoid cell-to-cell contact, i.e. in the 12-well transwells with the pore

size of 0.4 μm and the insert diameter of 6.5 mm (Corning Incorporated, Costar, Arizona, USA) for three days under the same conditions.

The HSC viability and proliferative activity were assessed using the WST-1 reagent (Takara Bio Inc., Kusatsu, Japan). The samples were analyzed by colorimetry using the Tecan Infinite F50 microplate reader (Austria) at the wavelength of 450 nm (standard 650 nm).

HSC cell cycle

HSCs were previously stained with the CFSE dye (Invitrogen, Eugene, Oregon, USA) in accordance with the manufacturer's protocol to ensure these would differ from tumor cells when co-cultured in the plate.

HSCs in a ratio of $1 : 1 - 1 \times 10^5$ cells/mL and $10 : 1 - 1 \times 10^6$ cells/mL to tumor cells were incubated in the 24-well plate as the co-culture to assess the influence of direct contact with tumor cells on the stem cells and in the 12-well transwells to assess the impact of humoral factors only for three days under the same conditions; the intact cells in the RPMI and STEM media were used as controls. Then the cells were transferred to flow cytometry tubes and fixed in the ice cold 70% alcohol on ice for 2 h, triple washed, then added 1 mg/mL of the staining solution based on EtBr (Serva Electrophoresis GmbH, Heidelberg, Germany), 5 μg/mL of RNAase A (Microgen, Russia), 10% fetal bovine serum and PBS + EDTA, and stained for 30 min at 37 °C. The ready-made samples were analyzed using the LongCyte 14-color flow cytofluorometer (Challenbio, China) with the ModelFlower software.

HSC differentiation

HSCs in a ratio of $10 : 1 - 1 \times 10^6$ cells/mL to tumor cells (since the larger number of cells is necessary for assessment of committed precursor cells) were incubated in the 24-well plate as the co-culture and in the 12-well transwells under the same conditions. Then the cells were transferred to flow cytometry tubes and stained using monoclonal antibodies against CD10 PE (BioLegend, USA), CD34 APC (BioLegend, USA), CD38 PE-Cy7 (ElabScience, China), CD45RA PerCP (ElabScience, China), CD90 APC-Cy7 (Cloud-Clone Corp., USA), Lin-(cocktail CD3/14/16/19/20/56) FITC (BioLegend, USA). The test samples were analyzed using the LongCyte 14-color flow cytofluorometer (Challenbio, China) with the ModelFlower

software. When assessing fluorescence for each monoclonal antibody, the fluorescent minus one (FMO) control was used. Precursor cells were typed based on the surface markers as follows: pluripotent hematopoietic stem cells (pHSCs) $Lin^-CD34^+CD38^-CD45RA^-CD90^+$; common multipotent progenitors (cMPPs) $Lin^- CD34^+CD38^-CD45RA^-CD90^-$; common lymphocyte progenitors (CLPs) $Lin^-CD34^+CD38^+CD45RA^+CD90^-$; myeloid and megakaryocyte-erythroid progenitors (MEPs) $Lin^-CD34^+CD38^+CD45RA^-CD10^-$; granulocyte-monocyte progenitors (GMPs) $Lin^-CD34^+CD38^+CD45RA^+CD10^-$; B cell and NK cell precursors (B-NKP) $Lin^-CD34^+CD38^+CD45RA^+CD10^+$. Furthermore, the relative number of progenitors was assessed before plating to ensure differentiation control ("before").

Statistical data processing was performed using the GraphPad Prism 9.0.0 software. The Friedman test was used for estimation of intergroup differences, and $p < 0.05$ was considered significant. The data were presented as median (25th percentile; 75th percentile) ± interquartile range.

RESULTS

In the first phase we assessed viability and proliferative activity of hematopoietic stem cells at three time points with different share of humoral factors from tumor cells line of various origin. Thus, we showed that HSC viability at the level of the control was maintained on day 3 in the conditioned media from the tumor cell lines of varying concentration. On day 5, not only viability was preserved, but also proliferation began in all dilutions of the conditioned media; almost the same proliferation level was maintained on day 7 (Fig. 1). Furthermore, on days 3 and 5, HSC viability was higher in the 50% and 100% conditioned medium from SK-mel37 (Fig.1A, B), however, HSC viability decreased rapidly on day 7 (Fig. 1C). Perhaps, this was due to the fact that HSC proliferation was more intense in the conditioned medium from SK-mel37, and the cells began to die by day 7 (presumably due to the lack of nutrients).

The importance of humoral influence on the HSC properties is also confirmed by the results obtained when culturing HSCs with tumor cell lines under conditions precluding the cell-to-cell contact; significant differences showed that proliferative activity of HSCs was higher in transwells, than in the control, with the almost equal number of cells (Fig. 2B). The fact that SK-mel 37 shows higher proliferative capacity in transwells with HSCs compared to the equivalent quantity of the 1301 cell line also attracts attention (Fig. 2A).
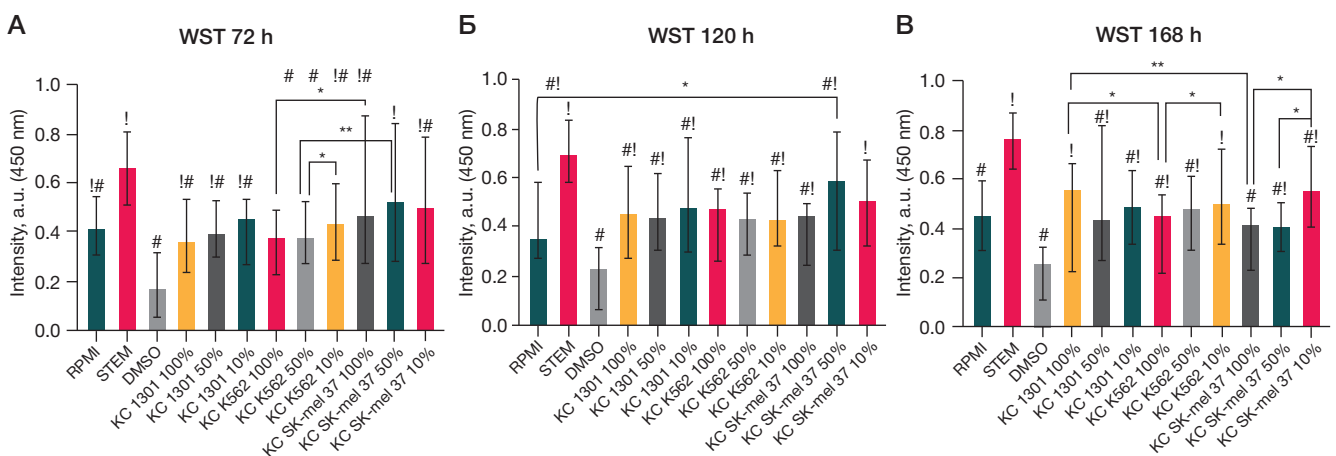
Fig. 1. Assessment of viability and proliferative activity of the hematopoietic stem cells co-cultured (c-c) with the conditioned media from the tumor cells lines 1301, K562, and SK-mel (10%, 50%, and 100% dilution) for 72 h **(A)**, 120 h **(B)**, and 168 h **(C)** (WST). Friedman test, significant differences $p < 0.05$, data are provided as median and interquartile range; # — significant differences from the control STEM; ! — significant differences from the control DMSO; * — significant differences, $p < 0.05$; ** — significant differences, $p < 0.005$
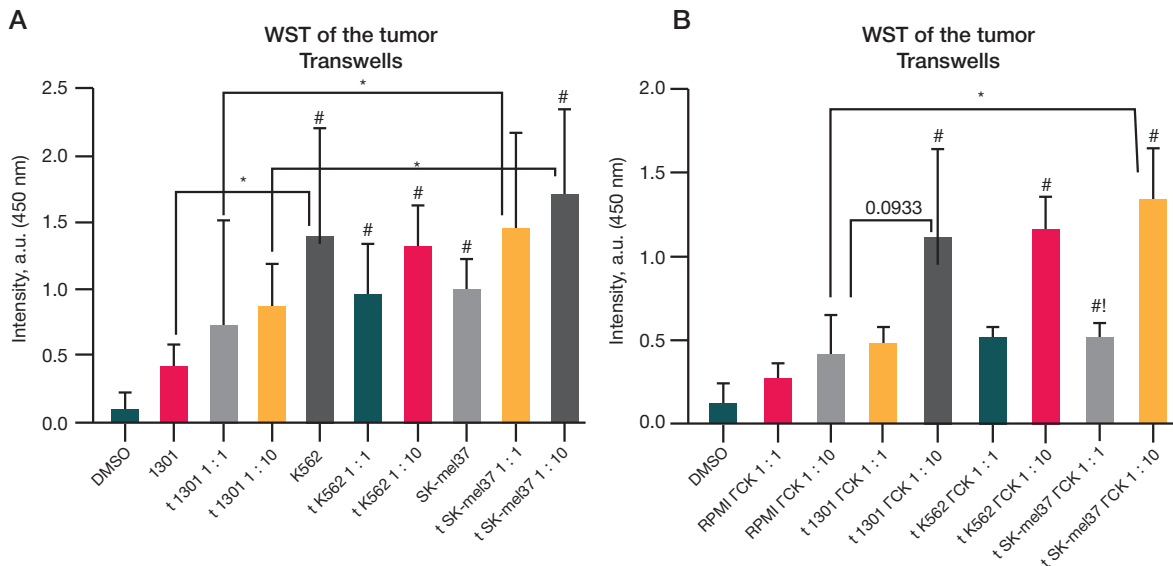
Fig. 2. Assessment of viability and proliferative activity of the tumor cell lines 1301, K562, and SK-mel37 **(A)** and hematopoietic stem cells **(B)** co-cultured in transwells (t) for 72 h. Friedman test, significant differences $p < 0.05$, data are provided as median and interquartile range; # — significant differences from the control DMSO; ! — trend compared to the SK-mel 37 HSC 1:10, $p = 0.05$; * — significant differences, $p < 0.05$

Then we assessed the influence of co-culturing on the HSC cell cycle phases. Thus, the number of cell being through the G2–M phase was higher in the co-culture with SK-mel37 compared to other tumor cell lines. The larger number of cells being through the S phase of the cell cycle was reported in cases of cell-to-cell contact with 1301. We also showed a rapid decrease in the number of HSCs cultured in transwells with SK-mel37. This was due to cell death, since 89.4% of cells were through the Sub-G1 phase (Table). It is interesting that HSC viability and proliferative activity also decreased in the conditioned media from SK-mel, but by day 7.

In the final phase, when assessing differentiation of hematopoietic stem cells, we found that the ratio of progenitors was different. Thus, after three days the number of HSCs and common multipotent progenitors increased (Fig. 3A), and the number of the latter increased much more (Fig. 3C), while the number of common lymphoid, megakaryocyte, erythroid, and myeloid progenitors decreased (Fig. 3B). It is interesting that

the number of HSCs and MPP was significantly lower (20.3%) in transwells with K562 compared to other tumors in transwells (Fig. 3A), while the value of pluripotent hematopoietic cells with the Lin⁻CD34⁺CD38⁻CD90⁺CD45RA⁻ phenotype was higher compared to both other tumors under the same conditions and control samples (Fig. 4). It should be noted that the larger relative number of granulocyte-monocyte progenitors was observed in the co-culture with 1301 and K562 compared to the cultures in transwells with the same tumors and the control medium (Fig. 4). The number of common progenitors of platelets, red blood cells, and cells of myeloid type decreased when cultured with the SK-mel-37 melanoma cells under conditions of both direct cell-to-cell contact and exchange of humoral factors. However, no significant differences between transwells and the co-culture in the plate were reported (Fig. 4).

Thus, the relative number of pluripotent HSCs increased under exposure to the K562 tumor humoral factors; the number

Table. Relative number of hematopoietic stem cells in various phases of the cell cycle during co-cultivation with the tumor cell lines 1301, K562, and SK-mel37 in the co-culture (c-c) and transwells (t) for 72 h.

	G2/M	S	G0–G1	Sub-G1
RPMI 1/1	3.1 (0.2–6.7)	8.6 (3.6–25.7)	77.4 (63.9–86.9)	3.5 (0.9–4.7)
RPMI 1/10	0.5 (0.4–1.9)	11.2 (5.1–13.9)	82.6 (74.1–87.0)	1.3 (1.1–4.3)
c-c 1301 1/1	15.7 (8.3–21.9)	3.9 (1.1–11.2)	76.8 (65.6–81.0)	5.1 (0.2–7.5)
c-c 1301 1/10	11.5 (3.0–20.9)	13.0 (5.9–31.3)#	79.6 (63.6–95.4)	2.2 (0.5–3.5)
t 1301 1/1	3.0 (2.5–9.2)!!	3.8 (2.2–24.1)	77.5 (69.1–88.9)	4.4 (0.8–6.8)
t 1301 1/10	3.2 (1.3–5.8)!	7.2 (1.9–11.3)	86.9 (84.5–93.3)	1.3 (0.5–2.3)!!
c-c K562 1/1	10.1 (0.4–27.2)	5.8 (1.8–32.1)	72.9 (59.1–83.5)	7.9 (3.7–12.6)
c-c K562 1/10	4.4 (1.3–7.3)	2.1 (1.4–3.8)**	83.9 (78.7–91.9)**	4.6 (1.9–6.6)
t K562 1/1	1.2 (0.4–4.4)	6.6 (3.5–22.6)	81.9 (72.9–88.7)	3.2 (0.9–5.6)
t K562 1/10	1.9 (1.2–16.6)	6.5 (3.6–7.6)	84.5 (72.7–89.6)	2.9 (1.1–3.6)
c-c SK-mel37 1/1	0.3 (0.1–0.6)*	7.2 (4.3–19.4)	71.9 (66.6–93.6)	6.8 (1.7–14.9)
c-c SK-mel37 1/10	1.0 (0.2–2.8)	12.5 (4.9–16.8)	86.1 (53.4–87.9)	3.8 (0.5–5.8)
t SK-mel37 1/1	1.6 (0.6–14.8)	6.4 (3.1–28.5)	78.9 (76.6–89.1)	1.2 (0.6–4.4)
t SK-mel37 1/10	0.5 (0.3–6.0)	4.7 (2.0–12.0)	1.6 (0–6.61)$	89.4 (84.9–91.8)***

Note: Friedman test, significant differences $p < 0.05$; * — significant differences compared to the c-c K562 1/1, c-c 1301 1/1; ** — significant differences compared to the c-c 1301 1/10, c-c SK-mel37 1/10, RPMI 1/10; *** — significant differences compared to the t SK-mel37 1/1, c-c SK-mel37 1/10, t K562 1/10, t 1301 1/10, RPMI 1/10; ! — significant differences from the control RPMI in equivalent concentrations; !! — significant differences compared to the t 1301 1/1; # — trend, $p = 0.05$ compared to c-c 1301 1/1, t 1301 1/10; $ — significant differences compared to the t SK-mel37 1/1, c-c SK-mel37 1/10, t K562 1/10, t 1301 1/10, RPMI 1/10

A

HSC + MPP (hematopoietic stem cell + MPP (Multipotent progenitor))
Lin⁻CD34⁺CD38⁻

B

MLP (multi-lymphoid progenitor) + CMP–MEP (common myeloid progenitor and megakaryocyte-erythroid progenitor)
Lin⁻CD34⁺CD38⁺

C

MPP (multipotent progenitor)
Lin⁻CD34⁺CD38⁻CD90⁻CD45RA⁻
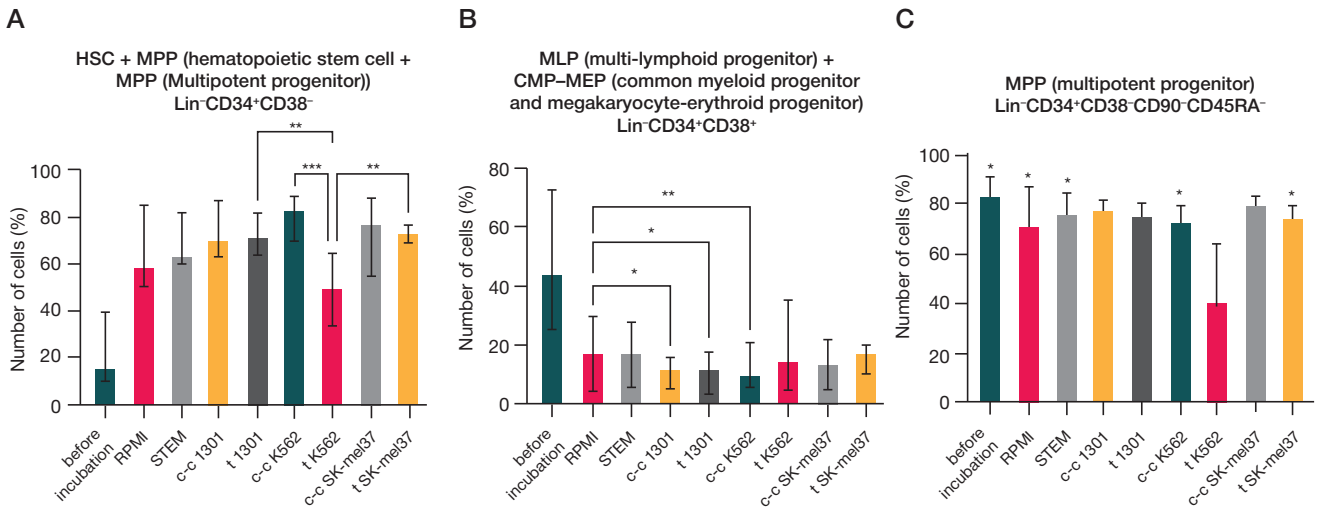
Fig. 3. Relative number of the common progenitors of hematopoietic stem cells co-cultured with the tumor cell lines 1301, K562, and SK-mel37 in the co-culture (c-c) and transwells (t) for 72 h. Friedman test, significant differences $p < 0.05$, data are provided as median and interquartile range; * — significant differences compared to t K562, $p < 0.05$

of granulocyte-monocyte progenitors increased in cases of cell-to-cell contact between HSCs and K562 or 1301.

DISCUSSION

Tumor microenvironment is a complex dynamic structure that represents the carcinogenesis regulator. The issue of studying tumor microenvironment in experimental models still remains relevant. Two major components of tumor microenvironment can be distinguished: synthesis and exchange of humoral factors, as well as formation of cross-links between cells under conditions of cellular neighborhood. Cells can change their properties and functions when influenced by the tumor. There

is information about specific cells having their own functions in the tumor microenvironment, these are the so-called tumor-associated macrophages, fibroblasts, dendritic cells, etc. [12–14] involved in carcinogenesis. Today, these cells can be considered as both informative marker and therapeutic target. Since we have discussed the fact that hematopoietic stem cells are found in the tumor microenvironment, it is important to assess the impact of the tumor on the HSC properties.

According to our data, HSC differentiation in the culture occurred on day 3, when the cells were activated and proliferation started by day 3, and differentiation started by day 7. It is noteworthy that HSCs can enter early differentiation on day 3 under exposure to various factors [15]. In general, the

	before incubation	RPMI	STEM	c-c 1301	t 1301	c-cK562	t K562	c-c SK-mel37	t SK-mel37
pHSC (pluripotent hematopoietic stem cell)	5.73	10.19	8.39	10.13	9.97	9.505	27.77	7.355	10.29
GMP (granulocyte–monocyte progenitor)	26.54	24.17	37.65	35.96	21.23	36,35	17.58	31.28	27.94
B-NKP (B-NK progenitor)	2.065	0.595	2.9	2.175	1.754	1.385	0.865	1.08	2.18
CMP–MEP (common myeloid progenitor and megakaryocyte-erythroid progenitor)	69.64	50.03	50.76	52.26	65.3	53.69	62.26	43.71	49.39

Fig. 4. Relative number of hematopoietic stem cell progenitors co-cultured with the tumor cell lines 1301, K562, and SK-mel37 in the co-culture (c-c) and transwells (t) for 72 h. Friedman test, significant differences $p < 0.05$, data are provided as median and interquartile range; * — significant differences from the control RPMI, t K562; ** — significant differences compared to all test groups, $p < 0.005$; ! — trend compared to the t K562, $p = 0.06$; # — trend compared to the control before incubation and RPMI, $p = 0.05$

HSC counts and differentiation depend on the fact, whether HSC interact with tumor cells directly or their interaction is mediated by humoral factors. The common HSC differentiation pattern was reported for 1301 and K562, most likely because both tumor types are clones of hematopoietic cells in origin. It should be also noted that the shift towards granulocyte-monocyte cells is associated with high risk of metastasis [16], which is generally typical for leukemia. However, HSCs cultured with a solid tumor, melanoma, showed a slightly different cell ratio with the decreased number of common progenitors of myelopoiesis and increased number of multipotent progenitors ($p = 0.05$). It is interesting that, according to the literature, in solid tumors HSC differentiation is directed not only towards myeloid cells, specifically myeloid suppressors [17], but also towards less differentiated cells with preserved multipotency [18], which is consistent with our data.

CONCLUSIONS

Proliferative activity, cell division and differentiation change depending on the tumor type. The K562 and 1301 leukemia tumor cell lines affect viability and differentiation of hematopoietic stem cells in the same way, while melanoma SK-mel-37, the solid tumor, has a different effect on the same processes, which teaches us about both isolated and common patterns of the tumor influence on the vital activity of the hematopoietic stem cell. For better understanding of the impact of tumors on the HSC properties it is necessary to use a more comprehensive approach involving assessment of the cell secretome, recruiting markers, and association with the tumor process, and to use more complex and relevant methods to co-culture cells taking into account the complex, dynamic, and heterogeneous structure of tumor microenvironment.

References

1. Treichel S, Filippi M-D. Linking cell cycle to hematopoietic stem cell fate decisions. Front Cell Dev Biol. 2020; 11:1231735. DOI: 10.3389/fcell.2023.1231735.
2. Szade K, Gulati GS, Chan CKF, Kao KS, Miyanishi M, Marjon KD, et al. Where Hematopoietic Stem Cells Live: The Bone Marrow Niche. Antioxid Redox Signal. 2018; 10; 29 (2): 191–204. DOI: 10.1089/ars.2017.7419.
3. Baldridge MT, King KY, Goodell M.A. Inflammatory signals regulate hematopoietic stem cells. Trends in Immunology. 2011; 32 (2), 57–65. DOI: 10.1016/j.it.2010.12.003.
4. Chavez JSPU, Loeffler D, Higa KC, Hernandez G, Mills TS. PU.1 enforces quiescence and limits hematopoietic stem cell expansion during inflammatory stress. Exp Med. 2011; 218 (6), e20201169. DOI: 10.1084/jem.20201169.
5. Pietras EM, Warr MR, Passegué E. Cell cycle regulation in hematopoietic stem cells. Cell Biol. 2011; 195 (5): 709–20. DOI: 10.1083/jcb.201102131.
6. Grinenko T, Eugster A, Thielecke L, et al. Hematopoietic stem cells can differentiate into restricted myeloid progenitors before cell division in mice. Nat Commun. 2018; 9, 1898. DOI: 10.1038/s41467-018-04188-7.
7. Han W, Yu Y, Liu XY. Local signals in stem cell-based bone marrow regeneration. Cell Res. 2006; 16: 189–95. DOI: 10.1038/sj.cr.7310026.
8. Lu IN, Dobersalske C, Rauschenbach L, et al. Tumor-associated hematopoietic stem and progenitor cells positively linked to glioblastoma progression. Nat Commun. 2021; 12, 3895. DOI: 10.1038/s41467-021-23995-z.
9. Hassan G, Seno M. Blood and Cancer: Cancer Stem Cells as Origin of Hematopoietic Cells in Solid Tumor Microenvironments. Cells. 2020; 9 (5): 1293. DOI: 10.3390/cells9051293.
10. Berz D, McCormack EM, Winer ES, Colvin GA, Quesenberry PJ. Cryopreservation of hematopoietic stem cells. Am J Hematol. 2007; 82 (6): 463–72. DOI: 10.1002/ajh.20707.
11. Katayama Y, Yano T, Bessho A, et al. The effects of a simplified method for cryopreservation and thawing procedures on peripheral blood stem cells. Bone Marrow Transplant. 1997; 19: 283–7. DOI: 10.1038/sj.bmt.1700644.
12. Bejarano L, Jordão MJC, Joyce JA. Therapeutic targeting of the tumor microenvironment. Cancer Discovery. 2021; 4 (11): 933–59. DOI: 10.1158/2159-8290.CD-20-1808.
13. Hinshaw DC, Shevde LA. The tumor microenvironment innately modulates cancer progression. Cancer Research. 2019; 18 (79): 4557–67. DOI: 10.1158/0008-5472.CAN-18-3962.
14. Najafi M, Goradel NH, Farhood B, et al. Tumor microenvironment: Interactions and therapy. Journal of Cellular Physiology. 2019; 5 (234): 5700–21. DOI: 10.1002/jcp.27425.
15. Edel MJ, Menchon C, Vaquero JM, et al. A protocol to assess cell cycle and apoptosis in human and mouse pluripotent cells. Cell Commun Signal. 2011; 9 (8): DOI: 10.1186/1478-811X-9-8.
16. Magidey-Klein K, Kveler K, Cooper TJ, Normand R, Zhang T, Timaner M, Raviv Z, et al. Tumor-educated uncommitted hematopoietic stem cells promote a metastatic switch BioRxiv. 2020; DOI: https://doi.org/10.1101/2020.08.25.266189.
17. Wang X, Li Y. The disruption of hematopoiesis in tumor progression. Blood Sci. 2019; 1 (1): 88–91. DOI: 10.1097/BS9.0000000000000001.
18. Lu IN, Dobersalske C, Rauschenbach L, et al. Tumor-associated hematopoietic stem and progenitor cells positively linked to glioblastoma progression. Nat Commun. 2021; 12, 3895. DOI: 10.1038/s41467-021-23995-z.

Литература

1. Treichel S, Filippi M-D. Linking cell cycle to hematopoietic stem cell fate decisions. Front Cell Dev Biol. 2020; 11:1231735. DOI: 10.3389/fcell.2023.1231735.
2. Szade K, Gulati GS, Chan CKF, Kao KS, Miyanishi M, Marjon KD, et al. Where Hematopoietic Stem Cells Live: The Bone Marrow Niche. Antioxid Redox Signal. 2018; 10; 29 (2): 191–204. DOI: 10.1089/ars.2017.7419.
3. Baldridge MT, King KY, Goodell M.A. Inflammatory signals regulate hematopoietic stem cells. Trends in Immunology. 2011; 32 (2), 57–65. DOI: 10.1016/j.it.2010.12.003.
4. Chavez JSPU, Loeffler D, Higa KC, Hernandez G, Mills TS. PU.1 enforces quiescence and limits hematopoietic stem cell expansion during inflammatory stress. Exp Med. 2011; 218 (6), e20201169. DOI: 10.1084/jem.20201169.
5. Pietras EM, Warr MR, Passegué E. Cell cycle regulation in hematopoietic stem cells. Cell Biol. 2011; 195 (5): 709–20. DOI: 10.1083/jcb.201102131.
6. Grinenko T, Eugster A, Thielecke L, et al. Hematopoietic stem cells can differentiate into restricted myeloid progenitors before cell division in mice. Nat Commun. 2018; 9, 1898. DOI: 10.1038/s41467-018-04188-7.
7. Han W, Yu Y, Liu XY. Local signals in stem cell-based bone marrow regeneration. Cell Res. 2006; 16: 189–95. DOI: 10.1038/sj.cr.7310026.
8. Lu IN, Dobersalske C, Rauschenbach L, et al. Tumor-associated hematopoietic stem and progenitor cells positively linked to glioblastoma progression. Nat Commun. 2021; 12, 3895. DOI: 10.1038/s41467-021-23995-z.
9. Hassan G, Seno M. Blood and Cancer: Cancer Stem Cells as Origin of Hematopoietic Cells in Solid Tumor Microenvironments. Cells. 2020; 9 (5): 1293. DOI: 10.3390/cells9051293.
10. Berz D, McCormack EM, Winer ES, Colvin GA, Quesenberry PJ.

Cryopreservation of hematopoietic stem cells. Am J Hematol. 2007; 82 (6): 463–72. DOI: 10.1002/ajh.20707.

11. Katayama Y, Yano T, Bessho A, et al. The effects of a simplified method for cryopreservation and thawing procedures on peripheral blood stem cells. Bone Marrow Transplant. 1997; 19: 283–7. DOI: 10.1038/sj.bmt.1700644.

12. Bejarano L, Jordão MJC, Joyce JA. Therapeutic targeting of the tumor microenvironment. Cancer Discovery. 2021; 4 (11): 933–59. DOI: 10.1158/2159-8290.CD-20-1808.

13. Hinshaw DC, Shevde LA. The tumor microenvironment innately modulates cancer progression. Cancer Research. 2019; 18 (79): 4557–67. DOI: 10.1158/0008-5472.CAN-18-3962.

14. Najafi M, Goradel NH, Farhood B, et al. Tumor microenvironment: Interactions and therapy. Journal of Cellular Physiology. 2019; 5 (234): 5700–21. DOI: 10.1002/jcp.27425.

15. Edel MJ, Menchon C, Vaquero JM, et al. A protocol to assess cell cycle and apoptosis in human and mouse pluripotent cells. Cell Commun Signal. 2011; 9 (8): DOI: 10.1186/1478-811X-9-8.

16. Magidey-Klein K, Kveler K, Cooper TJ, Normand R, Zhang T, Timaner M, Raviv Z, et al. Tumor-educated uncommitted hematopoietic stem cells promote a metastatic switch BioRxiv. 2020; DOI: https://doi.org/10.1101/2020.08.25.266189.

17. Wang X, Li Y. The disruption of hematopoiesis in tumor progression. Blood Sci. 2019; 1 (1): 88–91. DOI: 10.1097/BS9.0000000000000001.

18. Lu IN, Dobersalske C, Rauschenbach L, et al. Tumor-associated hematopoietic stem and progenitor cells positively linked to glioblastoma progression. Nat Commun. 2021; 12, 3895. DOI: 10.1038/s41467-021-23995-z.

MODIFIED MICRO TEST TUBES AS A PROMISING BASIS FOR IMMOBILIZATION OF ANTIBODIES FOR IMMUNOCAPTURE ON THE EXAMPLE OF SARS-COV-2

Roubalsky EO[1,2] ✉, Abdrakhmanova RA[1], Baeva GR[1], Rubalskaya TS[3], Lazko MV[1], Poroyskiy SV[1], Shcheblyakov DV[4], Favorskaya IA[4], Gushchin VA[4,5,6]

[1] Astrakhan State Medical University, Astrakhan, Russia
[2] Russian University of Medicine, Moscow, Russia
[3] Gabrichevsky Moscow Research Institute for Epidemiology and Microbiology of the Federal Service for Surveillance on Consumer Rights Protection and Human Wellbeing, Moscow, Russia
[4] Gamaleya National Research Centre for Epidemiology and Microbiology, Moscow, Russia
[5] Lomonosov Moscow State University, Moscow, Russia
[6] Sechenov First Moscow State Medical University, Moscow, Russia

The solid-phase immunocapture with antibodies is an important tool used in immunology studies, but conventional polystyrene plates are prone to deformation during thermal cycling and cross-contamination of samples, which reduces accuracy and reproducibility, when molecular genetic testing methods are included in the study. The development of alternative solutions, such as modified polystyrene-coated polypropylene tubes, makes it possible to eliminate these limitations. The study aimed to create a new approach to SARS-CoV-2 immunocapture involving the use of modified test tubes and to assess its efficacy. Monoclonal antibodies P2C5 and R107, as well as inactivated strains GK2020/1 (Wuhan) and hCoV-19/Russia/MOW-PMVL-51/2021 (Omicron) were used for analysis. Immobilization of antibodies, sorption of viral particles, and RNA extraction were accomplished using modified test tubes, standard plates, and uncoated test tubes. The key findings showed that the polystyrene-coated modified test tubes ensured better immunocapture compared to the plates ($p < 0.0001$), especially when using the P2C5 antibody effective against various SARS-CoV-2 lineages, including Omicron. The R107 antibody showed limited specificity, not exceeding that of the control group with bovine serum albumin. The cross-contamination analysis revealed contamination of 14 samples out of 288 in the plates, while no contamination of samples was reported for modified test tubes. Thus, modified test tubes used for high-precision molecular testing have some advantages, since these decrease the risk of cross-contamination and improve immunocapture efficacy.

Keywords: immunocapture, monoclonal antibodies, RT-PCR, modified surface, cross-contamination, SARS-CoV-2

✉ **Correspondence should be addressed:** Evgeny O. Roubalsky
Bakinskaya, 121, Astrakhan, 414000, Russia; e.o.rubalsky@gmail.com rubalsky@phage.pro

МОДИФИЦИРОВАННЫЕ МИКРОПРОБИРКИ — ПЕРСПЕКТИВНАЯ ОСНОВА ДЛЯ ИММОБИЛИЗАЦИИ АНТИТЕЛ ИММУНОЗАХВАТА НА ПРИМЕРЕ SARS-COV-2

Е. О. Рубальский[1,2] ✉, Р. А. Абдрахманова[1], Г. Р. Баева[1], Т. С. Рубальская[3], М. В. Лазько[1], С. В. Поройский[1], Д. В. Щебляков[4], И. А. Фаворская[4], В. А. Гущин[4,5,6]

[1] Астраханский государственный медицинский университет Министерства здравоохранения Российской Федерации, Астрахань, Россия
[2] Российский университет медицины Министерства здравоохранения Российской Федерации, Москва, Россия
[3] Московский научно-исследовательский институт эпидемиологии и микробиологии имени Г. Н. Габричевского Федеральной службы по надзору в сфере защиты прав потребителей и благополучия человека, Москва, Россия
[4] Национальный исследовательский центр эпидемиологии и микробиологии имени Н. Ф. Гамалеи Министерства здравоохранения Российской Федерации, Москва, Россия
[5] Московский государственный университет имени М. В. Ломоносова, Москва, Россия
[6] Первый Московский государственный медицинский университет имени И. М. Сеченова Министерства здравоохранения Российской Федерации, Москва, Россия

Иммунозахват антителами на твердой фазе является важным инструментом в иммунологических исследованиях, но традиционные полистироловые планшеты подвержены деформации при термоциклировании и перекрестной контаминации образцов, что снижает точность и воспроизводимость при включении в исследование молекулярно-генетических методов. Разработка альтернативных решений, таких как модифицированные полипропиленовые пробирки с полистироловым покрытием, позволяет устранить эти ограничения. Целью исследования было создать и оценить эффективность нового подхода к иммунозахвату SARS-CoV-2 с использованием модифицированных пробирок. Для анализа использовали моноклональные антитела Р2С5 и R107, а также инактивированные штаммы ГК2020/1 (Ухань) и hCoV-19/Russia/MOW-PMVL-51/2021 (Омикрон). Иммобилизацию антител, сорбцию вирусных частиц и выделение РНК проводили с применением модифицированных пробирок, стандартных планшетов и пробирок без покрытия. Основные результаты показали, что модифицированные пробирки с полистироловым покрытием обеспечивали лучший иммунозахват по сравнению с планшетами ($p < 0{,}0001$), особенно при использовании антител Р2С5, эффективных против различных генетических линий SARS-CoV-2, включая Омикрон. Антитела R107 продемонстрировали ограниченную специфичность, не превышающую уровня контрольной группы с бычьим сывороточным альбумином. Анализ перекрестной контаминации выявил ее наличие в 14 из 288 образцов в планшетах, тогда как в модифицированных пробирках контаминации образцов не было. Таким образом, использованные для высокоточных молекулярных исследований модифицированные пробирки имеют преимущества, так как обеспечивают снижение риска перекрестной контаминации и улучшение эффективности иммунозахвата.

Ключевые слова: иммунозахват, моноклональные антитела, ОТ-ПЦР, модифицированная поверхность, перекрестная контаминация, SARS-CoV-2

✉ **Для корреспонденции:** Евгений Олегович Рубальский
ул. Бакинская, д. 121, г. Астрахань, 414000, Россия; e.o.rubalsky@gmail.com rubalsky@phage.pro

Immunocapture based on specific antibodies is a key phase of many immunological laboratory testing methods. Polystyrene microplates that ensure the possibility of simultaneous processing of multiple samples are conventionally used for implementation of this method. Polystyrene usually can passively (in non-specific manner) immobilize almost all large molecules having accessible hydrophobic fragments, such as antibodies, on its surface [1]. However, this material is prone to deformation at temperatures above +70 °C (above +60 °C when heated over a long time) [2]. This is a serious technical issue of the use of additional molecular genetic phases of analysis, such as thermal nucleic acid extraction and thermal cycling (for example, in immuno-PCR [3]), which limits the widespread practical use of such methods. Polycarbonate strip tubes gathered in the 96-well plate that have been proposed as an alternative to polystyrene plates are resistant to heat and have high sorption capacity [4].

However, the use of plates is associated with high risk of cross-contamination [5, 6]. The risk can be leveled using various methodological approaches, such as the use of automated sample preparation systems. The use of conventional polypropylene test tubes for molecular genetic testing might potentially decrease the risk of contamination when working in accordance with the principle of "one open test tube". However, the use of test tubes is limited by low protein sorption capacity of polypropylene, including adsorption of antibodies [7], which prevents their use for high-sensitivity methods, such as immuno-PCR, that require stable immobilization of immunocapture antibodies [4].

The development of such methods, as immunomolecular assays, can significantly increase sensitivity and specificity of molecular genetic testing, which is especially important for the diagnosis and monitoring of viral infections showing high mutational variance of the pathogen, such as SARS-CoV-2 virus [8]. It should be noted that such reactions have not yet received wide practical application. To date, no studies of the COVID-19 causative agent by immuno-PCR have been reported in scientific literature. This is likely to be associated with complexity of the design and implementation of the reaction phases. That is why it is necessary to optimize their key components and overcome technical issues inherent to the existing reaction formats for successful practical use of such combination approaches [4, 9].

In this regard, we have proposed original polystyrene coating of polypropylene test tubes. This solution makes it possible to combine advantages of both materials: high sorption capacity of polystyrene and heat resistance of polypropylene, with the reduced risk of cross-contamination.

The study aimed to develop a simple production method and perform testing of new test tubes for immunocapture ensuring effective immobilization of primary antibodies and designed for universal use in molecular genetic testing on an example of SARS-CoV-2.

METHODS

SARS-CoV-2 strains and antibodies

The well-characterized samples of positive control of the strain GK2020/1 (GISAID identifier: EPI_ISL_421275, variant B.1.1.1, Wuhan) and strain hCoV-19/Russia/MOW-PMVL-51/2021 (GISAID identifier: EPI_ISL_12748382, variant B.1.1.529+BA.* of the Omicron lineage) of the SARS-CoV-2 coronavirus chemically inactivated using glutaraldehyde in the final concentration of 0.01% and then incubated at +4 °C for 24 h were used as an antigen.

To assess the effectiveness of primary antibody immobilization (immunocapture) we used the P2C5 experimental monoclonal antibodies against RBD of the coronavirus spike protein (produced at the Immunobiotechnology Laboratory of the Gamaleya National Research Centre for Epidemiology and Microbiology) having the broadest spectrum of activity covering inter alia certain variants of the Omicron lineage [10]. Furthermore, we tested the R107 monoclonal antibody (Hytest, Russia) showing specific activity mainly against RBD of the B.1.1.1 virus variant.

Assessing the effectiveness of immunocapture involving the use of polystyrene ELISA plates

To optimize immobilization of antibodies, we used the FEP-101-896 96-well flat bottom polystyrene immunological plates (Guangzhou Jet Bio-Filtration Co., Ltd., China). We added 100 µL of antibodies in a concentration of 10 µg/mL dissolved in the 0.5 M carbonate buffer (pH = 9.5) to each well of the plate, covered the plates with film and incubated at a temperature of +37 °C for 30 min. We used 100 µL of phosphate-buffered saline (PBS, pH = 7.4) supplemented with 2% bovine serum albumin (BSA) as a blocking buffer with incubation at +37 °C for 30 min. The washing buffer consisted of PBS (pH = 7.4) supplemented with 0.05% Tween 20.

After triple washing of the wells with 300 µL and incubation for 45 s, these were added 50 µL of the SARS-CoV-2 samples inactivated and preliminarily diluted with PBS to the concentration of 1×10^6 copies/mL and incubated at +37 °C for 30 min. Then washing was performed, followed by RNA extraction using the RIBO-prep kit (Central Research Institute of Epidemiology of Rospotrebnadzor, Russia) and quantitative RT-PCR.

RNA was extracted in accordance with the modified manufacturer's protocol: we added 50 µL of TE buffer to the wells of the polystyrene plate, then added 155 µL of the lysing solution, covered the wells with film for ELISA plates and incubated at +65 °C for 10 min. Then the content of the polystyrene plate wells was transferred to micro test tubes, and subsequent phases of RNA extraction were implemented in accordance with the manufacturer's instructions. Quantitative RT-PCR was conducted using the SARS-CoV-2-PCR reagent kit (MedipalTech, Russia) in combination with the samples of the chemically inactivated GK2020/1 strain used as a calibrator. All the experiments were conducted in ten replicates ($n = 10$).

Assessing immunocapture involving the use of modified micro test tubes

The 1.5 mL sterile micro test tubes made of transparent polypropylene, free from DNAses and RNAses (SPINWIN Tarsons, India) and polystyrene from the FEP-101-896 immunological plates (Guangzhou Jet Bio-Filtration Co., Ltd., China) dissolved in acetone were used as components for production of modified micro test tubes. A total of 50 µL of polystyrene solution were aseptically applied to the bottom of the test tubes and dried in a fume hood. Mechanical stability of the resulting polypropylene layer was visually estimated after the vortex mixing of the added 1 mL of water at 2500 rpm for 2 min by twenty-fold pipetting with the pipette tip touching the micro test tube bottom and centrifugation at 15,000 g for 15 min. A total of 100 µL of antibodies in the carbonate buffer (10 µg/mL) were added to the micro test tubes modified by this method and incubated at +37 °C for 30 min with the lids closed. After blocking the remaining antibody-free surface with
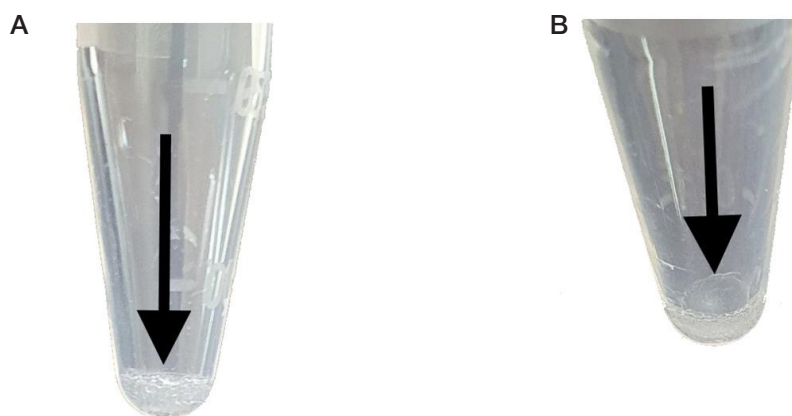
Fig. 1. Polypropylene micro test tube after modification with polystyrene: side view **(A)** and ≈45° view **(B)**

PBS supplemented with 2% BSA and washing (similar to that of plates), 50 μL of SARS-CoV-2 samples were added. Further washing, RNA extraction, and RT-PCR were performed in the same way, as when using polystyrene plates. All the RNA extraction phases were implemented in modified micro test tubes.

The non-modified polypropylene test tubes were used as controls. All the experiments were conducted in ten replicates ($n = 10$).

Assessing cross-contamination

To assess cross-contamination, 50 μL of the GK2020/1 (variant B.1.1.1) and hCoV-19/Russia/MOW-PMVL-51/2021 (Omicron) strains were added in a staggered manner to the 96-well plates and modified test tubes with the immobilized P2C5 antibody. After incubation, washing, and RNA extraction, genotyping was performed by RT-PCR. To detect the GK2020/1 strain, we conducted sequence-specific RT-PCR with original primers Wu_fw1mod 5'-CGTGGTTCCATGCTATACATG-3' and Wu_rv1mod 5'-CGTCCCTGTGGTAATAAACAC-3' in the ready-made reaction mixture OneTube RT-PCR SYBR (Evrogen, Russia) involving real-time detection in the SYBR-Green channel. The strain of the Omicron lineage was detected using the AmpliTest SARS-CoV-2 VOC v.3 kit (Centre for Strategic Planning and

Management of Biomedical Health Risks of FMBA of Russia, Russia) in accordance with the manufacturer's instructions. Three plates and 288 test tubes were used for the experiment. The experiment was conducted in the laminar airflow in the class II A2 biosafety cabinet (LamSystems, Russia).

Statistical analysis

The data were analyzed using the GraphPad PRISM v.10.4.0 software (Graphpad Software, Inc., USA). Distribution was estimated using the Shapiro–Wilk test. Two-way ANOVA with Tukey's test of additivity was used for multiple comparisons of parametric data; the significance level was set as $p < 0.05$ (confidence interval (95%).

RESULTS

Modified micro test tubes

A polypropylene micro test tube after modification with polystyrene is presented in Fig. 1. The modified micro test tubes obtained were mechanically stable during both vortex mixing and mixing by pipetting. Centrifugation also had no visible effect on the polystyrene layer integrity.
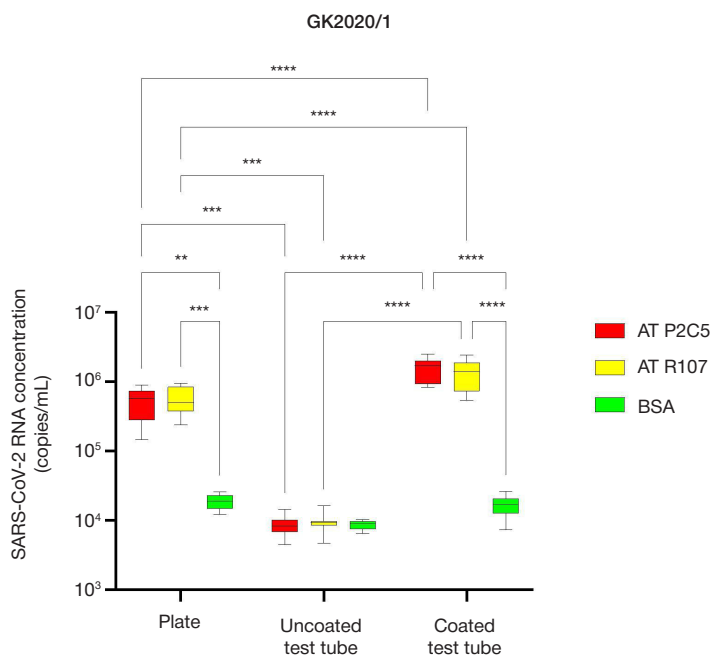
Fig. 2. The GK2020/1 strain immunocapture results. The P2C5 monoclonal antibody is highlighted in *red*, R107 is highlighted in *yellow*, control group with BSA is highlighted in green. ** — $p < 0.01$; *** — $p < 0.001$; **** — $p < 0.0001$

hCoV-19/Russia/MOW-PMVL-51/2021
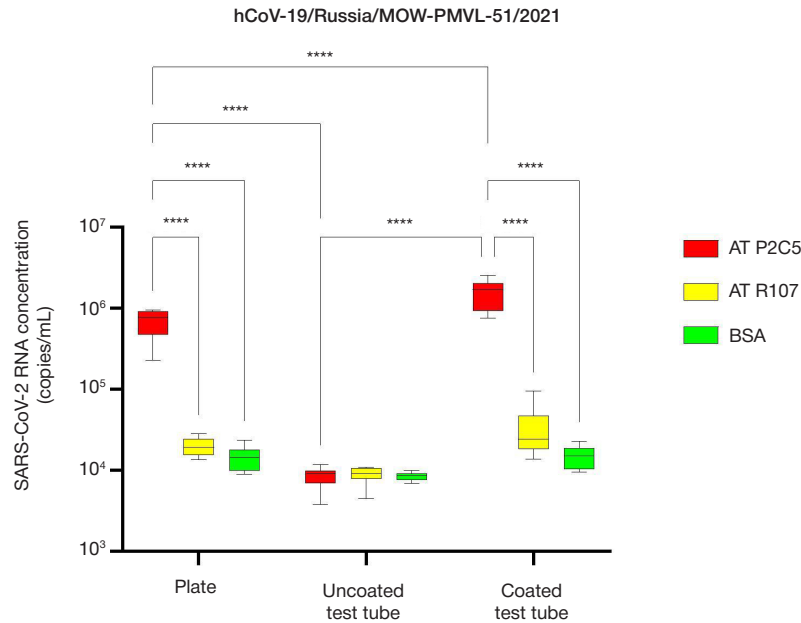
Fig. 3. The hCoV-19/Russia/MOW-PMVL-51/2021 strain immunocapture results. The P2C5 monoclonal antibody is highlighted in *red*, R107 is highlighted in *yellow,* control group with BSA is highlighted in green. **** — $p < 0.0001$

Immunocapture of inactivated SARS-CoV-2

When using the GK2020/1 strain (variant B.1.1.1) as an antigen, effective immunocapture was reported for both P2C5 and R107 antibodies (Fig. 2). The quantity of virus bound by antibodies turned out to be significantly higher when using modified test tubes compared to polystyrene plates ($p < 0.0001$). The number of SARS-CoV-2 RNA copies in the control groups, where BSA was used, was significantly lower, than the number reported for the groups with antibodies when using both plates and modified test tubes. When using the test tubes without coating, the equally low quantities of coronavirus RNA were determined in all groups ($p > 0.05$), which suggests the lack of specific antigen immunocapture, regardless of the use of antibodies.

When using the hCoV-19/Russia/MOW-PMVL-51/2021 strain (Omicron lineage), effective immunocapture was reported for the P2C5 antibody only (Fig. 3). The R107 antibody specific for RBD primarily of the Wuhan SARS-CoV-2 variant showed no significant differences from the control group with BSA. Thus, the strain of the Omicron lineage showed the ability to escape the R107 neutralizing antibody, which is consistent with the data of other researchers on the decreased efficacy of some monoclonal antibodies against new SARS-CoV-2 variants [11, 12]. The modified test tubes ensured better results, than polystyrene plates, for both B.1.1.1 and Omicron lineages.

Cross-contamination

Cross-contamination was found in 14 samples out of 288 when using polystyrene plates (Fig. 4). Contamination was represented by mixing of RNA of the GK2020/1 and hCoV-19/Russia/MOW-PMVL-51/2021 strains, which confirms the risk of material transfer between the wells under such conditions. No cross-contamination was reported for modified test tubes.

DISCUSSION

The findings show that polystyrene-coated modified polypropylene test tubes offer significant advantages over conventional polystyrene plates, including reduced risk of cross-contamination and improved immunocapture efficacy. These data are in line with the studies showing that polystyrene plates represent a good material for immobilization of antibodies, but their use is limited due to low heat resistance and the risk of contamination [2, 5, 6].

The differences in efficacy of the P2C5 and R107 antibodies reported when working with different SARS-CoV-2 strains are consistent with the data on significant mutations in RBD of the Omicron lineage, which reduce the efficacy of antibodies specific for the B.1.1.1 (Wuhan) virus variant [13, 14]. It is assumed that such mutations lead to conformational RBD alterations, thereby preventing binding of antibodies,
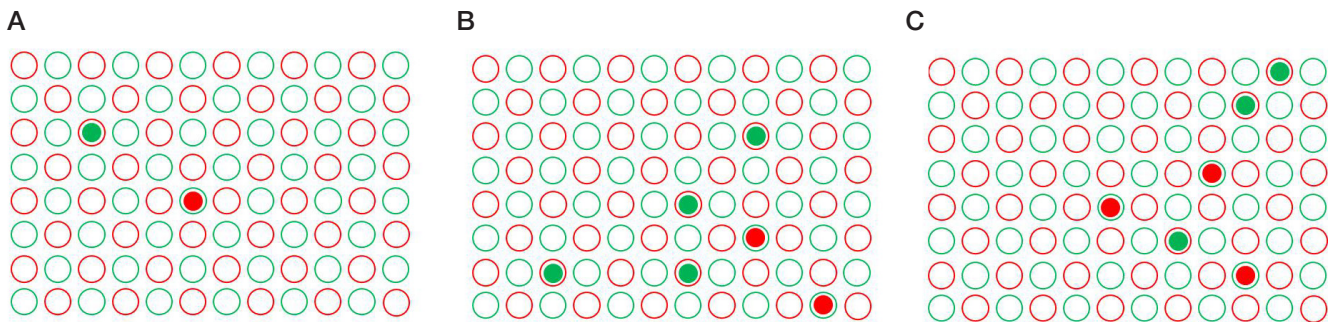
Fig. 4. Cross-contamination detected when extracting SARS-CoV-2 RNA in the 96-well plates. The wells depicted as *red circles* contain the GK2020/1 strain (variant B.1.1.1). The wells depicted as *green circles* contain the hCoV-19/Russia/MOW-PMVL-51/2021 strain (variant B.1.1.529+BA.*Omicron lineage). *Red dots* in *green circles* indicate contamination of the hCoV-19/Russia/MOW-PMVL-51/2021 strain with the GK2020/1 strain. *Green dots* in *red circles* indicate contamination of the GK2020/1 strain with the hCoV-19/Russia/MOW-PMVL-51/2021 strain. **(A–C)** Three sequential tests performed by three different operators

as previously reported for first-generation antibodies against SARS-CoV-2 [15]. High efficacy of P2C5 covering a broad range of variants, including Omicron, confirms their versatility and relevance for monitoring of new strains.

The lack of cross-contamination in modified test tubes can be explained by the lack of direct contact between samples and minimization of airborne transfer. Similar conclusions were drawn in the studies, in which other closed systems were used for molecular diagnosis [16].

Despite positive results, it is necessary to further optimize the conditions of antibody immobilization and RNA extraction in order to improve reproducibility of the method when using modified test tubes. Furthermore, for widespread use of the tubes, testing on other pathogens is necessary to confirm versatility of the method. Further testing and improvement of the test tubes can cover the following areas: study of the suitability and compatibility of polypropylene and polystyrene of various grades; reduction of non-specific signal through the use of polypropylene tubes with low adhesive capacity; polystyrene application automatization.

In general, modified test tubes represent a promising basis for combined immunological and molecular genetic testing requiring high sensitivity and accuracy, especially under conditions of high variability of pathogens, such as SARS-CoV-2.

CONCLUSIONS

The polystyrene-coated modified polypropylene test tubes have shown high immunocapture effectiveness and the lack of cross-contamination, being superior to conventional polystyrene plates. Such findings confirm that the goals of the study have been achieved. The P2C5 antibody have shown versatility when used against various SARS-CoV-2 lineages, including Omicron, which makes these promising for the diagnosis of new variants of the COVID-19 causative agents. Further research should be focused on testing the test tubes with other pathogens and improving their functional characteristics. Possible areas to use the polystyrene-coated modified polypropylene test tubes include clinical diagnosis and development of highly sensitive methods for virus detection, selection, and identification.

References

1. Butler JE, Ni L, Nessler R, Joshi KS, Suter M, Rosenberg B, et al. The physical and functional behavior of capture antibodies adsorbed on polystyrene. J Immunol Methods. 1992; 150 (1–2): 77–90. DOI: 10.1016/0022-1759(92)90066-3. PMID: 1613260.

2. Donald AM. The effect of temperature on crazing mechanisms in polystyrene. J Mater Sci. 1985; 20: 2630–8. DOI: 10.1007/BF00556095.

3. Sano T, Smith CL, Cantor CR. Immuno-PCR: very sensitive antigen detection by means of specific antibody-DNA conjugates. Science. 1992; 258 (5079): 120–2. DOI: 10.1126/science.1439758. PMID: 1439758.

4. Gorshkov AS, Pechenkin DV, Kuznecovskij AV, Balakin VA. PCR-amplificirovannyj immunoanaliz (immuno-PCR): princip metoda, varianty ispolnenija, vozmozhnosti i perspektivy ispol'zovanija dlja vyjavlenija patogennyh biologicheskih agentov. Vestnik vojsk RHB zashhity. 2021; 5 (4): 366–75. Dostupno po ssylke: https://doi.org/10.35825/2587-5728-2021-5-4-366-375. Russian.

5. Minich JJ, Sanders JG, Amir A, Humphrey G, Gilbert JA, Knight R. Quantifying and Understanding Well-to-Well Contamination in Microbiome Research. mSystems. 2019; 4 (4): e00186–19. DOI: 10.1128/mSystems.00186-19. PMID: 31239396; PMCID: PMC6593221.

6. Lou YC, Hoff J, Olm MR, West-Roberts J, Diamond S, Firek BA, et al. Using strain-resolved analysis to identify contamination in metagenomics data. Microbiome. 2023; 11 (1): 36. DOI: 10.1186/s40168-023-01477-2. PMID: 36864482; PMCID: PMC9979413.

7. Goebel-Stengel M, Stengel A, Taché Y, Reeve JR Jr. The importance of using the optimal plasticware and glassware in studies involving peptides. Anal Biochem. 2011; 414 (1): 38–46. DOI: 10.1016/j.ab.2011.02.009. Epub 2011 Mar 9. PMID: 21315060; PMCID: PMC3290000.

8. Wu X, Liu J, Zhang H, Zhou H, Wang W, Ma Y, et al. Immunomolecular assay based on selective virion capture by spike antibody and viral nucleic acid amplification for detecting intact SARS-CoV-2 particles. J Nanobiotechnology. 2022; 20 (1): 399. DOI: 10.1186/s12951-022-01558-8. PMID: 36064407; PMCID: PMC9444083.

9. Malou N, Raoult D. Immuno-PCR: a promising ultrasensitive diagnostic method to detect antigens and antibodies. Trends Microbiol. 2011; 19 (6): 295–302. DOI: 10.1016/j.tim.2011.03.004. PMID: 21478019.

10. Favorskaya IA, Shcheblyakov DV, Esmagambetov IB, Dolzhikova IV, Alekseeva IA, Korobkova AI, et al. Single-Domain Antibodies Efficiently Neutralize SARS-CoV-2 Variants of Concern. Front Immunol. 2022; 13: 822159. DOI: 10.3389/fimmu.2022.822159. PMID: 35281053; PMCID: PMC8907979.

11. Shah M, Woo HG. Omicron: A Heavily Mutated SARS-CoV-2 Variant Exhibits Stronger Binding to ACE2 and Potently Escapes Approved COVID-19 Therapeutic Antibodies. Front Immunol. 2022; 12: 830527. DOI: 10.3389/fimmu.2021.830527. PMID: 35140714; PMCID: PMC8819067.

12. Pochtovyi AA, Kustova DD, Siniavin AE, Dolzhikova IV, Shidlovskaya EV, Shpakova OG, et al. In Vitro Efficacy of Antivirals and Monoclonal Antibodies against SARS-CoV-2 Omicron Lineages XBB.1.9.1, XBB.1.9.3, XBB.1.5, XBB.1.16, XBB.2.4, BQ.1.1.45, CH.1.1, and CL.1. Vaccines (Basel). 2023; 11 (10): 1533. DOI: 10.3390/vaccines11101533. PMID: 37896937; PMCID: PMC10611309.

13. Calvaresi V, Wrobel AG, Toporowska J, Hammerschmid D, Doores KJ, Bradshaw RT, et al. Structural dynamics in the evolution of SARS-CoV-2 spike glycoprotein. Nat Commun. 2023; 14 (1): 1421. DOI: 10.1038/s41467-023-36745-0. PMID: 36918534; PMCID: PMC10013288.

14. Reuter N, Chen X, Kropff B, Peter AS, Britt WJ, Mach M, et al. SARS-CoV-2 Spike Protein Is Capable of Inducing Cell-Cell Fusions Independent from Its Receptor ACE2 and This Activity Can Be Impaired by Furin Inhibitors or a Subset of Monoclonal Antibodies. Viruses. 2023; 15 (7): 1500. DOI: 10.3390/v15071500. PMID: 37515187; PMCID: PMC10384293.

15. Chulanov VP, Shmakov RG, Lioznov DA, Abdulganieva DI, Valishin DA, Grabovsky VM, i dr. Rezoljucija Soveta jekspertov. Nejtralizujushhie monoklonal'nye antitela pri COVID-19 — mesto v terapii ujazvimyh kategorij bol'nyh. Infekcionnye bolezni. 2023; 21 (1): 152–61. DOI: 10.20953/1729-9225-2023-1-152-161. Russian.

16. Venkatesan G, Kushwaha A, Kumar A, Bora DP, Sasikumar P. An improved visual closed tube Loop mediated isothermal amplification (LAMP) assay for rapid identification of orf virus in sheep and goats. Vet Ital. 2022; 58 (2). DOI: 10.12834/VetIt.2426.15340.2. PMID: 36586114.

Литература

1. Butler JE, Ni L, Nessler R, Joshi KS, Suter M, Rosenberg B, et al. The physical and functional behavior of capture antibodies adsorbed on polystyrene. J Immunol Methods. 1992; 150 (1–2): 77–90. DOI: 10.1016/0022-1759(92)90066-3. PMID: 1613260.

2. Donald AM. The effect of temperature on crazing mechanisms in polystyrene. J Mater Sci. 1985; 20: 2630–8. DOI: 10.1007/BF00556095.
3. Sano T, Smith CL, Cantor CR. Immuno-PCR: very sensitive antigen detection by means of specific antibody-DNA conjugates. Science. 1992; 258 (5079): 120–2. DOI: 10.1126/science.1439758. PMID: 1439758.
4. Горшков А. С., Печенкин Д. В., Кузнецовский А. В., Балакин В. А. ПЦР-амплифицированный иммуноанализ (иммуно-ПЦР): принцип метода, варианты исполнения, возможности и перспективы использования для выявления патогенных биологических агентов. Вестник войск РХБ защиты. 2021; 5 (4): 366–75. Доступно по ссылке: https://doi.org/10.35825/2587-5728-2021-5-4-366-375.
5. Minich JJ, Sanders JG, Amir A, Humphrey G, Gilbert JA, Knight R. Quantifying and Understanding Well-to-Well Contamination in Microbiome Research. mSystems. 2019; 4 (4): e00186–19. DOI: 10.1128/mSystems.00186-19. PMID: 31239396; PMCID: PMC6593221.
6. Lou YC, Hoff J, Olm MR, West-Roberts J, Diamond S, Firek BA, et al. Using strain-resolved analysis to identify contamination in metagenomics data. Microbiome. 2023; 11 (1): 36. DOI: 10.1186/s40168-023-01477-2. PMID: 36864482; PMCID: PMC9979413.
7. Goebel-Stengel M, Stengel A, Taché Y, Reeve JR Jr. The importance of using the optimal plasticware and glassware in studies involving peptides. Anal Biochem. 2011; 414 (1): 38–46. DOI: 10.1016/j.ab.2011.02.009. Epub 2011 Mar 9. PMID: 21315060; PMCID: PMC3290000.
8. Wu X, Liu J, Zhang H, Zhou H, Wang W, Ma Y, et al. Immunomolecular assay based on selective virion capture by spike antibody and viral nucleic acid amplification for detecting intact SARS-CoV-2 particles. J Nanobiotechnology. 2022; 20 (1): 399. DOI: 10.1186/s12951-022-01558-8. PMID: 36064407; PMCID: PMC9444083.
9. Malou N, Raoult D. Immuno-PCR: a promising ultrasensitive diagnostic method to detect antigens and antibodies. Trends Microbiol. 2011; 19 (6): 295–302. DOI: 10.1016/j.tim.2011.03.004. PMID: 21478019.
10. Favorskaya IA, Shcheblyakov DV, Esmagambetov IB, Dolzhikova IV, Alekseeva IA, Korobkova AI, et al. Single-Domain Antibodies Efficiently Neutralize SARS-CoV-2 Variants of Concern. Front Immunol. 2022; 13: 822159. DOI: 10.3389/fimmu.2022.822159. PMID: 35281053; PMCID: PMC8907979.
11. Shah M, Woo HG. Omicron: A Heavily Mutated SARS-CoV-2 Variant Exhibits Stronger Binding to ACE2 and Potently Escapes Approved COVID-19 Therapeutic Antibodies. Front Immunol. 2022; 12: 830527. DOI: 10.3389/fimmu.2021.830527. PMID: 35140714; PMCID: PMC8819067.
12. Pochtovyi AA, Kustova DD, Siniavin AE, Dolzhikova IV, Shpakova OG, et al. In Vitro Efficacy of Antivirals and Monoclonal Antibodies against SARS-CoV-2 Omicron Lineages XBB.1.9.1, XBB.1.9.3, XBB.1.5, XBB.1.16, XBB.2.4, BQ.1.1.45, CH.1.1, and CL.1. Vaccines (Basel). 2023; 11 (10): 1533. DOI: 10.3390/vaccines11101533. PMID: 37896937; PMCID: PMC10611309.
13. Calvaresi V, Wrobel AG, Toporowska J, Hammerschmid D, Doores KJ, Bradshaw RT, et al. Structural dynamics in the evolution of SARS-CoV-2 spike glycoprotein. Nat Commun. 2023; 14 (1): 1421. DOI: 10.1038/s41467-023-36745-0. PMID: 36918534; PMCID: PMC10013288.
14. Reuter N, Chen X, Kropff B, Peter AS, Britt WJ, Mach M, et al. SARS-CoV-2 Spike Protein Is Capable of Inducing Cell-Cell Fusions Independent from Its Receptor ACE2 and This Activity Can Be Impaired by Furin Inhibitors or a Subset of Monoclonal Antibodies. Viruses. 2023; 15 (7): 1500. DOI: 10.3390/v15071500. PMID: 37515187; PMCID: PMC10384293.
15. Чуланов В. П., Шмаков Р. Г., Лиознов Д. А., Абдулганиева Д. И., Валишин Д. А., Грабовский В. М., и др. Резолюция Совета экспертов. Нейтрализующие моноклональные антитела при COVID-19 — место в терапии уязвимых категорий больных. Инфекционные болезни. 2023; 21 (1): 152–61. DOI: 10.20953/1729-9225-2023-1-152-161.
16. Venkatesan G, Kushwaha A, Kumar A, Bora DP, Sasikumar P. An improved visual closed tube Loop mediated isothermal amplification (LAMP) assay for rapid identification of orf virus in sheep and goats. Vet Ital. 2022; 58 (2). DOI: 10.12834/VetIt.2426.15340.2. PMID: 36586114.

T-CELL RECEPTOR CHAIN CENTRICITY IN THE PRIMARILY ACTIVATED EFFECTORS AND RE-STIMULATED MEMORY CELLS

Kalinina AA[1], Kubekina MV[2], Persiyantseva NA[1], Bruter AV[1,2], Khromykh LM[1], Kazansky DB[1]✉

[1] Blokhin National Medical Research Center of Oncology, Moscow, Russia
[2] Center for Precision Genome Editing and Genetic Technologies for Biomedicine, Institute of Gene Biology, Moscow, Russia

T cells, the adaptive immunity effectors, carry an antigen-recognizing T-cell receptor (TCR) that represents an αβ heterodimer. Functional dominance of one chain has been reported for a number of TCRs. This feature is called chain centricity. Today, it is unclear whether chain centricity is an inherent feature of some TCRs, and what mechanism underlies its development. The study aimed to determine the abundance of such receptors in the repertoire of primarily activated effectors and re-stimulated memory cells of mice specific to the allogeneic tumor antigens. The long-lived memory cells formed in the primary immune response *in vivo* were *in vitro* re-stimulated with the immunizing tumor cells. Primary effectors were obtained *in vitro* in the culture by stimulation of T cells of non-immunized mice with cells of the same allogeneic tumor. TCR libraries of effectors involved in the primary and secondary immune response were created by NGS sequencing. To identify chain-centric TCRs, 10 TCRα variants were selected from each repertoire. T cells of intact mice were modified with individual TCR α-chain variants by transduction, with subsequent assessment of T cell proliferation under exposure to specific allogeneic stimulators. *In vitro* screening revealed 10% of chain-centric receptors in the primary effector pool, and the proportion of such TCRs in the repertoire of re-activated memory cells was 30%. Thus, chain centricity is an inherent property of some TCRs, but secondary antigenic stimulation can be a factor for selection of clonotypes with such receptors.

Keywords: T-cell receptor, chain centricity, dominant-active α-chain, primarily activated effectors, memory T cells

ЦЕПЕЦЕНТРИЧНОСТЬ Т-КЛЕТОЧНЫХ РЕЦЕПТОРОВ У ПЕРВИЧНО АКТИВИРОВАННЫХ ЭФФЕКТОРОВ И РЕСТИМУЛИРОВАННЫХ КЛЕТОК ПАМЯТИ

А. А. Калинина[1], М. В. Кубекина[2], Н. А. Персиянцева[1], А. В. Брутер[1,2], Л. М. Хромых[1], Д. Б. Казанский[1]✉

[1] Национальный медицинский исследовательский центр онкологии имени Н. Н. Блохина, Москва, Россия
[2] Центр высокоточного редактирования и генетических технологий для биомедицины, Институт биологии гена, Москва, Россия

Т-клетки, эффекторы адаптивного иммунитета, оснащены антигенраспознающим Т-клеточным рецептором (ТКР), который представляет собой αβ-гетеродимер. Для ряда ТКР было показано функциональное доминирование одной цепи, и эта особенность рецептора получила название цепецентричности. В настоящее время неизвестно, является ли цепецентричность врожденным свойством некоторых ТКР и каков механизм ее формирования. Целью работы было установить частоту встречаемости подобных рецепторов в репертуаре эффекторов и рестимулированных клеток памяти мыши, специфичных к антигенам аллогенной опухоли. Сформированные в ходе первичного иммунного ответа *in vivo* долгоживущие клетки памяти рестимулировали клетками иммунизирующей опухоли *in vitro*. Первичные эффекторы получали в культуре *in vitro* путем стимуляции Т-клеток неиммунизированных мышей клетками этой же аллогенной опухоли. Методом NGS-секвенирования были созданы библиотеки ТКР эффекторов, вовлеченных в первичный и вторичный иммунный ответ. Для идентификации цепецентрических рецепторов были отобраны по 10 вариантов ТКРα из каждого репертуара. Путем трансдукции Т-клетки интактных мышей модифицировали индивидуальными вариантами α-цепей ТКР с последующей оценкой уровня их пролиферации в присутствии специфических аллогенных стимуляторов. В ходе скрининга *in vitro* выявлено 10% цепецентрических рецепторов в пуле первичных эффекторов, при этом доля таких ТКР в репертуаре реактивированных клеток памяти составила 30%. Таким образом, цепецентричность является исходно присущим свойством некоторых ТКР, но вторичная антигенная стимуляция может быть фактором селекции клонотипов с такими рецепторами.

Ключевые слова: Т-клеточный рецептор, цепецентричность, доминантно-активная α-цепь, первично активированные эффекторы, Т-клетки памяти

T cells are the most important adaptive immunity effectors. To ensure realization of their functions, T cells carry an antigen-recognizing T-cell receptor (TCR) involved in recognition of peptide antigens represented by self-major histocompatibility complex (MHC) molecules. TCR is a heterodimer, which consists of α- and β-chains in the predominant type of T cells. According to the classic paradigm, both TCR chains contribute equally to recognition of MHC/peptide complexes. However, it has been reported for a number of TCRs that α- or β-chain can predominate during interaction with antigen and determine the specificity of the entire receptor [1]. About a decade ago the term "TCR chain centricity" was introduced to describe this phenomenon, and TCRs showing asymmetric functional activity of the chains were named chain-centric receptors [2, 3]. This property of some TCRs can significantly simplify and increase the effectiveness of generating therapeutic T-cell products for immunotherapy of infectious diseases and cancer [1, 4].

Today, it is unclear whether chain centricity is an inherent feature of some TCRs, and what mechanism underlies its development. In the majority of studies, chain-centric TCRs were identified in the human or mouse immune repertoire [2, 3, 5–7], which may suggest that these receptors are expressed mainly by antigen-primed T cells. It has previously been shown that the naturally occurring pool of mouse memory T cells contains about 20% of chain-centric receptors [4], but their proportion in the repertoire of effectors involved in the primary immune response is still poorly understood. Clarification of this issue will help determine the important aspects of the chain-centric TCR nature: 1) whether chain centricity is an inherent property of some receptors; 2) what is the role of antigenic stimulation in the formation or selection of such TCRs.

The study aimed to determine the abundance of TCRs with the dominant-active α-chain in the repertoire of primarily activated effectors and re-stimulated memory cells of mice.

METHODS

The study involved inbred C57BL/6 (haplotype H2-K^b) female mice (body weight 18–20 g, age 6–8 weeks) obtained from the experimental biology laboratory of the Research Institute of Experimental Diagnostics and Therapy of Tumors (Blokhin National Medical Research Center of Oncology, Moscow, Russia). Animals were kept under standard conditions (20–24 °C, a 40% relative humidity, a 12-h light/dark cycle) and withdrawn from the experiment by cervical dislocation. To generate memory cells *in vivo*, nine C57BL/6 mice were immunized with P815 allogeneic mastocytoma cells (K^{d}D^d) via a single intraperitoneal injection of 1×10^7 tumor cells/mouse. Two months after immunization [8] the animals were withdrawn from the experiment as stated above, and the spleen was isolated under sterile conditions. Cells of the spleen were squeezed out carefully from the splenic stroma in the Potter homogenizer (DWK Life Sciences; Germany) in 3 mL of PBS. Then cytometry analysis of splenocytes was carried out in the FACScantoII system (BD; USA) using fluorescent labeled antibodies (BioLegend; USA) to T-cell surface markers: CD3-PE, CD8-Pacific blue, CD44-APC, and CD62L-APC-Cy7. Cell debris was excluded from analysis based on the light scattering values and propidium iodide (BD; USA) incorporation. The percentage of T cells (%) in the total population of live splenic leukocytes was determined based on the CD3 marker expression. The relative number (%) of cytotoxic CD8$^+$ T cells was assessed in the CD3$^+$ lymphocyte pool. The long-lived CD8$^+$ memory T cells generated *in vivo* after immunization were determined

based on co-expression of CD44 and CD62L markers (Fig. 1). Splenic cells of the P815-immunized mice were re-stimulated with the immunizing tumor antigens *in vitro* without pre-sorting [9]. For that splenocytes (4×10^5 cells/well) were seeded in triplets into 96-well round bottom plates (Corning Costar, Sigma Aldrich; USA). P815 mastocytoma cells were treated with cytostatic mitomycin C (Kyowa Hakko Kogyo Co., Ltd.; Japan) in a dose of 50 µg/mL for 60 min at 37 °C and added to splenocytes at a ratio of 1 : 10. Cells were cultured in 200 µL of the RPMI-1640 medium (PanEco; Russia) enriched with 10% fetal bovine serum (HyClone, GE Healthcare; USA), 0.01 mg/mL of ciprofloxacin (KRKA; Slovenia) and 10 µM of 2-mercaptoethanol (Merck; Germany) for 72 h at 37 °C, 5% CO$_2$. To induce primarily activated CD8$^+$ effectors, splenic cells of six intact (not immunized with mastocytoma P815) C57BL/6 mice were *in vitro* cultured with P815 cells for 72 h, as described above. To assess baseline proliferation, splenic cells of intact and immunized mice were similarly cultured without P815. Cell proliferation (counts per minute) in the splenocyte culture was measured based on incorporation of ^{3}H-thymidine (1 µCi/well) (Isotope; Russia) added for the last 8 h of cultivation. The antigen-induced response index was calculated as the ratio of splenocyte proliferation under exposure to P815 and corresponding baseline proliferation (Fig. 2).

The primarily activated effectors and re-stimulated memory cells obtained as described above from one intact (non-immunized) and one immunized mouse, respectively, were used to create the TCR cDNA libraries by NGS sequences on the MiSeq platform (Illumina; USA) [9].

The full-length cDNA of the TCR α-chain from each repertoire was cloned into the MigRI retroviral vector containing the PGK promoter [4]. Transfection of the HEK293T packaging cell line was performed using the calcium phosphate method. To obtain T cells transduced with an individual TCRα variant, preliminary activation of T cells of intact (non-immunized) mice was performed. For that animals were euthanized by cervical dislocation; the spleen and mesenteric lymph nodes were recovered under sterile conditions, and cells were isolated from these organs as described above. The cells obtained were then *in vitro* activated with the T-cell mitogen, concanavalin A (3 µg/mL) (Sigma Aldrich; USA), for 24 h and transduced by two spinoculations with the retroviruses containing an individual TCRα variant at 2000 × g for 2 h (22 °C) [10]. The lymphocyte modification levels were determined 48 h later by flow cytometry based on the GFP reporter protein expression measured in the control sample of T cells similarly transduced with the GFP retrovirus [10]. The transduction efficacy was 40–70% (data not shown).

T cells (1×10^5 cells/well) were seeded in triplets into the 96-well flat-bottom plates (Corning Costar, Sigma Aldrich; USA) 48 h after transduction. Cells of the EL-4 lymphoma syngeneic for C57BL/6 mice and of the immunizing mastocytoma P815 were treated with mitomycin C. To determine proliferation levels of modified T cells under exposure to syngeneic stimulators, EL-4 cells treated with the cytostatic were added to T cells at a ratio of 1 : 2. To assess specific antigen-induced proliferation, modified T cells were co-cultured with P815 cells treated with mitomycin C. Cells were cultured in 200 µL of the RPMI-1640 medium (PanEco; Russia) enriched as described above for 72 h at 37 °C, 5% CO$_2$. The non-transduced lymphocytes (NTLs) and GFP-modified T cells were used as controls. To assess baseline proliferation, T cells (NTLs, TCRα- and GFP-transduced) were similarly cultured without tumor cells. Cell proliferation levels were assessed using the CellTiter 96 AQueous Non-Radioactive Cell Proliferation Assay kit (Promega; USA) in accordance with
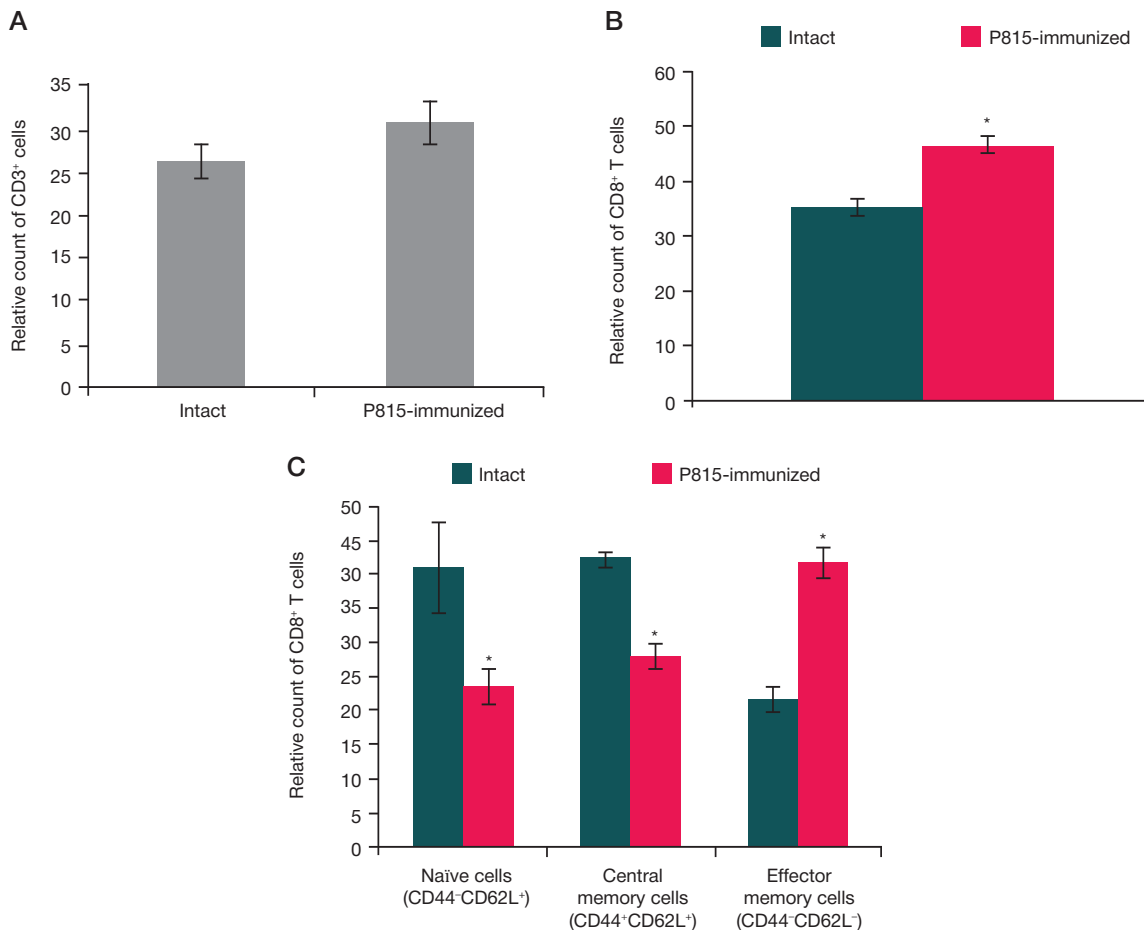
Fig. 1. Analysis of mouse splenic T cells after *in vivo* immunization with the allogeneic tumor cells. C57BL/6 mice (*n* = 9) were immunized intraperitoneally with allogeneic mastocytoma P815 cells. Spleen cells were analyzed by flow cytometry 2 months after immunization. Splenocytes of intact (not immunized with P815) C57BL/6 mice (*n* = 6) were used as a control. **A**) The relative count (%) of T cells (CD3+). **B**) The percentage (%) of cytotoxic CD8+ T cells. **C**) The percentage (%) of CD8+ T cells with the phenotype of naïve cells (CD44−CD62L+), central memory cells (CD44+CD62L+), and effector memory cells (CD44+CD62L−). The data are presented as m ± SEM (*n* = 6–9). *$p \leq 0.05$ compared to the intact control (Student's *t*-test)

the manufacturer's instructions. Optical density (OD) was measured using the Infinite F50 microplate spectrophotometer (Tecan; Switzerland). *In vitro* screening of each TCRα variant was conducted in at least two independent experiments.

Fig. 1 and 2 present the data of three independent experiments as mean ± standard error of the mean (mean ± SEM) (*n* = 6–9). Fig. 3 presents frequencies of unique TCRα clonotypes in each studied repertoire. Fig. 4 presents the data of one of the two representative experiments as mean ± SEM for three technical replicates. Statistical analysis was performed using the unpaired Student's t-test after testing the sample distribution for normality using the Kolmogorov–Smirnov test. The differences were considered significant at *p* < 0.05. Statistical analysis was performed using the Prism v.8.1.2 software (GraphPad; USA).

RESULTS

In this study, the experimental model of generating long-lived memory T cells was used involving *in vivo* immunization of C57BL/6 mice (H2-Kb) with P815 allogeneic mastocytoma cells (KdDd). Due to allogeneic differences in MHC class I molecules, the recipient develops predominantly CD8+ T-cell response to the transplanted tumor. No increase in the relative number of T cells in the spleen of immunized animals compared to intact mice was reported (Fig. 1A), however, the proportion of CD8+ T cells after immunization was significantly higher relative to the control (Fig. 1B). Furthermore, in the spleen of immunized mice, accumulation of CD8+ T cells with the phenotype of effector

memory cells (CD44+CD62L−) was reported, the percentage of which increased 1.9-fold relative to the same population of CD8+ T cells in the spleen of intact mice (Fig. 1C). The data obtained suggest that a pool of long-lived CD8+ memory cells is formed *in vivo* after contraction of primary immune response.

Considering the fact that the T cell surface activation phenotype is not directly correlated with the T cell experience of interaction with antigen and its functional status [11], splenic lymphocytes of the immunized mice were re-stimulated with the immunizing tumor antigens *in vitro* in order to confirm generation of true memory T cells during *in vivo* immunization. Primary proliferative response of splenocytes of intact mice was obtained *in vitro* in the culture with P815 allogeneic mastocytoma cells, which was twice higher compared to baseline proliferation values (Fig. 2). Furthermore, the antigen-induced proliferation level of splenocytes from the immunized animals was three times higher compared to that in the cell culture of intact mice (Fig. 2). Thus, the *in vitro* functional test showed the primary immune response to the allogeneic tumor cells and the enhanced secondary response of memory T cells.

This experimental system was used to generate effectors of the primary and secondary immune response to the allogeneic tumor cells and construct libraries of their TCR α-chains (TCRα). To identify TCRα clonotypes involved in the immune response to the P815 antigens, the repertoires of primarily activated effectors and re-stimulated memory cells were compared to the TCRα repertoires of non-immunized mice and immunized mice without antigenic stimulation *in vitro*, respectively. TCRα
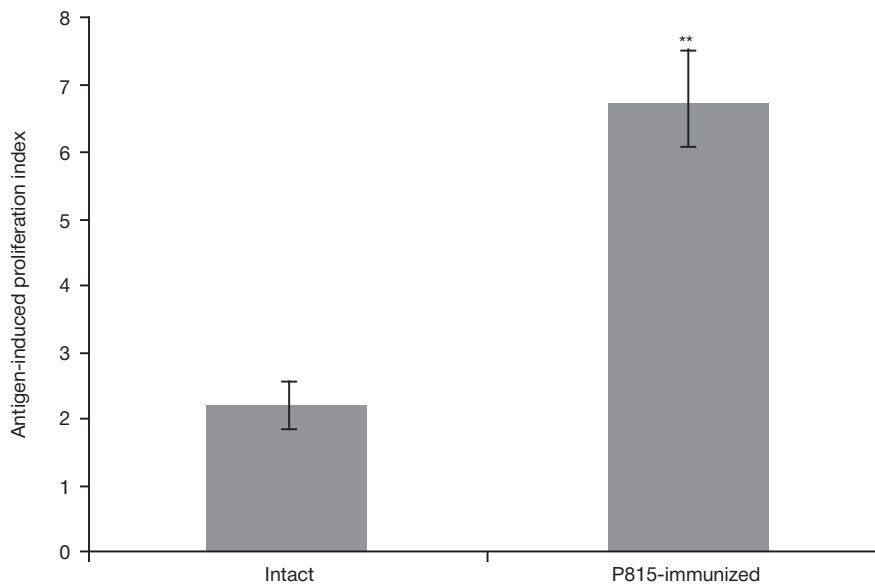
Fig. 2. Levels of antigen-induced proliferation *in vitro* of T-cells in the primary and secondary immune responses to the allogeneic tumor cells. Splenic cells of intact (not immunized with P815) and P815-immunized C57BL/6 mice were cultured in the presence of allogeneic mastocytoma P815 for 72 h. Splenocytes similarly cultured without antigenic stimulation were used to assess baseline proliferation. The index of antigen-induced proliferative response to alloantigens was calculated as described in the Methods section. The data are presented as m ± SEM (*n* = 6–9). **$p \leq 0.01$ (Student's *t*-test)

variants, the frequency of which after stimulation was at least three times higher compared to frequency of the same clonotype in the corresponding repertoire without antigenic stimulation, were determined in each library [9]. A total of 10 TCRα variants unique for the repertoire of primarily activated effectors or re-stimulated memory cells were selected for further research (Fig. 3).

The dominant-active TCRα were identified in an *in vitro* test system. For that T cells of the intact mice modified with each TCRα variant were introduced to the culture with syngeneic stimulators (EL-4 cells) or specific allogeneic stimulators (P815 cells) (Fig. 4). The appropriate α-chain was considered to be dominant-active, when the proliferation level of transduced lymphocytes under exposure to P815 was significantly higher, than the proliferation level of the same cells not subjected to antigenic stimulation (baseline), in the presence of EL-4 (stimulation with the syngeneic tumor), or when it was significantly higher, than the values of antigen-induced proliferation of NTLs and GFP-modified T cells (Fig. 4).

The screening revealed one dominant-active TCRα from the repertoire of primarily activated effectors (#3; Fig. 4A): the level of proliferative response of T cells modified with the α-chain TCR #3 in the presence of the specific allogeneic stimulator (P815 cells) was 1.3-fold ($p < 0.05$) higher, than the level of their proliferation in the culture with syngeneic stimulators (EL-4 cells). Three dominant-active TCRα variants were identified in the repertoire of re-activated memory cells: T cells transduced with TCRα #2, TCRα #5, and TCRα #9 had significantly 1.3-fold increased ($p < 0.05$) proliferation activity under specific antigenic stimulation with P815 cells compared to their proliferation in the presence of syngeneic EL-4 cells (Fig. 4B).

Thus, the study has shown that the primarily activated effector repertoire comprises 10% of chain-centric TCRs, while the proportion of such receptors in the repertoire of re-stimulated memory cells is 30%. This preliminary assessment is currently being refined with additional data.

In vitro screening also revealed distinct variants of TCR α-chains (#9 in the primarily activated effector repertoire (Fig. 4A) and #1 in the repertoire of re-stimulated memory T cells (Fig. 4B)), modification with which resulted in enhanced T cell proliferation in the presence of syngeneic EL-4. This may be explained by the generation of a receptor with the new specificity as a result of the interaction of the transduced α–chain with an endogenous TCR β-chain in a mature T cell.

DISCUSSION

Using the previously developed experimental model we traced sequential changes in the mouse TCR repertoire during the immune response to tumor alloantigens, from the primary response to immunological memory formation and induction of the secondary memory cell response [8, 9]. The data obtained have shown that both primarily activated effectors and re-stimulated memory T cells express TCRs with the dominant-active α-chain. Based on this finding, it can be assumed that chain centricity is an inherent property of some TCRs.

An interesting analogy for this phenomenon can be found in the paper by Dietrich et al. reporting the study of the pre-immune repertoire of T cells specific for the melanoma-associated autoantigen melan-A. It has been shown that melan-A-specific thymocytes and mature peripheral T cells preferentially use a particular V segment of the α-chain (Vα 2.1) [12]. Thus, narrowing of the repertoire in favor of using this α-chain variant occurs during intrathymic selection of melan-A-specific T cells, although the fact that they preferentially use this TCRα variant does not indicate the α-chain functional dominance. We believe that the reasons for this phenomenon can include the possibility of repeated rearrangements of the TCR α-chain genes during positive selection in the thymus, resulting in the selection of their variants capable of establishing multiple contacts with the endogenous MHC/peptide complexes and, therefore, of more effective positive selection.

It should be noted that in our experiments the proportion of chain-centric receptors in the repertoire of re-activated memory cells was higher (30% vs. 10% in the primarily activated effector repertoire), which can suggest selection of the TCR clonotypes with the dominant-active α-chains during secondary specific antigenic stimulation. Bioinformatics analysis of the entire TCR repertoire of these two functional groups has shown that physicochemical characteristics of TCRα in the pool of re-activated memory cells markedly differed from the properties of the TCR α-chains of effectors involved in the primary immune

A

B
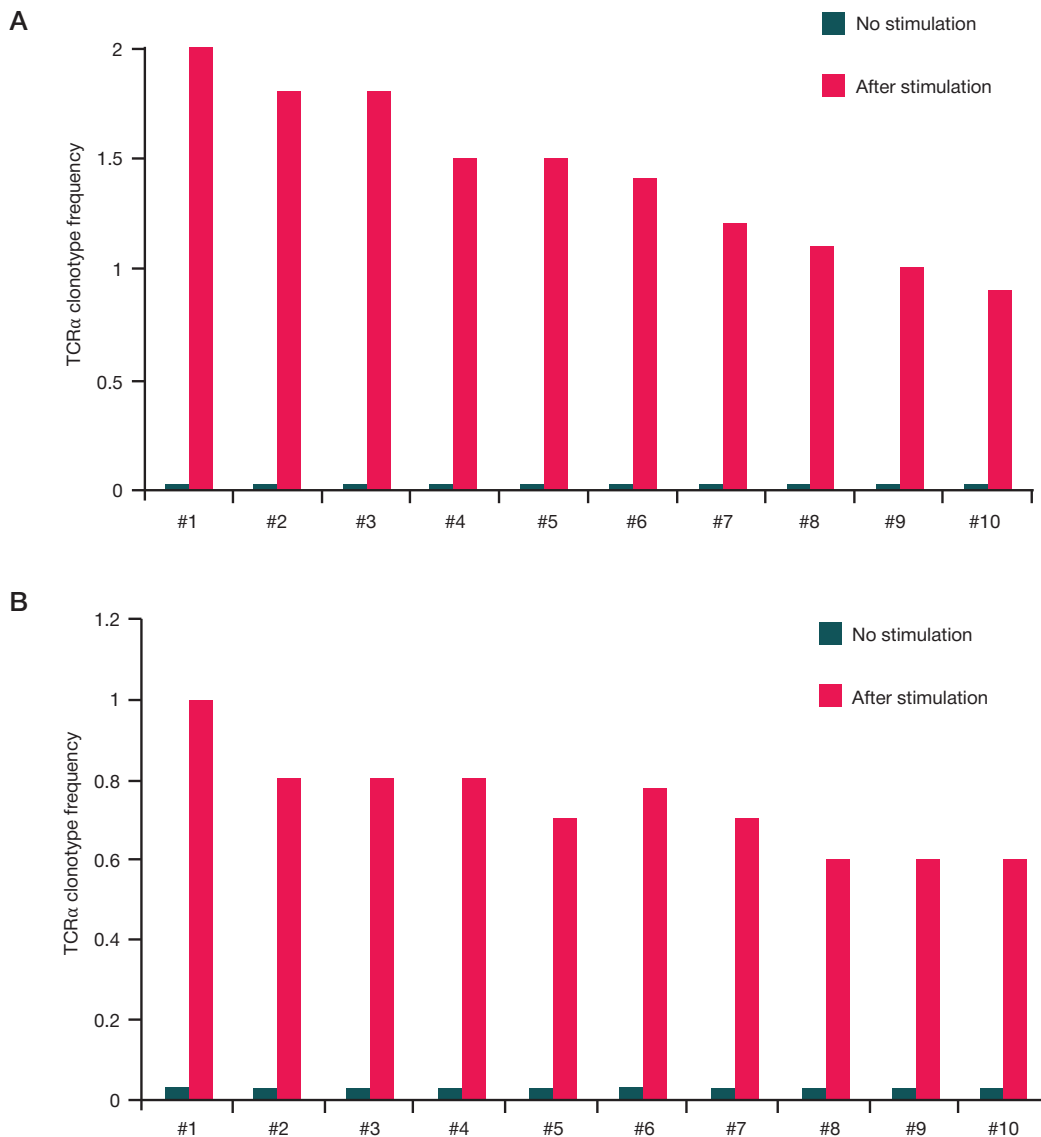
Fig. 3. T-cell receptor α-chain variants selected for *in vitro* screening. Frequency of the T-cell receptor α-chain clonotype in the repertoire of effectors involved in the primary immune response **(A)** and of re-stimulated memory T cells **(B)**

response [9]. According to the data obtained, in the secondary response, the TCR repertoire is enriched with receptors containing the α-chain with the increased strength of binding to the MHC/peptide complexes and cross-reactivity [9].

It is well known that TCRs of memory cells have the increased affinity for antigen [13, 14]. The results of our studies suggest that this can be also associated with the expression of the dominant-active TCRα. Thus, selection of chain-centric TCRs can represent one of the mechanisms underlying maturation of functional avidity of antigen-primed T cells [15–17].

In the light of the currently available data, we believe that the functionally true memory T cells can be the most promising source of therapeutic TCRs. It has been previously shown in the *in vivo* experimental models that the dominant-active α-chains of the memory cell chain-centric TCRs can be successfully used to generate T-cell products for adoptive immunotherapy of cancer and infectious diseases [4, 7].

The *in vitro* screening system described in this study can be also used to assess possible autoreactivity of modified T cells. During transduction of an individual TCR α-chain into T cells, the α-chain binds to endogenously rearranged β-chains, and this can result in the generation of receptors with new specificity, including potentially autoreactive TCR. Thus,

in our study we have revealed increased proliferative activity of T cells modified with two TCRα variants in the presence of syngeneic stimulators (Fig. 4A, #9; Fig. 4B, #1). However, determination of autoreactivity of these transduced T cells was outside the scope of this study. Meanwhile, we have earlier shown that T cells modified with the dominant-active TCRα do not show nonspecific cytotoxicity when adoptively transferred into syngeneic recipients, which confirms the lack or low rate of potentially autoreactive clones in the resulting T cell product [18].

CONCLUSIONS

In this study we developed an *in vitro* system for screening of mouse chain-centric TCRs. Using this system, the dominant-active antigen-specific α-chains were identified both in the repertoire of effectors involved in the primary immune response and in the repertoire of memory cells after the secondary specific antigenic stimulation. The study results have shown that 10% of the TCRs of primarily activated effectors are chain centric. Thus, this property is inherent to some T-cell receptors. Furthermore, in the secondary immune response, the proportion of such receptors increases 3-fold, which suggests that the repertoire is enriched with chain-centric TCRs due to antigen-induced
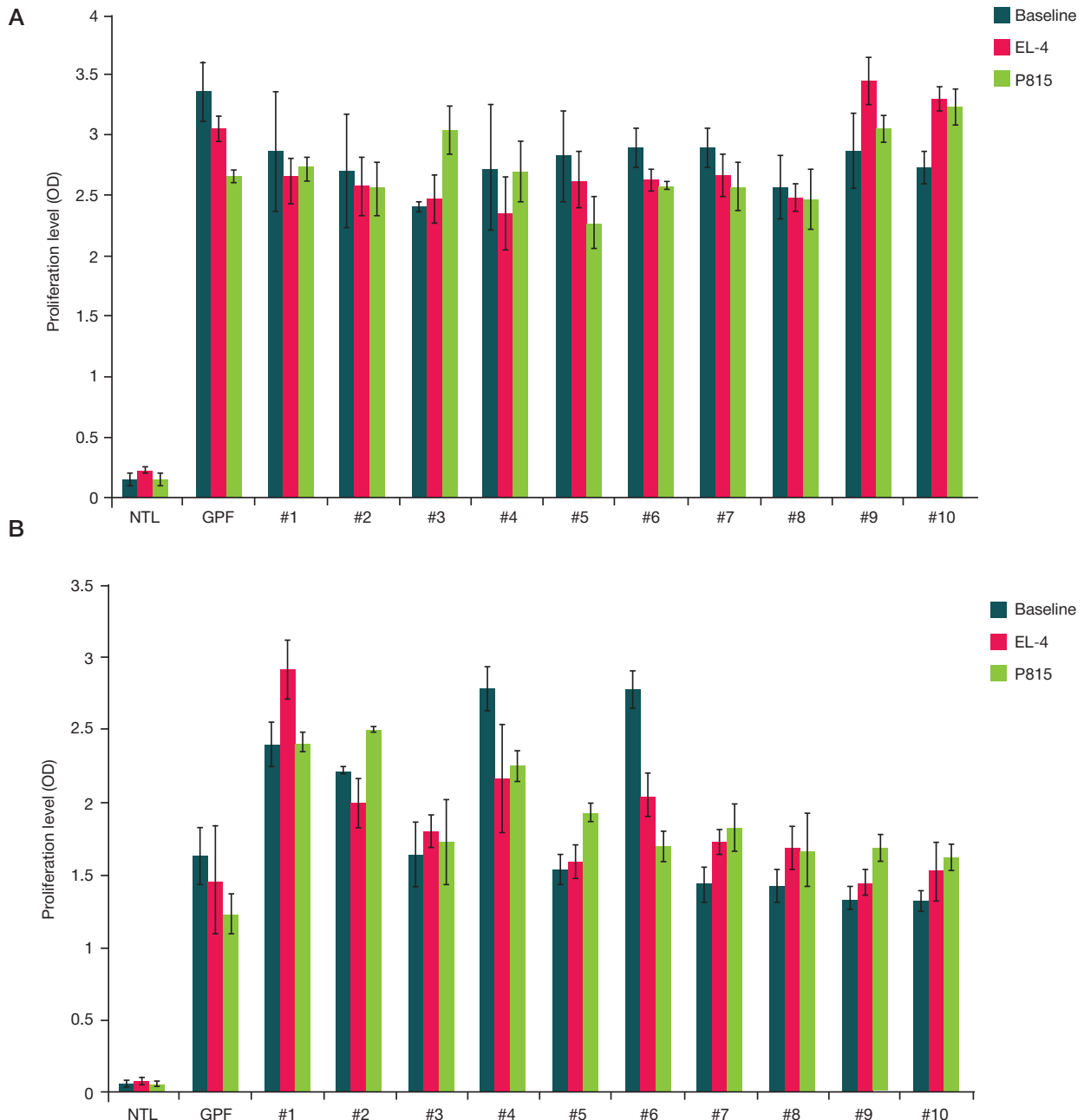
Fig. 4. *In vitro* antigen-induced proliferation levels of T cells transduced with individual T-cell receptor (TCR) α-chain variants. Activated T cells of an intact C57BL/6 mouse were transduced with the TCR α-chains from the repertoire of primarily activated effectors **(A)** or re-stimulated memory cells **(B)**. Modified lymphocytes were placed in the culture with syngeneic stimulators (EL-4 lymphoma cells) or allogeneic specific stimulators (P815 mastocytoma cells) for 72 h. To assess baseline proliferation levels, transduced T cells were cultured without tumor cells (baseline). Non-transduced activated lymphocytes (NTLs) and GFP-modified T cells were used as controls. The data of one representative experiment out of two are presented as m ± SEM for three technical replicates. *$p \leq 0.05$ (Student's *t*-test)

selection of clonotypes with such receptors. The findings will help to improve the process of identifying and selecting chain-centric antigen-specific TCRs, which are a promising source of therapeutic receptors for adoptive immunotherapy.

References

1. Kalinina AA, Khromykh LM, Kazansky DB. T Cell Receptor Chain Centricity: The Phenomenon and Potential Applications in Cancer Immunotherapy. Int J Mol Sci. 2023; 24: 15211.
2. Ochi T, Nakatsugawa M, Chamoto K, Tanaka S, Yamashita Y, Guo T, et al. Optimization of T-cell Reactivity by Exploiting TCR Chain Centricity for the Purpose of Safe and Effective Antitumor TCR Gene Therapy. Cancer Immunol Res. 2015; 3: 1070–81.
3. Nakatsugawa M, Yamashita Y, Ochi T, Tanaka S, Chamoto K, Guo T, et al. Specific roles of each TCR hemichain in generating functional chain-centric TCR. J Immunol. 2015; 194: 3487–500.
4. Kalinina AA, Nesterenko LN, Bruter AV, Balunets DV, Chudakov DM, Izraelson M, et al. Adoptive Immunotherapy Based on Chain-Centric TCRs in Treatment of Infectious Diseases. iScience. 2020; 23 (12): 101854.
5. Brändle D, Brduscha-Riem K, Hayday AC, Owen MJ, Hengartner H, Pircher H. T cell development and repertoire of mice expressing a single T cell receptor alpha chain. Eur J Immunol. 1995; 25: 2650–5.
6. Mori L, Loetscher H, Kakimoto K, Bluethmann H, Steinmetz M.

Expression of a transgenic T cell receptor beta chain enhances collagen-induced arthritis. J Exp Med. 1992; 176: 381–88.

7. Zamkova MA, Kalinina AA, Silaeva YY, Persiyantseva NA, Bruter AV, Deikin AV, et al. Dominant role of the α-chain in rejection of tumor cells bearing a specific alloantigen inTCR transgenic mice and in in vitro experiments. Oncotarget. 2019; 10: 4808–21.

8. Grinenko TS, Pobezinskaya EL, Pobezinskii LA, Baturina IA, Zvezdova ES, Kazanskii DB. Suppression of primary allogenic response by CD8+ memory cells. Bull Exp Biol Med. 2005; 140 (5): 545–9.

9. Kalinina AA, Persiyantseva NA, Britanova OV, Lupyr K, Shagina I, Khromykh LM et al. Unique features of the TCR repertoire of reactivated memory T cells in the experimental mouse tumor model. Comput Struct Biotechnol J. 2023; 21: 3196–209.

10. Kalinina A, Bruter A, Nesterenko L, Khromykh L, Kazansky D. Generation of TCRα-transduced T cells for adoptive transfer therapy of salmonellosis in mice. STAR Protoc. 2021; 2 (1): 100368.

11. Kalinina AA, Khromykh LM, Kazansky DB, Deykin AV, Silaeva YY. Suppression of the immune response by syngeneic splenocytes adoptively transferred to sublethally irradiated mice. Acta Nat. 2021; 13 (1): 116–26.

12. Dietrich PY, Le Gal FA, Dutoit V, Pittet MJ, Trautman L, Zippelius A,

et al. Prevalent role of TCR alpha-chain in the selection of the preimmune repertoire specific for a human tumor-associated self-antigen. J Immunol. 2003; 170: 5103–9.

13. Hebeisen M, Allard M, Gannon PO, Schmidt J, Speiser DE, Rufer N. Identifying individual T cell receptors of optimal avidity for tumor antigens. Front Immunol. 2015; 6: 582.

14. Mondino A, Manzo T. To remember or to forget: the role of good and bad memories in adoptive T cell therapy for tumors. Front Immunol. 2020; 11: 1915.

15. von Essen MR, Kongsbak M, Geisler C. Mechanisms behind functional avidity maturation in T cells. Clin Dev Immunol. 2012; 2012: 163453.

16. Gilfillan CB, Hebeisen M, Rufer N, Speiser DE. Constant regulation for stable CD8 T-cell functional avidity and its possible implications for cancer immunotherapy. Eur J Immunol. 2021; 51 (6): 1348–60.

17. Campillo-Davo D, Flumens D, Lion E. The quest for the best: how TCR affinity, avidity, and functional avidity affect TCR-engineered T-cell antitumor responses. Cells. 2020; 9(7): 1720.

18. Kalinina A, Bruter A, Persiyantseva N, Silaeva Y, Zamkova M, Khromykh L et al. Safety evaluation of the mouse TCRα -transduced T cell product in preclinical models in vivo and in vitro. Biomed Pharmacother. 2022; 145: 112480.

Литература

1. Kalinina AA, Khromykh LM, Kazansky DB. T Cell Receptor Chain Centricity: The Phenomenon and Potential Applications in Cancer Immunotherapy. Int J Mol Sci. 2023; 24: 15211.

2. Ochi T, Nakatsugawa M, Chamoto K, Tanaka S, Yamashita Y, Guo T, et al. Optimization of T-cell Reactivity by Exploiting TCR Chain Centricity for the Purpose of Safe and Effective Antitumor TCR Gene Therapy. Cancer Immunol Res. 2015; 3: 1070–81.

3. Nakatsugawa M, Yamashita Y, Ochi T, Tanaka S, Chamoto K, Guo T, et al. Specific roles of each TCR hemichain in generating functional chain-centric TCR. J Immunol. 2015; 194: 3487–500.

4. Kalinina AA, Nesterenko LN, Bruter AV, Balunets DV, Chudakov DM, Izraelson M, et al. Adoptive Immunotherapy Based on Chain-Centric TCRs in Treatment of Infectious Diseases. iScience. 2020; 23 (12): 101854.

5. Brändle D, Brduscha-Riem K, Hayday AC, Owen MJ, Hengartner H, Pircher H. T cell development and repertoire of mice expressing a single T cell receptor alpha chain. Eur J Immunol. 1995; 25: 2650–5.

6. Mori L, Loetscher H, Kakimoto K, Bluethmann H, Steinmetz M. Expression of a transgenic T cell receptor beta chain enhances collagen-induced arthritis. J Exp Med. 1992; 176: 381–88.

7. Zamkova MA, Kalinina AA, Silaeva YY, Persiyantseva NA, Bruter AV, Deikin AV, et al. Dominant role of the α-chain in rejection of tumor cells bearing a specific alloantigen inTCR transgenic mice and in in vitro experiments. Oncotarget. 2019; 10: 4808–21.

8. Grinenko TS, Pobezinskaya EL, Pobezinskii LA, Baturina IA, Zvezdova ES, Kazanskii DB. Suppression of primary allogenic response by CD8+ memory cells. Bull Exp Biol Med. 2005; 140 (5): 545–9.

9. Kalinina AA, Persiyantseva NA, Britanova OV, Lupyr K, Shagina I, Khromykh LM et al. Unique features of the TCR repertoire of reactivated memory T cells in the experimental mouse tumor model. Comput Struct Biotechnol J. 2023; 21: 3196–209.

10. Kalinina A, Bruter A, Nesterenko L, Khromykh L, Kazansky D. Generation of TCRα-transduced T cells for adoptive transfer therapy of salmonellosis in mice. STAR Protoc. 2021; 2 (1): 100368.

11. Kalinina AA, Khromykh LM, Kazansky DB, Deykin AV, Silaeva YY. Suppression of the immune response by syngeneic splenocytes adoptively transferred to sublethally irradiated mice. Acta Nat. 2021; 13 (1): 116–26.

12. Dietrich PY, Le Gal FA, Dutoit V, Pittet MJ, Trautman L, Zippelius A, et al. Prevalent role of TCR alpha-chain in the selection of the preimmune repertoire specific for a human tumor-associated self-antigen. J Immunol. 2003; 170: 5103–9.

13. Hebeisen M, Allard M, Gannon PO, Schmidt J, Speiser DE, Rufer N. Identifying individual T cell receptors of optimal avidity for tumor antigens. Front Immunol. 2015; 6: 582.

14. Mondino A, Manzo T. To remember or to forget: the role of good and bad memories in adoptive T cell therapy for tumors. Front Immunol. 2020; 11: 1915.

15. von Essen MR, Kongsbak M, Geisler C. Mechanisms behind functional avidity maturation in T cells. Clin Dev Immunol. 2012; 2012: 163453.

16. Gilfillan CB, Hebeisen M, Rufer N, Speiser DE. Constant regulation for stable CD8 T-cell functional avidity and its possible implications for cancer immunotherapy. Eur J Immunol. 2021; 51 (6): 1348–60.

17. Campillo-Davo D, Flumens D, Lion E. The quest for the best: how TCR affinity, avidity, and functional avidity affect TCR-engineered T-cell antitumor responses. Cells. 2020; 9(7): 1720.

18. Kalinina A, Bruter A, Persiyantseva N, Silaeva Y, Zamkova M, Khromykh L et al. Safety evaluation of the mouse TCRα -transduced T cell product in preclinical models in vivo and in vitro. Biomed Pharmacother. 2022; 145: 112480.

GENE POOL OF THE URAL-VOLGA REGION: GENETIC HISTORY OF MORDOVIA'S POPULATION BASED ON THE Y-CHROMOSOMAL HAPLOGROUP N3A1-Y23475 PHYLOGEOGRAPHY

Agdzhoyan AT[1]✉, Adamov DS[1], Potanina AYu[1], Voronina MM[1], Gorin IO[1], Shtrunov-Shlykov AG[1], Koshel SM[2], Balanovska EV[1], Ponomarev GYu[1]

[1] Research Centre for Medical Genetics, Moscow, Russia

[2] Lomonosov Moscow State University, Moscow, Russia

It has been shown that Y-haplogroup N3a1-B211 is common in the Finnish-speaking peoples of the Ural-Volga region. The study aimed to investigate gene geography and phylogeography of the westernmost variant of this haplogroup: the N3a1-Y23475 branch. Comprehensive genotyping of 395 haplogroup N3a1-B211 carriers from 29 populations of Eastern Europe, Ural-Volga region, and Siberia revealed 78 carriers of its western branch reaching its maximum frequency in Mordovia's populations (8% in Moksha, 9% in Erzya, 25% in Tengushevsky Erzya-Shoksha). Low N3a1-Y23475 frequencies in the Turkic-speaking and Slavic populations suggest the role of the Finnish-speaking substrate in their gene pools. According to the phylogenetic analysis data, the N3a1-Y23475 branch emerged 2.3–2.7 thousand years ago, but active accumulation of its current diversity took place mainly in the populations of Mordovia during the last millennium. We performed DNA genotyping in 74 haplogoup N3a1-Y23475 carriers using the 37 Y-STR panel. The Y-STR haplotype phylogenetic network created suggests two periods of population growth in ancestors of Mordovia's indigenous population: about 1000 years ago in the populations of proto-Erzya and proto-Shoksha, about 500 years ago in the populations of Moksha and Shoksha. The fact of finding haplogroup N3a1-Y23475 in the Northern and Southern Altaians requires further research. Position of Northern Altaians-Kumandins in the phylogenetic network presumably reflects migration of Mordovia's population to Altai in the 19th–20th centuries. The age estimates reported for Southern Altaians-Telengits can indicate the association with the haplogroup N3a1 ancestral homeland in South Siberia before resettlement of its ancient carriers in the Ural-Volga region about 1.7 thousand years ago.

Keywords: gene pool, gene geography, phylogeography, Ural region, Mordovia, Y chromosome, haplogroup N3a1-Y23475, TMRCA estimates

ГЕНОФОНД УРАЛО-ПОВОЛЖЬЯ: ГЕНЕТИЧЕСКАЯ ИСТОРИЯ НАСЕЛЕНИЯ МОРДОВИИ ПО ДАННЫМ ФИЛОГЕОГРАФИИ ГАПЛОГРУППЫ N3A1-Y23475 Y-ХРОМОСОМЫ

А. Т. Агджоян[1]✉, Д. С. Адамов[1], А. Ю. Потанина[1], М. М. Воронина[1], И. О. Горин[1], А. Г. Штрунов-Шлыков[1], С. М. Кошель[2], Е. В. Балановская[1], Г. Ю. Пономарёв[1]

[1] Медико-генетический научный центр имени Н. П. Бочкова, Москва, Россия

[2] Московский государственный университет имени М. В. Ломоносова, Москва, Россия

Показано, что Y-гаплогруппа N3a1-B211 распространена в популяциях финноязычных народов Урало-Поволжья. Целью исследования было изучение геногеографии и филогеографии самого западного варианта этой гаплогруппы: ветви N3a1-Y23475. При детальном генотипировании 395 носителей гаплогруппы N3a1-B211 из 29 популяций Восточной Европы, Урало-Поволжья и Сибири выявлено 78 носителей ее западной ветви, которая достигает максимальных частот в популяциях Мордовии (8% — у мокши, 9% — у эрзя, 25% — у теньгушевских эрзи-шокши). Низкие частоты N3a1-Y23475 в тюркоязычных и славянских популяциях могут указывать на роль финноязычного субстрата в их генофондах. По данным филогенетического анализа ветвь N3a1-Y23475 возникла 2,3–2,7 тыс. лет назад, но активное накопление ее современного разнообразия происходило преимущественно в популяциях Мордовии в течение последнего тысячелетия. Проведено генотипирование ДНК 74 носителей гаплогруппы N3a1-Y23475 по панели 37 Y-STR. Созданная филогенетическая сеть Y-STR гаплотипов указывает на два периода демографического роста у предков коренного населения Мордовии: около 1000 лет назад в популяциях праэрзи и прашокши, около 500 лет назад — в популяциях мокши и шокши. Выявленное наличие гаплогруппы N3a1-Y23475 у северных и южных алтайцев требует продолжения исследования. Положение северных алтайцев-кумандинцев на филогенетической сети предположительно отражает миграцию мордовского населения на Алтай в XIX–XX вв. Генетическая датировка для южных алтайцев-теленгитов может указывать на связь с прародиной гаплогруппы N3a1 в Южной Сибири до расселения ее древних носителей в Урало-Поволжье около 1,7 тыс. лет назад.

Ключевые слова: генофонд, геногеография, филогеография, Уральский регион, Мордовия, Y-хромосома, гаплогруппа N3a1-Y23475, генетические датировки TMRCA

Y-haplogroup N3 represents one of the basic components of the North Eurasian gene pool and is considered to be a marker of the ancient population expansion, during which the Uralic languages spread [1–2]. Most of the haplogroup N3 range is the territory of Russia, where there are currently more than 1.6 million speakers of languages of the Uralic linguistic group belonging to 20 ethnic groups [3]. More than 90% of the population of the Uralic language-speakers in the Russian Federation is represented by the Finnish-speaking peoples of the Ural-Volga region of three language groups: Mari (Mari), Mordovian (Moksha, Shoksha, Erzya), and Permic (Besermyan, Komi-Zyryans, Komi-Permyaks, Udmurts). Among branches of haplogroup N3 most common in Europe (N3a1, N3a3, N3a4), high significant correlation with the Uralic ancestral component of the autosomal genome was reported for haplogroup N3a1 only [4].

Haplogroup N3a1 is common in the gene pools of peoples of the Ural region and is rare outside the region: in Udmurts (67%), Komi-Zyryans (18–43%), Chuvash (20%), Khanty and Mansi (19%), Komi-Permyaks (12%), Mari (14%), and Mordvins (5–10%) [1]. The spread of N3a1 is characterized by considerable frequency variation within its range: from 1% on the outskirts of the range (in Bashkirs, Belarusians, Karelians, Russians, Khakas) to the world's maximum in Udmurts (67%). This haplogroup, like other N3 lineages, could be brought to Europe by the population related to the Seima-Turbino transcultural phenomenon in the Bronze Age, despite the fact that this hypothesis has not yet been confirmed by direct paleoDNA analysis [5–6].

The structure of haplogroup N3a1-B211, common in the Finnish-speaking peoples of the Ural-Volga region, and the time of origin of its branches are poorly understood, but basic understanding is ensured by the YFull open source data [7]. Among the commercial testing participants, a common one in the populations of the Ural-Volga region is the N3a1-Y23475 branch spread across the western part of the region: in Mordvins-Erzya, Volga Tatars, and Russians (Bryansk, Nizhny Novgorod, Penza, Kirov, and Sverdlovsk regions). According to the YFull data, active accumulation of today's diversity within N3a1-Y23475 took place on average in the last 2.4–2.7 thousand years.

The study aimed to investigate gene geography and phylogenetic structure of haplogroup N3a1-Y23475 based on the extensive data on the populations of North Eurasia.

METHODS

Biological samples were collected after obtaining the informed consent from the donors during the expedition surveys managed by Professor E.V. Balanovska and RAS Professor O.P. Balanovsky in accordance with the same program that had been described earlier [8]. The donors were unrelated adult males, whose ancestors for at least three generations considered themselves to belong to this ethnic group and were born into this population. In Mordovia, the Moksha and Erzya ethnic groups were assessed, including the distinct group of Erzya living in the Tengushevsky District, hereinafter referred to as Shoksha.

DNA was isolated from the venous blood samples using the QIAsymphony SP nucleic acid purification system or by phenol-chloroform extraction using proteinase K; the sample preparation phases had been described earlier [9]. Among 4051 samples (Table 1) there were 395 samples of the haplogroup N3a1-B211 carriers from 29 populations of Eastern Europe, Ural-Volga region, and Siberia. For these genotyping

of the Y23475 SNP marker was performed by real-time PCR using the TaqMan probes and the OpenArray technique in the QuantStudio 12 Flex thermocycler (Thermo Fisher Scientific, USA). A total of 78 carriers of the N3a1-Y23475 branch were identified. Of those the results of fragment analysis (37 YSTR markers) were obtained for 74 samples using the commercially available Yfiler Plus (Thermo Fisher Scientific, USA), Powerplex Y23 (Promega, USA) kits and the Nanophore 05 genetic analyzer (Syntol, Russia).

Cartographic analysis was performed using the original GeneGeo cartographic software package [10] developed under the leadership of E. V. Balanovska and O. P. Balanovsky. The gene geographic map of the haplogroup N3a1-Y23475 spread was created based on the genotyping data by the weighted average interpolation (radius 400 km, and weight function degree 3).

The N3a1-Y23475 phylogenetic network was constructed based on the median-joining principle [11] using the Network v.10.2.0.0 software tool (Fluxus Technology Ltd, UK). The network image was visualized in Network Publisher v.2.1.2.5 (Fluxus Technology Ltd, UK). The weight of each of 37 STR markers was considered to be 10 with $\varepsilon = 0$. The time to the most recent common ancestor (TMRCA) for the entire phylogenetic network and the clusters distinguished (Table 2) was calculated by the ASD method [12]. We excluded the DYF387S1b locus due to partial AZFc deletions in the P1 palindromic sequence in the haplogroup N3-M178 samples. The mutation rate constant for the 36-marker haplotype was selected based on the world's data [13–14]: 0.0038 per locus per generation. The average generation interval for males was considered to be 31.5 years [15].

RESULTS

Gene geography of haplogroup N3a1-Y23475

The range of haplogroup N3a1-Y23475 extends from northwest to southeast (from the Vologda Russians to Mongols), but shows intermittent and irregular frequency distribution (Table 1). Most of the haplogroup carriers (84%) are in the Finnish-speaking populations of the Ural-Volga region, where the N3a1-Y23475 frequency varies between 0.4% and 25% (Fig. 1). The haplogroup frequency reaches its maximum in the populations of Mordovia, where there more than 70% of its carriers with the following frequency values: 8% in Moksha, 9% in Erzya, and the maximum value (25%) in Tengushevsky Erzya-Shoksha (hereinafter, Shoksha). N3a1-Y23475 is almost an order of magnitude more rare in the neighbouring Turkic-speaking peoples: Mishar Tatars (2%), Kazan Tatars (1%), and extremely rare in Bashkirs (0.4%). The haplogroup is rare in the Russian populations: 3% in the Vologda Region and 1% in the Belgorod, Kaluga, Oryol regions (Table 1). In Siberia, haplogroup N3a1-Y23475 has been found in Altaians (6%) and one Mongol.

The reported haplogroup N3a1-Y23475 gene geography necessitates consideration of two issues: 1) of the factors that led to its accumulation in Mordovia's populations; 2) of its sources in Altaians. The search for answers to these questions was performed using phylogenetic analysis.

Phylogenetic structure and chronology of clusters/branches

The samples of the haplogroup N3a1-Y23475 carriers were assessed using the 37 Y-STR marker panel in all populations,

Table 1. Spread of haplogroup N3a1-Y23475 across the populations of the Ural-Volga region and adjacent regions

Linguistic characteristics	Populations	Total sample	Number of the N3a1 test samples	Number of the N3a1-Y23475 branch carriers	N3a1-Y23475 branch frequency, %
Eastern Europe					
Slavic group of Indo-European language family	Russians of Vologda Region	80	2	2	3
	Russians of Kaluga Region	96	1	1	1
	Russians of Belgorod Region	341	2	2	1
	Russians of Oryol Region	173	1	1	1
Ural-Volga region					
Mari group of Uralic language family	Mountain Mari	65	14	0	0
	Meadow Mari	161	33	0	0
Mordovian group of Uralic language family	Moksha Mordvins**	194	16	16	8
	Erzya Mordvins**	280	26	26	9
	Shoksha Mordvins**	52	13	13	25
Permic group of Uralic language family	Besermyan	45	20	0	0
	Eastern Udmurts	70	50	0	0
	Northern Udmurts	42	13	0	0
	Southern Udmurts	113	83	0	0
	Zyuzdinski Komi (Kirov Region)	32	8	0	0
	Northern Komi-Permyaks	74	7	0	0
	Southeastern Komi-Permyaks	74	23	0	0
	Southwestern Komi-Permyaks	175	19	0	0
Turkic branch of Altaic language family	Kazan Tatars	382	11	5	1
	Mishar Tatars	154	12	3	2
	Chuvash of Tatarstan	66	12	0	0
	Bashkirs of Bashkortostan	719	7	3	0.4
Siberia and Cenral Asia					
Ugric group of Uralic language family	Khanty	83	5	0	0
	Mansi	76	1	0	0
Turkic branch of Altaic language family	Siberian Tatars	544	6	0	0
	Northern Altaians-Kumandins	44	1	1	2
	Northern Altaians-Chelkans	56	1	0	0
	Southern Altaians-Telengits	54	4	4	7
	Tofalars people	51	1	0	0
Mongolic branch of Altaic language family	Buryats of Trans-Baikal Territory, Duldurginsky District	96	2	0	0
	Mongols	636	1	1	0.2
Total:		5028	395	78	

Note: ** — significant differences in haplogroup frequency between the Mordvin populations ($p < 0.01$)

where the haplogroup was found. A total of 74 haplotypes were obtained (Table in Appendix), based on which a phylogenetic network was constructed (Fig. 2).

The use of 37 Y-STR markers allowed us to achieve high phylogenetic resolution: most haplotypes were distributed across six clusters (Fig. 2). Four clusters (B, C, D, E) are characterized by absolute specificity: each cluster is formed by the samples belonging to only one Mordovia's ethnic group, i.e. Erzya, Moksha or Shoksha. Clusters A and F include three specific subclusters, two of which (A1 and F1) are formed by the haplotypes from Mordovia's populations. Chronology of their emergence was calculated for all clusters and subclusters (Table 2 — time to the most recent common ancestor, TMRCA).

Subcluster A1 and cluster B (Fig. 2) of Moksha were formed within the same period: about 500 years ago (Table 2). Subcluster A1 includes for different Moksha haplotypes from

the Insarsky District of Mordovia (hereinafter, birthplaces of the assessed individuals' paternal grandfathers are specified). Cluster B is represented by the Moksha samples from three neighboring districts of Mordovia: four samples from the Insarsky District, three samples from the Atyuryevsky District, and one sample from the Kovylkinsky District.

Clusters C and E (Fig. 2) of Erzya were formed about 900–1000 years ago (Table 2). Cluster C includes representatives of the Ichalkovsky District of Mordovia, and cluster E includes mostly those of the adjacent Chamzinsky District.

Cluster D and subcluster F1 of Shoksha are far from each other in the phypogenetic network, despite the fact that these originate from the populations of the Tengushevsky District in northwestern Mordovia. The dates differ almost two times: subcluster F1 was formed about 500 years ago, cluster D about 900 years ago (Table 2).
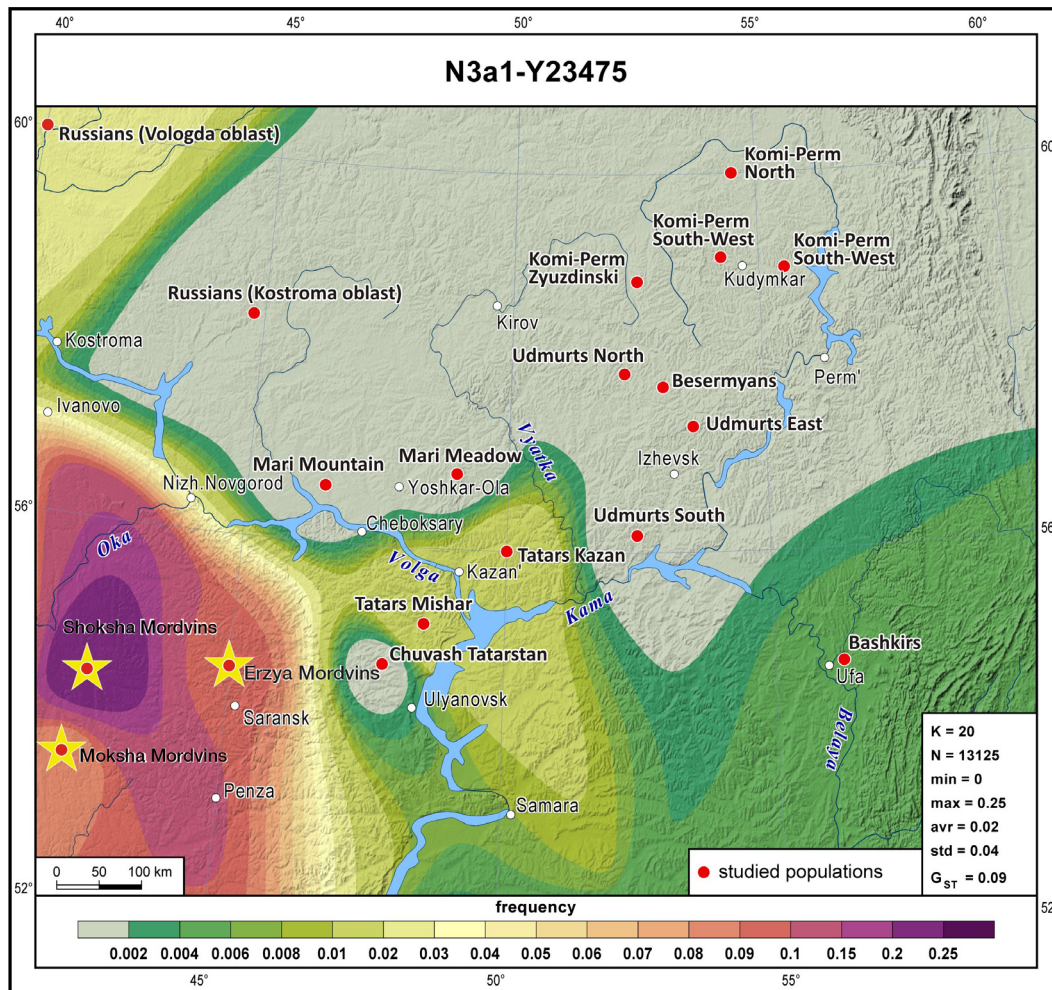
Fig. 1. Spread of haplogroup N3a1-Y23475 across indigenous populations of the Ural-Volga region. The studied populations are marked with *red dots*; *yellow dots* represent Mordovia's populations. The haplogroup frequency is shown according to the color chart in the map legend

All haplotypes of the Kazan Tatars and Mishar Tatars are located outside the clusters. A casual resemblance to these is reported for two Moksha samples and two Bashkir samples (Fig. 2), as well as for subcluster D of Shoksha.

The samples of Russians also do not form any separate subcluster; these are included in the most heterogeneous cluster F, along with the haplotypes of Moksha, Bashkir, and Mongol and subclusters of Shoksha and Telengit Altaians.

Haplotypes of Altaians are distributed across clusters A and F in the phylogenetic network. The age of cluster A including only one sample of the Kumandin Altaian is about 1150 years. This value twice exceeds the value of the Moksha subcluster A1, the Altaian haplotype originates from. Samples of southern Altaians-Telengits are merged into the specific subcluster F2, which suggests their descent from a common ancestor. The time to the most recent common ancestor for subcluster F2 is about 800 years (Table 2).

The age of the entire haplogroup N3a1-Y23475 calculated based on the Y-STR haplotypes (2340 ± 330 years) within the margins of error is consistent with the estimates of the YFull team [7] obtained based on SNP markers (2700 ± 300 years). Matches in the YFull phylogenetic tree can be found for a half of the Y-STR clusters identified in the population-based study (Table 2).

DISCUSSION

The detected accumulation of haplogroup N3a1-Y23475 in the gene pools of Mordovia's population and two population

growth momenta reflect their demographic history. The population growth about 500 years ago could result from liberation of the population from the system of dependence on the Mongol Empire and the Golden Horde (that lasted from mid-13th century to late 15th century). The population growth momentum about 1000 years ago is considered to be associated with the formation of ethnic foci of Moksha (on the Tsna River and in Prisurie) and Erzya (in Poteshie) in the 10th century. The late Ryazan-Oka traditions followed by the ceramic complex of the Shokshinsky burial ground developed within the Shoksha range in an isolated manner, inheriting and developing the features of ceramics of the preceding period [16].

Peculiarity of the Shoksha gene pool is traced through high frequency of N3a1-Y23475 (25% vs. 8–9% in Moksha and Erzya) and the analysis of autosomal gene pool. The ADMIXTURE method revealed two ancestral components [17]. The first ancestral component (Moksha-Erzya) merges the populations of Moksha and Erzya only, while the second (Shoksha) is typical only for Shoksha populations. Both ancestral components are found in the genomes of most Russian populations, suggesting the contribution of pre-Slavic population to the Russian gene pool (Table 3).

Accumulation of haplogroup N3a1-Y23475 in the population of Mordovia can be explained by consecutive effects of two factors: migration and the founder effect. The presence of this lineage in all Mordovia's populations suggests that it was inherited by the Mordvin proto-population from the same source (probably, from the alien carriers of haplogroup N3a1).
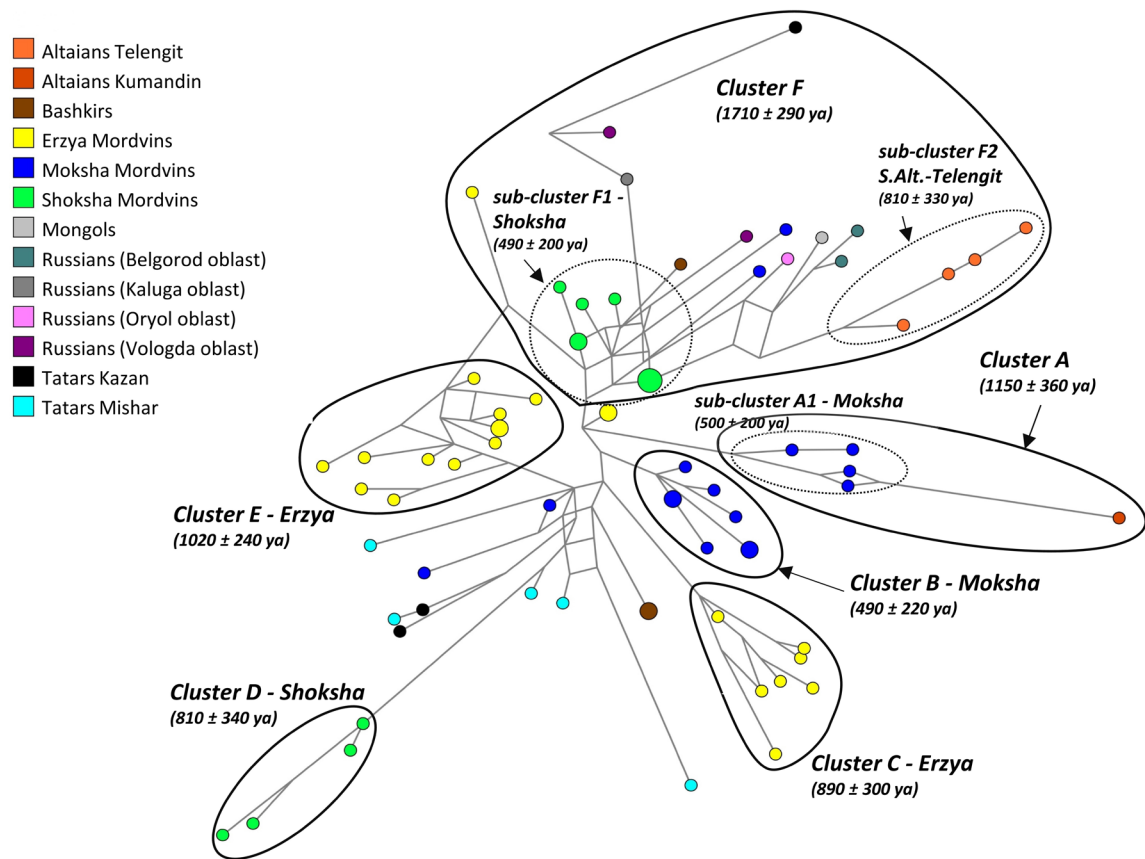
Fig. 2. Phylogenetic network of haplogroup N3a1-Y23475

The founder effect presumably manifested itself after isolation of Mordovia's ethnic groups. This explains high specificity of clusters and subclusters (accumulation of haplotype diversity within each population) and their structure in the phylogenetic network (Fig. 2).

The N3a1-Y23475 phylogenetic analysis results make it possible to give an interim answer to the question about the sources of origin of haplogroup N3a1-Y23475 in Altaians. Haplotype of the Northern Altaian-Kumandin is most close to the Moksha haplotypes (Fig. 2, cluster A). Since the population of Kumandins is small (2400 people), a single Moksha lineage could emerge in Kumandins due to mass resettlement of Mordvins to Altai in the 19th–20th centuries [18]: in the early 20th century, Mordvins ranked third (following Russian and

Ukranians) among ethnic groups based on the population size in the Altai Region.

The issue of the population being the source of branch N3a1-Y23475 in Southern Altaians is related to the issue of its ancestral homeland that could hypothetically be located in the Ural region ("Uralic ancestral homeland") or South Siberia ("Siberian ancestral homeland").

Southern Altaians-Telengits form their own subcluster F1 in the phylogenetic network, which, along with two Belgorod samples and the Mongol sample can be traced back to the most common Shoksha haplotype (Fig. 2, cluster F). The subcluster F2 chronology suggests that the ancestor of today's N3a1-Y23475 branch carriers could emerge within the range of Southern Altaians-Telengits about 800 years ago (500–1100 years ago).

Table 2. Genetic chronology (TMRCA) of the haplogroup N3a1-Y23475 clusters

Cluster	n	TMRCA, years ago	YFull estimate	Match between the STR cluster and the YFull tree branch
A (Moksha and the Kumandin Altaian)	5	1150 ± 360		not found
A1 (Moksha)	4	500 ± 200		not found
B (Moksha)	8	490 ± 220	800 ± 210	N-BY9737
C (Erzya)	7	890 ± 300	1400 ± 260	N-Y164241
D (Shoksha)	4	810 ± 340		not found
E (Erzya)	12	1020 ± 240		not found
E	25	1710 ± 290	1250 ± 260	N-Y39435
F1 (Shoksha)	9	490 ± 200	425 ± 110	N-Y39282
F2 (Altaians-Telengits)	4	810 ± 330		not found
N3a1-Y23475	74	2340 ± 330	2700 ± 300	N-Y23472
in general				

Note: n — number of samples the cluster consists of, TMRCA — time to the most recent common ancestor.

Таблица 3. Share of individual autosomal genomes (%) in Russian populations, where the ADMIXTURE ancestral components typical for Moksha and Erzya (Moksha-Erzya) and Shoksha (Shoksha) are found

Regions with the Russian population	Share of Mordovia's ancestral components in Russian populations	
	Moksha-Erzya (%)	Shoksha (%)
Tver	90	50
Kaluga	80	60
Smolensk	60	50
Oryol	65	25
Tambov	50	40
Kostroma	50	80
Ryazan	50	80
Nizhny Novgorod	45	80

Reasons for the "Uralic ancestral homeland" hypothesis. The greatest diversity of both clusters and single N3a1-Y23475 haplotypes is observed in today's populations of the Ural-Volga region, which indirectly indicates the haplogroup origin can be in this area. In this case the emergence of haplogroup N3a1-Y23475 in Southern Altaians and Mongols is associated with the eastward migration from the Ural region. Furthermore, migration to Altai had to occur no later as 500 years ago, since subcluster F2 is significantly isolated from the main pool of haplotypes from the populations of the Ural-Volga region.

Reasons for the "Siberian ancestral homeland" hypothesis. An alternative hypothesis places the haplogroup N3a1-Y23475 ancestral homeland to South Siberia. This hypothesis is supported by the previously reported general vector of the haplogroup N spread from east to west [1]. In this case, subcluster F2 of Southern Altaians-Telengits preserves genetic memories about the ancient haplogroup N3a1-Y23475 carriers, who migrated to the Ural region from South Siberia. Cluster F differs from other clusters of the phylogenetic network (Fig. 2) by the highest population heterogeneity and the most ancient date (1710 ± 290 years ago; Table 2). There is a large number of reticulations in the structure of cluster F, along with rather distant relationships between haplotypes from different regions and both subclusters. The chronology calculated suggests that cluster F was formed on average only 600 years later than the entire haplogroup N3a1-Y23475. Both observations suggest that in the past there were many clusters within cluster F, from which only distinct haplotypes survived by today.

The hypothesis about the South Siberian ancestral homeland of haplogroup N3a1-Y23475 is not contradicted by the pattern of its spread across today's populations, since high frequency and haplotype diversity in Mordovia's populations formed as late as in the last millennium. Chronology of cluster F suggests that the South Siberian, some Volga region, and all Russian populations had the same root about 1700 years ago. During this period N3a1-Y23475 could emerge in South Siberia in the population of haplogroup N3a1-B211 carriers, who migrated to the west. The subcluster F2 founder can be a descendant of this population, which left sporadic marks in the gene pool of today's Southern Altaians-Telengits.

The available data do not yet provide unambiguous confirmation of validity of one or another hypothesis. That is why it is planned to analyze the entire complex of the Y chromosome haplogroups and haplotypes in order to trace genetic links between the gene pools of the Ural region and South Siberia.

CONCLUSIONS

Haplogroup N3a1-Y23475 was formed 2.3–2.7 thousand years ago, but intense accumulation of the haplogroup took place mostly in Mordovia's populations since the 10th century. High share of the haplogroup in all Mordovia's populations suggests that it originates from the common source. Two population growth momenta in the ancestors of Mordvins can be traced: about 1000 years ago in Erzya, about 500 years ago in Moksha; both momenta have been reported for the Shoksha population. Low N3a1-Y23475 frequency in the populations of Tukcic-speaking and Slavic-speaking peoples is associated with the presence of the substrate layer of Finnish-speaking peoples in their gene pools. The presence of haplogroup N3a1-Y23475 in Northern Altaians-Kumandins is likely to be associated with migration of Mordovia's population to Altai in the 19th–20th centuries. The source of N3a1-Y23475 in Southern Altaians-Telengits requires verification of two hypotheses: of the "Uralic ancestral homeland" with negligible migration to the east and of the "Siberian ancestral homeland" with migration from South Siberia to the Ural-Vplga region about 1700 years ago.

References

1. Ilumäe AM, Reidla M, Chukhryaeva M, Järve M, Post H, Karmin M, et al. Human Y Chromosome Haplogroup N: A Non-trivial Time-Resolved Phylogeography that Cuts across Language Families. The American Journal of Human Genetics. 2016; 99 (1): 163–73.
2. Lamnidis TC, Majander K, Jeong C, Salmela E, Wessman A, Moiseyev V, et al. Ancient Fennoscandian genomes reveal origin and spread of Siberian ancestry in Europe. Nature Communications. 2018; 9 (1): 5018.
3. All-Russian Population Census 2020. Volume 5 National composition and language proficiency. Table 1. National composition of the population (cited 10 November 2024) Available from: https://rosstat. gov.ru/vpn/2020/Tom5_Nacionalnyj_sostav_i_vladenie_yazykami.

4. Tambets K, Yunusbayev B, Hudjashov G, Ilumäe AM, Rootsi S, Honkola T, et al. Genes reveal traces of common recent demographic history for most of the Uralic-speaking populations. Genome Biol. 2018; 19 (1): 139.
5. Zeng TC, Vyazov LA, Kim A, Flegontov P, Sirak K, Maier R, et al. Postglacial genomes from foragers across Northern Eurasia reveal prehistoric mobility associated with the spread of the Uralic and Yeniseian languages. bioRxiv. 2023.
6. Childebayeva A, Fricke F, Rohrlach AB, Huang L, Schiffels S, Vesakoski O, et al. Bronze age Northern Eurasian genetics in the context of development of metallurgy and Siberian ancestry. Communications Biology. 2024; 7 (1): 723.

7. Tree YTree v12.03.00 (cited 20 November 2024). Available from: https://www.yfull.com/sc/tree/.

8. Balanovska EV, Agdzhoyan AT, Chukhryaeva MI, Skhalyakho RA, Zaporozhchenko VV, Romanov AG, et al. Population biobanks: organizational models and prospects of application in gene geography and personalized medicine. Russian Journal of Genetics. 2016; 52 (12): 1371–87.

9. Agdzhoyan A, Iskandarov N, Ponomarev G, Pylev V, Koshel S, Salaev V, et al. Origins of East Caucasus Gene Pool: Contributions of Autochthonous Bronze Age Populations and Migrations from West Asia Estimated from Y-Chromosome Data Genes. 2023; 14 (9): 1780.

10. Koshel SM. Geoinformacionnye tehnologii v genogeografii. V knige: Sovremennaja geograficheskaja kartografija. M.: Data+, 2012; s. 158–166. Russian.

11. Bandelt HJ, Forster P, Röhl A. Median-joining networks for inferring intraspecific phylogenies. Molecular Biology and Evolution. 1999; 16 (1): 37–48.

12. Zhivotovsky LA, Underhill PA, Cinnioğlu C, Kayser M, Morar B, Kivisild T, et al. The effective mutation rate at Y chromosome short tandem repeats, with application to human population-divergence

time. American Journal of Human Genetics. 2004; 1: 50–61.

13. Willuweit S, Roewer L. The new Y Chromosome Haplotype Reference Database. Forensic Science International: Genetics. 2015; 15: 43–48.

14. Ballantyne KN, Goedbloed M, Fang R, Schaap O, Lao O, Wollstein A, et al. Mutability of Y-chromosomal microsatellites: rates, characteristics, molecular bases, and forensic implications. American Journal of Human Genetics. 2010; 87 (3): 341–53.

15. Fenner J. Cross-cultural estimation of the human generation interval for use in genetics-based population divergence studies. American Journal of Physical Anthropology. 2005; 128 (2): 415–23.

16. Grishakov V. V. Keramika pogrebal'nykh pamyatnikov Oksko-Surskogo Mezhdurech'ya v I tys. n.e. [dissertation]. M., 1993. Russian.

17. Balanovska EV, Gorin IO, Ponomarev GY, Pylev VY, Petrushenko VS, Markina NV, et al. Footprints of interaction among Finnic-speaking, Slavic, and Turkic-speaking populations in modern gene pool and their reflection in pharmacogenetics. Bulletin of RSMU. 2022; 2: 18–27.

18. Ovcharova MA. Mordva Altaya: istoriya i etnokul'turnye protsessy (XIX - nachalo XXI v.) [dissertation]. Barnaul, 2009. Russian.

Литература

1. Ilumäe AM, Reidla M, Chukhryaeva M, Järve M, Post H, Karmin M, et al. Human Y Chromosome Haplogroup N: A Non-trivial Time-Resolved Phylogeography that Cuts across Language Families. The American Journal of Human Genetics. 2016; 99 (1): 163–73.

2. Lamnidis TC, Majander K, Jeong C, Salmela E, Wessman A, Moiseyev V, et al. Ancient Fennoscandian genomes reveal origin and spread of Siberian ancestry in Europe. Nature Communications. 2018; 9 (1): 5018.

3. Итоги Всероссийской переписи населения 2020 года. Том 5 Национальный состав и владение языками. Таблица 1. Национальный состав населения (дата обращения: 10 November 2024). Доступно по ссылке: https://rosstat.gov.ru/vpn/2020/Tom5_Nacionalnyj_sostav_i_vladenie_yazykami.

4. Tambets K, Yunusbayev B, Hudjashov G, Ilumäe AM, Rootsi S, Honkola T, et al. Genes reveal traces of common recent demographic history for most of the Uralic-speaking populations. Genome Biol. 2018; 19 (1): 139.

5. Zeng TC, Vyazov LA, Kim A, Flegontov P, Sirak K, Maier R, et al. Postglacial genomes from foragers across Northern Eurasia reveal prehistoric mobility associated with the spread of the Uralic and Yeniseian languages. bioRxiv. 2023.

6. Childebayeva A, Fricke F, Rohrlach AB, Huang L, Schiffels S, Vesakoski O, et al. Bronze age Northern Eurasian genetics in the context of development of metallurgy and Siberian ancestry. Communications Biology. 2024; 7 (1): 723.

7. Tree YTree v12.03.00 (дата обращения: 20 November 2024). Доступно по ссылке: https://www.yfull.com/sc/tree/.

8. Балановская Е. В., Жабагин М. К., Агджоян А. Т., Чухряева М. И., Маркина Н. В., Балаганская О. А. и др. Популяционные биобанки: принципы организации и перспективы применения в геногеографии и персонализированной медицине. Генетика. 2016; 52 (12): 1371–87.

9. Agdzhoyan A, Iskandarov N, Ponomarev G, Pylev V, Koshel S,

Salaev V, et al. Origins of East Caucasus Gene Pool: Contributions of Autochthonous Bronze Age Populations and Migrations from West Asia Estimated from Y-Chromosome Data Genes. 2023; 14 (9): 1780.

10. Кошель С. М. Геоинформационные технологии в геногеографии. В книге: И. К. Лурье, В. И. Кравцова, редакторы. Современная географическая картография. М.: Дата+, 2012; с. 158–66.

11. Bandelt HJ, Forster P, Röhl A. Median-joining networks for inferring intraspecific phylogenies. Molecular Biology and Evolution. 1999; 16 (1): 37–48.

12. Zhivotovsky LA, Underhill PA, Cinnioğlu C, Kayser M, Morar B, Kivisild T, et al. The effective mutation rate at Y chromosome short tandem repeats, with application to human population-divergence time. American Journal of Human Genetics. 2004; 1: 50–61.

13. Willuweit S, Roewer L. The new Y Chromosome Haplotype Reference Database. Forensic Science International: Genetics. 2015; 15: 43–48.

14. Ballantyne KN, Goedbloed M, Fang R, Schaap O, Lao O, Wollstein A, et al. Mutability of Y-chromosomal microsatellites: rates, characteristics, molecular bases, and forensic implications. American Journal of Human Genetics. 2010; 87 (3): 341–53.

15. Fenner J. Cross-cultural estimation of the human generation interval for use in genetics-based population divergence studies. American Journal of Physical Anthropology. 2005; 128 (2): 415–23.

16. Гришаков В. В. Керамика погребальных памятников Окско-Сурского Междуречья в I тыс. н.э. [диссертация]. М., 1993.

17. Балановская Е. В., Горин И. О., Пономарев Г. Ю., Пылёв В. Ю., Петрушенко В. С., Маркина Н. В. и др. Следы взаимодействия финноязычного, славянского и тюркоязычного населения в современном генофонде и их отражение в фармакогенетике. Вестник РГМУ. 2022; 2: 20–9.

18. Овчарова М. А. Мордва Алтая: история и этнокультурные процессы (XIX — начало XXI в.) [диссертация]. Барнаул, 2009.

PROSPECTS OF GENE THERAPY WITH HEMATOPOIETIC STEM CELLS

Valieva YM[1], Popov KV[2] ✉

[1] Moscow Institute of Physics and Technology (National Research University), Moscow, Russia

[2] Kulakov National Medical Research Center for Obstetrics, Gynecology and Perinatology, Moscow, Russia

Gene therapy is subdivided into *in vivo* and *ex vivo* according to the tactics of delivery of therapeutic constructions. *In vivo* therapy, a vector containing a therapeutic construction is injected into the patient. In *ex vivo* therapy, cells are removed from the patient's body, genetically modified, and then returned. In *ex vivo* therapy for inherited diseases, hematopoietic stem cells are most often subjected to modification. Despite the advantage of *in vivo* therapy, which consists in the possibility of scale-up of production and convenience of use of ready-to-use drug, therapy based on transplantation of genetically modified hematopoietic stem cells remains relevant for a number of genetic diseases.

Keywords: hematopoietic stem cells, ex vivo gene therapy, in vivo gene therapy, lysosomal storage diseases, genetic disorder

✉ **Correspondence should be addressed:** Konstantin V. Popov
Akademika Oparina, 4, Moscow, 117997, Russia; popov_konst@mail.ru

ПЕРСПЕКТИВЫ ГЕННОЙ ТЕРАПИИ ГЕМОПОЭТИЧЕСКИМИ СТВОЛОВЫМИ КЛЕТКАМИ

Я. М. Валиева[1], К. В. Попов[2] ✉

[1] Московский физико-технический институт (Национальный исследовательский университет), Москва, Россия

[2] Национальный медицинский исследовательский центр акушерства, гинекологии и перинатологии имени В. И. Кулакова, Москва, Россия

По тактике доставки терапевтических конструкций генную терапию разделяют на i*n vivo* и *ex vivo*. При терапии *in vivo* вектор, содержащий терапевтическую конструкцию, вводят пациенту. При терапии *ex vivo* клетки извлекают из организма пациента, подвергают генетической модификации и возвращают обратно. В *ex vivo* терапии наследственных заболеваний модификации чаще всего подвергаются гемопоэтические стволовые клетки. Несмотря на преимущество терапии *in vivo*, состоящее в возможности масштабирования производства и удобства применения готового препарата, для ряда генетических заболеваний сохраняется актуальность терапии на основе трансплантации генетически модифицированных гемопоэтических стволовых клеток.

Ключевые слова: гемопоэтические стволовые клетки, генная клеточная терапия *ex vivo*, генная терапия *in vivo*, лизосомные болезни накопления, генные болезни

✉ **Для корреспонденции:** Константин Васильевич Попов
ул. Опарина, д. 4, г. Москва, 117997, Россия; popov_konst@mail.ru

According to the definition, the therapeutic effect of a gene therapy medicinal product is determined by the sequence of recombinant nucleic acid included in its composition or by the product of the expression of such a sequence [1]. Depending on the molecular mechanism underlying the disease, therapy may aim to correct genetic defects or give cells new properties. The strategy for dealing with a damaged gene function may include adding a working copy, suppressing expression or correcting the sequence. Adding a working copy of the gene is used to treat autosomal recessive disorders. Suppressing the expression of the damaged gene is used for autosomal dominant diseases [2]. With the development of genome editing techniques, correcting the sequence of a damaged gene is being considered a priority approach for the development of treatment for both autosomal recessive and autosomal dominant inherited diseases. CAR-T therapy is the most widely used gene therapy drug in clinical practice, is based on giving cells with new properties. In this case, a chimeric receptor is used to enable them to recognize and destroy cancer cells [3].

Current gene therapy methods

Regardless of the mechanism of action of the nucleic acid contained in the gene therapy drug, a key factor in the development of the manufacturing technology for the drug is the choice between *in vivo* and *ex vivo* delivery of the therapeutic construct to the target cells. In the *in vivo* application, the drug containing the vector is administered directly into the patient's body. For *ex vivo* application, specific cells are isolated from the patient's body, genetically modified, and then returned to the patient.

Currently, the use of viral vectors is the most studied method for delivering genes into cells. Viruses are used for targeted delivery of necessary genetic material to cells both *in vivo* and *ex vivo*. Leaders among modified gene carriers are adeno-associated viral (AAV) vectors and lentiviral vectors. AAV vectors are predominantly used *in vivo*, while lentiviral vectors are utilized for *ex vivo* therapy [4, 5].

RNA methods in gene therapy represent a rapidly evolving field with significant potential for treating various diseases. These

methods include therapy using antisense oligonucleotides, RNA interference and messenger RNA (mRNA). The development of non-viral RNA delivery systems, particularly those based on encapsulation in lipid nanoparticles, is expected to allow for the avoidance of viral delivery systems in the future. This advancement will help to mitigate risks associated with the immune system's reactions to viral proteins and the uncontrolled integration of transgenes into the patient's genome [6].

The development of a new method of genome editing, CRISPR/Cas9, has become a groundbreaking technology. CRISPR/Cas9 can be used to correct genetic mutations by precisely editing the defective gene. This approach is particularly relevant for monogenic diseases, where a specific gene mutation is responsible for the condition [7].

Gene therapy *in vivo* has a competitive advantage in most cases due to the ability to create ready-made drug products tailored to the main cohort of patients. This leads to ease of scaling, a reduction in cost per unit of production and readiness for on-demand use.

Gene therapy *ex vivo* is primarily used in the treatment of oncological diseases (in this case, immune cells are modified) and in the treatment of hereditary diseases using genetically modified hematopoietic stem cells (HSCs). HSCs are optimal target cells for therapeutic genome editing due to their ability to self-renew and differentiate. Thus, a prolonged expression level of the therapeutic construct is ensured, along with the delivery of its expression products to differentiated cells throughout most of the organism. Moreover, HSCs do not carry the risk of immunogenicity associated with the direct use of high doses of viral vectors *in vivo* [8].

Hematopoietic stem cell gene therapy

The methodology of *ex vivo* gene therapy using hematopoietic stem cells (HSC GT) is a multi-step process. First, HSCs are collected from the patient, then they are cultured, subjected to genetic modification, and the modified cells are reintroduced into the patient. The injected cells populate the HSC niche in the bone marrow [9]. HSC GT *ex vivo* appears to be a promising approach for treating monogenic genetic disorders, including primary immunodeficiencies, hemoglobinopathies and lysosomal storage diseases.

The most successful example of HSC GT is the gene therapy product registered in 2020 for the treatment of metachromatic leukodystrophy (MLD) — Libmeldy. The drug consists of autologous HSCs that have been transduced with a lentiviral vector carrying a functional copy of the ARSA gene. The treatment results showed a significant therapeutic effect and a long duration of action for the drug [10]. The use of lentivirus-based vectors ensures stable integration of genetic constructs into the genome, resulting in high and prolonged gene expression. However, utilizing viral vectors for modifying HSCs poses a risk of insertional mutagenesis. Treatment of X-linked severe combined immunodeficiency (X-SCID) with a similar HSC GT drug was found to be associated with an increased risk of T-cell acute lymphoblastic leukemia. Despite efforts to modify the design of lentiviral vectors to reduce the risk of cancer development due to transgene integration, similar complications were observed when using the therapy for treating adrenoleukodystrophy [11]. Increasing the safety of modified HSCs can be achieved by using non-viral delivery systems based on transposons and CRISPR/Cas genome editing systems.

The advantage of *ex vivo* HSCs gene therapy compared to *in vivo* therapy using viral vectors lies in the absence of the need to use high doses of the vector, thereby reducing the patient's risk of developing immune reactions. In particular, when using AAV vectors, a significant portion of particles remains in the liver due to the first-pass effect. In other words, if the target organ differs from the liver, AAV vectors do not reach it at the required therapeutic dose, and using higher doses leads to hepatotoxic and immunogenic effects [12]. Since autologous cells of the patient are used in HSC GT, the immunogenicity of these products is minimal. Transplantation of HSCs with stable integration of gene therapy constructs provides a long-lasting, theoretically lifelong therapeutic effect. In the case of hematopoietic diseases, such as Wiskott-Aldrich syndrome and other primary immunodeficiencies, HSCs themselves are the target cells. HSCs are capable of crossing the blood-brain barrier, differentiating into macrophages to occupy the microglial niche, and expressing necessary enzymes in brain tissues [13]. This explains the effect of allogeneic hematopoietic stem cell transplantation from a healthy donor for the treatment of a group of hereditary diseases caused by damage to brain nerve cells, including mucopolysaccharidoses, adrenoleukodystrophy, and MLD. The same effect is achieved when using autologous HSCs with corrected gene defects.

The improvement of *ex vivo* cultivation methods for HSCs allows for the production of significantly more HSCs for modification than what is available from directly using cells collected from the patient. High doses of HSCs used for transplantation raise hopes for the introduction of modified HSCs transplantation protocols that do not require genotoxic conditioning regimens. Currently, achieving a clinical effect from HSCs transplantation requires prior myeloablative conditioning through chemotherapy aimed at suppressing the patient's bone marrow. Such conditioning carries both short-term risks associated with the development of infectious diseases and long-term risks of growth impairment, intellectual development issues, loss of fertility, and the development of other diseases [14]. Currently, protocols are being developed for the formation of HSCs niches using antibody conjugates specific to HSCs combined with toxins.

Today, the most expensive drug in the world is Lenmeldy, an HSC-based medicine for MLD [15]. The use of patient-derived cells for the production of the drug means that there is no possibility of reducing the cost per dose by increasing the volume of the produced batch. In addition, *ex vivo* application also requires complex logistics and carries additional risks related to ensuring the quality and safety of the donor material. The possibility of reducing the production costs of these drugs is linked to optimizing the logistics of delivering donor material and the finished product, as well as automating the manufacturing process. A significant reduction in the cost of drugs can be expected from replacing the currently used viral vectors with non-viral systems for delivering gene therapy constructs. This approach will help reduce the time and costs associated with each unit of the drug. The creation of scientific and technological complexes for the development of personalized drugs based on HSC GT will help automate, accelerate, and scale the production process.

CONCLUSION

The development of *ex vivo* HSC GT is currently relevant and promising. The development of such therapy will provide opportunities for etiological treatment of many incurable genetic diseases. Further exploration of this direction in gene therapy, improvement of existing methods, and the development of new ones will expand the range of diseases for which treatment with HSC GT is effective from both clinical and economic perspectives.

References

1. Carvalho M, Sepodes B, Martins AP. Regulatory and Scientific Advancements in Gene Therapy: State-of-the-Art of Clinical Applications and of the Supporting European Regulatory Framework. Frontiers in Medicine [Internet]. 2017; 4. Available from: https://www.frontiersin.org/journals/medicine/articles/10.3389/fmed.2017.00182/full.
2. Wang D, Gao G. State-of-the-art human gene therapy: part ii. gene therapy strategies and applications. 2014. Available from: https://pmc.ncbi.nlm.nih.gov/articles/PMC4440458/.
3. CAR T Cells: Engineering Immune Cells to Treat Cancer [Internet]. Cancer gov. 2022. Available from: https://www.cancer.gov/about-cancer/treatment/research/car-t-cells.
4. Wang JH, Gessler DJ, Zhan W, Gallagher TL, Gao G. Adeno-associated virus as a delivery vector for gene therapy of human diseases. Signal Transduction and Targeted Therapy. 2024; 9 (1). Available from: https://pubmed.ncbi.nlm.nih.gov/38565561/.
5. Kohn DB, Booth C, Shaw KL, Xu-Bayford J, Garabedian E, Trevisan V, et al. Autologous Ex Vivo Lentiviral Gene Therapy for Adenosine Deaminase Deficiency. New England Journal of Medicine. 2021; 384 (21): 2002–13. Available from: https://www.nejm.org/doi/full/10.1056/NEJMoa2027675.
6. Zhu Y, Zhu L, Wang X, Jin H. RNA-based therapeutics: an overview and prospectus. Cell Death and Disease [Internet]. 2022 Jul 23;13(7). Available from: https://www.nature.com/articles/s41419-022-05075-2
7. Li T, Yang Y, Qi H, Cui W, Zhang L, Fu X, et al. CRISPR/Cas9 therapeutics: progress and prospects. Signal Transduction and Targeted Therapy. 2023; 8 (1). Available from: https://www.nature.com/articles/s41392-023-01309-7.
8. Ferrari S, Valeri E, Conti A, Scala S, Aprile A, Di Micco R, et al. Genetic engineering meets hematopoietic stem cell biology for next-generation gene therapy. Cell Stem Cell]. 2023; 30 (5): 549–70. Available from: https://pubmed.ncbi.nlm.nih.gov/37146580/.
9. Meaker GA, Wilkinson AC. Ex vivo hematopoietic stem cell expansion technologies: recent progress, applications, and open questions. Experimental Hematology]. 2023; 130: 104136. Available from: https://pmc.ncbi.nlm.nih.gov/articles/PMC11511678/.
10. Horgan C, Watts K, Ram D, Rust S, Hutton R, Jones S, et al. A retrospective cohort study of Libmeldy (atidarsagene autotemcel) for MLD: What we have accomplished and what opportunities lie ahead. JIMD Reports. 2023; 64 (5): 346–52. Available from: https://onlinelibrary.wiley.com/doi/full/10.1002/jmd2.12378.
11. Duncan CN, Bledsoe JR, Grzywacz B, Beckman A, Bonner M, Eichler FS, et al. Hematologic Cancer after Gene Therapy for Cerebral Adrenoleukodystrophy. New England Journal of Medicine. 2024; 391 (14): 1287–301. Available from: https://www.nejm.org/doi/full/10.1056/NEJMoa2405541.
12. Rabinowitz J, Chan YK, Samulski RJ. Adeno-Associated Virus (AAV) Versus Immune Response. Viruses. 2019; 11 (2): 102. Available from: https://www.mdpi.com/1999-4915/11/2/102.
13. de Vasconcelos P, Lacerda JF. Hematopoietic Stem Cell Transplantation for Neurological Disorders: A Focus on Inborn Errors of Metabolism. Front Cell Neurosci. 2022; 16: 895511. Available from: https://www.frontiersin.org/journals/cellular-neuroscience/articles/10.3389/fncel.2022.895511/full.
14. Mikulska M, Gualandi F, Anserini P. Early and late complications of hematopoietic stem cell transplantation. Handb Clin Neurol. 2024; 202: 135–51.
15. Maragkou I, Maragkou I. The most expensive drugs in the US. Pharmaceutical Technology. 2024. Available from: https://www.pharmaceutical-technology.com/features/the-most-expensive-drugs-in-the-us/.

Литература

1. Carvalho M, Sepodes B, Martins AP. Regulatory and Scientific Advancements in Gene Therapy: State-of-the-Art of Clinical Applications and of the Supporting European Regulatory Framework. Frontiers in Medicine [Internet]. 2017; 4. Available from: https://www.frontiersin.org/journals/medicine/articles/10.3389/fmed.2017.00182/full.
2. Wang D, Gao G. State-of-the-art human gene therapy: part ii. gene therapy strategies and applications. 2014. Available from: https://pmc.ncbi.nlm.nih.gov/articles/PMC4440458/.
3. CAR T Cells: Engineering Immune Cells to Treat Cancer [Internet]. Cancer gov. 2022. Available from: https://www.cancer.gov/about-cancer/treatment/research/car-t-cells.
4. Wang JH, Gessler DJ, Zhan W, Gallagher TL, Gao G. Adeno-associated virus as a delivery vector for gene therapy of human diseases. Signal Transduction and Targeted Therapy. 2024; 9 (1). Available from: https://pubmed.ncbi.nlm.nih.gov/38565561/.
5. Kohn DB, Booth C, Shaw KL, Xu-Bayford J, Garabedian E, Trevisan V, et al. Autologous Ex Vivo Lentiviral Gene Therapy for Adenosine Deaminase Deficiency. New England Journal of Medicine. 2021; 384 (21): 2002–13. Available from: https://www.nejm.org/doi/full/10.1056/NEJMoa2027675.
6. Zhu Y, Zhu L, Wang X, Jin H. RNA-based therapeutics: an overview and prospectus. Cell Death and Disease [Internet]. 2022 Jul 23;13(7). Available from: https://www.nature.com/articles/s41419-022-05075-2
7. Li T, Yang Y, Qi H, Cui W, Zhang L, Fu X, et al. CRISPR/Cas9 therapeutics: progress and prospects. Signal Transduction and Targeted Therapy. 2023; 8 (1). Available from: https://www.nature.com/articles/s41392-023-01309-7.
8. Ferrari S, Valeri E, Conti A, Scala S, Aprile A, Di Micco R, et al. Genetic engineering meets hematopoietic stem cell biology for next-generation gene therapy. Cell Stem Cell]. 2023; 30 (5): 549–70. Available from: https://pubmed.ncbi.nlm.nih.gov/37146580/.
9. Meaker GA, Wilkinson AC. Ex vivo hematopoietic stem cell expansion technologies: recent progress, applications, and open questions. Experimental Hematology]. 2023; 130: 104136. Available from: https://pmc.ncbi.nlm.nih.gov/articles/PMC11511678/.
10. Horgan C, Watts K, Ram D, Rust S, Hutton R, Jones S, et al. A retrospective cohort study of Libmeldy (atidarsagene autotemcel) for MLD: What we have accomplished and what opportunities lie ahead. JIMD Reports. 2023; 64 (5): 346–52. Available from: https://onlinelibrary.wiley.com/doi/full/10.1002/jmd2.12378.
11. Duncan CN, Bledsoe JR, Grzywacz B, Beckman A, Bonner M, Eichler FS, et al. Hematologic Cancer after Gene Therapy for Cerebral Adrenoleukodystrophy. New England Journal of Medicine. 2024; 391 (14): 1287–301. Available from: https://www.nejm.org/doi/full/10.1056/NEJMoa2405541.
12. Rabinowitz J, Chan YK, Samulski RJ. Adeno-Associated Virus (AAV) Versus Immune Response. Viruses. 2019; 11 (2): 102. Available from: https://www.mdpi.com/1999-4915/11/2/102.
13. de Vasconcelos P, Lacerda JF. Hematopoietic Stem Cell Transplantation for Neurological Disorders: A Focus on Inborn Errors of Metabolism. Front Cell Neurosci. 2022; 16: 895511. Available from: https://www.frontiersin.org/journals/cellular-neuroscience/articles/10.3389/fncel.2022.895511/full.
14. Mikulska M, Gualandi F, Anserini P. Early and late complications of hematopoietic stem cell transplantation. Handb Clin Neurol. 2024; 202: 135–51.
15. Maragkou I, Maragkou I. The most expensive drugs in the US. Pharmaceutical Technology. 2024. Available from: https://www.pharmaceutical-technology.com/features/the-most-expensive-drugs-in-the-us/.

TRANSCRIPTION PROFILE IN PREOPERATIVE AROMATASE INHIBITOR RESPONSE TEST IN BREAST CANCER PATIENTS

Burmenskaya OV ✉, Trofimov DYu, Kometova VV, Rodionova MV, Rodionov VV

Kulakov National Medical Research Center for Obstetrics, Gynecology and Perinatology, Moscow, Russia

Today, preoperative hormone therapy is a standard procedure in the context of treatment of ESR+/HER2-negative early-stage breast cancer. Transcription profiles of genes helps make assessment of effectiveness of this therapy more accurate. This study aimed to investigate the changes in gene expression caused by the preoperative aromatase inhibitor response test in postmenopausal women with ESR+/HER2-negative breast cancer. The participants were 100 breast cancer patients treated at the Department of Breast Pathology of Kulakov National Medical Research Center for Obstetrics, Gynecology and Perinatology. We did a pathomorphological study of FFPE blocks (trephine biopsied before the hormone response test was prescribed) and intraoperative samples, and immunohistochemical (Ki67, ER, PR, HER2/neu) and molecular genetic studies of 45 target genes (quantitative RT-PCR). Aromatase inhibitors in the preoperative hormone response test caused significant changes in the mRNA expression of 37 genes in breast tumors: for 35 of them (*ESR1, PGR, AR, ERBB2, FGFR4, MKI67, MYBL2, CCNB1, AURKA, BIRC5, CCND1, CCNE1, CDKN2A, KIF14, PPP2R2A, PTTG1, TMEM45B, TPX2, ANLN, MMP11, CTSL2, EMSY, PAK1, BCL2, BAG1, PTEN, TYMS, EXO1, UBE2T, NAT1, SCGB2A2, GATA3, FOXA1, ZNF703, CD274/PD-L1*) the level was decreased, and for 2 genes it increased (*SFRP1, KRT5*). The results of this study can be used in the development of a hormone sensitivity test and personification of adjuvant systemic treatment for breast cancer patients.

Keywords: ESR+/Her2-negative breast cancer, mRNA gene expression, aromatase inhibitors, letrozole, real-time reverse transcription polymerase chain reaction, RT-qPCR

ТРАНСКРИПЦИОННЫЙ ПРОФИЛЬ В ПРЕДОПЕРАЦИОННОМ ТЕСТЕ ИНГИБИТОРАМИ АРОМАТАЗЫ У БОЛЬНЫХ РАКОМ МОЛОЧНОЙ ЖЕЛЕЗЫ

О. В. Бурменская ✉, Д. Ю. Трофимов, В. В. Кометова, М. В. Родионова, В. В. Родионов

Национальный медицинский исследовательский центр акушерства, гинекологии и перинатологии имени В. И. Кулакова, Москва, Россия

Тестовая предоперационная гормонотерапия стала стандартной процедурой лечения ESR+/Her2-негативного рака молочной железы ранних стадий. Хорошим подспорьем в оценке эффективности данной терапии могут стать транскрипционные профили генов. Целью исследования было оценить изменения экспрессионной активности генов при проведении предоперационного теста на гормоночувствительность опухоли к ингибиторам ароматазы у женщин постменопаузального возраста при ESR+/HER2-негативном раке молочной железы. В исследование вошло 100 больных раком молочной железы, проходивших лечение в отделении патологии молочной железы ФГБУ «НМИЦ АГП им. В.И. Кулакова». Выполнено патоморфологическое исследование FFPE-блоков трепан-биопсии, проведенной до назначения теста на гормоночувствительность, и операционного материала, а также иммуногистохимическое (Ki67, ER, PR, HER2/neu) и молекулярно-генетическое исследование экспрессионной панели 45 целевых генов методом количественной полимеразной цепной реакции в режиме реального времени. Применение ингибиторов ароматазы в предоперационном тесте на гормоночувствительность сопровождается статистически значимыми изменениями в экспрессии мРНК 37 генов в опухолях молочной железы, из них снижение уровня экспрессии установлено для 35 генов (*ESR1, PGR, AR, ERBB2, FGFR4, MKI67, MYBL2, CCNB1, AURKA, BIRC5, CCND1, CCNE1, CDKN2A, KIF14, PPP2R2A, PTTG1, TMEM45B, TPX2, ANLN, MMP11, CTSL2, EMSY, PAK1, BCL2, BAG1, PTEN, TYMS, EXO1, UBE2T, NAT1, SCGB2A2, GATA3, FOXA1, ZNF703, CD274/PD-L1*), повышение для 2 генов (*SFRP1, KRT5*). Полученные результаты могут быть использованы в дальнейшем при разработке теста на гормоночувствительность и персонификации адъювантной системной терапии больных раком молочной железы.

Ключевые слова: ESR+/HER2-негативный рак молочной железы, экспрессия мРНК генов, ингибиторы ароматазы, летрозол, обратная транскрипция, количественная полимеразная цепная реакция в режиме реального времени, ОТ-кПЦР

Identification of five main molecular subtypes of breast tumors and formalization of differential approach to the treatment of breast cancer (BC) patients constituted a real breakthrough in oncology. Tumors expressing estrogen (ESR) and progesterone (PGR) receptors are of luminal subtypes; as a rule, they are susceptible to hormone therapy.

In postmenopausal women, estrogens are formed mainly with the participation of the aromatase enzyme, which converts androgens synthesized in the adrenal glands and adipose tissue (testosterone and androstenedione) into estradiol and estrone. Therefore, in the context of treatment of breast tumors of luminal subtypes, this cohort of patients receives selective aromatase inhibitors (letrozole, anastrozole), which block synthesis of estrogens through highly specific competitive binding to the aromatase subunit encoded by the cytochrome P450 CYP19A1 gene.

Tumors expressing estrogen receptor are prevalent among molecular subtypes of BC [1, 2]. However, even within this large group, there are significant differences in the features of the course of the disease and response to hormone therapy, which necessitates study of all learnable biological parameters of a malignant neoplasm with the aim to devise the optimal treatment tactics.

Preoperative hormone response test is one of the tools designed for the purpose. This test enables prescription of a short-term (2–4 weeks) hormonal drugs course before surgery. Evaluation of the dynamics of tumor proliferation by monitoring changes of the level of Ki67 and expression of hormonal receptors allows predicting clinical response to and effectiveness of endocrinotherapy in vivo, and consequently free some patients from unnecessary highly toxic chemotherapy. The recommendation to do hormone therapy testing was included in the St. Gallen International Consensus Guidelines for treatment of early breast cancer issued in 2021, and were kept in the 2023 edition of the paper [3, 4]; Russian breast cancer treatment guidelines contain similar recommendations [5, 6].

BC-specific transcription panels of genes involved in oncogenesis, such as Oncotype DX, PAM50, Mammaprint, and Russian products, can be a useful tool in evaluating the effectiveness of therapy [7, 8].

In this connection, this study aimed to investigate the changes in gene expression caused by the preoperative aromatase inhibitor response test in postmenopausal women with ESR+/HER2-negative breast cancer.

The study aimed to investigate the changes in gene expression caused by the preoperative aromatase inhibitor response test in postmenopausal women with ESR+/HER2-negative breast cancer.

METHODS

The study involved 100 breast cancer patients treated at the Department of Breast Pathology of Academician V. I. Kulakov National Medical Research Center for Obstetrics, Gynecology and Perinatology, from January, 2019 to August, 2024. We studied samples trephine biopsied from each participant before the hormone response test, and samples taken during surgery.

The inclusion criteria were: invasive breast cancer, luminal Her2-negative tumor subtype, postmenopausal age, preoperative test for tumor sensitivity to aromatase inhibitors. Exclusion criteria: inadequate quality of trephine biopsied samples (unfit for molecular genetic studies).

The preoperative hormone sensitivity test implied taking aromatase inhibitors (letrozole 2.5 mg or anastrozole 1 mg) once a day for 2–4 weeks.

We did histological and immunohistochemical studies of the biopsy and intrasurgery samples, which were taken within 30 minutes after tumor removal and preserved for 48 hours in neutral buffered formalin. After preservation, the samples were processed in an automatic LOGOS microwave histoprocessor (Milestone, Italy). The sections, 4–5 microns thick, were stained with hematoxylin and eosin. Microscopic preparations were subjected to survey microscopy enabled by an Olympus BX46 light microscope (Olympus Corp., Japan). For immunohistochemical diagnostics, we used a BenchMark ULTRA system (Ventana, Roche) employing antibodies to estrogen receptors (ER, clone SP1, VENTANA), progesterone (PgR, clone 1E2, VENTANA), to Ki67 (clone MIB–1, VENTANA), to the oncoprotein of the human epidermal growth factor type 2 gene (c–erbB2).

For molecular genetic studies, we used a transcription panel that included 45 target genes (ESR1, PGR, AR, ERBB2, GRB7, EGFR, FGFR4, MKI67, MYBL2, CCNB1, AURKA, BIRC5, MYC, CCND1, CCNE1, CDKN2A, KIF14, PPP2R2A, PTTG1, SFRP1, TMEM45B, TMEM45A, TPX2, MMP11, CTSL2, EMSY, PAK1, ANLN, BCL2, BAG1, PTEN, TYMS, EXO1, UBE2T, TPT1, SCGB2A2, KRT5, MIA, GATA3, FOXA1, ZNF703, NAT1 CD68, TRAC, CD274/PD-L1) and three reference genes (B2M, GUSB, HPRT1). Two to three paraffin sections 4-5 microns thick were placed in dry plastic 1.5 ml tubes. The material was selected and prepared by a pathomorphologist, with the results of the pathomorphological study factored in.

Total RNA was isolated after pretreatment of samples with proteinase K (PREP-PK kit; DNA-Technology LLC, Russia), then we used a PREP-NA PLUS kit (DNA-Technology LLC, Russia) to isolate nucleic acids in alcohol deposits. The resulting RNA preparations were immediately used to set up a reverse transcription reaction with a mixture of oligonucleotides specific to each gene. The reverse transcription reaction was maintained for 30 minutes at 40 °C, followed by a 10-minute reverse transcriptase inactivation at 95 °C.

The transcription profile of the genes was determined by multiplex Real-time reverse transcription polymerase chain reaction (RT-qPCR). The PCR was enabled by DTprime detecting amplifiers (DNA-Technology LLC, Russia); the program was as follows: 94 °C for 5 minutes; five cycles of 94 °C for 30 s — 64 °C for 15 s; then 45 cycles of 94 °C for 10 s — 64 °C 15 s, and storage.

The reaction mixtures included oligonucleotides specific to mRNA, not amplifying from genomic DNA template, flanking amplicons measuring up to 100–120 bp, which is important when working with DNA after preservation in formalin. The amplification products were detected at the primer annealing temperature by using fluorescently labeled TaqMan probes (Fam, Cy5).

After amplification, we calculated the abundance of transcript by comparing indicator cycles (ΔCt) with the norm relative to the reference genes B2M, GUSB, HPRT1. The data are given in relative units (RU) on the ln scale.

To improve perception of the results of the study, we calculated the ratio (R) of expression before and after therapy: R = Eb/Ea, where Eb is the normalized expression level before therapy, and Ea is the normalized expression level after therapy. R > 1 was regarded as dropping expression, R < 1 as rising expression.

Statistical methods

The results obtained are presented as Me [1Q–3Q] (median, 1st and 3rd quartiles). Comparing the transcription profiles of genes before and after aromatase inhibitor therapy, we employed

Table 1. Pathomorphological characteristics of tumors

Characteristic	Quantity (%)
Tumor size (sT)	
T1 (up to 2 cm): • T1a (> 0.1 cm, but ≤ 0.5 cm) • T1b (> 0.5 cm, but ≤ 1 cm) • T1c (> 1 cm, but ≤ 2 cm)	75 (75%)
	2 (2%)
	21 (21%)
	52 (52%)
T2 (> 2, but ≤ 5)	25 (25%)
Status of regional lymph nodes (rN)	
N0	76 (76%)
N1	17 (17%)
N2	4 (4%)
N3	3 (3%)
Histological variant	
Invasive cancer of a non-specific type	65 (65%)
Lobular cancer	23 (23%)
Special variants of cancer	12 (12%)
Degree of malignancy	
G1	18 (18%)
G2	74 (74%)
G3	8 (8%)

the Wilcoxon signed-rank test. The values were considered statistically significant at $p < 0.01$. The calculation was done in SPSS 17 statistical processing program (IBM, USA).

RESULTS

The study included 100 BC patients aged 49–84 years (63.3 [51–79]). Table 1 gives the pathomorphological characteristics of their tumors.

In 75% of cases, the tumor was smaller than 2 cm. In 2/3 (76%) of the patients, there were no metastases to the regional lymph nodes diagnosed. No cases involved distant metastases.

The nonspecific variant was the prevailing one: 65 cases (65%). Eighteen percent of samples were from low grade tumors (G1), 74% from intermediate grade cancers (G2), and 8% from high grade neoplasms (G3).

Using the IHC test, we established that 44 (44%) patients suffered a luminal A subtype of BC, and 56 (56%) participants had luminal B HER2-negative subtype of the tumor.

Aromatase inhibitors taken preoperatively as a hormone sensitivity test caused significant changes in the mRNA expression of 37 genes, as registered in the studied tumor samples, with the expression level dropping for 35 genes (*ESR1, PGR, AR, ERBB2, FGFR4, MKI67, MYBL2, CCNB1, AURKA, BIRC5, CCND1, CCNE1, CDKN2A, KIF14, PPP2R2A, PTTG1, TMEM45B, TPX2, ANLN, MMP11, CTSL2, EMSY, PAK1, BCL2, BAG1, PTEN, TYMS, EXO1, UBE2T, NAT1, SCGB2A2, GATA3, FOXA1, ZNF703, CD274/PD-L1*), and rising for two *SFRP1* and *KRT5* genes (Table 2).

Figure 1 shows the results for five proliferation markers, estrogen and progesterone receptors, the levels of which decreased after treatment.

A statistically significant drop of expression was registered in the group of markers of proliferation and regulation of the cell cycle. The most pronounced changes were noted for the *MYBL2, AURKA, PTTG1, TPX2,* and *ANLN* genes, with the expression decreasing 3.5-5.5 times in 96–97% of women.

We have also registered significant expression drops:

– in the group of markers of cell migration and cytoskeleton organization, with the most pronounced decrease observed for *MMP11*, the expression level of which went down 3.4 times on average (interquartile range 1.9–6.3) in 94% of women;

– in the group of DNA repair markers, with the most pronounced decrease observed for *EXO1*, the expression level of which went down 6.4 times on average (interquartile range 3.1–15.3) in 96% of women;

– in the group of transcription factors, with the most pronounced decrease observed for *ZNF703*, the expression level of which went down 6.6 times on average (interquartile range 2.9–12.6) in 97% of women;

– in the group of hormonal receptors, with a 2.3-fold (average) decrease of the expression of the *ESR1* mRNA gene in 84% of women, and the most pronounced decrease observed for the *PGR* and *AR* genes, the expression of which dropped more than 2-fold in over 90% of the participants;

– in the ungrouped markers of the ubiquitination gene of *UBE2T* proteins and the arylamine-N-acetyltransferase *NAT1* gene (more than 90% of women).

A slightly less impressive but statistically significant decrease in expression was observed for apoptosis markers (*BCL2, BAG*), growth factor receptors (*FGFR4, ERBB2*), secretory protein mammoglobin *SCGB2A2*, and *PTEN*.

The level of expression increased significantly for the marker of epithelial cell differentiation of cytokeratin *KRT5* and tumor suppressor *SFRP1*: this was observed in more than half of the patients, 67% and 57% of cases, respectively.

DISCUSSION

Estrogen-positive or luminal breast tumors account for up to 70–75% of all BC cases [1, 2], and ESR1-dependent signaling pathways regulated by estrogens play one of the key roles in tumor progression.

Table 2. Changes in the expression of mRNA markers after intake of aromatase inhibitors

Marker	Median expression level, ln			Expression level change, times			
	before therapy	after therapy	p-level	Median	quartile 1	quartile 3	Share of samples with a change in expression*
Markers of cell cycle proliferation and regulation (decreased expression*)							
MKI67	−4	−5.4	7.27E−16	3.7	1.9	8.3	91%
MYBL2	−3.1	−4.9	5.17E−18	5.5	3	10.7	97%
AURKA	−4.7	−6.1	3.67E−17	3.9	2.4	6.1	96%
CCNB1	−3.3	−4.2	3.15E−14	2.1	1.5	3.9	90%
BIRC5	−5	−7	9.99E−16	8.8	3.5	16.6	90%
CCND1	−0.4	−1.3	3.11E−16	2.4	1.8	3.3	92%
CCNE1	−5	−6	2.92E−15	3	2	4	91%
CDKN2A	−2.4	−2.6	5.14E−06	1.2	0.9	1.7	70%
KIF14	−6.5	−8.1	1.19E−13	3.7	2.1	7.2	85%
PPP2R2A	−2.9	−3.4	2.56E−09	1.7	1.1	2.7	77%
PTTG1	−3.4	−4.6	8.12E−18	3.5	2.1	5.1	97%
TMEM45B	−2.9	−3.3	4.50E−05	1.4	0.9	2.4	67%
TMEM45A	−4.2	−4.2	0.036	–	–	–	–
TPX2	−3.2	−4.6	7.09E−17	4.8	2.7	8	96%
TPT1	−6	−6.2	0.269	–	–	–	–
ANLN	−4.1	−5.7	6.03E−17	4.5	3	7.5	97%
Migration, invasion, cytoskeleton organization (decreased expression)							
EMSY	−2.8	−3.4	1.99E−14	1.6	1.3	2.1	88%
PAK1	−2.4	−3	1.20E−16	1.8	1.5	2.4	93%
MMP11	−1.6	−3.1	8.58E−15	3.4	1.9	6.3	94%
CTSL2	−4.4	−5	2.32E−08	1.7	1.1	2.5	77%
DNA replication and repair (decreased expression)							
EXO1	−5.4	−7.4	1.20E−17	6.4	3.1	15.3	
TYMS	−4.1	−5.2	5.18E−17	3	1.9	5	
Hormone receptors (decreased expression)							
ESR1	0.1	−0.7	6.11E−12	2.3	1.2	3.6	
PGR	−2.8	−4.7	1.90E−16	5.5	2.6	11.1	
AR	−1.9	−3	3.30E−16	3.4	2	5.7	
Tumor suppressors							
PTEN (decrease)	−2.1	−2.5	1.95E−09	1.4	1	2.1	
SFRP1 (increase*)	−4	−3.5	0.007	1.4	0.6	4.1	
Apoptosis (decreased expression)							
BCL2	−2.9	−3.5	5.09E−11	2	1.1	2.9	
BAG1	−2.9	−3.3	3.86E−15	1.6	1.2	2.2	
Growth factor receptors (decreased expression)							
GRB7	−2.2	−2.2	0.064	–	–	–	
FGFR4	−4.9	−5.5	2.18E−06	1.7	1	3.3	
ERBB2	−0.8	−1.2	2.55E−09	1.4	1	2.1	
EGFR	−3.7	−3.7	0.331	–	–	–	
Cell differentiation							
KRT5 (increase)	−5	−4.3	0.001	1.3	0.8	3.7	
SCGB2A2 (decrease)	−0.2	−1.2	0.002	2.2	0.5	6.1	
MIA	−6.1	−6.3	0.412	–	–	–	
Transcription factors (decreased expression)							
FOXA1	−0.7	−1.4	1.71E−13	1.9	1.5	2.7	
GATA3	−1.1	−1.9	1.65E−12	2.3	1.4	3.4	
ZNF703	−3.6	−5.3	8.43E−18	6.6	2.9	12.6	
MYC	−1.3	−1.2	0.029	–	–	–	
OTHER (decrease)							
NAT1	−3.6	−4.7	1.93E−15	2.9	1.6	4.9	
UBE2T	−3.4	−4.9	1.03E−17	3.9	2.3	5.9	
Immunity							
CD274 (decrease)	−5.7	−5.9	0.003	1.3	0.8	1.9	
TRAC	−2.4	−2.3	0.386	–	–	–	
CD68	−2	−2	0.4	–	–	–	

Note: * $R > 1$ — decreased expression, $R < 1$ — increased expression.
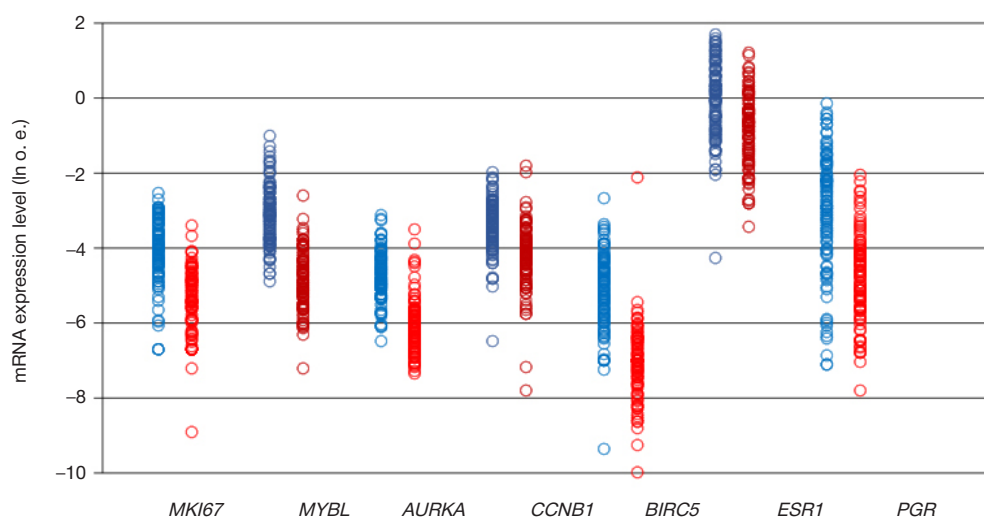
Fig. Changes in the mRNA expression of proliferation and hormonal reception genes during a test for tumor hormone sensitivity to aromatase inhibitors. Dots mark the individual indicators of the mRNA gene expression level in the tumor

The theory by E.V. Jensen, who described the model of action of the hormone, laid the foundation of the current understanding of how steroid hormones act. Within the framework of this model, a steroid hormone molecule, having penetrated into the target cell, binds to a specific receptor, and the resulting hormone-receptor complex is translocated into the cell nucleus, where it interacts with specific DNA sequences and changes the expression of the corresponding genes [9].

The ESR1 receptor is an estrogen-activated transcription factor. As such, it regulates the expression of genes involved in cell cycles, proliferation and apoptosis. Activation of *ESR1* triggers the expression of *MYC*, *Cyclin D1*, *FOXM1*, *GREB1*, *BCL2* or amphiregulin, *IGF-1* and *CXCL12*, which possess oncogenic potential [2]. It is believed that ligand-activated *ESR1* binds to estrogen responsive elements (ERE) in promoters of target genes, and it can also interact with transcription factors, i.e., activator protein 1 (AP1) and specific protein 1 (SP1). Thus, this genomic action regulates the transcription of hundreds of target genes involved in cell growth and differentiation [2, 10].

ESR1 can also embed in caveoles, special recesses in the cytoplasmic membrane of cells, and interact with G proteins, thus participating in the production of secondary messengers (cAMP) and stimulation of various signaling pathways, like *PI3K/AKT* or *Ras/MAPK*. This non-genomic activity of ERα eventually leads to the activation of transcription factors involved in the regulation of cell proliferation and survival [2, 10].

Therefore, there is no doubt that a complete lack or smaller amounts of the *ESR1* ligand (estrogens) associated with aromatase inhibitor therapy translate into an impressive drop of the level of expression of mRNA of a large number of genes. The results we received confirm a significant slowdown of mRNA expression for transcription factors *GATA3, FOXA1, ZNF703*, apoptosis *BCL2, BAG1*, proliferation and cell cycle regulation (*MKI67, MYBL2, CCNB1, AURKA, BIRC5, CCND1, CCNE1, CDKN2A, KIF14, PPP2R2A, PTTG1, TMEM45B, ANLN, TPX2*). Deterioration of proliferative activity also decelerates the expression of markers of replication and control of DNA repair (*TYMS, EXO1*), cytoskeleton and cell migration markers (*MMP11, CTSL2, EMSY, PAK*), and the process of ubiquitination of *UBE2T* proteins.

Interestingly, another study that focused on atypical breast hyperplasia showed an increase in the expression of mRNA genes from our panel, namely, *ESR1, AR*, epidermal growth factor receptor *ERBB2*, transcription factors *FOXA1, GATA3, ZNF703*, and decreasing amounts of cytokeratin *KRT5* and

tumor suppressor *SFRP1* [11]. The authors of that study associated these changes with activation of signaling pathways involved in oncogenesis.

In our study, aromatase inhibitor therapy caused a slowdown of the expression of mRNA of the *ESR1, AR, FOXA1, GATA3, ZNF703, ERBB2* genes, and acceleration of the expression of mRNA of the *KRT5* and *SFRP1* genes, which may indicate a positive effect the said therapy has on signaling pathways that participate in oncogenesis.

We registered significant acceleration of expression only for two markers, *KRT5* and *SFRP1*. High level of expression of the cytokeratin gene *KRT5* is characteristic of the breast basal epithelium. Luminal epithelium expresses cytokeratins *KRT8* and *KRT18* [2].

Currently, it is generally accepted that the main physiological regulator of the expression of nuclear receptors in the body is the concentration of circulating steroid hormones. Estrogens boost synthesis of their own receptors as well as receptors of progesterone androgen [10]. Therefore, the attenuating effect of the therapy on the expression of mRNA of *ESR1, PGR*, and *AR* was predictable. It should be noted that initially, we noted decreasing expression of the progesterone receptor in the first place, and the slowdown of expression of that for *ESR1* was registered secondary to that.

The mRNA expression of the *PGR* gene is directly regulated by the activated estrogen receptor. Some authors even consider *PGR* to be an indicator of the *ESR1* functionality [12]. Therefore, with dropping estrogens and the transcriptional activity of the *ESR1* gene in the background, the expression of the *PGR* gene's mRNA decreases, too.

CONCLUSIONS

Aromatase inhibitors taken preoperatively in the context of the hormone sensitivity test cause significant changes in the mRNA expression of 37 genes, with that for 35 genes (*MKI67, MYBL2, CCNB1, AURKA, BIRC5, CCND1, CCNE1, CDKN2A, KIF14, PPP2R2A, PTTG1, TMEM45B, TPX2, ANLN, ESR1, PGR, AR, ERBB2, FGFR4, MMP11, CTSL2, EMSY, PAK1, BCL2, BAG1, GATA3, FOXA1, ZNF703, TYMS, EXO1, PTEN, UBE2T, NAT1, SCGB2A2, CD274*) dropping, and for 2 genes (*KRT5* and *SFRP1*) growing. The results of this study can be used in the development of the hormone sensitivity test effectiveness assessment method and personification of adjuvant systemic treatment for breast cancer patients.

References

1. Ahn SG, Nam SJ, Ahn SH, Jung Y, Park HK, Lee SJ, et al. Clinical Outcomes Following Letrozole Treatment according to Estrogen Receptor Expression in Postmenopausal Women: LETTER Study (KBCSG-006). J Breast Cancer. 2021; 24 (2): 164–74. DOI: 10.4048/jbc.2021.24.e17.

2. Clusan L, Ferrière F, Flouriot G, Pakdel F. A Basic Review on Estrogen Receptor Signaling Pathways in Breast Cancer. Int J Mol Sci. 2023; 24 (7): 6834. DOI: 10.3390/ijms24076834.

3. Sparano JA, Gray RJ, Ravdin PM, et al. Clinical and genomic risk to guide the use of adjuvant therapy for breast cancer. N Engl J Med. 2019; 380 (25): 2395–405. Available from: https://doi.org/10.1056/NEJMoa1904819.

4. Burstein HJ, Curigliano G, Thürlimann B, et al. Customizing local and systemic therapies for women with early breast cancer: the St. Gallen International Consensus Guidelines for treatment of early breast cancer 2021. Ann Oncol. 2021; 32 (10): 1216–35. Available from: https://doi.org/10.1016/j.annonc.2021.06.023.

5. Zolotoj standart profilaktiki, diagnostiki, lechenija i reabilitacii bol'nyh RMZh. Rossijskoe obshhestvo onkomammologov. 2024; 297 s. Russian.

6. Tjuljandin SA, Stenina MB, Frolova MA. Prakticheskie instrumenty, oblegchajushhie vybor ad#juvantnoj lekarstvennoj terapii u bol'nyh operabel'nym ljuminal'nym HER2-negativnym rakom molochnoj zhelezy. Zlokachestvennye opuholi. 2024; 14 (2): 51–57. Dostupno po ssylke: https://doi.org/10.18027/2224-5057-2024-003. Russian.

7. Bozhenko VK, Trocenko ID , Kudinova EA, Vardanjan SG, Zaharenko MV, Solodkij VA, Makarova MV. Vozmozhnosti tipirovanija raka molochnoj zhelezy s ispol'zovaniem metodiki OT-PCR. Sibirskij onkologicheskij zhurnal. 2019; 18 (5): 61–67. DOI: 10.21294/1814-4861-2019-18-5-61-67. Russian.

8. Burmenskaya OV, Trofimov DYu, Kometova VV, Sergeev IV, Maerle AV, Rodionov VV, i dr. Razrabotka i opyt ispol'zovanija transkripcionnoj signatury genov v diagnostike molekuljarnyh podtipov raka molochnoj zhelezy. Akusherstvo i ginekologija. 2020; 2: 132–140. Dostupno po ssylke: https://dx.doi.org/10.18565/aig.2020.2.132-140. Russian.

9. Krasilnikov MA, Shherbakov AM. Signal'nye puti, reguliruemye jestrogenami, i ih rol' v opuholevoj progressii: novye fakty i napravlenija poiska. Uspehi molekuljarnoj onkologii. 2014; 1: 18–26. Russian.

10. Dovzhikova IV, Andrievskaja IA. Receptory jestrogenov (obzor literatury). Chast' 1. Bjulleten' fiziologii i patologii dyhanija. 2019; 72: 120–27. DOI: 10.12737/article_5d0ad2e5d54867.15780111. Russian.

11. Gregory KJ, Roberts AL, Conlon EM, Mayfield JA, Hagen MJ, Crisi GM, et al. Gene expression signature of atypical breast hyperplasia and regulation by SFRP1. Breast Cancer Res. 2019; 21 (1): 76. DOI: 10.1186/s13058-019-1157-5.

12. Kumar M, Salem K, Jeffery JJ, Yan Y, Mahajan AM, Fowler AM. Longitudinal Molecular Imaging of Progesterone Receptor Reveals Early Differential Response to Endocrine Therapy in Breast Cancer with an Activating ESR1 Mutation. J Nucl Med. 2021; 62 (4): 500–506. DOI: 10.2967/jnumed.120.249508. Epub 2020 Aug 28.

Литература

1. Ahn SG, Nam SJ, Ahn SH, Jung Y, Park HK, Lee SJ, et al. Clinical Outcomes Following Letrozole Treatment according to Estrogen Receptor Expression in Postmenopausal Women: LETTER Study (KBCSG-006). J Breast Cancer. 2021; 24 (2): 164–74. DOI: 10.4048/jbc.2021.24.e17.

2. Clusan L, Ferrière F, Flouriot G, Pakdel F. A Basic Review on Estrogen Receptor Signaling Pathways in Breast Cancer. Int J Mol Sci. 2023; 24 (7): 6834. DOI: 10.3390/ijms24076834.

3. Sparano JA, Gray RJ, Ravdin PM, et al. Clinical and genomic risk to guide the use of adjuvant therapy for breast cancer. N Engl J Med. 2019; 380 (25): 2395–405. Available from: https://doi.org/10.1056/NEJMoa1904819.

4. Burstein HJ, Curigliano G, Thürlimann B, et al. Customizing local and systemic therapies for women with early breast cancer: the St. Gallen International Consensus Guidelines for treatment of early breast cancer 2021. Ann Oncol. 2021; 32 (10): 1216–35. Available from: https://doi.org/10.1016/j.annonc.2021.06.023.

5. Золотой стандарт профилактики, диагностики, лечения и реабилитации больных РМЖ. Российское общество онкомаммологов. 2024; 297 с.

6. Тюляндин С. А., Стенина М. Б., Фролова М. А. Практические инструменты, облегчающие выбор адъювантной лекарственной терапии у больных операбельным люминальным HER2-негативным раком молочной железы. Злокачественные опухоли. 2024; 14 (2): 51–57. Доступно по ссылке: https://doi.org/10.18027/2224-5057-2024-003.

7. Боженко В. К., Троценко И. Д., Кудинова Е. А., Варданян С. Г., Захаренко М. В., Солодкий В. А., Макарова М. В. Возможности типирования рака молочной железы с использованием методики ОТ-ПЦР. Сибирский онкологический журнал. 2019; 18 (5): 61–67. DOI: 10.21294/1814-4861-2019-18-5-61-67.

8. Бурменская О. В., Трофимов Д. Ю., Кометова В. В., Сергеев И. В., Маерле А. В., Родионов В.В., и др. Разработка и опыт использования транскрипционной сигнатуры генов в диагностике молекулярных подтипов рака молочной железы. Акушерство и гинекология. 2020; 2: 132–140. Доступно по ссылке: https://dx.doi.org/10.18565/aig.2020.2.132-140.

9. Красильников М. А., Щербаков А. М. Сигнальные пути, регулируемые эстрогенами, и их роль в опухолевой прогрессии: новые факты и направления поиска. Успехи молекулярной онкологии. 2014; 1: 18–26.

10. Довжикова И. В, Андриевская И. А. Рецепторы эстрогенов (обзор литературы). Часть 1. Бюллетень физиологии и патологии дыхания. 2019; 72: 120–27. DOI: 10.12737/article_5d0ad2e5d54867.15780111.

11. Gregory KJ, Roberts AL, Conlon EM, Mayfield JA, Hagen MJ, Crisi GM, et al. Gene expression signature of atypical breast hyperplasia and regulation by SFRP1. Breast Cancer Res. 2019; 21 (1): 76. DOI: 10.1186/s13058-019-1157-5.

12. Kumar M, Salem K, Jeffery JJ, Yan Y, Mahajan AM, Fowler AM. Longitudinal Molecular Imaging of Progesterone Receptor Reveals Early Differential Response to Endocrine Therapy in Breast Cancer with an Activating ESR1 Mutation. J Nucl Med. 2021; 62 (4): 500–506. DOI: 10.2967/jnumed.120.249508. Epub 2020 Aug 28.

ROLE OF OXIDATIVE STRESS IN PATHOGENESIS OF BONE DESTRUCTION SYNDROME IN PATIENTS WITH CHRONIC LYMPHOCYTIC LEUKEMIA

Osikov MV[1,2] ✉, Korobkin EA[1,2]

[1] South Ural State Medical University, Chelyabinsk, Russia

[2] Chelyabinsk Regional Clinical Hospital, Chelyabinsk, Russia

Reduced bone mineral density (BMD), osteopenia, and osteoporosis are slightly more common in patients with chronic lymphocytic leukemia (CLL). The risk of osteoporotic fractures in individuals with CLL is higher, than in healthy individuals of the same age. The mechanism underlying the CLL-associated BMD reduction can be related to decreased antioxidant protection and oxidative stress (OS). The study aimed to assess the relationship between oxidative stress, antioxidant protection, and osteopenia indicators in patients with CLL. Males aged 50–70 years were examined. Group 1 consisted of 14 healthy men, group 2 consisted of 54 patients with CLL having no BMD alterations, and group 3 consisted of 22 patients with CLL having signs of osteopenia. A densitometer was used to estimate BMD, T- and Z-scores of the lumbar vertebrae, proximal femoral neck (PFN), proximal femoral bone in all groups. At the beginning of the study, the levels of lipid peroxidation (LPO) products were determined in blood serum in all groups and bone tissue homogenate in groups 2 and 3; the total antioxidant status (TAS) was also determined. Bone densitometry indicators, serum LPO and TAS were assessed in all groups after 6 months of follow-up. At the beginning of the study osteopenia in PFN based on bone densitometry data was revealed in 29% of patients, while 6 months later osteopenia of all localizations was observed in 55% of patients. At the beginning of the study patients with CLL and osteopenia showed OS and reduced TAS in both blood serum and bone tissue. After 6 months patients with CLL and osteopenia showed signs of OS progression and TAS reduction. In patients with CLL, serum and bone tissue OS indicators are comparable and can be used to predict the onset of osteopenia within 6 months.

Keywords: chronic lymphocytic leukemia, bone mineral density, osteopenia, oxidative stress, lipid peroxidation, redox status

РОЛЬ ОКИСЛИТЕЛЬНОГО СТРЕССА В ПАТОГЕНЕЗЕ ОСТЕОДЕСТРУКТИВНОГО СИНДРОМА У БОЛЬНЫХ С ХРОНИЧЕСКИМ ЛИМФОЛЕЙКОЗОМ

М. В. Осиков[1,2] ✉, Е. А. Коробкин[1,2]

[1] Южно-Уральский государственный медицинский университет Министерства здравоохранения России, Челябинск, Россия

[2] Челябинская областная клиническая больница, Челябинск, Россия

У пациентов с хроническим лимфоцитарным лейкозом (ХЛЛ) несколько чаще наблюдаются снижение минеральной плотности кости (МПК), остеопения и остеопороз. Риск остеопоротических переломов при ХЛЛ выше, чем у здоровых лиц того же возраста. Механизм снижения МПК при ХЛЛ может быть связан со снижением антиоксидантной защиты и окислительным стрессом (ОС). Целью работы было исследовать взаимосвязь между показателями окислительного стресса, антиоксидантной защиты и показателями остеопении у пациентов с ХЛЛ. Обследовали мужчин в возрасте 50–70 лет. Группу 1 составили 14 здоровых мужчин, группу 2 — 54 пациента с ХЛЛ без изменений МПК, группу 3 — 22 пациента с ХЛЛ с признаками остеопении. На денситометре оценивали МПК, Т- и Z-критерии в поясничных позвонках, шейке бедренной кости (ШПОБК), проксимальном отделе бедренной кости во всех группах. На старте исследования в сыворотке во всех группах и в гомогенате костной ткани в группах 2 и 3 определяли содержание продуктов перекисного окисления липидов (ПОЛ); общий антиоксидантный статус (ОАС). Показатели остеоденситометрии, ПОЛ и ОАС в сыворотке крови во всех группах оценивали через 6 месяцев наблюдения. На старте исследования по данным остеоденситометрии у 29% больных с ХЛЛ выявлена остеопения в ШПОБК, а через 6 месяцев остеопению наблюдали во всех локализациях у 55% больных. На старте исследования у пациентов с ХЛЛ и остеопенией в сыворотке и костной ткани зафиксированы ОС и сниженный ОАС. Через 6 месяцев у пациентов с ХЛЛ и остеопенией выявлены признаки прогрессии ОС и снижения ОАС. У пациентов с ХЛЛ показатели ОС в сыворотке и костной ткани сопоставимы и могут быть использованы для прогноза возникновения остеопении через 6 месяцев.

Ключевые слова: хронический лимфолейкоз, минеральная плотность кости, остеопения, окислительный стресс, перекисное окисление липидов, редокс-статус

Chronic lymphocytic leukemia (CLL) belonging to the class of malignant lymphomas originates from small B cells. CLL is divided into two clinical variants: lymphoid hyperplasia with clonal lymphocytosis ≥ 5000/µL; lymphoid organ hypertrophy without lymphocytosis. Enlarged lymph nodes, tonsils and the spleen represent a manifestation of small B cell lymphoma that belongs to the same disease entity as CLL [1]. According to epidemiological situation, the annual incidence of CLL in Europe is about 5 cases per 100,000 population, while in Russia it is about 3–4 cases per 100,000 population [2]. CLL is the second most common non-Hodgkin lymphoma. In individuals with CLL, the risk of bone loss reaches 66%, which later leads to fractures of the tubular bones and disability. Reduced bone mineral density (BMD) leads to osteoporosis in 16% of patients and osteopenia in 35% of patients with CLL [3]. In dynamics, skeletal bone destruction associated with CLL begins in the proximal femurs expanding to the spine and other bones; this is most likely to be associated with tumor cell localization in the bone marrow of pelvic bones and interaction with stromal cells [4].

Excess generation of reactive oxygen species (ROS) by leukemic cells, reduced functional activity of the antioxidant system can be the key mechanisms underlying bone loss associated with CLL [5]. The CLL-associated oxidative stress results from the large number of mitochondria in tumor cells, and their survival rate is related to resistance to oxidative stress and associated with high levels of intracellular antioxidants that bind ROS and inhibit apoptosis, which leads to the increase in the number of malignant lymphocytes [6].

The bone resorption process is related to oxidative stress, specifically to the effects of ROS on protein molecules resulting in damage to the surrounding cells in the bone tissue. The lipid peroxidation (LPO) products accumulating in the tissues are used as markers of oxidative stress in many cancers, and their tissue levels suggest functional activity of the antioxidant system in CLL [7]. Pathogenesis of the CLL-associated bone destruction is poorly understood, and the analysis of research on the subject has shown that BMD reduction represents a part of the complex of events involving the immune system, intracellular signaling pathways, and redox status, necessitating further investigation of the mechanism underlying bone loss aimed at improving diagnosis and treatment of such patients.

The study aimed to assess the relationship between the serum and bone tissue levels of lipid peroxidation products and antioxidant status, as well as bone mineral density values in patients with CLL.

METHODS

The study was conducted at the South Ural State Medical University and Chelyabinsk Regional Clinical Hospital. Inclusion criteria: males aged 50–70 years only, who had submitted the informed consent. Exclusion criteria: all diseases and conditions, for which BMD reduction was proven, specifically, end-stage renal disease, genetic disorders (cystic fibrosis, Ehlers–Danlos syndrome, osteogenesis imperfecta, porphyria, etc.), endocrine disorders (type 1 and 2 diabetes mellitus, thyroid diseases, etc.), long-term treatment with glucocorticosteroids, gastrointestinal disorders (Crohn's disease, non-specific ulcerative colitis, primary biliary cirrhosis, celiac disease, malabsorption, etc.), gastrointestinal surgery, oncohematological diseases, except chronic lymphocytic leukemia, rheumatic diseases, human immunodeficiency virus, impossibility of self-care.

The control group (group 1) consisted of 14 conditionally healthy males; group 2 consisted of 54 patients with CLL with normal bone system indicators; group 3 consisted of 22 patients with CLL showing significant BMD reduction. All groups were matched by age ($p > 0.05$): group 1 — 59.0 [55.7; 63.5] years, group 2 — 62.0 [59.7; 65.3] years, group 3 — 65.0 [59.0; 66.1] years. The diagnosis of CLL was verified using the BD FACSCanto II flow cytofluorometer (BD Biosciences; USA) by immunophenotyping of peripheral blood lymphocytes of the following clonality: $CD5^+$, $CD19^+$, $CD20^+$, $CD23^+$, $CD22^+$, $CD23^+$, $CD43^+$, $CD200^+$, immunoglobulin kappa or lambda light chains. Patients were distributed based on the stage (Binet staging system): stage A — 28 patients (37%), stage B — 36 patients (47%), stage C — 12 patients (16%) [1]. The average disease duration was 10.5 months, and the duration of the study was 6 months. At the beginning of the study we assessed BMD, T- and Z-scores of the lumbar spine (LS), proximal femoral neck (PFN), proximal femoral bone (PHB) using the DEXXUM 3 bone densitometer (OsteoSys Co; South Korea). The 10-year fracture risk was calculated using the internationally accepted Fracture Risk Assessment Tool (FRAX) [8]. All patients with CLL underwent trephine biopsy from the the posterior superior iliac spine for confirmation of the diagnosis. The bone tissue biopsy specimen was homogenized for 3 min at the temperature of 4 °C (1 : 10) with added 0.9% sodium chloride solution. The levels of LPO products were assessed in blood serum in all groups and in bone tissue homogenate in patients with CLL by the extraction spectrophotometric method using the SF-56 spectrophotometer (LOMO-Spectrum; Russia) [9]. Optical density of LPO products was determined in the heptane and isopropanol phases of the lipid extract vs. appropriate control at 220 nm (levels of products with isolated double bonds), 232 nm, 278 nm, 400 nm. The results were measured in the oxidative index units (OIU): E232/E220 — relative content of diene conjugates (DC), E278/E220 — relative content of ketodienes and conjugated trienes (KD and CT), and E400/E220 — relative content of Schiff bases (SB). The total antioxidant status (TAS) was assessed using the Chem Well 2910 Combi automated analyzer (Awereness Technology; USA) and the B-7501 Total Antioxidant Status test system (Vector-Best; Russia); the results were expressed as total antioxidant levels measured in mmol/L.

At the second point of the study, 6 months later, we assessed bone densitometry indicators, serum LPO and TAS indicators. Three mathematical models predicting BMD alterations based on bone tissue and serum LPO and TAS values were constructed based on the results obtained at two points of the study.

The results were processed using IBM SPSS Statistics v. 23 (SPSS: An IBM Company; USA) and presented as median and interquartile range (Me [Q_1; Q_3]). Significance of differences was assessed using the Mann–Whitney U test. The medians of several samples were compared using the Kruskal–Wallis test. The differences were considered significant at $p \leq 0.05$. Linear regression analysis was used to reveal statistical relationships between indicators. The quality of models was estimated based on the R^2 determination coefficient, residual distribution type. Correlation analysis was performed using Spearman's rank correlation coefficient (R).

RESULTS

At the beginning of the study, 29% of patients with CLL (group 3) showed a significant decrease in T-score of the lumbar spine (4.8-fold based on median relative to group 1), Z-score — by 100% based on median, BMD — by 10% based on median; decrease in proximal femoral neck T-score — 8-fold based on

Table 1. Bone mineral density indicators (Me [Q_1; Q_3])

Indicators	Group 1 (n = 14)	Group 2		Group 3	
		Beginning (n = 54)	6 months (n = 18)	Beginning (n = 22)	6 months (n = 12)
FRAX, %	28.50 [25.60; 30.00]	28.00 [26.80; 30.50]	27.10 [24.20; 28.70]	28.70 [23.00; 30.10]	28.55 [26.20; 31.10]
T-score of LS, SD	1.15 [0.70; 3.00]	1.30 [–0.10; 2.50]	0.20 [–0.50; 0.80]$	–0.30 [–0.60; 1.00]*#	–1.10 [–1.80; –1.00]*#&
Z-score of LS, SD	1.30 [0.80; 3.00]	1.60 [0.40; 2.90]	1.20 [0.00; 2.10]	0.00 [–1.10; 1.40]*#	–1.05 [–1.20; –0.55]*#&
BMD of LS, g/cm²	1.31 [1.06; 1.36]	1.37 [1.21; 1.52]	1.24 [1.16; –1.35]$	1.18 [1.06; 1.34]#	1.15 [1.11; 1.21]#
T-score of PFN, SD	0.20 [–0.20; 0.50]	–0.20 [–0.60; 0.10]	–0.80 [–1.20; –0.40]$	–1.40 [–2.00; –1.10]*#	–2.10 [–2.30; –1.60]*#&
Z-score of PFN, SD	0.90 [0.10; 1.10]	0.70 [0.40; 1.00]	0.00 [–0.40; 0.50]&	–0.60 [–1.00; 0.00]*#	–1.00 [–1.30; –0.60]*#&
BMD of PFN, g/cm²	1.05 [0.98; 1.10]	1.04 [0.99; 1.08]	0.96 [0.91; 1.02]&	0.88 [0.80; 0.93]*#	0.89 [0.85; 0.92]*#
T-score of PFB, SD	0.25 [–0.10; 0.50]	–0.10 [–0.30; 0.30]	–0.60 [–0.80; 0.20]&	–0.80 [–2.00; –0.60]*#	–1.65 [–2.50; –1.20]*#&
Z-score of PFB, SD	0.07 [0.88; 2.40]	0.70 [0.30; 1.10]	–0.10 [–0.30; 0.30]&	–0.20 [–1.30; –0.10]*#	–1.85 [–2.20; –1.50]*#&
BMD of PFB, g/cm²	1.07 [0.88; 1.12]	1.09 [1.05; 1.14]	1.01 [0.98; 1.05]&	0.93 [0.83; 1.01]#	0.94 [0.92; 0.97]*#

Note: * — significant ($p < 0.05$) differences from group 1 based on the Kruskal–Wallis test, # — from group 2; $ — differences in group 2; & — differences in group 3.

median relative to group 1, Z-score — 3-fold based on median, BMD — by 16% based on median; in the proximal femur bone, T-score decreased 4.2-fold based on median, Z-score — 1.3-fold, BMD — by 13% based on median (Table 1). According to the National Guidelines, the decrease in the PFN T-score in group 3 can be considered as osteopenia. When compared with group 2, patients with CLL and osteopenia showed a significant decrease in the LS indicators: T-score — 6-fold based on median, Z-score — by 100%, BMD — by 13.5%; PFN indicators: T-score — 7-fold based on median, Z-score — 2.1-fold, BMD — by 15% based on median, and PFB indicators: T-score — 8-fold based on median, Z-score — 4.5-fold based on median, BMD — by 14% based on median. The 10-year skeletal bone fracture risk calculated using the FRAX algorithm and including BMD values in all groups showed no significant differences ($p > 0.05$). In group 2 followed up for 6 months, significant changes were reported for LS: T-score decreased 6.5-fold based on median, BMD — by 9% based on median, and for PFN: T-score decreased 4-fold based on median. However, the bone densitometry characteristics, including T-scores of LS and PFN, were normal based on the parameters specified in the National Guidelines. After 6 months patients with CLL and osteopenia showed the following LS indicators that were significantly decreased compared to group 2: T-score —

3.7-fold based on median, Z-score — 1.05-fold, BMD — by 2% based on median; PFN: T-score — 1.5-fold based on median, Z-score — 1.7-fold, BMD — by 13% based on median; PFB: T-score — 22-fold based on median, Z-score — 1.2-fold, BMD — by 12% based on median. The in-depth analysis of the dynamic changes in bone densitometry indicators after 6 months in group 3 showed that BMD indicators were reduced to osteopenia values in all the studied localizations: in LS, the T-score was reduced 4-fold based on median, Z-score — 0.1-fold; in PFN: T-score — 1.5-fold based on median, Z-score — 1.2-fold; in PFB: T-score — 2.1-fold based on median, Z-score — 9.3-fold.

Oxidative stress in bone tissue of patients with CLL was assessed based on the levels of oxidized lipid molecule residues and total antioxidant status. At the beginning of the study group 3 showed a significant increase in the levels of ketodienes and conjugated trienes (by 5.5% based on median relative to group 2) and Schiff bases (24-fold based on median) in the heptane phase of the lipid extract (Table 2).

In the isopropanol phase of the lipid extract, there was a significant increase in Schiff base levels (by 41% based on median relative to group 2). In patients with CLL and osteopenia, no significant changes in the diene conjugate levels were found in the heptane and isopropanol phases of the bone tissue lipid

Table 2. Bone tissue oxidative stress indicators in patients with CLL (Me [Q_1; Q_3])

Indicators	Group 2 (n = 54)	Group 3 (n = 22)
DC (h), OIU	0.609 [0.602; 0.617]	0.612 [0.608; 0.626]
(KD and CT (h), OIU	0.073 [0.056; 0.077]	0.077 [0.076; 0.081]#
SB (h), OIU	0.003 [0.001; 0.007]	0.076 [0.038; 0.078]#
DC (i), OIU	0.504 [0.485; 0.526]	0.506 [0.489; 0.507]
(KD and CT (i), OIU	0.104 [0.097; 0.121]	0.100 [0.095; 0.109]
SB (i), OIU	0.061 [0.047; 0.065]	0.086 [0.084; 0.094]#
TAS, mmol/L	0.88 [0.81; 1.04]	0.61 [0.49; 0.62]#

Note: # — significant ($p < 0.05$) differences from group 2 based on the Mann–Whitney U test; (h) — heptane phase of the bone tissue lipid extract; (i) — isopropanol phase.

Table 3. Serum oxidative stress inficators (Me [Q_1; Q_3])

Indicators	Group 1 (*n* = 14)	Group 2		Group 3	
		Beginning (*n* = 54)	6 months (*n* = 18)	Beginning (*n* = 22)	6 months (*n* = 12)
DC (h), OIU	0.014 [0.013; 0.014]	0.582 [0.561; 0.613]*	0.800 [0.776; 0.804]*$	0.679 [0.534; 0.680]*#	1.126 [1.087; 1.309]*#&
KD and CT (h), OIU	0.001 [0.001; 0.002]	0.088 [0.077; 0.093]*	0.114 [0.109; 0.139]*$	0.097 [0.092; 0.103]*#	0.161 [0.137; 0.193]*#&
SB (h), OIU	0.003 [0.002; 0.004]	0.058 [0.040; 0.062]*	0.061 [0.026; 0.096]*	0.075 [0.048; 0.075]*	0.089 [0.043; 0.135]*#
DC (i), OIU	0.049 [0.047; 0.051]	0.518 [0.500; 0.527]*	0.932 [0.912; 0.942]*$	0.611 [0.608; 0.624]*#	1.312 [1.286; 1.547]*#&
KD and CT (i), OIU	0.025 [0.023; 0.027]	0.267 [0.235; 0.281]*	0.847 [0.829; 0.856]*$	0.305 [0.293; 0.317]*#	1.193 [1.169; 1.407]*#&
SB (i), OIU	0.012 [0.011; 0.016]	0.039 [0.033; 0.047]*	0.062 [0.041; 0.074]*$	0.031 [0.026; 0.046]*#	0.087 [0.042; 0.105]*#&
TAS, mmol/L	1.97 [1.89; 2.27]	1.73 [1.54; 2.01]*	2.03 [1.78; 2.35]*$	0.91 [0.85; 0.94]#	0.53 [0.43; 0.54]*#&

Note: * — significant ($p < 0.05$) differences from group 1 based on the Kruskal–Wallis test, # — from group 2; $ — differences in group 2; & — differences in group 3; (h) — heptane phase of the bone tissue lipid extract; (i) — isopropanol phase.

extract, as well as in the ketodiene and conjugated triene levels in the isopropanol phase. The bone tissue total antioxidant status was significantly reduced in group 3 (by 30% based on median relative to group 2).

Serum oxidative stress indicators for all groups are provided in Table 3.

It was found that at the beginning of the study patients with CLL and reduced BMD showed a significant increase in the diene conjugate levels (by 14% based on median), ketodiene and conjugated triene levels (by 9% based on median) in the heptane phase of the lipid extract relative to group 2. In the isopropanol phase, significantly increased serum levels of diene conjugates (by 15% based on median), ketodienes and conjugated trienes (by 13% based on median) were reported, however, SB levels were reduced by 20% based on median. At the beginning of the study group 3 showed a significantly reduced serum total antioxidant status (by 47% based on median) relative to group 2.

Group 3 showed a significant increase in the levels of diene conjugates — by 28%, ketodienes and conjugated trienes — by 29%, and Schiff bases — by 31% based on median in the heptane phase of the serum lipid extract, and diene conjugates, ketodienes and conjugated trienes — by 29% and Schiff bases — by 28% based on median in the isopropanol phase relative to group 2 after 6 months of follow-up. TAS of group 3 was significantly lower (by 74% based on median) relative to group 2 after 6 months of follow-up.

At the beginning of the study group 3 showed significantly increased levels of diene conjugates, ketodienes and conjugated trienes — by 98%, Schiff bases — by 95% in the heptane phase of the serum lipid extract, and diene conjugates, ketodienes and conjugated trienes — by 92%, Schiff bases — by 62% based on median in the isopropanol phase relative to group 1. Group 3 showed a significantly decreased TAS (by 53% based on median) relative to group 1.

After 6 months, patients with CLL and osteopenia showed significantly increased serum levels of DC — by 98.7%, KD and CT — by 99%, and SB — by 96% based on median in the heptane phase of the lipid extract, and DC — by 96%, KD and CT — by 98%, and SB — by 86% based on median in the isopropanol phase relative to group 1. The serum TAS of group 3 significantly decreased (by 73%) relative to group 1 after 6 months.

Group 3 showed a significant increase in the serum levels of DC, KD and CT — by 40% based on median in the heptane

phase, and DC — by 53% based on median, KD and CT — by 74.5%, SB — by 64% in the isopropanol phase of the extract after 6 months. Furthermore, group 3 showed a serum TAS decrease (by 43% based on median) during the 6-month follow-up.

The use of mathematical modeling based on the Spearman's rank correlation revealed a significant negative correlation between the femoral neck bone mineral density and the diene conjugate levels in the heptane phase of the serum lipid extract at the beginning of the study (Table 4). The model can be described by the following equation:

$$x = 1.396 - 0.62 \times DC\ (h),$$

where x is the PFN BMD value, DC (h) are diene conjugates in the heptane phase.

The linear regression analysis method allowed us to compare the bone tissue oxidative lipid destruction values and the serum LPO values at the beginning of follow-up using mathematical modeling, thereby making it possible to stand down from re-assessment of the dynamic changes in the bone tissue redox status and exclude extra medical traumatization of patients resulting from trephine biopsy from the posterior superior iliac spine. The model can be described by the following equation:

$$x = 0.5 - 0.41 \times KD\ and\ CT\ (h) + 0.66 \times SB\ (h),$$

where x is the bone tissue concentration of diene conjugates in the isopropanol phase, KD and CT (h) are ketodienes and conjugated trienes in the heptane phase, SB (h) are Schiff bases in the heptane phase.

According to another model, serum levels of diene conjugates in the heptane phase and the levels of Schiff bases in the isopropanol phase of the extract showed a significant negative correlation with the PFB BMD 6 months after the beginning of follow-up. The model can be described by the following equation:

$$x = 2.39 - 1.99 \times DC\ (h) - 3.12 \times SB\ (i) + 0.27 \times osteopenia,$$

where x is the likelihood of the PFB BMD (g/cm^2) reduction, DC (h) are diene conjugates in the heptane phase, SB (i) are Schiff bases in the isopropanol phase. The trait of having osteopenia was included in the model, since it improved the prediction

Table 4. Regression models

Models	Traits	Coefficients	p
Model of the relationship between PFN BMD and serum LPO at the beginning adjusted R^2 = 0.34; p = 0.001	Intercept	1.396	< 0.001*
	DC (h)	−0.620	0.00156*
Model of the relationship between bone LPO and serum LPO at the beginning adjusted R^2 = 0.36; p = 0.003	Intercept	0.49817	< 0.001*
	KD and CT (h)	−0.40958	0.03754*
	SB (h)	0.66482	0.00107*
Model to determine PFB BMD after 6 months based on the serum LPO values adjusted R^2 = 0.71; p = 0.002	Intercept	2.39	< 0.001*
	DC (h)	−1.99	0.024*
	SB (i)	−3.12	0.017*
Group 3		0.27	0.128

Note: * — significant (p < 0.05) differences.

quality, but it showed no statistical significance (1 — present, 0 — absent).

DISCUSSION

T-score is considered to be a standardized indicator when performing bone densitometry; it represents the number of standard deviations from the maximum BMD and is used in postmenopausal women and men over the age of 50. Z-score represents the number of standard deviations from the average BMD value in individuals of the same age group [8].

In CLL, the femoral neck is considered to be the most common localization of reduced BMD. However, in individuals with severe disease, alterations of BMD indicators can be found in other parts of the skeleton, including the spine [4].

The mechanism underlying the development of osteopenia of different localization is likely to be associated with the negative effect of the large number of free radical synthesized by tumor cells on protein and lipid molecules, as well as with generation of products of their oxidative destruction [10, 11].

As is well-known, diene conjugates, ketodienes and conjugated trienes are early stage lipid peroxidation products. Their levels reflect activity of the LPO processes and oxidative stress intensity. The non-metabolizable Schiff bases are markers of dystrophic processes in cells and tissues. Today, it is believed that the polyunsaturated fatty acid peroxide-derived carbonyl residues of oxidized lipids, such as 4-hydroxynonenal or malondialdehyde, are biomarkers of oxidative stress in tissues associated with CLL [7]. Survival of clonal B cells is associated with the oxidative phosphorylation (ROS conversion to less harmful forms), increased antioxidant protection, specifically activation of the superoxide dismutase isoforms (SOD, SOD1 (Cu/Zn SOD), SOD2 (Mn-SOD)), thioredoxin system, and the enzyme cascade inducing glutathione biosynthesis and recirculation [12]. In CLL, ROS are synthesized mainly in mitochondria, in contrast to other tumors, in which this function is performed by NADPH oxidases [12]. ROS are buffered under exposure to the antioxidant factors, the expression of which is controlled by the transcription factors regulated by oxidation and phosphorylation [12]. Oxidative stress is considered to be the main mechanism underlying bone loss [13–15]. Oxidative stress indirectly, via activation of signaling pathways (FGF23, Nrf-2, JNK, ERK1/2, NF-κB, RANKL/OPG), stimulates differentiation of osteoclasts, affects proliferation and life span, reduces activity of osteoblasts and takes part in their apoptosis [15]. In particular, excess Nrf-2 expression, activation of heme oxygenase-1 (HO-1) and RUNX2-dependent transcription activity in CLL are associated with the decrease in osteoblast differentiation [16, 17]. Furthermore, the mechanism of bone tissue mineralization reduction under conditions of oxidative stress is associated with increased FGF23 expression in the bone tissue due to apopotosis of osteocytes and osteoblasts, activation of mitogen-activated protein kinases (MAPK) [18, 19].

As a consequence, the tumor-induced oxidative stress results in the fact that mature osteoclasts resorb bone matrix allowing tumor cells to grow and migrate in the tissues. The antioxidant protection dysfunction associated with CLL contributes to apoptosis of osteoblasts and osteocytes, causing further decrease in BMD leading to osteopenia and osteoporosis [20].

A software tool "Modeling Changes in Bone Mineral Density Depending on Redox Status in Patients with Chronic Lymphocytic Leukemia" allowing one to predict osteopenia or osteoporosis in patients with CLL within 6 months based on the serum LPO indicators was created based on the data obtained. According to our results, testing of this model made it possible to demonstrate high sensitivity and specificity of the tool created and had high predictive value. Practical use of the tool by healthcare specialists will make it possible to determine the subgroup of patients with CLL at risk of developing osteopenia.

CONCLUSIONS

In patients with CLL, the rate of determining osteopenia based on the proximal neck of the femur bone densitometry is 29%. During the 6-month follow-up the signs of osteopenia are found in 55% of patients in all instrumental assessment localizations. Bone tissue of patients with CLL and osteopenia shows signs of oxidative stress: accumulation of secondary and end products in the heptane phase of the lipid extract, accumulation of lipid oxidation end products in the isopropanol phase, reduced total antioxidant status. Furthermore, systemic oxidative stress associated with the increased levels of primary and secondary products of oxidative lipid destruction in the heptane phase, levels of primary, secondary and end products in the isopropanol phase, reduced serum total antioxidant status has been discovered in patients with CLL and osteopenia. After 6 months, progression of oxidative stress in blood serum relative to the values reported at the beginning of the study is observed: the levels of primary, secondary and end products of oxidative lipid destruction in the heptane and isopropanol phases are increased, the total antioxidant status is decreased. The serum and bone tissue redox status indicators are comparable, and serum oxidative stress indicators can be used to predict the development of osteopenia. The study can have an impact on the choice of patient management tactics, preparation of treatment and preventive measures, such as prescription of antioxidant therapy or bisphosphonate therapy.

References

1. Nikitin EA, Bjalik TE, Zarickij AYu, Iseber L, Kaplanov KD, Lopatkina TN, i dr. Hronicheskij limfocitarnyj lejkoz/limfoma iz malyh limfocitov. Klinicheskie rekomendacii. Sovremennaja Onkologija. 2020; 22 (3): 24–44. DOI: 10.26442/18151434.2020.3.200385. Russian.
2. Kaprin AD, Starinskij VV, Shahzadova AO, Lisichnikova IV. Zlokachestvennye novoobrazovanija v Rossii v 2022 godu (zabolevaemost' i smertnost'). M-vo zdravoohranenija Rossijskoj Federacii, MNIOI im. P.A. Gercena — filial FGBU «NMIC radiologii». Moskva: Kollektiv avtorov, 2023; 275 s. Russian.
3. Petty L, Stephens D, Sharma A. Risk Factors for Fragility Fractures in Chronic Lymphocytic Leukemia. Cureus. 2024; 16 (2): e54774. DOI: 10.7759/cureus.54774.
4. Giannoni P, Marini C, Cutrona G, Sambuceti GM, Fais F, de Totero D. Unraveling the Bone Tissue Microenvironment in Chronic Lymphocytic Leukemia. Cancers (Basel). 2023; 15 (20): 5058. DOI: 10.3390/cancers15205058.
5. D'Arena G, Seneca E, Migliaccio I, De Feo V, Giudice A, La Rocca F, et al. Oxidative stress in chronic lymphocytic leukemia: still a matter of debate. Leuk Lymphoma. 2019; 60 (4): 867–5. DOI: 10.1080/10428194.2018.1509317.
6. Sciaccotta R, Gangemi S, Penna G, Giordano L, Pioggia G, Allegra A. Potential New Therapies "ROS-Based" in CLL: An Innovative Paradigm in the Induction of Tumor Cell Apoptosis. Antioxidants (Basel). 2024; 13 (4): 475. DOI: 10.3390/antiox13040475.
7. Jomova K, Raptova R, Alomar SY, Alwasel SH, Nepovimova E, Kuca K, et al. Reactive oxygen species, toxicity, oxidative stress, and antioxidants: chronic diseases and aging. Arch Toxicol. 2023; 97 (10): 2499–574. DOI: 10.1007/s00204-023-03562-9.
8. Belaja ZhE, Belova KYu, Birjukova EV, Dedov II, Dzeranova LK, Drapkina OM, i dr. Federal'nye klinicheskie rekomendacii po diagnostike, lecheniju i profilaktike osteoporoza. Osteoporoz i osteopatii. 2021; 24 (2): 4–47. DOI: org/10.14341/osteo12930. Russian.
9. Volchegorskij IA, Dolgushin II, Kolesnikov OL, Cejlikman VYe. Jeksperimental'noe modelirovanie i laboratornaja ocenka adaptivnyh reakcij organizma. Cheljabinsk: ChelGPU, 2000; 167 s. Russian.
10. Chaudhary P, Janmeda P, Docea AO, Yeskaliyeva B, Abdull Razis AF, Modu B, et al. Oxidative stress, free radicals and antioxidants: potential crosstalk in the pathophysiology of human diseases. Front Chem. 2023; 11: 1158198. DOI: 10.3389/fchem.2023.1158198.
11. Zhivodernikov IV, Kirichenko TV, Markina YV, Postnov AY, Markin AM. Molecular and Cellular Mechanisms of Osteoporosis. Int J Mol Sci. 2023; 24 (21): 15772. DOI: 10.3390/ijms242115772.
12. Pagano MA, Frezzato F, Visentin A, Trentin L, Brunati AM. Protein Phosphorylation and Redox Status: An as Yet Elusive Dyad in Chronic Lymphocytic Leukemia. Cancers (Basel). 2022;14 (19): 4881. DOI: 10.3390/cancers14194881.
13. Han J, Yang K, An J, Jiang N, Fu S, Tang X. The Role of NRF2 in Bone Metabolism — Friend or Foe? Front Endocrinol (Lausanne). 2022; 13: 813057. DOI: 10.3389/fendo.2022.813057.
14. Ma F, Luo S, Lu C, Jiang X, Chen K, Deng J, et al. The role of Nrf2 in periodontal disease by regulating lipid peroxidation, inflammation and apoptosis. Front Endocrinol (Lausanne). 2022; 13: 963451. DOI: 10.3389/fendo.2022.963451.
15. Marcucci G, Domazetovic V, Nediani C, Ruzzolini J, Favre C, Brandi ML. Oxidative Stress and Natural Antioxidants in Osteoporosis: Novel Preventive and Therapeutic Approaches. Antioxidants (Basel). 2023; 12 (2): 373. DOI: 10.3390/antiox12020373.
16. Gao Y, Patil S, Jia J. The Development of Molecular Biology of Osteoporosis. Int J Mol Sci. 2021; 22 (15): 8182. DOI: 10.3390/ijms22158182.
17. Zhou X, Yuan W, Xiong X, Zhang Z, Liu J, Zheng Y, et al. HO-1 in Bone Biology: Potential Therapeutic Strategies for Osteoporosis. Front Cell Dev Biol. 2021; 9: 791585. DOI: 10.3389/fcell.2021.791585.
18. Vervloet MG. Shedding Light on the Complex Regulation of FGF23. Metabolites. 2022; 12 (5): 401. DOI: 10.3390/metabo12050401.
19. Domazetovic V, Falsetti I, Ciuffi S, Iantomasi T, Marcucci G, Vincenzini MT, et al. Effect of Oxidative Stress-Induced Apoptosis on Active FGF23 Levels in MLO-Y4 Cells: The Protective Role of 17-β-Estradiol. Int J Mol Sci. 2022; 23 (4): 2103. DOI: 10.3390/ijms23042103.
20. El-Gazzar A, Högler W. Mechanisms of Bone Fragility: From Osteogenesis Imperfecta to Secondary Osteoporosis. Int J Mol Sci. 2021; 22 (2): 625. DOI: 10.3390/ijms22020625.

Литература

1. Никитин Е. А., Бялик Т. Е., Зарицкий А. Ю., Исебер Л., Капланов К. Д., Лопаткина Т. Н., и др. Хронический лимфоцитарный лейкоз/лимфома из малых лимфоцитов. Клинические рекомендации. Современная Онкология. 2020; 22 (3): 24–44. DOI: 10.26442/18151434.2020.3.200385.
2. Каприн А. Д., Старинский В. В., Шахзадова А. О., Лисичникова И. В. Злокачественные новообразования в России в 2022 году (заболеваемость и смертность). М-во здравоохранения Российской Федерации, МНИОИ им. П.А. Герцена — филиал ФГБУ «НМИЦ радиологии». Москва: Коллектив авторов, 2023; 275 с.
3. Petty L, Stephens D, Sharma A. Risk Factors for Fragility Fractures in Chronic Lymphocytic Leukemia. Cureus. 2024; 16 (2): e54774. DOI: 10.7759/cureus.54774.
4. Giannoni P, Marini C, Cutrona G, Sambuceti GM, Fais F, de Totero D. Unraveling the Bone Tissue Microenvironment in Chronic Lymphocytic Leukemia. Cancers (Basel). 2023; 15 (20): 5058. DOI: 10.3390/cancers15205058.
5. D'Arena G, Seneca E, Migliaccio I, De Feo V, Giudice A, La Rocca F, et al. Oxidative stress in chronic lymphocytic leukemia: still a matter of debate. Leuk Lymphoma. 2019; 60 (4): 867–5. DOI: 10.1080/10428194.2018.1509317.
6. Sciaccotta R, Gangemi S, Penna G, Giordano L, Pioggia G, Allegra A. Potential New Therapies "ROS-Based" in CLL: An Innovative Paradigm in the Induction of Tumor Cell Apoptosis. Antioxidants (Basel). 2024; 13 (4): 475. DOI: 10.3390/antiox13040475.
7. Jomova K, Raptova R, Alomar SY, Alwasel SH, Nepovimova E, Kuca K, et al. Reactive oxygen species, toxicity, oxidative stress, and antioxidants: chronic diseases and aging. Arch Toxicol. 2023; 97 (10): 2499–574. DOI: 10.1007/s00204-023-03562-9.
8. Белая Ж. Е., Белова К. Ю., Бирюкова Е. В., Дедов И. И., Дзеранова Л. К., Драпкина О. М., и др. Федеральные клинические рекомендации по диагностике, лечению и профилактике остеопороза. Остеопороз и остеопатии. 2021; 24 (2): 4–47. DOI: org/10.14341/osteo12930.
9. Волчегорский И. А., Долгушин И. И., Колесников О. Л., Цейликман В. Э. Экспериментальное моделирование и лабораторная оценка адаптивных реакций организма. Челябинск: ЧелГПУ, 2000; 167 с.
10. Chaudhary P, Janmeda P, Docea AO, Yeskaliyeva B, Abdull Razis AF, Modu B, et al. Oxidative stress, free radicals and antioxidants: potential crosstalk in the pathophysiology of human diseases. Front Chem. 2023; 11: 1158198. DOI: 10.3389/fchem.2023.1158198.
11. Zhivodernikov IV, Kirichenko TV, Markina YV, Postnov AY, Markin AM. Molecular and Cellular Mechanisms of Osteoporosis. Int J Mol Sci. 2023; 24 (21): 15772. DOI: 10.3390/ijms242115772.
12. Pagano MA, Frezzato F, Visentin A, Trentin L, Brunati AM. Protein Phosphorylation and Redox Status: An as Yet Elusive Dyad in Chronic Lymphocytic Leukemia. Cancers (Basel). 2022;14 (19): 4881. DOI: 10.3390/cancers14194881.
13. Han J, Yang K, An J, Jiang N, Fu S, Tang X. The Role of NRF2 in Bone Metabolism — Friend or Foe? Front Endocrinol (Lausanne). 2022; 13: 813057. DOI: 10.3389/fendo.2022.813057.
14. Ma F, Luo S, Lu C, Jiang X, Chen K, Deng J, et al. The role of Nrf2 in periodontal disease by regulating lipid peroxidation, inflammation and apoptosis. Front Endocrinol (Lausanne). 2022; 13: 963451. DOI: 10.3389/fendo.2022.963451.
15. Marcucci G, Domazetovic V, Nediani C, Ruzzolini J, Favre C, Brandi ML. Oxidative Stress and Natural Antioxidants in Osteoporosis: Novel

Preventive and Therapeutic Approaches. Antioxidants (Basel). 2023; 12 (2): 373. DOI: 10.3390/antiox12020373.

16. Gao Y, Patil S, Jia J. The Development of Molecular Biology of Osteoporosis. Int J Mol Sci. 2021; 22 (15): 8182. DOI: 10.3390/ijms22158182.

17. Zhou X, Yuan W, Xiong X, Zhang Z, Liu J, Zheng Y, et al. HO-1 in Bone Biology: Potential Therapeutic Strategies for Osteoporosis. Front Cell Dev Biol. 2021; 9: 791585. DOI: 10.3389/fcell.2021.791585.

18. Vervloet MG. Shedding Light on the Complex Regulation of FGF23.

Metabolites. 2022; 12 (5): 401. DOI: 10.3390/metabo12050401.

19. Domazetovic V, Falsetti I, Ciuffi S, Iantomasi T, Marcucci G, Vincenzini MT, et al. Effect of Oxidative Stress-Induced Apoptosis on Active FGF23 Levels in MLO-Y4 Cells: The Protective Role of 17-β-Estradiol. Int J Mol Sci. 2022; 23 (4): 2103. DOI: 10.3390/ijms23042103.

20. El-Gazzar A, Högler W. Mechanisms of Bone Fragility: From Osteogenesis Imperfecta to Secondary Osteoporosis. Int J Mol Sci. 2021; 22 (2): 625. DOI: 10.3390/ijms22020625.

INTRAOCULAR LENS STITCHING TO IRIS WITH FULL PRESERVATION OF ITS FUNCTIONS: MICRORECONSTRUCTIVE TECHNIQUES

Takhchidi KhP ✉

Pirogov Russian National Research Medical University, Moscow, Russia

Today, implantation of an intraocular lens (IOL) into the capsular bag is the standard approach to surgical treatment of cataracts and aphakia of various origins. However, there are several reasons and conditions that disallow this operation or increase the risk of instability of the implanted lens, such reasons and conditions including weakness of the lens ligaments; degradation of Zinn's zonule, including dislocation of the IOL–capsular bag complex post-surgery; damage to or removal of capsular bag during surgery; lack of capsular bag or its destruction during implantation in aphakia cases. To date, problems associated with fixation and centralization of IOL in non-standard cases involving weak or inexistent capsular support remain unresolved. This study aimed to develop techniques allowing to stitch IOL to the iris without compromising its functions in various situations when it is unfeasible or impossible to fix and center lens in the capsular bag. The patients (n = 12; 12 eyes), depending on the clinical situation, were divided into groups: group 1 — dislocations of the IOL–capsular bag complex (6 eyes); group 2 — complete lack of capsular support (3 eyes); group 3 — weakness of capsular support (3 eyes). A special stitching technique was developed for each of these situations. The results of the treatment were good from clinical and functional perspectives: the IOL was fixed securely and centered properly, and the iris's performance and cosmetic aspects were not compromised.

Keywords: lack or weakness of capsular support, IOL dislocation, destruction of lens ligaments, aphakia, avitria

МИКРОРЕКОНСТРУКТИВНЫЕ ТЕХНОЛОГИИ ПОДШИВАНИЯ ИНТРАОКУЛЯРНОЙ ЛИНЗЫ К РАДУЖКЕ С ПОЛНЫМ СОХРАНЕНИЕМ ЕЕ ФУНКЦИЙ

Х. П. Тахчиди ✉

Российский национальный исследовательский медицинский университет имени Н. И. Пирогова, Москва, Россия

Имплантация интраокулярной линзы (ИОЛ) в капсульный мешок на сегодняшний день признана стандартом в хирургическом лечении пациентов с катарактой и афакией различного генеза. Несмотря на это существует ряд причин и состояний, при которых имплантация линзы в капсульную сумку не представляется возможной или связана с высоким риском ее нестабильной фиксации: несостоятельность связочного аппарата хрусталика, разрушение цинновых связок, в том числе дислокация комплекса «ИОЛ — капсульный мешок» в послеоперационном периоде; повреждение или удаление капсульного мешка во время операции, а также его отсутствие или разрушение при имплантации на афакичных глазах. На сегодняшний день проблемы фиксации и центрации ИОЛ в случаях нестандартных ситуаций, связанных с несостоятельностью или отсутствием «капсульной поддержки», остаются нерешенными. Целью исследования было разработать технологии подшивания ИОЛ к радужке с полным сохранением ее функций, при различных ситуациях несостоятельности или отсутствии возможности фиксации и центрации линзы в капсульном мешке. Пациенты (n = 12; 12 глаз) в зависимости от клинической ситуации были разделены на группы: группа 1 — дислокации комплекса «ИОЛ — капсульный мешок» (6 глаз); группа 2 — полное отсутствие «капсульной поддержки» (3 глаза); группа 3 — несостоятельность «капсульной поддержки» (3 глаза). Для каждой ситуации из этих трех групп была разработана отдельная технология подшивания. В результате проведенного лечения получены высокие клинико-функциональные результаты за счет надежной фиксации и высококачественной центрации ИОЛ, а также полного сохранения объема функций и косметических свойств радужки.

Ключевые слова: несостоятельность или отсутствие капсульной поддержки, дислокация ИОЛ, разрушение связочного аппарата хрусталика, афакия, авитрия

Implantation of a posterior chamber intraocular lens (IOL) into the capsular bag is the standard approach to surgical treatment of cataracts and aphakia of various origins [1]. However, there are several reasons and conditions making this operation unfeasible or impossible. These reasons and conditions increase the risk of subsequent instability of the lens and include post-surgery weakness of capsular ligaments in cataract cases, aphakias involving a lacking or destroyed capsular bag, eye trauma of various origins, lens subluxations/dislocations, and a number of congenital diseases [2–5].

The weakness of lens ligaments can be congenital (Marfan syndrome, Weill-Marchesani syndrome, homocystinuria, dominant spherophakia, etc.) [6, 7] and acquired (consequences of trauma, glaucoma, pseudoexfoliative syndrome, high-grade myopia, etc.) [8–11]. According to various authors, 15–20% of cataract patients suffer from this condition, and 20% more have it in a latent form that is not always possible to detect before the surgery [2, 12, 13]. Defects of the zonule of Zinn's fibers discovered during the operation often force the surgeon to change the tactics and urgently decide upon an appropriate IOL that can be fixed in place adequately in the given situation [14–16].

Lack of complications with the lens suspensory ligaments occurring during cataract surgery does not exclude their

development afterwards [2, 17]. Dislocations of the IOL-capsular bag complex are some of the gravest complications in the late postoperative period; occurring in 0.2–2.8% of cases at various points of time post-surgery, they usually have an unfavorable prognosis [18–21]. The anatomical and topographic position of the said complex can become incorrect because of the weakness of suspensory ligaments or capsular bag, or fibrosis of the latter [22]. The main reasons behind such weakness are the pseudoexfoliation syndrome, high-grade axial myopia, various eyeball injuries, earlier vitreoretinal intervention, retinitis pigmentosa, diabetes mellitus, and various connective tissue diseases [15, 23–25]. Currently, there is no consensus on the optimal method of treating IOL dislocation in these situations, with the two discernible approaches involving repositioning of the dislocated IOL or its replacement with its subsequent attachment to the sclera or iris [22].

The displacement of the IOL–capsular bag complex relative to the optical axis not only worsens the visual functions of the operated eye but also causes severe complications, including ocular hypertension, secondary glaucoma, corneal dystrophy, indolent iridocyclitis [26]. In case the IOL moves to the posterior segment of the eye, the complications are developing there: recurrent vitrious hemorrage, destruction of the vitreous body with subsequent pathological adhesion and traction, epiretinal fibrosis, and retinal detachment [27, 28]. All of these complications are predictable and require prevention.

Aphakia against the background of complete or partial lack of capsular support is a difficult problem for ophthalmic surgeons. The choice of the optimal method of IOL implantation in such cases remains a debated matter.

Anterior chamber IOLs fixed in the corner of that chamber or attached to the iris are easy to implant, but the side effects and complications associated with them include optical aberrations, aniseikonia, visible shine from the edges of the lens, limited pupil mobility, development of chronic uveitis and glaucoma, and a high risk of loss of endothelial cells followed by bullous keratopathy [8, 29].

Scleral fixation of the IOL enables restoration of the iridolenticular diaphragm to an almost natural state, and the lens does not contact the endothelium of the cornea and structures of the anterior segment of the eye, which reduces the risk of corneal dystrophy, glaucoma, and chronic inflammation. Despite the benefits, transcleral stitching is a technically more complex method because it disallows visual control and, accordingly, prevents factoring in the individual anatomical and topographic features of the eye in the IOL fixation zone. This yields an unpredictable variability in position (tilt) and mobility (rotation) of the IOL relative to the optical axis, which affects the quality of vision and commonly causes complications, such as eruption and biodestruction of the fixing elements, vitrious hemorrhage, retinal detachment, endophthalmitis [30].

For an eye surgeon, stitching IOLs with supporting elements to the iris is the most frequently practiced and familiar manipulation, which is performed given the tissue of the iris is unchanged (due to injuries, uveitis, aniridia, dystrophy, etc.). The key advantages of this technique are better visualization of the process, possibility to stitch through small self-sealing incisions, alignment of the IOL and iris planes (prevents tilt and rotation of the lens, thus improving the quality of vision), a lower degree of biodegradation of suture material, and the applicability of various elastic IOLs. Among the most common complications associated with this method are hyphema, iridodialysis, iris injury, pupil shape deformation, iris function impairment [31, 32].

Thus, the problems of fixation and centering of IOL in non-standard situations involving weakness or lack of capsular support, which can be discovered during surgery or occur in the postoperative period, remain unresolved. Today, the urgent task is to develop affordable, safe, reliable, function-preserving techniques of IOL fixation and centering for cases complicated by weakness of the suspensory ligaments of the lens, including dislocations of the IOL–capsular bag complex in the postoperative period, and damage or removal of the capsular bag during cataract surgery and implantation on aphakic eyes (including cases of associated destruction of the anterior hyaloid membrane with partial or complete loss of the vitreous body).

This study aimed to develop microreconstructive techniques allowing to stitch IOL to the iris without compromising its functions in various situations when it is unfeasible or impossible to fix and center the lens relying on capsular support.

METHODS

The study included 12 patients (12 eyes) aged 53–85 years (mean age — 67.4 ± 11.7 years) who have undergone surgery at the Research Center for Ophthalmology of Pirogov Russian National Research Medical University.

The inclusion criteria were: dislocation of the IOL–capsular bag complex; complete lack of capsular support (no capsular bag, destroyed anterior hyaloid membrane, partially or completely lost vitreous body); capsular support weakness (partially compromised suspensory ligaments and/or capsular bag).

The exclusion criteria were: corneal dystrophy and opacities hindering visualization of the anterior segment of the eye; iris dystrophy; congenital and acquired iris defects; glaucoma (primary open-angle glaucoma, closed-angle glaucoma, secondary glaucoma); diabetic retinopathy; dystrophic diseases of the fundus (central chorioretinal retinal dystrophy, age-related macular dystrophy, dry and wet); occlusion of retinal vessels, acute inflammatory diseases of the eyeball; intraocular tumors.

We haven't registered a significant concomitant somatic pathology that could affect the results of the assessment of the functional state of the visual system.

All patients underwent a comprehensive ophthalmological examination, including: visometry to establish uncorrected visual acuity (UCVA) and best corrected visual acuity (BCVA); pneumotonometry (CT-80 Topcon, Japan), biomicroscopy (Carl Zeiss SL 120, Germany), ophthalmoscopy with a MaxField non-contact lens (Ocular Inc., USA), and special tests like eye and orbit ultrasound (Quantel Compact Touch AB, France), pupillography with a corneal topographer (C.S.O Sirius, Italy).

The results were processed using standard Microsoft Office Excel descriptive statistics tools. The data are given as M ± σ, where M is the arithmetic mean, and σ is the standard deviation.

The patients were divided into the following groups: group 1 — dislocation of the IOL–capsular bag complex (6 eyes); group 2 — complete lack of capsular support (3 eyes); group 3 — weakness of capsular support (3 eyes).

IOL–capsular bag complex dislocation was diagnosed when there was a rupture and stretching of the suspensory ligaments of the lens post-surgery as remote complications. The complex moves in a plane parallel to the plane of the iris and can also move in the plane of the optical axis (to determine this, the patient is examined in supine position).

Complete lack of capsular support was diagnosed when there was no capsular bag, the anterior hyaloid membrane was disrupted, vitreous body partially or completely corrupted.

Capsular support weakness was diagnosed when the ligaments and/or the capsular bag were compromised to a
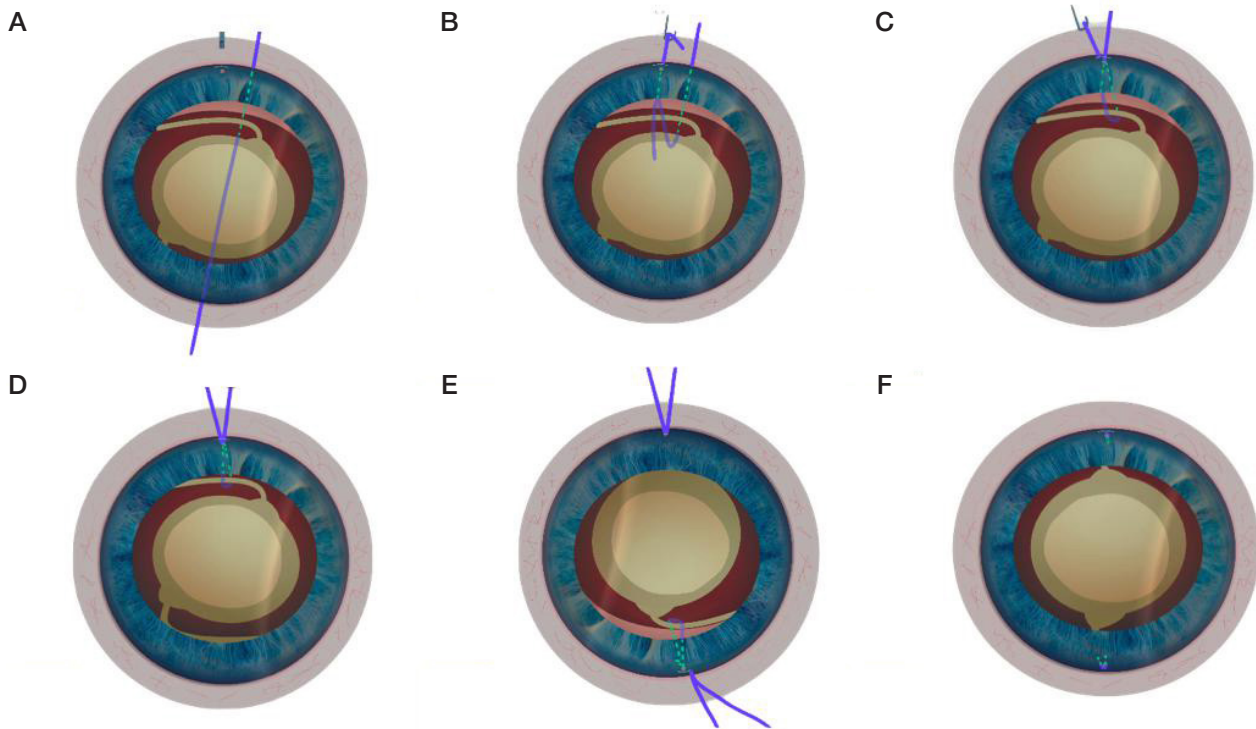
Fig. 1. IOL repositioning and stitching to the iris in cases involving dislocation of the IOL–capsular bag complex. A. Suture made on the top haptic element (*blue line*), needle with a thread passed through the corneal edge of the limb, root of the iris (*dotted line* shows the position of the needle behind the iris and the haptic element), and brought out; paracentesis made 2–3 mm from the needle injection point, microcoloboma made in the iris root in the projection of the paracentesis (highlighted pink). **B.** Output end of the thread brought out by a microhook through microcoloboma and paracentesis. **C.** The input second end of the thread is pulled through the same paracentesis. **D.** The IOL–capsular bag complex is pulled to the point when the base of the opposite haptic element appears. **E.** Similar manipulations performed on the opposite haptic element. **F.** The threads are pulled out, tied, and cut off, the incisions hydrated.

various degree but not fully destroyed; such conditions created a risk of IOL migration into the vitreal cavity during surgery.

The follow-up period was from 6 months to 2 years.

RESULTS

Examination of group 1

The average UCVA was 0.43 ± 0.17, the average BCVA was 0.63 ± 0.19, and the average intraocular pressure (IOP) was 18.1 ± 2.5 mmHg.

Biomicroscopy revealed iridodonesis with a displacement of the IOL–capsular bag complex relative to the plane of the iris, which brought IOL's haptics to different levels of the pupil area. In supine position, the displacement of the complex in the eyeball axis ranged from insignificant to almost vertical. At this stage, it is important to determine the projection of the meridians of location of the bases of IOL's haptics.

In cases involving displacement of the IOL–capsular bag complex, we applied the technique developed by us (patent No. RU 2817077 C1, 09.04.2024. Priority 07.04.2023).

The topography of the displaced complex and the projections of the meridians of haptic elements were additionally registered during surgery. It should be remembered that these parameters can change somewhat as the patient's head is repositioned. Next, with a needle carrying a thread, we punctured the corneal edge of the limb on the meridian of projection of the base of the haptic element visible in the pupil zone, pierced the iris root, moved the needle to the posterior chamber parallel to the iris into the visual zone of the pupil, then punctured the capsule and wound around the rear surface of the base of the visible haptic element in the pupil zone, and moved the needle out to the anterior chamber. Then, the needle was passed over the iris in the direction of the angle of the anterior chamber and

brought out, piercing the cornea in the prelimbal zone, and the thread was cut off above the eyeball. A 1.0 mm paracentesis was formed 2–3 mm from the needle injection site in the limb area, and the anterior chamber was filled with viscoelastic. Using a 27G vitreotome, we formed a microcoloboma at the root of the iris in the projection of paracentesis (Fig. 1A). Then, a microhook was introduced through the paracentesis and microcoloboma into the posterior chamber, moved along the iris through the pupil area to the anterior chamber, where we captured the output end of the thread and, reversely, brought it out through the paracentesis (Fig. 1B). After that, the microhook was introduced to the anterior chamber through the same paracentesis above the iris root, by the needle injection point, captured the second end of the thread and brought it out in reverse (Fig. 1C).

Thus, the resulting loop trapped the haptic element of the IOL and a fragment of the iris root 2–3 mm wide. Next, the captured haptic element of the IOL–capsular bag complex was pulled so that the base of the opposite haptic element appeared in the pupil area (Fig. 1D). If this technique fails to bring the opposite haptics from under the iris into the pupil area, visualization can be achieved with the help of iris hooks or mydriatics.

At the next stage, we repeated the routine at the opposite haptic element found on the opposite end of the meridian (Fig. 1E). The needle injection point and microcoloboma were positioned along the respective meridians, symmetrically in the projection of the previously made injection point and microcoloboma. Having completed manipulations on the opposite haptic element of the lens, we tied the threads pulled through the paracenteses and cut them off (Fig. 1F). Viscoelastic was washed out of the anterior chamber, the incisions were sealed by hydration.

Results of the control examination after 2 years: average UCVA — 0.86 ± 0.23, average BCVA — 0.96 ± 0.13, average IOP — 17.6 ± 1.63 mmHg.
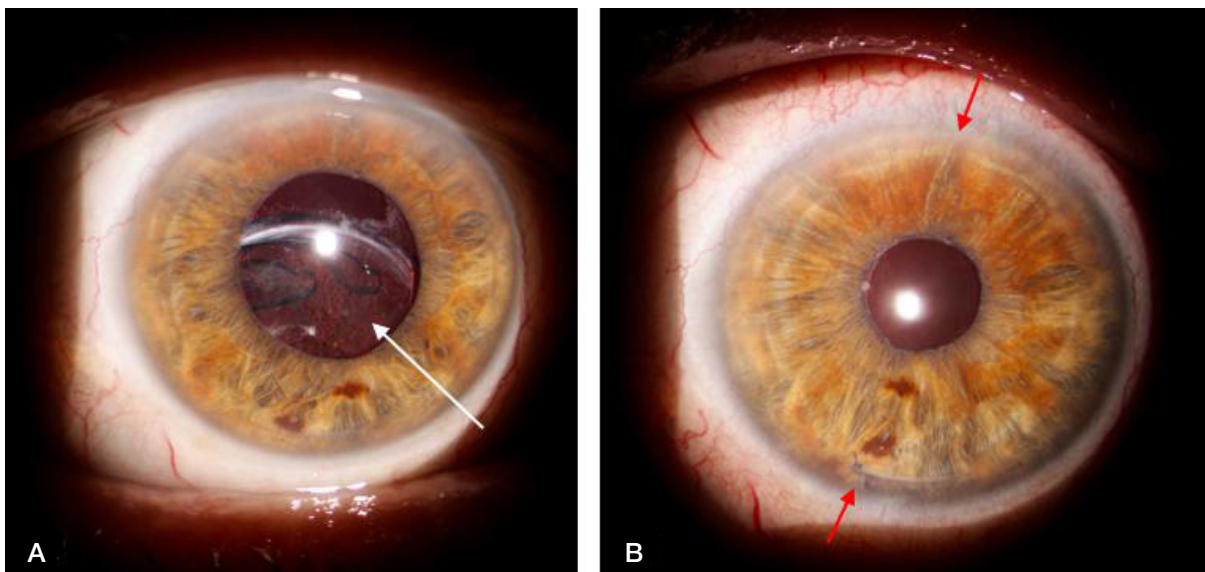
Fig. 2. Anterior segment of the eye with dislocated IOL–capsular bag complex. A. Before surgical treatment (drug-induced mydriasis): dislocation of the IOL (*white arrow*). **B.** After surgical treatment: round pupil, active reaction to light, solid fixing suture knots, IOL fixed and centered as expected from the suggested technique; *red arrows* point to the zones of suture knots and microcolobomas

Pupils of the operated eyes round, active reaction to light, suture knots solid, IOLs fixed and centered as expected from the suggested technique (Fig. 2A, B). Comparison to the fellow eye: similar size and shape of pupils, direct and coordinated reactions to light preserved in full.

Pupillography was performed at various times post-surgery on both the operated and the fellow eye. The diameter of the pupil was measured in scotopic (0.04 lux), mesopic (4 lux) and photopic (50 lux) conditions. Results of the control examination after 2 years: average pupil diameter in scotopic conditions — 4.45 ± 0.71 mm, in mesopic conditions — 4.27 ± 0.68 mm, in photopic conditions — 3.97 ± 0.59 mm. Pupillography of the fellow eye: average pupil diameter in scotopic conditions — 4.3 ± 0.83 mm, in mesopic conditions — 4.07 ± 0.76 mm, in photopic conditions — 3.81 ± 0.76 mm.

Examination of group 2

The average UCVA was 0.04 ± 0.01, the average BCVA was 0.28 ± 0.2, and the average IOP was 17.0 ± 2.64 mmHg.

Two cases involved postoperative aphakia with missing capsular bag and corrupted anterior hyaloid membrane, partial loss of the anterior parts of the vitreous body; one case had aphakia with missing capsular bag, avitria.

To implant the IOL with lacking capsular support, we applied the technique developed by us (patent application No. 2024116758 of 18.06.2024).

In the 12-hour zone, we made two parallel paracentesis (temporal and nasal) on the limb, 2–3 mm away from each other, perpendicular to the limb. Symmetrically, two similar paracentesis were made in the projection of these meridians in the 6-hour zone. The anterior chamber was filled with viscoelastic. Using a 27 G vitreotome, we made temporal and nasal microcolobomas in the projection of each paracentesis, 12-hour and 6-hour zones of the iris root (Fig. 3A). Depending on the conditions, paracenteses and microcolobomas can be made in other zones.

Outside the eye, we tied one fixing thread sequentially to the top and bottom haptic elements of the IOL (Fig. 3B). After that, the IOL with tied fixing threads on the top and bottom haptic elements was inserted into the injector and implanted into the

anterior chamber through a pre-made corneal tunnel. Thus, the IOL was positioned in the anterior chamber and anchored by the ends of the threads passing through the corneal tunnel and tied to the haptic outside the eye. Alternatively, the ends of the lower fixing thread can be pulled by a microhook into the lower paracentesis, and the IOL will be suspended by the ends of the upper fixing thread in the tunnel, those of the lower thread — in one of the lower paracenteses, so the lens could already be tucked through the pupil area behind the iris.

Then, in the 12-hour zone, we introduced a microhook through the temporal paracentesis and microcoloboma, moved it through the posterior chamber parallel to the iris, reached the anterior chamber through the pupil, captured the output end of the thread fixing to the top haptic element there, and pulled it out reversely through the paracentesis (Fig. 3C). After that, in a similar way, the inner end of the top haptic element's fixing thread was pulled outside through nasal microcoloboma and paracentesis. Next, we put a microhook through the temporal paracentesis into the corner of the anterior chamber above the nasal microcoloboma, captured the second inner end of the fixing thread and pulled it out through the temporal paracentesis. In the 6-hour zone, similar manipulations were performed with the thread fixing IOL's bottom haptic element (Fig. 3D).

The next step involved positioning the IOL through the pupil area behind the iris, pulling the ends of the haptics' fixing threads and knotting them (Fig. 3E). The remaining ends were cut off in the anterior chamber, the viscoelastic washed out, and the incisions sealed by hydration (Fig. 3F).

Thus, the IOL is constantly held inside the eye by fixing threads trapping haptic elements, and cannot independently move behind the iris and sink to the fundus. This means that during implantation, the surgeon can freely and safely manipulate the IOL inside the eye expecting no unplanned movements therefrom.

Alternatively, when avitria is complete, the vitreal cavity can be tamponed with a perfluorocarbon liquid (PFCL), and all of the above manipulations performed such conditions, with PFCL replaced at the end of the operation.

Results of the control examination after 1 year: average UCVA — 0.53 ± 0.15, average BCVA — 0.66 ± 0.05, average IOP — 18 ± 4.9 mmHg.
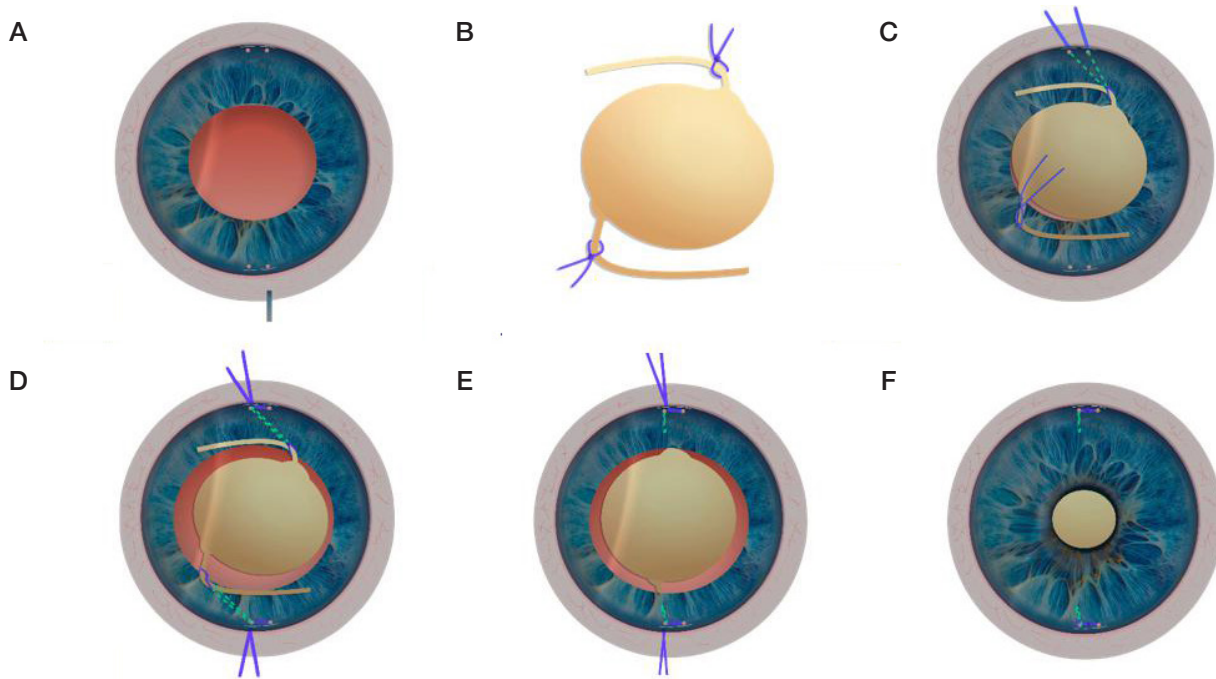
Fig. 3. IOL implantation in the absence of capsular support. A. Two paracenteses (temporal and nasal) made in the limb, 2–3 mm from each other, with similar paracenteses made at the opposite ends of the same meridians in symmetrical positions; next, microcolobomas made in the projection of each paracentesis (highlighted pink). **B.** Top and bottom haptic elements with fixing threads (blue color) tied to them, outside the eye. **C.** IOL with sutures implanted into the anterior chamber, the ends of the thread fixing top haptic element pulled through the respective microcoloboma and paracentesis (temporal and nasal). **D.** Similar manipulations done on the bottom haptic element (opposite): with the help of a microhook, both ends of the fixing threads pulled through the upper and lower temporal paracenteses. **E.** The IOL is positioned behind the iris, the ends of the fixing threads are pulled and knotted. **F.** The ends of the threads are cut off, viscoelastic washed, incisions hydrated

Pupils of the operated eyes round, active reaction to light, suture knots solid, IOLs fixed and centered as expected from the suggested technique (Fig. 4A, B). Comparison to the fellow eye: similar size and shape of pupils, direct and coordinated reactions to light preserved in full.

Pupillography results: average pupil diameter in scotopic conditions — 4.39 ± 1.02 mm, in mesopic conditions — 3.98 ± 0.97 mm, in photopic conditions — 3.53 ± 1.04 mm.

Pupillography of the fellow eye: average pupil diameter in scotopic conditions — 5.03 ± 0.7 mm, in mesopic conditions — 4.89 ± 0.73 mm, in photopic conditions — 4.61 ± 0.62 mm.

Examination of group 3

The average UCVA — 0.35 ± 0.27, average BCVA — 0.51 ± 0.43, average IOP — 13.6 ± 1.52 mmHg. In two cases, we registered total corruption of the ligaments and the lens capsule (top segments), aggravated by damaged anterior hyaloid membrane and partial loss of the vitreous body; in one case, there was no lens capsule with the preserved anterior hyaloid membrane of the vitreous body.

To implant the IOL with weak lacking capsular support in the background, we applied the technique developed by us (patent application No. 2809441 of 11.12.2023. Priority 07.04.2023). Essentially, this technique combines the two described above.

In the 12-hour zone of the limb, we made two parallel paracenteses, temporal and nasal, 2–3 mm apart, perpendicular to the limb (it is desirable, but not mandatory, to select the zone on the meridian opposite the best preserved remaining parts of the capsular support, which can act as additional suspension for the implanted IOL). The anterior chamber was filled with viscoelastic. Using a 27G vitreotome, we made temporal and
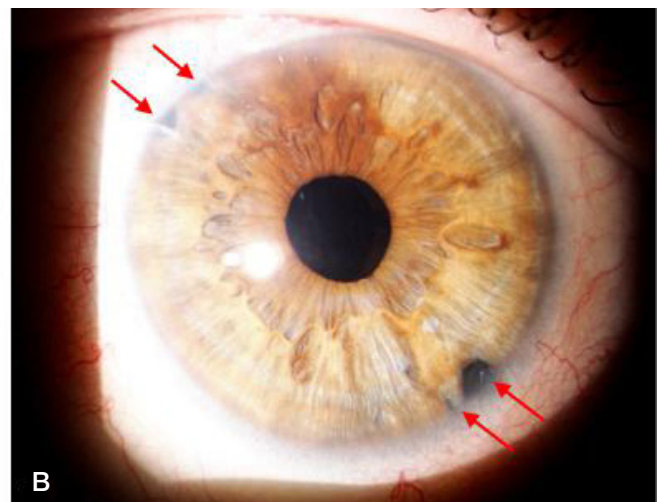
Fig. 4. Anterior segment of the eye with lacking capsular support. A. Before surgery. **B.** After surgery: round pupil, active reaction to light, solid fixing suture knots, IOL fixed and centered as expected from the suggested technique; red arrows point to the zones of suture knots and microcolobomas
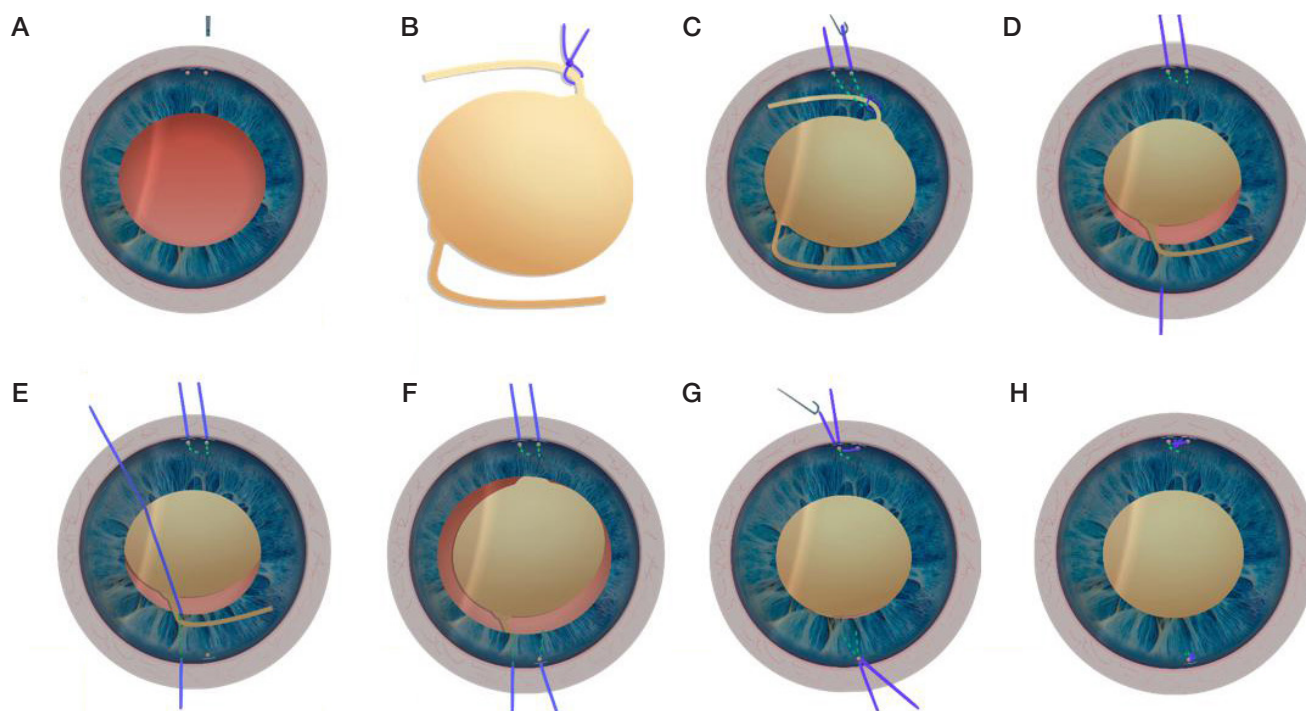
Fig. 5. IOL implantation and attachment to the iris against the background of weak capsular support (diagram). **A.** Two paracenteses (temporal and nasal) made in the limb, 2–3 mm from each other, then microcolobomas made in the projection of each paracentesis (highlighted pink). **B.** Outside the eye, the fixing thread is tied to the top haptic element (highlighted blue). **C.** The IOL with a suture is implanted into the anterior chamber, inner and outer ends of the thread fixing the lens to the top haptic element pulled out with a microhook through the respective microcoloboma and paracentesis. **D.** Top haptic element positioned behind the iris; the IOL is pulled up by the ends of the threads until the base of the bottom haptic element appears. **E.** Suture made on the bottom haptic element (blue line), needle with a thread passed through the corneal edge of the limb, root of the iris (dotted line shows the position of the needle behind the iris and the haptic element), and brought out; paracentesis made 2–3 mm from the needle injection point, microcoloboma made in the iris root in the projection of the paracentesis (highlighted pink). **F.** Bottom haptic element positioned, output end of the thread pulled out through the microcoloboma and the paracentesis with a microhook. **G.** Both input second ends of the threads pulled to the paracentesis and knotted. **H.** The ends of the threads are cut off, viscoelastic washed, incisions hydrated

nasal microcolobomas, 2–3 mm apart, in the projection of each paracentesis (Fig. 5A). Outside the eye, the fixing thread was tied to the top haptic element (Fig. 5B). The lens with the thread tied to the top haptic element was inserted in the injector and implanted into the anterior chamber through a pre-made corneal tunnel. Thus, the IOL was positioned in the anterior chamber and anchored there by the ends of the thread that passed through the corneal tunnel and was tied to the top haptic element.

Then, we introduced a microhook through the temporal paracentesis and microcoloboma, moved it through the posterior chamber parallel to the iris, reached the anterior chamber through the pupil, captured the output end of the thread fixing to the top haptic element there, and pulled it out in reverse order. After that, in a similar way, the inner end of the top haptic element's fixing thread was pulled outside through nasal microcoloboma and paracentesis (Fig. 5C). Having positioned the top haptic element behind the iris, we pulled both ends of the fixing thread and thus moved the optical part of the IOL behind the plane of the iris until the base of the bottom haptic element appeared in the pupil area, with the bottom haptic element remaining in the anterior chamber (Fig. 5D).

The next step involved manipulations from the first technique performed on the bottom haptic element. We injected the needle into the cornea and made microcolobomas at the opposite ends of the respective meridians, symmetrically in the projection of the previously made microcolobomas.

The needle was introduced into the cornea at the limb, then pierced the root of the iris, moved to the posterior chamber parallel to the iris, and brought into the pupil area, wound around the posterior surface of the base of the haptic element visible in the pupillary zone, and pulled out into the anterior chamber. The needle was passed over the iris in the direction

of the angle of the anterior chamber and brought out, piercing the cornea; next, the thread was cut off above the eyeball (Fig. 5E). Further, 2–3 mm from the needle injection point, we made a paracentesis in the limb zone, and using a 27G vitreotome created a microcoloboma in the root of the iris, then positioned the bottom haptic element behind the iris, and pushed a microhook through the paracentesis and the microcoloboma behind the iris and into the posterior chamber, parallel to the iris, through the pupil zone, and into the anterior chamber, over the IOL, to capture the output end of the thread there, after which the microhook with the thread was brought out through the paracentesis in reverse order. Next, the microhook was introduced to the anterior chamber through the paracentesis, moved above the iris root by the needle injection point, captured the second end of the thread and brought it out reversely (Fig.5F). Thus, the resulting loop trapped the bottom haptic element of the IOL. Once through with manipulations on the bottom haptic element, we pulled both ends of the thread fixing the top haptic element through a single paracentesis (Fig. 5G). The ends of the threads were tied and cut off, viscoelastic washed out of the anterior chamber, incisions sealed by hydration (Fig. 5H).

Results of the control examination after 6 months: average UCVA — 0.8 ± 0.17, average BCVA — 0.9 ± 0.17, average IOP — 13.3 ± 2.5 mmHg.

Pupils of the operated eyes round, active reaction to light, suture knots solid, IOLs fixed and centered as expected from the suggested technique. Comparison to the fellow eye: similar size and shape of pupils, direct and coordinated reactions to light preserved in full.

Pupillography results: average pupil diameter in scotopic conditions — 4.37 ± 0.29 mm, in mesopic conditions — 3.54 ± 0.58 mm, in photopic conditions — 3.09 ± 0.3 mm.

Pupillography of the fellow eye: average pupil diameter in scotopic conditions — 4.53 ± 0.44 mm, in mesopic conditions — 3.95 ± 0.61 mm, in photopic conditions — 3.45 ± 0.39 mm.

DISCUSSION

The problem of postoperative dislocation of the IOL–capsular bag complex in ophthalmic surgery retains its relevancy. An analysis of literature shows that today, there are no effective solutions thereto. There are two approaches to remedying this complication, one involving stitching the dislocated IOL to the membranes of the eyeball (iris or sclera), another suggesting replacement of the IOL with a lens attached differently; both approaches have several significant drawbacks [33]. Suturing to the iris offers the lowest risk of complications during and after surgery, that of repeated dislocations, and also allows positioning the IOL more centrally and stable relative to the optical axis of the eye.

Several authors have proposed various original methods of repositioning and stitching the IOL–capsular bag complex to the iris [1, 17, 21, 28, 34, 35]. The drawbacks of these methods include: lack of visualization during manipulations on haptic elements; putting fixing sutures in the most mobile areas of the iris stroma, which disrupts its diaphragmatic function and creates cosmetic defects associated with the shape, size and synchronicity of the pupils. Moreover, the suture area is constantly pulled by the antagonist muscles (sphincter and dilator of the pupil), which undermines strength, reliability, and durability of the fixing sutures in the long-term. Such methods of stitching jeopardize topographically accurate and symmetrical application of sutures fixing IOL to the opposite haptic elements while involving a similar, precisely measured volume of the iris tissue.

The microsurgery technique of stitching the IOL–capsular bag complex to the iris described in this paper, has a number of significant advantages over the said methods. Firstly, all manipulations that involve IOL haptics capturing and stitching to carried out under full visual microscopic control in the area of the pupil or anterior chamber, ensuring the process is accurate and atraumatic. The use of the iris root microcolobomas in the projection of the limb at opposite ends of the same meridian ensures topographically accurate and symmetrical application of fixing sutures to the IOL's opposite haptics, with the sutures placed on the said elements and involving a precisely measures volume of the iris root tissue (2–3 mm) at a planned location. This makes the centering of IOL accurate, even for toric and multifocal models.

The location of the fixing suture knots in the projection of the limb, where the iris root tissue, only 2–3 mm of which is used, is not essential functionally, leaves the structure of the iris virtually unchanged, and does not disrupt operation of its muscles, thus allowing to fully retain functions and cosmetic properties of the iris and the pupil. Moreover, the involved iris root tissue is exposed to minimal dynamic forces, which ensures reliability, strength, and durability of fixing sutures.

A positive feature of this technique is the possibility of repeated and additional manipulations aimed at achieving the set goals.

When removing cataracts, surgeons occasionally encounter weak of lacking capsular support. The most common cause of such weakness is the poor condition of the suspensory ligaments of the lens. The most popular solution in such cases is implantation of a capsule ring, which enables intraoperative stabilization of the capsular bag and IOL implantation. However, some authors note that the effectiveness of this technique is low [33, 36]. Often, patients that underwent such manipulations

develop the IOL–capsular bag complex dislocation post-surgery. In addition to the problems with ligaments, some of them also suffer breaches of integrity of the lens capsule during surgery, sometimes ending in the complete loss thereof. Patients with aphakias of various origins (postoperative, traumatic, etc.) form a separate group among those having problems with capsular support. For most of them, it is necessary to anchor the IOL during primary and delayed surgical interventions [37].

Back in the 1950s and 1960s, seamless fixation of IOLs to the iris became a topic of interest, when two ophthalmologists proposed similar techniques: E. Epstein with the "Maltese cross" or "cufflinks", and C.D. Binkhorst with the iris-clips lens [31, 38, 39].

Later, in 1968, S.N. Fedorov and V.D. Zakharov created the Sputnik iris-clip lens, which was the base model in clinical practice for several years. However, this type of fixation could entail a severe complication: dislocation of the IOL into the anterior chamber or into the vitreal cavity, triggered by any planned or unplanned pupil dilation, further aggravated by restriction of the diaphragmatic function of the iris [8, 40].

In 1970, J. Worst proposed an IOL model called "medallion," which had to be stitched to the iris beyond the equatorial zone of the lens, and in 1973, he developed a lens model with seamless attachment to the iris, the "claw lens." This method implied pinching the iris stroma at two points at the distal ends of the IOL, for which slits were made in the haptic part of the lens. The key points of the operation are the use of myotics to maximize pupil constriction and iris expansion, use of viscoelastics to minimize injury to the corneal endothelium, and use of a second instrument to hold the IOL during fixation [8, 41]. However, attaching the IOL to the functionally active zone of the iris stroma violated its functioning.

Most of the works covering stitching of IOLs to the iris describe the process of suturing the haptic elements of the lens to the mid-peripheral zone of the stroma of the iris using the M.A. McCannel method and Siepser knots (dead loop knots). The drawbacks of this technique include iris function impairment, as well as a high risk of iris atrophy, pigment dispersion, uveitis, and cystic macular edema [8, 42].

Some authors have demonstrated various ways of stitching the IOL to the iris when the capsular support is weak of absent [40, 43 , 44]. The main disadvantage of the proposed techniques is still the risk of unplanned IOL luxation into the vitreal cavity during surgery, with all the consequences and complications that follow. Technical drawbacks of the suggested methods: suturing in functionally active areas of the iris stroma, which leads to pupil deformation (violation of diaphragmatic and cosmetic functions); lack of complete visual control over the manipulations of capturing and stitching IOL haptics; difficulties with achievement of a topographically correct and symmetrical positions of the seams on opposing haptic elements; increased risk of unpredictable traumatism of the structures of the anterior segment of the eye given the extremely limited room for a maneuver available to the ophthalmic surgeon.

The technique of IOL implantation suggested in this paper, that which was developed for the cases of lacking capsular support, has a number of significant advantages over the mentioned methods.

In addition to the advantages described above (first technique), which are also useful in the context of similar microsurgical techniques and manipulations, application of fixing threads on both haptic elements of the IOL outside the eye with subsequent implantation ensures a fully controlled position thereof throughout the operation enabled by the threads pulled out. The suggested technique solves the key problem: it allows

full control over the IOL position inside the eye during surgery, eliminating the risks of lens luxation to the fundus. Thus, the surgeon feels confident and fully controls the process, and also can do additional reconstructive manipulations in the eye if necessary. Performing most steps in the anterior chamber means full visual control over the work with seams and reliable pulling of the threads' ends into the planned zones of knots.

The use of microhooks and microcolobomas to capture and pull out fixing threads' ends makes the process completely controllable, predictable, and atraumatic, ensuing accurate localization of the knots and precise capturing of the volume of the iris root tissue (2–3 mm) needed for the purpose. The symmetrical, precise topographic positioning of the fixing suture knots in the projection of the limb at opposite ends of the same meridian ensures high-quality fixation and centering of the IOL, and the iris retains its functions and anatomical and cosmetic properties in full.

The technique presented in this paper addresses cases of weak capsular support (partial corruption of the suspensory ligaments and/or capsular bag). Essentially, it is a combination of the first two techniques, with the first stage involving a set of manipulations from the second technique, and the second stage employing manipulations from the first technique, the former performed on one haptic element, the latter on the opposite one. Thus, the advantages of both techniques are realized. This combined technique is a preferred approach in cases when some parts of capsular support remain and can be used for IOL suspension during implantation. The technique is a safe method for doubtful situations when there is a risk of the IOL dropping into the vitreal cavity during surgery. Application of a fixing suture outside the eye to one of the haptic elements, followed by pulling its ends into the paracentesis, ensures controlled behavior of the IOL inside the eye throughout the operation and does not allow the lens to luxate onto the fundus.

With these techniques, the entire set of manipulations, which is carried out through self-sealing micro-punctures and micro-incisions with use of viscoelastics, creates conditions for anatomical and topographic stability of the structures and microspaces of the eye during surgery, thus enabling a more accurate, controlled, atraumatic work inside the eye at the micro level.

Thus, the developed and proposed set of micro-constructive techniques makes it possible to effectively stitch IOL to the iris while preserving of its functions; the techniques are applicable in various situations when the suspensory ligaments are weak, or it is impossible to anchor and enter the lens relying on the capsular support.

CONCLUSIONS

The developed micro-constructive techniques allow: 1. Transferring the basic manipulations of suturing to the haptic elements of the IOL to the visible zone of the pupil and anterior chamber, where the work is done under full microscopic control, which significantly improves the accuracy, controllability, safety of the process, and makes it atraumatic. 2. Making microcolobomas at the iris root in the projection of limbal paracentesis and to pass through them, using a microhook, the end of the thread capturing the haptic element, so the resulting loop embraces the haptic element of the IOL and a precisely measures volume (2–3 mm) of the iris root tissue. The precise topographic execution of this manipulation translates into symmetrical arrangement of fixing knots on the IOL's opposite haptic elements on one meridian, which means high-quality centering, including for toric and multifocal models. 3. Applying topographically oriented, precise fixing sutures in the projection of the limb, localized in the zone of the most functionally inert iris root tissue, and, as a result, ensure full preservation of the volume of functions and cosmetic properties of the iris and the pupil. Moreover, the involved iris root tissue is exposed to minimal dynamic forces, which ensures reliability, strength, and durability of fixing sutures. 4. Applying fixing threads to the haptic elements of the IOL outside the eye with subsequent implantation, in case of failure or absence of capsular support, which enables full control over the behavior of the IOL inside the eye throughout the operation, eliminating the risks of lens luxation into the vitreal cavity and empowering the surgeon with confidence. 5. Performing all manipulations through self-sealing micro-punctures and micro-incisions, using viscoelastics that create conditions for anatomical and topographic stability of structures and microspaces inside the eye throughout the operation and ensure improved microsurgical reconstruction. This opens up a new direction in ophthalmic surgery, enabling assembling of collapsible structures inside the eye from various micro-components (microconstruction), and, above all, the assembling and installation of the IOL from separate microelements.

References

1. Smirnov AK, Sokolov KV. Sravnitel'nyj analiz metodov podshivanija dislocirovannyh kompleksov «intraokuljarnaja linza–kapsul'nyj meshok» v razlichnyh klinicheskih situacijah. Tihookeanskij medicinskij zhurnal. 2019; 2: 70–73. Russian.

2. Avetisov SYe, Lipatov DV, Fedorov AA. Morfologicheskie izmenenija pri nesostojatel'nosti svjazochno-kapsuljarnogo apparata hrustalika. Vestnik oftal'mologii. 2002; 118 (4): 22–23. Russian.

3. Briszi A, Prahs P, Hillenkamp J, Helbig H, Herrmann W. Complication rate and risk factors for intraoperative complications in resident-performed phacoemulsification surgery. Graefes Arch Clin Exp Ophthalmol. 2012; 250: 1315–20.

4. Hennig A, Johnson GJ, Evans JR, Lagnado R, Poulson A, Pradhan D, et al. Long-term clinical outcome of a randomised controlled trial of anterior chamber lenses after high volume intracapsular cataract surgery. Br J Ophthalmol. 2001; 85: 11–17.

5. Konradsen TR, Zetterström C. A descriptive study of ocular characteristics in Marfan syndrome. Acta Ophthalmol. 2013; 91 (8): 751–5.

6. Jacqueline N. Review of surgical techniques for posterior chamber intraocular lens fixation in the absence of capsular lens support. US Ophthalmic Review. 2015; 8 (2): 86–91.

7. Ma X, Li Z. Capsular tension ring implantation after lens extraction for management of subluxated cataracts. Int J Clin Exp Pathol. 2014; 7 (7): 3733–8.

8. Kadatskaja NV. Mikrohirurgicheskie tehnologii shovnoj fiksacii IOL v hirurgii katarakty, oslozhnennoj slabost'ju ili polnym otsutstviem kapsul'noj podderzhki [dissertacija]. M., 2017. Russian.

9. Dureau P. Pathophysiology of zonular diseases. Curr Opin Ophthalmol. 2008; 19: 27–30.

10. Hoffman RS, Snyder ME, Devgan U, Allen QB, Yeoh R, Braga-Mele R. Management of the subluxated crystalline lens. Journal of Cataract & Refractive Surgery. 2013; 39 (12): 1904–15.

11. Kohnen T. Pseudoexfoliation: impact on cataract surgery and long-term intraocular lensposition. J Cataract Refract Surg. 2010; 36 (8): 1247–8.

12. Pashtaev NP. Klassifikacija dislokacij hrustalika, sovremennaja taktika lechenija. V kn.: S. N. Fedorov, redaktor. Aktual'nye problemy hirurgii hrustalika, steklovidnogo tela i setchatki: Sb. nauch. tr. Mosk. NII mikrohirurgii glaza. M., 1986; s. 34–37. Russian.

13. Pashtaev NP. Hirurgija podvyvihnutogo i vyvihnutogo v steklovidnoe telo hrustalika. Cheboksary: GOU IUV, 2006. Russian.

14. Belonozhenko YaV, Sorokin EL. Vozmozhnosti profilaktiki dislokacii kompleksa «IOL — kapsul'nyj meshok» u bol'nyh s legkoj stepen'ju podvyviha hrustalika pri vypolnenii fakojemul'sifikacii vozrastnoj katarakty. Oftal'mologicheskie vedomosti. 2012; 5 (3): 42–47. Russian.

15. Belonozhenko YaV, Sorokin EL. Variant vybora sposoba hirurgicheskoj korrekcii afakii pri vypolnenii fakojemul'sifikacii vozrastnoj katarakty s legkoj stepen'ju podvyviha hrustalika. Prakticheskaja medicina. 2012; 4 (59): 263–6. Russian.

16. Mamedov ShYu, Agaev MM, Sultanova MM. Sravnitel'naja ocenka techenija posleoperacionnogo perioda pri provedenii fakojemul'sifikacii u pacientov s oslozhnennoj kataraktoj. Oftalmologija. 2014; 1 (14): 81–83. Russian.

17. Rozanova OI. Otdalennye rezul'taty fiksacii zadnekamernoj IOL k raduzhke «obratnym hodom» pri zonuljarnyh defektah. Sovremennye tehnologii v oftal'mologii. 2018; 5: 123–5. Russian.

18. Davis D, Brubaker J, Espandar L, Stringham J, Crandall A, Werner L et al. Late in-the-bag spontaneous intraocular lens dislocation: evaluation of 86 consecutive cases. Ophthalmology. 2009; 116 (4): 664–70.

19. Krepste L, Kuzmiene L, Miliauskas A, Januleviciene I. Possible predisposing factors for late intraocular lens dislocation after routine cataract surgery. Medicina. 2013; 49 (5): 229–34.

20. Tereshhenko YuA, Krivko SV, Sorokin EL, Egorov VV. Spontannaja dislokacija zadnekamernyh intraokuljarnyh linz v pozdnem posleoperacionnom periode: chastota, prichiny, oslozhnenija. RMZh. Klinicheskaja oftal'mologija. 2010; 11 (3): 100–2. Russian.

21. Ivanov DI, Nikitin VN. Hirurgicheskoe lechenie pacientov s dislokaciej kompleksov IOL-fibrozirovannyj kapsul'nyj meshok. Oftal'mologija. 2022; 19 (2): 307–17. Russian.

22. Potemkin VV, Astahov SYu, Golcman EV, Van SYu. Ocenka faktorov riska razvitija pozdnej dislokacii intraokuljarnoj linzy. Oftal'mologija. 2021; 18 (1): 103–10. Russian.

23. Gross JG, Kokame GT, Weinberg DV. In-the-bag intraocular lens dislocation. Am J Ophthalmol. 2004; 137 (4): 630–5.

24. Ganesh SK, Sen P, Sharma HR. Late dislocation of in-the-bag intraocular lenses in uveitic eyes: An analysis of management and complications. Indian J Ophthalmol. 2017; 65 (2): 148–54.

25. Liu E, Cole S, Werner L, Hengerer F. Pathologic evidence of pseudoexfoliation in cases of in-the-bag intraocular lens subluxation or dislocation. Journal of Cataract and Refractive Surgery. 2015; 41 (5): 929–35.

26. Tereshhenko YuA, Krivko SV, Sorokin EL, Egorov VV. Vyjasnenie prichin dislokacii kompleksa «IOL — kapsul'nyj meshok» v pozdnem posleoperacionnom periode hirurgii katarakty. Sovremennye tehnologii kataraktal'noj i refrakcionnoj hirurgii. Sbornik nauchnyh rabot. M., 2010; s. 92–195. Russian.

27. Ivanova NV, Rasin OG, Savchenko AV, Litvinenko OA. Koncepcija stabil'noj fiksacii IOL pri avitrii i nesostojatel'nosti svjazochnogo apparata hrustalika. Sovremennye tehnologii v oftal'mologii. 2019; 1: 66–70. Russian.

28. Dajee KP, Abbey AM, Williams GA. Management of dislocated intraocular lenses in eyes with insufficient capsular support. Current Opinion in Ophthalmology. 2016; 27 (3): 191–5.

29. Donaldson KE, Gorscak JJ, Budenz DL. Anterior chamber and sutured posterior chamber intraocular lenses in eyes with poor capsular support. American Journal of Ophthalmology. 2005; 140 (5): 903–9.

30. Faria MY, Ferreira NP, Canastro M. Management of Dislocated Intraocular Lenses with Iris Suture. European Journal of Ophthalmology. 2017; 27 (1): 45–48.

31. Potemkin VV, Golcman EV. Sposoby hirurgicheskoj korrekcii dislokacij intraokuljarnyh linz i afakii (obzor literatury). Uchenye zapiski SPbGMU im. akad. I. P. Pavlova. 2019; 26 (1): 20–28. Russian.

32. Nottage JM, Bhasin V, Nirankari VS. Long-term safety and visual outcomes of transscleral sutured posterior chamber IOLs and penetrating keratoplasty combined with transscleral sutured posterior chamber IOLs. Trans Am Ophthalmol Soc. 2009; 107: 242–50.

33. Egorova AV, Vasilev AV, Smoljakova GP. Rezul'taty hirurgicheskogo lechenija dislokacii intraokuljarnyh linz. Oftal'mohirurgija. 2017; 1: 6–9. Russian.

34. Sorokoletov GV, Dibina DA, Arisov AA, Molova ZA, avtory; FGBU «MNTK «Mikrohirurgija glaza» im. akad. S.N. Fedorova Minzdrava Rossii», patentoobladatel'. Sposob repozicii i podshivanija dislocirovannoj intraokuljarnoj linzy k raduzhnoj obolochke. Patent RF № 2765539. 31.01.2022. Russian.

35. Teplovodskaja VV, Dibina DA, Sudakova EP, Nosirov PO, avtory; FGBU «MNTK «Mikrohirurgija glaza» im. akad. S.N. Fedorova Minzdrava Rossii», patentoobladatel'. Sposob repozicii i flancevoj fiksacii dislocirovannoj intraokuljarnoj linzy vmeste s kapsul'nym meshkom k raduzhnoj obolochke (varianty). Patent RF № 2773103. 30.05.2022. Russian.

36. Ioshin IYe, Egorova YeV. Vnutrikapsul'noe kol'co — profilaktika oslozhnenij jekstrakcii katarakty pri podvyvihe hrustalika. Oftal'mohirurgija. 2002; 1: 25–28. Russian.

37. Shhuko AG, Mishhenko OP, Senchenko NYa, Jureva TN. Faktory riska i oslozhnenija, voznikajushhie pri pozdnih spontannyh dislokacijah kompleksa «zadnekamernaja IOL — kapsul'nyj meshok» v steklovidnoe telo. Oftal'mohirurgija. 2017; 1: 21–26. Russian.

38. Binkhorst CD. Artificial pseudophakia. Long-term results obtained with the papillary lens (iris-clip lens) in the first twenty cases of unilateral aphakia. Br J Ophthalmol. 1962; 46: 947–56.

39. Epstein E. Modified Ridley lenses. Johannesburg, South Africa. Br J Ophthalmol.1959; 43: 29–33.

40. Maruhnenko AM, Kadatskaja NV. FGBU «MNTK «Mikrohirurgija glaza» im. akad. S. N. Fedorova Minzdrava Rossii», patentoobladatel'. Sposob shovnoj fiksacii k raduzhke intraokuljarnoj linzy pri ee ljuksacii v steklovidnoe telo. Patent RF №2619748. 17.05.2017. Russian.

41. Worst JGF. Extracapsular surgery in lens implantation (Birkhorst lection). Amer Intraocular Implant Soc J. 1977; 13 (2): 102–04.

42. Chang DF. Siepser slipknot for McCannel iris-suture fixation of subluxated intraocular lenses. Journal of Cataract and Refractive Surgery. 2004; 30: 1170–6.

43. Maruhnenko AM, patentoobladatel'. Sposob fiksacii mjagkih intraokuljarnyh linz. Patent RF № 2141295. 20.11.1999. Russian.

44. Fechin OB, avtory; Akcionernoe obshhestvo «Ekaterinburgskij centr MNTK "Mikrohirurgija glaza"», patentoobladatel'. Sposob implantacii i shovnoj fiksacii S-obraznoj intraokuljarnoj linzy k raduzhke. Patent RF №2017133687. 28.08.2018. Russian.

Литература

1. Смирнов А. К., Соколов К. В. Сравнительный анализ методов подшивания дислоцированных комплексов «интраокулярная линза–капсульный мешок» в различных клинических ситуациях. Тихоокеанский медицинский журнал. 2019; 2: 70–73.

2. Аветисов С. Э., Липатов Д. В., Федоров А. А. Морфологические изменения при несостоятельности связочно-капсулярного аппарата хрусталика. Вестник офтальмологии. 2002; 118 (4): 22–23.

3. Briszi A, Prahs P, Hillenkamp J, Helbig H, Herrmann W. Complication rate and risk factors for intraoperative complications in resident-performed phacoemulsification surgery. Graefes Arch Clin Exp Ophthalmol. 2012; 250: 1315–20.

4. Hennig A, Johnson GJ, Evans JR, Lagnado R, Poulson A, Pradhan D, et al. Long-term clinical outcome of a randomised controlled trial of anterior chamber lenses after high volume intracapsular cataract surgery. Br J Ophthalmol. 2001; 85: 11–17.

5. Konradsen TR, Zetterström C. A descriptive study of ocular characteristics in Marfan syndrome. Acta Ophthalmol. 2013; 91 (8): 751–5.

6. Jacqueline N. Review of surgical techniques for posterior chamber intraocular lens fixation in the absence of capsular lens support.

US Ophthalmic Review. 2015; 8 (2): 86–91.

7. Ma X, Li Z. Capsular tension ring implantation after lens extraction for management of subluxated cataracts. Int J Clin Exp Pathol. 2014; 7 (7): 3733–8.

8. Кадатская Н. В. Микрохирургические технологии шовной фиксации ИОЛ в хирургии катаракты, осложненной слабостью или полным отсутствием капсульной поддержки [диссертация]. М., 2017.

9. Dureau P. Pathophysiology of zonular diseases. Curr Opin Ophthalmol. 2008; 19: 27–30.

10. Hoffman RS, Snyder ME, Devgan U, Allen QB, Yeoh R, Braga-Mele R. Management of the subluxated crystalline lens. Journal of Cataract & Refractive Surgery. 2013; 39 (12): 1904–15.

11. Kohnen T. Pseudoexfoliation: impact on cataract surgery and long-term intraocular lensposition. J Cataract Refract Surg. 2010; 36 (8): 1247–8.

12. Паштаев Н. П. Классификация дислокаций хрусталика, современная тактика лечения. В кн.: С. Н. Федоров, редактор. Актуальные проблемы хирургии хрусталика, стекловидного тела и сетчатки: Сб. науч. тр. Моск. НИИ микрохирургии глаза. М., 1986; с. 34–37.

13. Паштаев Н. П. Хирургия подвывихнутого и вывихнутого в стекловидное тело хрусталика. Чебоксары: ГОУ ИУВ, 2006.

14. Белоноженко Я. В., Сорокин Е. Л. Возможности профилактики дислокации комплекса «ИОЛ — капсульный мешок» у больных с легкой степенью подвывиха хрусталика при выполнении факоэмульсификации возрастной катаракты. Офтальмологические ведомости. 2012; 5 (3): 42–47.

15. Белоноженко Я. В., Сорокин Е. Л. Вариант выбора способа хирургической коррекции афакии при выполнении факоэмульсификации возрастной катаракты с легкой степенью подвывиха хрусталика. Практическая медицина. 2012; 4 (59): 263–6.

16. Мамедов Ш. Ю., Агаев М. М., Султанова М. М. Сравнительная оценка течения послеоперационного периода при проведении факоэмульсификации у пациентов с осложненной катарактой. Oftalmologiya. 2014; 1 (14): 81–83.

17. Розанова О. И. Отдаленные результаты фиксации заднекамерной ИОЛ к радужке «обратным ходом» при зонулярных дефектах. Современные технологии в офтальмологии. 2018; 5: 123–5.

18. Davis D, Brubaker J, Espandar L, Stringham J, Crandall A. Werner L et al. Late in-the-bag spontaneous intraocular lens dislocation: evaluation of 86 consecutive cases. Ophthalmology. 2009; 116 (4): 664–70.

19. Krepste L, Kuzmiene L, Miliauskas A, Januleviciene I. Possible predisposing factors for late intraocular lens dislocation after routine cataract surgery. Medicina. 2013; 49 (5): 229–34.

20. Терещенко Ю. А., Кривко С. В., Сорокин Е. Л., Егоров В. В. Спонтанная дислокация заднекамерных интраокулярных линз в позднем послеоперационном периоде: частота, причины, осложнения. РМЖ. Клиническая офтальмология. 2010; 11 (3): 100–2.

21. Иванов Д. И., Никитин В. Н. Хирургическое лечение пациентов с дислокацией комплексов ИОЛ-фиброзированный капсульный мешок. Офтальмология. 2022; 19 (2): 307–17.

22. Потемкин В. В., Астахов С. Ю., Гольцман Е. В., Ван С. Ю. Оценка факторов риска развития поздней дислокации интраокулярной линзы. Офтальмология. 2021; 18 (1): 103–10.

23. Gross JG, Kokame GT, Weinberg DV. In-the-bag intraocular lens dislocation. Am J Ophthalmol. 2004; 137 (4): 630–5.

24. Ganesh SK, Sen P, Sharma HR. Late dislocation of in-the-bag intraocular lenses in uveitic eyes: An analysis of management and complications. Indian J Ophthalmol. 2017; 65 (2): 148–54.

25. Liu E, Cole S, Werner L, Hengerer F. Pathologic evidence of pseudoexfoliation in cases of in-the-bag intraocular lens subluxation or dislocation. Journal of Cataract and Refractive Surgery. 2015; 41 (5): 929–35.

26. Терещенко Ю. А., Кривко С. В., Сорокин Е. Л., Егоров В. В. Выяснение причин дислокации комплекса «ИОЛ — капсульный мешок» в позднем послеоперационном периоде хирургии катаракты. Современные технологии катарактальной и рефракционной хирургии. Сборник научных работ. М., 2010; с. 92–195.

27. Иванова Н. В., Расин О. Г., Савченко А. В., Литвиненко О. А. Концепция стабильной фиксации ИОЛ при авитрии и несостоятельности связочного аппарата хрусталика. Современные технологии в офтальмологии. 2019; 1: 66–70.

28. Dajee KP, Abbey AM, Williams GA. Management of dislocated intraocular lenses in eyes with insufficient capsular support. Current Opinion in Ophthalmology. 2016; 27 (3): 191–5.

29. Donaldson KE, Gorscak JJ, Budenz DL. Anterior chamber and sutured posterior chamber intraocular lenses in eyes with poor capsular support. American Journal of Ophthalmology. 2005; 140 (5): 903–9.

30. Faria MY, Ferreira NP, Canastro M. Management of Dislocated Intraocular Lenses with Iris Suture. European Journal of Ophthalmology. 2017; 27 (1): 45–48.

31. Потемкин В. В., Гольцман Е. В. Способы хирургической коррекции дислокаций интраокулярных линз и афакии (обзор литературы). Ученые записки СПбГМУ им. акад. И. П. Павлова. 2019; 26 (1): 20–28.

32. Nottage JM, Bhasin V, Nirankari VS. Long-term safety and visual outcomes of transscleral sutured posterior chamber IOLs and penetrating keratoplasty combined with transscleral sutured posterior chamber IOLs. Trans Am Ophthalmol Soc. 2009; 107: 242–50.

33. Егорова А. В. Васильев А. В., Смолякова Г. П. Результаты хирургического лечения дислокации интраокулярных линз. Офтальмохирургия. 2017; 1: 6–9.

34. Сороколетов Г. В., Дибина Д. А., Арисов А. А., Молова З. А., авторы; ФГБУ «МНТК «Микрохирургия глаза» им. акад. С.Н. Федорова Минздрава России», патентообладатель. Способ репозиции и подшивания дислоцированной интраокулярной линзы к радужной оболочке. Патент РФ № 2765539. 31.01.2022.

35. Тепловодская В. В., Дибина Д. А, Судакова Е. П., Носиров П. О., авторы; ФГБУ «МНТК «Микрохирургия глаза» им. акад. С.Н. Федорова Минздрава России», патентообладатель. Способ репозиции и фланцевой фиксации дислоцированной интраокулярной линзы вместе с капсульным мешком к радужной оболочке (варианты). Патент РФ № 2773103. 30.05.2022.

36. Иошин И. Э., Егорова Э. В. Внутрикапсульное кольцо — профилактика осложнений экстракции катаракты при подвывихе хрусталика. Офтальмохирургия. 2002; 1: 25–28.

37. Щуко А. Г., Мищенко О. П., Сенченко Н. Я., Юрьева Т. Н. Факторы риска и осложнения, возникающие при поздних спонтанных дислокациях комплекса «заднекамерная ИОЛ – капсульный мешок» в стекловидное тело. Офтальмохирургия. 2017; 1: 21–26.

38. Binkhorst CD. Artificial pseudophakia. Long-term results obtained with the papillary lens (iris-clip lens) in the first twenty cases of unilateral aphakia. Br J Ophthalmol. 1962; 46: 947–56.

39. Epstein E. Modified Ridley lenses. Johannesburg, South Africa. Br J Ophthalmol.1959; 43: 29–33.

40. Марухненко А. М., Кадатская Н. В. ФГБУ «МНТК «Микрохирургия глаза» им. акад. С. Н. Федорова Минздрава России», патентообладатель. Способ шовной фиксации к радужке интраокулярной линзы при ее люксации в стекловидное тело. Патент РФ №2619748. 17.05.2017.

41. Worst JGF. Extracapsular surgery in lens implantation (Birkhorst lection). Amer Intraocular Implant Soc J. 1977; 13 (2): 102–04.

42. Chang DF. Siepser slipknot for McCannel iris-suture fixation of subluxated intraocular lenses. Journal of Cataract and Refractive Surgery. 2004; 30: 1170–6.

43. Марухненко А. М., патентообладатель. Способ фиксации мягких интраокулярных линз. Патент РФ № 2141295. 20.11.1999.

44. Фечин О. Б., авторы; Акционерное общество «Екатеринбургский центр МНТК "Микрохирургия глаза"», патентообладатель. Способ имплантации и шовной фиксации S-образной интраокулярной линзы к радужке. Патент РФ №2017133687. 28.08.2018.

COMPARATIVE ANALYSIS OF METHODS FOR CALCULATION OF TORIC INTRAOCULAR LENSES IN PATIENTS AFTER PENETRATING KERATOPLASTY

Sinitsyn MV ✉, Voskresenskaya AA, Pozdeyeva NA

[1] Cheboksary branch of the Fyodorov Eye Microsurgery Federal State Institution, Cheboksary, Russia

[2] Postgraduate Doctors' Training Institute of the Ministry of Public Health of Chuvashia, Cheboksary, Russia

Calculation of toric intraocular lenses (tIOLs) in patients after penetrating keratoplasty (PK) is challenging. The study aimed to perform comparative retrospective analysis of various methods for calculation of tIOL during phacoemulsification in patients after PK. We analyzed case reports of 36 eyes (36 patients) after PK, which underwent phacoemulsification with tIOL implantation. All tIOLs were recalculated using four different methods. In group 1, tIOL calculation was performed using keratometry data of the anterior surface of the corneal graft measured using a corneal topographer, and the posterior surface of the corneal graft measured using optical coherence tomography of the cornea or the Scheimpflug keratotopographer. In group 2, keratometry of both corneal graft surfaces was measured using the Scheimpflug keratotopographer, in group 3 — using OCT of the cornea, in group 4 — using the keratotopographer. The online Barrett True — K Toric Calculator was used to calculate tIOLs in groups 1–3, and The Kane Formula was used in group 4. There were significant differences in the values of the spherical and cylindrical components of refraction between the studied groups ($p < 0.05$). The highest predictability of tIOL calculation was reported for group 1: the ensured postoperative refraction for the spherical component was within ±0.5 D in 58% of eyes, within ±1.0 D in 67% of eyes; postoperative refraction for the cylindrical component was within –0.5 D in 56% of eyes, within –1.0 D in 89% of eyes. Thus, the highest predictability of tIOL calculation is observed in patients of group 1.

Keywords: penetrating keratoplasty, postkeratoplastic ametropia, toric intraocular lens, calculation method

СРАВНИТЕЛЬНЫЙ АНАЛИЗ СПОСОБОВ РАСЧЕТА ТОРИЧЕСКОЙ ИНТРАОКУЛЯРНОЙ ЛИНЗЫ У ПАЦИЕНТОВ ПОСЛЕ СКВОЗНОЙ КЕРАТОПЛАСТИКИ

М. В. Синицын ✉, А. А. Воскресенская, Н. А. Поздеева

[1] Чебоксарский филиал Федерального государственного автономного учреждения «Национальный медицинский исследовательский центр «Межотраслевой научно-технический комплекс «Микрохирургия глаза» имени С. Н. Фёдорова» Минздрава России, Чебоксары, Россия

[2] Государственное автономное учреждение Чувашской Республики дополнительного профессионального образования «Институт усовершенствования врачей» Минздрава Чувашии, Чебоксары, Россия

Расчет торической интраокулярной линзы (тИОЛ) у пациентов после сквозной кератопластики (СКП) вызывает ряд сложностей. Целью исследования было провести сравнительный ретроспективный анализ различных способов расчета тИОЛ при факоэмульсификации катаракты (ФЭК) у пациентов после СКП. Был проведен анализ историй болезни 36 глаз (36 пациентов) после СКП, на которых была выполнена ФЭК с имплантацией тИОЛ. Все тИОЛ были пересчитаны четырьмя способами. В группе 1 расчет тИОЛ проводили с применением данных кератометрии передней поверхности роговичного трансплантата, измеренных при помощи кератотопографа, и задней поверхности роговичного трансплантата — при помощи оптической когерентной томографии роговицы или шаймпфлюг-кератотопографа). В группе 2 измерение кератометрии обеих поверхностей роговичного трансплантата выполняли при помощи шаймпфлюг-кератотопографа, в группе 3 — на ОКТ роговицы, в группе 4 — при помощи кератотопографа. Для расчета тИОЛ в группах 1–3 применяли онлайн-калькулятор Barrett True — K Toric Calculator, в группе 4 — The Kane Formula. Была отмечена статистически значимая разница по значениям сферического и цилиндрического компонентов рефракции между исследуемыми группами ($p < 0,05$). Наибольшая предсказуемость расчета тИОЛ обнаружена в группе 1: попадание в послеоперационную рефракцию по сферическому компоненту в пределах ±0,5 дптр — в 58% глаз и в пределах ±1,0 дптр — в 67% глаз, по цилиндрическому компоненту — в пределах –0,5 дптр — в 56% глаз и в пределах –1,0 дптр — в 89% глаз. Таким образом, наибольшая предсказуемость расчета тИОЛ была отмечена у пациентов группы 1.

Ключевые слова: сквозная кератопластика, посткератопластическая аметропия, торическая интраокулярная линза, способ расчета

Penetrating keratoplasty (PK) leads to the development of post-keratoplastic corneal astigmatism (CA) in almost all patients [1–3]. In cases of cataract development in patients after PK and the need for its extraction, the accuracy of the selected intraocular lens (IOL) calculation method is of great importance [4–6]. The best functional results are reported in patients with regular CA, who are through cataract extraction with the toric IOL (tIOL) implantation [7–9]. However, the method to calculate tIOL is still a matter of debate. Not all authors consider the posterior corneal graft curvature when calculating tIOL, since they believe that its refraction is similar to refraction of light by the anterior chamber fluid, like in the healthy cornea. That is why keratometry values of the anterior corneal graft surface only are often used [10, 11]. Currently, various online calculators and calculators by tIOL manufacturers are used, which consider curvature of both corneal graft surfaces. However, postoperative results vary considerably even when using keratometry data of both corneal graft surfaces due

to the use of different diagnostic equipment [12, 13]. In view of the above, selection of the most predictable method to calculate tIOL during cataract extraction in patients after PK has determined the relevance of the study.

The study aimed to perform comparative retrospective analysis of various methods for calculation of tIOL during cataract extraction in patients after PK.

METHODS

We performed retrospective analysis of case reports of 36 eyes (36 patients) after PK, which underwent phacoemulsification with tIOL implantation. All the patients were implanted the RayOne Toric RAO610T tIOL (Rayner; UK). The age of patients enrolled in clinical trial (12 males and 24 females) was 31–76 years (average age 57 ± 13 years). Past PK was performed due to congenital corneal dystrophy in six eyes, pellucid corneal degeneration in eight eyes, central corneal scar in six eyes, corneal opacity after the corneal ulcer in six eyes, stage IV keratoconus in six eyes, secondary keratectasia in four eyes. The interval between phacoemulsification and PK in patients was 4–15 years. All corneal grafts were transparent. The corneal graft diameter reached 7.5–8.5 mm (on average 8.14 ± 0.36 mm).

When calculating tIOL, the eye length, anterior chamber depth, lens thickness, white-to-white distance were measured by optical biometry using the IOL Master 500 system (Carl Zeiss AG; Germany). The values of keratometry data and orientation of the major meridians of the anterior corneal graft surface were determined using the TMS-5 corneal topographer (Tomey; Japan), Pentacam Scheimpflug keratotopographer (Oculus Optikgerate GmbH; Germany), by optical coherence tomography (OCT) of the cornea using the CASIA 2 system (Tomey; Japan). The values of keratometry data and orientation of the major meridians of the posterior corneal graft surface were determined using the Pentacam Scheimpflug keratotopographer and the CASIA 2 optical coherence tomography (OCT) system for the cornea. Regular CA was reported in all patients based on the keratotopography data before phacoemulsification.

When calculating tIOL, the following was entered in the calculator: values of the RayOne Toric RAO610T tIOL A-constant of 118.6, Lens Factor, induced astigmatism, orientation of the main surgical incision, target refraction, central corneal graft thickness. IOL was calculated using the online Barrett True-K Toric Calculator and The Kane Formula.

According to case reports, discrepancies in the values of the tIOL optical power and toric component were reported in some patients when calculating tIOL due to differences in the keratometry data of the anterior corneal graft surface measured using the keratotopographer, by corneal OCT, or using the Scheimpflug keratotopographer. In such cases, either mean values of keratometry parameters measured using the above diagnostic equipment, or mean values of similar keratometry parameters based on the results were taken.

We also took the values of the spherical (Sph) and cylindrical (Cyl) refraction components obtained three months

and later after phacoemulsification, when stabilization of these parameters was reported, from medical records.

To determine the most predictable tIOL calculation method, we divided the methods into four groups depending on the diagnostic equipment used to measure keratometry parameters (Table 1).

In group 1, keratometry parameters of the anterior corneal graft surface were measured using the keratotopographer (TMS-5), while that of the posterior surface were measured using the Scheimpflug keratotopographer (Pentacam) or corneal OCT (CASIA 2), considering comparable keratometry values reported for the posterior corneal graft surface when using these devices. In group 2, keratometry parameters of both corneal graft surfaces were measured with the Scheimpflug keratotopographer (Pentacam), and in group 3 these were measured by the corneal OCT (CASIA 2). In group 4, the anterior corneal graft surface curvature only was measured using the keratotopographer (TMS-5).

In groups 1–4, tIOLs were calculated using the online Barrett True-K Toric Calculator, since it allows one to consider keratometry data of both corneal graft surfaces. In group 4, tIOL calculation was performed using the online The Kane Formula calculator allowing one to analyze the anterior corneal graft surface keratometry data only.

The tIOL optical power was calculated for emmetropic target refraction in all groups, toric component for full correction of total CA in groups 1–3, and for correction of CA of the anterior corneal graft surface in group 4.

Comparative analysis of predictability of tIOL calculation by various methods was performed in groups 1–4 based on the data on the implanted tIOL optic power, toric component, as well as the postoperative refraction results.

Statistical data analysis was performed using IBM SPSS Statistics 20. The Shapiro–Wilk test was used to test the data distributions for normality. The values of the studied parameters were normally distributed in all groups, so significance of differences in the studied parameters between two groups were assessed using the parametric Student's t-test for independent variables, and the differences between three groups were assessed by one-way analysis of variance. The differences in the studied parameters between two groups were considered significant at $p < 0.05$, and the differences between three groups were considered significant at $p < 0.017$. The values of the studied parameters were presented as M ± σ, where M was the mean, σ was the standard deviation.

RESULTS

According to medical records, none of the patients had intra- or postoperative complications of phacoemulsification. The slit lamp examination performed on the next day after surgery showed that the eye media were transparent, and tIOLs were centered in all patients (Fig. 1).

Preoperative data on the average CA value and keratomery data (Km) of the anterior corneal graft surface showed significant differences based on the data obtained using the

Table 1. Methods for toric intraocular calculation during cataract extraction in patients after penetrating keratoplasty

Groups	Keratometry data measurement	
	Anterior corneal graft surface	Posterior corneal graft surface
1	Keratotopographer (TMS-5)	OCT (CASIA 2) or Scheimpflug keratotopographer (Pentacam)
2	Scheimpflug keratotopographer (Pentacam)	Scheimpflug keratotopographer (Pentacam)
3	Corneal OCT (CASIA 2)	Corneal OCT (CASIA 2)
4	Keratotopographer (TMS-5)	Keratometry was not taken into account
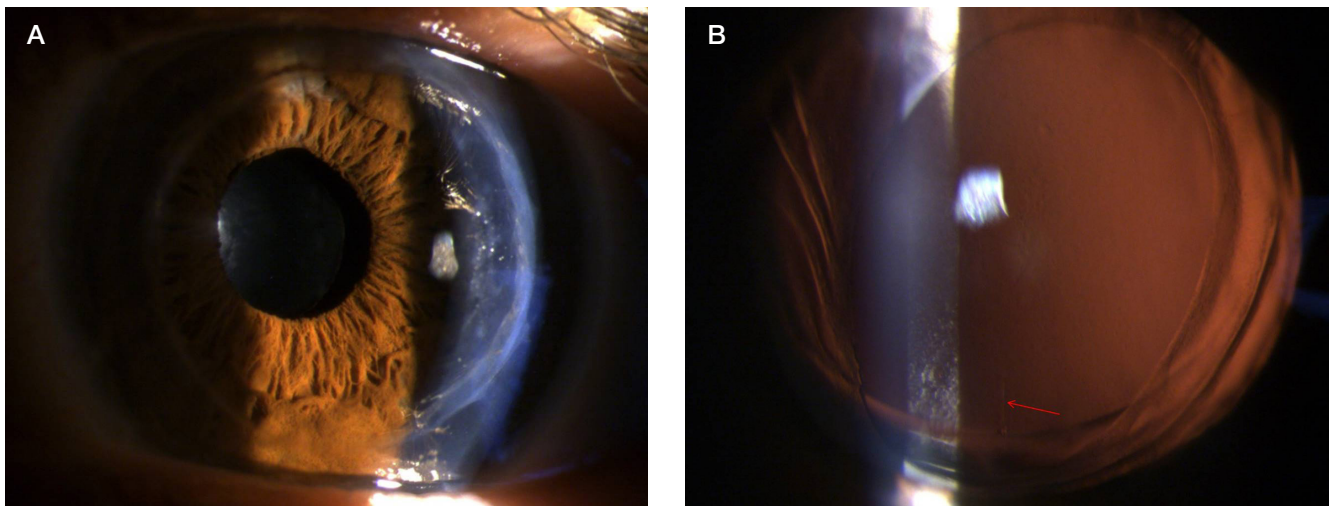
Fig. 1. View of the eye of patient N., 56 years, during slit lamp examination on day 1 after phacoemulsification with the toric intraocular lens implantation. **A**. A transparent corneal graft can be seen, along with the optic part of the toric intraocular lens in the projection of the pupil. **B**. View of the eye against the background of drug-induced mydriasis, a vertical mark of the intraocular lens toric axis (marked with a *red arrow*) located along the corneal graft keratometry strong meridian can be seen

corneal topographer (TMS-5), Scheimpflug keratotopographer (Pentacam), and OCT of the cornea (CASIA 2), while both CA and Km of the posterior corneal graft surface were comparable based on the data obtained using the Scheimpflug keratotopographer and OCT of the cornea (Tables 1, 2).

The difference in orientation of the axes of the major meridians of the corneal graft anterior and posterior surfaces exceeding 5° based on the data obtained using the Scheimpflug keratotopographer was reported for 12 eyes (33,3%), while that based on the data obtained using OCT of the cornea was reported for 15 eyes (41.7%).

The results of preoperative analysis of CA on the posterior corneal graft surface based on the Scheimpflug keratotopography and corneal OCT data are presented as a chart (Fig. 2).

The rate of CA on the posterior corneal graft surface based on the corneal OCT within ≤ –0.3 D was 11%, within ≤ –1.0 D — 56% (Fig. 1). The rate of CA on the posterior surface based on the Scheimpflug keratotopography data within ≤ –0.3 D was 11%, within ≤ –1.0 D — 44%. Thus, the average rate of CA on the posterior surface based on the data obtained using both devices within ≤ –0.3 D was 11%.

When calculating the tIOL optic power, getting into the planned target refraction for Sph in group 1 within ±0.5 D was reported for 58% of eyes, ±1.0 D for 66% of eyes, in group 2 that within ±0.5 D was reported for 33% of eyes, ±1.0 D for 49% of eyes, in group 3 that within ±0.5 D was reported for 17% of eyes, ±1.0 D for 25% of eyes, in group 4 that within ±0.5 D was not reported at all, ±1.0 D was reported for 17% of eyes (Fig. 3).

The highest predictability of getting into target refraction for Sph was reported when calculating the tIOL optic power in group 1, while the lowest predictability was reported for group 4 (Fig. 2).

When calculating the tIOL toric component, getting into target refraction for Cyl in group 1 within –0.5 D was reported for 56% of eyes, –1.0 D for 89% of eyes, in group 2 that within –0.5 D was reported for 22% of eyes, –1.0 D for 44% of eyes, in group 3 that within –0.5 D was reported for 22% of eyes, –1.0 D for 33% of eyes, in group 4 that within –0.5 was reported for 6% of eyes, –1.0 D for 17% of eyes (Fig. 4).

The highest predictability of getting into target refraction for Cyl was reported when calculating the tIOL toric component in group 1, while the lowest predictability was reported for group 4 (Fig. 3).

Table 2. Preoperative values of corneal astigmatism on both corneal graft surfaces measured using different equipment (M ± σ)

Astigmatism on the corneal graft	Equipment			*p*
	Keratotopographer (TMS-5), D	Scheimpflug keratotopographer (Pentacam), D	Corneal OCT (CASIA 2), D	
Anterior surface	–6.15 ± 3.28	–5.81 ± 2.89	–6.72 ± 3.23	0.0105
	(from –2.5 to –10.5)	(from –2.1 to –10.8)	(from –1.8 to –11.7)	
Posterior surface	no data	–1.05 ± 0.63	–1.04 ± 0.60	0.4115
		(from –0.1 to –1.8)	(from –0.3 to –1.9)	

Table 3. Preoperative average keratometry values of both corneal graft surfaces measured using different equipment (M ± σ)

Km of the corneal graft	Equipment			*p*
	Keratotopographer (TMS-5), D	Scheimpflug keratotopographer (Pentacam), D	Corneal OCT (CASIA 2), D	
Anterior surface	44.07 ± 4.20 (from 39.16 to 49.72)	44.69 ± 4.14 (from 39.5 to 49.1)	45.89 ± 4.34 (from 39.2 to 49.9)	0.0122
Posterior surface	no data	5.77 ± 0.75 (from 4.4 to 6.8)	7.24 ± 1.08 (from 5.9 to 8.6)	0.1225
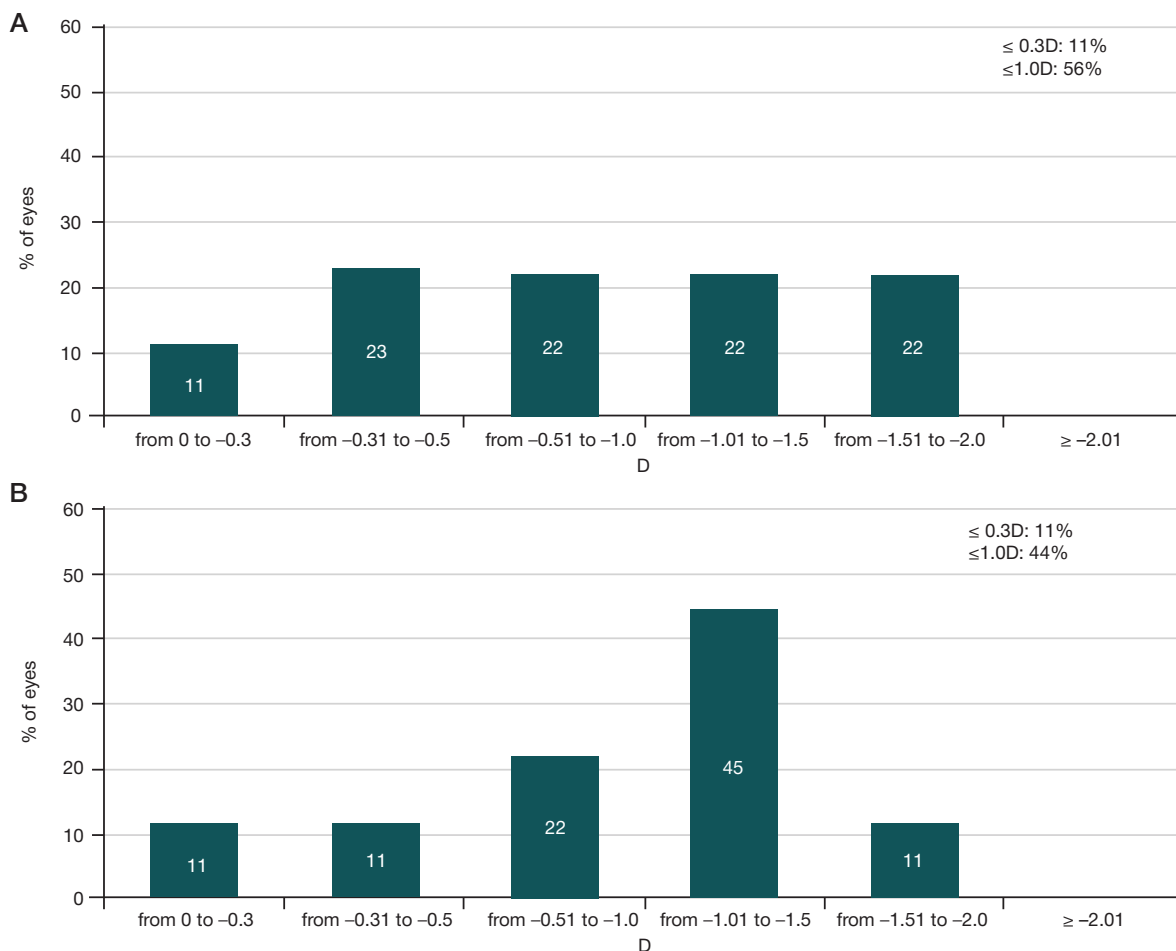
Fig. 2. Diagrams of the distribution of pre-operative values of corneal astigmatism on the posterior corneal graft surface based on the corneal OCT data (CASIA 2) **(A)**, Scheimpflug keratotopography data (Pentacam) **(B)**

DISCUSSION

Considering the fact that almost all patients develop CA after PK, performing cataract extraction with tIOL implantation allows one to solve a problem of cataract through one surgical procedure and at the same time correct CA. However, the accuracy of tIOL calculation in patients after PK has a lot of features. First, the tIOL calculation complexity results from trouble selecting the most accurate calculator. Currently, there are two types of tIOL calculators: those considering curvature of the anterior corneal surface only and those considering curvature of both corneal surfaces. As is well known, refraction of the posterior corneal surface is normally similar to light refraction of the anterior chamber fluid, due to which many authors neglect keratometry of the posterior corneal surface. However, keratometry parameters of the posterior surface of the cornea can change when performing corneal surgery. According to certain data, CA on the posterior corneal surface is normally on average –0.3 D, and only 9% of eyes have CA on the posterior corneal surface exceeding –0.5 D [14]. In our study, patients after PK have shown the opposite. Only 11% of eyes have CA on the posterior corneal graft surface within ≤ –0.3 D; CA exceeds –1.0 D in 44% of eyes based on the OCT data and in 56% of eyes based on the Scheimpflug keratotopography data. That is why it should be considered to accurately select the tIOL toric component.

The next thing that can lead to the tIOL calculation errors is orientation of the major meridians of the corneal graft anterior and posterior surfaces. As is well known, in case of matching axes of the major meridians of both corneal graft surfaces, CA

on the posterior surface compensates for the value of CA on the anterior surface by its own value, which results in reduction of total CA. This, along with the induced astigmatism value, must be considered when calculating the tIOL toric component in order not to overcorrect and not to flip the CA axis to the opposite. Orientation of the major meridians of both corneal graft surfaces is also very important. If these differ by no more than 5°, tIOL can immediately correct the entire total CA, otherwise CA on the posterior corneal surface will persist and will be capable of affecting vision after surgery, depending on its value (in our study the value reached 1.8–1.9 D). In this study, the difference in orientation of the major meridians of both corneal graft surfaces exceeded 5° based on the Scheimpflug keratotopography data in 33.3% of eyes, based on the corneal OCT in 41.7% of eyes. In such cases, CA on the posterior surface persists after the tIOL implantation.

The next thing is selection of the device, the results of using which will be most accurate when calculating tIOL. According to the results of this study, keratometry parameters of the posterior corneal graft surface are comparably measured by corneal OCT and by using the Scheimpflug keratotopographer. The difference is in measuring keratometry of the anterior corneal graft surface. According to the findings, the highest predictability for the spherical and cylindrical refraction components was demonstrated by the tIOL calculation method used in group 1, where keratometry parameters of the anterior corneal graft surface were measured using the keratotopographer operating based on the Placido ring principle, and that of the posterior corneal graft surface were measured by corneal OCT or using
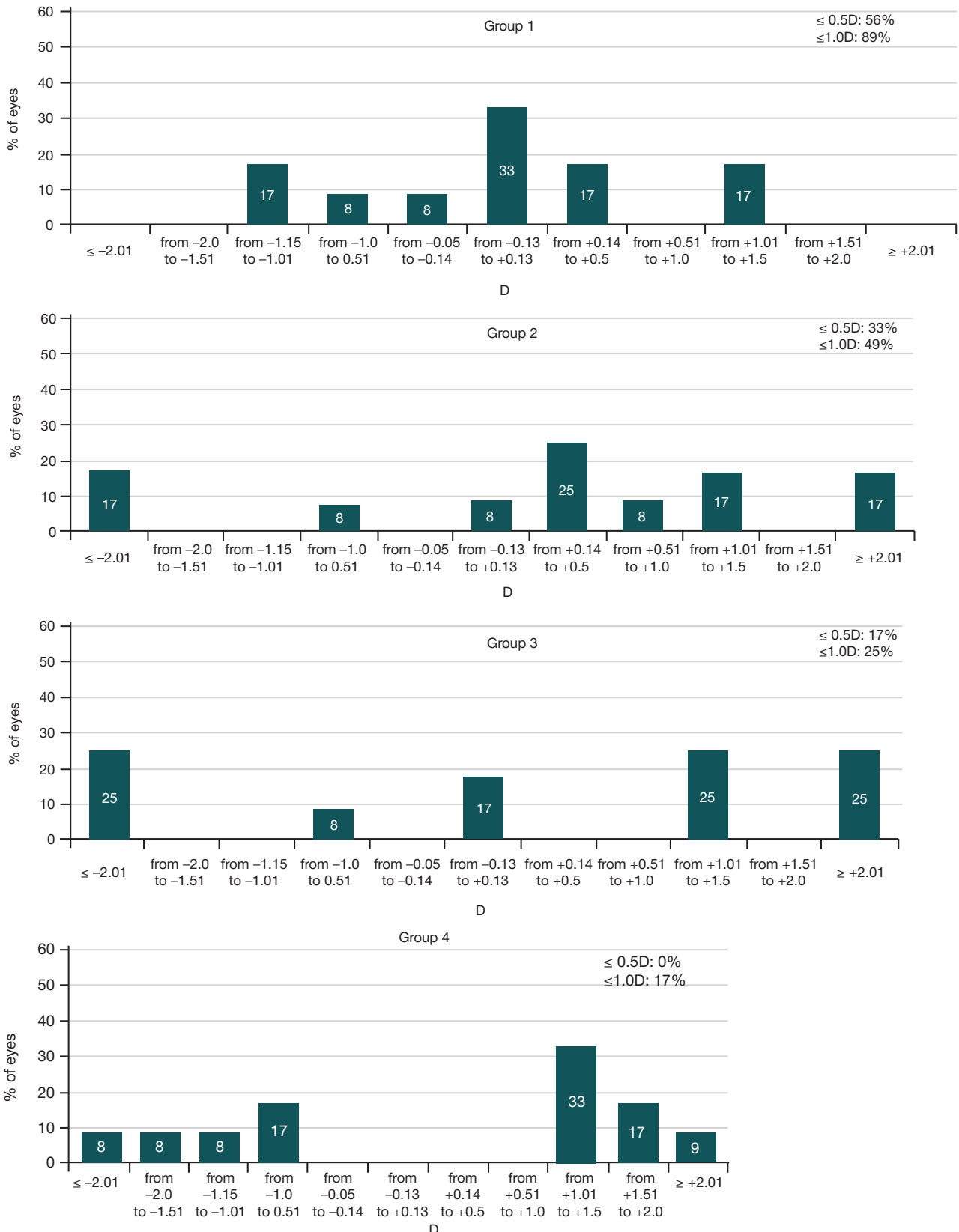
Fig. 3. Predictability of the spherical refraction component when calculating the tIOL optic power in groups 1–4

the Scheimpflug keratotopographer. The lowest tIOL calculation predictability was reported for group 4, which can be explained by the fact that tIOL calculation did not take into account the posterior corneal graft surface curvature.

Today, there are several tIOL calculators taking into account keratometry of both corneal graft surfaces. In our study, the

value of one of the major meridians of the posterior corneal graft surface exceeded 7.5 D in 12 eyes (34.3%), which made it possible to enter these in the online Barrett True-K Toric Calculator only.

According to the literature data, the refraction results of the cataract extraction with tIOL implantation differ due to the facts that the authors used different tIOL calculators and keratometry
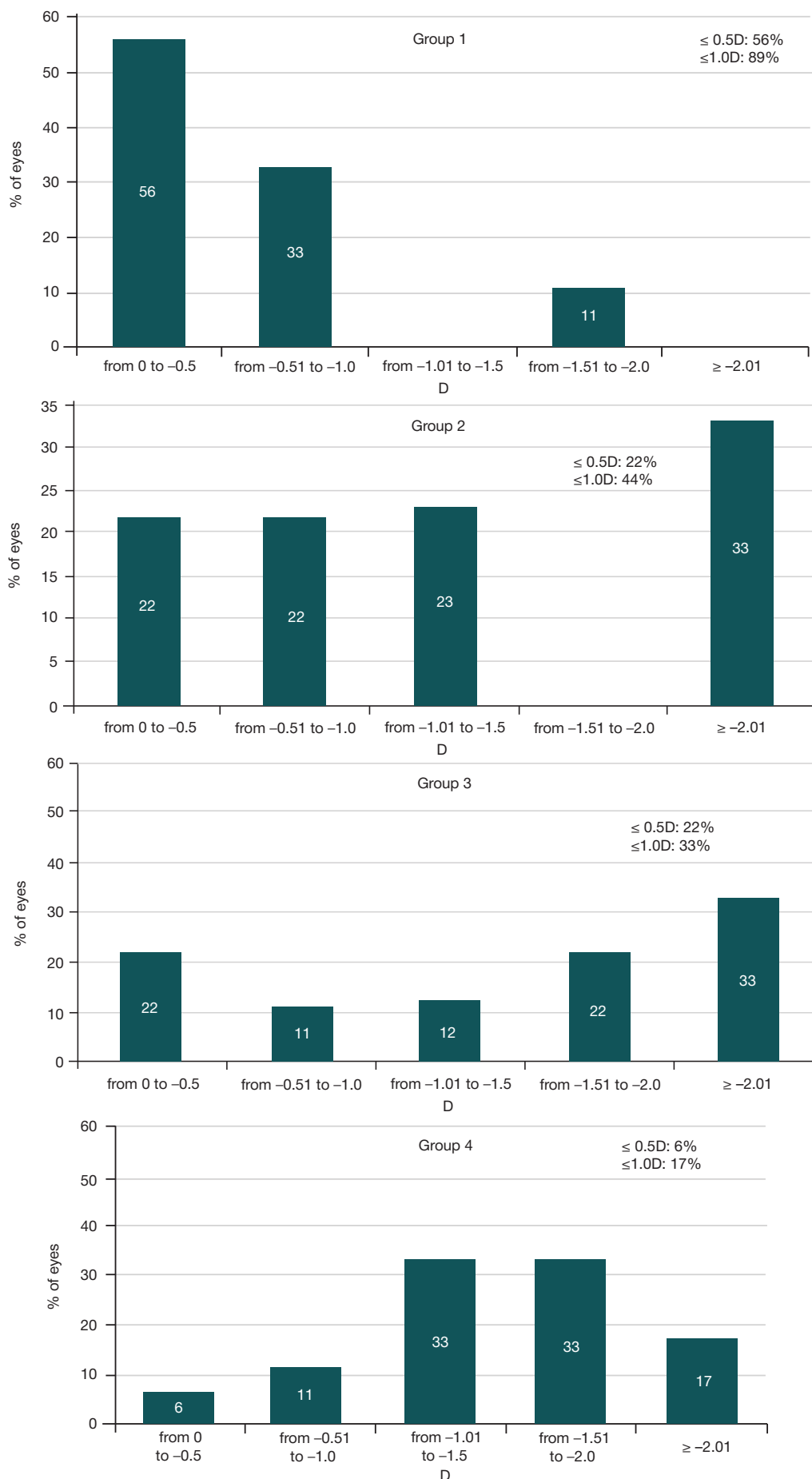
Fig. 4. Predictability of the cylindrical refraction component when calculating the tIOL optic power in groups 1–4

data obtained using different diagnostic devices. Thus, a clinical trial was conducted focused on correction of post-PK CA exceeding 2.25 D in 67 eyes (45 patients) with cataract by phacoemulsification with the Acrysof Toric SN60T6- SN60T9 tIOL implantation [15]. After surgery, UDVA was 0.61 ± 0.26, CDVA was 0.81 ± 0.21. Postoperative cylindrical refraction component (CRC) was below 0.75 D in 62% of eyes and below 1.00 D in 81% of eyes [15]. In 2021, the results of the clinical trial focused on correction of high corneal astigmatism (6–10 D) after PK in patients with cataract by phacoemulsification with tIOL implantation were published. After surgery, the average UDVA increased from 0.04 ± 0.02 to 0.6 ± 0.14, CRC reduced from –9.0 ± 1.80 to –1.1 ± 0.45 D, and postoperative average spherical equivalent was 0.75 ± 0.5 D [7]. In 2022, the results of phacoemulsification with tIOL implantation in patients after PK with the regular form of corneal astigmatism exceeding 1.5 D were provided. After surgery, UDVA increased from 0.1 ± 0.02 to 0.38 ± 0.11, CDVA increased from 0.23 ± 0.07 to 0.78 ± 0.12, and postoperative CRC was 0.93 ± 0.87 D [5].

Thus, the tIOL calculation method, in which the data of the anterior corneal graft surface measured using the keratotopographer operating based on the Placido ring principle and that of the posterior corneal graft surface measured by corneal OCT or the Scheimpflug keratotopographer are entered in the calculator taking into account keratometry data of both corneal graft surfaces, will be the most predictable.

CONCLUSIONS

Comparative retrospective analysis of various tIOL calculation methods used during cataract extraction in patients after PK showed the highest predictability of getting into planned target refraction in group 1. When calculating the intraocular lens optic power and toric component, it is reasonable to use the calculators taking into account keratometry data of both corneal graft surfaces, specifically keratometry data of the anterior corneal graft surface measured using the keratotopographer operating based on the Placido ring principle and keratometry data of the posterior corneal graft surface measured using the corneal optical coherence tomography scanner or the Scheimpflug keratotopographer.

References

1. Deshmukh R, Nair S, Vaddavalli PK, Agrawal T, Rapuano CJ, Beltz J, et al. Post-penetrating keratoplasty astigmatism. Surv Ophthalmol. 2022; 67 (4): 1200–28. DOI: 10.1016/j.survophthal.2021.11.005.
2. Kijonka M, Nowińska A, Wylęgała E, Wylęgała A, Wróblewska-Czajka E, Kryszan K, et al. Postoperative Astigmatism after Keratoplasty: A Systematic Review Meta-Analysis Based on PRISMA. J Clin Med. 2024; 13 (11): 3306. DOI: 10.3390/jcm13113306.
3. Alió JL, Niazi S, Doroodgar F, Barrio JLAD, Hashemi H, Javadi MA. Main issues in penetrating keratoplasty. Taiwan J Ophthalmol. 2024; 14 (1): 50–58. DOI: 10.4103/tjo.TJO-D-24-00001.
4. Den S, Shimmura S, Shimazaki J. Cataract surgery after deep anterior lamellar keratoplasty and penetrating keratoplasty in age- and disease-matched eyes. J Cataract Refract Surg. 2018; 44 (4): 496–503. DOI: 10.1016/j.jcrs.2018.01.024.
5. Pellegrini M, Furiosi L, Yu AC, Giannaccare G, Scuteri G, Gardeli I, et al. Outcomes of cataract surgery with toric intraocular lens implantation after keratoplasty. J Cataract Refract Surg. 2022; 48 (2): 157–61. DOI: 10.1097/j.jcrs.0000000000000730.
6. Tang Q, Yao K. Challenges in cataract surgery after penetrating keratoplasty managed using femtosecond laser: A series of 3 case reports. Medicine (Baltimore). 2024; 103 (25): e38614. DOI: 10.1097/MD.0000000000038614.
7. Reddy JK, Pooja CM, Prabhakar GV. High power custom toric intraocular lens for correcting high corneal astigmatism in post-keratoplasty and keratoconus patients with cataract. Indian J Ophthalmol. 2021; 69 (7): 1766–68. DOI: 10.4103/ijo.IJO_2640_20.
8. Moreno-Martínez A, Martín-Melero O, Andrés-Pretel F, Gómez-Cortés A, Granados-Centeno JM. Outcomes of Phacoemulsification With Toric Intraocular Lenses in Addressing Postkeratoplasty Astigmatism. Cornea. 2024; 43 (1): 76–82. DOI: 10.1097/ICO.0000000000003288.
9. Jeeva IK, Masud S, Ali TS, Siddiqui MAR, Waheed AA, Awan A. Evaluation of visual outcomes with toric intraocular lens implantation using digital marker during cataract surgery. J Pak Med Assoc. 2024; 74 (3): 450–5. DOI: 10.47391/JPMA.8008.
10. Alfonso-Bartolozzi B, Fernández-Vega-Cueto L, Fernández-Vega L, Martínez-Alberquilla I, Madrid-Costa D, Alfonso JF. Triple Procedure: A Stepwise Combination of Deep Anterior Lamellar Keratoplasty and Cataract Surgery. Cornea. 2024; 43 (3): 301–6. DOI: 10.1097/ICO.0000000000003364.
11. Krysik K, Lyssek-Boron A, Janiszewska-Bil D, Wylegala E, Dobrowolski D. Impact of ultrasound and optical biometry on refractive outcomes of cataract surgery after penetrating keratoplasty in keratoconus. Int J Ophthalmol. 2019; 12 (6): 949–53. DOI: 10.18240/ijo.2019.06.11.
12. Lin H, Zhang J, Niu GZ, Huang XY, Zhang YS, Liu CY, et al. Phacoemulsification in eyes with corneal opacities after deep anterior lamellar keratoplasty. Int J Ophthalmol. 2019; 12 (8): 1344–47. DOI: 10.18240/ijo.2019.08.17.
13. Sinitsyn MV, Pozdeeva NA. Correction of irregular postkeratoplastic astigmatism in patients with cataract. The EYE GLAZ. 2023; 25 (2): 99–107. Russian.
14. Koch DD, Ali SF, Weikert MP, Shirayama M, Jenkins R, Wang L. Contribution of posterior corneal astigmatism to total corneal astigmatism. J Cataract Refract Surg. 2012; 38 (12): 2080–87. DOI: 10.1016/j.jcrs.2012.08.036.
15. Visser N, Ruíz-Mesa R, Pastor F, Bauer NJ, Nuijts RM, Montés-Micó R. Cataract surgery with toric intraocular lens implantation in patients with high corneal astigmatism. J Cataract Refract Surg. 2011; 37 (8): 1403–10. DOI: 10.1016/j.jcrs.2011.03.034.

Литература

1. Deshmukh R, Nair S, Vaddavalli PK, Agrawal T, Rapuano CJ, Beltz J, et al. Post-penetrating keratoplasty astigmatism. Surv Ophthalmol. 2022; 67 (4): 1200–28. DOI: 10.1016/j.survophthal.2021.11.005.
2. Kijonka M, Nowińska A, Wylęgała E, Wylęgała A, Wróblewska-Czajka E, Kryszan K, et al. Postoperative Astigmatism after Keratoplasty: A Systematic Review Meta-Analysis Based on PRISMA. J Clin Med. 2024; 13 (11): 3306. DOI: 10.3390/jcm13113306.
3. Alió JL, Niazi S, Doroodgar F, Barrio JLAD, Hashemi H, Javadi MA. Main issues in penetrating keratoplasty. Taiwan J Ophthalmol. 2024; 14 (1): 50–58. DOI: 10.4103/tjo.TJO-D-24-00001.
4. Den S, Shimmura S, Shimazaki J. Cataract surgery after deep anterior lamellar keratoplasty and penetrating keratoplasty in age- and disease-matched eyes. J Cataract Refract Surg. 2018; 44 (4): 496–503. DOI: 10.1016/j.jcrs.2018.01.024.
5. Pellegrini M, Furiosi L, Yu AC, Giannaccare G, Scuteri G, Gardeli I, et al. Outcomes of cataract surgery with toric intraocular lens implantation after keratoplasty. J Cataract Refract Surg. 2022; 48 (2): 157–61. DOI: 10.1097/j.jcrs.0000000000000730.

6. Tang Q, Yao K. Challenges in cataract surgery after penetrating keratoplasty managed using femtosecond laser: A series of 3 case reports. Medicine (Baltimore). 2024; 103 (25): e38614. DOI: 10.1097/MD.0000000000038614.

7. Reddy JK, Pooja CM, Prabhakar GV. High power custom toric intraocular lens for correcting high corneal astigmatism in post-keratoplasty and keratoconus patients with cataract. Indian J Ophthalmol. 2021; 69 (7): 1766–68. DOI: 10.4103/ijo.IJO_2640_20.

8. Moreno-Martínez A, Martín-Melero O, Andrés-Pretel F, Gómez-Cortés A, Granados-Centeno JM. Outcomes of Phacoemulsification With Toric Intraocular Lenses in Addressing Postkeratoplasty Astigmatism. Cornea. 2024; 43 (1): 76–82. DOI: 10.1097/ICO.0000000000003288.

9. Jeeva IK, Masud S, Ali TS, Siddiqui MAR, Waheed AA, Awan A. Evaluation of visual outcomes with toric intraocular lens implantation using digital marker during cataract surgery. J Pak Med Assoc. 2024; 74 (3): 450–5. DOI: 10.47391/JPMA.8008.

10. Alfonso-Bartolozzi B, Fernández-Vega-Cueto L, Fernández-Vega L, Martínez-Alberquilla I, Madrid-Costa D, Alfonso JF. Triple Procedure: A Stepwise Combination of Deep Anterior Lamellar Keratoplasty and Cataract Surgery. Cornea. 2024; 43 (3): 301–6.

DOI: 10.1097/ICO.0000000000003364.

11. Krysik K, Lyssek-Boron A, Janiszewska-Bil D, Wylegala E, Dobrowolski D. Impact of ultrasound and optical biometry on refractive outcomes of cataract surgery after penetrating keratoplasty in keratoconus. Int J Ophthalmol. 2019; 12 (6): 949–53. DOI: 10.18240/ijo.2019.06.11.

12. Lin H, Zhang J, Niu GZ, Huang XY, Zhang YS, Liu CY, et al. Phacoemulsification in eyes with corneal opacities after deep anterior lamellar keratoplasty. Int J Ophthalmol. 2019; 12 (8): 1344–47. DOI: 10.18240/ijo.2019.08.17.

13. Синицын М. В., Поздеева Н. А. Коррекция иррегулярного посткератопластического астигматизма у пациентов с катарактой. The EYE ГЛАЗ. 2023; 25 (2): 99–107. DOI: 10.33791/2222-4408-2023-2-99-107.

14. Koch DD, Ali SF, Weikert MP, Shirayama M, Jenkins R, Wang L. Contribution of posterior corneal astigmatism to total corneal astigmatism. J Cataract Refract Surg. 2012; 38 (12): 2080–87. DOI: 10.1016/j.jcrs.2012.08.036.

15. Visser N, Ruíz-Mesa R, Pastor F, Bauer NJ, Nuijts RM, Montés-Micó R. Cataract surgery with toric intraocular lens implantation in patients with high corneal astigmatism. J Cataract Refract Surg. 2011; 37 (8): 1403–10. DOI: 10.1016/j.jcrs.2011.03.034.

EFFECT OF ENDOILLUMINATION DURING VITRECTOMY ON OXIDATIVE PROCESSES IN RABBIT BLOOD

Yamgutdinov RR[1,2] ✉, Mukhamadeev TR[1], Ahmadeev RR[1], Mochalov KS[1]

[1] Bashkir State Medical University, Ufa, Russia

[2] City Clinical Hospital No. 8, Ufa, Russia

Investigation of the mechanisms underlying retinal photodamage occurring during vitreoretinal interventions is a topical issue of ophtalmology. The study aimed to assess the effect of endoillumination of varying intensity and duration on alteration of oxidative processes in rabbit blood. The experiment involved 16 rabbits, with their retinas exposed to endoillumination of different duration (30 and 60 min) and intensity (8 and 16 cd/m²). Blood samples were collected from the rabbits' ear vein before and after light exposure. Whole blood and serum biochemiluminescence was measured in order to assess oxidative processes. The data were analyzed using the Mann–Whitney U-test, and the results were considered significant at $p \leq 0.05$. A 30-minute light exposure resulted in a significant increase in whole blood biochemiluminescence: 1.5-fold at the intensity of 8 cd/m² and 2.5-fold at the intensity of 16 cd/m² relative to control values ($p < 0.05$), indicating enhanced reactive oxygen species generation by blood cells. In contrast, a significant decrease in serum biochemiluminescence was revealed: 1.2-fold at the intensity of 8 cd/m² and 2-fold at the intensity of 16 cd/m² compared to control ($p < 0.05$) , which likely indicates a compensatory increase in antioxidant activity in response to hyperactivation of free radical processes. With the 60-minute exposure, the changes in biochemiluminescence were more pronounced: 3- and 7-fold increase in whole blood biochemiluminescence and 2- and 3-fold decrease in serum biochemiluminescence, respectively. Thus, intense light exposure resulted in the oxidative process alterations determined by the intensity and duration of exposure.

Keywords: endoillumination, vitreoretinal surgery, phototoxicity, biochemiluminescence, oxidative processes

ВЛИЯНИЕ ЭНДОВИТРЕАЛЬНОЙ ИЛЛЮМИНАЦИИ НА ОКСИДАТИВНЫЕ ПРОЦЕССЫ В КРОВИ КРОЛИКОВ

Р. Р. Ямгутдинов[1,2] ✉, Т. Р. Мухамадеев[1], Р. Р. Ахмадеев[1], К. С. Мочалов[1]

[1] Башкирский государственный медицинский университет, Уфа, Россия

[2] Городская клиническая больница № 8, Уфа, Россия

Актуальной проблемой офтальмологии является исследование механизмов фотоповреждений сетчатки, происходящих во время витреоретинальных вмешательств. Цель исследования — оценить влияние эндоиллюминации различной интенсивности и продолжительности на изменение оксидативных процессов в крови кроликов. Эксперимент проводили на 16 кроликах, сетчатку которых подвергали воздействию эндоиллюминации разной продолжительности (30 и 60 мин) и интенсивности (8 и 16 кд/м²). Образцы крови из ушной вены кролика забирали до и после светового воздействия. Для оценки оксидативных процессов измеряли биохемилюминесценцию в цельной крови и сыворотке крови. Данные анализировали с использованием U-теста Манна–Уитни, а результаты считали достоверными при $p \leq 0,05$. При 30-минутной световой экспозиции в цельной крови было зафиксировано статистически значимое увеличение биохемилюминесценции: в 1,5 раза при интенсивности 8 кд/м² и в 2,5 раза при интенсивности 16 кд/м² по сравнению с контрольными показателями ($p < 0,05$), что отражает усиление генерации активных форм кислорода клетками крови. В сыворотке, напротив, выявлено достоверное снижение уровней биохемилюминесценции: в 1,2 раза при интенсивности 8 кд/м² и в 2 раза при интенсивности 16 кд/м² относительно контроля ($p < 0,05$), что, очевидно, может свидетельствовать о компенсаторном увеличении антиокислительной активности в ответ на гиперактивацию свободнорадикальных процессов. При 60-минутной экспозиции изменения биохемилюминесценции имели более выраженный характер: усиление в цельной крови в 3 и 7 раз, и снижение в сыворотке крови в 2 и 3 раза соответственно. Таким образом, при интенсивном световом воздействии отмечено изменение оксидативных процессов, определяемое временем и длительностью воздействия.

Ключевые слова: эндоиллюминация, витреоретинальная хирургия, фототоксичность, биохемилюминесценция, оксидативные процессы

Adequate intraoperative visualization of intraocular structures accomplished using external light sources for intraocular illumination is an important prerequisite for conducting vitreoretinal surgery [1–3]. The development of new light sources for endoillumination (EI) is also associated with the transition to minor surgical approaches (25 G, 27 G, 29 G), however, the luminous flux enhancement accompanying such transition inevitably increases the risk of phototoxic damage to the retina and pigment epithelium [4, 5].

The following major parameters affecting phototoxicity of the sources of endovitreal illumination are distinguished: light source type, aphakic hazard indicator, brightness, numerical aperture of a fiber (light cone), light exposure duration, working distance (between endoilluminator and the retina), and the retinal zone affected by the luminous flux [2, 3].

Thanks decades of experimental research, the key components of pathogenesis of photodamage to the eye

structures and tissues have been uncovered. Destructive photochemical reactions can occur as a result of oxidative process enhancement due to high concentrations of photosensitizers in photoreceptors, high partial pressure of oxygen in the retina and high polyunsaturated fatty acid levels [6–12]. It has been shown that the retinal pigment epithelial cells contain lipofuscin granules comprising bisretinoid fluorophores that begin to produce reactive oxygen species when exposed to light, which leads eventually to the formation of oxidized products [13].

First of all, photosensitizers, such as retinal and its metabolites, are potentially dangerous in terms of phototoxicity. These can generate singlet oxygen and superoxide radicals when exposed to light [14]. Other pathogenetic factors include high oxygen tension reaching 100 mmHg at the level of the apices of the outer photoreceptor segments. Finally, it should be noted that oxidative destruction of melanosomes can result in formation of toxic aldehydes and ketones, as well as in protein modification [15].

Thus, according to the published data, all the potentially dangerous conditions for photodamage to the eye structures and tissues, especially the photoreceptor–pigment epithelium complex, arise during vitreoretinal interventions.

The study aimed to assess the effect of endoillumination of varying intensity and duration on oxidative process alteration in rabbit blood.

METHODS

The study involving 16 rabbits (males) aged 6–9 months with the body weight of 2–3 kg was conducted at the Chair of Ophtalmology and the Central Research Laboratory of the Bashkir State Medical University. The animals were bought from specialized breeding nursery (SP Tulupov; Russia). Rabbits were kept in the controlled environment ensuring optimal temperature, humidity, and illumination; these were given a balanced diet including specialized foods and fresh water. The animals were administered 2% xylazine solution (Alfasan International B.V.; Netherlands) intramuscularly in a dose of 1 mg per 1 kg of body weight half an hour before surgery in order to ensure a pronounced sedative effect. Zoletil 100 (Virbac; France) in a dose of 7.5 mg per 1 kg of rabbit's body weight was used intramuscularly for general anesthesia. The Mydrimax drops (Sentiss Pharma; India) were instilled into the conjunctival sac 15–20 min before the procedure to dilate pupils. Local anesthesia was achieved using the 0.5% proxymetacaine hydrochloride solution.

The test samples were represented by blood collected from the rabbits' ear vein (EV). Such an approach was used due to the fact that we collected samples from the central retinal vein (CRV) using the 27–40 G MedOne cannula earlier, at the pilot stage of the study. However, in our experiments, blood collection directly from the CRV had serious methodological limits, since the procedure is associated with further alteration of intraocular media. The analysis of biochemiluminescence (BCL) parameters involving samples collected from the rabbits' CRV and EV revealed no significant differences, which allowed us to use blood from EV as test samples.

A 25 G port installed in the projection of the pars plana part of the ciliary body was used to model endovitreal exposure. A xenon light source integrated into the Optimed Profi ophtalmological miscrosurgical system (Optimedservice; Russia) was used as an illuminator. The endoilluminator was introduced via the port, and its tip was placed at a distance of 8 mm (light cone 30°) from the retina in the direction of the macular zone.

The experimental animals were divided into two groups.

Group 1: exposure to light with the intensity of 8 cd/m^2 (50%) for 30 min (4 rabbits, 4 eyes) and 60 min (4 rabbits, 4 eyes).

Group 2: exposure to light with the intensity of 16 cd/m^2 (100%) for 30 min (4 rabbits, 4 eyes) and 60 min (4 rabbits, 4 eyes).

The follow-up collection of blood from the ear vein was performed after the end of the light exposure.

The BHL recording method was used to assess the effects of endoillumination during vitrectomy on oxidative processes. The use of BCL in vitreoretinal surgery for estimation of photodamage to the eye tissues is based on the fact that biochemiluminescence reflects light emission from the electronically excited atoms and molecules emerging during chemical reactions. Furthermore, free radical processes are the only biochemiluminescence sources [16].

We recorded blood BCL with the HLM-003 system (Ufa State Aviation Technical University; Russia) measuring the light sum S and maximum slow-flash amplitude Imax in quanta per second for 3 min [17]. The whole blood BCL was used as an indicator of the oxidative processes of reactive oxygen species generation by blood cells, primarily neutrophils. We used luminol (10-4 M) in the dimethyl sulfoxide (DMSO) solution to record luminol-dependent chemiluminescence (LDBCL). A total of 0.1 mL of blood were mixed with 2 mL of luminol solution, then the mixture was put in the chamber of the unit at 37 °C. In addition to LDBCL, we assessed iron-induced biochemiluminescence (IIBCL) of blood serum in order to determine the levels of oxidative processes of lipid peroxidation (LPO). Blood was centrifuged to obtain serum, and serum was diluted with phosphate buffer. Luminescence was indiced by adding the $FeSO_4 \times 7H_2O$ solution, the intensity of which reflected the LPO level.

The data were analyzed using the nonparametric Mann–Whitney U-test. The results were considered significant at $p \leq 0.05$ and presented as median (Me) and interquartile range (IQR).

RESULTS

A significant increase in biochemiluminescence with luminol was observed after the 30-min exposure to light with the 50% intensity (8 cd/m^2; group 1). During the experiment LDBCL increased from the baseline level of 26.4×10^5 quanta/s to 38.2×10^5 quanta/s. This increase corresponds to the almost 50% intensity growth, which suggests a significant effect of moderately intense radiation on this indicator. There was a rather more pronounced increase in LDBCL (up to 62.2×10^5 quanta/s) under exposure to radiation with greater intensity 100% (16 cd/m^2; group 2). Such an increase is equivalent to the almost 2.5-fold intensity growth relative to baseline. The data obtained show that the more intense radiation has a stronger effect on LDBCL. This confirms the fact that the effect depends on the intensity of radiation used. We also conducted appropriate measurement of LDBCL for the 60-min exposure in order to assess the longer EI. The data are provided in Table 1.

According to the table, EI leads to the LDBCL enchancement, which reflects the increased generation of free radicals by blood cells. The exposure time increase results in the LDBCL parameter enchancement, which suggests intensification of oxidative processes in blood.

The LDBCL value increased 3-fold after the 60-min exposure: the control value was 26.4×10^5 quanta/s, and the value after the exposure was 79.1×10^5 quanta/s. There was an almost 7-fold increase in LDBCL, when the intensity increased to 100% (16 cd/m^2).

Table 1. LDBCL parameters (Me (IQR)) before and after the 30-min and 60-min exposure to aphakic light of varying intensity, 10^5 quanta/s

Studied parameter	Before	30 min		60 min	
		50% EI intensity	100% EI intensity	50% EI intensity	100% EI intensity
S	26.4 (21.4–29.2)	38.2 (36.5–39.0)*	62.2 (61.4–64.7)*	79.1 (78.8–79.6)*	179.5 (179.5–180.6)*
Imax	7.6(7.4–8.8)	12.7 (11.2–14.3)*	17.1 (16.1–17.9)*	25.06 (24.9–25.5)*	53.3 (52.5–53.5)*

Note: * — the difference from control is significant at $p \leq 0.05$.

Table 2. IIBCL parameters (Me (IQR)) before and after the 30-min and 60-min exposure to aphakic light of varying intensity, 10^5 quanta/s

Studied parameter	Before	30 min		60 min	
		50% EI intensity	100% EI intensity	50% EI intensity	100% EI intensity
S	408.2 (379.2–416.6)	333.5 (327.2–335.8)*	206.0 (188.7–220.8)*	204.0 (197.9–209.8)*	137.1 (136.4–138.7)*
Imax	205.3 (197.9–213.7)	170.9 (169.3–172.1)*	127.5 (117.3–135.2)*	102.1 (102.0–112.20)*	68.1 (66.8–74.2)*

Note * — the difference from control is significant at $p \leq 0.05$.

The following patterns were revealed when recording IIBCL of the samples exposed to EI: the 30-min EI source exposure resulted in the significantly decreased IIBCL parameters: 1.2-fold in the first group relative to control. The intensity increase to the full value of 100% (16 cd/m²; group 2) resulted in the 2-fold decrease in luminosity parameters. Control — 408.2×10^5 quanta/s, after the exposure — 206.1×10^5 quanta/s.

When the exposure duration increased to 60 min, the decrease in IIBCL parameters became more noticeable. At 50% intensity (8 cd/m²; group 1) IIBCL decreased to 204.0×10^5 quanta/s, which was 2 times lower. At 100% intensity (16 cd/m²; group 2) IIBCL dropped to 137.1×10^5 quanta/s, which was 3 times lower. These findings demonstrate that the illumination duration and intensity have a significant effect on blood serum biochemiluminescence (Table 2).

DISCUSSION

Our findings show that alterations of oxidative processes in blood are clearly of dose-dependent nature associated with the endoillumination intensity and duration. With increasing EI intensity and duration, enhancement of LDBCL of the test samples has been reported, which suggests enhancement of oxidative processes in blood cells. It is clear that at first the oxygen-dependent cellular mechanisms ensuring realization of reactive oxygen species generation are activated.

The findings are in line with the general conclusions that oxidative processes yielding the oxidative degradation products are triggered in molecular structures of the eye under exposure to light [13, 18].

The low IIBCL values revealed reflect the antioxidant activity increase and lipid peroxidation decrease. This may be due to the fact the enhancement of oxidative processes causes activation of antioxidant enzyme systems. Certain studies show that inhibitory effect on the oxidative photodestruction products is associated with antioxidant activity [19]. The antioxidant activity increase in blood serum can probably be explained by compensatory rearrangement of the antioxidant systems caused by free radical accumulation resulting from endoillumination. This process can be considered as an adaptive mechanism allowing the body to neutralize excess free radicals and maintain cellular homeostasis.

Thus, the effects of EI exposure lead to complex adaptive response of the hemic system that is intended to reduce damage caused by free radical oxidation and maintain cell viability. The studies of mechanisms underlying light-induced damage to the eye show that the oxidative degradation products can diffuse into the cell cytoplasm and cause toxic effects even when there is no light exposure [13]. According to our study, the EI time and intensity represent an important factor of the LDBCL and IIBCL parameter alteration. The longer and more intense is EI, the more severe are alterations in the form of increased LDBCL and decreased IIBCL.

CONCLUSIONS

The data provided make it possible to conclude that the duration and intensity of exposure to light emitted by endoillumination sources lead to considerable alterations of oxidative processes in blood. The most severe alterations of oxidative processes are reported after the 60-min exposure to endoillumination of 100% intensity. Further morphological and electrophysiological testing will help determine the contribution and temporary pattern of the identified alterations of oxidation processes to the development of phototoxic risk of endoillumination sources.

References

1. Kaziev SN, Borzenok SA, Saburina IN, Kosheleva NV, Tonaeva HD. Jendoilljuminacija v hode vitreal'noj hirurgii — jevoljucija voprosa i osobennosti primenenija na sovremennom jetape. Prakticheskaja medicina. 2013; 70: 10–2. Russian.
2. de Oliveira PR, Berger AR, Chow DR. Vitreoretinal instruments: vitrectomy cutters, endoillumination and wide-angle viewing systems. Int J Retina Vitreous. 2016; 2: 28.
3. McCannel CA. Advanced in endoillumination. Retinal Physician. 2015; 12: 9–10.
4. Totsuka K, Ueta T, Uchida T, Roggia MF, Nakagawa S, Vavvas DG, et al. Exp Eye Res. 2019; 181: 316–24.
5. Sun Y, Zheng Y, Wang C, Liu Y. Glutathione depletion induces ferroptosis, autophagy, and premature cell senescence in retinal pigment epithelial cells. Cell Death Dis. 2018; 9 (7): 753.
6. Tang Z, Ju Y, Dai X, Ni N, Liu Y, Zhang D, et al. HO-1-mediated ferroptosis as a target for protection against retinal pigment

epithelium degeneration. Redox Biol. 2021; (43): 101971.

7. Upadhyay M, Milliner C, Bell BA, Bonilha VL. Oxidative stress in the retina and retinal pigment epithelium (RPE): Role of aging, and DJ-1. Redox Biol. 2020; 37: 101623.

8. Rossino MG, Lulli M, Amato R, Cammalleri M, Monte MD et al. Oxidative Stress Induces a VEGF Autocrine Loop in the Retina: Relevance for Diabetic Retinopathy. Cells. 2020; 9 (6): 1452.

9. Wang S, Ji LY, Li L, Li JM. Oxidative stress, autophagy and pyroptosis in the neovascularization of oxygeninduced retinopathy in mice. Mol Med Rep. 2019; 19 (2): 927–34.

10. Ozawa Y. Oxidative stress in the light-exposed retina and its implication in age-related macular degeneration. Redox Biol. 2020; 37: 101779.

11. Datta S, Cano M, Ebrahimi K, Wang L, Handa JT. The impact of oxidative stress and inflammation on RPE degeneration in non-neovascular AMD. Prog Retin Eye Res. 2017; 60: 201–18.

12. Guo KX, Huang C, Wang W, Zhang P, Li Y, et al. Oxidative stress and mitochondrial dysfunction of retinal ganglion cells injury exposures in long-term blue light. Int J Ophthalmol. 2020; 13 (12): 1854–63. https://doi.org/10.18240/ijo.2020.12.03.

13. Yakovleva MA, Ostrovsky DS, Khubetsova MH, Borzenok SA, Feldman TB, Ostrovsky MA. Study of the cytotoxic properties of unoxidized and oxidized bisretinoids of lipofuscin granules

in retinal pigment epithelium cells. Pathological Physiology and Experimental Therapy. 2023; 67 (3): 76–87. Russian.

14. Zhuravlev AI. Kvantovaja biofizika zhivotnyh i cheloveka: uchebnoe posobie. M.: Izd-vo «BINOM. Laboratorija znanij», 2015. Russian.

15. Gulin AA, Dontsov AE, Yakovleva MA, Trofimova NN, Aybush AV et al. Oxidative destruction of human RPE melanosomes induced by superoxide radicals leads to the formation of reactive aldehydes and ketones. St. Petersburg State Polytechnical University Journal. Physics and Mathematics. 2022; 15 (3.2): 311–6.

16. Zakoteev JuA. Hemiljuminescencija Principy i metodiki registracii, oborudovanie, zadachi. M., 2015. Russian.

17. Farhutdinov RR., Tevdoradze SI. Metodiki issledovanija hemiljuminescencii biologicheskogo materiala na hemiljuminomere HL-003. Metody ocenki antioksidantnoj aktivnosti biologicheski aktivnyh veshhestv. M.: RUDN, 2005. Russian.

18. Dontsov AE, Yakovleva MA, Vasin AA, Gulin AA, Aybush AV, et al. Understanding the mechanism of light-induced age-related decrease in melanin concentration in retinal pigment epithelium cells. Int J Mol Sci. 2023; 24 (17): 13099.

19. Dontsov AE, Aronstam NL, Ostrovsky MA. Inhibitory effect of oxybiol on the modification of proteins by water-soluble products of photooxidative destruction of bisretinoid A2E. Biophysics. 2024; 69 (2): 257–63. Russian.

Литература

1. Казиев С. Н., Борзенок С. А., Сабурина И. Н., Кошелева Н. В., Тонаева Х. Д. Эндоиллюминация в ходе витреальной хирургии — эволюция вопроса и особенности применения на современном этапе. Практическая медицина. 2013; 70: 10–2.

2. de Oliveira PR, Berger AR, Chow DR. Vitreoretinal instruments: vitrectomy cutters, endoillumination and wide-angle viewing systems. Int J Retina Vitreous. 2016; 2: 28.

3. McCannel CA. Advanced in endoillumination. Retinal Physician. 2015; 12: 9–10.

4. Totsuka K, Ueta T, Uchida T, Roggia MF, Nakagawa S, Vavvas DG, et al. Exp Eye Res. 2019; 181: 316–24.

5. Sun Y, Zheng Y, Wang C, Liu Y. Glutathione depletion induces ferroptosis, autophagy, and premature cell senescence in retinal pigment epithelial cells. Cell Death Dis. 2018; 9 (7): 753.

6. Tang Z, Ju Y, Dai X, Ni N, Liu Y, Zhang D, et al. HO-1-mediated ferroptosis as a target for protection against retinal pigment epithelium degeneration. Redox Biol. 2021; (43): 101971.

7. Upadhyay M, Milliner C, Bell BA, Bonilha VL. Oxidative stress in the retina and retinal pigment epithelium (RPE): Role of aging, and DJ-1. Redox Biol. 2020; 37: 101623.

8. Rossino MG, Lulli M, Amato R, Cammalleri M, Monte MD et al. Oxidative Stress Induces a VEGF Autocrine Loop in the Retina: Relevance for Diabetic Retinopathy. Cells. 2020; 9 (6): 1452.

9. Wang S, Ji LY, Li L, Li JM. Oxidative stress, autophagy and pyroptosis in the neovascularization of oxygeninduced retinopathy in mice. Mol Med Rep. 2019; 19 (2): 927–34.

10. Ozawa Y. Oxidative stress in the light-exposed retina and its implication in age-related macular degeneration. Redox Biol. 2020; 37: 101779.

11. Datta S, Cano M, Ebrahimi K, Wang L, Handa JT. The impact of oxidative stress and inflammation on RPE degeneration in non-neovascular AMD. Prog Retin Eye Res. 2017; 60: 201–18.

12. Guo KX, Huang C, Wang W, Zhang P, Li Y, et al. Oxidative stress and mitochondrial dysfunction of retinal ganglion cells injury exposures in long-term blue light. Int J Ophthalmol. 2020; 13 (12): 1854–63. https://doi.org/10.18240/ijo.2020.12.03.

13. Яковлева М. А., Островский Д. С., Хубецова М. Х., Борзенок С. А., Фельдман Т. Б., Островский М. А. Изучение цитотоксичных свойств неокисленных и окисленных бисретиноидов липофусциновых гранул в клетках ретинального пигментного эпителия. Патологическая физиология и экспериментальная терапия. 2023; 67 (3): 76–87.

14. Журавлев А. И. Квантовая биофизика животных и человека: учебное пособие. 4-е изд., перераб. и доп. М.: Изд-во «БИНОМ. Лаборатория знаний», 2015.

15. Gulin AA, Dontsov AE, Yakovleva MA, Trofimova NN, Aybush AV et al. Oxidative destruction of human RPE melanosomes induced by superoxide radicals leads to the formation of reactive aldehydes and ketones. St. Petersburg State Polytechnical University Journal. Physics and Mathematics. 2022; 15 (3.2): 311–6.

16. Закотеев Ю. А. Хемилюминесценция. Принципы и методики регистрации, оборудование, задачи. М., 2015.

17. Фархутдинов Р. Р., Тевдорадзе С. И. Методики исследования хемилюминесценции биологического материала на хемилюминомере ХЛ-003. Методы оценки антиоксидантной активности биологически активных веществ. М.: РУДН, 2005.

18. Dontsov AE, Yakovleva MA, Vasin AA, Gulin AA, Aybush AV, et al. Understanding the mechanism of light-induced age-related decrease in melanin concentration in retinal pigment epithelium cells. Int J Mol Sci. 2023; 24 (17): 13099.

19. Донцов А. Е., Аронштам Н. Л., Островский М. А. Ингибирующее действие оксибиола на процесс модификации белков водорастворимыми продуктами фотоокислительной деструкции бисретиноида А2Е. Биофизика. 2024; 69 (2): 257–63.

STRAINS OF *MYCOBACTERIUM TUBERCULOSIS* WITH MUTATIONS IN *gyrA* DIFFER IN THEIR LEVEL OF COMPETITIVE FITNESS

Andreevskaya SN[1]✉, Smirnova TG[1], Chernousova LN[1], Larionova EE[1], Sevastyanova EV[1], Ustinova VV[1], Kiselyova EA[1], Ergeshov A[1,2]

[1] Central Tuberculosis Research Institute, Moscow, Russia

[2] Yevdokimov Moscow State University of Medicine and Dentistry, Moscow, Russia

As *M. tuberculosis* strains develop resistance to fluoroquinolones, pools of *M. tuberculosis* sensitive to drugs of this group and pools of *M. tuberculosis* with different resistance determinants can simultaneously coexist in the host organism. The goal of this research was to run an *in vitro* investigation of growth characteristics of *M. tuberculosis* strains which have different genetic determinants of resistance to fluoroquinolones, in the setting of competition for nutrients. The research used five clinical strains of multidrug-resistant *M. tuberculosis* differing in *gyrA* structure. Strains were cultured in pairs and individually under optimal conditions (Middlebrook 7H9 medium) and under conditions of multistress (50% Middlebrook 7H9 medium, 2 mM KNO_2, 0.02% H_2O_2). The experiment took 21 days. The number of cells of each co-cultured strain was estimated from calibration curves. These curves showed the dependence of the threshold cycle of the polymerase chain reaction — respective to the channel targeted by the mutation — on the concentration of *M. tuberculosis* cells. The competitive fitness value and specific growth rate were calculated from the number of cells of each strain when co-cultured. *M. tuberculosis* strains with mutations in *gyrA* were found to be inferior in growth rate to the wild-type *gyrA* strain, which was particularly pronounced under multistress conditions. The strain with the most common *gyrA*_D94G mutation had the lowest growth rate of all strains examined. It has been hypothesised that the slow growth of *M. tuberculosis* with this mutation may lead to tolerance to anti-tuberculosis drugs, and as a result, the strain gains an advantage under chemotherapy conditions compared to other *gyrA* mutant variants.

Keywords: *Mycobacterium tuberculosis*, *gyrA*, fluoroquinolones, competitive fitness, resistance, heteroresistance

ШТАММЫ *MYCOBACTERIUM TUBERCULOSIS* С МУТАЦИЯМИ В *gyrA* РАЗЛИЧАЮТСЯ ПО УРОВНЮ КОНКУРЕНТНОГО ФИТНЕСА

С. Н. Андреевская[1]✉, Т. Г. Смирнова[1], Л. Н. Черноусова[1], Е. Е. Ларионова[1], Э. В. Севастьянова[1], В. В. Устинова[1], Е. А. Киселева[1], А. Эргешов[1,2]

[1] Центральный научно-исследовательский институт туберкулеза, Москва, Россия

[2] Московский государственный медико-стоматологический университет имени А. И. Евдокимова, Москва, Россия

В процессе формирования устойчивости *M. tuberculosis* к фторхинолонам в организме хозяина могут одновременно сосуществовать пулы *M. tuberculosis*, чувствительные к препаратам этой группы, и пулы *M. tuberculosis* с различными детерминантами устойчивости. Целью исследования было изучить особенности роста *in vitro* штаммов *M. tuberculosis*, отличающихся генетическими детерминантами устойчивости к фторхинолонам, в условиях конкуренции за питательные вещества. Исследование проведено на пяти клинических штаммах *M. tuberculosis* с множественной лекарственной устойчивостью, различающихся структурой *gyrA*. Штаммы культивировали попарно и индивидуально в оптимальных условиях (среда Middlebrook 7H9) и в условиях мультистресса (50% среда Middlebrook 7H9, 2 мМ KNO_2, 0,02% H_2O_2). Время эксперимента составило 21 сутки. Число клеток каждого из совместно культивируемых штаммов оценивали по калибровочным кривым зависимости порогового цикла полимеразной цепной реакции по целевому для мутации каналу от концентрации клеток *M. tuberculosis*. По числу клеток каждого штамма при совместном культивировании вычисляли величину конкурентного фитнеса и удельную скорость роста. Было установлено, что штаммы *M. tuberculosis* с мутациями в *gyrA* уступали в скорости роста штамму с диким типом *gyrA*, что было особенно сильно выражено в условиях мультистресса. Штамм с наиболее распространенной мутацией *gyrA*_D94G имел наименьшую скорость роста из всех исследованных штаммов. Была высказана гипотеза, что медленный рост *M. tuberculosis* с этой мутацией может приводить к толерантности к противотуберкулезным препаратам и в результате этого штамм получает преимущество в условиях химиотерапии по сравнению с другими мутантными по *gyrA* вариантами.

Ключевые слова: *Mycobacterium tuberculosis*, *gyrA*, фторхинолоны, конкурентный фитнес, устойчивость, гетерорезистентность

Mycobacteria of a tuberculosis complex form a genetically homogeneous group of bacteria with a low mutagenesis rate compared to other bacteria [1]. Although the frequency of mutations in *Mycobacterium tuberculosis* (MTB) is low, it must be considered that tuberculosis disease lasts from several months to several years, and the size of the bacterial population in the host during this time can reach more than 1 billion CFU. Over the course of the disease, there is an increased likelihood of spontaneous mutations, including mutations in genes associated with drug resistance, which may result in the emergence of clones with new genotypes [2, 3].

The coexistence of drug-sensitive and drug-resistant MTB pools in the same organism is called bacterial heteroresistance [4, 5]. Heteroresistance can occur not only in the case of microevolution of a single clone, as described above (monoclonal heteroresistance), but also as a result of mixed infection, when a person is infected with several MTB strains with different drug resistance (polyclonal heteroresistance) [6–8]. Monoclonal heteroresistance is considered one of the major steps in the development of drug resistance in bacterial isolates [5, 9]. Several studies have linked the presence of heteroresistance to poor outcome of TB treatment [10, 11].

Multidrug-resistant tuberculosis (MDR TB) is currently on the rise worldwide, when the pathogen is resistant to the two main first-line drugs, Rifampicin and Isoniazid, at the same time [12]. Fluoroquinolones are the most effective drugs for MDR TB therapy [13–15]. According to different authors, the frequency of MTB heteroresistance to fluoroquinolones varies from 1 to 35% depending on the region studied [16–20].

The already mentioned formation of drug resistance through heteroresistance, failure of TB therapy in the presence of pathogen heteroresistance, and fluoroquinolones becoming the most effective drugs for MDR TB — all this provides relevance to the studies aimed at understanding the mechanisms of MTB heteroresistance to fluoroquinolones, also helping to understand the evolutionary perspectives of MTBs with different genetic determinants of resistance to drugs of this group.

The goal of this research was to run an *in vitro* investigation of growth characteristics of *M. tuberculosis* strains which have different genetic determinants of resistance to fluoroquinolones, in the setting of competition for nutrients.

METHODS

The subject of the study

The study was conducted on five clinical strains of MTBs that were maximally similar in phenotypic resistance, had an identical MDR genotype (rpoB_S531L + katG_S315T) and belonged to the spoligygous SIT1 of Beijing sublineage, but differed

in genetic determinants of resistance to fluoroquinolones (four strains with different mutations in the *gyrA* gene and one strain with wild-type gyrA; Table 1).

Culturing MTB strains

MTB strains were cultured in pairs and individually on Middlebrook 7H9 liquid nutrient medium and under multistress conditions (50% Middlebrook 7H9 medium, 2 mM KNO_2, 0.02% H_2O_2). The time of the experiment was 21 days.

Determining the number of MTB cells in a sample

To determine the number of cells of each strain in the sample, we followed an approach using multiplex PCR using the Amplitub-FQ-PV kit (Syntol, Russia), which detects key mutations associated with fluoroquinolone resistance. For this purpose, serial dilutions of each of the MTB strains from 10^2 to 10^8 CFU/ml were prepared and calibration curves were plotted, showing the dependence of the threshold cycle of amplification — respective to the channel targeted by the mutation — on the concentration of MTB cells in the sample. According to the calibration curves, the concentration of each of the co-cultured mutants was determined by the value of the threshold cycle. All studies were performed in triplicate.

Competitive fitness

Competitive fitness (W) of MTB strains, reflecting the total culture growth of each strain during the experiment in paired cultivation, was determined according to the formula [21]:

$$W = \frac{ln\dfrac{S1(f)}{S1(i)}}{ln\dfrac{S2(f)}{S2(i)}},$$

where W — Competitive fitness level;
$S1(i)$ — initial concentration of strain 1;
$S1(f)$ — final concentration of strain 1;
$S2(i)$ — initial concentration of strain 2;
$S2(f)$ — final concentration of strain 2.

When W > 1, the competitive fitness of strain 1 is higher than that of strain 2;

W < 1, the competitive fitness of strain 1 is lower than that of strain 2;

W = 1, strains 1 and 2 have similar competitive fitness.

To compare the growth of MTB strains cultured in pairs with individual growth on the medium, we determined the *specific growth rate of the culture* (μ), i.e. the accumulation of bacterial mass per unit time during the exponential phase of growth, according to the formula [22]:

Table 1. Characteristics of MTB strains

Strain code	Phenotypic resistance	Mutations in genes			SIT
		rpoB	*katG*	*gyrA*	
90V	HREZEthLfx	S531L	S315T	A90V	SIT1
94Y	HREZLfx	S531L	S315T	D94Y	SIT1
94G	HREZEthLfx	S531L	S315T	D94G	SIT1
94A	HREZEthLfx	S531L	S315T	D94A	SIT1
WT	HREZEth	S531L	S315T	WT	SIT1

Note: the strain code was assigned based on the mutation in the *gyrA* gene (codon and amino acid substitution); WT — MTB strain with wild type *gyrA*; H — isoniazid; R — rifampicin; E — ethambutol; Z — pyrazinamide; Eth — ethionamide; Lfx — levofloxacin; SIT (Spoligotype International Type) — international code of the spoligotype as per the SITVIT2 database (http://www.pasteur-guadeloupe.fr:8081/SITVIT2/).

Table 2. Competitive fitness (W) of MTB strains with different genetic determinants of resistance to pharmaceutical chemicals, determined on the 21st day of the experiment

Co-cultivated strains	Optimal conditions		Multistress	
	W	interpretation	W	interpretation
WT + 90V	1.34	WT > 90V	2.07	WT > 90V
WT + 94A	1.32	WT > 94A	1.42	WT > 94A
WT + 94G	1.13	WT > 94G	1.58	WT > 94G
WT + 94Y	0.87	WT < 94Y	1.28	WT > 94Y
94Y + 90V	1.29	94Y > 90V	0.96	94Y < 90V
94Y + 94A	1.16	94Y > 94A	0.86	94Y < 94A
94Y + 94G	1.3	94Y > 94G	1.05	94Y > 94G
94G + 90V	0.93	94G < 90V	0.93	94G < 90V
94G + 94A	0.99	94G = 94A	0.65	94G < 94A
94A + 90V	0.92	94A < 90V	1.01	94A = 90Va
Strains rating by competitive fitness, in ascending order				
Optimal conditions	94A, 94G → 90V → WT → 94Y			
Multistress	94G → 94Y → 90V, 94A → WT			

Note: signs < and > indicate which strain has less/more fitness when co-cultivated, and sign = shows that the level of competitive fitness of a pair of strains is similar

$$\mu = \frac{ln2}{g},$$

where g — generation time, defined as:

$$g = \frac{t_2 - t_1}{n},$$

where t_1 and t_2 — parameter estimation time during the exponential growth phase; n — number of generations, defined as:

$$n = \frac{log_{10}N_2 - log_{10}N_1}{log_{10}2},$$

where N_1 and N_2 — number of CFU at time points t_1 and t_2, respectively.

RESULTS

The level of competitive fitness was determined for 10 pairs of MTB strains with different determinants of resistance to fluoroquinolones (Table 2). It was shown that under competition for nutrients during growth under optimal conditions, MTB strains with wild-type *gyrA* accumulated biomass more intensively compared to strains 90V, 94A and 94G. Strain 94Y, when cultured under optimal conditions, had the highest competitive fitness of all strains examined, including strain WT. MTB strains 94A and 94G had the lowest competitive fitness under optimal culture conditions.

Under multistress conditions on depleted Middlebrook 7H9 medium in the presence of active oxygen and nitrogen, the ability of the studied MTB strains to compete for nutrients differed from optimal culture conditions. Under multistress, the wild-type gyrA strain was more competitive compared to MTB strains with mutations in *gyrA*. The competitive fitness of strain 94Y decreased dramatically under multistress conditions, while in contrast, strain 94A improved compared to optimal culturing conditions. The competitive fitness of strain 94G under multistress conditions, as well as under optimal conditions, was the lowest among all strains studied.

The specific growth rate of MTB culture with different genetic determinants of resistance to fluoroquinolones also depended on the culture conditions (Table 3). When individually cultured under optimal conditions, the wild-type *gyrA* strain and the 94Y / 90V mutants had similar specific growth rates. The specific growth rate of the 94G and 94A mutants was lower.

When paired culturing was performed under optimal conditions, the specific growth rate of MTB strains was generally the same as that of individual culturing. A lower value of specific growth rate in paired culturing, compared to individual culturing, was observed only for strain WT when co-cultured with strain 94A and for strain 94G when co-cultured with strain WT and with strain 94A.

Under multistress conditions of individual culturing, the specific growth rate of MTB strains WT and 90V was at the same level as under optimal conditions, while that of strain 94A increased. The specific growth rate of strains 94G and 94Y was lower under multistress conditions when individually cultured than under optimal conditions.

When strains were co-cultured under multistress conditions, the specific growth rate of strains WT, 90V, 94A, and 94Y did not differ significantly from that of strains cultured under optimal conditions, or, in some combinations, was higher. The specific growth rate of strain 94G when cultured with other strains either did not change compared to the optimal conditions, remaining at the same low level, or decreased even more compared to the optimal conditions.

The specific growth rate of strains when cultured individually and when cultured under multistress conditions tended to differ. Strain 94G when co-cultured with strains WT and 94A and strain 94A when co-cultured with strain WT had a specific rate more than 10% lower than that of individual cultivation. But more often the specific rate was higher when strains were co-cultured under multistress conditions than when they were cultured individually (strain WT co-cultured with 94A; strain 90V co-cultured with WT, 94G and 94A, strain 94A co-cultured with 94Y and 90V; strain 94G co-cultured with 90V and 94Y, strain 94Y co-cultured with 90V and WT).

It was also found that MTB strains with mutations in *gyrA* differed in their ability to replicate when co-cultured, and this parameter for most strains varied depending on the culture conditions.

Thus, under optimal conditions, MTB strain 94Y multiplied more intensively than strains 94A and 94G, while under multistress conditions, the best growth rates in pairs were demonstrated by strain 94A, and the fission rate of strains 94Y and 94G in paired cultivation was identical. Similarly, cultivation conditions affected the level of competitive fitness in pairs 94G + 90V, 94G + 94A and 94A + 90V. The only exception was the pair of strains 94Y + 90V, in which both under optimal

Table 3. Specific growth rate (μ) of MTB strains with different genetic determinants of resistance to pharmaceutical chemicals

Strain	Co-cultivation with	μ (hour-1)	
		optimal conditions	multistress
WT	–	0.021	0.024
	94Y	0.021	0.024
	94G	0.021	0.024
	94A	0.018*	0.029**
	90 V	0.021	0.022
94Y	–	0.024	0.015
	WT	0.023	0.018**
	94G	0.024	0.017
	94A	0.024	0.015
	90V	0.024	0.019**
94G	–	0.016	0.012
	WT	0.012*	0.008*
	94Y	0.016	0.014**
	94A	0.012*	0.007*
	90V	0.016	0.014**
94A	–	0.017	0.022
	WT	0.016	0.015*
	94Y	0.015	0.026**
	94G	0.017	0.02
	90V	0.015	0.025**
90V	–	0.018	0.016
	WT	0.016	0.019**
	94Y	0.019	0.017
	94G	0.018	0.02**
	94A	0.02	0.02**

Note: * — μ is more than 10% lower than in individual cultivation; ** — μ is more than 10% higher than in individual cultivation

and multistress conditions the strain 94Y had a higher culture growth rate.

DISCUSSION

The study examined the culture growth characteristics of five MTB strains differing in genetic determinants of resistance to fluoroquinolones, in individual and paired cultivation. The *gyrA*-mutant MTB variants studied are represented in the population as follows: strains with a mutation in *gyrA* D94G are the most common (40%), followed by strains with mutation A90V (20%), then strains with mutation D94A (15%) and D94Y (5%). [20]. There are other *gyrA*-mutant variants of MTB, but they are very rarely exuded by patients, which prevented us from including these strains in the study.

Heteroresistance of the MTB population in the host organism can be considered as a special case of intraspecies competition, as there is competition for a limited resource between representatives of the same species with insignificant differences (in our case, the different structure of the alpha subunits of DNA gyrase encoded by the *gyrA* gene). The result of such competition may be the disappearance of the least adapted MTB pool and the proliferation of the most adapted pool in the population. Since the competitiveness of mutant MTB variants was to be studied, one of the parameters we evaluated was the competitive fitness of MTB strains when co-cultured. MTB competitive fitness is traditionally determined by culturing a resistant strain together with a susceptible strain,

followed by reinoculation of the strain mixture on medium with an antituberculosis drug, thereby determining the number of CFU of the resistant strain in the mixture. [23]. However, this approach does not allow us to compare the competitive fitness of two resistant strains, so for the first time we used a multiplex PCR method to determine competitive fitness, which allowed us to quantify the number of CFU of each mutant variant in a sample. Since the study was performed in dynamics rather than by endpoint, the approach we used also allowed us to estimate the specific growth rate of each mutant when co-cultured.

In addition, we studied the growth of co-cultured strains not only under optimal conditions but also in a multistress model, being able to create *in vitro* — to some extent — the conditions that the pathogen encounters in the macroorganism: lack of nutrients and presence of active nitrogen and oxygen as bactericidal agents produced by macrophages [24].

We have demonstrated that the competitive fitness of MTB strains with mutations in *gyrA* is lower than that of strains with wild-type *gyrA*. The only exception when cultured under optimal conditions was strain 94Y with a rare mutation, however under conditions as close as possible to in vivo conditions in the multistress model, its fission rate decreased significantly.

The low fission rate of *gyrA*-mutant MTB strains was generally predictable, as the gene encodes the alpha-subunit of DNA gyrase [25]. Changes in the structure of this enzyme due to mutations in *gyrA* can inhibit DNA replication and transcription in the MTB cell and lead to a decrease in the growth rate of the pathogen.

The frequency of *gyrA*-mutant MTB variants occurrence in a population associates with the level of competitive fitness in a multistress culturing model as follows: the strain with the frequent mutation *gyrA*_A90V had high competitive fitness values, while the strain with the rare mutation *gyrA*_D94Y had low values. The fitness of the strain with the *gyrA*_D94A mutation in the multistress model was comparable to that of strain 90V, but was less frequent in the population, possibly because the *gyrA*_D94A mutation is not strictly associated with resistance to fluoroquinolones and, therefore, the pool of MTBs carrying this mutation could be eliminated during chemotherapy [20, 26, 27].

Surprisingly, the strain with the most common *gyrA*_D94G mutation had the lowest competitive fitness and lowest specific growth rate of all strains examined. However, a reduced rate of fission *in vivo* is not always a disadvantage, especially under selection pressure due to chemotherapy. Most TB drugs are effective against MTBs demonstrating active fission, while pools of slow fission pose a major challenge to the efficacy of chemotherapy [28, 29].

Consequently, it can be assumed that the high prevalence of fluoroquinolone-resistant MTBs with the *gyrA*_D94G mutation is related to the low fission rate of such strains, which allows them to avoid exposure to anti-TB drugs.

In summarising the results of this study, it appears that the evolutionary success of the most common *gyrA*-mutant variant of MTB lies in its tolerance to anti-TB drugs due to slow growth. MTBs with the *gyrA*_A90V mutation, which are twice as rare, have good growth properties and have been favoured by this feature. Strains with the *gyrA*_D94A mutation are even rarer because, having a high level of competitive fitness, they are not always resistant to fluoroquinolones. MTBs with the *gyrA*_D94Y mutation have the lowest fitness under multistress conditions and are rarely found in the population.

In conclusion, it should be noted that the article presents data from a pilot study on a limited group of strains; therefore, the findings can be regarded as preliminary and should not be generalised at this stage to the entire population of MTBs resistant to fluoroquinolones. A full-scale study on a large sample of strains is planned to confirm the findings.

CONCLUSIONS

This study found that MTB strains with mutations in *gyrA* differ in their ability to adapt to nutrient competition *in vitro*. Strain cultivation conditions influence the level of competitive fitness of MTB strains with different genetic determinants of resistance to fluoroquinolones. Most MTB strains demonstrate a direct association between the level of competitive fitness under multistress conditions and the frequency of occurrence in the population. Mutations in *gyrA* reduce the rate of MTB growth; maybe it helps the pathogen survive chemotherapy.

References

1. Eldholm V, Balloux F. Antimicrobial Resistance in *Mycobacterium tuberculosis:* The Odd One Out. Trends Microbiol. 2016; 24 (8): 637–48.
2. O'Neill MB, Mortimer TD, Pepperell CS. Diversity of *Mycobacterium tuberculosis* across Evolutionary Scales. PLoS Pathog. 2015; 11 (11): e1005257.
3. Vargas R, Freschi L, Marin M, Epperson LE, Smith M, Oussenko I, et al. In-host population dynamics of *Mycobacterium tuberculosis* complex during active disease. Elife. 2021; 10: e61805.
4. McIvor A, Koornhof H, Kana BD. Relapse, re-infection and mixed infections in tuberculosis disease. Pathog Dis. 2017; 75 (3).
5. Ye M, Yuan W, Molaeipour L, Azizian K, Ahmadi A, Kouhsari E. Antibiotic heteroresistance in *Mycobacterium tuberculosis* isolates: a systematic review and meta-analysis. Ann Clin Microbiol Antimicrob. 2021; 20 (1): 73.
6. Zetola NM, Shin SS, Tumedi KA, Moeti K, Ncube R, Nicol M et al. Mixed *Mycobacterium tuberculosis* complex infections and false-negative results for rifampin resistance by GeneXpert MTB/RIF are associated with poor clinical outcomes. J Clin Microbiol. 2014; 52 (7): 2422–9.
7. Andersson DI, Nicoloff H, Hjort K. Mechanisms and clinical relevance of bacterial heteroresistance. Nat Rev Microbiol. 2019; 17 (8): 479–96.
8. Ford C, Yusim K, Ioerger T, Feng S, Chase M, Greene M, et al. *Mycobacterium tuberculosis*–heterogeneity revealed through whole genome sequencing. Tuberculosis (Edinb). 2012; 92 (3): 194–201.
9. Chen J, Huang F, Yin X, Gu D. Assessments of Different Methods for Testing Heteroresistance to Rifampicin in Tubercle Bacillus. J Nanosci Nanotechnol. 2018; 18 (12): 8414–8.
10. Chen L, Zhang J, Zhang H. Heteroresistance of *Mycobacterium tuberculosis* Strains May Be Associated More Strongly With Poor Treatment Outcomes Than Within-Host Heterogeneity of M. tuberculosis Infection. J Infect Dis. 2016; 214 (8): 1286–7.
11. Rigouts L, Miotto P, Schats M, Lempens P, Cabibbe AM, Galbiati S, et al. Fluoroquinolone heteroresistance in *Mycobacterium tuberculosis:* detection by genotypic and phenotypic assays in experimentally mixed populations. Sci Rep. 2019; 9 (1): 11760.
12. Global tuberculosis report 2023. Geneva: World Health Organization, 2023; 75 p.
13. Huo F, Ma Y, Li S, Xue Y, Shang Y, Dong L, et al. Specific gyrA gene mutations correlate with high prevalence of discordant levofloxacin resistance in Mycobacterium tuberculosis isolates from Beijing, China. J Mol Diagn. 2020; 22 (9): 1199–204.
14. WHO consolidated guidelines on drug-resistant tuberculosis treatment. Geneva: World Health Organization, 2019; 104 p.
15. Nahid P, Mase SR, Migliori GB, Sotgiu G, Bothamley GH, Brozek JL, et al. Treatment of Drug-Resistant Tuberculosis. An Official ATS/CDC/ERS/IDSA Clinical Practice Guideline. Am J Respir Crit Care Med. 2019; 200 (10): e93–e142.
16. Jouet A, Gaudin C, Badalato N, Allix-Béguec C, Duthoy S, Ferré A, et al. Deep amplicon sequencing for culture-free prediction of susceptibility or resistance to 13 anti-tuberculous drugs. Eur Respir J. 2021; 57 (3): 2002338.
17. Zhang X, Zhao B, Liu L, Zhu Y, Zhao Y, Jin Q. Subpopulation analysis of heteroresistance to fluoroquinolone in *Mycobacterium tuberculosis* isolates from Beijing, China. J Clin Microbiol. 2012; 50 (4): 1471–4.
18. Campbell PJ, Morlock GP, Sikes RD, Dalton TL, Metchock B, Starks AM, et al. Molecular detection of mutations associated with first- and second-line drug resistance compared with conventional drug susceptibility testing of *Mycobacterium tuberculosis*. Antimicrob Agents Chemother. 2011; 55 (5): 2032–41.
19. Baffoe-Bonnie A, Houpt ER, Turner L, Dodge D, Heysell SK. Drug-Susceptible and Multidrug-Resistant *Mycobacterium tuberculosis* in a Single Patient. Emerg Infect Dis. 2019; 25 (11): 2120–1.
20. Andreevskaya SN, Smirnova TG, Chernousova LN, Larionova EE, Kiseleva EA, Ergeshov A. The nature of genotypic resistance to fluoroquinolones in Mycobacterium tuberculosis circulating in Russian Federation. Bulletin of RSMU. 2022; (5): 15–22.
21. Kodio O, Georges Togo AC, Sadio Sarro YD, Fane B, Diallo F, Somboro A. et al. Competitive fitness of *Mycobacterium tuberculosis in vitro*. Int J Mycobacteriol. 2019; 8 (3): 287–91.
22. Aleshina ES, Drozdova EA, Romanenko NA. Kul'tivirovanie mikroorganizmov kak osnova biotehnologicheskogo processa: uchebnoe posobie. Orenburg: OOO IPK «Universitet», 2017; 191

s. Russian.

23. Gagneux S, Long CD, Small PM, Van T, Schoolnik GK, Bohannan BJ. The competitive cost of antibiotic resistance in *Mycobacterium tuberculosis*. Science. 2006; 312 (5782): 1944–6.

24. Peddireddy V, Doddam SN, Ahmed N. Mycobacterial Dormancy Systems and Host Responses in Tuberculosis. Front Immunol. 2017; 8: 84.

25. An Q, Lin R, Yang Q, Wang C, Wang D. Evaluation of genetic mutations associated with phenotypic resistance to fluoroquinolones, bedaquiline, and linezolid in clinical *Mycobacterium tuberculosis*: A systematic review and meta-analysis. J Glob Antimicrob Resist. 2023; 34: 214–26.

26. Chan RC, Hui M, Chan EW, Au TK, Chin ML, Yip CK, et al. Genetic and phenotypic characterization of drug-resistant *Mycobacterium tuberculosis* isolates in Hong Kong. J Antimicrob Chemother 2007; 59 (5): 866–73.

27. Casali N, Nikolayevskyy V, Balabanova Y, Harris SR, Ignatyeva O, Kontsevaya I, et al. Evolution and transmission of drug-resistant tuberculosis in a Russian population. Nat Genet. 2014; 46 (3): 279–86.

28. Gomez JE, McKinney JD. *M. tuberculosis* persistence, latency, and drug tolerance. Tuberculosis (Edinb). 2004; 84 (1–2): 29–44.

29. Mitchison DA, Coates AR. Predictive in vitro models of the sterilizing activity of anti-tuberculosis drugs. Curr Pharm Des. 2004; 10 (26): 3285–95.

Литература

1. Eldholm V, Balloux F. Antimicrobial Resistance in *Mycobacterium tuberculosis:* The Odd One Out. Trends Microbiol. 2016; 24 (8): 637–48.

2. O'Neill MB, Mortimer TD, Pepperell CS. Diversity of *Mycobacterium tuberculosis* across Evolutionary Scales. PLoS Pathog. 2015; 11 (11): e1005257.

3. Vargas R, Freschi L, Marin M, Epperson LE, Smith M, Oussenko I, et al. In-host population dynamics of *Mycobacterium tuberculosis* complex during active disease. Elife. 2021; 10: e61805.

4. McIvor A, Koornhof H, Kana BD. Relapse, re-infection and mixed infections in tuberculosis disease. Pathog Dis. 2017; 75 (3).

5. Ye M, Yuan W, Molaeipour L, Azizian K, Ahmadi A, Kouhsari E. Antibiotic heteroresistance in *Mycobacterium tuberculosis* isolates: a systematic review and meta-analysis. Ann Clin Microbiol Antimicrob. 2021; 20 (1): 73.

6. Zetola NM, Shin SS, Tumedi KA, Moeti K, Ncube R, Nicol M et al. Mixed *Mycobacterium tuberculosis* complex infections and false-negative results for rifampin resistance by GeneXpert MTB/RIF are associated with poor clinical outcomes. J Clin Microbiol. 2014; 52 (7): 2422–9.

7. Andersson DI, Nicoloff H, Hjort K. Mechanisms and clinical relevance of bacterial heteroresistance. Nat Rev Microbiol. 2019; 17 (8): 479–96.

8. Ford C, Yusim K, Ioerger T, Feng S, Chase M, Greene M, et al. *Mycobacterium tuberculosis*–heterogeneity revealed through whole genome sequencing. Tuberculosis (Edinb). 2012; 92 (3): 194–201.

9. Chen J, Huang F, Yin X, Gu D. Assessments of Different Methods for Testing Heteroresistance to Rifampicin in Tubercle Bacillus. J Nanosci Nanotechnol. 2018; 18 (12): 8414–8.

10. Chen L, Zhang J, Zhang H. Heteroresistance of *Mycobacterium tuberculosis* Strains May Be Associated More Strongly With Poor Treatment Outcomes Than Within-Host Heterogeneity of M. tuberculosis Infection. J Infect Dis. 2016; 214 (8): 1286–7.

11. Rigouts L, Miotto P, Schats M, Lempens P, Cabibbe AM, Galbiati S, et al. Fluoroquinolone heteroresistance in *Mycobacterium tuberculosis:* detection by genotypic and phenotypic assays in experimentally mixed populations. Sci Rep. 2019; 9 (1): 11760.

12. Global tuberculosis report 2023. Geneva: World Health Organization, 2023; 75 p.

13. Huo F, Ma Y, Li S, Xue Y, Shang Y, Dong L, et al. Specific gyrA gene mutations correlate with high prevalence of discordant levofloxacin resistance in Mycobacterium tuberculosis isolates from Beijing, China. J Mol Diagn. 2020; 22 (9): 1199–204.

14. WHO consolidated guidelines on drug-resistant tuberculosis treatment. Geneva: World Health Organization, 2019; 104 p.

15. Nahid P, Mase SR, Migliori GB, Sotgiu G, Bothamley GH, Brozek JL, et al. Treatment of Drug-Resistant Tuberculosis. An Official ATS/CDC/ERS/IDSA Clinical Practice Guideline. Am J Respir Crit Care Med. 2019; 200 (10): e93–e142.

16. Jouet A, Gaudin C, Badalato N, Allix-Béguec C, Duthoy S, Ferré A,

et al. Deep amplicon sequencing for culture-free prediction of susceptibility or resistance to 13 anti-tuberculous drugs. Eur Respir J. 2021; 57 (3): 2002338.

17. Zhang X, Zhao B, Liu L, Zhu Y, Zhao Y, Jin Q. Subpopulation analysis of heteroresistance to fluoroquinolone in *Mycobacterium tuberculosis* isolates from Beijing, China. J Clin Microbiol. 2012; 50 (4): 1471–4.

18. Campbell PJ, Morlock GP, Sikes RD, Dalton TL, Metchock B, Starks AM, et al. Molecular detection of mutations associated with first- and second-line drug resistance compared with conventional drug susceptibility testing of *Mycobacterium tuberculosis*. Antimicrob Agents Chemother. 2011; 55 (5): 2032–41.

19. Baffoe-Bonnie A, Houpt ER, Turner L, Dodge D, Heysell SK. Drug-Susceptible and Multidrug-Resistant *Mycobacterium tuberculosis* in a Single Patient. Emerg Infect Dis. 2019; 25 (11): 2120–1.

20. Андреевская С. Н., Смирнова Т. Г., Черноусова Л. Н., Ларионова Е. Е., Киселева Е. А., Эргешов А. Особенности генотипической резистентности к фторхинолонам у *Mycobacterium tuberculosis*, циркулирующих в Российской Федерации. Вестник РГМУ. 2022; (5): 23–31.

21. Kodio O, Georges Togo AC, Sadio Sarro YD, Fane B, Diallo F, Somboro A. et al. Competitive fitness of *Mycobacterium tuberculosis in vitro*. Int J Mycobacteriol. 2019; 8 (3): 287–91.

22. Алешина Е. С., Дроздова Е. А., Романенко Н. А. Культивирование микроорганизмов как основа биотехнологического процесса: учебное пособие. Оренбург: ООО ИПК «Университет», 2017; 191 с.

23. Gagneux S, Long CD, Small PM, Van T, Schoolnik GK, Bohannan BJ. The competitive cost of antibiotic resistance in *Mycobacterium tuberculosis*. Science. 2006; 312 (5782): 1944–6.

24. Peddireddy V, Doddam SN, Ahmed N. Mycobacterial Dormancy Systems and Host Responses in Tuberculosis. Front Immunol. 2017; 8: 84.

25. An Q, Lin R, Yang Q, Wang C, Wang D. Evaluation of genetic mutations associated with phenotypic resistance to fluoroquinolones, bedaquiline, and linezolid in clinical *Mycobacterium tuberculosis*: A systematic review and meta-analysis. J Glob Antimicrob Resist. 2023; 34: 214–26.

26. Chan RC, Hui M, Chan EW, Au TK, Chin ML, Yip CK, et al. Genetic and phenotypic characterization of drug-resistant *Mycobacterium tuberculosis* isolates in Hong Kong. J Antimicrob Chemother 2007; 59 (5): 866–73.

27. Casali N, Nikolayevskyy V, Balabanova Y, Harris SR, Ignatyeva O, Kontsevaya I, et al. Evolution and transmission of drug-resistant tuberculosis in a Russian population. Nat Genet. 2014; 46 (3): 279–86.

28. Gomez JE, McKinney JD. *M. tuberculosis* persistence, latency, and drug tolerance. Tuberculosis (Edinb). 2004; 84 (1–2): 29–44.

29. Mitchison DA, Coates AR. Predictive in vitro models of the sterilizing activity of anti-tuberculosis drugs. Curr Pharm Des. 2004; 10 (26): 3285–95.

EFFECTS OF LYTIC BACTERIOPHAGES OF THE FAMILIES *HERELLEVIRIDAE* AND *ROUNTREEVIRIDAE* ON THE *STAPHYLOCOCCUS AUREUS* BIOFILMS

Abdraimova NK ✉, Shitikov EA, Malakhova MV, Gorodnichev RB, Kornienko MA

Lopukhin Federal Research and Clinical Center of Physical-Chemical Medicine of the Federal Medical Biological Agency, Moscow, Russia

Staphylococcus aureus causes a broad range of infections and is often characterized by multidrug resistance (MDR). Treatment of staphylococcal infections is further complicated by the ability of bacterium to form biofilms protecting it against antimicrobial agents and the immune system. The use of bacteriophages is one of the promising strategies for combating the bacteria showing MDR and biofilm formation activity. The study aimed to assess the effects of the lytic phages vB_SauM-515A1 (genus *Kayvirus*, family *Herelleviridae*) and vB_SauP-436A (genus *Rosenblumvirus*, family *Rountreeviridae*) on biofilms of the *S. aureus* clinical strains. The study involved 20 strains of eight sequence types, among which 45% (9/20) belonged to MRSA, and 35% (7/20) showed MDR. All the strains demonstrated the ability to form biofilms, and 65% (13/20) were strong biofilm producers. Genes of the *ica*ADBC operon responsible for synthesis of polysaccharide intercellular adhesin were found in genomes of all samples. The exposure of planktonic bacterial cells to bacteriophages showed that 70% (14/20) of strains were sensitive to phage vB_SauM-515A1 and 50% (10/20) were sensitive to phage vB_SauP-436A. Furthermore, the 24-h treatment of biofilms of sensitive strains with phage vB_SauM-515A1 led to the biofilm biomass increase in 64.3% (9/14) of cases, while phage vB_SauP-436A, on the contrary, significantly reduced the quantity of biofilm in 40% (4/10) of strains. The results obtained highlight the ambiguity of interaction between bacteriophages and S. aureus biofilms and suggest the need for further research aimed at optimizing phage therapy targeting the biofilm-forming strains.

Keywords: *Staphylococcus aureus*, bacteriophage, phage therapy, biofilm, *Herelleviridae*, *Rountreeviridae*

ВОЗДЕЙСТВИЕ ЛИТИЧЕСКИХ БАКТЕРИОФАГОВ СЕМЕЙСТВ *HERELLEVIRIDAE* И *ROUNTREEVIRIDAE* НА БИОПЛЕНКИ *STAPHYLOCOCCUS AUREUS*

Н. К. Абдраймова✉, Е. А. Шитиков, М. В. Малахова, Р. Б. Городничев, М. А. Корниенко

Федеральный научно-клинический центр физико-химической медицины имени Ю. М. Лопухина Федерального медико-биологического агентства, Москва, Россия

Staphylococcus aureus вызывает широкий спектр инфекций и часто характеризуется множественной лекарственной устойчивостью (МЛУ). Лечение стафилококковых инфекций дополнительно осложнено способностью бактерии формировать биопленку, которая защищает ее от антимикробных агентов и иммунной системы. Одной из перспективных стратегий борьбы с бактериями, обладающими МЛУ и биопленкообразующей активностью, является применение бактериофагов. Целью исследования было оценить влияние литических фагов vB_SauM-515A1 (род *Kayvirus*, семейство *Herelleviridae*) и vB_SauP-436A (род *Rosenblumvirus*, семейство *Rountreeviridae*) на биопленки клинических штаммов *S. aureus*. Исследование включало 20 штаммов восьми сиквенс-типов, из которых 45% (9/20) относились к MRSA, а 35% (7/20) обладали МЛУ. Все штаммы продемонстрировали способность к биопленкообразованию, причем 65% (13/20) являлись сильными продуцентами биопленки. В геномах всех образцов обнаружены гены icaADBC-оперона, ответственного за синтез полисахаридного межклеточного адгезина. Воздействие бактериофагов на планктонные клетки бактерий показало, что 70% (14/20) штаммов были чувствительны к фагу vB_SauM-515A1, а 50% (10/20) — к фагу vB_SauP-436A. При этом 24-часовая обработка биопленок чувствительных штаммов фагом vB_SauM-515A1 в 64,3% (9/14) случаев приводила к увеличению биомассы биопленки, тогда как фаг vB_SauP-436A, напротив, достоверно снижал количество биопленки у 40% (4/10) штаммов. Полученные результаты подчеркивают неоднозначность взаимодействия бактериофагов с биопленками *S. aureus* и указывают на необходимость дальнейших исследований для оптимизации фаговой терапии в отношении биопленкообразующих штаммов.

Ключевые слова: *Staphylococcus aureus*, бактериофаг, фаговая терапия, биопленки, Herelleviridae, *Rountreeviridae*, *Kayvirus, Rosenblumvirus*

Staphylococcus aureus is one of the leading bacterial pathogens responsible for a broad range of infections: from superficial inflammation of the skin to severe life-threatening conditions, such as pneumonia, sepsis, and endocarditis [1]. The microorganism attracts special attention due to its resistance to a broad spectrum of antibiotics, and the most important are methicillin-resistant *S. aureus* strains (MRSA).

Treatment of staphylococcal infections is hampered not only by antibiotic resistance, but also by plenty of virulence factors, among which is the ability of staphylococci to form biofilms. Like biofilms of other bacteria, the *S. aureus* biofilm consists of two main components: water (about 97%) and organic matter represented by extracellular polymers and colonies of microorganisms. Extracellular polymers constitute 50–90% of all organic mass of the biofilm and include a combination of various compounds, such as extracellular DNA (eDNA), proteins, and polysaccharides. The remainder of biofilm is represented by bacterial cells [2, 3].

The biofilm ensures firm attachment of bacteria to various surfaces, including tissues of the body and medical equipment [2]. Furthermore, biofilms considerably increase resistance of bacteria to the immune system factors and antimicrobial drugs: the minimum inhibitory concentrations (MICs) of antibiotics necessary for disruption of bacteria in biofilms can 1000-fold exceed the concentrations that are enough to destroy planktonic cells [3, 4].

Bacteriophages increasingly considered as a promising remedy to treat bacterial infections caused by antibiotic-resistant strains. Only virulent bacteriophages that realize the lytic cycle only are used in medical practice. Such phages capable of infecting and destroying the *S. aureus* cells include members of the families *Herelleviridae* and *Rountreeviridae*. These demonstrate high efficacy in both *in vitro* experiments and *in vivo* models, are successfully used for therapy, which ensures reduction of bacterial load and improvement of clinical outcomes [5].

In this context, of special interest are the studies focused on assessing the effects of phages on biofilms. It has been shown that some S. aureus phages can effectively reduce the biofilm biomass [6, 7]. Nevertheless, a number of studies show that biofilm generation can be stimulated under exposure to phages, which can be associated with the features of interplay between phages and bacterial cells [8, 9]. Such effects are likely to depend on a number of factors: bacterial strain itself, bacteriophage used and its concentration, physiological state of cells, as well as morphological and structural characteristics of the biofilm.

The study aimed to assess the effects of the lytic bacteriophages vB_SauM-515A1 (family *Herelleviridae*) and vB_SauP-436A (family *Rountreeviridae*) on biofilms formed by the *S. aureus* clinical isolates.

METHODS

Bacterial strains and bacteriophages

In this study, we used 20 *S. aureus* strains, most different based on the origin and isolation locus, from the collection of the Lopukhin Federal Research and Clinical Center of Physical-Chemical Medicine of the Federal Medical Biological Agency. The strains were collected in 2015–2020 from hospitals in various regions of Russia.

Bacterial culture was grown in the liquid LB (lysogeny broth) medium (Oxoid; UK) or Miller LB agar (Oxoid) at 37 °C for 18 h. Cells grown in the liquid medium were used to produce overnight cultures, which were later used for inoculation in both experiments on determining antibiotic resistance and all the tests related to assessment of biofilm formation and the effects of antibacterial agents on biofilm formation. Bacteria were cultured in LB agar in order to maintain the bacterial culture, as well as to enumerate cells in the experiments on assessing the effects of bacteriophages on the biofilms formed.

Sensitivity to oxacillin (beta-lactam antibiotic), vancomycin (glycopeptide), gentamicin (aminoglycoside), tetracycline (tetracycline antibiotic), levofloxacin (fluoroquinolone), and erythromycin (macrolide) (all drugs manufactured by Sigma-Aldrich, USA) was determined by the serial dilution method in accordance with the EUCAST guidelines (v.14.0) [10]. The strains showing multidrug resistance (MDR) were determined as resistant to three or more antibiotics of different classes.

The study involved lytic bacteriophages vB_SauM-515A1 (genus *Kayvirus,* family *Herelleviridae*) and vB_SauP-436A (genus *Rosenblumvirus,* family *Rountreeviridae*) used in the form of sterile filtrates of phage lysates in the LB medium. Bacteriophages were earlier isolated from the commercially available combination phage product "Staphylococcal Bacteriophage" of the series P332 (Microgen; Russia) in the *S. aureus* SA515 (ST8 (ST, sequence type)) and SA436 (ST1) strains and characterized in detail [11]. Phages were grown in appropriate host strains.

Molecular genetic characteristics of bacterial strains

DNA was extracted using the DNA-Express kit (Lytech; Russia) following the manufacturer's instructions. DNA samples were stored at –20°C.

Strain typing was performed by multilocus sequence typing (MLST) in accordance with the standard scheme [12]. The *icaA, icaB, icaC,* and *icaD* genes responsible for biofilm formation were detected by polymerase chain reaction (PCR) using the previously reported primers [13]. The PCR reaction mixture (25 µL) contained 66 mM Tris-HCl (pH = 9), 16.6 mM $(NH_4)_2SO_4$, 2.5 mM $MgCl_2$, 250 µM of each dNTP, 1 unit of Taq DNA polymerase (Lytech; Russia) and 10 pmol of each appropriate primer. Amplification was performed using the DNA Engine Tetrad 2 kit (MJ Research; USA) in accordance with the previously proposed regimes [13]. The amplification products were assessed by horizontal 2% agarose gel electrophoresis with ethidium bromide visualization.

Assessment of biofilm formation

Assessment was performed by the previously reported method [14] with certain modifications. For that the suspension of bacterial cells being in their exponential growth phase (optical density (OD) at 620 nm was 0.12) was inoculated into the wells of the uncoated 96-well flat bottom ventilated plate (Thermo Scientific; USA) containing TSBg (tryptic soy broth supplemented with 1% glucose) (Himedia; India) to the final concentration of 10^4 cells per well and incubated at 37 °C for 24 h without shaking. The final volume in each well was 200 µL. The sterile medium was used as a negative control. After incubation the wells were carefully triple washed with the sterile phosphate buffer (PBS, pH = 7.4) to remove planktonic cells, then stained with the 0.1% crystal violet (CV) aqueous-alcohol solution (Sigma-Aldrich; USA) for 30 min at room temperature. After incubation the dye was triple washed with the sterile PBS. To perform further analysis, the dye bound in each well was eluted by adding 200 µL of 96% ethanol, and optical density of the solution was measured using the Microplate Reader

Table. Biofilm formation patterns of the *S. aureus* strains

Strain	Origin	Locus	ST	Antibiotic resistance						Biofilm production type	EOP (vB_SauM-515A1),%	EOP (vB_SauP-436A),%
				OXA	VAN	GEN	TET	LFX	ERY			
SA515	Novosibirsk	Wound discharge	8	R	I	R	R	S	S	strong	100	–
SA64	Saint Petersburg	Blood	8	R	S	S	R	R	S	strong	267	400
SA412	Lipetsk	Skin and soft tissues	8	R	S	R	I	S	R	strong	–	150
SA2242	Novosibirsk	Bones and joints	239	R	S	R	S	S	S	strong	300	–
SA191	Moscow	Cerebrospinal fluid	239	R	S	R	R	R	R	strong	–	–
SA364	Saint Petersburg	Skin and soft tissues	764	R	S	R	R	n/d	R	strong	–	–
SA436	Nizhny Novgorod	Nasopharyngeal discharge	1	R	S	R	R	S	S	moderate	–	100
SA402	Lipetsk	Bones and joints	5	R	S	R	R	R	R	moderate	183	83
SA88	Krasnodar	Wound discharge	25	R	S	S	S	S	S	moderate	183	167
SA103	Krasnodar	Blood	1	S	S	S	S	S	S	strong	250	133
SA172	Moscow	Wound discharge	1	S	S	S	S	S	S	strong	–	200
SA2153	Smolensk	Sputum	5	S	S	S	S	S	R	strong	250	–
SA2464	Yakutsk	Skin and soft tissues	5	S	S	S	S	S	S	strong	190	–
SA54	Irkutsk	Conjunctival discharge	25	S	n/d	S	S	S	S	strong	500	90
SA2003	Voronezh	Skin and soft tissues	25	S	S	S	S	S	S	strong	245	–
SA837	Smolensk	Skin and soft tissues	8	S	S	S	S	S	S	strong	200	–
SA117	Vologda	Eyelid discharge	121	S	n/d	S	S	S	S	moderate	90	75
SA156	Smolensk	Conjunctival discharge	121	S	n/d	S	S	S	S	moderate	383	–
Sa226	Moscow	Eyelid discharge	121	S	n/d	n/d	n/d	n/d	n/d	moderate	150	200
SA606	Oryol	Skin and soft tissues	398	S	S	S	S	S	S	moderate	–	–

Note: «–» — the strain is resistant to the bacteriophage; S — the strain is sensitive to the antibiotic; R — the strain is resistant to the antibiotic; OXA — oxacillin; VAN — vancomycin; GEN — gentamicin; TET — tetracycline; LFX — levofloxacin; ERY — erythromycin.

Flex-A (Allsheng; China) at 570 nm. All the experiments were conducted in three biological replicates.

The ability of the bacterium to form biofilms was determined in accordance with the earlier proposed criteria: OD ≤ ODc — the strain does not produce biofilms; ODc < OD ≤ 2 × ODc — the strain is a weak biofilm producer; 2 × ODc < OD ≤ 4 × ODc — the strain is a moderate biofilm producer; 4 × ODc < OD — the strain is a strong biofilm producer, where ODc — is the average OD of the negative control + 3 × SD (standard deviation). The sterile medium was used as a negative control [15].

Sensitivity of planktonic forms of strains to bacteriophages

The strains' sensitivity to bacteriophages was determined when assessing the efficiency of plating (EOP), as previously reported [11]. EOP is a ratio of the bacteriophage titer in the test strain to the bacteriophage titer in the host strain (*S. aureus* SA515 for phage vB_SauM-515A1; *S. aureus* SA436 for phage vB_SauP-436A) expressed as a percentage. Bacteriophage titer in the test strain was determined by the Gracia titration method, as previously reported [16]. For that aliquots (5 µL) of the 10-fold serial dilutions of each bacteriophage product (stock of 2×10^9 plaque-forming units/mL or PFU/mL) were applied to the surface of the plates with the semi-solid LB agar (0.6% agar) containing 0.1 mL of the test strain overnight culture (10^6 CFU/mL) and incubated at 37 °C for 24 h. Concentration of phage particles in PFU/mL was estimated for each strain. The efficacy of plating was assessed in three replicates.

Assessment of the impact of bacteriophages on the biofilms formed

The experiments involved the 24-h biofilms produced and washed in accordance with the above method. After washing, phage lysate in TSBg was added to the well to the final

concentration of 10^8 PFU/mL, the volume in each well was 200 µL. Sterile PBS was added to the control samples instead of phage lysate. Incubation was carried out for 24 h at 37 °C. Then CV staining was performed as described above, with subsequent OD measurement at 570 nm. All the experiments were conducted in three biological replicates.

In preliminary experiments, we determined the number of cells in the biofilm by adding 200 µL of sterile PBS to the pre-washed biofilm and destroying the biofilm by active pipetting. Serial dilutions of the cell suspension were sown on the LB agar. Colonies were enumerated after the 24-h incubation at 37 °C.

Statistical analysis

Statistical analysis was performed using the GraphPad Prism v. 8.0.1 software (GraphPad Software Inc.; USA) based on the *t*-test data. During the analysis we compared optical density values obtained after the 24-h incubation of the biofilms treated and not treated with the bacteriophage. The differences were considered significant at $p < 0.05$. The Shapiro–Wilk test was used to confirm normal distribution of data, the data on the samples were considered to be almost normally distributed at $p > 0.05$.

Fisher's exact test was used to reveal significant correlations based on two nominal traits in small samples. The correlations were considered significant at $p < 0.05$.

RESULTS

Characteristics of strains and their ability to form biofilms

According to the MLST results, strains of the collection belonged to eight sequence types, among which the most abundant was ST8 (4/20, 20%) (Table). ST1, ST121, ST5, and ST25 accounted for three strains each (15%). As for
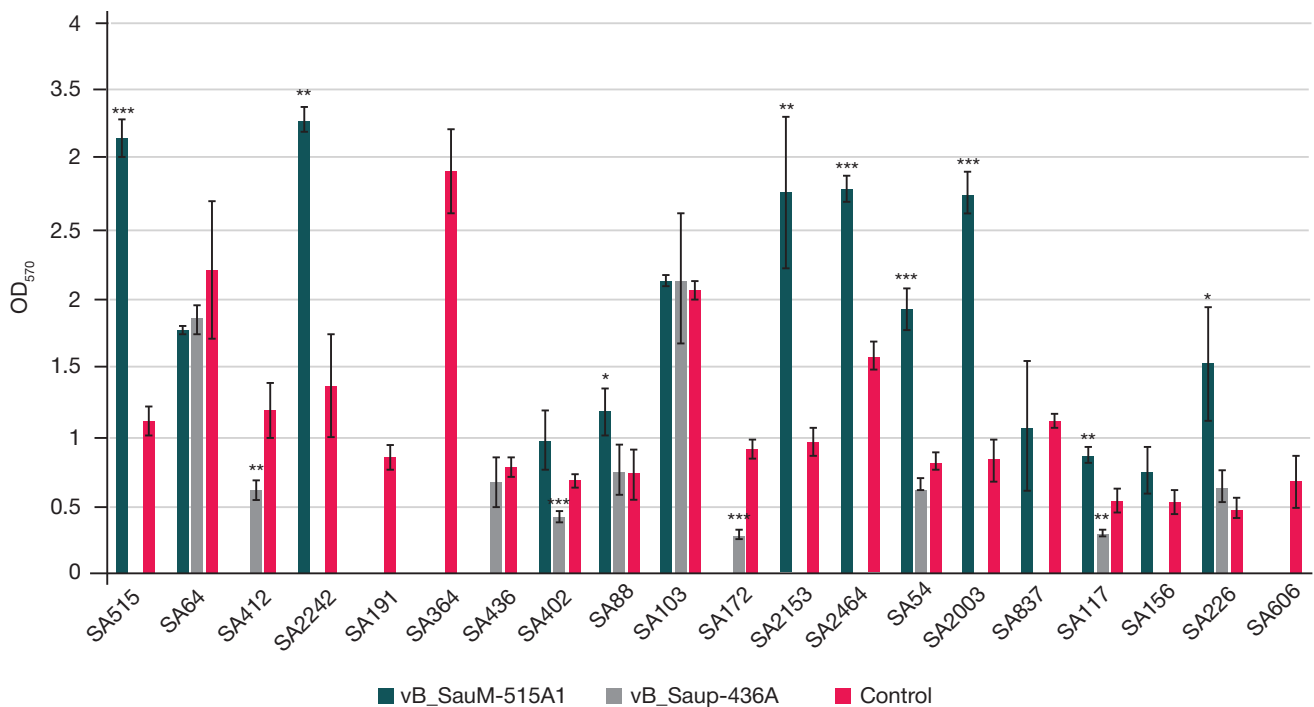
Fig. Effects of bacteriophages vB_SauM-515A1 and vB_SauP-436A on the biofilm biomass. Biofilms treated with bacteriophage vB_SauM-515A1 are highlighted in *green*; those treated with bacteriophage vB_SauP-436A are highlighted in *blue*; the untreated control is highlighted in *orange*. The lack of data in the column indicates that the strain is resistant to the effects of appropriate bacteriophage. The ranges show standard deviation. * — $p \leq 0.05$; ** — $p \leq 0.01$; *** — $p \leq 0.001$

sensitivity to antibiotics, a large number of strains belonged to MRSA (9/20, 45%). Furthermore, seven strains (35%) were characterized by MDR.

All the tested strains were able to form biofilms, and more than a half were strong biofilm producers (13/20, 65%). In the remaining cases (7/20, 35%), the strains were moderate biofilm producers. CFU enumeration showed that the number of cells in the 24-h biofilms reached 10^8 CFU/mL for all the studied strains. The amplification results demonstrated that all the isolates contained a complete set of the *icaADBC* operon genes.

Effects of bacteriophages of various taxonomic groups on the *S. aureus* planktonic cells and biofilms

Based on the results of assessing the effects of bacteriophages vB_SauM-515A1 and vB_SauP-436A on the planktonic cells of strains of the collection it was determined that 14 strains (70%) were sensitive to phage vB_SauM-515A1, while 10 strains (50%) were sensitive to phage vB_SauP-436A. Three strains of the collection (15%) turned out to be resistant to both phages. The phage vB_SauM-515A1 efficiency of plating in sensitive strains varied between 90 and 500%, while that of phage vB_SauP-436A varied between 75 and 400%.

The effect of bacteriophages on biofilm was assessed only for strains sensitive to the corresponding bacteriophage, based on data from experiments with planktonic cells. Biofilms were treated with the bacteriophage titer of 10^8 PFU/mL, which, based on CFU enumeration in the untreated biofilms, corresponds to the multiplicity of infection (MOI) value of 1.

According to the experimental results (Figure), in the majority of cases (9/14, 64.3%), the 24-h treatment with the vB_SauM-515A1 bacteriophage did not cause reduction of the biofilm biomass but, on the contrary, stimulated biomass production. As for remaining five strains (5/14, 35.7%), the exposure to the vB_SauM-515A1 bacteriophage had no significant effect on the biofilm. The exposure to bacteriophage vB_SauP-436A, on the contrary, significantly reduced the biofilm biomass in four

strains (4/10, 40%). This bacteriophage had no effect on the biofilms formed by other strains.

It should be noted that statistical analysis has revealed no significant correlations between the fact that the strain belongs to MRSA or certain sequence type and the ability of bacteriophage to stimulate biofilm formation (in the case of vB_SauM-515A1) or destroy biofilms (in the case of vB_SauP-436A). These effects also did not depend on the baseline strains' ability to form biofilms.

DISCUSSION

In this study, the strains were considered isolated from the heterogeneous clinical material that belonged to epidemiologically significant sequence types (Table). Among them the most abundant was ST8, one of the most common sequence types in Russia and all over the world among hospital strains [17, 18]. Strains of this sequence type include the pandemic clones, such as USA300, causing multiple infection outbreaks and often belonging to MRSA [19]. Along with ST8, the ST1, ST5, and ST121 strains were identified, which, according to the literature data, are characterized by antibiotic resistance and are capable of causing severe infections [20–22].

The findings showed that all the studied samples could form biofilms, regardless of the origin and sequence type. Furthermore, all strains were characterized by the presence of the *icaADBC* operon responsible for biosynthesis of polysaccharide intercellular adhesin, the major and best studied component of the *S. aureus* clinical strains' biofilm matrix, in the genome [23, 24]. It should also be noted that the majority of strains turned out to be strong biofilm producers. In combination with antibiotic resistance, this once again emphasizes severity of the problem of treating the infections caused by these strains.

Members of the families *Herelleviridae* and *Rountreeviridae* were used to assess the efficacy of bacteriophages. Phages were selected based on the differences in their morphological

(myoviruses and podoviruses), microbiological (host spectrum, parameters of infection based on the single-step growth curve), and genetic (genome size and the number of genes encoded) characteristics [11]. According to the findings, vB_SauM-515A1 (genus *Kayvirus*, family *Herelleviridae*) showed higher efficacy against planktonic cells compared to vB_SauP-436A (genus *Rosenblumvirus*, family *Rountreeviridae*), which is consistent with the earlier reported data on these bacteriophages [11]. As for other lytic bacteriophages of the family *Herelleviridae* (earlier referred to as *Myoviridae*), it has been also shown that their lytic spectrum varies between 85.3 and 99.2% depending on the collection, while in members of the family *Rountreeviridae* (earlier referred to as *Podoviridae*) this indicator is 64–68% [11, 25, 26].

As for biofilms, it was shown that bacteriophage vB_SauM-515A1 stimulated the biofilm biomass increase, while phage vB_SauP-436A reduced its quantity (Figure). It was earlier reported that myovirus phiIPLA-RODI belonging to the same genus, as vB_SauM-515A1, could stimulate biofilm formation in S. aureus [9]. The authors explain the findings by the increased eDNA content in the matrix, which, in turn, is associated with high lytic activity of bacteriophages of this family. The increased eDNA content contributes to the biofilm structural integrity and stability, as well as modulates formation of amyloid fibers essential for the biofilm architecture maintenance [27]. In another study, the researchers have shown that the use of phages of the genera *Kayvirus* и *Rosenblumvirus* (separately or in combination) in initial phases of biofilm formation or in mature biofilms does not result in the decrease in biofilm quantity [8]. The authors observed such an effect when using phages at both low (0.1) and high (10) MOI values. Furthermore, the increase in biofilm quantity was observed after the 24-h incubation, except for the case of treating the mature biofilm with the mixture of phages at MOI 10.

It should be noted that in the studies discussed the authors confined themselves to testing one and two bacterial isolates, which limits comprehensive comparison of the results. Nevertheless, the available data suggest the trend towards stimulation of biofilm formation in the *S. aureus* strains shown by phages of the genus *Kayvirus*. According to our data, reduction of the biomass quantity or the lack of significant effect was observed, when treating biofilms with bacteriophage of the genus *Rosenblumvirus*. Perhaps, vB_SauP-436A causes less intense cell lysis and lower eDNA release, which hampers stimulation of biofilm formation. In this regard, the combination use of bacteriophages, either in the form of the cocktail comprising several phages, or in combination with the agents destroying the matrix, such as depolymerases, seems to be a promising approach to combating biofilms [28].

It should also be noted that in this study phage efficacy was assessed by staining the biofilm biomass consisting of matrix and cells (both live and dead) with crystal violet. This method makes it impossible to assess the share of viable cells after treatment with antibacterial agents, so it is necessary to conduct further research for better understanding of the effects of phages on biofilms.

CONCLUSIONS

The study emphasizes complexity and ambiguity of the effects of bacteriophages on the *S. aureus* biofilm, especially in the case of clinical isolates showing high antibiotic resistance. Despite the ability of phages of the families vB_SauM-515A1 and vB_SauP-436A to inhibit growth of planktonic cells, their efficacy against biofilms of the *S. aureus* strains turned out to be low. The findings emphasized the importance of selecting phages based on their specific characteristics and efficacy against biofilms, as well as possible need for combination approaches involving bacteriophages and the agents destroying the biofilm matrix. At the same time, it should be considered that the results of this study have been obtained in the *in vitro* experiments by the limited number of methods. Further research is required to translate the findings into clinical practice, including the experiments involving *in vivo* models, which will make it possible to more accurately assess the efficacy and safety of the proposed approaches under conditions close to reality.

References

1. Ikuta KS, Swetschinski LR, Robles Aguilar G, Sharara F, Mestrovic T, et al. Global Mortality Associated with 33 Bacterial Pathogens in 2019: A Systematic Analysis for the Global Burden of Disease Study 2019. The Lancet. 2022; 400: 2221–48.
2. Idrees M, Sawant S, Karodia N, Rahman A. Staphylococcus Aureus Biofilm: Morphology, Genetics, Pathogenesis and Treatment Strategies. Int J Environ Res Public Health. 2021; 18: 7602.
3. Tuon FF, Suss PH, Telles JP, Dantas LR, Borges NH, Ribeiro VST. Antimicrobial Treatment of Staphylococcus Aureus Biofilms. Antibiotics. 2023; 12: 87.
4. Liu K, Wang C, Zhou X, Guo X, Yang Y, Liu W, et al. Bacteriophage Therapy for Drug-Resistant Staphylococcus Aureus Infections. Front. Cell. Infect. Microbiol. 2024; 14.
5. Plumet L, Ahmad-Mansour N, Dunyach-Remy C, Kissa K, Sotto A, Lavigne J-P, et al. Bacteriophage Therapy for Staphylococcus Aureus Infections: A Review of Animal Models, Treatments, and Clinical Trials. Front Cell Infect Microbiol. 2022; 12: 907314.
6. Gordina E, Bozhkova S, Smirnova LN. Effects of Bacteriophages on Biofilms Formed by Staphylococcus Aureus Isolated from Patients with Orthopedic Infection. Clinical Microbiology and Antimicrobial Chemotherapy. 2022; 24: 283–8.
7. Totten KMC, Patel R. Phage Activity against Planktonic and Biofilm Staphylococcus Aureus Periprosthetic Joint Infection Isolates. Antimicrobial Agents and Chemotherapy. 2022; 66: e01879.
8. Hosseinidoust Z, Tufenkji N, van de Ven TGM. Formation of Biofilms under Phage Predation: Considerations Concerning a Biofilm Increase. Biofouling. 2013; 29: 457–68.
9. Fernández L, González S, Campelo AB, Martínez B, Rodríguez A, García P. Low-Level Predation by Lytic Phage phiIPLA-RODI Promotes Biofilm Formation and Triggers the Stringent Response in Staphylococcus Aureus. Scientific Reports. 2017; 7: 40965.
10. Eucast: EUCAST Available from: https://www.eucast.org/ (accessed on 13 November 2024).
11. Kornienko M, Kuptsov N, Gorodnichev R, Bespiatykh D, Guliaev A, Letarova M, et al. Contribution of Podoviridae and Myoviridae Bacteriophages to the Effectiveness of Anti-Staphylococcal Therapeutic Cocktails. Sci Rep. 2020; 10: 18612.
12. Enright MC, Day NP, Davies CE, Peacock SJ, Spratt BG. Multilocus sequence typing for characterization of methicillin-resistant and methicillin-susceptible clones of Staphylococcus aureus. J Clin Microbiol. 2000; 38 (3): 1008–15.
13. Ghasemian A, Peerayeh SN, Bakhshi B, Mirzaee M. High Prevalence of Icaadbc Genes Responsible for Biofilm Formation in Clinical Isolates of Staphylococcus Aureus From Hospitalized Children. Archives of Pediatric Infectious Diseases. 2015; 3.
14. Cassat JE, Lee CY, Smeltzer MS. Investigation of Biofilm Formation in Clinical Isolates of Staphylococcus Aureus. Methods

Mol Biol. 2007; 391: 127–44.

15. Stepanović S, Vuković D, Hola V, Di Bonaventura G, Djukić S, Cirković I, et al. Quantification of Biofilm in Microtiter Plates: Overview of Testing Conditions and Practical Recommendations for Assessment of Biofilm Production by Staphylococci. APMIS. 2007; 115: 891–9.

16. Mazzocco A, Waddell TE, Lingohr E, Johnson RP. Enumeration of Bacteriophages Using the Small Drop Plaque Assay System. Methods Mol Biol. 2009; 501: 81–85.

17. Gostev V, Kruglov A, Kalinogorskaya O, Dmitrenko O, Khokhlova O, Yamamoto T, et al. Molecular Epidemiology and Antibiotic Resistance of Methicillin-Resistant Staphylococcus Aureus Circulating in the Russian Federation. Infection, Genetics and Evolution. 2017; 53: 189–94.

18. Wang X, Zhao H, Wang B, Zhou Y, Xu Y, Rao L, et al. Identification of Methicillin-Resistant Staphylococcus Aureus ST8 Isolates in China with Potential High Virulence. Emerg Microbes Infect. 2022; 11: 507–18.

19. Strauß L, Stegger M, Akpaka PE, Alabi A, Breurec S, Coombs G, et al. Origin, Evolution, and Global Transmission of Community-Acquired Staphylococcus Aureus ST8. Proceedings of the National Academy of Sciences. 2017; 114: E10596–E10604.

20. Xu K, Wang Y, Jian Y, Chen T, Liu Q, Wang H, et al. Staphylococcus Aureus ST1 Promotes Persistent Urinary Tract Infection by Highly Expressing the Urease. Front Microbiol. 2023; 14: 1101754.

21. Smith JT. Eckhardt EM, Hansel NB, Rahmani Eliato T, Martin IW, Andam CP. Genome Evolution of Invasive Methicillin-Resistant Staphylococcus Aureus in the Americas. Microbiol Spectr. 2022;

22. Kurt K, Rasigade J-P, Laurent F, Goering RV, Žemličková H, Machova I, et al. Subpopulations of Staphylococcus Aureus Clonal Complex 121 Are Associated with Distinct Clinical Entities. PLoS One. 2013; 8: e58155.

23. Cramton SE, Gerke C, Schnell NF, Nichols WW, Götz F. The Intercellular Adhesion (Ica) Locus Is Present in Staphylococcus Aureus and Is Required for Biofilm Formation. Infect Immun. 1999; 67: 5427–33.

24. Peng Q, Tang X, Dong W, Sun N, Yuan W. A Review of Biofilm Formation of Staphylococcus aureus and Its Regulation Mechanism. Antibiotics (Basel). 2022; 12 (1): 12.

25. Moller AG. Winston K, Ji S, Wang J, Davis MNH, Solís-Lemus CR, et al. Genes Influencing Phage Host Range in Staphylococcus Aureus on a Species-Wide Scale. mSphere. 2021; (6): e01263.

26. Göller PC. Elsener T, Lorgé D, Radulovic N, Bernardi V, Naumann A, et al. Multi-Species Host Range of Staphylococcal Phages Isolated from Wastewater. Nat Commun. 2021; 12: 6965.

27. Schwartz K, Ganesan M, Payne DE, Solomon MJ, Boles BR. Extracellular DNA facilitates the formation of functional amyloids in Staphylococcus aureus biofilms. Molecular microbiology. 2016; 99 (1): 123–34.

28. Duarte AC, Fernández L, Jurado A, Campelo AB, Shen Y, Rodríguez A, et al. Synergistic Removal of Staphylococcus Aureus Biofilms by Using a Combination of Phage Kayvirus Rodi with the Exopolysaccharide Depolymerase Dpo7. Front Microbiol. 2024; 15: 1438022.

10: e0020122.

Литература

1. Ikuta KS, Swetschinski LR, Robles Aguilar G, Sharara F, Mestrovic T, et al. Global Mortality Associated with 33 Bacterial Pathogens in 2019: A Systematic Analysis for the Global Burden of Disease Study 2019. The Lancet. 2022; 400: 2221–48.

2. Idrees M, Sawant S, Karodia N, Rahman A. Staphylococcus Aureus Biofilm: Morphology, Genetics, Pathogenesis and Treatment Strategies. Int J Environ Res Public Health. 2021; 18: 7602.

3. Tuon FF, Suss PH, Telles JP, Dantas LR, Borges NH, Ribeiro VST. Antimicrobial Treatment of Staphylococcus Aureus Biofilms. Antibiotics. 2023; 12: 87.

4. Liu K, Wang C, Zhou X, Guo X, Yang Y, Liu W, et al. Bacteriophage Therapy for Drug-Resistant Staphylococcus Aureus Infections. Front. Cell. Infect. Microbiol. 2024; 14.

5. Plumet L, Ahmad-Mansour N, Dunyach-Remy C, Kissa K, Sotto A, Lavigne J-P, et al. Bacteriophage Therapy for Staphylococcus Aureus Infections: A Review of Animal Models, Treatments, and Clinical Trials. Front Cell Infect Microbiol. 2022; 12: 907314.

6. Gordina E, Bozhkova S, Smirnova LN. Effects of Bacteriophages on Biofilms Formed by Staphylococcus Aureus Isolated from Patients with Orthopedic Infection. Clinical Microbiology and Antimicrobial Chemotherapy. 2022; 24: 283–8.

7. Totten KMC, Patel R. Phage Activity against Planktonic and Biofilm Staphylococcus Aureus Periprosthetic Joint Infection Isolates. Antimicrobial Agents and Chemotherapy. 2022; 66: e01879.

8. Hosseinidoust Z, Tufenkji N, van de Ven TGM. Formation of Biofilms under Phage Predation: Considerations Concerning a Biofilm Increase. Biofouling. 2013; 29: 457–68.

9. Fernández L, González S, Campelo AB, Martínez B, Rodríguez A, García P. Low-Level Predation by Lytic Phage phiIPLA-RODI Promotes Biofilm Formation and Triggers the Stringent Response in Staphylococcus Aureus. Scientific Reports. 2017; 7: 40965.

10. Eucast: EUCAST Available from: https://www.eucast.org/ (accessed on 13 November 2024).

11. Kornienko M, Kuptsov N, Gorodnichev R, Bespiatykh D, Guliaev A, Letarova M, et al. Contribution of Podoviridae and Myoviridae Bacteriophages to the Effectiveness of Anti-Staphylococcal Therapeutic Cocktails. Sci Rep. 2020; 10: 18612.

12. Enright MC, Day NP, Davies CE, Peacock SJ, Spratt BG. Multilocus sequence typing for characterization of methicillin-resistant and methicillin-susceptible clones of Staphylococcus aureus. J Clin Microbiol. 2000; 38 (3): 1008–15.

13. Ghasemian A, Peerayeh SN, Bakhshi B, Mirzaee M. High Prevalence of Icaadbc Genes Responsible for Biofilm Formation in Clinical Isolates of Staphylococcus Aureus From Hospitalized Children. Archives of Pediatric Infectious Diseases. 2015; 3.

14. Cassat JE, Lee CY, Smeltzer MS. Investigation of Biofilm Formation in Clinical Isolates of Staphylococcus Aureus. Methods Mol Biol. 2007; 391: 127–44.

15. Stepanović S, Vuković D, Hola V, Di Bonaventura G, Djukić S, Cirković I, et al. Quantification of Biofilm in Microtiter Plates: Overview of Testing Conditions and Practical Recommendations for Assessment of Biofilm Production by Staphylococci. APMIS. 2007; 115: 891–9.

16. Mazzocco A, Waddell TE, Lingohr E, Johnson RP. Enumeration of Bacteriophages Using the Small Drop Plaque Assay System. Methods Mol Biol. 2009; 501: 81–85.

17. Gostev V, Kruglov A, Kalinogorskaya O, Dmitrenko O, Khokhlova O, Yamamoto T, et al. Molecular Epidemiology and Antibiotic Resistance of Methicillin-Resistant Staphylococcus Aureus Circulating in the Russian Federation. Infection, Genetics and Evolution. 2017; 53: 189–94.

18. Wang X, Zhao H, Wang B, Zhou Y, Xu Y, Rao L, et al. Identification of Methicillin-Resistant Staphylococcus Aureus ST8 Isolates in China with Potential High Virulence. Emerg Microbes Infect. 2022; 11: 507–18.

19. Strauß L, Stegger M, Akpaka PE, Alabi A, Breurec S, Coombs G, et al. Origin, Evolution, and Global Transmission of Community-Acquired Staphylococcus Aureus ST8. Proceedings of the National Academy of Sciences. 2017; 114: E10596–E10604.

20. Xu K, Wang Y, Jian Y, Chen T, Liu Q, Wang H, et al. Staphylococcus Aureus ST1 Promotes Persistent Urinary Tract Infection by Highly Expressing the Urease. Front Microbiol. 2023; 14: 1101754.

21. Smith JT. Eckhardt EM, Hansel NB, Rahmani Eliato T, Martin IW, Andam CP. Genome Evolution of Invasive Methicillin-Resistant Staphylococcus Aureus in the Americas. Microbiol Spectr. 2022; 10: e0020122.

22. Kurt K, Rasigade J-P, Laurent F, Goering RV, Žemličková H, Machova I, et al. Subpopulations of Staphylococcus Aureus Clonal Complex 121 Are Associated with Distinct Clinical Entities. PLoS One. 2013; 8: e58155.

23. Cramton SE, Gerke C, Schnell NF, Nichols WW, Götz F. The Intercellular Adhesion (Ica) Locus Is Present in Staphylococcus Aureus and Is Required for Biofilm Formation. Infect Immun. 1999; 67: 5427–33.

24. Peng Q, Tang X, Dong W, Sun N, Yuan W. A Review of Biofilm Formation of Staphylococcus aureus and Its Regulation Mechanism. Antibiotics (Basel). 2022; 12 (1): 12.

25. Moller AG. Winston K, Ji S, Wang J, Davis MNH, Solís-Lemus CR, et al. Genes Influencing Phage Host Range in Staphylococcus Aureus on a Species-Wide Scale. mSphere. 2021; (6): e01263.

26. Göller PC. Elsener T, Lorgé D, Radulovic N, Bernardi V, Naumann A, et al. Multi-Species Host Range of Staphylococcal Phages Isolated from Wastewater. Nat Commun. 2021; 12: 6965.

27. Schwartz K, Ganesan M, Payne DE, Solomon MJ, Boles BR. Extracellular DNA facilitates the formation of functional amyloids in Staphylococcus aureus biofilms. Molecular microbiology. 2016; 99 (1): 123–34.

28. Duarte AC, Fernández L, Jurado A, Campelo AB, Shen Y, Rodríguez A, et al. Synergistic Removal of Staphylococcus Aureus Biofilms by Using a Combination of Phage Kayvirus Rodi with the Exopolysaccharide Depolymerase Dpo7. Front Microbiol. 2024; 15: 1438022.

EVALUATION OF THE EFFECTIVENESS OF ETIOTROPIC THERAPY WITH LINEZOLID AND BACTERIOPHAGE IN A MOUSE MODEL FOR STAPHYLOCOCCAL INFECTION

Kornienko MA[1] ✉, Kuzin VV[2], Abdraimova NK[1], Gorodnichev RB[1], Shitikov EA[1]

[1] Lopukhin Federal Research and Clinical Center of Physical-Chemical Medicine of Federal Medical Biological Agency, Moscow, Russia
[2] State Research Center for Applied Microbiology and Biotechnology, Obolensk, u.d. Serpukhov, Moscow region, Russia

Staphylococcus aureus is the causative agent of a wide range of infections, including severe systemic diseases, which is often multidrug resistant. Given the growing overall antibiotic resistance, a promising approach to treating staphylococcal infections is administration of bacteriophages, especially in combination with antibiotics. This study aimed to evaluate the synergistic effect of linezolid and bacteriophage vB_SauM-515A1 in combating a systemic infection in BALB/c mice. Using 36 animals, we established the optimal way of administration and the infecting dose of the microorganism (5×10^8 CFU/mouse intravenously), and identified the threshold concentrations of antimicrobial agents for monotherapy. The evaluation was based on the revealed contamination of internal organs (kidneys, spleen) and blood. To learn the etiotropic effect of linezolid (10 mg/kg animal weight) combined with the phage (2×10^7 PFU/mouse), we worked with a control group and a test group, 12 mice in each; 2, 8, 18, and 24 hours after infection, the former received the drug only, the latter — the investigated combination. Combined therapy had a more pronounced effect, decreasing the bacterial load in the kidneys by two to three orders of magnitude compared with monotherapy on the first day of treatment. Thus, the combined use of linezolid and bacteriophages is promising for the treatment of infections caused by *S. aureus*, and may increase the effectiveness of treatment and reduce the risk of side effects of high-dose antibiotics.

Keywords: *Staphylococcus aureus*, bacteriophages, phage therapy, combination therapy, linezolid, synergism, synergy between antibiotics and bacteriophages, mouse model, multidrug resistance

✉ Correspondence should be addressed: Maria A. Kornienko
Malaya Pirogovskaya, 1a, Moscow, 119435; kornienkomariya@gmail.com

ОЦЕНКА ЭФФЕКТИВНОСТИ ЭТИОТРОПНОЙ ТЕРАПИИ ЛИНЕЗОЛИДОМ И БАКТЕРИОФАГОМ НА МЫШИНОЙ МОДЕЛИ СТАФИЛОКОККОВОЙ ИНФЕКЦИИ

М. А. Корниенко[1] ✉, В. В. Кузин[2], К. Н. Абдраймова[1], Р. Б. Городничев[1], Е. А. Шитиков[1]

[1] Федеральный научно-клинический центр физико-химической медицины имени Ю. М. Лопухина Федерального медико-биологического агентства, Москва, Россия
[2] Государственный научный центр прикладной микробиологии и биотехнологии Роспотребнадзора, Оболенск, Россия

Staphylococcus aureus — возбудитель широкого спектра инфекций, включая тяжелые системные заболевания, и часто характеризуется множественной лекарственной устойчивостью. В условиях растущей антибиотикорезистентности перспективным методом лечения стафилококковых инфекций является применение бактериофагов, особенно в сочетании с антибиотиками. Целью работы было оценить синергетический эффект линезолида и бактериофага vB_SauM-515A1 при лечении системной инфекции у мышей BALB/c. С использованием 36 животных были подобраны оптимальный способ введения и инфицирующая доза микроорганизма (внутривенно 5×10^8 КОЕ/мышь), а также установлены пороговые концентрации антимикробных агентов при монотерапии. Оценку проводили по результатам исследования обсемененности внутренних органов (почки, селезенка) и крови. Для оценки комбинированного эффекта этиотропного действия линезолида (10 мг/кг массы животного) и фага (2×10^7 БОЕ/мышь) эксперимент проводили на контрольной и экспериментальных группах (по 12 особей в группе), получавших внутрибрюшинно монотерапию и комбинированное лечение через 2, 8, 18, 24 ч после заражения. Комбинированная терапия продемонстрировала более выраженный эффект: снижение бактериальной нагрузки в почках на два–три порядка по сравнению с монотерапией в первые сутки терапии. Таким образом, совместное использование линезолида и бактериофагов перспективно для лечения инфекций, вызванных *S. aureus*, и может повысить эффективность лечения и снизить риск побочных эффектов применения высоких доз антибиотиков.

Ключевые слова: *Staphylococcus aureus*, бактериофаги, фаговая терапия, комбинированная терапия, линезолид, синергизм, синергизм антибиотиков и бактериофагов, мышиные модели, множественная лекарственная устойчивость

✉ Для корреспонденции: Мария Андреевна Корниенко
ул. Малая Пироговская, д. 1а, г. Москва, 119435, Россия; kornienkomariya@gmail.com

Staphylococcus aureus is a major causative agent of both hospital-acquired and community-acquired infections, ranging from mild skin infections to life-threatening systemic diseases [1, 2]. In 2019, *S. aureus* caused more than 1 million deaths worldwide, largely because of the antibiotic resistance of strains of this species [3]. Clinically, the most significant of them are the methicillin-resistant strains of *S. aureus* (MRSA), which are resistant to beta-lactam antibiotics and often exhibit multidrug resistance (MDR) [2].

Recently, virulent bacteriophages, or phages, are increasingly considered as agents against infections caused by resistant bacteria [4]. One of the most promising applications of the phages is in combination with antibiotics. This approach promises increased effectiveness of etiotropic treatment, smaller doses of antibiotics, minimized side effects, and reduced likelihood of acquired resistance on the part of the pathogens because of the intercomplementary effects of the antimicrobial agents [4]. There are two types of such effects, additive and synergistic. The additive effect is defined as the cumulative action of drugs equal to the sum of their individual effects. Synergism means amplification of the combined antimicrobial effect to the level exceeding that of the additive effect. However, the drugs can also be antagonistic to each other, i.e., their combined efficacy is below the effect achieved when they are use separately [5, 6].

In vitro studies have shown that in most cases, combined use of staphylophages and most antibiotics yields synergy [4]. Combining linezolid and staphylophages of the *Herelleviridae family* is a particularly interesting approach. Phages of this family have a wide lytic range, which supports their potential therapeutic applications [7–9]. Linezolid is a drug used against staphylococcal infections, those resistant to vancomycin in particular [10].

Linezolid inhibits protein synthesis by disrupting the formation of a functionally active complex needed to initiate the translation [10]. However, its use is associated with a number of limitations. First, prolonged administration of the antibiotic can cause serious side effects [11]. Secondly, the use of linezolid against microorganisms that require concentrations upwards of 4 µgr/ml or higher to suppress their growth may lead to deterioration of clinical efficacy [10] due to the peculiarities of its administration and possible fluctuations in blood plasma concentrations [12]. Thus, the combined linezolid-staphylophages therapy can increase the effectiveness of treatment and mitigate the risk of side effects by reducing the dose of the antibiotic, which makes this approach promising for clinical practice.

The synergy in the combination of linezolid and *Herelleviridae* family bacteriophages was previously demonstrated in vitro by us and other researchers [13–15]. The synergistic effect has also been confirmed in mouse models of staphylococcal infection [16–18]. Nevertheless, several studies describe antagonistic interaction between phages and linezolid [19, 20], which probably stems from the concentration of the antibiotic and the sequence of administration of the agents (in case of biofilms).

The purpose of this study was to expand knowledge of the synergy of linezolid and the vB_SauM-515A1 bacteriophage (*Herelleviridae* family) [13] by evaluating the effect of their combined and separate use in the context of treatment of systemic staphylococcal infection in BALB/c mice. The resulting data may be key to optimizing combination therapy for MRSA infections and may boost its effectiveness in clinical practice.

METHODS

Bacterial strains, phages, storage and cultivation conditions

The study used *S. aureus* SA413, a previously described strain, taken from the collection of Yu. M. Lopukhin Federal Research and Clinical Center for Physical-Chemical Medicine. The strain, isolated from purulent discharge of soft tissues, was classified as methicillin-sensitive *S. aureus* sequence type 8 (ST8); the minimum inhibitory concentration of linezolid for it was 8 µg/ml. This strain was selected because a previous in vitro study has shown the bacteriophage and linezolid to produce synergistic effect when acting thereon [13]. The strain was cultured on a meat peptone agar (MPA) nutrient medium (State Research Center for Applied Biotechnology and Microbiology, Obolensk, Russia).

The bacteriophage vB_SauM-515A1 was previously isolated from the commercially available P332 series Staphylococcal bacteriophage preparation (Microgen; Russia). Its detailed description was given earlier. The bacteriophage was grown on the SA413 strain of *S. aureus*, in an LB broth (Miller's modification) (Oxoid; Great Britain), at 37 °C. The phage lysate was then filtered through a 0.22 µm syringe filter with a hydrophilic polyethersulfone membrane (Millipore, USA), and purified by ultracentrifugation in a sucrose gradient as described earlier [7]. After purification, the bacteriophage was resuspended in a sterile saline solution. The titer of the bacteriophage in the preparation was assessed using the standard Grazia titration method [22]. The bacteriophage preparation was stored at 4 °C.

Animals

Female BALB/c mice weighing 18–22 g, 68 weeks old, were used as model animals. They were taken from the laboratory animal nursery of the Stolbovaya branch of the Research Center for Biomedical Technologies (Series Certificate No. 20353 of 30.05.2024). The mice were kept in groups, under standard conditions, as per the international standards and requirements, with unrestricted access to water and feed (Laboratorkorm; Russia). The animals were euthanized through CO_2 inhalation.

Parenchymal organs (spleen, liver) from the dead mice were examined for staphylococcal infection using the dense nutrient surface imprinting method; the medium was *Staphylococcagar* (State Research Center for Applied Microbiology and Biotechnology; Russia).

Modeling of staphylococcal infection in mice

Modeling simulate staphylococcal infection, we tested various infectious doses of the *S. aureus* SA413 strain and two approaches of administration, intravenous and intraperitoneal. The bacterial inoculum was grown in a liquid nutrient medium to an optical density (OD_{620}) of 0.75 (5×10^9 CFU/ml), and diluted with saline to the desired concentration. The animals were divided into six groups, three mice in each: group 1 — intravenous administration of 5×10^6 CFU/mouse; group 2 — intravenous administration of 5×10^7 CFU/mouse; group 3 — intravenous administration of 5×10^8 CFU/mouse; group 4 — intraperitoneal administration of 5×10^6 CFU/mouse; group 5 — intraperitoneal administration of 5×10^7 CFU/mouse; group 6 — intraperitoneal administration of 5×10^8 CFU/mouse. The volumes of the injected inoculum were 200 µl (intraperitoneal) and 100 µl (intravenous). The animals were monitored for three days to account for deaths. On the third day, bacterial
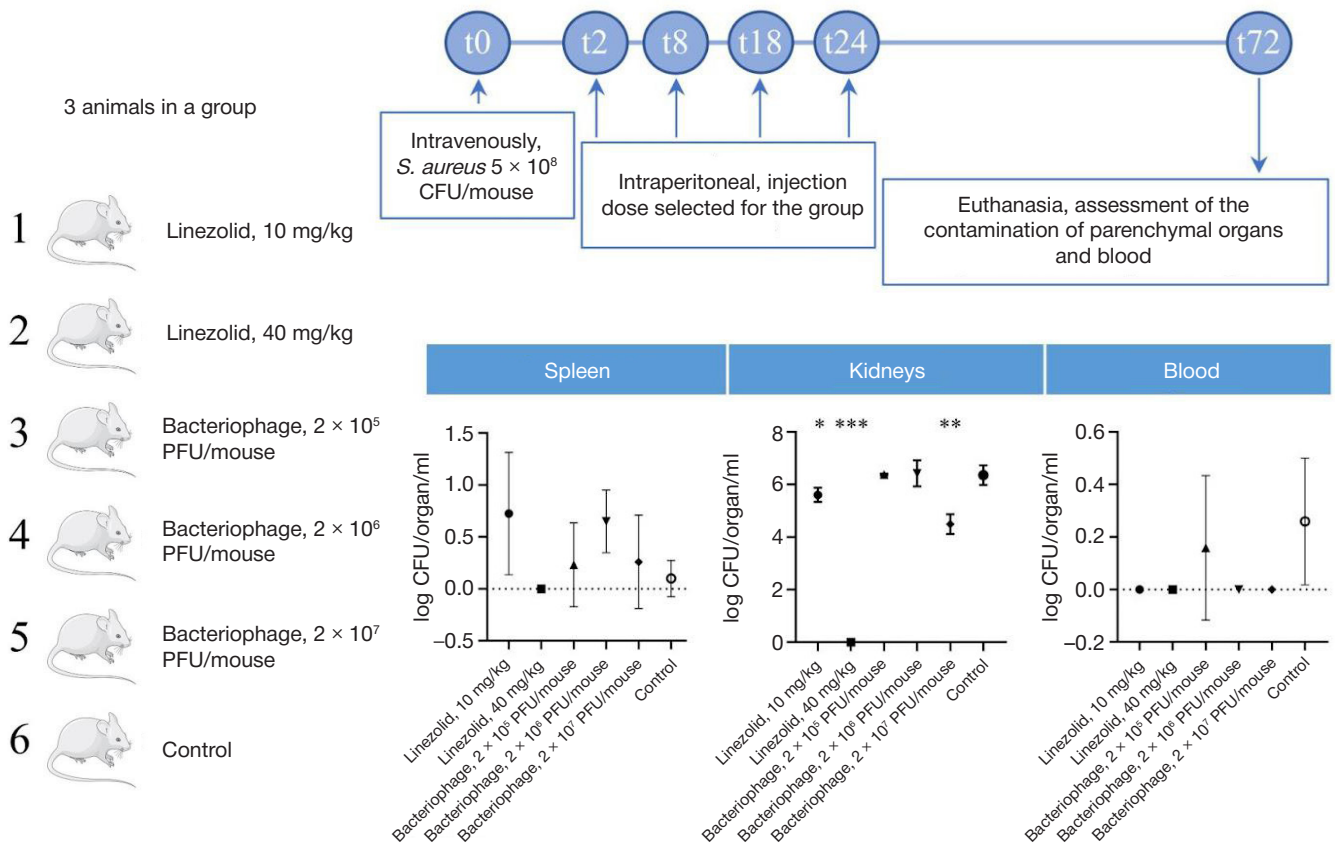
Fig. 1. Identification of the minimum inhibitory and therapeutic doses of linezolid and bacteriophage against staphylococcal infection * — $p < 0.05$; ** — $p < 0.001$; *** — $p < 0.0001$

contamination of parenchymal organs and blood was assessed in the surviving animals.

Selection of doses of antimicrobial agents

To assess the therapeutic and minimum inhibitory doses of linezolid and the bacteriophage vB_SauM-515A1, we divided the mice into 6 groups, three mice in each. Two, eight, eighteen, and twenty-four hours after infection, mice were injected with either linezolid (Sigma-Aldrich; USA) at concentrations of 10 mg/kg of animal weight or 40 mg/kg of animal weight, or the vB_SauM-515A1 bacteriophage at doses of 2×10^5, 2×10^6, and 2×10^7 PFU/mouse. Sterile saline solution was used to dilute the preparations to the necessary concentrations. Control group received saline solution without treatment, similar administration patterns as the test groups. The preparations (200 µl) were injected intraperitoneally. The animals were observed for three days, then euthanized. Parenchymal organs (spleen, kidneys) and blood were collected from them and examined for bacterial contamination and phage content. Blood (1 ml) was sampled from the heart through a puncture into sterile vacuum tubes with sodium heparin (no gel) (Improvacuter; China) designed for blood plasma testing.

Evaluation of the effectiveness of the combined effect of linezolid and bacteriophage

To assess the effectiveness of the combination, we used the antibacterial agents in minimal inhibitory doses. The experiment employed four experimental groups of animals, 12 mice in each, infected with the *S. aureus* SA413 strain. The infectious dose and the pattern of administration were selected based on the results of preliminary experiments. For the monotherapy

stage, the animals received 200 µl of drugs intraperitoneally 2, 8, 18 and 24 hours post-infection. For the combined therapy stage (similar to the monotherapy stage time-wise), the mice were first injected with 200 µl of he antibiotic in one side of the peritoneum, then with 200 µl of the phage in the other side of the peritoneum. The first group of mice was treated with linezolid; the second group was treated with bacteriophage; the third group received the combination of the two; the fourth group (control) was injected with saline solution. Subsequently, three mice from each group were euthanized on the first and second days, and six mice on the third day. Their organs anfd blood were collected and examined for bacterial contamination.

Examination for bacterial contamination bacteriophages in parenchymal organs and blood

The organs were homogenized in sterile mortars, with 1 ml of saline solution added per organ. Next, blood samples and suspension samples were diluted tenfold in saline solution and plated on the Staphylococcagar dense nutrient medium (State Research Center for Applied Microbiology and Biotechnology; Russia). In parallel, we measured bacteriophage content in the suspensions using the Grazia titration method and Staphylococcagar medium (State Research Center for Applied Microbiology and Biotechnology; Russia); the samples made for the purpose were 100 µl serial dilutions. The measurements were done in five technical repetitions.

Data presentation and statistical analysis

For statistical analysis, we used Prism software (GraphPad Software 8; USA). The Shapiro-Wilk test allowed assessing the normalcy of data distribution, and the Student's *t*-test was used
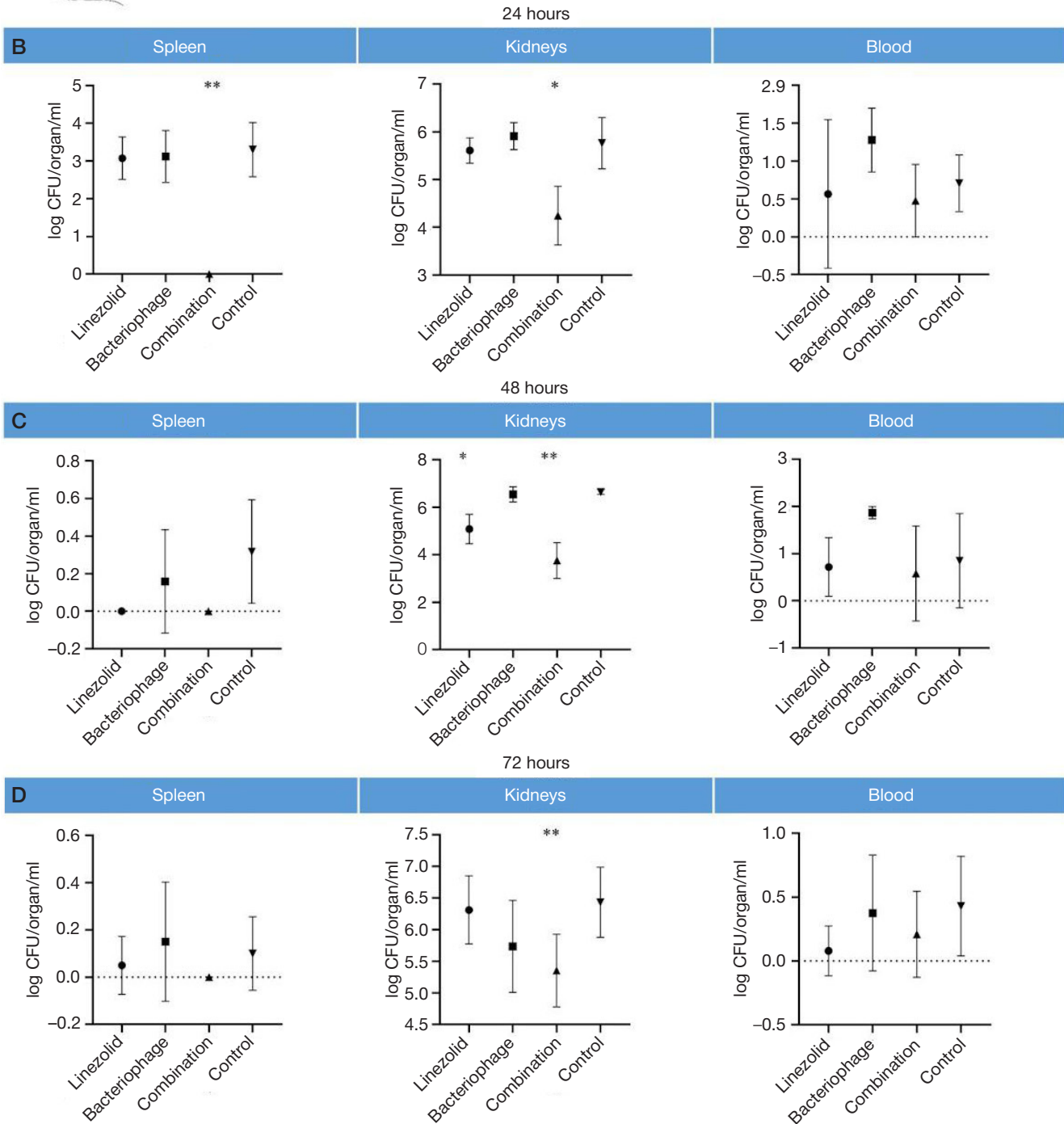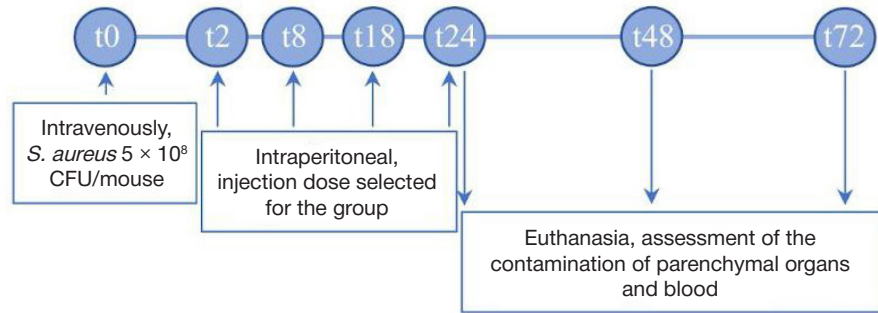
Fig. 2. Evaluation of the effectiveness of the combined effect of linezolid and bacteriophage: experiment design and results. **A**. Experiment design. **B–D**. Contamination of parenchymal organs and blood 24, 48, and 72 hours after infection, respectively. * — $p < 0.05$, ** — $p < 0.001$.

to compare the means between the groups. The differences were considered significant for $p < 0.05$.

Statement of compliance with ethical standards

All experiments with laboratory animals were approved by the Bioethics Commission of the State Research Center for Applied Microbiology and Biotechnology and conducted in accordance with the Guide for the Care and Use of Laboratory Animals [23].

RESULTS

Staphylococcal infection model

To build an adequate model of staphylococcal infection in laboratory animals, we conducted preliminary studies to select and infecting dose that ensures contamination of parenchymal organs (spleen, kidneys) and blood with the *S. aureus* strain SA413 on the third day after infection while avoiding animal mortality.

According to the results of those studies, intraperitoneal administration of bacteria at a dose of 5×10^8 CFU/mouse yielded death of all animals on the first day after infection, which is presumably due to the high concentration of the investigated strain in the area of administration and the subsequent toxic shock. Intraperitoneal administration of the bacterial culture at concentrations of 5×10^6 and 5×10^7 CFU/mouse, same as intravenous administration at any of the concentrations studied, left the mice alive three days after the infection. Only the mice that received a dose of 5×10^8 CFU/mouse intravenously exhibited downed motor activity and drowsiness, tousled hair and eyelid hyperemia, which indicate the development of an infectious process.

According to the autopsy, on the third day after intravenous injection of 5×10^8 CFU/mouse the animals had staphylococci in the kidneys ($8.9 \times 10^5 - 3.6 \times 10^6$ CFU/organ/ml) and a small amount of the pathogen in the spleens (37–52 CFU/organ/ml) and blood ($3.4 \times 10^2 - 1.3 \times 10^3$ CFU/ml). Smaller doses produced either isolated bacterial colonies or none at all, regardless of the method of infection.

Identification of the minimum inhibitory and therapeutic doses of linezolid and bacteriophage against staphylococcal infection

The minimum inhibitory and therapeutic doses of antimicrobial agents were evaluated for two concentrations of linezolid and three variants of bacteriophage doses. Eighteen mice were used for the purpose (Fig. 1).

Visual examination showed physical depression, tousled hair, and eyelid hyperemia in mice in the control group and four of the five experimental groups (linezolid 10 mg/kg of animal weight, and all doses of bacteriophage). No animals died through the entire experiment. Animals that received linezolid in the dose of 40 mg/kg of weight did not have the above symptoms.

An autopsy on the third day revealed low spleen contamination (0–25 CFU/organ/ml) in all groups and no bacteria in the blood, with the exception of the control group (0–3 CFU/ml) and the group that received the bacteriophage in the dose of 2×10^5 PFU/mouse. Kidney contamination was the most illustrative indicator. A dose of linezolid 40 mg/kg of animal weight ensured the pathogen was eliminated from the kidneys, indicating this was the therapeutic dose. A dose of 10 mg/kg of animal weight slowed formation of the bacterial

colonies by one order of magnitude, made it a minimum inhibitory dose. The doses of bacteriophage 2×10^5 and 2×10^6 PFU/mouse did not deliver results significantly different from those registered in the control group, and were considered ineffective. The dose of bacteriophage 2×10^7 PFU/mouse reduced kidney contamination by one order of magnitude, and was recognized as the minimum inhibitory dose. An amount that could constitute a therapeutic dose was not found.

We detected phage particles only in the kidneys of mice that received a dose of 2×10^7 PFU/mouse (30–70 PFU/organ). There were no bacteriophages found in the blood and spleens of the animals.

Evaluation of the effectiveness of the combined effect of linezolid and bacteriophage

We used 48 mice to assess the combined effect of antimicrobial agents in minimum inhibitory concentrations (linezolid: 10 mg/kg animal weight; bacteriophage: 2×10^7 PFU/mouse) (Fig. 2).

By visual indicators, animals in all groups had the infectious process developing, and their condition was depressed, as described in the previous experiment.

On the first day, we detected no differences in the contamination of parenchymal organs between the monotherapy groups and the control group (Fig. 2B). In the combined therapy group, the spleen contamination dropped to almost zero values ($p = 0.0014$), and that of the kidneys was by one to two orders of magnitude lower than in the control group ($p = 0.0318$), while blood contamination remained comparable to that in the control group.

The results registered on the second day are shown in Fig. 2B. There were insignificant amounts of staphylococci in the spleens of animals of all groups, except those receiving linezolid, where the spleens were clean of the bacteria. Kidney contamination in the bacteriophage group remained at the level of the control group, and in the antibiotic group it significantly decreased by less than an order of magnitude ($p = 0.0127$); combined therapy pushed the value of this indicator down by two to three orders of magnitude compared to the control group ($p = 0.0028$). Blood contamination in all groups remained at the level of up to 10^2 CFU/ml.

On the third day after infection, we registered insignificant amounts of staphylococci in platings from spleen homogenates sampled in all the groups, which points to this organ's ability to independently eliminate the pathogen (Fig. 2D). Kidney contamination in mice treated with linezolid returned to the level peculiar to the control group, while in mice treated with bacteriophage it remained at that level throughout. In the combined therapy group, the contamination rate was an order of magnitude lower than the control values ($p = 0.0079$). Blood contamination in all groups remained at the control level.

As for the bacteriophage, its content was insignificant during the entire experiment (20–250 PFU/organ/ml) in the kidneys of the animals that received 2×10^7 PFU/mouse thereof as monotherapy, and in the combined use scenario. We registered no significant differences between the groups. No bacteriophage was detected in the spleens and blood.

DISCUSSION

Combined bacteriophages and antibiotics therapy is, presumably, one of the most promising approaches to the treatment of MDR pathogens. Numerous in vitro studies show promising results, demonstrating the synergistic effect of these agents. However, it is important to conduct *in vivo* experiments

to confirm their effectiveness and practical potential. Animal model studies allow assessing the possibilities and limitations of such therapy in conditions close to those of real-life clinical practice, and enable identification of the aspects that require further study before a full-fledged adoption.

To evaluate the effectiveness of the combined use of the bacteriophage vB_SauM-515A1 and linezolid, we chose a model of systemic infection in BALB/c mice, which aligns with the approaches practiced in similar studies [24, 25]. In the preliminary experiments, special attention was paid to the choice of the method of administration, selection of the infecting dose, and establishment of the minimum inhibitory concentrations of active agents. Previously published studies have shown that the infecting dose of *S. aureus* varies depending on the strain in the range from 10^6 to 10^8 CFU/mouse [24, 26, 27]. For example, a dose of 10^6 CFU/mouse was selected for the USA300 strain, known for its high virulence; in this case, the observation period was limited to 24 hours [28]. At the same time, a dose of 10^8 CFU/mouse used in the studies dedicated to the MDR strains partially killed the animals within 10–24 hours and, in some cases, by the third day [24, 27]. We focused on the sequence type 8 SA413 strain, one of the most common and associated with hospital infections worldwide, and found the optimal dose to be 5×10^8 CFU/mouse, administered intravenously. The dose ensured stable organ contamination after three days, thus creating adequate conditions for registration of the effects of therapy. Consistent with the findings reported by other authors, we have established that the results are most reliably reproducible when the injections are intravenous [27, 29].

The identified minimum inhibitory concentration of linezolid that does not cause pathogen elimination in monotherapy regimens and, consequently, should be investigated further, is 10 mg/kg of animal weight. This concentration of the antibiotic reduced bacterial contamination minimally, which is also consistent with the results reported by other researchers [10]. The concentration of 40 mg/kg of animal weight completely eliminated bacteria from the kidneys by the third day of the experiment, which is also similar to the data registered by other authors [29]. It should be noted that linezolid and bacteriophage were administered intraperitoneally to avoid vascular damage and the risk of hemorrhages associated with repeated injections. In particular, the effectiveness of this way was demonstrated in staphylococcal infection mice models that have thus received K-like phage ɸSA039 [30].

According to the published data on therapeutic use of bacteriophages in mouse models, the amount of antimicrobial agent varies from 10^6 to 10^{10} PFU/mouse [27, 31]. In our study, the minimum inhibitory dose of the bacteriophage was 2×10^7 PFU/mouse. This dose only partially decreased the level of bacterial contamination of kidneys, which underscores the need to use high concentrations of bacteriophages in monotherapy regimens. Moreover, lack of phages in blood and spleen indicates that there probably are some limitations to the system-wide spread of bacteriophages, which once again points to the need for an integrated approach in therapy.

Compared to monotherapy, combined use of linezolid and bacteriophage in minimum inhibitory doses had a more pronounced effect: within the first 24 hours, kidney contamination level decreased by two to three orders of magnitude versus the control values, a fact that backs the synergistic potential of antimicrobial agents. However, by the third day, bacterial contamination damping effect produced by the combination was not as strong as initially, which may indicate the need for a longer course of treatment to achieve the full therapeutic effect.

The evidence of the greater effectiveness of combination therapy compared with monotherapy are consistent with a number of reports covering animal model studies that investigated the effectiveness of the combined use of linezolid and *Herelleviridae* bacteriophages against other types of infections caused by *S. aureus*. Previously, it was demonstrated in a mouse model of a diabetic foot staphylococcal infection that a single injection of a Herelleviridae family phage delivers results comparable to those produced by linezolid, and combination therapy was much more effective in stopping the entire infectious process (bacterial load, number of lesions, foot myeloperoxidase activity, and histopathology), as well as accelerating the general tissue healing process [16]. A study that assessed the effectiveness of a linezolid and bacteriophage MR-5 (family *Herelleviridae*) combination against a skin infection modeled in mice has shown its potency: the agents, taken together, have significantly decreased the bacterial load and, consequently, boosted recovery [17]. There is also a report describing a combined therapy success in a modeled S. aureus infection case after arthroplasty. Mice were implanted with a wire coated with phage (10^9 PFU/ml) and/or linezolid into the intramedullary canal of the femur, and then inoculated with MRSA. In the group that received wire with a combination of agents, bacterial adhesion was reduced, and the limb's motor functions restored faster [18].

CONCLUSIONS

This study confirmed the promise held by the combined therapy with linezolid and bacteriophage vB_SauM-515A1 for treatment of systemic infections caused by *S. aureus*. Minimum inhibitory doses of the antibiotic and the bacteriophage were established to significantly decrease the level of bacterial contamination of parenchymal organs, which indicates a synergistic effect. The results of this study demonstrate that combination therapy is more effective than monotherapy, especially at the early stages, and can help reduce the dosage of the antibiotic, thus minimizing the possible side effects.

References

1. Cheung GYC, Bae JS; Otto M. Pathogenicity and Virulence of Staphylococcus Aureus. Virulence 2021; 12: 547–69, DOI: 10.1080/21505594.2021.1878688.

2. Guo Y, Song G, Sun M, Wang J, Wang Y. Prevalence and Therapies of Antibiotic-Resistance in Staphylococcus Aureus. Front Cell Infect Microbiol. 2020; 10: 107, DOI: 10.3389/fcimb.2020.00107.

3. Ikuta KS, Swetschinski LR, Robles Aguilar G, Sharara F, Mestrovic T, et al. Global Mortality Associated with 33 Bacterial Pathogens in 2019: A Systematic Analysis for the Global Burden of Disease Study 2019. The Lancet. 2022; 400: 2221–48, DOI: 10.1016/S0140-6736(22)02185-7.

4. Łusiak-Szelachowska M, Międzybrodzki R, Drulis-Kawa Z, Cater K Knežević P, Winogradow C, Amaro K, et al. Bacteriophages and Antibiotic Interactions in Clinical Practice: What We Have Learned so Far. J Biomed Sci. 2022; 29: 23, DOI: 10.1186/s12929-022-00806-1.

5. Dickey J, Perrot V. Adjunct Phage Treatment Enhances the Effectiveness of Low Antibiotic Concentration against Staphylococcus Aureus Biofilms in Vitro. PLoS ONE. 2019; 14:

e0209390, DOI: 10.1371/journal.pone.0209390.

6. Kumaran D, Taha M, Yi Q, Ramirez-Arcos S, Diallo J-S, Carli A, et al. Does Treatment Order Matter? Investigating the Ability of Bacteriophage to Augment Antibiotic Activity against Staphylococcus Aureus Biofilms. Front Microbiol. 2018; 9: 127, DOI: 10.3389/fmicb.2018.00127.

7. Kornienko M, Kuptsov N, Gorodnichev R, Bespiatykh D, Guliaev A, Letarova M, et al. Contribution of Podoviridae and Myoviridae Bacteriophages to the Effectiveness of Anti-Staphylococcal Therapeutic Cocktails. Sci Rep. 2020; 10: 18612, DOI: 10.1038/s41598-020-75637-x.

8. Leskinen K, Tuomala H, Wicklund A, Horsma-Heikkinen J, Kuusela P, Skurnik M, et al. Characterization of vB_SauM-fRuSau02, a Twort-Like Bacteriophage Isolated from a Therapeutic Phage Cocktail. Viruses. 2017; 9: 258, DOI: 10.3390/v9090258.

9. Abatángelo V, Peressutti Bacci N, Boncompain CA, Amadio AF, Carrasco S, Suárez CA, et al. Correction: Broad-Range Lytic Bacteriophages That Kill Staphylococcus Aureus Local Field Strains. PLoS ONE. 2017; 12: e0187387, DOI: 10.1371/journal.pone.0187387.

10. Liu C, Bayer A, Cosgrove SE, Daum RS, Fridkin SK, Gorwitz RJ, et al. Clinical practice guidelines by the infectious diseases society of america for the treatment of methicillin-resistant Staphylococcus aureus infections in adults and children: executive summary. Clinical infectious diseases: an official publication of the Infectious Diseases Society of America. 2011; 52 (3): 285–92. Available from: https://doi.org/10.1093/cid/cir034.

11. Bozdogan B, Appelbaum PC. Oxazolidinones: Activity, Mode of Action, and Mechanism of Resistance. International Journal of Antimicrobial Agents. 2004; 23: 113–9. DOI: 10.1016/j.ijantimicag.2003.11.003.

12. Hui L-A, Bodolea C, Vlase L, Hiriscau EI, Popa A. Linezolid Administration to Critically Ill Patients: Intermittent or Continuous Infusion? A Systematic Literature Search and Review. Antibiotics. 2022; 11: 436. DOI: 10.3390/antibiotics11040436.

13. Abdraimova NK, Kornienko MA, Bespiatykh DA, Kuptsov NS, Gorodnichev RB, Shitikov EA. Combined effects of bacteriophage vB_SauM-515A1 and antibiotics on the Staphylococcus aureus clinical isolates. Bulletin of RSMU. 2022; DOI: 10.24075/brsmu.2022.052.

14. Kaur S, Harjai K, Chhibber S. Bacteriophage Mediated Killing of Staphylococcus Aureus In Vitro on Orthopaedic K Wires in Presence of Linezolid Prevents Implant Colonization. PLoS ONE. 2014; 9: e90411. DOI:10.1371/journal.pone.0090411.

15. Wang B, Xu Y, Zhao H, Wang X, Rao L, Guo Y, et al. Methicillin-Resistant Staphylococcus Aureus in China: A Multicentre Longitudinal Study and Whole-Genome Sequencing. Emerging Microbes & Infections. 2022; 11: 532–42. DOI: 10.1080/22221751.2022.2032373.

16. Chhibber S, Kaur T. Sandeep Kaur Co-Therapy Using Lytic Bacteriophage and Linezolid: Effective Treatment in Eliminating Methicillin Resistant Staphylococcus Aureus (MRSA) from Diabetic Foot Infections. PLoS ONE. 2013; 8: e56022. DOI: 10.1371/journal.pone.0056022.

17. Kaur S, Chhibber S. A Mouse Air Pouch Model for Evaluating the Anti-Bacterial Efficacy of Phage MR-5 in Resolving Skin and Soft Tissue Infection Induced by Methicillin-Resistant Staphylococcus Aureus. Folia Microbiol. 2021; 66: 959–72, DOI: 10.1007/s12223-021-00895-9.

18. Kaur S, Harjai K, Chhibber S. In Vivo Assessment of Phage and Linezolid Based Implant Coatings for Treatment of Methicillin Resistant S. Aureus (MRSA) Mediated Orthopaedic Device Related Infections. PLoS ONE.

19. Berryhill BA, Huseby DL, McCall IC, Hughes D, Levin BR. Evaluating the Potential Efficacy and Limitations of a Phage for Joint Antibiotic and Phage Therapy of Staphylococcus Aureus Infections. Proc Natl Acad Sci USA. 2021; 118, e2008007118. DOI: 10.1073/pnas.2008007118.

20. Kumaran D, Taha M, Yi Q, Ramirez-Arcos S, Diallo J-S, Carli A, Abdelbary H. Does Treatment Order Matter? Investigating the Ability of Bacteriophage to Augment Antibiotic Activity against Staphylococcus Aureus Biofilms. Front Microbiol. 2018; 9: 127. DOI: 10.3389/fmicb.2018.00127.

21. Kornienko M, Fisunov G, Bespiatykh D, Kuptsov N, Gorodnichev R, Klimina K, et al. Transcriptional Landscape of Staphylococcus Aureus Kayvirus Bacteriophage vB_SauM-515A1. Viruses. 2020; 12: 1320. DOI: 10.3390/v12111320.

22. Mazzocco A, Waddell TE, Lingohr E, Johnson RP. Enumeration of Bacteriophages Using the Small Drop Plaque Assay System. In: Clokie MRJ, Kropinski AM, editors. Bacteriophages. Methods in Molecular Biology. Humana Press: Totowa, NJ. 2009; p. 81–85.

23. Guide for the Care and Use of Laboratory Animals. National Academies Press: Washington, D.C., 2011.

24. García P, Moscoso M, Fernández MC, Fuentes-Valverde V, Pérez A, Bou G. Comparison of the in Vivo Efficacy of Ceftaroline Fosamil, Vancomycin and Daptomycin in a Murine Model of Methicillin-Resistant Staphylococcus Aureus Bacteraemia. International Journal of Antimicrobial Agents. 2023; 62: 106836. DOI: 10.1016/j.ijantimicag.2023.106836.

25. Suligoy CM, Díaz RE, Gehrke A-K, Ring N, Yebra G, Alves J, et al. Acapsular Staphylococcus Aureus with a Non-Functional Agr Regains Capsule Expression after Passage through the Bloodstream in a Bacteremia Mouse Model. Sci Rep. 2020; 10: 14108 DOI: 10.1038/s41598-020-70671-1.

26. Kim HK, Missiakas D, Schneewind O. Mouse Models for Infectious Diseases Caused by Staphylococcus Aureus. Journal of Immunological Methods. 2014; 410: 88–99, DOI: 10.1016/j.jim.2014.04.007.

27. Oduor JMO, Onkoba N, Maloba F, Arodi WO, Nyachieo A. Efficacy of Lytic Staphylococcus Aureus Bacteriophage against Multidrug-Resistant Staphylococcus Aureus in Mice. J Infect Dev Ctries. 2016; 10: 1208–13. DOI: 10.3855/jidc.7931.

28. Sharma-Kuinkel BK, Zhang Y, Yan Q, Ahn SH, Fowler VG. Host Gene Expression Profiling and In Vivo Cytokine Studies to Characterize the Role of Linezolid and Vancomycin in Methicillin-Resistant Staphylococcus Aureus (MRSA) Murine Sepsis Model. PLoS ONE. 2013; 8: e60463. DOI: 10.1371/journal.pone.0060463.

29. Gordon O, Dikeman DA, Ortines RV, Wang Y, Youn C, Mumtaz M, et al. The Novel Oxazolidinone TBI-223 Is Effective in Three Preclinical Mouse Models of Methicillin-Resistant Staphylococcus Aureus Infection. Microbiol Spect. 2022; 10: e02451-21, DOI: 10.1128/spectrum.02451-21.

30. Fujiki J, Nakamura T, Nakamura K, Nishida K, Amano Y, Watanabe Y, et al. Biological properties of Staphylococcus virus –SA012 for phage therapy. Scientific reports. 2022; 12 (1): 21297. Available from: https://doi.org/10.1038/s41598-022-25352-6.

31. Plumet L, Ahmad-Mansour N, Dunyach-Remy C, Kissa K, Sotto A, Lavigne J-P, et al. Bacteriophage Therapy for Staphylococcus Aureus Infections: A Review of Animal Models, Treatments, and Clinical Trials. Front Cell Infect Microbiol. 2022; 12: 907314. DOI: 10.3389/fcimb.2022.907314.

Литература

1. Cheung GYC, Bae JS; Otto M. Pathogenicity and Virulence of Staphylococcus Aureus. Virulence 2021; 12: 547–69, DOI: 10.1080/21505594.2021.1878688.

2. Guo Y, Song G, Sun M, Wang J, Wang Y. Prevalence and Therapies of Antibiotic-Resistance in Staphylococcus Aureus. Front Cell Infect Microbiol. 2020; 10: 107, DOI: 10.3389/fcimb.2020.00107.

3. Ikuta KS, Swetschinski LR, Robles Aguilar G, Sharara F, Mestrovic T, et al. Global Mortality Associated with 33 Bacterial Pathogens in 2019: A Systematic Analysis for the Global Burden of Disease Study 2019. The Lancet. 2022; 400: 2221–48, DOI:

10.1016/S0140-6736(22)02185-7.

4. Łusiak-Szelachowska M, Międzybrodzki R, Drulis-Kawa Z, Cater K Knežević P, Winogradow C, Amaro K, et al. Bacteriophages and Antibiotic Interactions in Clinical Practice: What We Have Learned so Far. J Biomed Sci. 2022; 29: 23, DOI: 10.1186/s12929-022-00806-1.

5. Dickey J, Perrot V. Adjunct Phage Treatment Enhances the Effectiveness of Low Antibiotic Concentration against Staphylococcus Aureus Biofilms in Vitro. PLoS ONE. 2019; 14: e0209390, DOI: 10.1371/journal.pone.0209390.

6. Kumaran D, Taha M, Yi Q, Ramirez-Arcos S, Diallo J-S, Carli A, et

al. Does Treatment Order Matter? Investigating the Ability of Bacteriophage to Augment Antibiotic Activity against Staphylococcus Aureus Biofilms. Front Microbiol. 2018; 9: 127, DOI: 10.3389/fmicb.2018.00127.

7. Kornienko M, Kuptsov N, Gorodnichev R, Bespiatykh D, Guliaev A, Letarova M, et al. Contribution of Podoviridae and Myoviridae Bacteriophages to the Effectiveness of Anti-Staphylococcal Therapeutic Cocktails. Sci Rep. 2020; 10: 18612, DOI: 10.1038/s41598-020-75637-x.

8. Leskinen K, Tuomala H, Wicklund A, Horsma-Heikkinen J, Kuusela P, Skurnik M, et al. Characterization of vB_SauM-fRuSau02, a Twort-Like Bacteriophage Isolated from a Therapeutic Phage Cocktail. Viruses. 2017; 9: 258, DOI: 10.3390/v9090258.

9. Abatángelo V, Peressutti Bacci N, Boncompain CA, Amadio AF, Carrasco S, Suárez CA, et al. Correction: Broad-Range Lytic Bacteriophages That Kill Staphylococcus Aureus Local Field Strains. PLoS ONE. 2017; 12: e0187387, DOI: 10.1371/journal.pone.0187387.

10. Liu C, Bayer A, Cosgrove SE, Daum RS, Fridkin SK, Gorwitz RJ, et al. Clinical practice guidelines by the infectious diseases society of america for the treatment of methicillin-resistant Staphylococcus aureus infections in adults and children: executive summary. Clinical infectious diseases: an official publication of the Infectious Diseases Society of America. 2011; 52 (3): 285–92. Available from: https://doi.org/10.1093/cid/cir034.

11. Bozdogan B, Appelbaum PC. Oxazolidinones: Activity, Mode of Action, and Mechanism of Resistance. International Journal of Antimicrobial Agents. 2004; 23: 113–9. DOI: 10.1016/j.ijantimicag.2003.11.003.

12. Hui L-A, Bodolea C, Vlase L, Hiriscau EI, Popa A. Linezolid Administration to Critically Ill Patients: Intermittent or Continuous Infusion? A Systematic Literature Search and Review. Antibiotics. 2022; 11: 436. DOI: 10.3390/antibiotics11040436.

13. Абдраймова Н. К., Корниенко М. А. Беспятых Д. А., Купцов Н. С., Городничев Р. Б., Шитиков Е. А. Комбинированное воздействие бактериофага VB_SAUM-515A1 и антибиотиков на клинические изоляты Staphylococcus aureus. Вестник РГМУ. 2022; DOI: 10.24075/vrgmu.2022.052.

14. Kaur S, Harjai K, Chhibber S. Bacteriophage Mediated Killing of Staphylococcus Aureus In Vitro on Orthopaedic K Wires in Presence of Linezolid Prevents Implant Colonization. PLoS ONE. 2014; 9: e90411. DOI:10.1371/journal.pone.0090411.

15. Wang B, Xu Y, Zhao H, Wang X, Rao L, Guo Y, et al. Methicillin-Resistant Staphylococcus Aureus in China: A Multicentre Longitudinal Study and Whole-Genome Sequencing. Emerging Microbes & Infections. 2022; 11: 532–42. DOI: 10.1080/22221751.2022.2032373.

16. Chhibber S, Kaur T. Sandeep Kaur Co-Therapy Using Lytic Bacteriophage and Linezolid: Effective Treatment in Eliminating Methicillin Resistant Staphylococcus Aureus (MRSA) from Diabetic Foot Infections. PLoS ONE. 2013; 8: e56022. DOI: 10.1371/journal.pone.0056022.

17. Kaur S, Chhibber S. A Mouse Air Pouch Model for Evaluating the Anti-Bacterial Efficacy of Phage MR-5 in Resolving Skin and Soft Tissue Infection Induced by Methicillin-Resistant Staphylococcus Aureus. Folia Microbiol. 2021; 66: 959–72, DOI: 10.1007/s12223-021-00895-9.

18. Kaur S, Harjai K, Chhibber S. In Vivo Assessment of Phage and Linezolid Based Implant Coatings for Treatment of Methicillin Resistant S. Aureus (MRSA) Mediated Orthopaedic Device Related Infections. PLoS ONE.

2016; 11: e0157626, DOI: 10.1371/journal.pone.0157626.

19. Berryhill BA, Huseby DL, McCall IC, Hughes D, Levin BR. Evaluating the Potential Efficacy and Limitations of a Phage for Joint Antibiotic and Phage Therapy of Staphylococcus Aureus Infections. Proc Natl Acad Sci USA. 2021; 118, e2008007118. DOI: 10.1073/pnas.2008007118.

20. Kumaran D, Taha M, Yi Q, Ramirez-Arcos S, Diallo J-S, Carli A, Abdelbary H. Does Treatment Order Matter? Investigating the Ability of Bacteriophage to Augment Antibiotic Activity against Staphylococcus Aureus Biofilms. Front Microbiol. 2018; 9: 127. DOI: 10.3389/fmicb.2018.00127.

21. Kornienko M, Fisunov G, Bespiatykh D, Kuptsov N, Gorodnichev R, Klimina K, et al. Transcriptional Landscape of Staphylococcus Aureus Kayvirus Bacteriophage vB_SauM-515A1. Viruses. 2020; 12: 1320. DOI: 10.3390/v12111320.

22. Mazzocco A, Waddell TE, Lingohr E, Johnson RP. Enumeration of Bacteriophages Using the Small Drop Plaque Assay System. In: Clokie MRJ, Kropinski AM, editors. Bacteriophages. Methods in Molecular Biology. Humana Press: Totowa, NJ. 2009; p. 81–85.

23. Guide for the Care and Use of Laboratory Animals. National Academies Press: Washington, D.C., 2011.

24. García P, Moscoso M, Fernández MC, Fuentes-Valverde V, Pérez A, Bou G. Comparison of the in Vivo Efficacy of Ceftaroline Fosamil, Vancomycin and Daptomycin in a Murine Model of Methicillin-Resistant Staphylococcus Aureus Bacteraemia. International Journal of Antimicrobial Agents. 2023; 62: 106836. DOI: 10.1016/j.ijantimicag.2023.106836.

25. Suligoy CM, Díaz RE, Gehrke A-K, Ring N, Yebra G, Alves J, et al. Acapsular Staphylococcus Aureus with a Non-Functional Agr Regains Capsule Expression after Passage through the Bloodstream in a Bacteremia Mouse Model. Sci Rep. 2020; 10: 14108 DOI: 10.1038/s41598-020-70671-1.

26. Kim HK, Missiakas D, Schneewind O. Mouse Models for Infectious Diseases Caused by Staphylococcus Aureus. Journal of Immunological Methods. 2014; 410: 88–99, DOI: 10.1016/j.jim.2014.04.007.

27. Oduor JMO, Onkoba N, Maloba F, Arodi WO, Nyachieo A. Efficacy of Lytic Staphylococcus Aureus Bacteriophage against Multidrug-Resistant Staphylococcus Aureus in Mice. J Infect Dev Ctries. 2016; 10: 1208–13. DOI: 10.3855/jidc.7931.

28. Sharma-Kuinkel BK, Zhang Y, Yan Q, Ahn SH, Fowler VG. Host Gene Expression Profiling and In Vivo Cytokine Studies to Characterize the Role of Linezolid and Vancomycin in Methicillin-Resistant Staphylococcus Aureus (MRSA) Murine Sepsis Model. PLoS ONE. 2013; 8: e60463. DOI: 10.1371/journal.pone.0060463.

29. Gordon O, Dikeman DA, Ortines RV, Wang Y, Youn C, Mumtaz M, et al. The Novel Oxazolidinone TBI-223 Is Effective in Three Preclinical Mouse Models of Methicillin-Resistant Staphylococcus Aureus Infection. Microbiol Spect. 2022; 10: e02451-21, DOI: 10.1128/spectrum.02451-21.

30. Fujiki J, Nakamura T, Nakamura K, Nishida K, Amano Y, Watanabe Y, et al. Biological properties of Staphylococcus virus –SA012 for phage therapy. Scientific reports. 2022; 12 (1): 21297. Available from: https://doi.org/10.1038/s41598-022-25352-6.

31. Plumet L, Ahmad-Mansour N, Dunyach-Remy C, Kissa K, Sotto A, Lavigne J-P, et al. Bacteriophage Therapy for Staphylococcus Aureus Infections: A Review of Animal Models, Treatments, and Clinical Trials. Front Cell Infect Microbiol. 2022; 12: 907314. DOI: 10.3389/fcimb.2022.907314.

COMPLEX ANTIBACTERIAL ACTION OF ENZYMES ACTING ON *STAPHYLOCOCCUS AUREUS* BIOFILMS

Zagoskin AA[1], Avakova RA[1], Rezvykh LF[1], Zakharova MV[2], Mubarakshina EK[1], Ivanov RA[1], Nagornykh MO[1,2]✉

[1] Sirius University of Science and Technology, Sochi, Russia

[2] Institute of Biochemistry and Physiology of Microorganisms, Russian Academy of Sciences, Pushchino, Russia

The widespread use of antibiotics in medicine and agriculture has significantly accelerated the emergence rate of bacterial infections showing multiple antibiotic resistance. Since resistance to conventional antibiotics is developed rather quickly, designing alternative antimicrobial drugs with other mechanisms underlying their effects on bacteria is a promising. The enzymes possessing bactericidal activity may be one option for such antibacterial agents. The study aimed to produce the combination recombinant protein-based products active against bacteria and their biofilms. Soluble forms of five recombinant proteins were produced using the genetic engineering approaches. Two of these have a bacteriolytic effect (endolysins LysK and PM9 from the *Staphylococcus aureus* bacteriophages), the other are capable of disrupting extracellular DNA matrix in biofilms (two nonspecific nucleases NucA, as well as the DNA-specific deoxyribonuclease I). It has been shown that natural endolysin PM9 with the truncated catalytic domain shows 4 times lower bacteriolytic efficacy compared to the full-size LysK version. Comparative analysis revealed 1.5–2 timed higher efficacy of nonspecific nucleases in terms of bacterial biofilm disruption compared to the DNA-specific deoxyribonuclease I. It has been shown that simultaneous use of endolysins and nucleases has a synergistic antibacterial effect and disrupts biofilms of the pathogenic bacterium *Staphylococcus aureus*. The findings show the prospects of developing the recombinant protein-based antibacterial drugs.

Keywords: endolysin, nuclease, biofilms, *Staphylococcus aureus*

КОМПЛЕКСНОЕ АНТИБАКТЕРИАЛЬНОЕ ДЕЙСТВИЕ ФЕРМЕНТОВ НА БИОПЛЕНКИ *STAPHYLOCOCCUS AUREUS*

А. А. Загоскин[1], Р. А. Авакова[1], Л. Ф. Резвых[1], М. В. Захарова[2], Э. К. Мубаракшина[1], Р. А. Иванов[1], М. О. Нагорных[1,2]✉

[1] Научно-технологический университет «Сириус», Сочи, Россия

[2] Институт биохимии и физиологии микроорганизмов Российской академии наук, Пущино, Россия

Широкое использование антибиотиков в медицине и сельском хозяйстве значительно ускорило темпы возникновения бактерий со множественной устойчивостью к антибиотикам. Поскольку к традиционным антибиотикам довольно быстро возникает резистентность, одним из перспективных направлений является разработка альтернативных антимикробных препаратов, обладающих иными механизмами действия на бактерии. Ферменты с бактерицидным действием могут быть одним из вариантов таких антибактериальных средств. Целью работы было получить комбинированные препараты рекомбинантных белков, активных в отношении бактерий и их биопленок. С помощью подходов генной инженерии были получены растворимые формы пяти рекомбинантных белков. Два из них обладают бактериолитическим эффектом (эндолизины LysK и PM9 из бактериофагов *Staphylococcus aureus*), остальные способны разрушать внеклеточный ДНК-матрикс у биопленок (две неспецифические нуклеазы NucA, а также ДНК-специфичная дезоксирибонуклеаза I). Показано, что природный эндолизин PM9 с усеченным каталитическим доменом обладает меньшей в 4 раза бактериолитической эффективностью по сравнению с полноразмерным вариантом LysK. С помощью сравнительного анализа выявлена в 1,5–2 раза большая эффективность неспецифических нуклеаз для разрушения бактериальных биопленок по сравнению с ДНК-специфичной дезоксирибонуклеазой I. Продемонстрировано, что одновременное использование эндолизинов и нуклеаз оказывает синергичное антибактериальное действие и разрушает биопленки патогенной бактерии *Staphylococcus aureus*. Полученные результаты показывают перспективность разработки антибактериальных препаратов на основе рекомбинантных белков.

Ключевые слова: эндолизин, нуклеаза, биопленки, *Staphylococcus aureus*

Drug resistance of pathogenic bacteria is growing rapidly, turning into a global issue of the world's healthcare system. According to the last data of the World Health Organization, the number of antimicrobial drugs being at various stages of their development has increased from 80 (2021) to 97 (2023). However, there is the question about creating novel, innovative agents for treatment of infectious diseases caused by antibiotic-resistant strains, which might complement the existing antibiotics that lose their efficacy due to widespread use [1].

The drugs based on the enzymes possessing antibacterial activity represent one such option. Today, the lytic enzymes of bacteriophages (endolysins) that cause lysis of pathogenic bacteria and can be used as therapeutic molecules are well-known [2]. Endolysins are the enzymes encoded by the bacteriophage genomes and used by bacteriophages for lysis of bacterial cells during viral infection. Since all bacteria have bacteriophages, and bacteriophage diversity is great, their endolysins represent a very promising class of bacteriolytic enzymes. Currently, there is a large amount of scientific research and antibacterial drugs developed based on such enzymes that are through pre-clinical and clinical trials [3]. Endolysins as therapeutic substances often have a broader specificity spectrum, than phages, and their specificity is manifested at the genus or species level. The endolysins' selectivity for bacterial targets is due to the cell wall-binding domain, which recognizes and binds receptors, regardless of certain substrate in the cell wall of the target. Thus, the cell wall-binding domain (CBD-domain) located usually in the C-terminal part of the endolysin molecule is responsible for specific recognition and binding. That is why gram-negative lysins have a broader range of targets, while gram-positive ones often have a narrow host range [4]. The catalytic domain (CD-domain) is responsible for catalytic activity, and its activity can be further enhanced by the presence of amidase domain [5]. The fact that bacteria do not develop resistance and the possibility of influencing various chemical bonds within the cell wall represent one more advantage of bacteriolytic enzymes over conventional antibiotics. However, endolysins cannot effectively disrupt stable biofilms formed by many pathogenic bacteria, which is one of the major challenges of modern antibacterial therapy. Biofilms are complex extracellular structures stabilized by multiple bonds between organic molecules [6]. The enzymes that destroy biofilms also represent a promising class of antibacterial agents that differ in enzyme activity type depending on the target biofilm component [7]. In particular, matrix of extracellular DNA that can be destroyed by nucleases is typical for many bacterial biofilms. It has been earlier shown that deoxyribonuclease I possessed such activity [8]. In this regard, the search for and characterization of novel nucleases possessing antibacterial activity are relevant. The use of bacteriolytic enzymes and their combinations with the enzymes having a destructing effect on biofilms can make it possible to increase the effectiveness of bacterial infection therapy. For example, such cumulative effect has been reported for antibacterial activity against *Mycobacterium tuberculosis* [9]. The enzymes that disrupt bonds within biofilms can become a component of the combination antibacterial drug together with endolysins, having a synergistic antibacterial effect. That is why the development of such antibacterial drugs based on the recombinant proteins showing different catalytic activity is a promising area. Such drugs are most effective against gram-positive bacteria, in particular, methicillin-resistant Staphylococcus aureus (MRSA), the fight against which in clinical settings is a priority [10].

The study aimed to perform comparative analysis of antibacterial effects of several combinations of the enzymes possessing antibacterial activity or activity against bacterial biofilms.

METHODS

Constructing plasmids

All the plasmids used in this study were produced by restriction enzyme DNA cloning. DNA sequences of the endolysin genes and DNA nucleases were *de novo* synthesized; this involved codon optimization of nucleotide sequences for *E. coli* (IDT, https://www.idtdna.com/). The nucleotide sequences were taken from the PhaLP (www.phalp.org) and Uniprot (www.uniprot.org) databases. Amplification of all DNA sequences involving the use of the Pfu high-fidelity polymerase (Takara, USA) was performed in accordance with the manufacturer's protocol. The target genes were cloned into the pET21a vector (Novagen, UK), as well as into the set of vectors with auxiliary peptides [11] based on pET28a (Novagen, UK) at the NdeI and NotI restriction sites through the enzyme reaction involving two appropriate restriction endonucleases (SibEnzyme, Russia) for 1 h at 37 °C. After electrophoresis, DNA fragments were purified from agarose gel using the commercially available GeneJet Gel Extraction Kit (Thermo Scientific, USA). Then the purified DNA fragments were mixed and used in the ligation reaction with the T4 DNA ligase (NEB, USA) for 30 min at room temperature. After that the *E. coli* 10G competent cells (Lucigen, UK) were transformed by electroporation (Bio-Rad, USA) in accordance with the protocol of the device manufacturer. Plasmid DNA was extracted from the clones comprising the correct inserts, and correctness was confirmed by Sanger sequencing.

Recombinant protein production in *E. coli*

Proteins were produced in the following strains designed for recombinant protein production: *E. coli* BL21 (DE3) (Novagen, UK), *E. coli* Rosetta gami 2 (Novagen, UK), *E. coli* SHuffle T7express (NEB, USA). Thus, plasmids comprising the genes encoding nucleases or endolysins were used to transform the selected strain by the heat shock method, the transformation mixture (100 µL) was seeded in liquid LB medium contained in the test tubes (3–5 mL) with selective antibiotics. Incubation was performed for 12–14 h at 37 °C with mixing at 180 rpm. Then the culture grown was passaged at the ratio of 1 : 200 in the flasks containing appropriate amounts of the LB culture medium (100–500 mL) with selective antibiotics. The cell culture was grown to the optical density $OD_{600} = 0.5$–0.6 on the shaker at 180 rpm and 37 °C. After reaching the target optical density, the culture was cooled on ice for 10 min, supplemented the inducer to the final concentration of 1 mM IPTG, incubated at different temperatures (18 °C and 37 °C) with mixing at 180 rpm for 18 h (18 °C) or 6 h (37 °C). The bacterial cells were then precipitated by centrifugation for 20 min at 4000 g and 4 °C.

To assess solubility of the protein obtained, the cells precipitated were transferred to buffer A for destruction (50 mM Tris-HCl pH 7.5; 0.3 M NaCl; 0.005 M imidazole) and destructed using the Qsonica Q700 ultrasonic homogenizer (Qsonica, USA) until the cell suspension became clear on ice (ultrasonic pulses 3 s, cooling 6 s, 40 cycles). The destructed cells were precipitated by centrifugation (17,000 g) for 20 min at 4 C°. Then supernatant containing the soluble form of the target protein was sampled, and precipitate containing the aggregated form was dissolved in the 2M urea for further analysis by electrophoresis. Proteins were separated by PAGE (10%) electrophoresis under denaturing conditions by standard methods. After the One-Step Blue® staining (Biotium, USA) and washing off the dye, the gels were imaged, and the distribution of soluble and insoluble protein forms was quantified. Densitometry analysis of the gels was performed using the Image Lab application (Bio-Rad, USA).

Purification of proteins by affinity chromatography

After ultrasonic destruction of biomass and cell debris centrifugation, supernatant was filtered through the membrane

with the pore size of 0.22 μm. Thus the preparation for chromatographic purification was obtained that contained soluble protein fraction in buffer A (50 mM Tris-HCl pH 7.5; 0.3 M NaCl; 0.005 M imidazole) for application onto the IMAC chromatographic sorbent (Bio-Rad® Nuviatm IMAC Resin, USA). Protein was eluted with the chromatographic buffer B (50 mM Tris-HCl pH 7.5; 0.5 M imidazole). When necessary, the preparation obtained by purification involving the use of IMAC was concentrated using the Vivaspin® 500 centrifugal concentrator (Sartorius, Germany) (pore size 3.5 kDa) 30–50 times. If necessary, then the purified protein preparation was treated with the TEV protease in accordance with the manufacturer's instructions overnight at 4 °C; after that chromatographic purification was performed again, but the fraction not bound to sorbent, which contained purified endolysin, was collected. The resulting preparation was used to estimate antibacterial activity.

Testing of the resulting protein preparation antibacterial activity against *Staphylococcus aureus*

The *Staphylococcus aureus* colony was taken and put in 3–5 mL of liquid LB medium and incubated for 12–14 h at 37 °C with mixing at 180 rpm. Then 1 mL of the overnight culture was transferred to the test tube, centrifuged for 3 min at 4000 g; the cell sediment was resuspended in PBS; the procedure was repeated 3 times. The cells washed were diluted with PBS to 0.1 at OD_{600}; 100 μL of the diluted cells were placed in the 96-well plate and added 100 μL of the test protein or 100 μL of PBS in the positive control. The plate was incubated at room temperature for 30 min with constant mixing at 200 rpm. After incubation, the cells were 100-fold diluted with PBS, after which 100 μL of the resulting mixture were seeded on the agar plates without any antibiotic. The plates were incubated overnight at 37 °C. On the next day colonies were enumerated in the control plates and plates with test proteins; antibacterial activity was calculated using the following formula:

$$X = 100 - ((CFU \text{ of the sample} \times 100)/ CFU \text{ of the control}),$$

where X is antibacterial activity of the test protein in %; CFU of the sample is the number of colony-forming units per plate after incubation of cells with the test protein; CFU of the control is the number of plaque-forming units per plate untreated with the test protein.

To assess anti-biofilm activity of the test proteins, the *S. aureus* colony was placed in 3–5 mL of the liquid TBS medium (glucose free) and incubated for 12–14 h at 37 °C with mixing at 180 rpm. Then the overnight culture was diluted with TBS supplemented with 1% glucose to the value of 0.08 at OD_{600}. After that 200 μL of cell suspension were poured in the 96-well plate and incubated at 37 °C without mixing for 48 h. After incubation, the resulting biofilms were triple washed with PBS by pipetting. Thus planktonic cells were eliminated. Then biofilms were added 200 μL of each studied enzyme and incubated for 2 h at 37 °C without mixing. After incubation, the wells were triple washed with PBS by pipetting and dried for 5 min at room temperature. The remaining biofilms were stained by adding 200 μL of the 0.1% crystal violet and incubating for 15 min at room temperature. After staining, the cells were triple washed with PBS by pipetting again and dried for 45 min. Then these were added 200 μL of the 33% acetic acid and incubated for 10 min at room temperature. The analysis performed using the Multiskan SkyHigh system (Thermo Scientific, USA) involved optical density measurement at OD_{600}. The effectiveness of biofilm destruction was calculated relative to control.

RESULTS

Production of the enzyme-based combination antibacterial drugs is a promising method to combine different enzyme activities against bacterial pathogens in the same medicinal product. This makes it possible to not only increase the efficacy of antimicrobial activity, including against biofilms, but also reduce the drug dose. To produce single components of such drugs, it is necessary to produce homogenous protein preparations for each enzyme. In this study we produced different recombinant protein preparations and then tested their antibacterial activity against single *Staphylococcus aureus* cells and biofilms. The general scheme of the experimental study is provided in Fig. 1. The first phase of the study involved production of the genetic constructs encoding the following proteins: 1) endolysin LysK of the staphylococcal phage K; 2) not previously annotated endolysin PM9_074 of the staphylococcal phage PM9 with the truncated catalytic domain; 3) human deoxyribonuclease I (DNAse I); 4) nonspecific nuclease NucA1 from *Serratia marcescens*; 5) nonspecific nuclease NucA2 from *Anabaena sp.*

All the nucleotide sequences were codon optimized for expression in *Escherichia coli* and encoded the histidine tag at the N-terminus for further purification by affinity chromatography. After *de novo* synthesis of genes these were cloned into the pET21a plasmid vector for further expression of the genes encoding recombinant proteins. The genetic constructs obtained were used to transform cells of the *E. coli* BL21 (DE3) strain designed for recombinant protein production. After induction and incubation, we estimated the extent of target protein production in the soluble and insoluble forms. Protein production at 37 °C and 20 °C failed to yield positive results, since all the target enzymes formed insoluble aggregates (inclusion bodies). Replacement of the strain with two alternative ones (*E. coli Rosetta gami 2*, *E. coli SHuffle T7express*) yielded no positive results (Table 1).

That is why later is was decided to turn to production involving auxiliary polypeptides potentially increasing protein solubility and ensuring their correct folding in space in order to obtain soluble forms of proteins [12]. The nucleotide sequences encoding the selected endolysins and nucleases were cloned into a number of the earlier constructed vectors comprising various auxiliary polypeptides. We had earlier used this approach in practice to produce the homogenous ribonuclease inhibitor preparation in the soluble form [13]. The system represents the set of plasmids, each of which contains certain helper polypeptide and the TEV protease cleavage site at the N-terminus of the target gene nucleotide sequence. Production of chimeric protein using such vector increases the likelihood of obtaining the soluble protein preparation. The following auxiliary polypeptides were used in the system: MBP, GST, TIG, YrhB, PpiB, TRX, TSF, SUMO, FH8. Verification of recombinant protein production using this set of plasmids was also performed in the *E. coli* BL(DE3) strain at two temperatures, as earlier reported. Protein production at 37 °C, regardless of the presence of partner polypeptide, yielded mainly insoluble aggregates, in contrast to protein production at 18 °C, where certain auxiliary polypeptides considerably increased yield of the target protein soluble form (Fig. 2, Table 2).

Thus, the most productive "auxiliary polypeptide-target protein" combinations were obtained; we also managed to select appropriate production conditions that allowed us to produce target proteins in the soluble form. The highest yield of endolysins and nucleases was reported when using auxiliary polypeptides MBP and TIG (Table 2).

Then we assessed antibacterial activity of the enzymes obtained, as well as their ability to destroy the bacterial
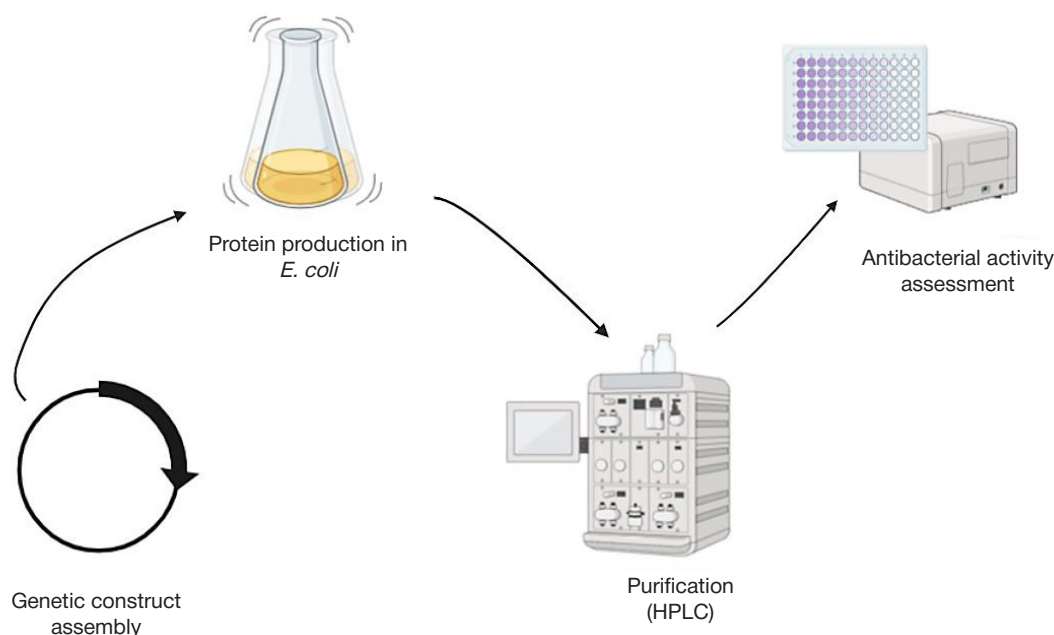
Fig. 1. Scheme of the experimental study involving production of enzybiotic drugs and testing their antibacterial activity

Staphylococcus aureus biofilms both in the form of monodrugs and in the form of enzyme activity combinations. First, we compared activity of two endolysins against bacterial cells (Fig. 3). The identical recognition domains of both endolysins allow one to compare catalytic activity of these molecules in the direct experiment. The findings demonstrate that both enzymes possess antibacterial activity and can cause lysis of the Staphylococcus aureus cells, but endolysin of bacteriophage PM9 with the truncated catalytic domain yet shows lower activity (almost four times lower relative to endolysin LysK). Presumably, such variants are less evolutionarily advantageous for viruses, so their number in the genome is significantly lower compared to the number of full-size endolysin genes. It is possible that the genes encoding such molecules represent "evolutionary waste" in bacteriophage genomes, but their exact biological role is poorly understood. These data suggest that it is reasonable to select endolysins with the full-fledged catalytic

domain (or several molecules with the catalytic domains showing different specificity) to create effective antibacterial drugs.

In the next phase we tested three nucleases obtained for the ability to disrupt *Staphylococcus aureus* biofilms via destruction of the matrix consisting of extracellular DNA. It was earlier shown that deoxyribonuclease I could destroy bacterial biofilms [8], however, no such research was conducted for nonspecific nucleases. All three nucleases, we have isolated in the form of recombinant protein preparations, specifically human deoxyribonuclease I, nonspecific nuclease NucA1 from *Serratia marcescens*, and nonspecific nuclease NucA2 from *Anabaena sp.,* can degrade bacterial biofilms (Fig. 4). The results obtained show that both nonspecific nucleases show higher biofilm destruction effectiveness, which can be due to their mechanism of action. Their higher nuclease activity has led to broader use of nonspecific nucleases for solving scientific and biotechnology tasks, specifically for the

Table 1. Estimation of the recombinant endolysin and nuclease production in *E. coli* strains

Temperatures of protein biosynthesis	*Escherichia coli* BL21 (*DE3*)	*Escherichia coli* Rosetta gami 2	*Escherichia coli* SHuffle T7express
pET21-LysK			
37 °C (6 h)	I	I	I
18 °C (16–18 h)	I	I	S+
pET21-PM9			
37 °C (6 h)	I	I	I
18 °C (16–18 h)	I	S+	S+
pET21-DnaseI			
37 °C (6 h)	I	I	I
18 °C (16–18 h)	I	I	I
pET21-NucA1			
37 °C (6 h)	I	I	I
18 °C (16–18 h)	I	I	I
pET21-NucA2			
37 °C (6 h)	I	I	I
18 °C (16–18 h)	I	I	S+

Note: S — soluble, I — insoluble, "+" — extent of soluble protein production.
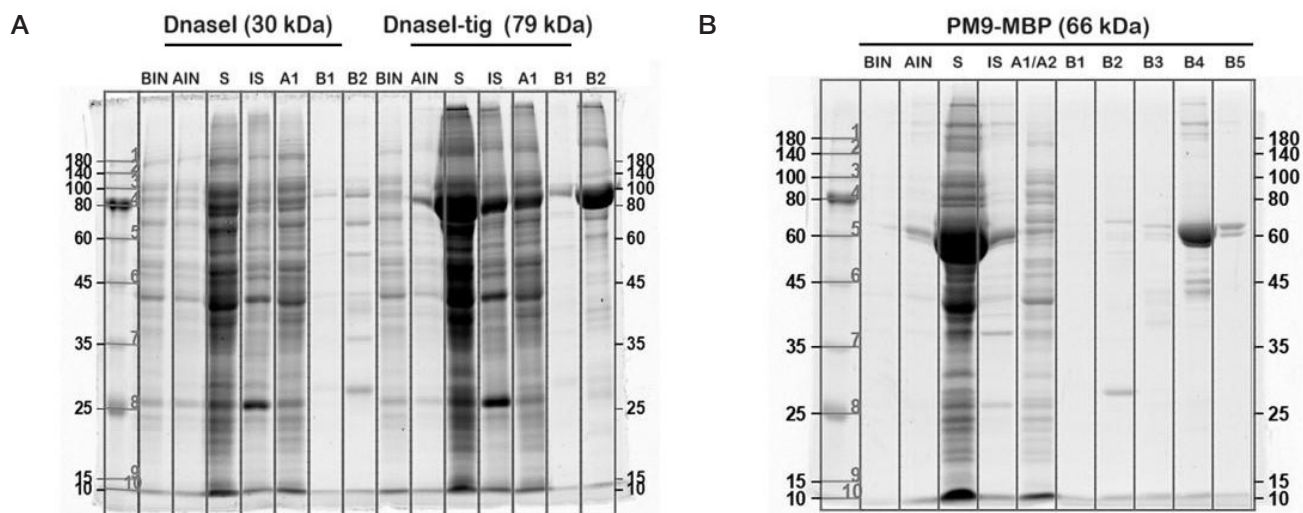
Fig. 2. Strategy of obtaining recombinant proteins prone to aggregation via production in the form of the chimeric molecule, in which there is an auxiliary polypeptide increasing the target protein solubility at the N-terminus. In particular, PAGE electropherogram demonstrates the examples of the TIG auxiliary polypeptide effects on the DNAse I solubility **(A)** and MBP auxiliary polypeptide effects on the endilysin PM9 solubility **(B)**

development of the commercially available *Benzonase* drug by *Merck*. Thus, nonspecific nucleases can be appropriate for the creation of antibacterial drugs capable of destroying bacterial biofilms. That is why it is reasonable to focus on the physical and chemical properties of such enzymes, as well as on the results of pre-clinical trials during further development of the combination antibacterial drug. Despite the fact that the DNAse I enzyme shows lower activity, the advantage is its origin, which potentially minimizes the drug immunogenicity. It should be also noted that there are already commercially available drugs based on this recombinant enzyme (Dornase Alfa and analogues), which are used for treatment.

The last fundamental objective of this study was to test the antibacterial activity effectiveness of the combination drug combining at least two different catalytic activities against the *Staphylococcus aureus* biofilms. Thus, we planned to test various combinations of two endolysin molecules and three nucleases. In our situation the best results were reported for the combinations of full-size endolysin LysK and nucleases, which can be explained by higher lytic activity of this enzyme compared

to endolysin PM9 with the truncated catalytic domain (Fig. 4). All three nucleases used were active in the combination drug, but the best results were shown by nonspecific nucleases. This was possibly due to experimental conditions, and DNAse I could show comparable efficacy in case of optimal reaction buffer selection. However, the difference in the enzyme activity mechanisms can play a major role during practical use of drugs. Thus, nonspecific nucleases can be used in the recombinant protein-based combination drugs or can potentiate the effects of antibiotics on bacterial biofilms.

Summarizing the findings, we selected conditions for production and chromatographic purification of two endolysins (LysK and PM9) possessing activity against *Staphylococcus aureus*, as well as of three nucleases (NucA1, NucA2, and DNAse I) capable of destroying the bacterial biofilm DNA matrix. For that we used a screening approach to production of enzymes in combination with helper polypeptides. Then we demonstrated antibacterial activity of these enzymes, as well as their complex activity against the *Staphylococcus aureus* biofilms.

Table 2. Estimation of the recombinant endolysin and nuclease production in *E. coli* strains

Temperatures of protein biosynthesis	Protein solubility degree	Yield of protein after purification (mg/L)
pET28MBP-LysK		
37 °C (6 h)	I	
18 °C (16–18 h)	S+	2.55
pET28MBP-PM9		
37 °C (6 h)	I	
18 °C (16–18 h)	S++	4.95
pET28TIG-DnaseI		
37 °C (6 h)	I	
18 °C (16–18 h)	S+++	7.4
pET28MBP-NucA1		
37 °C (6 h)	I	
18 °C (16–18 h)	S+++	6.7
pET28TIG-NucA2		
37 °C (6 h)	I	
18 °C (16–18 h)	S++	4.8

Note: S — soluble, I — insoluble, "+" — extent of soluble protein production.
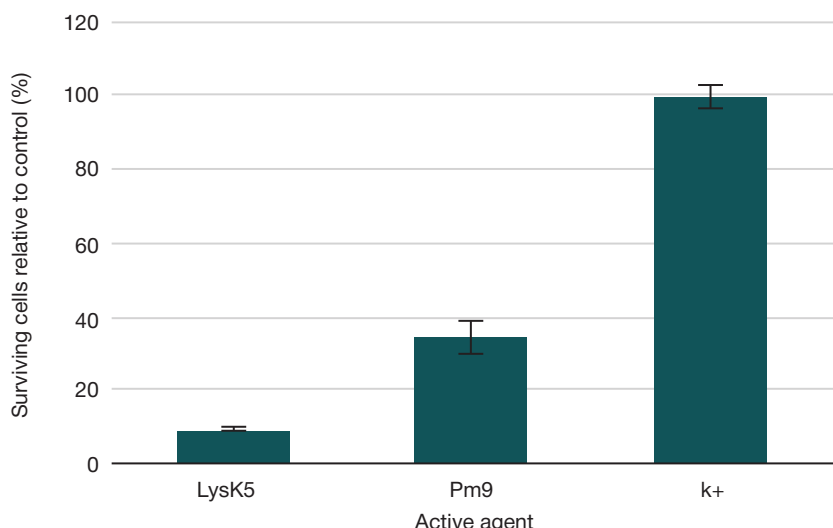
Fig. 3. Catalytic activity of two endolysins against the *Staphylococcus aureus* bacterial cell wall. Both recombinant enzymes possess antibacterial activity disrupting the cell wall. Endolysin LysK having a full-fledged catalytic domain possess significantly higher antibacterial activity against the gram-positive *Staphylococcus aureus* pathogen compared to endolysin PM9 having a truncated catalytic domain

DISCUSSION

The current antibiotic-resistance crisis caused by the widespread use of antibiotics in medicine and agriculture makes it necessary to seek for alternative therapeutic agents to fight against pathogenic bacteria. Such drugs might be used to support therapy with conventional antibiotics or as monotherapy, precluding the use of antibiotics in certain cases. Developing antibacterial drugs based on the recombinant proteins possessing bacteriolytic activity is a promising area [14]. The most interesting are endolysins, the bacteriolytic proteins used by bacteriophages to lyse infected bacterial cells during viral infection. Endolysins have a modular structure and usually comprise two or three domains responsible for recognition of certain bacteria, as well as for catalytic activity against the cell wall components. To date, these molecules are rather well understood; attempts are made to develop antimicrobial drugs, enzybiotics, based on these molecules [14]. As genomes of bacteriophages are discovered and described, the data on the uncharacterized viral proteins, including endolysins, are accumulated. Some of these endolysins have truncated catalytic domains, but biological meaning of this phenomenon is poorly understood. In this study we compared two endolysins encoded by two *Staphylococcus aureus* bacteriophages, K and PM9. One of these is well-known, it has a full-fledged three-domain structure, including catalytic domains (peptidase

and amidase), as well as the recognition domain [15], while the second represents an uncharacterized endolysin with the significantly truncated catalytic domain and the binding domain with the identical sequence. When produced in the *E. coli* heterologous system, both endolysins aggregate and form the inclusion bodies. To obtain functional preparations of such proteins possessing activity, we used a methodological approach, in which solubility of the target recombinant protein is ensured by auxiliary polypeptide located at the N-terminus of the chimeric protein molecule (Fig. 2, Table 2). After successful production of chimeric molecules in the soluble form, the auxiliary peptide was cleaved using the TEV protease, and the proteins were used to conduct tests for antimicrobial activity against the *Staphylococcus aureus* cells. Our findings suggest that the phage PM9 endolysin with the truncated catalytic domain exerts significantly lower activity against the *Staphylococcus aureus* cells (Fig. 3). Furthermore, both endolysins have the recognition domains that are completely identical based on the amino acid compositions, which balances the differences when the molecules bind to receptors of bacterial cells. The use of such enzymes is unjustified due to low activity, regardless of their greater compactness and some beneficial differences in physical and chemical properties from full-size molecules. That is why it is necessary to select variants with full-size domains for the development of endolysin-based
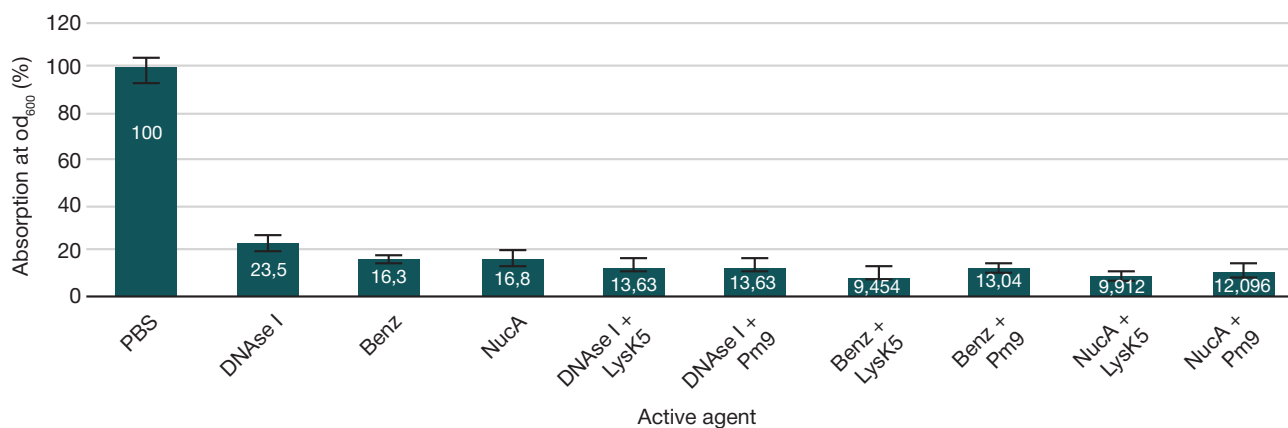
Fig. 4. Destruction of the *Staphylococcus aureus* bacterial biofilms with the recombinant nuclease drugs and the combination drugs combining different catalytic activities (endolysin + nuclease). Nonspecific nucleases show higher activity in terms of bacterial biofilm disruption compared to DNAse I. Combining the enzymes showing different specificity in the same drug enhances antibacterial effects

drugs. Research and development in the field of combinatorial engineering of endolysins show the potential of such proteins used as antibacterial agents [4, 14]. Endolysins with the full-fledged catalytic domain predictably possess higher antibacterial activity compared to variants with the truncated catalytic domain. Furthermore, the binding domain of such truncated endolysin variants is fully functional, which targets these molecules towards cellular receptors of bacteria during infection, but biological role of this phenomenon is poorly understood. It can be assumed that such forms of endolysin molecules represent either evolutionarily transitional variants, or rudimentary enzymes, on which the life cycle of the virus no longer depends very much, but they are preserved in the viral genome.

However, it should be noted that antibacterial activity of endolysins against bacterial biofilms that are often formed by pathogenic bacteria is limited. Since the structure of bacterial biofilms is stabilized by extracellular matrix consisting of various bioorganic molecules, the bonds between molecules represent a potential target for biofilm destruction [6]. Extracellular DNA forming sustainable structures that stabilize biofilms represents one component of such biofilm matrix [16, 17]. It has been earlier shown that catalytic activity of deoxyribonuclease I (DNAse I), hydrolyzing phosphodiester bonds between the nucleic acid subunits, can ensure disruption of bacterial biofilms formed in the presence of infection [8]. We decided to test two more nucleases possessing nonspecific activity against DNA and RNA (nuclease NucA from the bacterium *Serratia marcescens* and nuclease NucA from *Anabaena sp.*) for similar activity and compare their efficacy with that of human DNAse I. For that we produced all three nucleases in the form of homogenous protein preparations; since these proteins also aggregate when produced in *E. coli*, we conducted screening and selected appropriate auxiliary proteins for production of nucleases in the soluble form (Fig. 2, Table 2). The proteins isolated show activity against the *Staphylococcus aureus* biofilms, and both nonspecific nucleases, NucA1 from *Serratia marcescens* and NucA2 from *Anabaena sp.*, show the highest activity among three in the biofilm destruction test (Fig. 4). Thus, any nucleases could potentially be used to develop antibacterial drugs; in this case, it is possible to focus on more suitable physical and chemical properties of enzymes and the safety profile based on the results of preclinical trials. Perhaps, human DNAse I is preferable in such preparation, despite its lower catalytic activity, because the immune response to it would be negligible, in contrast to foreign recombinant proteins. Moreover, there are already commercially available drugs based on this enzyme to alleviate the symptoms of cystic fibrosis, as well as bacterial complications of viral infections [18].

Combining two (or more) catalytic activities in the same antibacterial drug makes it possible to target different bacterial biofilm structures during infection [19]. Thus, the enzymes destroying extracellular structural components of biofilms can provide access to the internal layers of bacterial cells for bacteriolytic enzymes and improve the efficacy of their activity against distinct bacterial cells [9]. Then we tried to combine endolysins with the nucleases obtained in our study. We assessed the effects of these combination drugs on the *Staphylococcus aureus* biofilms and estimated their lytic activity against cells of this gram-positive bacterial pathogen. The predictably best results in case of joint action were yielded by the pairs, were endolysin LysK functioned in combination with one of three nucleases (Fig. 4). The combinations of endolysin with the truncated catalytic domain and nucleases did not yield such good results, which was predictable based on testing antimicrobial activity of this endolysin against the *Staphylococcus aureus* cells (Fig. 3). It can be concluded that the use of two (or more) catalytic activities ensured by different enzymes in the same antibacterial drug is promising for treatment of bacterial infections complicated by biofilm formation. It seems feasible to use nucleases (both nonspecific and DNA-specific) in such drugs, since their activity significantly degrades bacterial biofilms, ensuring potentiating effect of antibacterial activity of both endolysins and conventional antibiotics.

CONCLUSIONS

The findings demonstrate the possibility of producing the combination antibacterial enzyme drugs based on the bacteriophage endolytic enzymes and the enzymes that degrade bacterial biofilms. We have shown that endolysin PM9 with the truncated catalytic domain exerts lower bacteriolytic activity compared to endolysin LysK with the full-fledged catalytic domain, while nonspecific nucleases possess higher destructive activity against bacterial biofilms. We have also conducted comparative analysis of efficacy of the activity of several enzyme combinations against the *Staphylococcus aureus* bacteria and their biofilms. The results show synergistic antimicrobial effect of the purified preparations of recombinant endolysins LysK and PM9, as well as of nonspecific (NucA1 and NucA2) and DNA-specific (DNAse I) nucleases. In the future, this approach to engineering combination drugs that combine two or three different types of catalytic activity will help to produce therapeutic agents with enhanced antibacterial properties against multidrug-resistant microorganisms that are prone to biofilm formation during infections.

References

1. Naghavi Mohsen, et al. Global burden of bacterial antimicrobial resistance 1990–2021: a systematic analysis with forecasts to 2050. The Lancet. 2024; 404 (10459), 1199–226.

2. Liu H, Hu Z, Li M, et al. Therapeutic potential of bacteriophage endolysins for infections caused by Gram-positive bacteria. J Biomed Sci. 2023; 30, 29. DOI:10.1186/s12929-023-00919-1.

3. Haddad Kashani H, Schmelcher M, Sabzalipoor H, Seyed Hosseini E, Moniri R. Recombinant Endolysins as Potential Therapeutics against Antibiotic-Resistant Staphylococcus aureus: Current Status of Research and Novel Delivery Strategies. Clin Microbiol Rev. 2018; 31: Available from: 10.1128/cmr.00071-17.https://doi.org/10.1128/cmr.00071-17

4. Wang Y, Wang X, Liu X, Lin B. Research Progress on Strategies for Improving the Enzyme Properties of Bacteriophage Endolysins. J Microbiol Biotechnol. 2024; 34: 1189–96. Available from: https://doi.org/10.4014/jmb.2312.12050.

5. Abdelrahman F, Easwaran M, Daramola OI, Ragab S, Lynch S, Oduselu TJ, et al. Phage-Encoded Endolysins. Antibiotics (Basel). 2021; 10 (2): 124. DOI: 10.3390/antibiotics10020124. PMID: 33525684; PMCID: PMC7912344.

6. Sauer K, Stoodley P, Goeres DM, et al. The biofilm life cycle: expanding the conceptual model of biofilm formation. Nat Rev Microbiol. 2022; 20: 608–620. Available from: https://doi.org/10.1038/s41579-022-00767-0.

7. Wang S, Zhao Y, Breslawec AP, et al. Strategy to combat biofilms: a focus on biofilm dispersal enzymes. npj Biofilms Microbiomes. 2023; 9: 63 Available from: https://doi.org/10.1038/s41522-023-00427-y.

8. Kaplan JB, LoVetri K, Cardona ST, Madhyastha S, Sadovskaya I, Jabbouri S, et al. Recombinant human DNase I decreases biofilm and increases antimicrobial susceptibility in staphylococci. J Antibiot (Tokyo). 2012; 65 (2): 73–7. DOI: 10.1038/ja.2011.113. Epub 2011 Dec 14. PMID: 22167157; PMCID: PMC3288126.

9. Bartlett HP, Dawson CC, Glickman CM, Osborn DW, Evans CR, Garcia BJ, et al. Targeting intracellular nontuberculous mycobacteria and M. tuberculosis with a bactericidal enzymatic cocktail. Microbiol Spectr. 2024; 12 (5): e0353423. DOI: 10.1128/spectrum.03534-23. Epub 2024 Mar 27. PMID: 38534149; PMCID: PMC11064574.

10. Howden BP, Giulieri SG, Wong Fok Lung T, et al. Staphylococcus aureus host interactions and adaptation. Nat Rev Microbiol. 2023; 21: 380–395. Available from: https://doi.org/10.1038/s41579-023-00852-y.

11. Zakharova MV, Mubarakshina EK, Nagornykh MO. Construction of Expression Vectors for Efficient Production of Recombinant Proteins in E. coli for the Development of Therapeutic Drugs. Biochem. Moscow Suppl. Ser. B. 2024; 18: 254–62. Available from: https://doi.org/10.1134/S1990750823600516.

12. Costa S, Almeida A, Castro A, Domingues L. Fusion tags for protein solubility, purification and immunogenicity in Escherichia coli: the novel Fh8 system. Front Microbiol. 2014; 5: 63. DOI: 10.3389/fmicb.2014.00063. PMID: 24600443; PMCID: PMC3928792.

13. Zakharova MV, Zagoskin AA, Ivanov RA, Nagornykh MO. Preparation of a recombinant ribonuclease inhibitor in E. coli for use in mRNA synthesis in vitro. Bulletin of RSMU. 2023; (6): 34–41. DOI: 10.24075/brsmu.2023.058.

14. Murray E, Draper LA, Ross RP, Hill C. The Advantages and Challenges of Using Endolysins in a Clinical Setting. Viruses. 2021; 13 (4): 680. DOI: 10.3390/v13040680. PMID: 33920965; PMCID: PMC8071259.

15. O'Flaherty S, Coffey A, Meaney W, Fitzgerald GF, Ross RP. The recombinant phage lysin LysK has a broad spectrum of lytic activity against clinically relevant staphylococci, including methicillin-resistant Staphylococcus aureus. J Bacteriol. 2005; 187 (20): 7161–4. DOI: 10.1128/JB.187.20.7161-7164.2005. PMID: 16199588; PMCID: PMC1251611.

16. Flemming HC, Wingender J. The biofilm matrix. Nat Rev Microbiol. 2010; 8: 623–33. Available from: https://doi.org/10.1038/nrmicro2415.

17. Karygianni L, Ren Z, Koo H, Thurnheer T. Biofilm Matrixome: Extracellular Components in Structured Microbial Communities. Trends Microbiol. 2020; 28 (8): 668–81. DOI: 10.1016/j.tim.2020.03.016. Epub 2020 Apr 21. PMID: 32663461.

18. Gustafson AM, Larrain CM, Friedman LR, Repkorwich R, Anidi IU, Forrest KM, et al. Novel management of pseudomonas biofilm-like structure in a post-pneumonectomy empyema. Front Cell Infect Microbiol. 2024; 14: 1458652. DOI: 10.3389/fcimb.2024.1458652. PMID: 39483118; PMCID: PMC11525003.

19. Quan Lin, Maokun Sheng, Yanjun Tian, Bing Li, Zhaodi Kang, Yingying Yang, et al. Antibiofilm activity and synergistic effects of DNase I and lysostaphin against Staphylococcus aureus biofilms. Food Quality and Safety. 2024; 8: fyae024. Available from: https://doi.org/10.1093/fqsafe/fyae024.

Литература

1. Naghavi Mohsen, et al. Global burden of bacterial antimicrobial resistance 1990–2021: a systematic analysis with forecasts to 2050. The Lancet. 2024; 404 (10459), 1199–226.

2. Liu H, Hu Z, Li M, et al. Therapeutic potential of bacteriophage endolysins for infections caused by Gram-positive bacteria. J Biomed Sci. 2023; 30, 29. DOI:10.1186/s12929-023-00919-1.

3. Haddad Kashani H, Schmelcher M, Sabzalipoor H, Seyed Hosseini E, Moniri R. Recombinant Endolysins as Potential Therapeutics against Antibiotic-Resistant Staphylococcus aureus: Current Status of Research and Novel Delivery Strategies. Clin Microbiol Rev. 2018; 31: Available from: 10.1128/cmr.00071-17.https://doi.org/10.1128/cmr.00071-17

4. Wang Y, Wang X, Liu X, Lin B. Research Progress on Strategies for Improving the Enzyme Properties of Bacteriophage Endolysins. J Microbiol Biotechnol. 2024; 34: 1189–96. Available from: https://doi.org/10.4014/jmb.2312.12050.

5. Abdelrahman F, Easwaran M, Daramola OI, Ragab S, Lynch S, Oduselu TJ, et al. Phage-Encoded Endolysins. Antibiotics (Basel). 2021; 10 (2): 124. DOI: 10.3390/antibiotics10020124. PMID: 33525684; PMCID: PMC7912344.

6. Sauer K, Stoodley P, Goeres DM, et al. The biofilm life cycle: expanding the conceptual model of biofilm formation. Nat Rev Microbiol. 2022; 20: 608–620. Available from: https://doi.org/10.1038/s41579-022-00767-0.

7. Wang S, Zhao Y, Breslawec AP, et al. Strategy to combat biofilms: a focus on biofilm dispersal enzymes. npj Biofilms Microbiomes. 2023; 9: 63 Available from: https://doi.org/10.1038/s41522-023-00427-y.

8. Kaplan JB, LoVetri K, Cardona ST, Madhyastha S, Sadovskaya I, Jabbouri S, et al. Recombinant human DNase I decreases biofilm and increases antimicrobial susceptibility in staphylococci. J Antibiot (Tokyo). 2012; 65 (2): 73–7. DOI: 10.1038/ja.2011.113. Epub 2011 Dec 14. PMID: 22167157; PMCID: PMC3288126.

9. Bartlett HP, Dawson CC, Glickman CM, Osborn DW, Evans CR, Garcia BJ, et al. Targeting intracellular nontuberculous mycobacteria and M. tuberculosis with a bactericidal enzymatic cocktail. Microbiol Spectr. 2024; 12 (5): e0353423. DOI: 10.1128/spectrum.03534-23. Epub 2024 Mar 27. PMID: 38534149; PMCID: PMC11064574.

10. Howden BP, Giulieri SG, Wong Fok Lung T, et al. Staphylococcus aureus host interactions and adaptation. Nat Rev Microbiol. 2023; 21: 380–395. Available from: https://doi.org/10.1038/s41579-023-00852-y.

11. Zakharova MV, Mubarakshina EK, Nagornykh MO. Construction of Expression Vectors for Efficient Production of Recombinant Proteins in E. coli for the Development of Therapeutic Drugs. Biochem. Moscow Suppl. Ser. B. 2024; 18: 254–62. Available from: https://doi.org/10.1134/S1990750823600516.

12. Costa S, Almeida A, Castro A, Domingues L. Fusion tags for protein solubility, purification and immunogenicity in Escherichia coli: the novel Fh8 system. Front Microbiol. 2014; 5: 63. DOI: 10.3389/fmicb.2014.00063. PMID: 24600443; PMCID: PMC3928792.

13. Захарова М. В., Загоскин А. А., Иванов Р. А., Нагорных М. О. Получение рекомбинантного ингибитора рибонуклеаз в E. coli для использования в синтезе мРНК in vitro. Вестник РГМУ. 2023; (6): 36–44. DOI: 10.24075/vrgmu.2023.058.

14. Murray E, Draper LA, Ross RP, Hill C. The Advantages and Challenges of Using Endolysins in a Clinical Setting. Viruses. 2021; 13 (4): 680. DOI: 10.3390/v13040680. PMID: 33920965; PMCID: PMC8071259.

15. O'Flaherty S, Coffey A, Meaney W, Fitzgerald GF, Ross RP. The recombinant phage lysin LysK has a broad spectrum of lytic activity against clinically relevant staphylococci, including methicillin-resistant Staphylococcus aureus. J Bacteriol. 2005; 187 (20): 7161–4. DOI: 10.1128/JB.187.20.7161-7164.2005. PMID: 16199588; PMCID: PMC1251611.

16. Flemming HC, Wingender J. The biofilm matrix. Nat Rev Microbiol. 2010; 8: 623–33. Available from: https://doi.org/10.1038/nrmicro2415.

17. Karygianni L, Ren Z, Koo H, Thurnheer T. Biofilm Matrixome: Extracellular Components in Structured Microbial Communities. Trends Microbiol. 2020; 28 (8): 668–81. DOI: 10.1016/j.tim.2020.03.016. Epub 2020 Apr 21. PMID: 32663461.

18. Gustafson AM, Larrain CM, Friedman LR, Repkorwich R, Anidi IU, Forrest KM, et al. Novel management of pseudomonas biofilm-like structure in a post-pneumonectomy empyema. Front Cell Infect Microbiol. 2024; 14: 1458652. DOI: 10.3389/fcimb.2024.1458652. PMID: 39483118; PMCID: PMC11525003.

19. Quan Lin, Maokun Sheng, Yanjun Tian, Bing Li, Zhaodi Kang, Yingying Yang, et al. Antibiofilm activity and synergistic effects of DNase I and lysostaphin against Staphylococcus aureus biofilms. Food Quality and Safety. 2024; 8: fyae024. Available from: https://doi.org/10.1093/fqsafe/fyae024.

COMPARATIVE ANALYSIS OF THE RESULTS OF TESTING CERVICAL EPITHELIAL SAMPLES AND CERVICAL BIOPSY SPECIMENS FOR HPV

Bayramova GR ✉, Trofimov DYu, Andreev AO, Bourmenskaya OV, Asaturova AV, Piven VD

Kulakov National Medical Research Center for Obstetrics, Gynecology and Perinatology, Moscow, Russia

Currently, testing for human papillomavirus (HPV) DNA is more and more often used as a primary diagnosis method when conducting screening for cervical cancer. However, HPV genotypes reported when assessing cervical smears can differ from the results of testing cervical biopsy specimens. The study aimed to assess the features of detecting HPV DNA in the paired cervical canal epithelium samples and cervical biopsy specimens. HPV-positive patients (n = 99) underwent targeted cervical biopsy. The HPV DNA was detected 175 times in biomaterial obtained from the cervical canal and 111 times in histologic blocks. In the group of patients with chronic cervicitis, the rate of HPV DNA testing results match was 28.3%, in the group with LSIL it was 45%, and in the group with HSIL it was 67.7%. When the HPV viral load was low, the results were matched in 27.1% of cases, when the viral load was moderate in 35.4%, and when the viral load was high these were matched in 82.3% of cases. We revealed a relatively strong correlation between the viral load and the probability of the HPV test results match: the percentage of HPV DNA test results match between paired samples increases by 9.3% with the increase in the HPV viral load by 1 lg.

✉ **Correspondence should be addressed:** Gyuldana R. Bayramova
Akademika Oparina, 4B, Moscow, 117513, Russia; bayramova@mail.ru

СРАВНИТЕЛЬНЫЙ АНАЛИЗ РЕЗУЛЬТАТОВ ВПЧ-ТЕСТИРОВАНИЯ В ОБРАЗЦАХ ЦЕРВИКАЛЬНОГО ЭПИТЕЛИЯ И БИОПСИЙНОГО МАТЕРИАЛА ШЕЙКИ МАТКИ

Г. Р. Байрамова ✉, Д. Ю. Трофимов, А. О. Андреев, О. В. Бурменская, А. В. Асатурова, В. Д. Пивень

Национальный медицинский исследовательский центр акушерства, гинекологии и перинатологии имени В. И. Кулакова, Москва, Россия

В настоящее время при проведении скрининга на рак шейки матки в качестве первичного метода диагностики все чаще применяют тестирование на ДНК ВПЧ. Однако генотипы вируса папилломы человека (ВПЧ), регистрируемые при исследовании цервикальных мазков, могут отличаться от результатов тестирования в биоптированных фрагментах шейки матки. Целью исследования было изучить особенности детекции ДНК ВПЧ парных образцов эпителия цервикального канала и биопсийного материала шейки матки. ВПЧ-позитивным пациенткам (n = 99) была выполнена прицельная биопсия шейки матки. Регистрация ДНК ВПЧ произошла 175 раз в биоматериале, полученном из цервикального канала, и 111 раз в гистологических блоках. В группе пациенток с хроническим цервицитом показатель совпадения результатов тестирования на ДНК ВПЧ составил 28,3%, для группы с LSIL — 45%, для группы с HSIL — 67,7%. При низкой вирусной нагрузке ВПЧ соответствие результатов наблюдалось в 27,1% случаев, при умеренной вирусной нагрузке — в 35,4%, при высокой вирусной нагрузке — в 82,3%. Обнаружена относительно сильная корреляционная связь между уровнем вирусной нагрузки и вероятностью совпадения результатов ВПЧ-тестирования: при увеличении уровня вирусной нагрузки ВПЧ на 1 lg наблюдается увеличение процента соответствия результатов тестирования на ДНК ВПЧ между парными образцами на 9,3%.

✉ **Для корреспонденции:** Гюльдана Рауфовна Байрамова
ул. Академика Опарина, д. 4Б, г. Москва, 117513, Россия; bayramova@mail.ru

Cervical cancer (CC) is the second most common tumor found in women of reproductive age [1]. Human papillomavirus (HPV) was proven be a mandatory prerequisite for most malignant neoplasms (MN) of the cervix [2, 3]. In recent years, most countries have changed the paradigm of national CC screening programs and chose HPV testing over cytological examination as a more sensitive method. Up to 90% of HPV infections are transient: the virus self-eliminates within 1–2 years [3, 4]. However, in 10% of cases, it persists, and sometimes cause development of a tumor [5, 6]. The global prevalence of HPV varies from 43% to 72.8% [7, 8]. In the USA alone, more than 14 million new cases of HPV infection are registered every year [9]. It should be noted that the development CC is preceded by squamous intraepithelial lesions of the cervix. Among HPV-positive women, low-grade squamous intraepithelial lesions of the cervix (LSIL) occur in 11.5% of cases, while 10.3% of them suffer from high-grade squamous intraepithelial lesions (HSIL) [10].

Currently, the detection of DNA of HPV directly in the affected cervical tissue is perceived as an important marker of viral activity that is fundamentally important for the prognosis of the likelihood of development of precancerous and cancerous lesions of the cervix [11–13]. The detection of HPV in a histological sample is a reliable sign of the level of contamination because the said sample originates from the affected part of the tissue, where the registered virus of a certain genotype and in a certain amount acts as the etiological cause of the pathological process. However, there is still no accurate understanding of the difference between finding DNA of HPV in a cervical smear and in a cervical biopsy.

This study aimed to investigate the specifics and patterns peculiar to the detection of DNA of HPV in the paired cervical canal smears and cervix histological samples.

METHODS

For this cross-sectional study, we used the biological material from 99 HPV-positive patients who sought cervical pathology diagnosing at the Scientific Outpatient Department of the V. I. Kulakov National Medical Research Center for Obstetrics,

Gynecology and Perinatology from January to December 2023. In the context of the comparative analysis aimed at learning the diagnostic value of detecting HPV DNA, the genotype of the virus was identified in a pair of samples taken from each participant, one being the secretions of the cervical canal, another — cervix biopsy (colposcopy-guided). All patients were divided into three groups depending on the histological verification of the diagnosis:

1) Group 1 — diagnosed with LSIL (*n* = 34);
2) Group 2 — diagnosed with HSIL (*n* = 31);
3) Group 3 — diagnosed with chronic cervicitis (*n* = 34) (control group).

The inclusion criteria were: age 18–65 years; HPV-positive status confirmed by the cervical canal secretion test; LSIL, HSIL, chronic cervicitis confirmed by the histopathological examination of the cervix biopsy.

The exclusion criteria were: pregnancy, lactation; malignant neoplasms of the cervix; non-specific inflammatory diseases at the decompensation stage.

In the context of this single-stage cross-sectional study, all patients underwent the following:

1) medical history taking, clinical examination (general and bimanual examinations);
2) real-time PCR testing for DNA of HPV using a diagnostic panel with 21 HPV genotypes (6, 11, 16, 18, 26, 31, 33, 35, 39, 44, 45, 51, 52, 53, 56, 58, 59, 66, 68, 73, 82);
3) extended colposcopy to visualize a potentially pathological area of the cervical epithelium for subsequent targeted cervical biopsy;
4) cytological examination (liquid-based cytology);
5) colposcopy-guided cervical biopsy followed by histological verification of the diagnosis;
6) identification of DNA of HPV, its genotyping and assessment of the viral load by real-time PCR (in histological samples).

For the real-time PCR test for DNA of HPV, we used an array designed to detect 21 genotypes of HPV. The materials for the test were cervical canal secretion samples and cervix bioptates harvested under CT guidance. The bioptates were fixed in neutral buffered formalin (pH = 7.0) for 24 hours. After
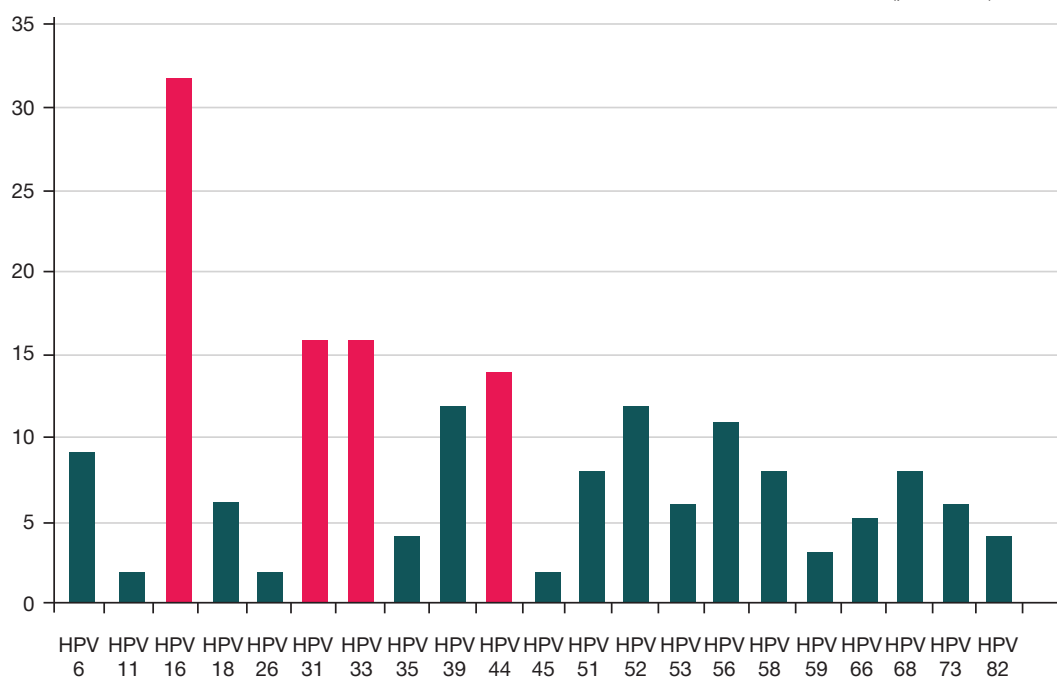
Fig. 1. Distribution of HPV genotypes in cervical canal smears
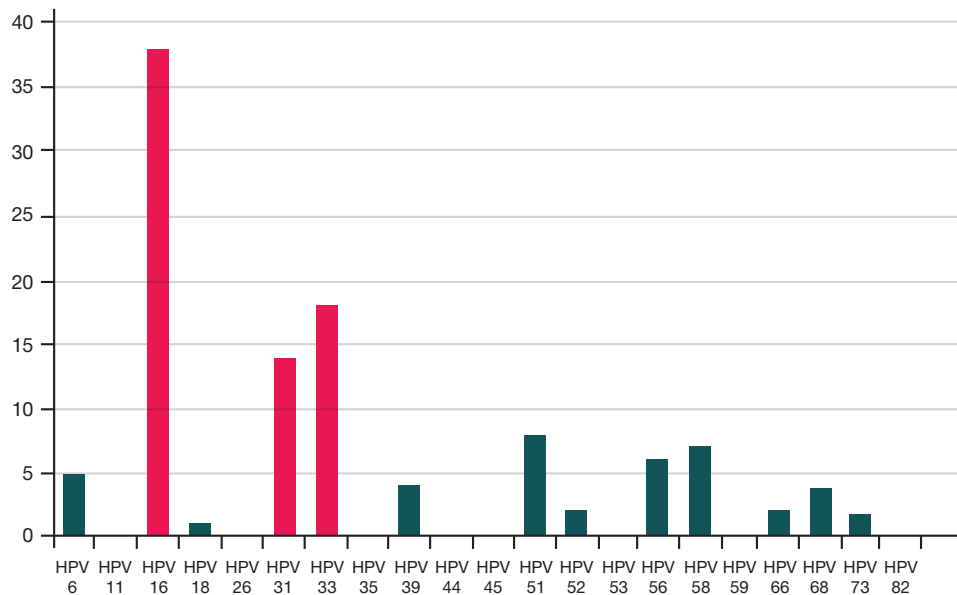
Fig. 2. Distribution of HPV genotypes in the biopsy specimens

fixation, the samples were put into Histo-Tek VP1 (Sakura, Japan) for tissue processing, and semi-automatic paraffin embedding station (Leica HistoCore Arcadia, Germany) was used to form paraffin blocks. Paraffin sections 5 μm thick were put into 1.5 ml dry tubes and transported for HPV DNA testing, same as the tubes with the cervical canal secretion samples. To prevent compromising of the results of comparison of HPV DNA identification in smears and bioptates, all samples were harvested within a single menstrual cycle. Before DNA isolation from the bioptates, paraffin was removed and samples treated with proteinase K using the Proba-PK kit (DNA Technology, Russia), then we isolated the DNA with the help of the Proba-NK kit that precipitates nucleic acids in alcohol. The viral load in the range from 0 to 3.0 lg was regarded as low, in the range from 3.1 to 5 lg — moderate, and values from 5.1 lg and up were considered to represent a high viral load [14].

Statistical data processing methods

For statistical data analysis, we used the IBM SPSS Statistics Version 20 software package (IBM, USA). The normality of distribution of the variables (under the Gaussian law) was checked with the help of the Kolmogorov–Smirnov test. At this step, it was established that most variables do not distribute normally, therefore, as is customary for data violating the Gaussian law, we used the median, which is less susceptible to extreme variations. The dispersion measures were represented by the upper and lower quartiles (Me (Q_1; Q_3)). Categorical data were presented as a percentage with a 95% confidence interval (95% CI) calculated using the Wilson method. Nonparametric Mantel-Haenszel chi-square value tests were used to compare variables depending on their properties (quantitative or categorical). The level of significance was set at $p < 0.05$.

RESULTS

Among the 99 pairs of samples, we registered DNA of HPV in 175 cervical canal smears and 111 biopsy specimens. In the smears, the distribution was as follows: chronic cervicitis — 53/175 (30.3%), LSI — 60/175 (34.3%), HSIL — 62/175 (35.4%). In the biopsy specimens, this characteristic was less uniform: chronic cervicitis — 22/111 (19.8%), LSIL — 40/111 (36.0%),

HSIL — 49/111 (44.1%). A noteworthy fact is that in the biopsy samples from patients diagnosed with chronic cervicitis and HSIL, we registered HPV DNA significantly less frequently than in the secretion samples paired with the respective biopsy specimens ($p = 0.048$ and $p = 0.034$, respectively). We have also considered the distribution of HPV genotypes through the lens of the method of sampling (Fig. 1, 2). For 25/111 (22.5%) cases of HPV DNA detection in the biopsy specimens, we failed to find identify HPV genotypes in the paired smears. In 8/25 (32%) of such cases, the registered genotype was HPV-16, in 7/25 (28%) cases — HPV-33, and in 6/25 (24%) cases — HPV-51. It is important to note that HPV-16 was most frequently identified in the biopsy specimens of the patients from Group 1 (6/8, 75%).

The comparative analysis has revealed that in 49.1% of cases HPV DNA was detected in both the cervical canal smears and the paired cervical biopsy specimens. It is also important to take into account the intra-group overlap of the HPV testing data. In Group 3 (chronic cervicitis), the level of coincidence of detection of HPV DNA in both samples of the pair was 28.3%, in Group 1 *(LSIL) — 45%, in Group 2 (HSIL) — 67.7% (Fig. 3).

One of the important components of this study was the assessment of the prevalence of simultaneous detection of two or more HPV genotypes. Several HPV genotypes were detected in 46/99 (46.5%) of the cervical canal smears. However, the respective tests made on the biopsy specimens returned only 13/99 (13.1%) of such cases. This difference is statistically significant ($p < 0.001$).

Analyzing the correlations between HPV test results, we discovered a noteworthy phenomenon. HPV-44, which is one of the three most prevalent genotypes (14/175. 8%) and is more associated with HSIL than with LSIL or chronic cervicitis (50% vs 28.6% vs 21.4%, respectively), was not detected in of the cervical biopsy specimens. At the same time, for other most common types, the matches within the pairs were frequent: HPV-16 — 30/32 (93.8%), HPV-33 — 13/16 (81.3%), HPV-31 — 11/16 (68.8%) (Fig. 4).

The aspects of the study that are of particular interest are investigation of the effect of HPV viral load on the various indicators, such as the incidence, frequency of simultaneous detection of several genotypes, and the degree of cervical
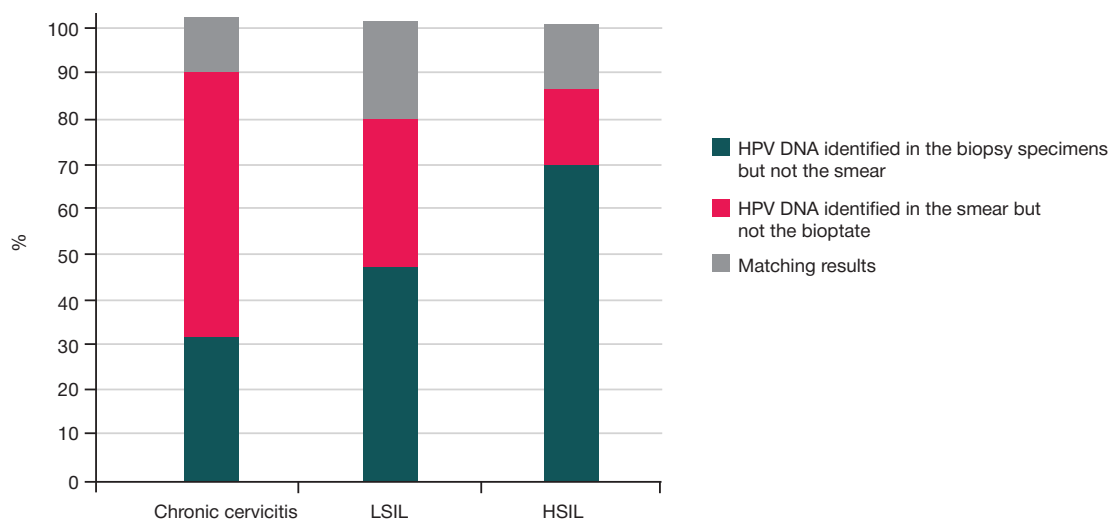
Fig. 3. Coincidence of registration of HPV DNA in both samples of a pair (comparative analysis)

lesion. In particular, we analyzed how the amounts of HPV affect the frequency of matching results in sample pairs. Among cervical canal smears, 62 exhibited high HPV viral load, 65 — moderate, and 48 low viral load. Among the biopsy specimens, the distribution was as follows: high viral load — 52 samples, moderate viral load — 37 samples, low viral load — 23 samples. It should be borne in mind that 22.5% of HPV DNA detections in the biopsy specimens were first-time, which means that these cases were not factored into the calculation of correlations between quantitative HPV test results. The analysis has shown that when the viral load is low, the results of the HPV DNA detection tests matched in 27.1% of sample pairs, when the load was moderate — in 35.4% of the pairs, and when it was high, 82.3% of sample pairs exhibited matching results (Fig. 5). It is important to note that the differences in the amounts of matching results in high vs. moderate viral load, and in high vs. low viral load cases was significant ($p < 0.001$ for both comparisons). Cramér's V showed a relatively strong correlation between the level of viral load and the probability of matching HPV test results (Table). Comparison of the frequency of matching HPV DNA detections in moderate and low viral load cases revealed no significant differences ($p = 0.456$).

In addition, we calculated the correlation of HPV test results depending on each viral load range, taking 1 lg as the increment. It was established that an increase of 1 lg raises the probability of confirmation of infection with the HPV genotype detected in the cervical canal smear (in an initially determined quantitative ratio) by 9.3%.

DISCUSSION

There are very few studies dedicated to this subject. For our study, we took as a reference an experiment that paired 74 paired cytological and histological samples of cervical cancer and tested them using a 51 HPV genotype diagnostic array [13]. In that experiment, the HPV test results matched in 93% of cases, but when the viral load was low, the results differed in 78% of cases. In addition, two or more types of HPV were detected significantly less often in bioptates than in smears (14% vs 47%; $p < 0.001$). It should be noted that the results of our study confirm and largely complement these findings. In Group 2 (HSIL), the proportion of matching results of HPV DNA tests was 67.7%, in Group 1 (LSIL) — 45%, and in Group 3 (chronic cervicitis) is was 28.3%. The values reported by the authors of the mentioned experiment support the upward
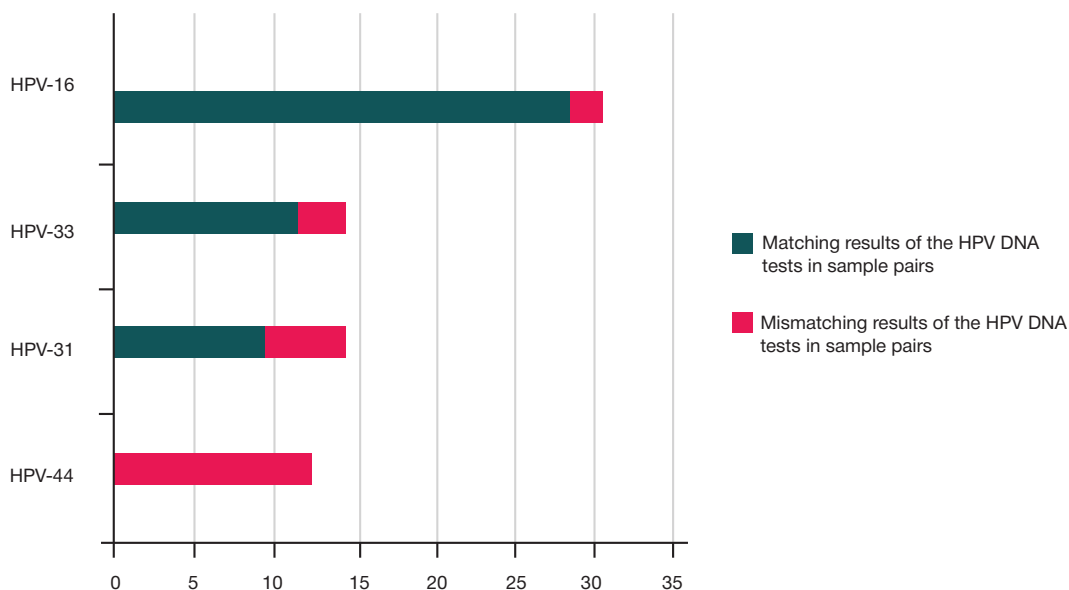
Fig. 4. Comparative analysis of the most common HPV genotypes, cervical canal smears and cervix biopsy specimens

Table. Correlation of the level of viral load and the proportion of matching HPV DNA detections in the sample pairs

Gradation of HPV viral load	Matching test results cases	Mismatching test results cases	Cramér's V	*p* value
High/low viral load	51/13	11/35	0.555	*p* < 0.001
High/moderate viral load	51/23	11/42	0.445	*p* < 0.001
Moderate/low viral load	23/13	42/35	0.074	*p* = 0.456

trend reflecting the dependence of the amount of matching results on the degree of damage to the cervix, which we registered. Our analysis shows that when the HPV viral load is low, the detection results in the sample pairs match in 27.1% of cases, when the load is moderate, this value goes up to 35.4%, and in high viral load circumstances, it increases to 82.3%. This is also consistent with what was reported in the foreign study. Another noteworthy aspect in which our findings coincide with those reported in the referenced experiment concerns registration of several HPV genotypes in a single sample: we encountered such situations significantly less often in cervix bioptates than in the cervical canal smears (13.1% vs 46.5%; *p* < 0.001). It is also important to note the specific distribution of HPV-44 we have identified: this genotype was the most common in

cervical canal smears, but it was not found in any of the cervix bioptates. This probably indicates that HPV-44 has a tropism for columnar epithelial cells. Given the results of our retrospective study, which demonstrate the association between this genotype and precancerous condition of the cervix, HPV-44 should probably be studied further.

CONCLUSIONS

Thus, increasing HPV viral load translates into a growing probability of detection of HPV genotypes in the diseased cervical tissue. In addition, the amount of matching results of HPV tests in paired samples depends on the pathomorphological conclusion: the more severe the cervical lesion, the more likely HPV is to be detected in the bioptates.
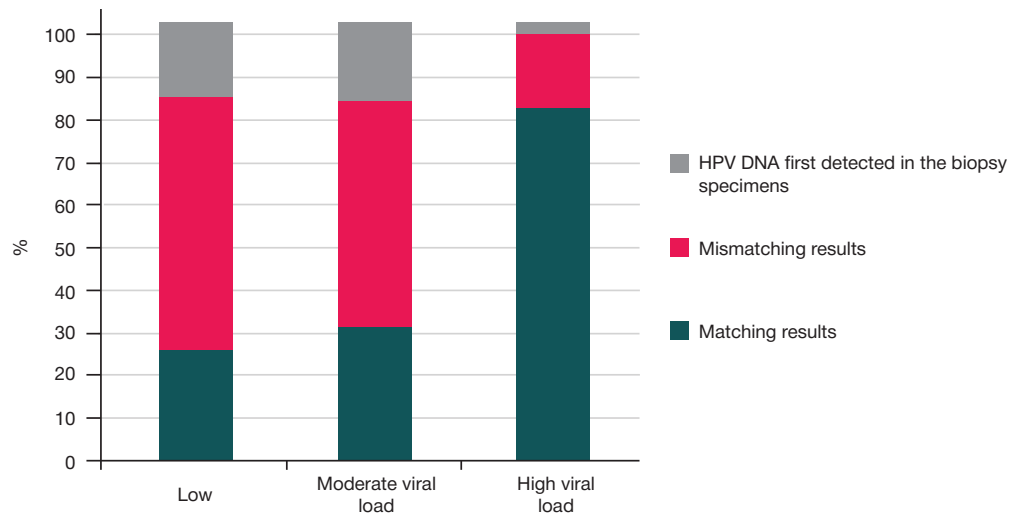
Fig. 5. Comparative analysis of HPV test results based on the established viral loads

References

1. Sung H, Ferlay J, Siegel RL, Laversanne M, Soerjomataram I, Jemal A, et al. Global Cancer Statistics 2020: GLOBOCAN Estimates of Incidence and Mortality Worldwide for 36 Cancers in 185 Countries. CA Cancer J Clin. 2021; 71 (3): 209–49. DOI: 10.3322/caac.21660.
2. Kyrgiou M, Mitra A, Moscicki AB. Does the vaginal microbiota play a role in the development of cervical cancer? Translational Research. 2017; 179: 168–82. DOI: 10.1016/j.trsl.2016.07.004.
3. Plisko O, Zodzika J, Jermakova I, Pcolkina K, Prusakevica A, Liepniece-Karele I, et al. Prediction of high-grade cervical precancerous abnormalities: The role of personal factors, vaginal microflora, sexually transmitted infections, and high-risk human papillomavirus. PLoS One. 2024; 19 (11): e0313004. DOI: 10.1371/journal.pone.0313004.
4. Gravitt PE. The known unknowns of HPV natural history. J Clin Invest. 2011; 121 (12): 4593–9. DOI: 10.1172/JCI57149.
5. Adams AK, Wise-Draper TM, Wells SI. Human papillomavirus induced transformation in cervical and head and neck cancers. Cancers (Basel). 2014; 6 (3): 1793–820. DOI: 10.3390/cancers6031793.
6. Khumalo PG, Carey M, Mackenzie L, Sanson-Fisher R. Cervical

cancer screening knowledge and associated factors among Eswatini women: A cross-sectional study. PLoS One. 2024; 19 (4): e0300763. DOI: 10.1371/journal.pone.0300763. PMID: 38635684; PMCID: PMC11025751.
7. Hu H, Wu Y, Zhao M, Liu J, Xie P. Sleep duration time and human papillomavirus infection risk: The U-shaped relationship revealed by NHANES data. PLoS One. 2024; 19 (4): e0301212. DOI: 10.1371/journal.pone.0301212.
8. Gomes FC, Galhardo DDR, Navegante ACG, Santos GSD, Dias HAAL, Dias Júnior JRL et al. Bioinformatics analysis to identify the relationship between human papillomavirus-associated cervical cancer, toll-like receptors and exomes: A genetic epidemiology study. PLoS One. 2024; 19 (8): e0305760. DOI: 10.1371/journal.pone.0305760.
9. Scott-Wittenborn N, Fakhry C. Epidemiology of HPV Related Malignancies. Semin Radiat Oncol. 2021; 31 (4): 286–96. DOI: 10.1016/j.semradonc.2021.04.001.
10. Huiyun J, Jie D, Huan W, Yuebo Y, Xiaomao L. Prevalence and characteristics of cervical human papillomavirus genotypes

and cervical lesions among 58630 women from Guangzhou, China. J Infect Public Health. 2023; 16 (10): 1531–6. DOI: 10.1016/j.jiph.2023.07.013. Epub 2023 Jul 21. PMID: 37562080.

11. Guo M, Sneige N, Silva EG, Jan YJ, Cogdell DE, Lin E, et al. Distribution and viral load of eight oncogenic types of human papillomavirus (HPV) and HPV 16 integration status in cervical intraepithelial neoplasia and carcinoma. Mod Pathol. 2007; 20 (2): 256–66. DOI: 10.1038/modpathol.3800737. Epub 2006 Dec 22. PMID: 17192787.

12. Yoshida T, Sano T, Oyama T, Kanuma T, Fukuda T. Prevalence, viral load, and physical status of HPV 16 and 18 in cervical adenosquamous carcinoma. Virchows Arch. 2009; 455 (3): 253–9. DOI: 10.1007/s00428-009-0823-x. PMID: 19727809.

13. Halec G, Schmitt M, Dondog B, Sharkhuu E, Wentzensen N,

Gheit T, Tommasino M, Kommoss F, Bosch FX, Franceschi S, Clifford G, Gissmann L, Pawlita M. Biological activity of probable/possible high-risk human papillomavirus types in cervical cancer. Int J Cancer. 2013; 132 (1): 63–71. DOI: 10.1002/ijc.27605. Epub 2012 Jul 9. PMID: 22514107.

14. Andreev AO. Taktika vedenija pacientok s ploskokletochnymi porazhenijami shejki matki s uchetom opredelenija genotipa i virusnoj nagruzki VPCh [dissertacija]. M., 2024. Russian.

15. Halec G, Schmitt M, Dondog B, Sharkhuu E, Wentzensen N, Gheit T, Tommasino M, Kommoss F, Bosch FX, Franceschi S, Clifford G, Gissmann L, Pawlita M. Biological activity of probable/possible high-risk human papillomavirus types in cervical cancer. Int J Cancer. 2013; 132 (1): 63–71. DOI: 10.1002/ijc.27605. Epub 2012 Jul 9. PMID: 22514107.

Литература

1. Sung H, Ferlay J, Siegel RL, Laversanne M, Soerjomataram I, Jemal A, et al. Global Cancer Statistics 2020: GLOBOCAN Estimates of Incidence and Mortality Worldwide for 36 Cancers in 185 Countries. CA Cancer J Clin. 2021; 71 (3): 209–49. DOI: 10.3322/caac.21660.

2. Kyrgiou M, Mitra A, Moscicki AB. Does the vaginal microbiota play a role in the development of cervical cancer? Translational Research. 2017; 179: 168–82. DOI: 10.1016/j.trsl.2016.07.004.

3. Plisko O, Zodzika J, Jermakova I, Pcolkina K, Prusakevica A, Liepniece-Karele I, et al. Prediction of high-grade cervical precancerous abnormalities: The role of personal factors, vaginal microflora, sexually transmitted infections, and high-risk human papillomavirus. PLoS One. 2024; 19 (11): e0313004. DOI: 10.1371/journal.pone.0313004.

4. Gravitt PE. The known unknowns of HPV natural history. J Clin Invest. 2011; 121 (12): 4593–9. DOI: 10.1172/JCI57149.

5. Adams AK, Wise-Draper TM, Wells SI. Human papillomavirus induced transformation in cervical and head and neck cancers. Cancers (Basel). 2014; 6 (3): 1793–820. DOI: 10.3390/cancers6031793.

6. Khumalo PG, Carey M, Mackenzie L, Sanson-Fisher R. Cervical cancer screening knowledge and associated factors among Eswatini women: A cross-sectional study. PLoS One. 2024; 19 (4): e0300763. DOI: 10.1371/journal.pone.0300763. PMID: 38635684; PMCID: PMC11025751.

7. Hu H, Wu Y, Zhao M, Liu J, Xie P. Sleep duration time and human papillomavirus infection risk: The U-shaped relationship revealed by NHANES data. PLoS One. 2024; 19 (4): e0301212. DOI: 10.1371/journal.pone.0301212.

8. Gomes FC, Galhardo DDR, Navegante ACG, Santos GSD, Dias HAAL, Dias Júnior JRL et al. Bioinformatics analysis to identify the relationship between human papillomavirus-associated cervical cancer, toll-like receptors and exomes: A genetic epidemiology study. PLoS One. 2024; 19 (8): e0305760. DOI: 10.1371/journal.pone.0305760.

9. Scott-Wittenborn N, Fakhry C. Epidemiology of HPV Related

Malignancies. Semin Radiat Oncol. 2021; 31 (4): 286–96. DOI: 10.1016/j.semradonc.2021.04.001.

10. Huiyun J, Jie D, Huan W, Yuebo Y, Xiaomao L. Prevalence and characteristics of cervical human papillomavirus genotypes and cervical lesions among 58630 women from Guangzhou, China. J Infect Public Health. 2023; 16 (10): 1531–6. DOI: 10.1016/j.jiph.2023.07.013. Epub 2023 Jul 21. PMID: 37562080.

11. Guo M, Sneige N, Silva EG, Jan YJ, Cogdell DE, Lin E, et al. Distribution and viral load of eight oncogenic types of human papillomavirus (HPV) and HPV 16 integration status in cervical intraepithelial neoplasia and carcinoma. Mod Pathol. 2007; 20 (2): 256–66. DOI: 10.1038/modpathol.3800737. Epub 2006 Dec 22. PMID: 17192787.

12. Yoshida T, Sano T, Oyama T, Kanuma T, Fukuda T. Prevalence, viral load, and physical status of HPV 16 and 18 in cervical adenosquamous carcinoma. Virchows Arch. 2009; 455 (3): 253–9. DOI: 10.1007/s00428-009-0823-x. PMID: 19727809.

13. Halec G, Schmitt M, Dondog B, Sharkhuu E, Wentzensen N, Gheit T, Tommasino M, Kommoss F, Bosch FX, Franceschi S, Clifford G, Gissmann L, Pawlita M. Biological activity of probable/possible high-risk human papillomavirus types in cervical cancer. Int J Cancer. 2013; 132 (1): 63–71. DOI: 10.1002/ijc.27605. Epub 2012 Jul 9. PMID: 22514107.

14. Андреев А. О. Тактика ведения пациенток с плоскоклеточными поражениями шейки матки с учетом определения генотипа и вирусной нагрузки ВПЧ [диссертация]. М., 2024.

15. Halec G, Schmitt M, Dondog B, Sharkhuu E, Wentzensen N, Gheit T, Tommasino M, Kommoss F, Bosch FX, Franceschi S, Clifford G, Gissmann L, Pawlita M. Biological activity of probable/possible high-risk human papillomavirus types in cervical cancer. Int J Cancer. 2013; 132 (1): 63–71. DOI: 10.1002/ijc.27605. Epub 2012 Jul 9. PMID: 22514107.

ASSOCIATION BETWEEN THE *NANOSYNBACTER LYTICUS* EPIBIOTIC BACTERIA AND INFLAMMATORY PERIODONTAL DISEASES

Pobozhieva LV ✉, Skvortsov-Igralov GA, Bocharova YuA, Kopetskiy IS, Chebotar IV

Pirogov Russian National Research Medical University, Moscow, Russia

The inflammatory periodontal disease pathogenesis is determined by microorganisms of the oral cavity. Along with the well-studied periodontopathogens, microbial agents of unproven clinical significance, including epibiotic bacteria, are found in individuals with gingivitis and periodontitis. The study aimed to determine the association between the N*anosynbacter lyticus* epibiont and inflammatory periodontal diseases. Conservative DNA sequences specific for the genera *Nanosynbacter*, *Schaalia* and the *Bacteria* domain were identified using PCR in 47 study participants (31 females and 16 males) aged 18–45 years. The results were expressed as indices determining the quantitative relationships between *N. lyticus* and *Schaalia spp*. (NS index), as well as between *N. lyticus* and representatives of the *Bacteria* domain (NB index). *Schaalia spp*. were not found in a large share (11/27, 40.7%) of patients with no periodontitis. All patients with moderate-to-severe periodontitis, as well as 75% of patients with mild periodontitis were carriers of *Schaalia spp*. All the *Schaalia*-positive samples from patients with periodontitis showed higher NS indices ($p < 0.05$) compared to *Schaalia*-positive samples from patients with no periodontitis: the median NS values were Me = 0.89 (0.79; 0.93) and Me = 0.63 (0.00; 0.73), respectively. The patients suffering from chronic generalized periodontitis had significantly higher NB indices (Me = 0.83 (0.79; 0.85)) ($p < 0.05$) compared to patients with no periodontitis, Me = 0.67 (0.00; 0.81).

✉ **Correspondence should be addressed:** Ludmila V. Pobozhieva
ludmila-stomatolog@mail.ru

ВЗАИМОСВЯЗЬ МЕЖДУ БАКТЕРИЯМИ-ЭПИБИОНТАМИ *NANOSYNBACTER LYTICUS* И ВОСПАЛИТЕЛЬНЫМИ ЗАБОЛЕВАНИЯМИ ПАРОДОНТА

Л. В. Побожьева ✉, Г. А. Скворцов-Игралов, Ю. А. Бочарова, И. С. Копецкий, И. В. Чеботарь

Российский национальный исследовательский медицинский университет имени Н. И. Пирогова, Москва, Россия

Патогенез воспалительных заболеваний пародонта детерминируется микроорганизмами полости рта. Кроме хорошо изученных пародонтопатогенов, при гингивите и пародонтите обнаруживаются микробные агенты с недоказанным клиническим значением, к числу которых принадлежат бактерии-эпибионты. Целью работы было определить взаимосвязь между присутствием эпибионта *Nanosynbacter lyticus* и воспалительными заболеваниями пародонта. У 47 участников исследования (среди них 31 женщина и 16 мужчин) в возрасте 18–45 лет с помощью ПЦР определяли наличие консервативных последовательностей ДНК, специфичных для родов N*anosynbacter, Schaalia*, а также домена *Bacteria*. Результаты выражали в виде индексов, определяющих количественные соотношения между *N. lyticus* и *Schaalia spp*. (индекс NS), а также между *N. lyticus* и представителями домена *Bacteria* (индекс NB). У значительной доли (11/27, 40,7%) пациентов без пародонтита *Schaalia spp*. не были обнаружены. Все пациенты со средней и тяжелой степенью пародонтита, а также 75% пациентов с легкой степенью пародонтита были носителями *Schaalia spp*. Для всех *Schaalia*-позитивных образцов от пациентов с пародонтитом индекс NS был более высоким ($p < 0,05$), чем у *Schaalia*-позитивных образцов без пародонтита: медианы показателя NS составляли соответственно Ме = 0,89 (0,79; 0,93) и Ме = 0,63 (0,00; 0,73). Индекс NB у пациентов, страдающих хроническим генерализованным пародонтитом (Ме = 0,83 (0,79; 0,85)), был достоверно выше ($p < 0,05$), чем у пациентов без пародонтита, Ме = 0,67 (0,00; 0,81).

✉ **Для корреспонденции:** Людмила Владимировна Побожьева
ludmila-stomatolog@mail.ru

Inflammatory periodontal diseases are among the most common diseases of the oral cavity. Severe forms of periodontitis are found in more than 700 million people all over the world [1]. Despite the fact that periodontitis is considered to be a multifaceted process, the key role of microorganisms in the development of periodontitis is indisputable. Contemporary metagenomic studies show that periodontitis is not associated with the presence of several specific periodontal pathogens, it results from polymicrobial synergy of dozens of microbial species [2, 3].

To date, pathogenetic significance of many representatives of the *Bacteria* domain is poorly understood. Along with typical periodontopathogens, which include *Porphyromonas gingivalis*, *Prevotella spp*., *Treponema denticola*, *Fusobacterium nucleatum*, *Aggregatibacter actinomycetemcomitans*, *Filifactor alocis*, *Peptostreptococcus spp*., etc. [4–7], many resident bacteria with poorly understood properties inhabit the oral cavity. The group of nonculturable bacteria, specifically epibionts living in symbiosis on the surface of other bacteria, is

of special interest. *Nanosynbacter lyticus* is a typical example of epibiotic bacterium of the oral cavity being an episymbiont of the *Schaalia* odontolytica periodontopathogen (formerly known as *Actinomyces odontolyticus*) [8]. Currently, *N. lyticus* is the only species of the genus *Nanosynbacter*, the presence of which in the oral cavity has been confirmed by certain studies. There are very conflicting reports concerning the role of *N. lyticus* in pathogenesis. According to some reports, the number of *N. lyticus* is positively correlated to inflammatory diseases of the oral cavity: periodontitis, pericoronitis [9, 10]. Other authors have discovered the opposite: the increase in the number of *N. lyticus* is associated with reduction of inflammation due to suppression of bacterial pathogens [11].

The study aimed to determine the association between the presence of *N. lyticus* bacteria and inflammatory periodontal diseases.

METHODS

The study involved 47 people (31 females and 16 males). Inclusion criteria: individuals of both genders, age 18–45 years; no history of dental treatment within at least six months. Exclusion criteria: taking antibiotics or using oral antiseptics within the last three months; pregnancy, postpartum period; age under 18 and over 45 years; acute inflammatory disorder; exacerbation of chronic somatic disorder, decompensated somatic disorder; cancer, refusal to participate in the study. General information about the patients is provided in Table 1. The informed consent to participation in the study was submitted by all subjects.

The clinical part of the study included collection of complaints, history taking, and oral cavity examination. Diseases of hard dental tissues and periodontal tissues were diagnosed based on ICD-10 (K05.31 — chronic periodontitis, K05.10 — chronic gingivitis, K02.1 — dental caries), as well as based on the Periodontal Disease Classification System of the Russian Dental Association.

Among surveyed individuals, chronic generalized catarrhal gingivitis (K05.10) was revealed in 21.3% of cases, mild chronic generalized periodontitis (K05.31) in 8.5% of cases, moderate chronic generalized periodontitis (K05.1) in 17% of cases, severe chronic generalized periodontitis (K05.31) in 17% of cases. The share of individuals having no inflammatory periodontal diseases in the entire surveyed population was 36.2%.

Subgingival samples were collected from the gingival sulcus or periodontal pocket for laboratory testing. The samples were transported to the laboratory for DNA extraction in a cold state within 6 h.

The samples were incubated with the lysozyme solution (Sisce Research Laborataries; India) with the final concentration of 1 mg/m at 37 °C for 60 min prior to DNA extraction [12]. Genomic DNA was extracted from the samples using the SKYAmp Micro DNA kit (SkyGene; Russia). The extraction quality control was ensured using the Equalbit 1x dsDNA HS Assay Kit (Vazyme; China) and the Fluo-200 fluorometer (Allsheng; China).

The extracted DNA samples were analyzed by real-time polymerase chain reaction (PCR). Conservative DNA sequences specific for the genera *Nanosynbacter*, *Schaalia* and the Bacteria domain were identified using three pairs of primers and three probes in different fluorescence channels (Table 2).

Nuclease-free Water (New England BioLabs; USA) was used as a negative control. The positive controls used were represented by the following: 1) artificially synthesized oligo-DNA identical to the fragment of the *Nanosynbacter* 23S rRNA (this group of bacteria was earlier referred to as Saccharibacteria or TM7) constructed based on the sequences from the GenBank database [13]; 2) DNA of bacteria of the genus *Schaalia spp.* (formerly known as *Actinomyces spp.*); 3) mixture of bacterial DNA from the *Staphylococcus aureus* ATCC 29213; *Pseudomonas aeruginosa* ATCC 27853; *Escherichia coli* ATCC 25922 cultures.

PCR mixture composition: 10 µL of BioMaster HS-qPCR (HS-Taq DNA polymerase, mixture of dNTP, PCR buffer, Mg^{2+}, and sterile water) (Biolabmix; Russia); 2 µL of each specific primer (5 µM), 1 µL of specific probe (5 µM), 5 µL 0.1 ng/µL. The PCR mixture was prepared in accordance with the manufacturer's instructions. Reaction protocol: 5 min activation at 95 °C, then 35 cycles 15 s each at 94 °C, 15 s at 62 °C and 20 s at 72 °C. The reaction was carried out using the DT Prime thermal cycler (DNA-Technology; Russia).

To estimate the amount of DNA of each studied species, we determined the threshold cycle (Cp) value. Then we used Microsoft Excel 2010 tools to calculate the conditional indicators reflecting quantitative ratios of: 1) representatives of *Nanosynbacter* and the genus *Schaalia* (NS index) based on Cp values; 2) bacteria of the genus Nanosynbacter and the *Bacteria* domain (NB index) based on Cp values. The NS and NB values were calculated using the following formulae:

$$NS = \frac{Cp^{-1}_{Nanosynbacter} * 100}{Cp^{-1}_{positive\ control\ Nanosynbacter}} / \frac{Cp^{-1}_{Schaalia} * 100}{Cp^{-1}_{positive\ control\ Schaalia}}$$

$$NB = \frac{Cp^{-1}_{Nanosynbacter} * 100}{Cp^{-1}_{positive\ control\ Nanosynbacter}} / \frac{Cp^{-1}_{Bacteria} * 100}{Cp^{-1}_{positive\ control\ Bacteria}}$$

Statistical analysis of the results was performed using IBM SPSS Statistics for Windows, version 27.0 (IBM Corp.; USA).

RESULTS

When assessing 47 samples, no correlations between the NS and NB indices and the patients' age and gender were revealed. No nucleotide sequences specific for the genus *Schaalia* were found in 12 samples out of 47 (25.5%). All the *Schaalia*-negative samples were obtained from patients having no signs of moderate-to-severe periodontitis; only one *Schaalia*-negative sample was obtained from the patient with mild periodontitis. *N. lyticus* were found in 7 *Schaalia*-negative samples out of 12.

No *Schaalia spp.* were found in a large share (11/27, 40.7%) of patients having no periodontitis. All patients (100%) with moderate-to-severe periodontitis, as well as 3 patients with mild periodontitis out of 4 (75%) were carriers of *Schaalia spp.*

Table 1. Gender and age distribution of subjects

Total surveyed population, individuals	*n* = 47	
Average age of surveyed individuals, years	34.2 (± 8.36) (min 18 – max 45)	
Gender distribution of surveyed population, individuals	Males *n* = 16	Females *n* = 31
Average age of surveyed individuals depending on gender, years	34.8 (± 9.41) (min 20 – max 45)	32.6 (± 8.54) (min 18 – max 43)

Table 2. Primers and probes used in the study

	Oligonucleotide	*Nanosynbacter*	*Schaalia spp.*	Total bacterial DNA
Forward primer		5'-GGCTTATAGCGCCCAATAG-3'	5'- GGTCTCTGGGCCGTTACTGA -3'	5'-TCCTACGGGAGGCAGCAGT-3'
	Reverse primer	5'-CGGATATAAACCGAACTGTC-3'	5'-CCCCCACACCTAGTGCCC -3'	5'-GGACTACCAGGGTATCTAATCC TGTT-3'
	Probe	(FAM) –5'-CATAGACGGCGCTGTTTGGCAC-3'-(RTQ1)	(FAM)-5'-CGTGGGGAGCGAACAGGATTAGATACC-3'-(TAMRA)	(ROX)-5'-CGTATTACCGCGGCTGCTGGCAC-3'-(RTQ2)
	Reference	[14]	[15]	[16]

The NS index reflecting the ratio of the genus *Nanosynbacter* representatives and *Schaalia spp*. was zero in 8 samples out of 47 (17%); none of these samples was obtained from patient with periodontitis. High NS indices were reported for all *Schaalia*-positive samples from patients with periodontitis (K05.31): Me = 0.89 (0.79; 0.93), which is significantly higher ($p < 0.05$) compared to other Schaalia-positive samples, for which Me = 0.63 (0.00; 0.73) is reported.

Among 10 samples obtained from patients with chronic generalized catarrhal gingivitis, three samples contained no genetic markers specific for the genus *Schaalia* and one sample contained no *Nanosynbacter*-specific markers. That is why no positive correlation between the NS index values and the diagnosis of chronic generalized catarrhal gingivitis (K05.10) was revealed ($p > 0.05$).

More interesting results were obtained when assessing the NB index (see Figure). The NB indices of patients suffering from chronic generalized periodontitis (K05.31) (Me = 0.83 (0.79; 0.85)) were significantly higher ($p < 0.05$), than that of patients with no periodontitis (Me = 0.67 (0.00; 0.81)). The samples from patients with mild periodontitis showed the NB index values (Me = 0.77 (0.38; 0.78)) that were not significantly different ($p > 0.05$) from the NB values reported for the samples from patients with no periodontitis, but were significantly lower ($p < 0.05$), than the NB values reported for the samples from patients with moderate-to-severe chronic generalized periodontitis (Me 0.85 (0.81; 0.85) and Me 0.84 (0.81; 0.88), respectively). The NB values of patients with moderate-to-severe periodontitis showed no significant differences ($p > 0.05$).

No significant correlations of the NB index with other groups of patients (gingivitis, patients with no inflammatory diseases of the oral cavity) were identified.

DISCUSSION

The first interesting observation made when assessing the results is related to discrepancies in the presence of *N. lyticus* and *Schaalia spp*. bacteria in the test samples. This proves that *S. odontolytica* is not the only host of *N. lyticus*. The fact of the *N. lyticus* symbiosis with representatives of other taxons, including *Actinomyces oris*, *Fusobacterium nucleatum*, was predicted earlier [17–19].

The second finding confirms a negative contribution of the *Schaalia spp.* bacteria to pathogenesis of moderate-to-severe periodontitis. Actually, 100% of patients with moderate-to-severe chronic generalized periodontitis (K05.31) were carriers of *Schaalia spp*., while a large share of patients (40.7%) with no periodontitis were not carriers of this group of bacteria. This finding complements the literature data suggesting that *S. odontolytica* (formerly known as *A. odontolyticus*) actively forms biofilms in periodontal pockets, but is not a significant periodontopathogen [20].

The most important finding of our study is related to positive correlation between the NS index (showing the ratio between representatives of *Nanosynbacter* and *Schaalia spp*.) and the severity of chronic generalized periodontitis. The *S. odontolytica* virulence increase under the influence of the increasing number of *N. lyticus* epibionts secured on these bacteria can be the most logical explanation of this fact. A similar observation was made by other researchers, who reported increased biofilm formation by *A. odontolyticus* (now named *S. odontolytica*) induced by epibionts via regulators of the quorum sensing system [21].

An observation related to no relationship between the number of *Nanosynbacter* and chronic generalized gingivitis can be considered a useful result.
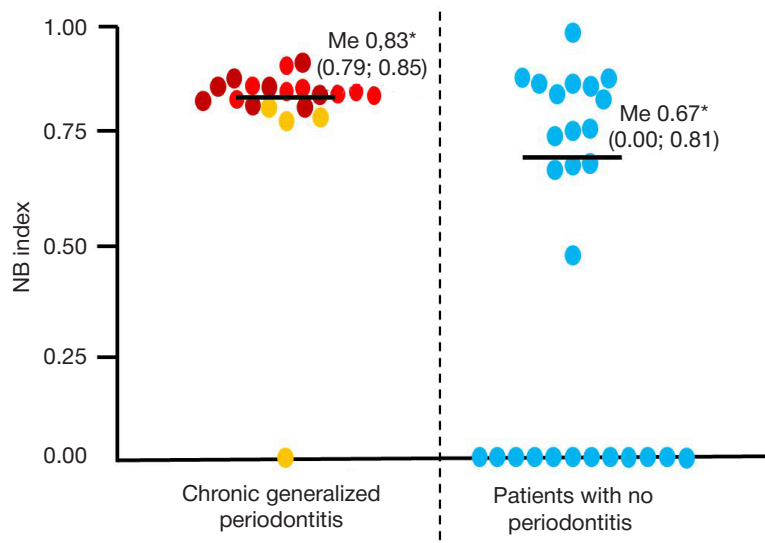
Fig. NB index showing the ratio of representatives of the genus *Nanosynbacter* and the *Bacteria* domain in patients with chronic generalized periodontitis and individuals with periodontitis. Mild periodontitis is highlighted in *orange*, moderate periodontitis is highlighted in *red*, severe form is highlighted in *maroon*. Me — median (lower and upper quartiles); * — significant differences between the values, $p < 0.05$

CONCLUSION

N. lyticus are likely to be symbionts of not only bacteria of the genus *Schaalia*, but also representatives of other taxons. Our findings foster a conversation about conducting a prospective study aimed to search for new *N. lyticus* hosts. Bacteria of the genus *Schaalia spp*. are involved in pathogenesis of chronic generalized forms of moderate-to-severe periodontitis. The NB index reflecting the ratio between representatives of the genus *Nanosynbacter* and the total number of bacteria increases in chronic generalized periodontitis, it can result from the increase in the virulence of pathogenetically significant bacteria under the influence of *N. lyticus* epibionts. The NS index reflecting the ratio between representatives of the genus *Nanosynbacter* and *Schaalia spp*. cannot be useful in terms of assessing the disease severity in patients with chronic generalized gingivitis.

References

1. Yixin Li, Yonggang Xiang, Haixia Ren, et al. Association between periodontitis and dental caries: a systematic review and meta-analysis. Clinical Oral Investigations. 2024; 28: 306. 10; 28 (6): 306. DOI: 10.1007/s00784-024-05687-2.
2. Krutyhołowa A, Strzelec K, Dziedzic A, Bereta GP, Łazarz-Bartyzel K, Potempa J, et al. Host and bacterial factors linking periodontitis and rheumatoid arthritis. Front Immunol. 2022; 13: 980805. DOI: 10.3389/fimmu.2022.980805.
3. Cai Z, Lin S, Hu S, Zhao L. Structure and function of oral microbial community in periodontitis based on integrated data. Front Cell Infect Microbiol. 2021; 11: 663756. DOI: 10.3389/fcimb.2021.663756.
4. Jiao Y, Hasegawa M, Inohara N. The role of oral pathobionts in dysbiosis during periodontitis development. Journal of Dental Research. 2014; 93 (6): 539–46. DOI: 10.1177/0022034514528212.
5. Antezack A, Etchecopar-Etchart D, La Scola B, Monnet-Corti V. New putative periodontopathogens and periodontal health-associated species: a systematic review and meta-analysis. 2023; 58: 893–906. DOI: 10.1111/jre.13173.
6. Valm AM. The structure of dental plaque microbial communities in the transition from health to dental caries and periodontal disease. J Mol Biol. 2019; 431 (16): 2957–69. DOI: 10.1016/j.jmb.2019.05.016.
7. Hajishengallis G. Immunomicrobial pathogenesis of periodontitis: keystones, pathobionts, and host response. Trends in Immunology. 2014; 35 (1): 3–11. DOI: 10.1016/j.it.2013.09.001.
8. Daniel R Utter, Xuesong He, Colleen M Cavanaugh, et al. The saccharibacterium TM7x elicits differential responses across its host range. The ISME Journal. 2020; 14 (12): 3054–67. DOI: 10.1038/s41396-020-00736-6.
9. Bo Liu, Faller LL, Klitgord N, et al. Deep sequencing of the oral microbiome reveals signatures of periodontal disease. PLOS one. 2012; 7 (6): 37919. DOI: 10.1371/journal.pone.0037919.
10. Mansfield JM, Campbell JH, Bhandari AR, et al. Molecular analysis of 16S rRNA genes identifies potentially periodontal pathogenic bacteria and archaea in the plaque of partially erupted third molars. J Oral Maxillofac Surg. 2012; 70 (7): 1507–14. DOI: 10.1016/J.JOMS.2011.09.049.
11. Chipashvili O, Utter DR, Bedree JK, et al. Episymbiotic Saccharibacteria suppresses gingival inflammation and bone loss in mice through host bacterial modulation. Cell Host & Microbe. 2021; 29 (11): 1649–62. DOI: 10.1016/J.CHOM.2021.09.009.
12. Rosenbaum J, Usyk M, Chen Z, et al. Evaluation of oral cavity DNA extraction methods on bacterial and fungal microbiota. Scientific Reports. 2019; 9 (1): 1531. DOI: 10.1038/s41598-018-38049-6.
13. Benson DA, Cavanaugh M, Clark K, Karsch-Mizrachi I, Lipman DJ, Ostell J, Sayers EW. GenBank. Nucleic Acids Res. 2013; 41: D36-42. DOI: 10.1093/nar/gks1195.
14. Ahmad Ibrahim, Mohamad Maatouk, Andriamiharimamy Rajaonison, et al. Adapted protocol for Saccharibacteria cocultivation: two new members join the club of candidate phyla radiation. Microbiol Spectr. 2021; 9 (3): e0106921. DOI: 10.1128/spectrum.01069-21.
15. Bilgilier C. Fuereder T, Kastner M-T, et al. Oral abundance of actinomyces spp. in breast cancer patients. Oncology. 2022; 100 (4): 221–7. DOI: 10.1159/000522070.
16. Nadkarni MA, Martin FE, Jacques NA, et al. Determination of bacterial load by real-time PCR using a broad-range (universal) probe and primers set. Microbiology. 2002; 148 (Pt 1): 257–66. DOI: 10.1099/00221287-148-1-257.
17. Ying Qi, Sheng-qi Zang, Juan Wei, et al. High-throughput sequencing provides insights into oral microbiota dysbiosis in association with inflammatory bowel disease. Genomics. 2021; 113 (1): 664–76. DOI: 10.1016/j.ygeno.2020.09.063.
18. Utter DR, He X, Cavanaugh CM, et al. The saccharibacterium TM7x elicits differential responses across its host range. The ISME Journal. 2020; 14 (12): 3054–67. DOI: 10.1038/s41396-020-00736-6.
19. Jie Nie, Utter DR, Kerns KA. Strain-Level Variation and diverse host bacterial responses in Episymbiotic Saccharibacteria. mSystems. 2022; 7 (2): e0148821. DOI: 10.1128/msystems.01488-21.
20. Könönen E, Wade WG. Actinomyces and related organisms in human infections. Clinical Microbiology Reviews. 2015; 28 (2): 419–42. DOI: 10.1128/CMR.00100-14.
21. Bedree JK, Bor B, Sen J, et al. Quorum sensing modulates the epibiotic-parasitic relationship between Actinomyces odontolyticus and its Saccharibacteria epibiont, a Nanosynbacter lyticus Strain, TM7x. Front Microbiol. 2018; 9: 2049. DOI: 10.3389/fmicb.2018.02049.

Литература

1. Yixin Li, Yonggang Xiang, Haixia Ren, et al. Association between periodontitis and dental caries: a systematic review and meta-analysis. Clinical Oral Investigations. 2024; 28: 306. 10; 28 (6): 306. DOI: 10.1007/s00784-024-05687-2.
2. Krutyhołowa A, Strzelec K, Dziedzic A, Bereta GP, Łazarz-Bartyzel K, Potempa J, et al. Host and bacterial factors linking periodontitis and rheumatoid arthritis. Front Immunol. 2022; 13: 980805. DOI: 10.3389/fimmu.2022.980805.
3. Cai Z, Lin S, Hu S, Zhao L. Structure and function of oral microbial community in periodontitis based on integrated data. Front Cell Infect Microbiol. 2021; 11: 663756. DOI: 10.3389/fcimb.2021.663756.
4. Jiao Y, Hasegawa M, Inohara N. The role of oral pathobionts in dysbiosis during periodontitis development. Journal of Dental Research. 2014; 93 (6): 539–46. DOI: 10.1177/0022034514528212.
5. Antezack A, Etchecopar-Etchart D, La Scola B, Monnet-Corti V. New putative periodontopathogens and periodontal health-associated species: a systematic review and meta-analysis. 2023; 58: 893–906. DOI: 10.1111/jre.13173
6. Valm AM. The structure of dental plaque microbial communities in the transition from health to dental caries and periodontal disease. J Mol Biol. 2019; 431 (16): 2957–69. DOI: 10.1016/j.jmb.2019.05.016.
7. Hajishengallis G. Immunomicrobial pathogenesis of periodontitis: keystones, pathobionts, and host response. Trends in Immunology. 2014; 35 (1): 3–11. DOI: 10.1016/j.it.2013.09.001.
8. Daniel R Utter, Xuesong He, Colleen M Cavanaugh, et al. The saccharibacterium TM7x elicits differential responses across its host range. The ISME Journal. 2020; 14 (12): 3054–67. DOI: 10.1038/s41396-020-00736-6.
9. Bo Liu, Faller LL, Klitgord N, et al. Deep sequencing of the oral microbiome reveals signatures of periodontal disease. PLOS one. 2012; 7 (6): 37919. DOI: 10.1371/journal.pone.0037919.
10. Mansfield JM, Campbell JH, Bhandari AR, et al. Molecular

analysis of 16S rRNA genes identifies potentially periodontal pathogenic bacteria and archaea in the plaque of partially erupted third molars. J Oral Maxillofac Surg. 2012; 70 (7): 1507–14. DOI: 10.1016/J.JOMS.2011.09.049.

11. Chipashvili O, Utter DR, Bedree JK, et al. Episymbiotic Saccharibacteria suppresses gingival inflammation and bone loss in mice through host bacterial modulation. Cell Host & Microbe. 2021; 29 (11): 1649–62. DOI: 10.1016/J.CHOM.2021.09.009.

12. Rosenbaum J, Usyk M, Chen Z, et al. Evaluation of oral cavity DNA extraction methods on bacterial and fungal microbiota. Scientific Reports. 2019; 9 (1): 1531. DOI: 10.1038/s41598-018-38049-6.

13. Benson DA, Cavanaugh M, Clark K, Karsch-Mizrachi I, Lipman DJ, Ostell J, Sayers EW. GenBank. Nucleic Acids Res. 2013; 41: D36-42. DOI: 10.1093/nar/gks1195.

14. Ahmad Ibrahim, Mohamad Maatouk, Andriamiharimamy Rajaonison, et al. Adapted protocol for Saccharibacteria cocultivation: two new members join the club of candidate phyla radiation. Microbiol Spectr. 2021; 9 (3): e0106921. DOI: 10.1128/spectrum.01069-21.

15. Bilgilier C. Fuereder T, Kastner M-T, et al. Oral abundance of actinomyces spp. in breast cancer patients. Oncology. 2022; 100 (4): 221–7. DOI: 10.1159/000522070.

16. Nadkarni MA, Martin FE, Jacques NA, et al. Determination of bacterial load by real-time PCR using a broad-range (universal) probe and primers set. Microbiology. 2002; 148 (Pt 1): 257–66. DOI: 10.1099/00221287-148-1-257.

17. Ying Qi, Sheng-qi Zang, Juan Wei, et al. High-throughput sequencing provides insights into oral microbiota dysbiosis in association with inflammatory bowel disease. Genomics. 2021; 113 (1): 664–76. DOI: 10.1016/j.ygeno.2020.09.063.

18. Utter DR, He X, Cavanaugh CM, et al. The saccharibacterium TM7x elicits differential responses across its host range. The ISME Journal. 2020; 14 (12): 3054–67. DOI: 10.1038/s41396-020-00736-6.

19. Jie Nie, Utter DR, Kerns KA. Strain-Level Variation and diverse host bacterial responses in Episymbiotic Saccharibacteria. mSystems. 2022; 7 (2): e0148821. DOI: 10.1128/msystems.01488-21.

20. Könönen E, Wade WG. Actinomyces and related organisms in human infections. Clinical Microbiology Reviews. 2015; 28 (2): 419–42. DOI: 10.1128/CMR.00100-14.

21. Bedree JK, Bor B, Sen J, et al. Quorum sensing modulates the epibiotic-parasitic relationship between Actinomyces odontolyticus and its Saccharibacteria epibiont, a Nanosynbacter lyticus Strain, TM7x. Front Microbiol. 2018; 9: 2049. DOI: 10.3389/fmicb.2018.02049.

ASSESSMENT OF THE EFFECT OF HYPOTHERMIA AFTER SIMULATED HYPOXIC ISCHEMIC ENCEPHALOPATHY BASED ON BLOOD METABOLOME

Eldarov CM[1,2] ✉, Starodubtseva NL[1], Shevtsova YuA[1,2], Goryunov KV[1], Ionov OV[1], Silachev DN[1,2]

[1] Kulakov National Medical Research Center for Obstetrics, Gynecology and Perinatology, Moscow, Russia

[2] Belozersky Institute Of Physico-Chemical Biology, Moscow State University, Moscow, Russia

Hypoxic ischemic encephalopathy (HIE) is a severe neonatal condition causing various neurological disorders and one of the main causes of mortality among full-term babies. Therapeutic hypothermia (TH), i.e. the newborn's body temperature decrease that significantly reduces the risk of fatality and contributes to improvement of long-term outcomes in infants with HIE is the key treatment method for moderate-to-severe HIE. However, the timely diagnosis and disease severity determination are crucial for this method to be used, and the method has a number of limitations and requirements. Assessment of the mechanism underlying the effects of TH and the search for the major metabolic pathways and potential targets for HIE therapy are relevant. The study aimed to assess metabolome of dried blood spots by HPLC-MS, since it is the least invasive to patients test for the search for markers and metabolic pathways most active in TH that are likely to mediate its positive effects. As a result, alterations in the class of phosphoglycerolipids were found, which suggests an important role of endocannabinoid metabolism in protection of the body against HIE. Furthermore, metabolic pathways of ubiquinone, certain fatty acids, and bile acids were altered. The targeted quantitative studies of these metabolites will make it possible to optimize HIE diagnosis and treatment based on the potential targets identified.

Keywords: mass spectrometry, neonatal asphyxia, metabolomics, diagnosis, hypoxic ischemic encephalopathy

ОЦЕНКА ЭФФЕКТА ГИПОТЕРМИИ ПОСЛЕ МОДЕЛИРОВАННОЙ ИШЕМИЧЕСКОЙ ГИПОКСИЧЕСКОЙ ЭНЦЕФАЛОПАТИИ ПО МЕТАБОЛОМУ КРОВИ

Ч. М. Эльдаров[1,2] ✉, Н. Л. Стародубцева[1], Ю. А. Шевцова[1,2], К. В. Горюнов[1], О. В. Ионов[1], Д. Н. Силачев[1,2]

[1] Национальный медицинский исследовательский центр акушерства, гинекологии и перинатологии имени В. И. Кулакова, Москва, Россия

[2] Научно-исследовательский институт физико-химической биологии имени А. Н. Белозерского Московского государственного университета, Москва, Россия

Гипоксически-ишемическая энцефалопатия (ГИЭ) — тяжелая неонатальная патология, вызывающая различные неврологические нарушения, одна из основных причин смертности доношенных детей. Ключевым методом лечения умеренной и тяжелой ГИЭ является терапевтическая гипотермия (ТГ) — снижение температуры тела новорожденных, которая существенно уменьшает риск летального исхода и способствует улучшению долгосрочных исходов у детей с ГИЭ. Однако для применения этого метода критически важна своевременная диагностика и определение тяжести заболевания, кроме того он имеет ряд ограничений и требований. Актуальны изучение механизма действия ТГ, поиск основных метаболических путей и потенциальных мишеней для терапии ГИЭ. Целью работы было с помощью методов ВЭЖХ-МС исследовать метаболом сухих пятен крови как менее инвазивной для пациента пробы для поиска маркеров и метаболических путей, наиболее активных при ТГ и, вероятно, опосредующих ее положительные эффекты. В результате были обнаружены изменения в классе фосфоглицеролипидов, что может свидетельствовать о важной роли метаболизма эндоканнабиноидов в защите организма от ГИЭ. Кроме того, были изменены пути метаболизма убихинона, ряда жирных кислот, а также желчных кислот. Таргетные количественные исследования данных метаболитов позволят оптимизировать диагностику ГИЭ и ее терапию на основе выявленных потенциальных мишеней.

Ключевые слова: масс-спектрометрия, неонатальная асфиксия, метаболомика, диагностика, гипоксически-ишемическая энцефалопатия

Hypoxic ischemic encephalopathy (HIE) is a severe neurological condition resulting from the lack of oxygen and insufficient blood supply to the brain of a newborn before and during labor. The rate of moderate-to-severe HIE forms is 1–8 cases per 1000 live births in the countries with advanced medicine, it shows no downward trend. HIE causes 6–9% of deaths among newborns and 21–23% of deaths among full-term babies, and 25% affected individuals develop severe neurological disorders (cerebral palsy, epilepsy, seizures, and developmental delay) [1].

The timely diagnosis and accurate determination of HIE severity are crucial for improvement of outcomes and the children's quality of life [2]. Therapeutic hypothermia (TH) is the key treatment method for moderate-to-severe HIE widely used in intensive care units. This approach significantly decreases the risk of fatality and contributes to improvement of long-term outcomes in infants with HIE [3].

The body or head temperature decrease occurring during TH slows down metabolic processes, reduces the neurons' oxygen demands, as well as the levels of oxidative stress and its mediators, i.e. glutamate and free radicals. Furthermore, inflammatory response is suppressed and apoptosis is prevented, which mitigates the effects of primary hypoxic ischemic stroke [4]. However, it is necessary to start TH within the first six hours of life (acute phase of hypoxic ischemic injury), before activation of secondary injury mechanisms, such as inflammation and apoptosis, for optimal results [5]. Unfortunately, despite proven efficacy of TH, about 20% of newborns with moderate or severe HIE do not receive treatment they need due to delayed diagnosis [6]. TH has a number of limitations and the use of TH can be dangerous in cases of erroneous diagnosis [7]. This emphasizes the importance of rapid intervention and improvement of diagnostic procedures in neonatology, including the analysis of biochemical markers associated with brain damage.

The search for HIE markers is hampered by both low prevalence of the disorder in the population and difficulty distinguishing from concomitant disorders, such as sepsis and congenital metabolic disorders [2, 8]. The use of noninvasive (urine, feces) and minimally invasive (blood, dried blood spots) samples makes it possible to effectively assess the dynamic changes in molecular composition of body fluids. The samples remaining after the routine procedures can be used for further testing without any additional interventions.

Assessment under the controlled conditions in model systems is performed to identify the markers associated exclusively with brain damage [8, 9]. The Rice–Vannucci model proposed in 1981 is most often used as a pre-clinical model for HIE assessment; it is used in laboratory settings all over the world over the last four decades [9, 10].

The omics technologies, including genomics, transcriptomics, proteomics, and metabolomics, contributed greatly to clarification of the pathophysiological mechanisms underlying HIE. These processes include alterations in energy metabolism of brain cells, oxidative stress, disturbed metabolism of neurotransmitters and hormones, as well as apoptosis of neurons and activation of neuroprotective (defensive) mechanisms [5, 8, 11–13]. The analysis of metabolic alterations in dried blood spots by liquid chromatography–mass spectrometry (HPLC-MS) is a promising strategy for improving the diagnosis and prediction of HIE in newborns. Together with multivariate analysis techniques, HPLC-MS allows one to isolate the whole patterns of biomolecules specific for hypoxic ischemic (HI) brain injury [5].

The study aimed to clarify the molecular mechanisms and identify the brain damage markers triggered in hypothermia during recovery after the HI brain injury using the modified Rice–Vannucci model by untargeted metabolomics (HPLC-MS) of dried blood spots in negative mode.

METHODS

HIE simulation

The animal handling protocol was approved by the local Ethics Committee in accordance with the principles of the Federation of European Laboratory Animal Science Associations (FELASA). The experiments involved outbred white rats obtained from the animal facility of the Belozersky Institute Of Physico-Chemical Biology, MSU.

The modified Rice–Vannucci model was used to simulate HI brain injury [26–27]. The 7-day-old male and female pups were anesthetized with 1% isoflurane, after which the left carotid artery was surgically isolated and subjected to electrocoagulation. After 1.5 h the pups were placed in the CO_2 incubator (Binder; Tuttlingen, Germany) with the gas mixture containing 8% of oxygen and 92% of nitrogen at 37 °C for 2 h.

Therapeutic hypothermia

Rats were randomly distributed into normothermic and hypothermic groups immediately after the end of HI for 6 h, then the dried blood spot samples were obtained. The experiment involved three groups of animals: control group ($n = 13$), rats with HIE and subsequent 6-h hypothermia ($n = 16$), rats with HIE and subsequent 6-h normothermia ($n = 14$). Normothermia was maintained at the level of 37 °C, hypothermic recovery took place at 30 °C. Pups were placed in an open container in a water bath in order to maintain the specified temperature.

Dried blood spot collection

The pups' blood was collected from the subclavian artery 6 h after normothermia/hypothermia, 40 µL of blood were applied to the PerkinElmer 226 filter paper test sheet. When applying blood to the sheet, we made sure that the tip of the syringe did not touch the paper. Once dry, blood spots were tested for suitability for analysis (the area of the paper impregnated with blood had to be at least 3 mm in diameter). The samples were considered unsuitable, when the blood spot area was insufficient or, in case of small samples, when blood didn't soak through the paper. The spots were also considered to be unsuitable, when there were microclots in the sample suggesting patchy distribution of the spot across the paper.

Sample preparation for HPLC-MS

Metabolites were extracted from the dried blood spots by the Folch's method [14]. Each sample (three circular fragments of the dried blood spot, 5 mm in diameter each) were added 480 µL of the chloroform and methanol mixture (2 : 1 ratio) and 250 µL of water. The extraction mixture was vortexed for 10 min, and then centrifuged at 15,000 g for 10 min. The organic phase (150 mL) from the lower part of the Eppendorf tube was transferred to a separate tube. This extraction phase was repeated with adding one more portion of the chloroform–methanol mixture. A total of 100 µL of the organic phase after the second centrifugation was mixed with the previously collected organic phase. The resulting mixture was dried under a nitrogen stream at room temperature, and then dissolved in 100 mL of the acetonitrile and isopropanol mixture (1 : 1 ratio) again.

Scores Plot
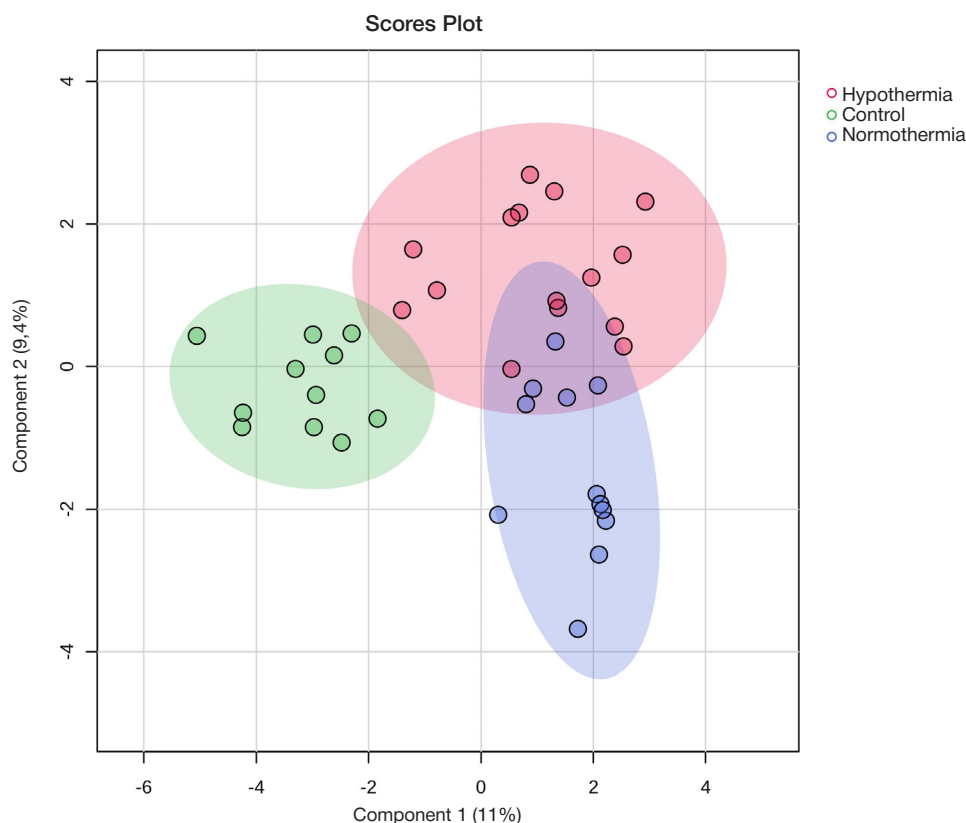
Fig. 1. Results of multivariate analysis by sPLS-DA for three studied groups of animals

HPLC-MS analysis and identification of substances

Further analysis was performed by HPLC-MS. The reverse-phased Atlantis T3 C18 column (particle size 3 μm, length 15 cm, inner diameter 1 mm; Waters, Milford, Massachusetts, USA) and the Ultimate 3000 Nano LC chromatography system (Thermo Scientific; Waltham, Massachusetts, USA) were used for chromatographic separation of the complex mixture of substances [30–31]. The mobile phase A consisted of the ACN : H$_2$0 mixture (60 : 40), and the mobile phase B consisted of IPA : ACN : H$_2$O (90 : 8 : 2). Both phases contained modifiers (0.1% of formic acid and 5 mm of ammonium formate). Elution was performed with the mobile phase B gradient at the flow rate of 40 μL/min: 0–0.5 min at 10%, then the 20-minute gradient from 10% to 99%. After that the 10-minute washing with the 99% phase B was performed, then the phase was returned to its initial concentration (10% of phase B) within 1 min, and the column was equilibrated for 3 min. The total chromatographic run time per sample was 34.5 min at the flow rate of 40 μL/min and the column temperature of 50 °C. Metabolites were determined using the Bruker MaXis Impact hybrid quadrupole time-of-flight mass spectrometer (Bruker Daltoniks; Bremen, Germany), with two repeats per sample and the following device settings: capillary voltage 4500 V; nebulizer pressure 0.6 Pa, drying gas flow rate 5.0 L/min at 200 °C. Mass spectra were acquired at the 50,000 resolution within the range of 50–1700 m/z, with negative polarity.

Peak detection and grouping, as well as retention time adjustment were performed using the xcms software package. The Centwave algorithm was used to detect peaks with certain parameters: the maximum m/z deviation was 15 ppm, and the peak width was 10–45 s. Peaks were grouped by the Peak Density method with the default parameters [15–16]. Metabolites were identified based on the Human Metabolome database (https://www.hmdb.ca).

Statistical methods

To identify and visualize the differences between groups, we conducted multivariate analysis by the partial least squares method (sPLS-DA) for multiple groups and the orthogonal partial least squares method (OPLS-DA) for pairwise comparison implemented in the Metaboanalyst 6.0.0 package (https://metaboanalyst.ca). Significance of intergroup differences in relative concentrations (average integrated peak areas) of certain metabolites was estimated using the t-test, and p-value below 0.05 was considered to be significant. As an additional criterion for identification of potential biomarkers, the fold change was limited to the value of 1.5. The analysis of enrichment pathways was performed using the over-representation analysis function of the Metaboanalyst 6.0.0 package.

RESULTS

The analysis of mass spectra conducted in the negative ion mode allowed us to identify 3425 molecular ions. To assess the differences between the groups of animals, we used the multivariate partial least squares method (sPLS-DA). According to the results provided in Fig. 1, the groups can be clearly distinguished, which is indicative of significant metabolic alterations typical for each group. This highlights that there are specific molecular differences underlying the dividing factors (Fig. 2).

To search for potential biomarkers, we conducted univariate statistical analysis of the normothermia-hypothermia pair (Fig. 2). A total of 55 molecular ions were found, among which 27 showed the concentration increase in the samples of animals subjected to hypothermia relative to the normothermic group. At the same time, concentrations of 28 molecular ions were decreased. We took into account significant differences in concentrations only (at least 1.5-fold with the significance level
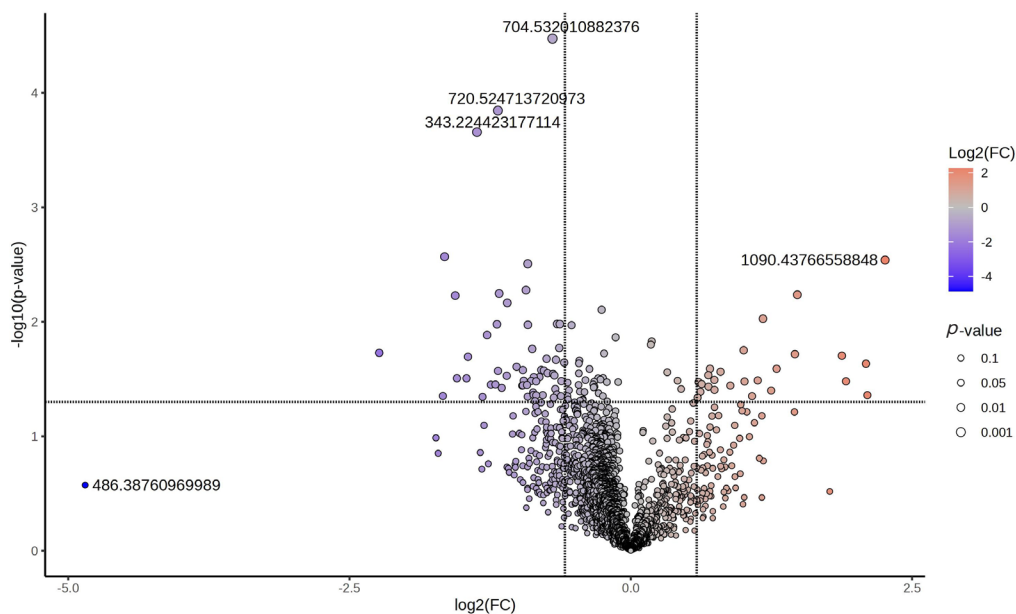
Fig. 2. Results of pairwise univariate statistical analysis of the dried blood spot metabolome for hypothermic and normothermic animals

$p < 0.05$). The compounds detected were identified using the LIPID MAPS and HMDB databases; the results are provided in Table 1. The data obtained show significant changes in metabolism of phosphoethanolamines and phosphatidic acids in hypothermia compared to normothermia, while the fatty acid levels remain relatively stable. Extensive analysis was conducted using the multivariate statistical method (orthogonal partial least squares (OPLS)), which allowed us to clearly delineate normothermic and hypothermic groups. The findings confirm that there are significant metabolic differences between

Table 1. List of potential biomarkers showing significant differences between the therapeutic hypothermia group and the control group

m/z	Name	Fold change	Adduct
294.157	CAR 6:0	2.32	[M+Cl]–
343.224	17-HDoHE	–2.34	M–H
353.308	FA 22:1;O	–4.58	[M–H]–
611.385	PA 30:4	–2.78	[M–H]–
677.386	PA 32:3	–2.09	[M+Cl]–
720.524	PS O-32:0	–1.9	[M–H]–
750.475	PE 36:6–OH	–2.42	M–H
802.503	PE 40:8–OH	2.26	M–H
812.523	PE 42:9	2.13	M–H
826.501	PE 42:10–OH	2.4	M–H
829.52	PG 38:4–2OH	3.09	M–H
833.478	PA 40:5–3OH	–1.6	M+Cl
841.577	PG 38:0	–2.64	[M+Cl]–
856.601	PE 42:3–2OH	–3.16	M–H
873.621	PA 46:3	–2.14	M+Cl
878.53	PE 40:4–3OH	4.01	M+Cl
883.471	PGP 36:3–2OH	3.68	M–H
885.485	PI 16:2–2OH	1.7	M–H
933.672	TG 56:5	–2.32	M+Cl
952.447	MIPC 29:2;O5	–2.55	M+Cl
953.468	PGP 40:6–OH	1.71	M+Cl
1021.451	PIP 36:4–3OH	1.68	M+Cl
627.343	LysoPI 20:0	0.63325	M–H
704.532	PE-Nme 32:0	0.66455	M–H
803.506	PA 40:3–O	1.9181	M+Cl
838.536	PE 44:10	3.5626	M–H
854.53	PE 44:10–OH	2.1599	M–H
902.476	PS 42:10–3OH	0.59297	M–H

Scores Plot
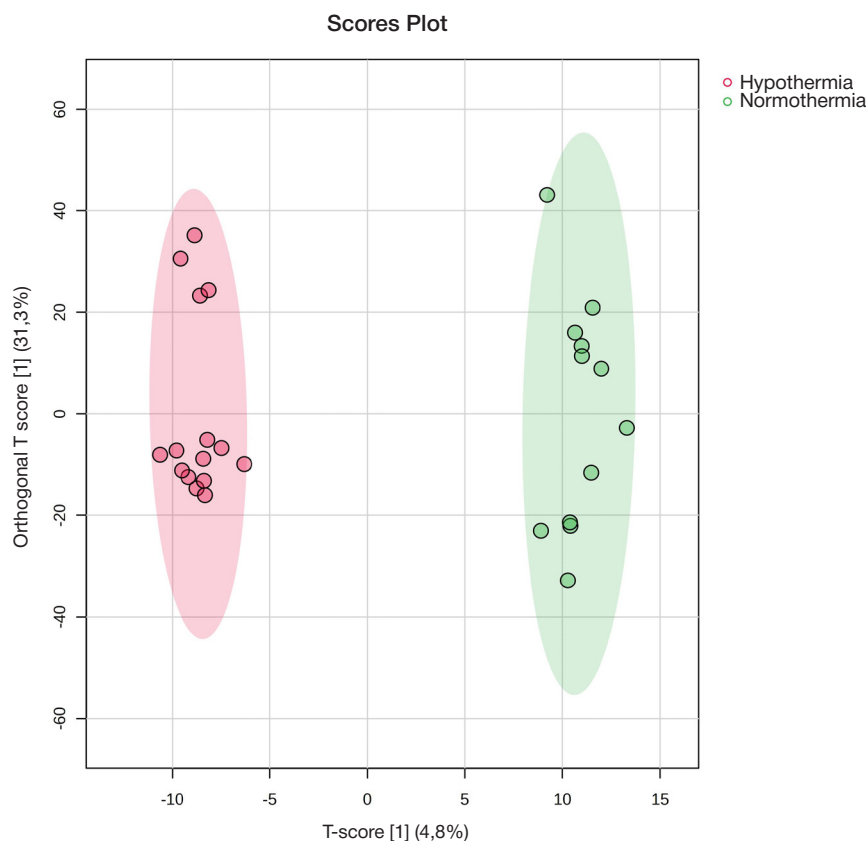
Fig. 3. Delineation of groups based on multivariate statistical analysis by the orthogonal partial least squares (OPLS-DA) method

these physiological states (Fig. 3). We selected molecular ions (top 200) that made the greatest contribution to delineation of the groups (VIP score >1) based on the analysis results; identification and search for the most involved metabolic pathways in the SMPDB database were performed for these ions. The changes in activity of biosynthesis pathways of bile acids, ubiquinone and plasmalogens, as well as in metabolism of a number of fatty acids, estrogens and androgens associated with hypothermia were identified (Table 2).

DISCUSSION

HIE is a major cause of neurological disorders and neonatal mortality. Ischemia followed by hypoxia leads to neuronal death within 12–36 h, which makes the timely diagnosis of HIE and estimation of injury severity one of the factors important for successful prediction of outcomes and selection of adequate therapy. MRI and aEEG of the brain that allow one to somehow estimate physical and functional brain damage represent the standard methods to diagnose HIE. However, these methods have limited informative value: thus, MRI is often impossible in newborns with severe conditions, it is associated with the need for sedation and is conducted 24 h or more after birth, while aEEG has insufficient sensitivity for early diagnosis. Furthermore, these methods involve no quantitative markers

allowing one to reliably determine HIE severity. Therefore, prediction of outcomes remains a challenging task.

At the same time, therapeutic hypothermia, during which the newborn's head is cooled to 32–35 °C for 48–72 h, represents one of the main HIE therapy methods. To ensure the neuroprotective effect, it is necessary to start the procedure within the first 6 h of the newborn's life. Assessment of blood biomarkers represents one of the HIE early diagnosis methods, since HIE is associated with not only brain damage, but also damage to the heart, liver, and other organs causing alterations of their metabolism. When assessing the dynamic changes in blood biomarkers, it is possible to correlate the changes with the developing injury and body's response, later adapting the therapy received by the patient to these changes. The use of changes in pro-inflammatory and other blood markers for the diagnosis of HIE has been previously reported. While venous blood collection for further testing is a gold standard in medicine, the use of this method is associated with a number of nuisance due to its invasive nature, the need to teach personnel, and difficulty ensuring conditions for storage and transportation of the samples collected. This is particularly true when working with newborns having severe disorders. In this study we used dried blood spots to assess metabolome. This method representing one of blood microsampling methods is becoming increasingly common due to low invasiveness,

Table 2. Metabolic pathways to the greater extent determining the differences between the normothermia and therapeutic hypothermia groups based on the OPLS-DA data

Name	Matches	*P*-value
Bile acid biosynthesis	4	0.0016
Ubiquinone biosynthesis	2	0.0125
Metabolism of alpha-linolenic and linoleic acids	1	0.143
Plasmalogen synthesis	1	0.211
Metabolism of estrogens and androgens	1	0.261

protocol simplicity, and easy storage of the acquired material collections. To use the method, it is important to estimate the effectiveness of its use for identification of early blood biomarkers.

The use of multivariate statistical analysis methods revealed significant differences both from the intact group and between normothermic and hypothermic groups (Fig. 2), which reflects metabolic changes associated with HIE and HIE under conditions of normothermia. Pairwise statistical analysis with subsequent identification made it possible to reveal changes in the classes of phosphatidic acids (PA), phosphatidylinositols (PI) and phosphatidylethanolamines (PE) that belong to glycerophospholipids, as well as triglycerides and acylcarnitines. Furthermore, we revealed elevated PI levels. According to the literature data, brain ischemia leads to degradation of PI and diacylglycerols. Thus, expansion of the pool of PI and phosphatidylinositol diphosphate in the group with therapeutic hypothermia can indicate inhibition of its degradation in hypothermia, which has a neuroprotective effect. The hypothermic group also showed elevated levels of short-chain acylcarnitines (C6). It has been earlier shown in the cell-based model that short-chain acylcarnitines increase the expression of genes associated with antioxidant activity under conditions of oxidative stress [17]. As for phosphatidic acids, these are messengers and intermediates of other glycerolipids, such as PE and phosphatidylserines (PS) [18]. In the normothermic group we can see the decreased levels of intermediates in the form of phosphatidic acids, as well as the elevated PE and PS levels. In turn, PE are precursors of a number of endocannabinoids, the neuroprotective role of which is well known [19–22]. Thus, the use of therapeutic hypothermia led to the increase in concentrations of a number of metabolites associated with reduction of the oxidative stress resulting from ischemia-reperfusion and neuroprotectors, as well as their precursors, which definitely can reduce the overall damage resulting from HIE.

During the study we also analyzed the major metabolic pathways altered in hypothermia relative to the normothermic group. For that we identified molecular ions that had made the greatest contribution to the differences between groups in the OPLS-DA multivariate statistical analysis model (VIP, 200 most "weighty" molecular ions) and revealed metabolic pathways, these belonged to. The most involved pathways included synthesis of ubiquinone, bile acids, unsaturated fatty acids and plasmalogens (Table 2). The presence of bile acids in the list can seem extraordinary. However, a number of studies have already shown that bile acids can cross the blood-brain barrier, performing the important functions of messengers and neuromodulators [23–24]. Bile acids have neuroprotective properties, these attenuate inflammation and the effects of oxidative stress, such as apoptosis [23–24], which is of special interest in the context of extensive oxidative stress resulting from ischemia-reperfusion associated with HIE [25–27]. The same is true for unsaturated fatty acids: both linoleic and alpha-linolenic fatty acids play an important role in body's response and adaptation to acute ischemia through regulation of the neuronal signaling pathways by using oxylipins, the oxidized derivatives [28], show well-defined neuroprotective and even antidepressant properties [29]. As for ubiquinone, its role in protection against oxidative stress is widely known ([30], etc.).

CONCLUSIONS

Thus, our study has revealed a number of metabolome alterations when using therapeutic hypothermia, suggesting mitigation of brain damage caused by HIE, along with involvement of pathways responsible for synthesis of various neuroprotectors and neuromodulators. These findings confirm understanding of therapeutic hypothermia as an effective method for therapy of the HIE sequelae. The use of mass spectrometry makes it possible to obtain information about metabolic alterations as early as within the first hours after birth. At the same time, the targeted quantitative studies of the metabolites identified (glycerophospholipids, bile acids, etc.) in patients with HIE of varying severity can make it possible to develop an effective system for early classification of HIE severity and prediction of outcomes.

References

1. Törn AE, Hesselman S, Johansen K, Ågren J, Wikström A-K, Jonsson M. Outcomes in Children after Mild Neonatal Hypoxic Ischaemic Encephalopathy: A Population-Based Cohort Study. BJOG Int. J Obstet Gynaecol. 2023.
2. Caramelo I, Coelho M, Rosado M, Cardoso CMP, Dinis A, Duarte CB, et al. Biomarkers of hypoxic-ischemic encephalopathy: a systematic review. World J Pediatr. 2023; 19: 505–48.
3. Abate BB, Bimerew M, Gebremichael B, Mengesha Kassie A, Kassaw M, Gebremeskel T, et al. Effects of therapeutic hypothermia on death among asphyxiated neonates with hypoxic-ischemic encephalopathy: A systematic review and meta-analysis of randomized control trials. PLoS One. 2021; 16 (2); e0247229.
4. Sun YJ, Zhang ZY, Fan B, Li GY. Neuroprotection by Therapeutic Hypothermia. Front Neurosci. 2019; 13; 586.
5. Korf JM, McCullough LD, Caretti V. A narrative review on treatment strategies for neonatal hypoxic ischemic encephalopathy. Transl Pediatr. 2023; 12: 1552–71.
6. DuPont TL, Chalak LF, Morriss MC, Burchfield PJ, Christie L, Sánchez PJ. Short-Term Outcomes of Newborns with Perinatal Acidemia Who Are Not Eligible for Systemic Hypothermia Therapy. J Pediatr. 2013; 162: 35–41.
7. Prempunpong C, Chalak LF, Garfinkle J, Shah B, Kalra V, Rollins N, et al. Prospective Research on Infants with Mild Encephalopathy: The PRIME Study. J Perinatol. 2018; 38: 80–85.
8. She HQ, Sun YF, Chen L, Xiao QX, Luo BY, Zhou HS, et al. Current analysis of hypoxic-ischemic encephalopathy research issues and future treatment modalities. Front Neurosci. 2023; 17: 1136500.
9. Landucci E, Pellegrini-Giampietro DE, Facchinetti F. Experimental Models for Testing the Efficacy of Pharmacological Treatments for Neonatal Hypoxic-Ischemic Encephalopathy. Biomedicines. 2022; 10 (5): 937.
10. Tokareva A, Starodubtseva N, Frankevich V, Silachev D. Minimizing Cohort Discrepancies: A Comparative Analysis of Data Normalization Approaches in Biomarker Research. Computation. 2024; 12: 137.
11. Eldarov C, Starodubtseva N, Shevtsova Y, Goryunov K, Ionov O, Frankevich V, et al. Dried Blood Spot Metabolome Features of Ischemic–Hypoxic Encephalopathy: A Neonatal Rat Model Int J Mol Sci. 2024; 25: 8903.
12. Shevtsova Y, Starodubtseva N, Tokareva A, Goryunov K, Sadekova A, Vedikhina I, et al. Metabolite Biomarkers for Early Ischemic–Hypoxic Encephalopathy: An Experimental Study Using the NeoBase 2 MSMS Kit in a Rat Model. Int J Mol Sci. 2024; 25: 2035.
13. Shevtsova Y, Eldarov C, Starodubtseva N, Goryunov K, Chagovets V, Ionov O, et al. Identification of Metabolomic Signatures for Ischemic Hypoxic Encephalopathy Using a Neonatal Rat Model. Children. 2023; 10: 1693.
14. Folch J, Lees M, Sloane Stanley GH. A Simple Method for the Isolation and Purification of Total Lipides from Animal Tissues. J Biol Chem. 1957; 226: 497–509.

15. Tokareva AO, Chagovets VV, Kononikhin AS, Starodubtseva NL, Nikolaev EN, Frankevich VE. Normalization Methods for Reducing Interbatch Effect without Quality Control Samples in Liquid Chromatography-Mass Spectrometry-Based Studies. Anal Bioanal Chem. 2021; 413: 3479–86.

16. Tokareva AO, Chagovets VV, Kononikhin AS, Starodubtseva NL, Nikolaev EN, Frankevich VE. Comparison of the Effectiveness of Variable Selection Method for Creating a Diagnostic Panel of Biomarkers for Mass Spectrometric Lipidome Analysis. J Mass Spectrom. 2021; 56: e4702.

17. Calò LA, Pagnin E, Davis PA, Semplicini A, Nicolai R, Calvani M, et al. Antioxidant effect of l-carnitine and its short chain esters: Relevance for the protection from oxidative stress related cardiovascular damage. International Journal of Cardiology. 2006; 54–60.

18. Fantini J, Yahi N. Chapter 3 — Lipid Metabolism and Oxidation in Neurons and Glial Cells. In: Jacques Fantini, Nouara Yahi, editors. Brain Lipids in Synaptic Function and Neurological Disease. Academic Press, 2015; p. 53–85.

19. Hahnefeld L, Vogel A, Gurke R, Geisslinger G, Schäfer MKE, Tegeder I. Phosphatidylethanolamine Deficiency and Triglyceride Overload in Perilesional Cortex Contribute to Non-Goal-Directed Hyperactivity after Traumatic Brain Injury in Mice. Biomedicines. 2022; 10: 914.

20. Duranti A, Beldarrain G, Álvarez A, Sbriscia M, Carloni S, Balduini W. et al. The Endocannabinoid System as a Target for Neuroprotection/Neuroregeneration in Perinatal Hypoxic-Ischemic Brain Injury. Biomedicines. 2022; 11 (1): 28.

21. Sagredo O, Palazuelos J, Gutierrez-Rodriguez A, Satta V, Galve-Roperh I, Martínez-Orgado J. Cannabinoid signalling in the immature brain: Encephalopathies and neurodevelopmental disorders. Biochem Pharmacol. 2018; 157: 85–96.

22. Fernández-Ruiz J, Moro MA, Martínez-Orgado J. Cannabinoids in neurodegenerative disorders and stroke/brain trauma: From preclinical models to clinical applications. Neurotherapeutics. 2015; 12: 793–806.

23. Xing C, Huang X, Wang D, et al. Roles of bile acids signaling in neuromodulation under physiological and pathological conditions. Cell Biosci. 2023; 13: 106.

24. Yeo Xin Yi , Tan Li Yang , Chae Woo Ri , Lee Dong-Yup , Lee Yong-An, Wuestefeld Torsten. Liver's influence on the brain through the action of bile acids. Frontiers in Neuroscience. 2023; 17.

25. Kletkiewicz H., Wojciechowski MS., Rogalska J. Cannabidiol effectively prevents oxidative stress and stabilizes hypoxia-inducible factor-1 alpha (HIF-1α) in an animal model of global hypoxia. Sci Rep. 2024; 14 (1): 15952.

26. Kong W, Lu C. Role of mitochondria in neonatal hypoxic-ischemic encephalopathy. Histol Histopathol. 2024; 39 (8): 991–1000.

27. Baldari B, De Simone S, Cipolloni L, Frisoni P, Alfieri L, D'Errico S, et al. Oxidative Stress Markers in Human Brain and Placenta May Reveal the Timing of Hypoxic-Ischemic Injury: Evidence from an Immunohistochemical Study. Int J Mol Sci. 2023; 24 (15): 12221.

28. Hennebelle M, Zhang Z, Metherel AH, et al. Linoleic acid participates in the response to ischemic brain injury through oxidized metabolites that regulate neurotransmission. Sci Rep. 2017; 7: 4342.

29. Blondeau N, Lipsky RH, Bourourou M, Duncan MW, Gorelick PB, Marini AM, Alpha-Linolenic Acid: An Omega-3 Fatty Acid with Neuroprotective Properties — Ready for Use in the Stroke Clinic? BioMed Research International. 2015; 519830.

30. Obolenskaia ON, Gorodetskaya EA, Kalenikova EI, Belousova MA, Gulyaev MV, Makarov VG, et al. Intravenous Administration of Coenzyme Q10 in Acute Period of Cerebral Ischemia Decreases Mortality by Reducing Brain Necrosis and Limiting Its Increase within 4 Days in Rat Stroke Model. Antioxidants (Basel). 2020; 9 (12): 1240.

Литература

1. Törn AE, Hesselman S, Johansen K, Ågren J, Wikström A-K, Jonsson M. Outcomes in Children after Mild Neonatal Hypoxic Ischaemic Encephalopathy: A Population-Based Cohort Study. BJOG Int. J Obstet Gynaecol. 2023.

2. Caramelo I, Coelho M, Rosado M, Cardoso CMP, Dinis A, Duarte CB, et al. Biomarkers of hypoxic-ischemic encephalopathy: a systematic review. World J Pediatr. 2023; 19: 505–48.

3. Abate BB, Bimerew M, Gebremichael B, Mengesha Kassie A, Kassaw M, Gebremeskel T, et al. Effects of therapeutic hypothermia on death among asphyxiated neonates with hypoxic-ischemic encephalopathy: A systematic review and meta-analysis of randomized control trials. PLoS One. 2021; 16 (2): e0247229.

4. Sun YJ, Zhang ZY, Fan B, Li GY. Neuroprotection by Therapeutic Hypothermia. Front Neurosci. 2019; 13; 586.

5. Korf JM, McCullough LD, Caretti V. A narrative review on treatment strategies for neonatal hypoxic ischemic encephalopathy. Transl Pediatr. 2023; 12: 1552–71.

6. DuPont TL, Chalak LF, Morriss MC, Burchfield PJ, Christie L, Sánchez PJ. Short-Term Outcomes of Newborns with Perinatal Acidemia Who Are Not Eligible for Systemic Hypothermia Therapy. J Pediatr. 2013; 162: 35–41.

7. Prempunpong C, Chalak LF, Garfinkle J, Shah B, Kalra V, Rollins N, et al. Prospective Research on Infants with Mild Encephalopathy: The PRIME Study. J Perinatol. 2018; 38: 80–85.

8. She HQ, Sun YF, Chen L, Xiao QX, Luo BY, Zhou HS, et al. Current analysis of hypoxic-ischemic encephalopathy research issues and future treatment modalities. Front Neurosci. 2023; 17: 1136500.

9. Landucci E, Pellegrini-Giampietro DE, Facchinetti F. Experimental Models for Testing the Efficacy of Pharmacological Treatments for Neonatal Hypoxic-Ischemic Encephalopathy. Biomedicines. 2022; 10 (5): 937.

10. Tokareva A, Starodubtseva N, Frankevich V, Silachev D. Minimizing Cohort Discrepancies: A Comparative Analysis of Data Normalization Approaches in Biomarker Research. Computation. 2024; 12: 137.

11. Eldarov C, Starodubtseva N, Shevtsova Y, Goryunov K, Ionov O, Frankevich V, et al. Dried Blood Spot Metabolome Features of Ischemic–Hypoxic Encephalopathy: A Neonatal Rat Model Int J Mol Sci. 2024; 25: 8903.

12. Shevtsova Y, Starodubtseva N, Tokareva A, Goryunov K, Sadekova A, Vedikhina I, et al. Metabolite Biomarkers for Early Ischemic–Hypoxic Encephalopathy: An Experimental Study Using the NeoBase 2 MSMS Kit in a Rat Model. Int J Mol Sci. 2024; 25: 2035.

13. Shevtsova Y, Eldarov C, Starodubtseva N, Goryunov K, Chagovets V, Ionov O, et al. Identification of Metabolomic Signatures for Ischemic Hypoxic Encephalopathy Using a Neonatal Rat Model. Children. 2023; 10: 1693.

14. Folch J, Lees M, Sloane Stanley GH. A Simple Method for the Isolation and Purification of Total Lipides from Animal Tissues. J Biol Chem. 1957; 226: 497–509.

15. Tokareva AO, Chagovets VV, Kononikhin AS, Starodubtseva NL, Nikolaev EN, Frankevich VE. Normalization Methods for Reducing Interbatch Effect without Quality Control Samples in Liquid Chromatography-Mass Spectrometry-Based Studies. Anal Bioanal Chem. 2021; 413: 3479–86.

16. Tokareva AO, Chagovets VV, Kononikhin AS, Starodubtseva NL, Nikolaev EN, Frankevich VE. Comparison of the Effectiveness of Variable Selection Method for Creating a Diagnostic Panel of Biomarkers for Mass Spectrometric Lipidome Analysis. J Mass Spectrom. 2021; 56: e4702.

17. Calò LA, Pagnin E, Davis PA, Semplicini A, Nicolai R, Calvani M, et al. Antioxidant effect of l-carnitine and its short chain esters: Relevance for the protection from oxidative stress related cardiovascular damage. International Journal of Cardiology. 2006; 54–60.

18. Fantini J, Yahi N. Chapter 3 — Lipid Metabolism and Oxidation in Neurons and Glial Cells. In: Jacques Fantini, Nouara Yahi, editors. Brain Lipids in Synaptic Function and Neurological Disease. Academic Press, 2015; p. 53–85.

19. Hahnefeld L, Vogel A, Gurke R, Geisslinger G, Schäfer MKE,

Tegeder I. Phosphatidylethanolamine Deficiency and Triglyceride Overload in Perilesional Cortex Contribute to Non-Goal-Directed Hyperactivity after Traumatic Brain Injury in Mice. Biomedicines. 2022; 10: 914.

20. Duranti A, Beldarrain G, Álvarez A, Sbriscia M, Carloni S, Balduini W. et al. The Endocannabinoid System as a Target for Neuroprotection/Neuroregeneration in Perinatal Hypoxic-Ischemic Brain Injury. Biomedicines. 2022; 11 (1): 28.

21. Sagredo O, Palazuelos J, Gutierrez-Rodriguez A, Satta V, Galve-Roperh I, Martínez-Orgado J. Cannabinoid signalling in the immature brain: Encephalopathies and neurodevelopmental disorders. Biochem Pharmacol. 2018; 157: 85–96.

22. Fernández-Ruiz J, Moro MA, Martínez-Orgado J. Cannabinoids in neurodegenerative disorders and stroke/brain trauma: From preclinical models to clinical applications. Neurotherapeutics. 2015; 12: 793–806.

23. Xing C, Huang X, Wang D, et al. Roles of bile acids signaling in neuromodulation under physiological and pathological conditions. Cell Biosci. 2023; 13: 106.

24. Yeo Xin Yi , Tan Li Yang , Chae Woo Ri , Lee Dong-Yup , Lee Yong-An, Wuestefeld Torsten. Liver's influence on the brain through the action of bile acids. Frontiers in Neuroscience. 2023; 17.

25. Kletkiewicz H., Wojciechowski MS., Rogalska J. Cannabidiol effectively prevents oxidative stress and stabilizes hypoxia-inducible factor-1 alpha (HIF-1α) in an animal model of global hypoxia. Sci Rep. 2024; 14 (1): 15952.

26. Kong W, Lu C. Role of mitochondria in neonatal hypoxic-ischemic encephalopathy. Histol Histopathol. 2024; 39 (8): 991–1000.

27. Baldari B, De Simone S, Cipolloni L, Frisoni P, Alfieri L, D'Errico S, et al. Oxidative Stress Markers in Human Brain and Placenta May Reveal the Timing of Hypoxic-Ischemic Injury: Evidence from an Immunohistochemical Study. Int J Mol Sci. 2023; 24 (15): 12221.

28. Hennebelle M, Zhang Z, Metherel AH, et al. Linoleic acid participates in the response to ischemic brain injury through oxidized metabolites that regulate neurotransmission. Sci Rep. 2017; 7: 4342.

29. Blondeau N, Lipsky RH, Bourourou M, Duncan MW, Gorelick PB, Marini AM, Alpha-Linolenic Acid: An Omega-3 Fatty Acid with Neuroprotective Properties — Ready for Use in the Stroke Clinic? BioMed Research International. 2015; 519830.

30. Obolenskaia ON, Gorodetskaya EA, Kalenikova EI, Belousova MA, Gulyaev MV, Makarov VG, et al. Intravenous Administration of Coenzyme Q10 in Acute Period of Cerebral Ischemia Decreases Mortality by Reducing Brain Necrosis and Limiting Its Increase within 4 Days in Rat Stroke Model. Antioxidants (Basel). 2020; 9 (12): 1240.

EXPERIENCE OF IMPLEMENTATION OF ECMM EQUAL SCORES IN TREATMENT OF CHILDREN AT RISK OF INVASIVE MYCOSIS

Lukash UV[1,2], Vlasova AV[1,2] ✉, Gorev VV[1], Tiganova OA[1], Bystrova AA[1], Kamenev MM[1], Khasanova KA[1], Denisenko NP[2], Sychev DA[2]

[1] Morozovskaya Children's City Clinical Hospital under the Moscow City Department of Health, Moscow, Russia

[2] Russian Medical Academy of Continuous Professional Education under the Ministry of Health of the Russian Federation, Moscow, Russia

The ECMM EQUAL Scores tool was proposed in 2018 as a way to improve the quality of treatment of invasive mycoses and assess compliance with the diagnostic algorithm. Currently, there are no reports of its practical application in pediatrics. This study aimed to assess the prevalence of invasive mycosis in a pediatric hospital, the attributed mortality in children with invasive mycosis, and to analyze the dynamics of consumption of antifungal drugs. By design, the study was multidirectional observational, and spanned two years, with retrospective part over the period from 01.01.2022 to 31.12.2022, and prospective part — from 01.01.2023 to 31.08.2024. We used ECMM EQUAL Scores to evaluate the conformity of the fungal infection prevention measures and the empirical therapy to the established risk tier the patients were allocated to, and calculated the ATC/DDD index to measure the consumption of antifungal drugs. During the 20-month follow-up period, 78 children survived, 20 died; supervision continues. The attributed mortality rate was 25.6%. The weighted average absolute ECMM EQUAL Scores were as follows: for candidiasis — 8.4 (38%), for aspergillosis — 6.6 (24%), and for mucormycosis — 9.85 (31%). With the help of the ATC/DDD index, we assessed the dynamics of consumption of antifungal drugs in 2022 and 2023, the "before" and "after" periods. It was concluded that introduction of the ECMM tool into the invasive mycosis diagnostic routine significantly raised the number of detected cases (from 5 to 98 per year), and pushed down the attributed mortality from 60% to 25.6%. With ECMM EQUAL Scores, the NNT index was 2.9. Before introduction of the ECMM tool, in 2022, antifungal drugs were given for 30.3 DDD per 100 bed-days, after the introduction in 2023 — 54.7 DDD per 100 bed-days.

Keywords: pediatrics, mycosis, invasive, clinical trial, antifungal, mycosis risks

ОПЫТ ВНЕДРЕНИЯ ПРОТОКОЛА У ДЕТЕЙ С РИСКОМ ИНВАЗИВНОГО МИКОЗА ECMM EQUAL SCORES

У. В. Лукаш[1,2], А. В. Власова[1,2] ✉, В. В. Горев[1], О. А. Тиганова[1], А. А. Быстрова[1], М. М. Каменев[1], К. А. Хасанова[1], Н. П. Денисенко[2], Д. А. Сычев[2]

[1] Морозовская детская городская клиническая больница Департамента здравоохранения города Москвы, Москва, Россия

[2] Российская медицинская академия непрерывного профессионального образования Министерства здравоохранения Российской Федерации, Москва, Россия

Для улучшения качества лечения инвазивных микозов и оценки соблюдения диагностического алгоритма в 2018 г. предложен метод ECMM (EQUAL Scores). Практический опыт применения у детей в настоящее время не представлен. Целью работы было оценить распространенность инвазивного микоза в детском стационаре, атрибутивную летальность у детей с инвазивным микозом и проанализировать динамику потребления противогрибковых препаратов. Разнонаправленное наблюдательное исследование выполнено в течение двух лет: ретроспективная часть в период с 01.01.2022 по 31.12.2022 и проспективная — с 01.01.2023 по 31.08.2024. Оценку соответствия противогрибковой профилактики и эмпирической терапии инвазивного микоза установленной группе риска пациента проводили методом ECMM (EQUAL Scores), оценку потребления противогрибковых препаратов — методом ATC/DDD-анализа. За период наблюдения в течение 20 месяцев выжили 78 детей, умерли — 20, наблюдение продолжается. Атрибутивная летальность составила 25,6%. Средневзвешенная абс. оценка по методу ECMM (EQUAL Scores) для кандидоза составила 8,4 (38%), для аспергиллеза — 6,6 (24%) и для мукормикоза — 9,85 (31%) от допустимой. Изучена динамика потребления противогрибковых препаратов методом ATC/DDD-анализа за 2022 и 2023 г. «до» и «после». Сделан вывод, что внедрение метода ECMM для диагностики инвазивного микоза привело к значительному увеличению числа выявленных случаев с 5 случаев в год до 98 случаев в год со снижением атрибутивной летальности с 60% до 25,6% соответственно. Индекс NNT при использовании метода ECMM составил 2,9. До внедрения метода ECMM потребление противогрибковых препаратов в 2022 г. составляло 30,3 ЧДТ (в стандартизованной суточной дозе) на 100 койко-дней, после внедрения в 2023 г. — 54,7 ЧДТ (в стандартизованной суточной дозе) на 100 койко-дней.

Ключевые слова: педиатрия, микоз, инвазивный, клиническое исследование, противогрибковый, риски микоза

Invasive mycoses account for a significant part of complications and deaths in patients with malignant neoplasms and impaired immunity in the background, or in cases of allogeneic hematopoietic stem cell transplantation (HSCT) [1].

No invasive mycoses management clinical recommendations have been published in Russia. Moreover, not every medical institution can verify an invasive mycosis diagnosis and establish its etiology [2, 3]. "Crawling" antifungal therapy is the

prescription of antifungal drugs that are not recommended for empirical antifungal therapy to patients who have not went through the complete diagnostic algorithm and thus have the lesion loci unidentified and the etiology unclear [4]. In patients with suspected invasive mycosis, such treatment regimen increases the risk of adverse reactions and drug interactions due overprescription of antifungal medications. Ultimately, crawling antifungal therapy may prolong inpatient stay, adversely affect the outcome of treatment of the underlying disease, and decrease the survival rate of patients [1, 3].

In 2018, European Confederation of Medical Mycology (ECMM) developed EQUAL Scores, a tool enabling systematic approach to diagnosing and improving the quality of treatment of patients with invasive mycoses. According to multicenter studies, introduction of this tool into protocols designed for adults helped raise the rate of invasive mycoses survival in this population [5-7]. As for children, there are currently no reports describing the use of ECMM EQUAL Scores in their treatment. Optimized amounts of antifungal drugs prescribed is one of the indicators of successful application of the principles of adequate diagnosing. Earlier, optimization of consumption of antibiotics confirmed this statement [8]. The degree of optimization of prescription of antifungal drugs can be one of the indicators in the dynamic assessment of the effectiveness of ECMM EQUAL Scores [1–3]. This study was organized to investigate applicability of ECMM EQUAL Scores in pediatrics, where the tool has not been used before.

The purpose of this study was to assess the prevalence of invasive mycosis in patients of a multidisciplinary pediatric hospital, determine the attributed mortality in this group, and analyze the dynamics of consumption of antifungal drugs against the background of adoption of ECMM EQUAL Scores as a tool to assess/categorize the risk of invasive mycosis in patients.

METHODS

Protocol of the study

The observational multidirectional study consists of retrospective and prospective parts. The retrospective component included patients of both sexes, aged from one month to 18 years, diagnosed with invasive mycosis, treated from 01.01.2022 to 31.12.2022. The prospective component includes 130 patients aged from one month to 18 years, diagnosed with invasive mycosis, treated from 01.01.2023 to 31.12.2025. Inclusion criteria: invasive mycosis diagnosed as per the CDC criteria. Non-inclusion criteria: terminal failure of organs and systems as competing with the infection for the main diagnosis or condition. Exclusion criteria: foster care; previous/concomitant therapy is not relevant for inclusion in the study. The diagnosis of invasive mycosis should be established under the CDC guidelines, with at least one host factor meeting the clinical and radiological criteria. The medical histories of inpatients diagnosed with invasive mycosis were analyzed in KIS EMIAS, a consolidated medical information system, and ECMM EQUAL Scores enabled assessment of the adequacy of treatment and invasive mycosis control to the diagnosis. The diagnosing methods were microbiological and microscopy examinations of liquid and dense substrates (tissue and fluid samples), including calcofluor white staining that allows detecting septic and unseptated mycelium. All patients had various organs, including those in the chest, scanned with high-resolution computed tomography, since typical signs of invasive pulmonary mycosis are often lacking, and even atypical pulmonary infiltrates may indicate

presence of this disease [4]. To diagnose aspergillosis, we tested biological fluids for galactomannan antigen (GalMAg-ELISA).

All patients diagnosed with invasive mycosis underwent a genetic study that employed iPLEX Pro PGx panel (Agena Bioscience, USA) 68 SNP/INDEL. VeriDose® Core Panel allows detecting of the relevant variants in the genes *ABCB1, APOE, CYP1A2, CYP2B6, CYP2C19, CYP2D6, CYP3A4, CYP3A5, PNPLA5, SLCO1B1, SULI4A1*, which can potentially affect drug metabolism. In addition, using real-time allele-specific PCR, we sought for clinically significant variants of the *TPMT, ATIC*, and *SLC19A1* genes in patients.

Throughout the study, up to 31.12.2025, we shall monitor patients to register possible ineffectiveness of therapy, development of adverse reactions, and deaths. Registration of an adverse reaction includes assessment of the severity of manifestations, the cause, and association with the antifungal drug.

It is planned to gather a control group of 30 patients with oncological or oncohematological diseases but not diagnosed with invasive mycosis; in this group, we shall also look for the polymorphisms of candidate genes. The subsequent analysis of the associations between such polymorphisms and ineffectiveness of antimycotic therapy, development of adverse reactions, and fatalities will be based on the results of this genetic study.

The comprehensive observational study was conducted at the Pediatric Oncology, Onco-Hematology and Hematopoietic Stem Cell Transplantation (HSCT) Department of Morozovskaya Children's City Clinical Hospital; it lasted two years, including the retrospective analysis part from 01.01.2022 to 31.12.2022, and the prospective analysis part 01.01.2023 to 31.08.2024. In both parts, we used ECMM EQUAL Scores to assess the adequacy of antifungal preventive measures and empirical invasive mycosis therapy to the established risk tiers. DDD analysis enabled assessment of the dynamics of antifungal drug consumption over the 12 months of 2022 and 2023. The effort to improve the invasive mycosis diagnostic methods included development of internal protocols and algorithms approved by the management order (Fig. 1). To diagnose aspergillosis, we looked for galactomannan antigen in biological fluids. In addition, microscopic examination of biological fluids with calcofluor white staining was introduced [8–10].

A patient was diagnosed with invasive mycosis if there were factors affecting the host and clinical and radiological criteria were met [12–14]. The criteria confirming the presence of invasive mycosis include at least one positive result returned by the following studies: microscopic, histopathological, cytopathological, microbiological, serological, or genetic, followed by verification of the fungal agent [15–17]. We stratified the patients into the invasive mycoses development risk tiers based on host factors for mycelial and yeast invasive mycoses:

– grade 4 neutropenia (< 0.5×10^9 neutrophils for >10 days);

– hematological tumors;

– recipient of allo-HSCT or a solid organ transplant;

– over three weeks of taking glucocorticosteroids (GCS) at an average minimum dose of 0.3 mg/kg/day (prednisone equivalent);

– treatment with T-cell immunosuppressants within the last 90 days;

– treatment with B-cell immunosuppressants (only for mycelial invasive mycoses);

– hereditary severe immunodeficiency (chronic granulomatous disease or severe combined immunodeficiency, deficiency of signaling protein and activating transcription factor 3);

– acute graft-versus-host disease (grade III or IV) with intestinal, lung, or liver damage, resistant to first-line therapy with GCS [3, 8, 11].

Table. ECMM EQUAL Scores assessment criteria

Invasive mycoses assessment criteria (98 patients)	Candidiasis (n = 98)	Aspergillosis (n = 98)	Mucormycosis (n = 98)
	Maximum ECMM EQUAL Scores values, points		
Patient's risk tier Radiological studies Platings Microscopy, preferably using optical brighteners Molecular diagnostics Histology Galactomannan test (aspergillosis identification)	10	15	18
TREATMENT Drug therapy (administration of an etiotropic antifungal drug without or after prior mould prophylaxis) Surgical treatment (removal of affected tissues according to indications)	10	5	8
FOLLOW-UP Radiological examination of the lesion locus (dynamical registration) Blood plating	2	7	6
Total	22	27	32

Using ECMM EQUAL Scores, we quantified the quality of diagnosis and treatment of invasive mycosis of various types based on medical records of inpatients. Table gives the quality assessment criteria and maximum scores for each section.

There is evidence of candidemia having the mortality rate of up to 40% in the adult population despite antifungal therapy. In case of *Candida*, the overall mortality rate varies significantly depending on the species; it averages at 7.7% for *C. albicans*, 23.7% for *C. glabrata*, 7.7% for *C. parapsilosis*, and 63.6% for *C. tropicalis* [18]. As for the paediatric population, there is currently no general mortality rate data describing cases of candidemia and other types of mycosis. In this study, at the time of introduction of the ECMM algorithms, the attributed mortality was 25.6%

We analyzed (ATC/DDD approach) the consumption of antifungal drugs in 2022 and 2023.

Figure 1 gives the principles of diagnosis of invasive mycoses under this protocol.

Statistical procedures

The IBM SPSS Statistics v26 software package (IBM, USA) was used for statistical processing of the research results.

Urgent recommendations
Solid evidence base

CT/MRI Scan*
• Chest
• Head
• Abdominal cavity and small pelvis

Suspected invasive mycosis or confirmed case of mycosis = medical emergency (!!!)

48 hours

48 hours

Staging of visualized changes
• Sinuses
• Thoracic organs
• Abdominal organs
• Pelvic organs

96 hours

Collection of biological samples
• Endoscopic biopsy, including under CT control
•! Careful treatment of samples (mechanical processing makes the pathogen inviable)

* Moderately urgent recommendation
Ultrasound examination (typical findings: enlarged kidneys without hydronephrosis, with slit–like areas of reduced density in the cortical layer)

Fig. 1. Invasive mycoses diagnosing algorithm. Adapted from: Duane R. Hospenthal et al., 2023 [3]
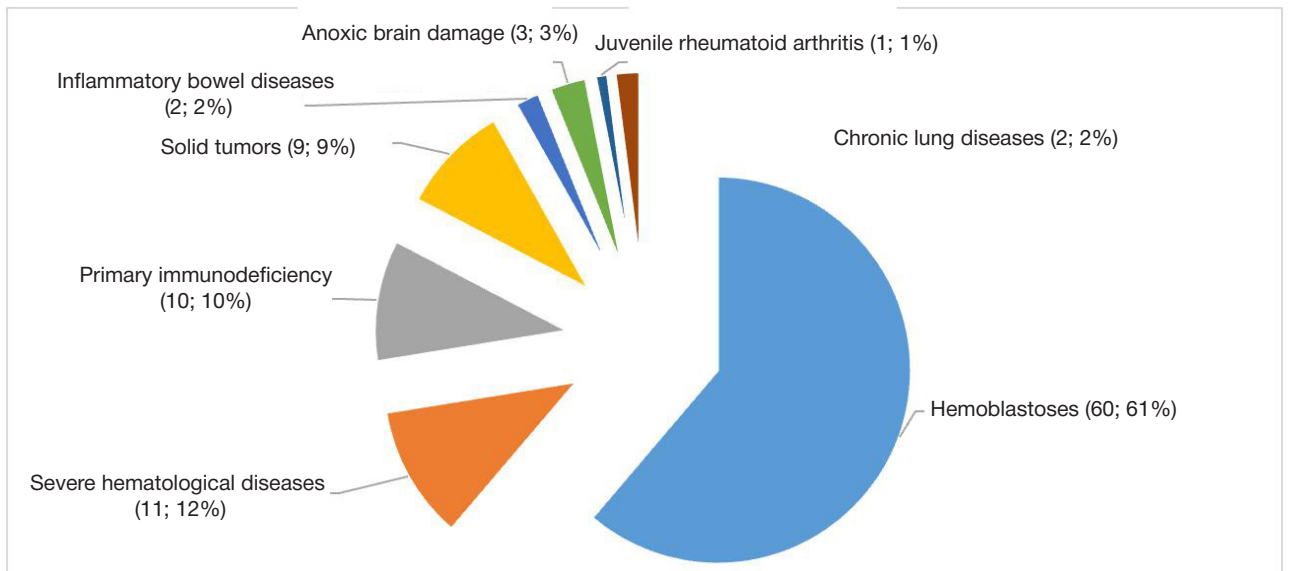
Fig. 2. Characteristics of the main diseases in patients diagnosed with invasive mycosis

RESULTS

In 2022, invasive mycosis was diagnosed in five children aged one month to 18 years (three boys and two girls), mean age of 7.6 years. Of them, two children are being treated against invasive aspergillosis, and three children have died (two with invasive mucormycosis and one with aspergillosis). The diagnosis of invasive mycosis was established in accordance with the CDC criteria. All patients included in the retrospective analysis had host factors characteristic of mycelial and yeast invasive mycosis: two of them underwent allogeneic HSCT in the first year without T-cell immunity restoration, and three children suffered from oncohematological diseases and had long-term neutropenia, receiving high doses of steroids.

From 01.01.2023 to 31.08.2024, the diagnosis of invasive mycosis was established in 98 patients (56 boys and 42 girls) aged from one month to 18 years, mean age of 12.4 years (13.0 years). Of them, 36 patients underwent allogeneic HSCT transplantation in the first year without T-cell immunity restoration; they also took steroids or several immunosuppressive drugs. 45 patients suffered from long neutropenia, and 17 were taking high doses of steroids. During the 20-month follow-up period, 78 children survived, 20 patients died; supervision continues. The attributed mortality rate was 25.6%. In one case involving a prevented fatality, the effectiveness of preventive intake of antifungal drugs was assessed using the EQUAL Scores and the NNT (number needed to treat) calculator, as described in [19].
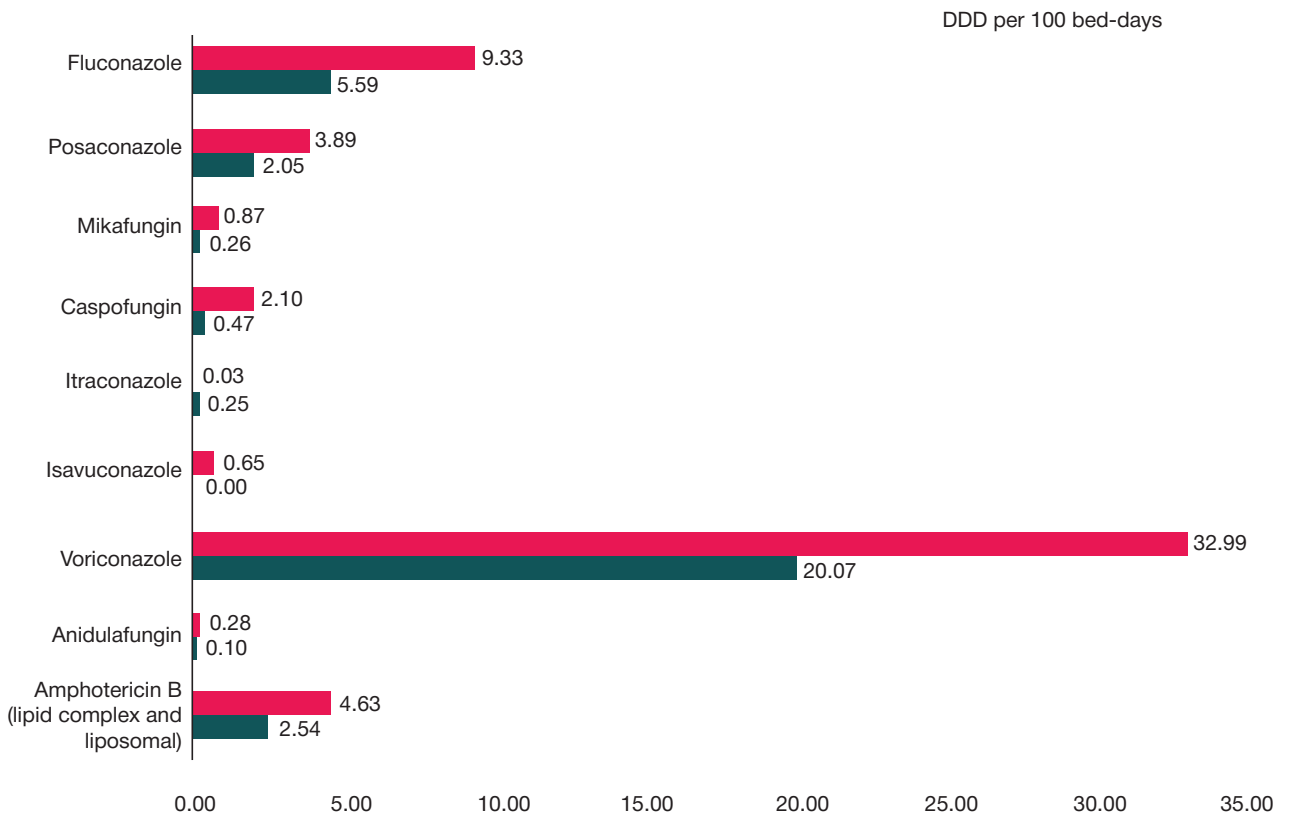
Fig. 3. Dynamics of consumption of antifungal drugs before and after introduction of the ECMM EQUAL Scores tool in 2022–2023

The median ECMM EQUAL Scores value for invasive candidiasis was 8.4 points, which is equivalent to 38% of the maximum. For invasive aspergillosis, this value was 6.6 points (24% of the maximum), and for invasive mucormycosis — 9.85 points, which is 31% of the maximum. Figure 2 presents the distribution of patients by main diseases.

Invasive mycosis was diagnosed in accordance with criteria 1–6 of the standard invasive mycosis case definition [3]. In real practice, the process of diagnosing potential invasive mycosis with clarification of its localization and etiology in a patient exhibiting host factors begins almost simultaneously with empirical and preventive (diagnostic) antifungal therapy, so the key aspects that can be improved in this context are the current diagnostic algorithms, which should be standardized, and administration of antifungal drugs, which can be rationalized. These changes will play an important role in ousting ineffective approaches, including the irrational practice of crawling antifungal therapy.

In 2022, voriconazole was the most consumed antifungal drug (20.07 DDD per 100 bed-days) (Figure 3). It was followed by fluconazole (4.59 DDD per 100 bed-days), amphotericin B liposome and lipid complex (2.54 DDD per 100 bed-days), posaconazole (2.05 DDD per bed-days), caspofungin (0.47 DDD per 100 bed-days), and anidulafungin (0.10 DDD per 100 bed-days).

In 2023, after the introduction of the ECMM EQUAL Scores tool, voriconazole consumption remained dominant (32.9 DDD per 100 bed-days), followed by fluconazole (9.33 DDD per 100 bed-days), amphotericin B (liposomal and lipid complex) (4.63 DDD per 100 bed-days), posaconazole (3.89 DDD per 100 bed-days), caspofungin (2.10 DDD per 100 bed-days), isavuconazole (0.65 DDD per 100 bed-days), and micafungin (0.28 DDD per 100 bed-days).

DISCUSSION

The retrospective part of this study has shown that before adoption of the ECMM EQUAL Scores tool, the frequency of inappropriate use of antifungal drugs in the context of crawling therapy was 78%. After the said adoption, this figure decreased to 32%, but overall consumption of the antifungal drugs has grown significantly: in 2022, the total use was 30.3 DDD per 100 bed-days, and in 2023, after introduction of ECMM EQUAL Scores, this value increased to 54.7 therapy days per 100 bed-days. The growth of consumption of antifungal drugs may be associated with improvements in the fungal infections diagnosing routines or changes in clinical practice that boosted preventive use of antifungal drugs.

While crawling therapy became less common, the total consumption of antifungal drugs increased 1.8 times compared to 2022, because they were prescribed for preventive purposes.

The number of children who could benefit from the ECMM EQUAL Scores in the context of prevention of one fatality by invasive mycosis was 2.9 (NNT), therefore, this study shows that the tool is effective and should be considered for use in paediatric clinical practice.

Study limitations

There are no voriconazole and posaconazole concentrations monitoring reagents registered in the Russian Federation, which disallows realizing the full potential of the ECMM EQUAL Scores tool. Despite this, the results of the study conducted under these conditions remain significant.

CONCLUSIONS

The prevalence of invasive mycosis in 2023–2024, within the scope of this study, was 1.5 cases per 100,000 hospitalized patients. Introduction of the ECMM EQUAL Scores tool into invasive mycosis diagnosing routines significantly increased the number of detected cases (from 5 to 98 patients from 01.01.2023 to 31.08.2024), and decreased the attributed mortality from 60% to 25.6%. The NNT index of 2.9 indicates that approximately three patients must be treated using the ECMM tool to prevent one death from invasive mycosis. In the adult population, the total candidemia mortality is 40%, but for the pediatric population, there is no data on the invasive mycoses mortality rate. After adoption of the ECMM EQUAL Scores tool, the use of antifungal drugs increased from 30.3 DDD per 100 bed-days in 2022 to 54.7 DDD per 100 bed-days in 2023. Thus, the tool boosted consumption of antifungal drugs by 80% within a year. Diagnosis and treatment of invasive mycoses in children are based on the same principles as in adults. This study has shown that ECMM EQUAL Scores significantly increases the effectiveness of invasive mycoses diagnosing in children. We have observed an improvement in the detection of invasive mycoses, which, in turn, allows a more accurate adherence to the current clinical guidelines. Although introduction of the ECMM EQUAL Scores tool decreased the number of crawling therapy cases from 78% in 2022 to 32% in 2023, this practice remains quite common. The analysis of consumption of antifungal drugs (ATC/DDD) before and after adoption of this tool revealed that approximately half of the hospitalized patients required antifungal drugs for prevention and therapy. In this study, we have shown the effectiveness of the ECMM EQUAL Scores for children: to prevent one fatal case of invasive mycosis, it was necessary to preventively give apply antifungal drugs to 3 patients (NNT index of 2.9). Thus, the ECMM EQUAL Scores tool should be recommended for wider application in paediatric clinical practice.

References

1. Lehrnbecher T, Robinson PD, Ammann RA, Fisher B, Patel P, Phillips R, et. al. Guideline for the Management of Fever and Neutropenia in Pediatric Patients With Cancer and Hematopoietic Cell Transplantation Recipients: 2023 Update. J Clin Oncol. 2023.
2. Koenig C, Lehrnbecher T. Diagnostics and Therapy of Paediatric Patients with Febrile Neutropenia. EJC Paediatric Oncology, 2023.
3. Hospenthal DR, Rinaldi MG, J Thomas. Walsh Diagnosis and Treatment of Fungal Infections, 2023.
4. Groll AH, et al. 8th European Conference on Infections in Leukaemia: 2020 guidelines for the diagnosis, prevention, and treatment of invasive fungal diseases in paediatric patients with cancer or post-haematopoietic cell transplantation. Lancet Oncol. 2021; 22: e254–e269.
5. Hoenigl M, Salmanton-García J, et al. Guideline adherence and survival of patients with candidaemia in Europe: results from the ECMM Candida III multinational European observational cohort study. Lancet Infect Dis. 2023; 23 (6): 751–61.
6. Cornely OA, Koehler P, Arenz D, C Mellinghoff S. EQUAL Aspergillosis Score 2018: An ECMM score derived from current guidelines to measure QUALity of the clinical management of invasive pulmonary aspergillosis. Mycoses, 2018.
7. El Zakhem A, El Eid R, Istambouli R, Tamim H, Kanj SS. The Utility

of EQUAL Candida Score in Predicting Mortality in Patients with Candidemia. J Fungi (Basel). 2022; 8 (3): 238.

8. Vlasova AV, Smirnova EV, Volkova NN, Dymnova LV, Andzhel AE, Romanova YuV, i dr. Rezul'taty pilotnogo proekta upravlenija antimikrobnoj terapiej v detskom stacionare. Zdravoohranenie Rossijskoj Federacii. 2023; 67 (5). Russian.

9. EQUAL Score 2018: An ECMM Score Derived From Current Guidelines to Measure QUALity of Clinical Invasive Mycosis.

10. Warris A, Lehrnbecher T, Roilides E, Castagnola E, Brüggemann RJM, Groll AH. ESCMID-ECMM guideline: diagnosis and management of invasive aspergillosis in neonates and children.

11. Ullmann AJ, Aguado JM, Arikan-Akdagli S, Vehreschild MJGT, et al. Diagnosis and management of Aspergillus diseases: executive summary of the 2017 ESCMID-ECMM-ERS guideline

12. 8-ja Evropejskaja konferencija po infekcijam pri lejkozah: rukovodstvo 2020 goda po diagnostike, profilaktike i lecheniju invazivnyh mikozov u pediatricheskih pacientov so zlokachestvennymi novoobrazovanijami ili posle transplantacii gemopojeticheskih stvolovyh kletok (Peresmotr ot 2023 goda). Russian.

13. Keighley C, Cooley L, Morris AJ, Ritchie D, Clark JE, Boan P, Worth LJ. Consensus guidelines for the diagnosis and management of invasive candidiasis in haematology, oncology and intensive care

settings, 2021.

14. Invasive candidiasis and candidaemia in neonates and children: update on current guidelines, 2014.

15. Clinical Practice Guideline for the Management of Candidiasis: 2016 Update by the Infectious Diseases Society of America.

16. ESCMID Fungal Infection Study Group. ESCMID* guideline for the diagnosis and management of Candida diseases 2012: prevention and management of invasive infections in neonates and children caused by Candida spp.

17. Cornely OA, Alastruey-Izquierdo A, Arenz D, Chen SCA, et al. Global guideline for the diagnosis and management of mucormycosis: an initiative of the European Confederation of Medical Mycology in cooperation with the Mycoses Study Group Education and Research Consortium.

18. Salmanton-García J, Cornely OA, Stemler J, etc. Attributable mortality of candidemia — Results from the ECMM Candida III multinational European Observational Cohort Study. J Infect. 2024; 89 (3): 106229. DOI: 10.1016/j.jinf.2024.106229. Epub 2024 Jul 16. PMID: 39025408.

19. Kane SP. Number Needed to Treat (NNT) Calculator. Available from: https://clincalc.com/stats/nnt.aspx. Updated June 23, 2024. Accessed October 24, 2024.

Литература

1. Lehrnbecher T, Robinson PD, Ammann RA, Fisher B, Patel P, Phillips R, et. al. Guideline for the Management of Fever and Neutropenia in Pediatric Patients With Cancer and Hematopoietic Cell Transplantation Recipients: 2023 Update. J Clin Oncol. 2023.

2. Koenig C, Lehrnbecher T. Diagnostics and Therapy of Paediatric Patients with Febrile Neutropenia. EJC Paediatric Oncology, 2023.

3. Hospenthal DR, Rinaldi MG, J Thomas. Walsh Diagnosis and Treatment of Fungal Infections, 2023.

4. Groll AH, et al. 8th European Conference on Infections in Leukaemia: 2020 guidelines for the diagnosis, prevention, and treatment of invasive fungal diseases in paediatric patients with cancer or post-haematopoietic cell transplantation. Lancet Oncol. 2021; 22: e254–e269.

5. Hoenigl M, Salmanton-García J, et al. Guideline adherence and survival of patients with candidaemia in Europe: results from the ECMM Candida III multinational European observational cohort study. Lancet Infect Dis. 2023; 23 (6): 751–61.

6. Cornely OA, Koehler P, Arenz D, C Mellinghoff S. EQUAL Aspergillosis Score 2018: An ECMM score derived from current guidelines to measure QUALity of the clinical management of invasive pulmonary aspergillosis. Mycoses, 2018.

7. El Zakhem A, El Eid R, Istambouli R, Tamim H, Kanj SS. The Utility of EQUAL Candida Score in Predicting Mortality in Patients with Candidemia. J Fungi (Basel). 2022; 8 (3): 238.

8. Власова А. В., Смирнова Е. В., Волкова Н. Н., Дымнова Л. В., Анджель А. Е., Романова Ю. В., и др. Результаты пилотного проекта управления антимикробной терапией в детском стационаре. Здравоохранение Российской Федерации. 2023; 67 (5).

9. EQUAL Score 2018: An ECMM Score Derived From Current Guidelines to Measure QUALity of Clinical Invasive Mycosis.

10. Warris A, Lehrnbecher T, Roilides E, Castagnola E, Brüggemann RJM, Groll AH. ESCMID-ECMM guideline: diagnosis and management of invasive aspergillosis in neonates and children.

11. Ullmann AJ, Aguado JM, Arikan-Akdagli S, Vehreschild MJGT, et al. Diagnosis and management of Aspergillus diseases: executive summary of the 2017 ESCMID-ECMM-ERS guideline

12. 8-я Европейская конференция по инфекциям при лейкозах: руководство 2020 года по диагностике, профилактике и лечению инвазивных микозов у педиатрических пациентов со злокачественными новообразованиями или после трансплантации гемопоэтических стволовых клеток (Пересмотр от 2023 года).

13. Keighley C, Cooley L, Morris AJ, Ritchie D, Clark JE, Boan P, Worth LJ. Consensus guidelines for the diagnosis and management of invasive candidiasis in haematology, oncology and intensive care settings, 2021.

14. Invasive candidiasis and candidaemia in neonates and children: update on current guidelines, 2014.

15. Clinical Practice Guideline for the Management of Candidiasis: 2016 Update by the Infectious Diseases Society of America.

16. ESCMID Fungal Infection Study Group. ESCMID* guideline for the diagnosis and management of Candida diseases 2012: prevention and management of invasive infections in neonates and children caused by Candida spp.

17. Cornely OA, Alastruey-Izquierdo A, Arenz D, Chen SCA, et al. Global guideline for the diagnosis and management of mucormycosis: an initiative of the European Confederation of Medical Mycology in cooperation with the Mycoses Study Group Education and Research Consortium.

18. Salmanton-García J, Cornely OA, Stemler J, etc. Attributable mortality of candidemia — Results from the ECMM Candida III multinational European Observational Cohort Study. J Infect. 2024; 89 (3): 106229. DOI: 10.1016/j.jinf.2024.106229. Epub 2024 Jul 16. PMID: 39025408.

19. Kane SP. Number Needed to Treat (NNT) Calculator. Available from: https://clincalc.com/stats/nnt.aspx. Updated June 23, 2024. Accessed October 24, 2024.

ASSESSMENT OF LOWER URINARY TRACT DYSFUNCTION IN WOMEN WITH MULTIPLE SCLEROSIS

Luzanova EI[1] ✉, Karpova MI[1], Abramovskikh OS[1], Chetvernina EA[1], Kupriyanov SV[1,2], Zotova MA[1], Bershadskiy AV[3]

[1] South Ural State Medical University, Chelyabinsk, Russia

[2] National Research Tomsk State University, Tomsk, Russia

[3] Medical Rehabilitation Center, Clinical Institute of Brain LLC, Berezovsky, Russia

Multiple sclerosis (MS) is a chronic disorder of the central nervous system affecting primarily young women. Neurogenic lower urinary tract dysfunction (NLUTD) represents one of the disease manifestations creating the risk of infectious complications and kidney disease. Today, there is insufficient data on the urinary microflora composition obtained by advanced high-tech diagnosis methods. The study aimed to perform clinical assessment of NLUTD associated with MS and its impact on the quality of life (QOL), as well as to clarify the data on the urinary microflora composition. A total of 33 women with MS aged 36 [39.5; 30.5] years were assessed using the customized questionnaires for estimation of the NLUTD prevalence and severity, as well as for QOL evaluation. Qualitative determination and quantification of urinary opportunistic microflora (OM) were performed using the real-time polymerase chain reaction. A total of 19 (57.6%) women with MS had symptoms of NLUTD: symptoms of the storage (15 individuals, 45.5%) and emptying (16 individuals, 48.5%) phases. In almost half of women with MS, the complaints included abnormalities of both bladder functioning phases (12 individuals, 36.4%); moderate abnormalities prevailed (12 individuals, 34.6%). Women with MS and NLUTD were more disabled based on the EDSS score (3.5 [5.0; 3.0] points; $p < 0.001$) and had longer disease duration (13 [20.0; 5.0] years; $p < 0.001$). The QOL index of women with NLUTD showed dissatisfaction with bladder function. The study revealed bacteriuria in patients with MS and NLUTD. The data on the urinary microflora composition are provided: OM members (bacteria of the ESKAPE group) have been found in 8 samples obtained from women with MS and NLUTD. Bacteriuria was asymptomatic.

Keywords: multiple sclerosis, bacteriuria, urinary tract infections, neurogenic bladder dysfunction, nocturia, urinary microflora

✉ Correspondence should be addressed: Ekaterina I. Luzanova
Vorovsky, 64, Chelyabinsk, 454092, Russia; estrochikova@yandex.ru

ИССЛЕДОВАНИЕ ДИСФУНКЦИИ НИЖНИХ МОЧЕВЫВОДЯЩИХ ПУТЕЙ У ЖЕНЩИН С РАССЕЯННЫМ СКЛЕРОЗОМ

Е. И. Лузанова[1] ✉, М. И. Карпова[1], О. С. Абрамовских[1], Е. А. Четвернина[1], С. В. Куприянов[1,2], М. А. Зотова[1], А. В. Бершадский[3]

[1] Южно-Уральский государственный медицинский университет, Челябинск, Россия

[2] Национальный исследовательский Томский государственный университет, Томск, Россия

[3] Центр медицинской реабилитации ООО «Клиника Института Мозга», Березовский, Россия

Рассеянный склероз (РС) — хроническое заболевание центральной нервной системы, преимущественно поражающее молодых женщин. Нейрогенная дисфункция нижних мочевыводящих путей (ДНМП) — одно из проявлений заболевания, оно создает риски инфекционных осложнений и поражения почек. В настоящее время недостаточно данных о составе микрофлоры мочи, полученных современными высокотехнологичными методами диагностики. Целью исследования было дать клиническую оценку ДНМП при РС, влияния ее на качество жизни (КЖ), а также уточнить данные о составе микрофлоры мочи. Для обследования 33 женщин с РС в возрасте 36 [39,5; 30,5] лет использовали специализированные опросники для оценки частоты и степени тяжести ДНМП, оценки уровня КЖ. Качественный и количественный состав условно-патогенной микрофлоры (УПМ) мочи определяли методом полимеразной цепной реакции в режиме реального времени. У 19 (57,6%) женщин с РС были симптомы ДНМП: симптомы фазы накопления (15 человек, 45,5%) и фазы опорожнения (16 человек, 48,5%). Почти у половины женщин с РС жалобы включали симптомы нарушения обеих фаз работы мочевого пузыря (12 человек, 36,4%), преобладали среднетяжелые нарушения (12 человек, 34,6%). Женщины с РС и ДНМП были более инвалидизированы согласно шкале EDSS (3,5 [5,0; 3,0] баллов; $p < 0,001$) и имели больший стаж болезни (13 [20,0; 5,0] лет; $p < 0,001$). Индекс КЖ у женщин с ДНМП отражал неудовлетворенность функцией мочевого пузыря. В результате исследования выявлено наличие бактериурии у пациенток с РС и ДНМП. Представлены данные о составе микрофлоры мочи: в 8 образцах от женщин с РС и ДНМП обнаружены представители УПМ (бактерии группы ESKAPE). Бактериурия имела бессимптомный характер.

Ключевые слова: рассеянный склероз, бактериурия, инфекции мочевых путей, нейрогенная дисфункция мочеиспускания, ноктурия, микрофлора мочи

✉ Для корреспонденции: Екатерина Игоревна Лузанова
ул. Воровского, д. 64, г. Челябинск, 454092, Россия; estrochikova@yandex.ru

Multiple sclerosis (MS) is a chronic demyelinating neuroinflammatory and autoimmune disease of the central nervous system (CNS) associated with degenerative phenomena and having a variable course. It usually affects young people, has a great effect on the quality of life (QOL), and places considerable burden on public health services.

Lower urinary tract dysfunction (LUTD) is a common symptom of multifocal CNS lesion underlying the development of MS. Neurogenic lower urinary tract dysfunction (NLUTD) develops on average 8 years after establishing the diagnosis of MS; up to 10% of patients complain of alterations in urination associated with the disease manifestation [1, 2]. In the course of the disease more than 80% of individuals with MS experience NLUTD symptoms, up to 91% have appropriate urodynamic abnormalities [2, 3]. In 35% of patients with MS, focal lesions damaging reticulospinal tracts usually result in detrusor sphincter dyssynergia [4–6]. This syndrome is characterized by impaired coordination between detrusor contraction and relaxation of bladder sphincters resulting urinary retention [7]. Clinical manifestations of such abnormal urodynamics are uncontrolled overactive detrusor contractions with or without urinary incontinence, sphincter dysfunction, which often result in considerable residual urine volume and high intravesical bladder pressure. Within the framework of obstructive symptoms the most common manifestations are weak urine stream, difficulty starting urinating, and the need to force urination. This creates conditions for functional odstruction and abnormal urinary outflow. Complete and partial urinary retention representing the extreme forms of obstructive disorder results in residual urine accumulation [4]. As a result, negative effects on the upper and lower urinary tract can be expected. High intravesical bladder pressure pressure contributes to reflux into the upper urinary tract and secondary kidney injury. Urinary tract infections (UTIs) represent a major challenge of treatment of individuals suffering from MS. Neurogenic urodynamic disturbances worsen the patients' QOL and ensure the increased risk of UTIs [8]. When discussing UTIs in MS, it is important to consider the issues of prevention. Risk factors of UTIs in patients with MS require thorough clinical assessment. The long-term immunosuppressive therapy with disease-modifying drugs for MS (DMDs), female sex, pelvic abnormalities and disability, treatment with corticosteroids, dysbiotic processes in the urogenital tract are discussed as predictors of UTIs in individuals with MS [1, 8]. To date, the composition of microflora of the lower urinary tract (LUT) and adjacent loci in patients with MS is poorly understood. The study aimed to perform clinical assessment of lower urinary tract dysfunction to assess its impact on the QOL using the customized questionnaires validated in Russia, as well as to perform qualitative assessment and quantitatifification of the LUT microflora composition by molecular genetic methods in women with MS.

METHODS

We performed observational clinical and laboratory study of 33 non-pregnant women. Inclusion criteria: definite diagnosis of MS based on the McDonald criteria (2017); EDSS up to 6.5 points; age 18–45 years; no corticosteroid therapy and antibacterial drugs at the moment of sample collection or within a month before enrollment; no sexually transmitted infections; no history of any urinary tract disorder or follow-up by urologist or nephrologist. Exclusion criteria: pregnancy and lactation, acute infection, history of surgery within a month before the study, participation in other studies, mental disorders, refusal of submitting the informed consent. Outpatients followed-

up at the consulting and diagnostic clinics for demyelinating disorders and MS in Chelyabinsk and Chelyabinsk Region were randomly enrolled. Inclusion criteria for the control group ($n = 20$): conditionally healthy non-pregnant women of fertile age with no nervous system disorder, pelvic organ function impairment or the history of urogenital infection; the median age was 35 [37.5; 30.0] years. Clinical assessment of women with MS involved the use of the generally accepted methods available to neurologists: neurological status assessment using the Expanded Disability Status Scale (EDSS), pelvic organ function assessment using the Pelvic Organ Function Questionnaire [9, 10], and the Neurogenic Bladder Symptom Score (NBSS) [11]. The median age of women with MS was 36 [39.5; 30.5] years. The majority of patients received DMDs for MS: 11 individuals (33.3%) used interferon beta, 11 (33.3%) used ocrelizumab, 6 (18.2%) used cladribine, and 5 (15.2%) were naïve. The median EDSS was 2.5 [4.0; 2.0] points; all the patients had the relapsing-remitting disease course.

Urinary microflora composition was assessed using the reagent kit for detection of DNA of opportunistic bacteria of the classes Bacilli, Betaproteobacteria and Gammaproteobacteria (BacScreen; BacScreen OM REAL-TIME PCR Detection Kit, DNA-Technology, Russia) by real-time polymerase chain reaction. Bacterial contamination of urine (total bacterial mass (TBM)) was quantified; the amount of DNA of the identified microorganism was presented as a logarithm Lg, the values of which were proportionate to microbial contamination of the biotope. The kit used in this study enables detection of 25 bacterial representatives of opportunistic microflora (OM): *Enterococcus spp., Streptococcus spp., Streptococcus agalactiae, Streptococcus pyogenes, Streptococcus pneumoniae, Staphylococcus spp., Staphylococcus aureus; Achromobacter ruhlandii, Achromobacter xylosoxidans, Burkholderia spp.; Acinetobacter spp., Citrobacter freundii, Citrobacter koseri, Enterobacteriales, Enterobacter cloacae, Escherichia coli, Haemophilus spp., Haemophilus influenzae, Klebsiella oxytoca, Klebsiella pneumoniae, Morganella morganii, Proteus spp., Pseudomonas aeruginosa, Serratia marcescens, Stenotrophomonas maltophilia*. All the patients complaining of LUTD and having the symptoms of LUTD were advised to consult urologist, undergo bladder ultrasound involving determination of post void residual urine. Statistical analysis was performed using Windows 10, Excel 2016 (Microsoft; USA), IBM SPSS Statistics 26 (IBM; USA). Descriptive statistics included frequency indicators, median values, 25th and 75th percentiles (Me [LQ; UQ]). The Mann–Whitney U test, Kruskal–Wallis test, and χ^2 test were used to compare the groups. The correlation analysis was performed using the Spearman's rank correlation coefficient (ρ); the correlation strength was estimated using the Chaddock scale. The differences were considered significant at $p < 0.05$.

RESULTS

The use of the Pelvic Organ Function Questionnaire revealed signs of urination disorder of varying severity in 19 individuals (57.6%). Patients with MS and LUTD were included in the study group; the age range was 21-45 years. The comparison group included 14 women with MS having no bladder dysfunction aged 19–42 years. The EDSS of patients with LUTD were different from that of patients having preserved bladder function (3.5 [5.0; 3.0] and 2.0 [2.0; 1.0] points, respectively; $p < 0.001$); there were no differences in age. Women with LUTD had longer MS duration (13 [20.0; 5.0] years) compared to patients with no urination disorder (4 [7.0; 2.75] years; $p < 0.001$).

Fig. 1. Frequency of storage phase symptoms in women with remittent MS based on the Pelvic Organ Function Questionnaire

The storage symptoms were found in 15 individuals (45.5%), while the voiding symptoms were reported in 16 individuals (48.5%) (Fig. 1, 2). The combination of symptoms of abnormalities of both urination phases was observed in 12 individuals (36.4%). All the patients developed symptoms of bladder dysfunction after the MS onset. The bladder symptoms were presented near 3 [5.0; 2.0] years after the MS onset, the latest time of the LUTD onset was 10 years since the diagnosis, and the minimum duration of bladder disorder was 1 year. The urgency more frequent than once a week was experienced by 12 women (36.4%) with varying frequency, 12 women (36.4%) reported they «can't hold urine because of urgency». A total of 7 individuals urinated 10 or more times per day (21.2%). Three women (9.1%) complained of the storage symptoms only. Six women with MS (18.2%) woke up to urinate more than once a night, but all of them had other bladder disorder symptoms. Nocturia was not found in patients having no symptoms of LUTD.

Persistent voiding symptoms occurring at least several times per week was reperesented by complaints of slower urine flow — in 14 individuals (42.4%), weak stream sensation, increase in the time needed to urinate — in 13 (39.4%); 13 individuals (39.4%) described their interrupted urine flow, 11 (33.3%) felt the need to strain to empty the bladder, feeling of incomplete bladder emptying after voiding was reported by 12 individuals (36.4%). Four women (12.1%) complained of the voiding symptoms only. Stress incontinence was experienced by 4 women with MS (12.1%), aged 35–46 years (median age 40.5 [44.25; 36.0] years), furthermore, 3 women had other bladder symptoms. One patient suffered from the storage abnormalities, 2 other patients had a combination of complaints. Among 19 women, 10 paients had a consultation of urologist, all of them were diagnosed with LUTD based on bladder ultrasound involving estimation of residual urine volume, the volume of 160 mL was revealed in one case.

According to the QOL index, women with MS and bladder disorder were dissatisfied with their bladder condition, in contrast to women having no such symptoms, $p < 0.05$ (Fig. 3). The median QOL index was 2.0 [2.0; 1.0] points. The worst values of the urological QOL index were reported in patients having the storage symptoms and a combination of bladder dysfunction symptoms (2.0 [2.75; 2.0]; 2.0 [2.0; 1.0] points, respectively; $p > 0.05$).

The bladder disorder severity assessment results are provided in Table. The increased average scores were reported for all NBSS domains. The total NBSS score exceeding 20 was reported in 12 women (34.6%), which suggests moderate bladder dysfunction, 10–20 (mild form) — in 4 women (12.1%), other patients had the values below 10. Weak positive correlations between the LUTD severity based on the NBSS score, disability score ($\rho = 349$; $p > 0.05$), and disease duration ($\rho = 145$; $p > 0.05$) were revealed.

The QOL index reflected negative impact on the well-being of patients with any clinical manifestations of bladder disorder; the worst values were reported in women having a combination of symptoms (3.0 [3.0; 2.0] points; $p > 0.05$). Almost one third of women with MS (9 individuals, 27.3%) and LUTD said that they would feel unhappy and dissatisfied, "if the bladder would function like now for the rest of life".

Molecular genetic testing of urine in women with MS revealed DNA of opportunistic microorganisms (OM) in 8 individuals (24.2%). We identified microorganisms of the order *Enterobacterales* (4 individuals), including *Enterobacter cloacae* (1 individual), *Escherichia coli* (1 individual), *Klebsiella pneumoniae + Klebsiella oxytoca* (1 individual); species of the order *Pseudomonadales: Acinetobacter spp.* (1 individual), and species of the class *Bacilli: Staphylococcus spp.* (3 individuals) and *Streptococcus spp.* (2 individuals). A combination of members of all the bacterial classes indetified was found in 3 women (9%). Variation in the amount of OM detected was 2.5–5.7 Lg, which corresponded to $10^{2.5}$–$10^{5.7}$ GE/sample. The questionnaire survey revealed obstructive symptoms manifested by weak urine stream, the need to strain, and intermittent urination, in all 8 patients, among them 5 (62.5%) had a combination of the storage and emptying phase symptoms, and 6 (75%) had episodes of cystitis in their urological history. A total of 12 women (36.4%) had episodes of UTIs since the moment of establishing the diagnosis of MS: cystitis, including recurrent form, and one case of pyelonephritis. No microorganisms were found in urine of the control group ($p < 0.001$).
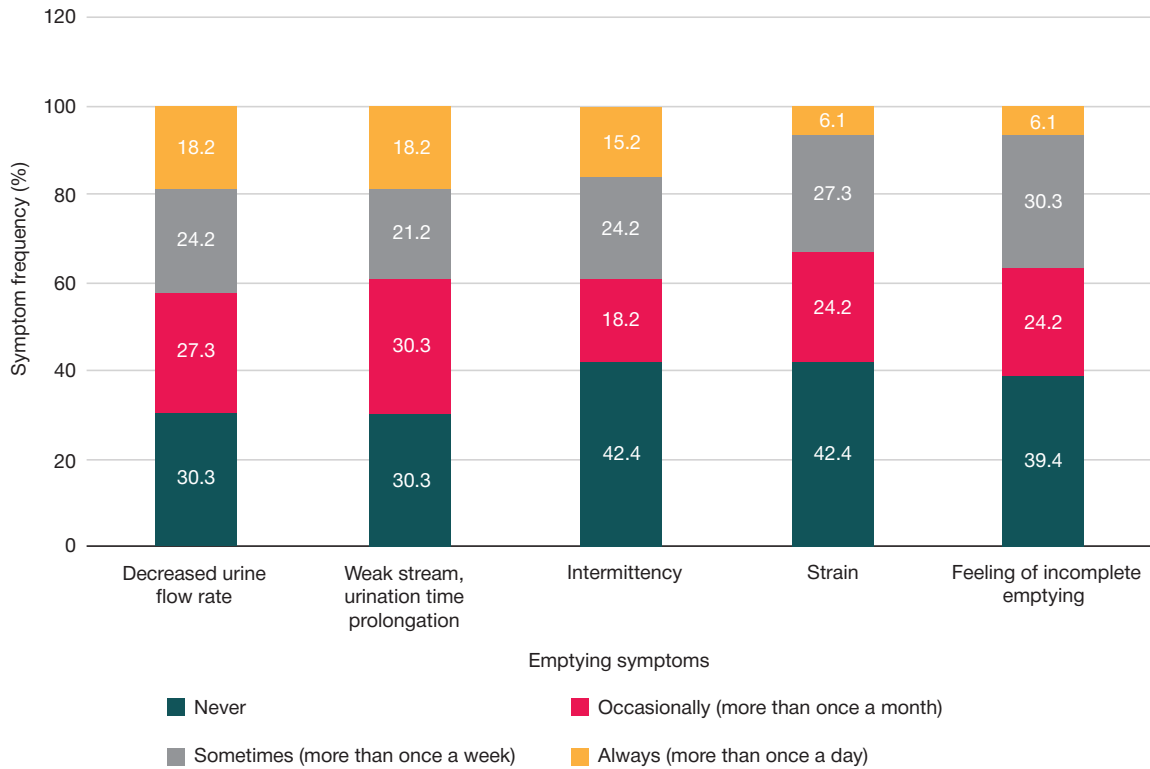
Fig. 2. Frequency of voiding symptoms in women with relapsing-remitting MS based on the Pelvic Organ Function Questionnaire

DISCUSSION

Patients with MS and healthcare professionals often face an important interdisciplinary problem: neurourological disorders. A number of foreign authors report that the type of bladder disorder associated with MS varies between detrusor hyperactivity (34–91% of patients) and areflexia (20–37% of patients) [1, 2]. In the recent study focused on the epidemiology and nature of bladder disorders associated with MS, NLUTD

was found in 65% of patients [12]. Among our patients more than a half (57.6%) had various symptoms of bladder dysfunction. The most common neurourologic symptoms are urinary frequency and detrusor overactivity [13]. In the surveyed women with MS, the storage and voiding symptoms were almost equally represented (45.5% and 48.5%, respectively), which resulted primarily from the CNS lesion localization. Perhaps, this can explain the lack of significant correlation between the disease duration and the bladder dysfunction
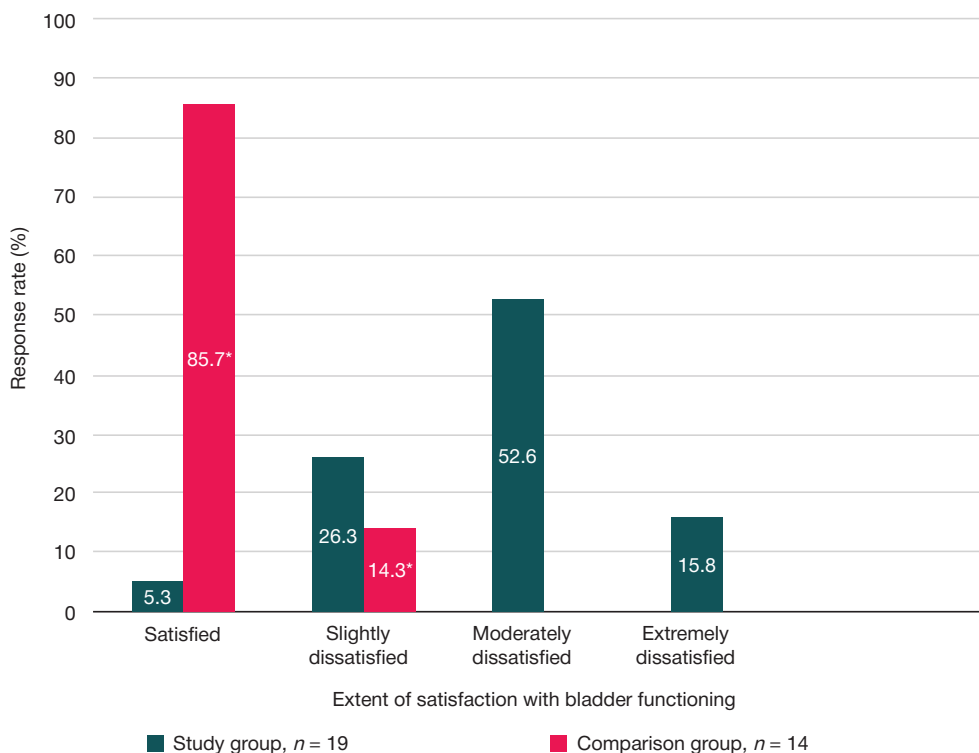
Fig. 3. Frequency of satisfaction with bladder functioning (QOL index) based on the Pelvic Organ Function Questionnaire. * — $p < 0.05$, χ^2 test

Table. Bladder disorder severity in women with remittent MS based on the Neurogenic Bladder Symptom Score (NBSS)

Women with MS and NLUTD $n = 19$	Average scores by domains				Total score
	Incontinence (0–29)	Storage and voiding	Complications	Quality of life	
	6.05 ± 5.43	10.08 ± 2.93	4.95 ± 4.36	2.1 ± 1.07	2.1 ± 8.85

severity. The severity of this or that MS symptom is determined by localization of demyelination lesion, exacerbation severity, and the quality of functional recovery after relapse. The bladder disorder associated with MS contributes greatly to the patients' disadaptation, increasing the disability score [12]. Women with MS and LUTD were more disabled compared to women with normal voiding. At the same time, they had mild-to-moderate bladder dysfunction, and no correlation between the EDSS and NBSS scores was found. This is consistent with the features of using the bladder and gut functional system scale and the algorithm to determine the total EDSS score.

It is important that a large share of women (39.4%) had bladder disorders, in which the symptoms associated with both urine retention and bladder voiding occur. Such variant of neurogenic bladder disorder develops in case of focal spinal cord lesion below the pons (or medulla oblongata) and above the sacral region [14]. It should be noted that about 80% of patients with MS have lesion in the spinal cord, mostly in the cervical region, which are more often symptomatic compared to brain lesions and can cause considerable disadaptation in the form of the gait, coordination, bladder and gut function disturbances [3, 15, 16]. The patients having a combination of the storage and voiding symptoms usually pay attention to the increase in urinary frequency and episodes of urge incontinence, while voiding symptoms remain out of sight, and the conditions for the upper urinary tract injury are preserved. Impossibility of adequate severity estimation based on the patient's subjective complaints represents one of the major challenges of the diagnosis of urinary hesitancy. In this regard, it is feasible to regularly conduct screening aimed to identify the voiding disturbances, ensure timely referral for urological counseling, perform uroflowmetry to quantify urine flow rate and bladder ultrasound to determine residual urine volume [5, 6].

In turn, the storage symptoms that usually reflect neurogenic detrusor overactivity can also lead to the upper urinary tract injury, as well as to the development of nonreflux pyelonephritis. This is associated with the detrusor tissue fibrosis, impaired bladder dynamics [7, 17].

The increase in the rate of urination at night in individuals with MS is one more manifestation of the urine storage and voiding dysfunction. Nocturia disturbes night sleep, leads to fatigue, daytime drowsiness, decreases the QOL [18, 19]. The prevalence of nocturia in individuals with MS is higher, than in general population, it varies between 20.9% and 48.8% [18]. We noted that 18.2% of women with MS woke up more than once a night and went to the bathroom for voiding. Currently, three various mechanisms underlying the development of nocturia (reduced bladder capacity, general polyuria and nocturnal polyuria) are discussed [20, 21]. The range of causes underlying these three pathogenetic variants of nocturia is well-known; the MS-associated specific factors not observed in patients having no neurological disorders have been reported [20, 21].

Specific questionnaires determining the QOL index have been developed to assess QOL in individuals with neurogenic bladder dysfunction. The majority of MS researchers agree that the symptoms of bladder dysfunction have a significant impact on the patients' QOL, regardless of the assessment tool used [2, 12]. In the Russian population of individuals with

MS the issue of the impact of bladder dysfunction on the QOL is still poorly understood, which is likely to be due to the fact that specific questionnaires have been translated into Russian and validated not so long ago [9, 11]. According to the data of the Russian study focused on validation of the short QOL questionnaire for patients with neurogenic bladder dysfunction (SF-Qualiveen), patients with MS and neurogenic LUTD had much worse QOL scores [22]. In our study, every third woman with MS having bladder dysfunction reported that the issue was very important for her. The QOL index from the Pelvic Organ Function Questionnaire also reflected low satisfaction with the urination quality in women with LUTD compared to patients having no such disorder.

Not only primary disease, but also comorbidities and lifestyle factors affect the QOL and mortality in individuals with MS. A large share of such factors is constituted by infections, especially pneumonia, influenza, and UTIs [2]. UTIs in patients with MS are strongly associated with bladder dysfunction. UTIs are among three major causes of hospital admission in patients with MS and reach 30–50% of all indications for hospitalization [2, 8]. According to the data of epidemiological study of MS comorbidity, among 815 patients 3.5% had UTIs [23]. In our patients, the reported rate of the history of UTIs was 36.4%. In the large-scale retrospective study of the causes of death in people with MS conducted in Canada in 1986–2013, UTIs were noted in 8% of 2153 death cases as one of the major causes of death, while in general population UTIs constituted only 2% of the causes of death [24].

Testing of the MS patients' urine by culture-based microbiological diagnosis methods showed that Escherichia coli, *Streptococcus* beta-hemolytic B, *Klebsiella pneumoniae*, *Proteus mirabilis*, and *Staphylococcus* coagulase-negative were the most common causative agents of UTIs [8, 25]. We have found no scientific literature data obtained by modern methods that would allow one to determine nonculturable bacteria in urine of patients with MS and neurogenic dysfunction. In this study we performed molecular genetic identification of OM in women with MS using the BacScreen OM test system. Asymptomatic bacteriuria was observed in 24.2% of cases. The following representatives were found: *Enterobacter cloacae*, *Escherichia coli*; *Klebsiella pneumonia*, *Klebsiella oxytoca*, *Acinetobacter spp*, as well as *Staphylococcus spp.*, and *Streptococcus spp*. All these microorganisms can cause UTIs [25, 26]. Moreover, *Enterobacter spp.*, *Klebsiella pneumonia*, *Staphylococcus spp.* found in the urine of women with MS belong to the group of most important bacteria referred to as ESKAPE: *Enterococcus faecium*, *Staphylococcus aureus*, *Klebsiella pneumoniae*, *Acinetobacter baumannii, Pseudomonas aeruginosa*, and *Enterobacter spp*. [27]. These bacteria that often cause severe infections show multidrug resistance to various classes of antibiotics [28, 29]. ESKAPE pathogens were included in the WHO priority list of pathogens for the development of new antibacterial drugs or alternative treatment methods [27–29]. The range of the quantity of OM revealed was $10^{2.5}$–$10^{5.7}$ GE/sample. The microbiological pattern associated with NLUTD changed depending on the urine drainage method [30]. All the women we examined urinated unaided. Despite the limited number of patients with the OM detected, we performed in-depth

analysis of bladder dysfunction symptoms in this group. This approach turned out to be relevant in the context of understanding the relationship between UTIs and various LUT dysfunction types. In our study, all women with MS and bacteriuria detected had urination disturbances with obstructive symptoms, as well as the history of UTI episodes. These symptoms can indicate disturbances of the mechanism underlying urination, which, according to modern studies can be associated with detrusor sphincter dyssynergia. Such a bladder disorder form conbines the storage symptoms and the signs of obstruction, including residual urine volume. While urinary retention and weak urine stream can attract the patient's attention, post-void residual volume often remains unnoticed. That is why it is important to timely detect the signs of voiding disturbances. To estimate the severity of such disturbances more accurately, it is necessary to conduct comprehensive urodynamic assessment allowing one to obtain detailed information abour the LUT functional state, including the dynamics of intra-bladder pressure and bladder volume [2]. It is impossible to draw definitive conclusion about the disease severity and nature without such assessment. In one of the studied cases, significant residual urine volume (160 mL) and pseudodiverticula were revealed in patient with bacteriuria based on ultrasound data. These findings can suggest a prolonged course of chronic urinary retention, which, in turn, can negatively affect the patient's health and ensure susceptibility to infectious complications. Joint monitoring of patients with NLUTD by neurologist and urologist is important for preservation of renal function and prevention of severe, often fatal, urological complications [2, 8].

CONCLUSIONS

Bladder disorders were found in 57.6% of women with relapsing-remitting MS. Clinical assessment of this category of patients involved the use of specific Pelvic Organ Function Questionnaire allowing the neurologist to thoroughly assess the system functioning quality and perform diagnostic screening. The storage and voiding symptoms were equally frequent, and the majority of patients had a combination of those. Moderate LUTD significantly affecting the QOL prevailed. The use of the diagnostic kit enabling comprehensive qualitative assessment and quantification of microflora composition with the emphasis on detection of the broad spectrum of OM of three classes (*Bacilli*, *Betaproteobacteria*, and *Gammaproteobacteria*) most often causing community-acquired and hospital-acquired infections was the feature of the study. Preliminary results of urinary microflora assessment suggest the presence of not only well-known *Escherichia coli*, but also other OM representatives, including those belonging to the ESKAPE group of most important bacteria that are often resistant to antibacterial drugs. Symptoms of obstruction prevailed in women with the OM detected. This emphasizes the importance of timely detection and adjustment of functional LUT disorders aimed at preventing infectious inflammatory diseases. Bladder voiding disturbances are likely to be one of the causes of intense bacterial growth. Further research is required to determine additional risk factors of infectious complications affecting LUT in individuals with MS.

References

1. Sakakibara R. Urinary Dysfunction in Multiple Sclerosis, Neuromyelitis Optica, and Related Disorders. Handbook of Neurourology. Singapore. 2023: 737–45.
2. Averbeck MA, Mehnert U, Al Mousa RT, Kessler TM. Epidemiology of Neurogenic Lower Urinary Tract Dysfunction. Handbook of Neurourology. Singapore. 2023: 135–40.
3. Vecchio M, Chiaramonte R, DI Benedetto P. Management of bladder dysfunction in multiple sclerosis: a systematic review and meta-analysis of studies regarding bladder rehabilitation. Eur J Phys Rehabil Med. 2022; 58 (3): 387–96. DOI: 10.23736/S1973-9087.22.07217-3.
4. de Sèze M, Ruffion A, Denys P, Joseph PA, Perrouin-Verbe B. The neurogenic bladder in multiple sclerosis: review of the literature and proposal of management guidelines. Mult Scler. 2007; 13 (7): 915–28. DOI: 10.1177/1352458506075651.
5. Shvarts PG, Popov SV, Zavalishin IA. Patofiziologicheskie i nejrofarmakologicheskie osobennosti terapii hronicheskoj zaderzhki mochi pri rassejannom skleroze. Farmateka. 2017; 6 (339): 51–60. Russian.
6. Shvarts PG, Popov SV. Nejrogennaja hronicheskaja zaderzhka mochi u bol'nyh rassejannym sklerozom. Trudnyj pacient. 2018; 16 (6): 61–64. Russian.
7. Ozkan B, Demirkesen O, Durak H, Uygun N, Ismailoglu V, Cetinel B. Which factors predict upper urinary tract deterioration in overactive neurogenic bladder dysfunction? Urology. 2005; 66 (1): 99–104. DOI: 10.1016/j.urology.2005.02.009.
8. Filippova ES, Bazhenov IV, Zyrianov AV, Borzunov IV, et al. Infekcii mochevyvodjashhih putej u bol'nyh nejrogennym mochevym puzyrem. Consilium Medicum. 2019; 21 (12): 139–44. DOI: 10.26442/20751753.2019.12.190676. Russian.
9. Korshunova ES, Yusupova DG, Zimin AA, Pyatnitskaya TM, Zaitsev AB, Yatsko KA, et al. Validacija oprosnika po funkcijam tazovyh organov (Questionnaire on pelvic organ function) u nevrologicheskih bol'nyh v Rossii. Andrologija i genital'naja hirurgija. 2023; 24 (1): 90–99. DOI: 10.17650/2070-9781-2023-24-1-90-99. Russian.
10. Sakakibara R, Shinotoh H, Uchiyama T, Sakuma M, Kashiwado M, Yoshiyama M, Hattori T. Questionnaire-based assessment of pelvic organ dysfunction in Parkinson's disease. Auton. Neurosci. 2001; 92 (1–2): 76–85. DOI: 10.1016/S1566-0702(01)00295-8.
11. Philippova ES, Bazhenov IV, Volkova LI, Moskvina EY, Turova EL, Popova YV. Russkojazychnaja versija shkaly simptomov nejrogennogo mochevogo puzyrja (NBSS). Urologija. 2018; 6: 5–13. DOI: 10.18565/urology.2018.6.5-13. Russian.
12. Ziryanov AV, Bazhenov IV, Philippova ES, Ustinov GS, Turova EL, Toreyev IO, et al. Jepidemiologija i harakter rasstrojstv mocheispuskanija u bol'nyh rassejannym sklerozom. Vestnik urologii. 2020; 8 (2): 29–36. DOI: 10.21886/2308-6424-2020-8-2-29-36. Russian.
13. Bientinesi R, Campetella M, Nociti V, Bassi PF, Sacco E. Identification of brain structures involved in lower urinary tract symptoms and sexual dysfunctions in patients with multiple sclerosis. Glob J Med Res. 2021; 21 (2): 42–48.
14. Mehnert U, van der Lely S, Seif M, Leitner L, Liechti MD, Michels L. Neuroimaging in Neuro-Urology. Eur Urol Focus. 2020; 6 (5): 826–37. DOI: 10.1016/j.euf.2019.12.006.
15. Kreiter D, Postma AA, Hupperts R, Gerlach O. Hallmarks of spinal cord pathology in multiple sclerosis. J Neurol Sci. 2024; 456: 122846. DOI: 10.1016/j.jns.2023.122846.
16. Sastre-Garriga J, Pareto D, Battaglini M, Rocca MA, Ciccarelli O, Enzinger C, et al. MAGNIMS consensus recommendations on the use of brain and spinal cord atrophy measures in clinical practice. Nat Rev Neurol. 2020; 16 (3): 171–82. DOI: 10.1038/s41582-020-0314-x.
17. Vega-P JM, Pascual LA. High-pressure bladder: an underlying factor mediating renal damage in the absence of reflux? BJU Int. 2001; 87 (6): 581–4. DOI: 10.1046/j.1464-410x.2001.00082.x.
18. Peyronnet B, Krupp LB, Reynolds WS, Gamé X, Amarenco G, Cornu JN, et al. Nocturia in Patients With Multiple Sclerosis. Rev Urol. 2019; 21 (2–3): 63–73.
19. Andersson K-E, Madersbacher H, Altaweel W, Vasudeva P, Igawa Y. Drug Treatment. Handbook of Neurourology. Singapore, 2023; p. 281–315.
20. Van Kerrebroeck P, Andersson KE. Terminology, epidemiology,

etiology, and pathophysiology of nocturia. Neurourol Urodyn. 2014; 33 (Suppl.1): S2–5. DOI: 10.1002/nau.22595.

21. Kowalik CG, Cohn JA, Delpe S, Reynolds WS, Kaufman MR, Milam DF, et al. Nocturia: Evaluation and Current Management Strategies. Rev Urol. 2018; 20 (1): 1–6. DOI: 10.3909/riu0797.

22. Filippova ES, Bazhenov IV, Moskvina EYu, Zyryanov AV, Borzunov IV. Perevod i aprobacija russkojazychnoj versii oprosnika SF-Qualiveen. Urologicheskie vedomosti. 2019; 9: 100. Russian.

23. Kapica-Topczewska K, Tarasiuk J, Chorąży M, Czarnowska A, Brola W, Szczepański M, et al. The epidemiology of comorbidities among multiple sclerosis patients in northeastern Poland. Mult Scler Relat Disord. 2020; 41: 102051. DOI: 10.1016/j.msard.2020.102051.

24. Harding K, Zhu F, Alotaibi M, Duggan T, Tremlett H, Kingwell E. Multiple cause of death analysis in multiple sclerosis: A population-based study. Neurology. 2020; 94 (8): e820–e829. DOI: 10.1212/WNL.0000000000008907.

25. Medeiros Junior WLG, Demore CC, Mazaro LP, de Souza MFN, Parolin LF, Melo LH, et al. Urinary tract infection in patients with multiple sclerosis: An overview. Mult Scler Relat Disord. 2020; 46: 102462. DOI: 10.1016/j.msard.2020.102462.

26. Grebenkina PV, Selkov SA, Kraeva LA, Sokolov DI. Vzaimodejstvie bakterij gruppy ESKAPE i NK-kletok: vzaimnaja reguljacija i rol' v razvitii reproduktivnyh patologij. Infekcija i immunitet. 2023; 13 (4): 609–26. DOI: 10.15789/2220-7619-CBE-15452.

27. Miller WR, Arias CA. ESKAPE pathogens: antimicrobial resistance, epidemiology, clinical impact and therapeutics. Nat Rev Microbiol. 2024; 22 (10): 598–616. DOI: 10.1038/s41579-024-01054-w.

28. Yarets YuI. Patogennyj potencial bakterij gruppy ESKAPE, vydelennyh iz ran: harakteristika feno- i genotipicheskih markerov i vozmozhnost' ih prakticheskogo primenenija. Zhurnal Grodnenskogo gosudarstvennogo medicinskogo universiteta. 2022; 20 (4): 400–13. DOI: 10.25298/2221-8785-2022-20-4-400-413. Russian.

29. Phé V, Chartier-Kastler E, Panicker JN Management of neurogenic bladder in patients with multiple sclerosis. Nat Rev Urol. 2016; 13 (5): 275–88. DOI: 10.1038/nrurol.2016.53.

30. Panicker JN, Fowler CJ. Lower urinary tract dysfunction in patients with multiple sclerosis. Handb Clin Neurol. 2015; 130: 371–81. DOI: 10.1016/B978-0-444-63247-0.00021-3.

Литература

1. Sakakibara R. Urinary Dysfunction in Multiple Sclerosis, Neuromyelitis Optica, and Related Disorders. Handbook of Neurourology. Singapore, 2023: 737–45.

2. Averbeck MA, Mehnert U, Al Mousa RT, Kessler TM. Epidemiology of Neurogenic Lower Urinary Tract Dysfunction. Handbook of Neurourology. Singapore, 2023: 135–40.

3. Vecchio M, Chiaramonte R, DI Benedetto P. Management of bladder dysfunction in multiple sclerosis: a systematic review and meta-analysis of studies regarding bladder rehabilitation. Eur J Phys Rehabil Med. 2022; 58 (3): 387–96. DOI: 10.23736/S1973-9087.22.07217-3.

4. de Sèze M, Ruffion A, Denys P, Joseph PA, Perrouin-Verbe B. The neurogenic bladder in multiple sclerosis: review of the literature and proposal of management guidelines. Mult Scler. 2007; 13 (7): 915–28. DOI: 10.1177/1352458506075651.

5. Шварц П. Г., Попов С. В., Завалишин И. А. Патофизиологические и нейрофармакологические особенности терапии хронической задержки мочи при рассеянном склерозе. Фарматека. 2017; 6 (339): 51–60.

6. Шварц П. Г., Попов С. В. Нейрогенная хроническая задержка мочи у больных рассеянным склерозом. Трудный пациент. 2018; 16 (6): 61–64.

7. Ozkan B, Demirkesen O, Durak H, Uygun N, Ismailoglu V, Cetinel B. Which factors predict upper urinary tract deterioration in overactive neurogenic bladder dysfunction? Urology. 2005; 66 (1): 99–104. DOI: 10.1016/j.urology.2005.02.009.

8. Филиппова Е. С., Баженов И. В., Зырянов А. В. и др. Инфекции мочевыводящих путей у больных нейрогенным мочевым пузырем. Consilium Medicum. 2019; 21 (12): 139–44. DOI: 10.26442/20751753.2019.12.190676.

9. Коршунова Е. С., Юсупова Д. Г., Зимин А.А. и др. Валидация опросника по функциям тазовых органов (Questionnaire on pelvic organ function) у неврологических больных в России. Андрология и генитальная хирургия. 2023; 24 (1): 90–99. DOI: 10.17650/2070-9781-2023-24-1-90-99.

10. Sakakibara R, Shinotoh H, Uchiyama T, Sakuma M, Kashiwado M, Yoshiyama M, Hattori T. Questionnaire-based assessment of pelvic organ dysfunction in Parkinson's disease. Auton Neurosci. 2001; 92 (1–2): 76–85. DOI: 10.1016/S1566-0702(01)00295-8.

11. Филиппова Е. С., Баженов И. В., Волкова Л. И., Москвина Е. Ю., Турова Е. Л., Попова Ю. В. Русскоязычная версия шкалы симптомов нейрогенного мочевого пузыря (NBSS). Урология. 2018; 6: 5–13. DOI: 10.18565/urology.2018.6.5-13.

12. Зырянов А. В., Баженов И. В., Филиппова Е. С., Устинов Г. С., Турова Е. Л., Тореев И. О., Леушин Е. К. Эпидемиология и характер расстройств мочеиспускания у больных рассеянным склерозом. Вестник урологии. 2020; 8 (2): 29–36. DOI: 10.21886/2308-6424-2020-8-2-29-36.

13. Bientinesi R, Campetella M, Nociti V, Bassi PF, Sacco E. Identification of brain structures involved in lower urinary tract symptoms and sexual dysfunctions in patients with multiple sclerosis. Glob J Med Res. 2021; 21 (2): 42–48.

14. Mehnert U, van der Lely S, Seif M, Leitner L, Liechti MD, Michels L. Neuroimaging in Neuro-Urology. Eur Urol Focus. 2020; 6 (5): 826–37. DOI: 10.1016/j.euf.2019.12.006.

15. Kreiter D, Postma AA, Hupperts R, Gerlach O. Hallmarks of spinal cord pathology in multiple sclerosis. J Neurol Sci. 2024; 456: 122846. DOI: 10.1016/j.jns.2023.122846.

16. Sastre-Garriga J, Pareto D, Battaglini M, Rocca MA, Ciccarelli O, Enzinger C, et al. MAGNIMS consensus recommendations on the use of brain and spinal cord atrophy measures in clinical practice. Nat Rev Neurol. 2020; 16 (3): 171–82. DOI: 10.1038/s41582-020-0314-x.

17. Vega-P JM, Pascual LA. High-pressure bladder: an underlying factor mediating renal damage in the absence of reflux? BJU Int. 2001; 87 (6): 581–4. DOI: 10.1046/j.1464-410x.2001.00082.x.

18. Peyronnet B, Krupp LB, Reynolds WS, Gamé X, Amarenco G, Cornu JN, et al. Nocturia in Patients With Multiple Sclerosis. Rev Urol. 2019; 21 (2–3): 63–73.

19. Andersson K-E, Madersbacher H, Altaweel W, Vasudeva P, Igawa Y. Drug Treatment. Handbook of Neurourology. Singapore, 2023; p. 281–315.

20. Van Kerrebroeck P, Andersson KE. Terminology, epidemiology, etiology, and pathophysiology of nocturia. Neurourol Urodyn. 2014; 33 (Suppl.1): S2–5. DOI: 10.1002/nau.22595.

21. Kowalik CG, Cohn JA, Delpe S, Reynolds WS, Kaufman MR, Milam DF, et al. Nocturia: Evaluation and Current Management Strategies. Rev Urol. 2018; 20 (1): 1–6. DOI: 10.3909/riu0797.

22. Филиппова Е. С., Баженов И. В., Москвина Е. Ю., Зырянов А. В., Борзунов И. В. Перевод и апробация русскоязычной версии опросника SF-Qualiveen. Урологические ведомости. 2019; 9: 100.

23. Kapica-Topczewska K, Tarasiuk J, Chorąży M, Czarnowska A, Brola W, Szczepański M, et al. The epidemiology of comorbidities among multiple sclerosis patients in northeastern Poland. Mult Scler Relat Disord. 2020; 41: 102051. DOI: 10.1016/j.msard.2020.102051.

24. Harding K, Zhu F, Alotaibi M, Duggan T, Tremlett H, Kingwell E. Multiple cause of death analysis in multiple sclerosis: A population-based study. Neurology. 2020; 94 (8): e820–e829. DOI: 10.1212/WNL.0000000000008907.

25. Medeiros Junior WLG, Demore CC, Mazaro LP, de Souza MFN, Parolin LF, Melo LH, et al. Urinary tract infection in patients with multiple sclerosis: An overview. Mult Scler Relat Disord. 2020; 46: 102462. DOI: 10.1016/j.msard.2020.102462.

26. Гребенкина П. В., Сельков С. А., Краева Л. А., Соколов Д. И. Взаимодействие бактерий группы ESKAPE и NK-клеток: взаимная регуляция и роль в развитии репродуктивных патологий. Инфекция и иммунитет. 2023; 13 (4): 609–626. DOI: 10.15789/2220-7619-CBE-15452.

27. Miller WR, Arias CA. ESKAPE pathogens: antimicrobial resistance, epidemiology, clinical impact and therapeutics. Nat Rev Microbiol. 2024; 22 (10): 598–616. DOI: 10.1038/s41579-024-01054-w.

28. Ярец Ю. И. Патогенный потенциал бактерий группы ESKAPE, выделенных из ран: характеристика фено- и генотипических маркеров и возможность их практического применения. Журнал Гродненского государственного медицинского университета.

2022; 20 (4): 400–13. DOI: 10.25298/2221-8785-2022-20-4-400-413.

29. Phé V, Chartier-Kastler E, Panicker JN Management of neurogenic bladder in patients with multiple sclerosis. Nat Rev Urol. 2016; 13 (5): 275–88. DOI: 10.1038/nrurol.2016.53.

30. Panicker JN, Fowler CJ. Lower urinary tract dysfunction in patients with multiple sclerosis. Handb Clin Neurol. 2015; 130: 371–81. DOI: 10.1016/B978-0-444-63247-0.00021-3.

SYNERGISTIC EFFICACY OF LOW-INTENSITY EXTRACORPOREAL SHOCK WAVE AND PLATELET-RICH PLASMA ON ERECTILE DYSFUNCTION

Lee YC[#,1,2], Yang TD[#,3,4], Chen WC[2,3,4], Dubey NK[5,6], Chaturvedi H[7], Huang AC[8,9], Chang CH[3,4,10], Lin CC[3,4], Liu MC[2,3,4,11,12] ✉

[1] Nursing Department, Taipei Medical University Hospital, Taipei, Taiwan
[2] Graduate Institute of Clinical Medicine, School of Medicine, College of Medicine, Taipei Medical University, Taipei, Taiwan
[3] Department of Urology, Taipei Medical University Hospital, Taipei, Taiwan
[4] TMU Research Center of Urology and Kidney, Taipei Medical University, Taipei, Taiwan
[5] Victory Biotechnology Co., Ltd., Taipei, Taiwan
[6] Executive Programme in Healthcare Management, Indian Institute of Management Lucknow, Lucknow, India
[7] Baba Kinaram Autonomous State Medical College Chandauli, Uttar Pradesh, India
[8] Institute of Traditional Medicine, School of Medicine, National Yang-Ming Chiao Tung University, Taipei, Taiwan
[9] Department of Urology, Department of Surgery, Taipei City Hospital Ren-Ai Branch, Taipei, Taiwan
[10] Institute of Microbiology and Immunology, National Yang Ming Chiao Tung University, Hsinchu, Taiwan
[11] Clinical Research Center, Taipei Medical University Hospital, Taipei, Taiwan
[12] School of Dental Technology, College of Oral Medicine, Taipei Medical University, Taipei, Taiwan

Erectile dysfunction (ED), an unusual sexual condition in which the person fails to attain or sustain an erectile penis, severely impacts personal relationships, confidence, and efficiency. To date, low-intensity extracorporeal shock wave therapy (Li-ESWT) is an option to manage ED; however, it is associated with adverse events such as bruising, redness, and pain. Hence, in this study, we applied platelet-rich plasma (PRP), a blood-derived biomaterial containing cargo of growth factors, to enhance the therapeutic efficacy of Li-ESWT on ED. We assessed the synergistic effect of PRP+Li-ESWT, in which Li-ESWT was extracorporeally applied simultaneously with PRP. They were evaluated clinically at 22 ± 2, 50 ± 2 and 78 ± 2 days. Statistical analysis was performed using a non-parametric test, Friedman repeated measures as an alternative non-parametric test of ANOVA test. The international index of erectile function (IIEF-5) and erection hardness score (EHS) were recorded. IIEF-5 score in the pre-treated group was 8.36 ± 1.44. After 22 ± 2 days of synergistic PRP+Li-ESWT treatment, the score was 14.45 ± 2.12 ($p < 0.028$). This score further increased to 15.45 ± 1.93 ($p < 0.008$) and 16.18 ± 1.48 ($p < 0.001$) after 50 ± 2 days and 78 ± 2 days of treatment, respectively. The mean pre-treated EHS was 1.64 ± 0.20 ($p < 0.002$), which increased to 2.81 ± 0.26 ($p < 0.002$), 3.09 ± 0.25 ($p < 0.0002$) and 3.18 ± 0.12 ($p < 0.000$) on day 22 ± 2, 50 ± 2 and 78 ± 2 days, respectively. Conclusively, our study demonstrated potent synergistic therapy of PRP+Li-ESWT in ED treatment by improving IIEF-5 and EHS scores. However, extensive mechanism-based clinical studies are needed to reach a consensus.

Keywords: erectile dysfunction, Li-ESWT, platelet-rich plasma (PRP), IIEF-5, EHS

СИНЕРГИЧЕСКАЯ ЭФФЕКТИВНОСТЬ НИЗКОИНТЕНСИВНОЙ ЭКСТРАКОРПОРАЛЬНОЙ УДАРНО-ВОЛНОВОЙ ТЕРАПИИ И ОБОГАЩЕННОЙ ТРОМБОЦИТАМИ ПЛАЗМЫ ПРИ ЭРЕКТИЛЬНОЙ ДИСФУНКЦИИ

Й. Ч. Ли[#,1,2], Т. Д. Янг[#,3,4], У. Ч. Чен[2,3,4], Н. К. Дуби[5,6], Х. Чатурведи[7], А. Ч. Хуанг[8,9], Ч. Х. Чанг[3,4,10], Ч. Ч. Лин[3,4], М. Ч. Лю[2,3,4,11,12] ✉

[1] Отделение сестринского ухода, Больница Медицинского университета Тайбея, Тайбей, Тайвань
[2] Академический институт клинической медицины, Школа медицины, Медицинский колледж, Медицинский университет Тайбея, Тайбей, Тайвань
[3] Отделение урологии, Больница Медицинского университета Тайбея, Тайбей, Тайвань
[4] Научно-исследовательский центр урологии и нефрологии, Медицинский университет Тайбея, Тайбей, Тайвань
[5] Victory Biotechnology Co., Ltd., Тайбей, Тайвань
[6] Программа для руководителей по управлению здравоохранением, Индийский институт менеджмента Лакхнау, Лакхнау, Индия
[7] Медицинский колледж Чандаули Бабы Кинарама, Уттар-Прадеш, Индия
[8] Институт традиционной медицины, Школа медицины, Национальный университет Ян Мин Цзяо Дун, Тайбей, Тайвань
[9] Хирургическое отделение, Городская больница Тайбея, филиал Рен-Ай, Тайбей, Тайвань
[10] Институт микробиологии и иммунологии, Национальный университет Ян Мин Цзяо Дун, Синьчжу, Тайвань
[11] Научно-клинический центр, Больница Медицинского университета Тайбея, Тайбей, Тайвань
[12] Стоматологический колледж, Медицинский университет Тайбея, Тайбей, Тайвань

Эректильная дисфункция (ЭД) — патологическое состояние репродуктивной системы, при котором нарушается способность достижения или поддержания эрекции. Оно губительно сказывается на взаимоотношениях, уверенности в себе и эффективности. Метод лечения ЭД — низкоинтенсивная ударно-волновая терапия (низкоинтенсивная УВТ). Однако ее применение связано с нежелательными явлениями, такими как синяки, покраснения и боль. В ходе настоящего исследования применяли обогащенную тромбоцитами плазму (PRP) — полученный из крови биоматериал, содержащий большое количество факторов роста, для повышения терапевтической эффективности низкоинтенсивной УВТ при ЭД. Оценивали синергический эффект PRP и низкоинтенсивной УВТ, при этом низкоинтенсивную УВТ применяли экстракорпорально одновременно с PRP. Оценку клинических показателей проводили через 22 ± 2, 50 ± 2 и 78 ± 2 дней. Статистический анализ выполняли с помощью непараметрического критерия Фридмана для повторных измерений (альтернатива дисперсионному анализу (ANOVA)). Фиксировали показатели Международного индекса эректильной функции (МИЭФ-5) и показатели твердости полового члена при эрекции (EHS). Показатель по шкале МИЭФ-5 до лечения составил $8,36 \pm 1,44$ баллов. Через 22 ± 2 дня комбинированного лечения с применением PRP и низкоинтенсивной УВТ показатель составил $14,45 \pm 2,12$ баллов ($p < 0,028$), а в дальнейшем увеличился до $15,45 \pm 1,93$ ($p < 0,008$) и $16,18 \pm 1,48$ ($p < 0,001$) баллов — через 50 ± 2 и 78 ± 2 дней лечения соответственно. Средний показатель по шкале EHS до лечения составил $1,64 \pm 0,20$ ($p < 0,002$). Он увеличился до $2,81 \pm 0,26$ ($p < 0,002$), $3,09 \pm 0,25$ ($p < 0,0002$) и $3,18 \pm 0,12$ ($p < 0,000$) через 22 ± 2, 50 ± 2 и 78 ± 2 дней соответственно. Комбинированное лечение с применением PRP и низкоинтенсивной УВТ продемонстрировало мощный синергический эффект, улучшив показатели МИЭФ-5 и EHS. Однако для достижения консенсуса необходимы широкомасштабные клинические исследования механизмов этого явления.

Ключевые слова: эректильная дисфункция, низкоинтенсивная УВТ, обогащенная тромбоцитами плазма (PRP), МИЭФ-5, EHS

Erectile dysfunction (ED) is an unusual sexual condition in which the person fails to attain or sustain an erectile penis [1]. It could severely affect sexual health and activity, which negatively impacts personal relationships, psychological status, and quality of life [1, 2]. Penile erection is regulated by oxygen tension, and its lower levels decrease cavernous trabecular smooth muscle content, resulting in venous leakage, oxidative stress, inflammation, structural change in the penile interstitium and neural structures due to vasoconstriction, endothelial dysfunction, veno-occlusive disease, and in the long-term may cause initiation and progression of ED [3].

It has been projected that the incidence of ED may influence the population of 322 million by 2025 [1, 4]. Recent longitudinal epidemiological data suggest that the prevalence of ED could range from 32–80%, depending on the age [5]. As the age increases, the risk and incidence of ED also elevate, particularly in the age group of 40–70 years [5]. To date, though various traditional ED therapies, including pharmaceutical and surgical alternatives, have been employed, the results either demonstrated an inadequate efficacy or adverse events. Hence, a complete therapeutic solution is urgently needed.

Low-intensity extracorporeal shockwave therapy (Li-ESWT) is a therapeutic approach that has the potential to regenerate endothelium, smooth muscle cells, and neuronal nitric oxide synthase-positive nerves [6]. Shock waves are acoustic waves with a frequency range of 16–20 MHz with a period of up to 10 microseconds and are collected in the focal zone, which could be a targeted tissue or organ for therapeutic purposes [7]. Low-intensity shockwaves are low-energy waves of less than 0.1mJ/mm^2 energy flux density (EFD), though no consensus has yet been reached on the EFD range [8]. Additional changes include the proliferation of T cells, recruitment of stem cells, increase in endothelial capillary connections, regeneration of nerve and axonal cells, collagen matrix alteration, and decrease in inflammation and oxidative stress [9].

PRP is a blood-derived product rich in growth factors such as vascular endothelial growth factor (VEGF), basic fibroblast growth factor (bFGF), transforming growth factor β-1 (TGF-β1), platelet-derived growth factors (PDGF), hepatocyte growth factor (HGF), insulin-like growth factor-1 (IGF-1), epidermal growth factor (EGF), and various cytokines. These factors participate in tissue growth and healing through activation and the proliferation of fibroblasts, smooth muscle cells, and neutrophils, in addition to mesenchymal stem cell differentiation [1, 10]. PRP also contains biomolecules such as adenosine triphosphate, adenosine diphosphate, dopamine, serotonin, histamine, and Ca^{+2} ions, which play a crucial role in tissue homeostasis [11]. Based on the above-mentioned therapeutic activities, the potential of PRP is being explored in ED treatment. However, a few studies have suggested that PRP therapeutic efficacy could be enhanced by supplementing other alternative therapies, such as low-intensity extracorporeal shockwave therapy (Li-ESWT). Moreover, pre-clinical and clinical studies limit their wide therapeutic applications in ED. Therefore, we examined the synergistic impact of PRP and Li-ESWT-based regenerative treatment for ED.

METHODS

Patients

Between 20 May 2020 and 22 Feb 2022, 11 ED patients underwent a combination therapy of Li-ESWT and PRP for 78 ± 2 days. All patients were informed in detail about the synergistic treatment of Li-ESWT and PRP, as illustrated in the schematic design of the study (Fig. 1).

The patients' demographic characteristics such as age, material status, ED duration, mean body mass index (BMI), triglyceride level, high-density lipoprotein (HDL), prostate serum antigen (PSA), and testosterone levels were evaluated. Additionally, hypertension, diabetes mellitus (DM), BPH, dyslipidemia, and antiplatelet therapy use were also recorded.

Inclusion and exclusion criteria

This study included patients suffering from impotence for more than 3 months, with an international index of erectile function (IIEF) less or equal to 21, erectile hardness score (EHS) of 0, ≤ 3, and age over 30 years old. Whereas the patients were excluded if they patients have characteristics such as hypogonadism, bleeding tendency, could not cooperate with the treatment, AIDS, syphilis, condyloma victim, received radical prostatectomy, prostate cancer or pelvis malignant tumor victim, gonad dysfunction, penis deformities, penile prosthesis implantation, psychiatric disease victim, neural disease (multiple myeloma, brain atrophy, etc.), pacemaker implantation, not suitable to join this trial judged by the investigation, alcohol or drug abuse.

Li-ESWT application

Treatment of Li-ESWT using PiezoWave 2 (Richard Wolf GmbH, Knittlingen, Germany) machine was performed on days 1, 8, 15, 29, 36, and 43. In each treatment, 2,000 shockwaves (SW) (0.16 mJ/ mm^2, 6–8 hertz (Hz) were applied to the penile shafts and 2,000 SW to the perineal corpus cavernosum.

Preparation and injection of human platelet-rich plasma (PRP)

To prepare PRP, we employed a specialized platelet concentrate separator containing ACD-A as an anticoagulant and a specific
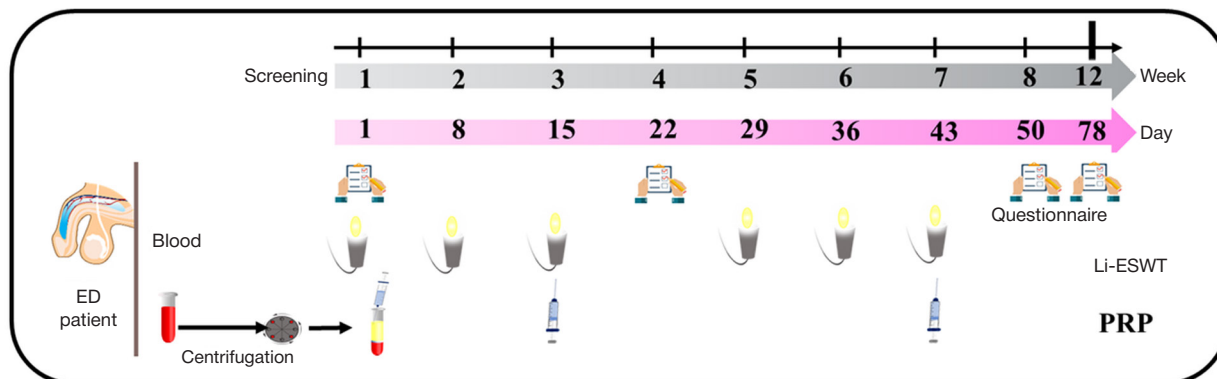
Fig. 1. The experimental schedule. ED — Erectile dysfunction. Li-ESWT — Extracorporeal shockwave therapy. PRP — Platelet-rich plasma.

Table 1. Patients' demographics. ED — Erectile dysfunction, BMI — Body mass index, DM — Diabetes melli-tus, HDL — High-density lipoprotein, TG — Triglycerides, BPH — Benign prostate hyperplasia, PSA — Prostate-specific antigen

Variable	N	Value	*p*-value (Shapiro–Wilk)
Age (years)	11	60.3 ± 10.4	0.154
Duration ED (year)	11	2 [1–8]	0.001
Mean BMI (kg/m^2)	11	25.2 ± 3.06	0.391
TG (mg/dl)	9	187 ± 119	0.198
HDL (mg/dl)	8	47.3 ± 10.8	0.524
PSA	10	1.10 [0.925–2.60]	0.005
Testosterone level	11	5.02 ± 1.55	0.322
Marital status (y/n)	11	8 d / 3 n	
Hypertension (y/n)	11	5 d / 6 n	
DM	11	5 d / 6 n	
Dyslipidemia	11	4 d / 7 n	
Usage antiplatelets	11	3 d / 8 n	
BPH	11	10 d / 1 n	

separator gel to harvest platelets and plasma to prevent contamination from other blood components, including red blood cells and leukocytes. In brief, we collected 7 milliliters (mL) of autologous human peripheral blood into a PLTenus PLUS Platelet Concentrate Separator (TCM Biotech International Corp., Taipei, Taiwan) through a sterile venipuncture. Then, the collected blood was centrifuged at 500~1200G for 8 minutes. Thereafter, approximately 4 mL of mixed plasma and platelets, which remained over the thixotropic gel layer, were isolated and then collected in a falcon tube for therapeutic application. The 0.5 ml PRP was then injected intracorporeally at 6 sites on the penile shaft, and the therapeutic efficacy was evaluated using IIEF-5 and EHS scores.

Outcome measurements

We evaluated treatment outcomes using the IIEF-5 and EHS scores. IIEF-5 is a self-assessment score-based questionnaire to determine the erectile function and severity of ED [12]. It specifically employs five domains to measure erectile function, sexual desire, orgasmic function, intercourse satisfaction, and overall satisfaction. Erection hardness is assessed through EHS, a four-point scale self-report based on a single item [13]. This reliable score system also indicates a direct relation between erection hardness and intercourse. Pre-treatment scores were compared with post-treatment scores to assess the efficacy of this synergistic treatment. The post-treatment scores were measured at 22 ± 2 and 50 ± 2 days and 78 ± 2 days.

Statistical analysis

The statistical analysis was performed using non-parametric test, Friedman repeated measures as an alternative non-parametric test of ANOVA test, which is suitable for non-normal distribution data/small sample. Further, pairwise comparison by Durbin-Conovar tests was done as post-hoc test (alternative non-parametric test of student *t*-test). The values were considered significant only when less than 0.05.
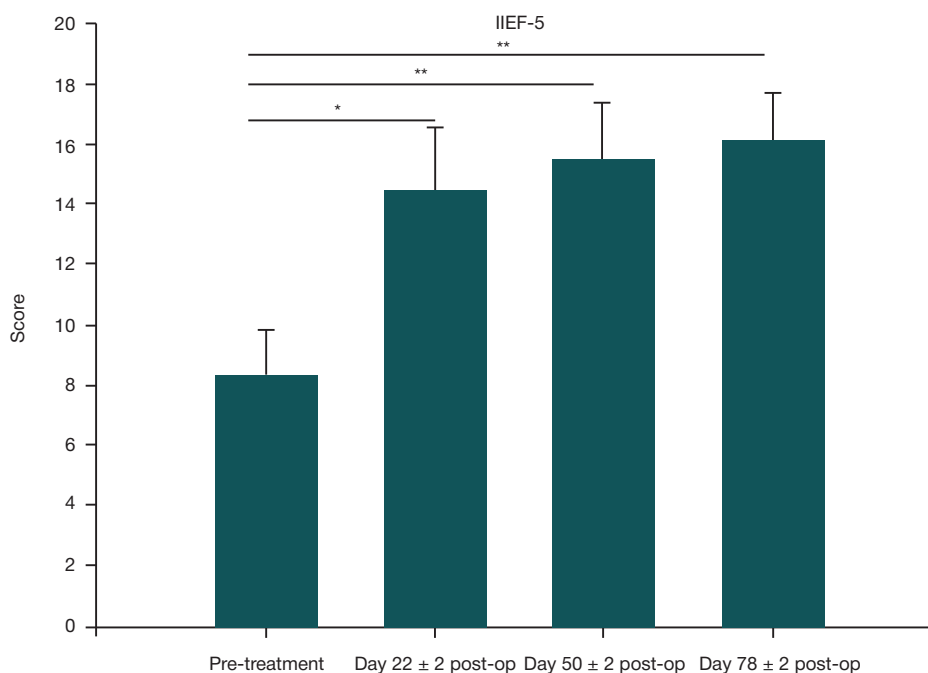
Fig. 2. IIEF-5 score at pre-treatment, 22 ± 2, 50 ± 2, and 78 ± 2 days post-treatment. IIEF-5 — International index erectile function-5. * *p* < 0.05 and *** *p* < 0.001

Table 2. Pre-treatment and post-treatment scores of IIEF-5 and EHS

Timeline / Variable	t1 median [q1–q3]; mean ± SD	t2 median [q1–q3]; mean ± SD	t3 median [q1–q3]; mean ± SD	t4 median [q1–q3]; mean ± SD	Q (p-value)	Significant post-hoc (p-value)
IIEF-5	7 [5–10.5]; 8.36 ± 4.80	13 [10–20.5]; 14.5 ± 7.05	15 [13–20.5]; 15.5 ± 6.42	17 [13–19.5]; 16.2 ± 4.92	22.5 < 0.001)	t1–t2 (<0.001). t2–t3 (<0.001). t1–t4 (<0.001). t2–t4 (0.011)
EHS	2 [1–2]; 1.64 ± 0.674	3 [2.5–3]; 2.82 ± 0.874	3 [3–3.5]; 3.09 ± 0.831	3 [3–3]; 3.18 ± 0.405	22.2 (0.001)	t1–t2 (<0.001). t2–t3 (<0.001). t1–t4 (<0.001). t2–t4 (0.043)

RESULTS

Demographics of patients

The study involved 11 patients treated with a combination of Li-ESWT and PRP. As shown in Table 1, no significant difference was observed for the age, BMI, TG, HDL, PSA, and testosterone; however, ED duration was significant. Out of 11 patients, 8 (72.73%) were married, and 5 (45.46%) suffered from hypertension and DM. Three patients (27.27%) had been using antiplatelets. After the treatment, the IIEF-5 and EHS scores were assessed.

Effect of PRP+Li-ESWT on IIEF-5 scores

The median [q1–q3] and mean±SD value of IIEF-5 (Fig. 2) at different time points are shown in Table 2 for the two groups (pre-treatement and PRP+Li-ESWT treatment). In the PRP+Li-ESWT group, the median [q1–q3] IIEF-5 scores significantly increased during t1–t2, t1–t3 and t1–t4 ($p < 0.001$).

Impact of PRP+Li-ESWT on erection hardness

Further, erection hardness score (EHS) (Fig. 3) also showed similar pattern the median [q1–q3] values significantly during t1–t2, t1–t3 and t1–t4 ($p < 0.001$), indicating the efficacy of PRP+Li-ESWT in gaining erection hardness, which is a fundamental component of erectile function.

DISCUSSION

Li-ESWT is considered a safer alternative in ED treatment, especially in the case of mild vasculogenic ED or when patients are less responsive to PDE-5i [6]. It promotes neo-angiogenesis, improves blood circulation in cavernosal tissues, and suppresses inflammation and stress [14]. In DM patients, Li-ESWT mimics shear stress, affects membrane permeabilization, and regulates signal cascades, resulting in an inhibited inflammatory response, secretion of nitric oxide, mobilization of endothelial and stem cells, and improved nNOS-positive nerves in corpora cavernosa and endothelial content in cavernous arteries and sinusoids [15]. Based on this evidence, we anticipate that all the therapeutic impacts, particularly neovascularization, could be elevated through supplementing PRP.

PRP is rich in trophic growth factors and regenerative molecules, which may promote stem cell recruitment, angiogenesis, nitric oxide synthesis, and cavernosal nerve regeneration. In the murine model, PRP has been demonstrated with neuroprotective and neuro-regenerative effects by lowering the expression of caspase-3 and TGF-β1, resulting in PDGF
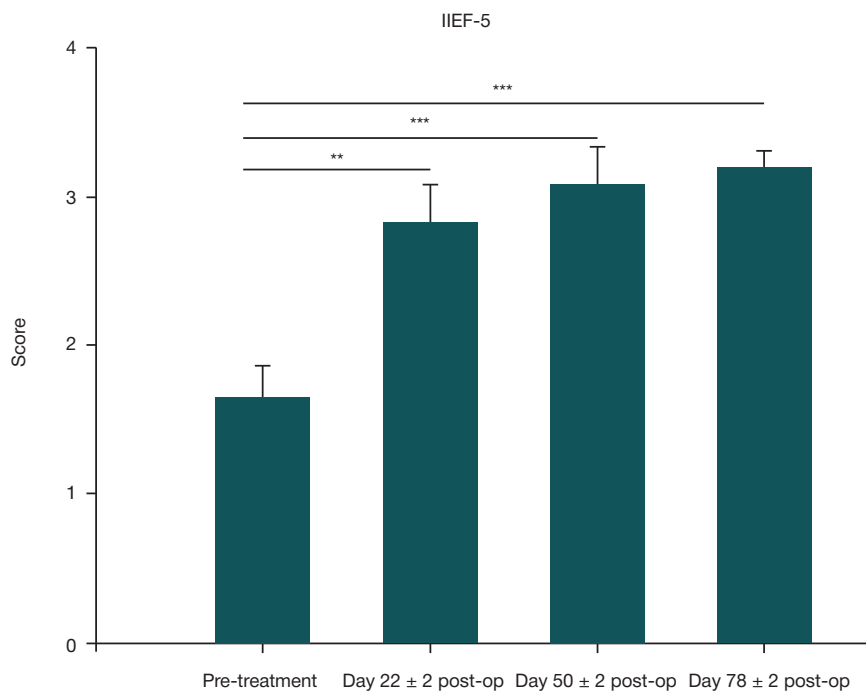
Fig. 3. EHS at pre-treatment, 22 ± 2, 50 ± 2, and 78 ± 2 days post-treatment. EHS: Erection hardness score
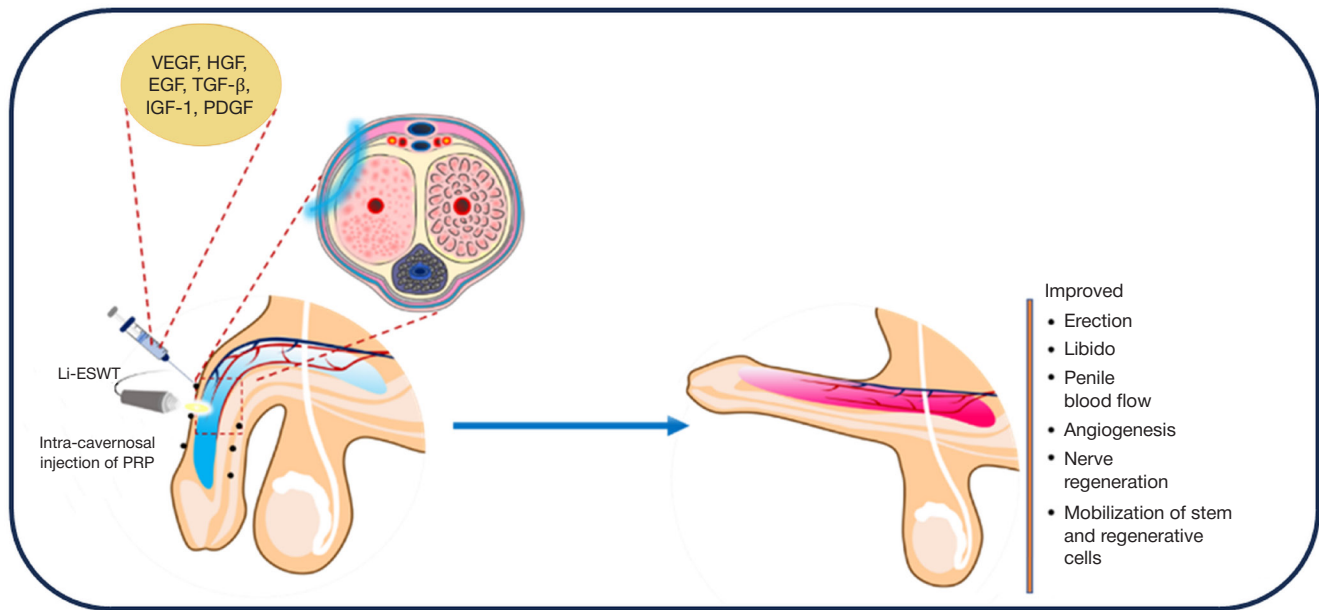
Fig. 4. Possible therapeutic outcomes of PRP and Li-ESWT. Intracavernosal administration of PRP at 6 sites with Li-LWST. PRP was administered on the penial shaft from the corona sulcus to the penoscrotal junction, and a black dot indicates the injection sites. PRP — Platelet-rich plasma, Li-ESWT — Low-intensity extracorporeal shock wave

levels [16]. The PRP-contained VEGF and BDNF promote nerve regeneration, upregulation of nNOS, and axon growth [17]. Li-ESWT also induces the expression of VEGF and its receptor Flt-1(vascular endothelial growth factor receptor-1)[18], which could be further accelerated through PRP-contained VEGF. In addition, BDNF activates the Janus kinase signal transducer and activator of the transcription (JAK-STAT) pathway, which promotes neurite growth in the pelvic ganglion region [17, 19]. The BDNF, IGF-1, VEGF, and bFGF present in PRP have effectively restored penile hemodynamics in the pre-clinical models [20].

In our study, some of the patients showed characteristics of hypertension, diabetes, and high triglyceride levels (Table 1). It has been evident that 25% and 60% of patients treated for hypertension and diabetes, respectively, suffered from ED [21]. Aging reduces the level of testosterone, smooth muscle cells in the penis, and elastic fibers in tunica albuginea, which results in ED [22]. Endothelial dysfunction due to dyslipidemia is a prominent cause of ED [23]. It has been further observed that ED is associated with at least one of the co-morbidities such as depression (11.1%), DM (20.2%), hyperlipidemia (42.4%), and hypertension (41.6%). Thus, the presence of above-mentioned characteristics/demographics in our patients is associated with ED.

Our study combined both Li-ESWT and PRP therapies to evaluate the synergistic effect of the combination therapy. The therapeutic outcomes, i.e., erectile function and hardness, were assessed using IIEF-5 and EHS scores, respectively (Table 2). The median changes in IIEF-5 score using Li-ESWT among ED patients are +3.5 ($p = 0.0049$) and +1 ($p = 0.046$) after 1 month and 1 year post-treatment [24]. Li-ESWT improved the baseline IIEF-5 score from 8.27±2.741 to 10.43 ± 8.43 after one month of the treatment, and the therapeutic effect was sustained for 6 months at a similar level [25]. Another randomized clinical study indicates that weekly Li-ESWT treatment for five weeks of courses improves EHS and IIEF-5 scores. The EHS score increases by 0.35 and 0.50, whereas the IIEF-5 score improves by 2.40 and 3.45 after 4 and 12 weeks of treatment [26]. A 14-week Li-ESWT treatment (once a week), which includes a gap of 4 weeks after 5 weeks, reported improvement in IIEF-EF score from baseline 11.5 to 13 and 12.6 after 5 and

10 sessions, respectively [27]. The above-mentioned studies showed an improvement in IIEF-5 and EHS in the range of 2–5 and 0.3–2 points, respectively. However, our study has recorded an increment of 6-8 points in the mean baseline IIEF-5 score of 8.36 ± 1.44, which was significantly elevated to 14.45 ± 2.12, 15.45 ± 1.93, and 16.18 ±1.48 after 22 ± 2, 50 ± 2 and 78 ± 2 days post-treatment, respectively. Similarly, the mean EHS baseline score of 1.64 ± 0.20 increased to 2.81 ± 0.26, 3.09 ± 0.25, and 3.18 ± 0.12 at 22 ± 2, 50 ± 2, and 78 ± 2 days post-treatment, respectively. This data indicates improvement in erectile function in our combined treatment of Li-ESWT+PRP, which is comparatively better than previously reported monotherapy of Li-ESWT.

The enhanced therapeutic impact may be attributed to PRP, which promotes natural healing. The IIEF score is improved without adverse events when used to treat ED [28]. A prospective study showed the significant efficacy of PRP in improving IIEF score after treatment ($p = 0.02$)[1]. However, a fibrotic plaque develops on the ventral side in the middle of the penile shaft. However, intravaginal ejaculatory latency time significantly improved due to the combination treatment. The regenerative therapeutic efficacy of PRP has been widely evaluated among various disorders and is linked to the growth factor and other bioactive molecules present in the PRP. VEGF, a PRP component, has shown that it could effectively recover erectile function among CN injury animal models [29]. In coherence, a double-blinded, randomized, placebo-controlled clinical trial evidenced that PRP significantly attained minimal clinically important difference (MCID) in the IIEF-EF (erectile domain) post 6 months of treatment [30]. Moreover, the satisfaction level was evident without any hemorrhagic adverse events.

It has been demonstrated that PRP improves erectile function among diabetic rat models by inhibiting the atrophy of corporal smooth muscle cells, corpus cavernosum safety, and regenerating CN fiber [16]. In addition, PRP also restores tissue and improves all parameters of erectile function and myelinated nerve regeneration among DM rats [16]. Thus, PRP could effectively minimize post-surgical complications due to DM in ED treatment. Similarly, the PRP treatment significantly improves intracavernous pressure, mean arterial pressure, IGF-1,

BDNF, and VEGF levels among hyperlipidemia-associated ED rats [31]. Moreover, the PRP treatment also improves endothelial cells, neuronal nitric oxide synthase, and endothelial nitric oxide synthase in the corporal tissues, resulting in lower oxidative stress and apoptotic index. Based on our results, we infer that PRP could improve the Li-ESWT-treated ED owing to its wound-healing potential for microtrauma developed during Li-ESWT (Fig. 4).

Limitations of the study

Apart from various positive therapeutic outcomes, our study includes limitations like the lack of a control group such as Li-ESWT, which will be investigated in the future. However, a previous study on monotherapy of Li-ESWT [32] demonstrated an effective and safer profile for diabetic as well as non-diabetic ED patients. Hence, combined Li-ESWT and PRP treatment is anticipated to offer an enhanced therapeutic efficacy on ED. The pain score while injecting PRP was not recorded, which will also be the focus of our future study. Small sample size is another limitation of the study; however, we have conducted statistical analysis using non-parametric test, Friedman repeated measures as alternative non-parametric test of ANOVA test, which is suitable for non-

normal distribution data/small sample. We further did pairwise comparison by Durbin-Conovar tests as post-hoc test (alternative non-parametric test of student t-test). Notwithstanding, replicating the study with a larger population is recommended. Age is also a significant factor in maintaining healthy sexual activity. As per epidemiological evidence, the prevalence of moderate to complete erectile dysfunction (ED) increases with age, and the data indicates that in men, ED prevalence is 5.1%, 14.8% and 44% in men aged 29–30, 40–59, and 60–69, respectively [33]. Additionally, over 50% of men aged 70 and above are diagnosed with ED. Therefore, we did not specify the maximum age; however, our sample population showed the maximum age of 70–71, which coincides with the previous studies.

CONCLUSIONS

Our study demonstrates the synergistic potential of PRP and Li-ESWT in treating ED through enhancing IIIEF-5 and EHS. However, PRP's augmentative impact on Li-ESWT should be corroborated through extensive multi-center clinical trials. Further, due to a lack of established protocols, more efforts are needed to develop an effective regenerative treatment procedure to achieve the highest clinical benefits.

References

1. Taş T, Çakıroğlu B, Arda E, Onuk Ö, Nuhoğlu B. Early Clinical Results of the Tolerability, Safety, and Efficacy of Autologous Platelet-Rich Plasma Administration in Erectile Dysfunction. Sex Med. 2021; 9: 100313.
2. Vance G, Zeigler-Hill V, Shackelford TK. Erectile Dysfunction and Sexual Coercion: The Role of Sperm Competition Risk. Archives of Sexual Behavior. 2022; 51 (6): 2781–90.
3. Trebatický B, Žitňanová I, Dvořáková M, Országhová Z, Paduchová Z, Ďuračková Z, et al. Role of oxidative stress, adiponectin and endoglin in the pathophysiology of erectile dysfunction in diabetic and non-diabetic men. Physiol Res. 2019; 68: 623–31.
4. Ayta I, McKinlay J, Krane R. The likely worldwide increase in erectile dysfunction between 1995 and 2025 and some possible policy consequences. BJU international. 1999; 84: 50–56.
5. Colson MH, Cuzin B, Faix A, Grellet L, Huyghes E. Current epidemiology of erectile dysfunction, an update. Sexologies, 2018; 27: e7–e13.
6. Geyik S. Comparison of the efficacy of low-intensity shock wave therapy and its combination with platelet-rich plasma in patients with erectile dysfunction. Andrologia. 2021; 53: e14197.
7. Lei H, Liu J, Li H, Wang L, Xu Y, Tian W, et al. Low-Intensity Shock Wave Therapy and Its Application to Erectile Dysfunction. wjmh, 2013; 31: 208–14.
8. Liu J, Zhou F, Li G-Y, Wang L, Li H-X, Bai G-Y, et al. Evaluation of the Effect of Different Doses of Low Energy Shock Wave Therapy on the Erectile Function of Streptozotocin (STZ)-Induced Diabetic Rats. International Journal of Molecular Sciences. 2013; 14: 10661–73.
9. Sun D, Junger WG, Yuan C, Zhang W, Bao Y, Qin D, et al. Shockwaves Induce Osteogenic Differentiation of Human Mesenchymal Stem Cells Through ATP Release and Activation of P2X7 Receptors. Stem Cells; 2013; 31: 1170–80.
10. Mijiritsky E, Assaf HD, Peleg O, Shacham M, Cerroni L, Mangani L. Use of PRP, PRF and CGF in Periodontal Regeneration and Facial Rejuvenation-A Narrative Review. Biology. 2021; 10: 317.
11. Bos-Mikich A, de Oliveira R, Frantz N. Platelet-rich plasma therapy and reproductive medicine. Journal of Assisted Reproduction and Genetics. 2018; 35: 753–6.
12. Mark KP, Arenella K, Girard A, Herbenick D, Fu J, Coleman E. Erectile dysfunction prevalence in the United States: report from the 2021 National Survey of Sexual Wellbeing. J Sex Med. 2024;

21: 296–303.
13. Mulhall JP, Goldstein I, Bushmakin AG, Cappelleri JC, Hvidsten K. Validation of the Erection Hardness Score. The Journal of Sexual Medicine. 2007; 4: 1626–34.
14. Sokolakis I, Dimitriadis F, Teo P, Hatzichristodoulou G, Hatzichristou D, Giuliano F. The Basic Science Behind Low-Intensity Extracorporeal Shockwave Therapy for Erectile Dysfunction: A Systematic Scoping Review of Pre-Clinical Studies. J Sex Med. 2019; 16: 168–94.
15. Spivak L, Shultz T, Appel B, Verze P, Yagudaev D, Vinarov A. Low-Intensity Extracorporeal Shockwave Therapy for Erectile Dysfunction in Diabetic Patients. Sex Med Rev. 2021; 9: 619–27.
16. Liao C-H, Lee K-H, Chung S-D, Chen K-C, Praveen Rajneesh C, Chen B-H, et al. Intracavernous Injection of Platelet-Rich Plasma Therapy Enhances Erectile Function and Decreases the Mortality Rate in Streptozotocin-Induced Diabetic Rats. International journal of molecular sciences. 2022; 23: 3017.
17. Ding X-G, Li S-W, Zheng X-M, Hu L-Q, Hu W-L, Luo Y. The effect of platelet-rich plasma on cavernous nerve regeneration in a rat model. Asian journal of andrology. 2009; 11: 215–21.
18. Vardi Y, Appel B, Jacob G, Massarwi O, Gruenwald I. Can low-intensity extracorporeal shockwave therapy improve erectile function? A 6-month follow-up pilot study in patients with organic erectile dysfunction. Eur Urol. 2010; 58: 243–8.
19. Bella AJ, Lin G, Tantiwongse K, Garcia M, Lin CS, Brant W, et al. Brain–derived neurotrophic factor (BDNF) acts primarily via the JAK/STAT pathway to promote neurite growth in the major pelvic ganglion of the rat: Part I. The journal of sexual medicine. 2006; 3: 815–20.
20. Huang Y-C, Wu C-T, Chen M-F, Kuo Y-H, Li J-M, Shi C-S. Intracavernous Injection of Autologous Platelet-Rich Plasma Ameliorates Hyperlipidemia-Associated Erectile Dysfunction in a Rat Model. Sexual Medicine. 2021; 9: 100317.
21. Hafez ES, Hafez SD. Erectile dysfunction: anatomical parameters, etiology, diagnosis, and therapy. Arch Androl. 2005; 51: 15–31.
22. Seftel AD. Erectile dysfunction in the elderly: epidemiology, etiology and approaches to treatment. J Urol. 2003; 169: 1999–2007.
23. Miner M, Billups KL. Erectile Dysfunction and Dyslipidemia: Relevance and Role of Phosphodiesterase Type-5 Inhibitors and Statins. The Journal of Sexual Medicine. 2008; 5: 1066–78.
24. Frey A, Sønksen J, Fode M. Low-intensity extracorporeal shockwave

therapy in the treatment of postprostatectomy erectile dysfunction: a pilot study. Scand J Urol. 2016; 50: 123–7.

25. Akande TO, Akinwunmi OM, Adebayo SA, Akinyinka AO, Shittu OB. Efficacy and safety of low-intensity extracorporeal shockwave therapy for treatment of vascular erectile dysfunction in nigerian men: Report of a study in Ibadan, South-West Nigeria. Ann Ib Postgrad Med. 2021; 19: 8–14.

26. Ladegaard PBJ, Mortensen J, Skov-Jeppesen SM, Lund L. Erectile Dysfunction A Prospective Randomized Placebo-Controlled Study Evaluating the Effect of Low-Intensity Extracorporeal Shockwave Therapy (LI-ESWT) in Men With Erectile Dysfunction Following Radical Prostatectomy. Sex Med. 2021; 9: 100338.

27. Fojecki GL, Tiessen S, Osther PJS. Effect of Low-Energy Linear Shockwave Therapy on Erectile Dysfunction—A Double-Blinded, Sham-Controlled, Randomized Clinical Trial. The Journal of Sexual Medicine. 2017; 14: 106–12.

28. Banno JJ, Kinnick TR, Roy L, Perito P, Antonini G, Banno D. 146 The Efficacy of Platelet-Rich Plasma (PRP) as a Supplemental Therapy for the Treatment of Erectile Dysfunction (ED): Initial Outcomes. The Journal of Sexual Medicine. 2017; 14: e59–e60.

29. Chen KC, Minor TX, Rahman NU, Ho HC, Nunes L, Lue TF. The additive erectile recovery effect of brain–derived neurotrophic factor combined with vascular endothelial growth factor in a rat model of neurogenic impotence. BJU international. 2005; 95: 1077–80.

30. Poulios E, Mykoniatis I, Pyrgidis N, Zilotis F, Kapoteli P, Kotsiris D, et al. Platelet-Rich Plasma (PRP) Improves Erectile Function: A Double-Blind, Randomized, Placebo-Controlled Clinical Trial. The Journal of Sexual Medicine. 2021; 18: 926–35.

31. Huang Y-C, Wu C-T, Chen M-F, Kuo Y-H, Li J-M, Shi C-S. Intracavernous Injection of Autologous Platelet-Rich Plasma Ameliorates Hyperlipidemia-Associated Erectile Dysfunction in a Rat Model. Sexual medicine. 2021; 9: 100317.

32. Geyik S. A single-centre result of two courses of low-intensity shockwave therapy (Li-SWT) in erectile dysfunction. Andrologia. 2022; 54: e14324.

33. Pang K, Pan D, Xu H, Ma Y, Wang J, Xu P, et al. Advances in physical diagnosis and treatment of male erectile dysfunction. Front Physiol. 2022; 13: 1096741.

Литература

1. Taş T, Çakıroğlu B, Arda E, Onuk Ö, Nuhoğlu B. Early Clinical Results of the Tolerability, Safety, and Efficacy of Autologous Platelet-Rich Plasma Administration in Erectile Dysfunction. Sex Med. 2021; 9: 100313.

2. Vance G, Zeigler-Hill V, Shackelford TK. Erectile Dysfunction and Sexual Coercion: The Role of Sperm Competition Risk. Archives of Sexual Behavior. 2022; 51 (6): 2781–90.

3. Trebatický B, Žitňanová I, Dvořáková M, Országhová Z, Paduchová Z, Ďuračková Z, et al. Role of oxidative stress, adiponectin and endoglin in the pathophysiology of erectile dysfunction in diabetic and non-diabetic men. Physiol Res. 2019; 68: 623–31.

4. Ayta I, McKinlay J, Krane R. The likely worldwide increase in erectile dysfunction between 1995 and 2025 and some possible policy consequences. BJU international. 1999; 84: 50–56.

5. Colson MH, Cuzin B, Faix A, Grellet L, Huyghes E. Current epidemiology of erectile dysfunction, an update. Sexologies, 2018; 27: e7–e13.

6. Geyik S. Comparison of the efficacy of low-intensity shock wave therapy and its combination with platelet-rich plasma in patients with erectile dysfunction. Andrologia. 2021; 53: e14197.

7. Lei H, Liu J, Li H, Wang L, Xu Y, Tian W, et al. Low-Intensity Shock Wave Therapy and Its Application to Erectile Dysfunction. wjmh, 2013; 31: 208–14.

8. Liu J, Zhou F, Li G-Y, Wang L, Li H-X, Bai G-Y, et al. Evaluation of the Effect of Different Doses of Low Energy Shock Wave Therapy on the Erectile Function of Streptozotocin (STZ)-Induced Diabetic Rats. International Journal of Molecular Sciences. 2013; 14: 10661–73.

9. Sun D, Junger WG, Yuan C, Zhang W, Bao Y, Qin D, et al. Shockwaves Induce Osteogenic Differentiation of Human Mesenchymal Stem Cells Through ATP Release and Activation of P2X7 Receptors. Stem Cells; 2013; 31: 1170–80.

10. Mijiritsky E, Assaf HD, Peleg O, Shacham M, Cerroni L, Mangani L. Use of PRP, PRF and CGF in Periodontal Regeneration and Facial Rejuvenation-A Narrative Review. Biology. 2021; 10: 317.

11. Bos-Mikich A, de Oliveira R, Frantz N. Platelet-rich plasma therapy and reproductive medicine. Journal of Assisted Reproduction and Genetics. 2018; 35: 753–6.

12. Mark KP, Arenella K, Girard A, Herbenick D, Fu J, Coleman E. Erectile dysfunction prevalence in the United States: report from the 2021 National Survey of Sexual Wellbeing. J Sex Med. 2024; 21: 296–303.

13. Mulhall JP, Goldstein I, Bushmakin AG, Cappelleri JC, Hvidsten K. Validation of the Erection Hardness Score. The Journal of Sexual Medicine. 2007; 4: 1626–34.

14. Sokolakis I, Dimitriadis F, Teo P, Hatzichristodoulou G, Hatzichristou D, Giuliano F. The Basic Science Behind Low-Intensity Extracorporeal Shockwave Therapy for Erectile Dysfunction: A Systematic Scoping Review of Pre-Clinical Studies. J Sex Med. 2019; 16: 168–94.

15. Spivak L, Shultz T, Appel B, Verze P, Yagudaev D, Vinarov A. Low-Intensity Extracorporeal Shockwave Therapy for Erectile Dysfunction in Diabetic Patients. Sex Med Rev. 2021; 9: 619–27.

16. Liao C-H, Lee K-H, Chung S-D, Chen K-C, Praveen Rajneesh C, Chen B-H, et al. Intracavernous Injection of Platelet-Rich Plasma Therapy Enhances Erectile Function and Decreases the Mortality Rate in Streptozotocin-Induced Diabetic Rats. International journal of molecular sciences. 2022; 23: 3017.

17. Ding X-G, Li S-W, Zheng X-M, Hu L-Q, Hu W-L, Luo Y. The effect of platelet-rich plasma on cavernous nerve regeneration in a rat model. Asian journal of andrology. 2009; 11: 215–21.

18. Vardi Y, Appel B, Jacob G, Massarwi O, Gruenwald I. Can low-intensity extracorporeal shockwave therapy improve erectile function? A 6-month follow-up pilot study in patients with organic erectile dysfunction. Eur Urol. 2010; 58: 243–8.

19. Bella AJ, Lin G, Tantiwongse K, Garcia M, Lin CS, Brant W, et al. Brain–derived neurotrophic factor (BDNF) acts primarily via the JAK/STAT pathway to promote neurite growth in the major pelvic ganglion of the rat: Part I. The journal of sexual medicine. 2006; 3: 815–20.

20. Huang Y-C, Wu C-T, Chen M-F, Kuo Y-H, Li J-M, Shi C-S. Intracavernous Injection of Autologous Platelet-Rich Plasma Ameliorates Hyperlipidemia-Associated Erectile Dysfunction in a Rat Model. Sexual Medicine. 2021; 9: 100317.

21. Hafez ES, Hafez SD. Erectile dysfunction: anatomical parameters, etiology, diagnosis, and therapy. Arch Androl. 2005; 51: 15–31.

22. Seftel AD. Erectile dysfunction in the elderly: epidemiology, etiology and approaches to treatment. J Urol. 2003; 169: 1999–2007.

23. Miner M, Billups KL. Erectile Dysfunction and Dyslipidemia: Relevance and Role of Phosphodiesterase Type-5 Inhibitors and Statins. The Journal of Sexual Medicine. 2008; 5: 1066–78.

24. Frey A, Sønksen J, Fode M. Low-intensity extracorporeal shockwave therapy in the treatment of postprostatectomy erectile dysfunction: a pilot study. Scand J Urol. 2016; 50: 123–7.

25. Akande TO, Akinwunmi OM, Adebayo SA, Akinyinka AO, Shittu OB. Efficacy and safety of low-intensity extracorporeal shockwave therapy for treatment of vascular erectile dysfunction in nigerian men: Report of a study in Ibadan, South-West Nigeria. Ann Ib Postgrad Med. 2021; 19: 8–14.

26. Ladegaard PBJ, Mortensen J, Skov-Jeppesen SM, Lund L. Erectile Dysfunction A Prospective Randomized Placebo-Controlled Study Evaluating the Effect of Low-Intensity Extracorporeal Shockwave Therapy (LI-ESWT) in Men With Erectile Dysfunction Following Radical Prostatectomy. Sex Med. 2021; 9: 100338.

27. Fojecki GL, Tiessen S, Osther PJS. Effect of Low-Energy Linear Shockwave Therapy on Erectile Dysfunction—A Double-Blinded, Sham-Controlled, Randomized Clinical Trial. The Journal of Sexual Medicine. 2017; 14: 106–12.

28. Banno JJ, Kinnick TR, Roy L, Perito P, Antonini G, Banno D. 146 The Efficacy of Platelet-Rich Plasma (PRP) as a Supplemental Therapy for the Treatment of Erectile Dysfunction (ED): Initial Outcomes. The Journal of Sexual Medicine. 2017; 14: e59–e60.

29. Chen KC, Minor TX, Rahman NU, Ho HC, Nunes L, Lue TF. The additive erectile recovery effect of brain–derived neurotrophic factor combined with vascular endothelial growth factor in a rat model of neurogenic impotence. BJU international. 2005; 95: 1077–80.

30. Poulios E, Mykoniatis I, Pyrgidis N, Zilotis F, Kapoteli P, Kotsiris D, et al. Platelet-Rich Plasma (PRP) Improves Erectile Function: A Double-Blind, Randomized, Placebo-Controlled Clinical Trial. The Journal of Sexual Medicine. 2021; 18: 926–35.

31. Huang Y-C, Wu C-T, Chen M-F, Kuo Y-H, Li J-M, Shi C-S. Intracavernous Injection of Autologous Platelet-Rich Plasma Ameliorates Hyperlipidemia-Associated Erectile Dysfunction in a Rat Model. Sexual medicine. 2021; 9: 100317.

32. Geyik S. A single-centre result of two courses of low-intensity shockwave therapy (Li-SWT) in erectile dysfunction. Andrologia. 2022; 54: e14324.

33. Pang K, Pan D, Xu H, Ma Y, Wang J, Xu P, et al. Advances in physical diagnosis and treatment of male erectile dysfunction. Front Physiol. 2022; 13: 1096741.

DYNAMIC CHANGES OF INFLAMMATORY MARKERS IN THE EARLY STAGES OF CHRONIC KIDNEY DISEASE IN PATIENTS WITH TYPE 1 DIABETES MELLITUS

Osikov MV[1,2], Efros LA[1,2], Zhuravleva LYu[1,2] ✉, Fedosov AA[3]

[1] South Ural State Medical University, Chelyabinsk, Russia

[2] Chelyabinsk Regional Clinical Hospital, Chelyabinsk, Russia

[3] Peoples' Friendship University of Russia, Moscow, Russia

Diabetes mellitus (DM) is one of the major factors contributing to the development and aggravation of chronic kidney disease (CKD). The accurate and convenient markers for early detection, estimation of progression, and adequate control of CKD therapy in individuals with DM are limited to glomerular filtration rate (GFR) and albuminuria. Given the role of chronic inflammation in the pathogenesis of DM and CKD, the study aimed to assess indicators of inflammation and the correlation of those with GFR in patients with type 1 DM (T1D) and early stage CKD. The study involved healthy individuals ($n = 14$), patients with T1D showing no signs of CKD ($n = 30$), as well as patients with T1D and stage 1 CKD ($n = 60$), stage 2 CKD ($n = 38$), and stage 3 CKD ($n = 31$). GFR was calculated using the formula CKD-EPI (eGFR); serum levels of IL1β and TNFα, C-reactive protein (CRP), and ceruloplasmin (CP) were determined by enzyme immunoassay; the neutrophil-to-lymphocyte index and the leukocyte intoxication index (LII) were calculated. It has been found that serum concentrations of IL1β, TNFα, CRP, and CP are elevated; LII and the neutrophil-to-lymphocyte index are increased. The inflammation and acute phase response severity progresses and reaches its maximum in stage 3b CKD, when the serum concentration of IL1β is increased 2.4-fold ($p = 0.042$), TNFα concentration by 34% ($p = 0.005$), CRP concentration 33-fold ($p < 0.000$), CP concentration by 73% ($p = 0.008$), LII 8.4-fold ($p < 0.000$), neutrophil-to-lymphocyte index 5-fold ($p = 0.013$). The integral kidney function indicator, eGFR, decreases with increasing serum levels of the above indicators. Thus, IL1β, TNFα, CRP, CP, LII, and the neutrophil-to-lymphocyte index can be considered as affordable and informative indicators for estimation of inflammation, the levels of which increase with progression of early stage CKD in patients with T1D.

Keywords: type I diabetes mellitus, chronic kidney disease, progression, C-reactive protein, ceruloplasmin, IL1β, TNFα, neutrophils

ДИНАМИКА МАРКЕРОВ ВОСПАЛЕНИЯ НА НАЧАЛЬНЫХ СТАДИЯХ ХРОНИЧЕСКОЙ БОЛЕЗНИ ПОЧЕК ПРИ САХАРНОМ ДИАБЕТЕ 1-ГО ТИПА

М. В. Осиков[1,2], Л. А. Эфрос[1,2], Л. Ю. Журавлева[1,2] ✉, А. А. Федосов[3]

[1] Южно-Уральский государственный медицинский университет Министерства здравоохранения Российской Федерации, Челябинск, Россия

[2] Челябинская областная клиническая больница, Челябинск, Россия

[3] Российский университет дружбы народов имени Патриса Лумумбы, Москва, Россия

Сахарный диабет (СД) — один из основных факторов, способствующих развитию и усугублению хронической болезни почек (ХБП). Точные и удобные маркеры для раннего выявления, оценки прогрессирования и надлежащего контроля терапии ХБП у лиц с СД ограничены показателями скорости клубочковой фильтрации (СКФ) и альбуминурией. В связи с ролью хронического воспаления в патогенезе СД и ХБП целью работы было изучить показатели воспалительного процесса и их взаимосвязь с СКФ у больных СД 1-го типа (СД1) при ранних стадиях ХБП. В исследовании участвовали здоровые люди ($n = 14$), больные СД1 без признаков ХБП ($n = 30$), а также больные СД1 с 1-й стадией ХБП ($n = 60$), 2-й стадией ХБП ($n = 38$) и 3-й стадией ХБП ($n = 31$). СКФ рассчитывали по формуле CKD-EPI (рСКФ), в сыворотке иммуноферментным методом определяли концентрацию IL1β и TNFα, С-реактивного белка (С-РБ), а также концентрацию церулоплазмина (ЦП), рассчитывали индекс нейтрофилы/лимфоциты, лейкоцитарный индекс интоксикации (ЛИИ). Установлено, что в сыворотке повышается концентрация IL1β, TNFα, С-РБ и ЦП, увеличивается ЛИИ, индекс нейтрофилы/лимфоциты. Выраженность воспалительного процесса и острофазового ответа прогрессирует и максимальна при 3б стадии ХБП, когда концентрация в сыворотке IL1β увеличивается в 2,4 раза ($p = 0,042$), TNFα — на 34% ($p = 0,005$), С-РБ — в 33 раза ($p < 0,000$), ЦП — на 73% ($p = 0,008$), ЛИИ — в 8,4 раза ($p < 0,000$), индекс нейтрофилы/лимфоциты — в 5 раз ($p = 0,013$). Интегральный показатель функции почек рСКФ снижается по мере увеличения содержания в сыворотке вышеперечисленных показателей. Таким образом IL1β, TNFα, С-РБ, ЦП, ЛИИ и индекс нейтрофилы/лимфоциты можно считать доступными и информативными показателями оценки воспалительного процесса, возрастающими по мере прогрессирования начальных стадий ХБП у больных СД1.

Ключевые слова: сахарный диабет 1-го типа, хроническая болезнь почек, прогрессирование, С-реактивный белок, церулоплазмин, IL1β, TNFα, нейтрофилы

Diabetes mellitus (DM) is one of the main causes of premature death from chronic non-communicable disorders; it accounts for about 1.5 million deaths annually. In 2023, the total number of patients with DM in Russia was 4.9 million or 3.31% of the population, among them 277.1 thousand had type 1 DM (T1D). Despite advances in diagnosis and treatment, the increase in the prevalence of T1D by about 2–3% a year is observed; in 2022, the prevalence was 191 cases per 100,000 population [1].

The majority of patients with T1D are in their prime work years (30–39 years); the average age of death from T1D is 53.2 years. Diabetic nephropathy is a common microvascular complication of DM, it occurs on average in 40% of affected individuals, and the rate of diabetic nephropathy associated with T1D is 50% after 10 years and 75% after 20 years [2]. According to the United Nations, chronic kidney disease (CKD) requires special attention and represents one of the indicators of progress in achieving global goals of reducing premature mortality from non-communicable diseases by 2030 [1, 3]. The importance of risk factor detection aimed at CKD progression prevention is emphasized considering the growing influence of CKD on public health [4]. It has been proven that targeted interventions in early-stage CKD associated with T1D effectively prevent kidney failure progression and improve treatment outcomes in patients; regular CKD screening represents the basic principle of the DM patient management [5]. To date, pathogenesis of CKD associated with DM is poorly understood, it includes such mechanisms, as endothelial dysfunction, chronic inflammation and thrombosis, mitochondrial dysfunction and oxidative stress, histone hypermethylation, DNA methylation, atherogenic dyslipidemia and arterial hypertension, etc. Understanding synergetic cellular molecular mechanisms underlying DM and CKD is crucial for assessment of the DM-associated CKD progression and development of effective diagnostic and therapeutic approaches [3, 6].

Inflammation is a standard disease process underlying many disorders and syndromes, including DM and CKD. Special attention is paid to low-grade chronic systemic inflammation and its markers: pro-inflammatory cytokines (interleukin 1β (IL1β) and tumor necrosis factor α (TNFα), IL6, etc.), acute phase reactant (highly sensitive C-reactive protein (CRP), serum amyloid A, ceruloplasmin (CP), etc.) [7, 8]. Chronic inflammation is considered as a key factor of pathogenesis of macrovascular and microvascular DM complications, including CKD [9]. At the same time, in clinical settings, calculation of the white blood cell differential (increased immature neutrophils) and its derivatives (leukocyte intoxication index (LII), neutrophil-to-lymphocyte index) remains the most affordable method to assess severity of inflammatory and acute phase response, which is very informative in terms of predicting the long-term survival, mortality, as well as ranking the factors contributing to cardiovascular disorders [10]. Most information about the relationship between inflammatory markers in blood and diabetic nephropathy worsening was acquired from patients suffering from T2D, which was due to its high prevalence.

The study aimed to assess indicators of inflammation and their correlation with the glomerular filtration rate in patients with T1D and early stage chronic kidney disease.

METHODS

The study was conducted at the Chelyabinsk Regional Clinical Hospital. The study involved females aged 18–54, males aged 18–60. Inclusion criteria: 1) having T1D for more than 6 months in accordance with the national clinical guidelines [11]; 2) informed consent to participation in the study. Exclusion criteria: 1) age over 60; 2) eGFR $\leq$ 29 mL/min/1.73 m^2; 2) T2D or other endocrine disorder; 3) severe concomitant diseases of the liver, lung, tuberculosis, rheumatic diseases, autoimmune kidney diseases, postmenopausal osteoporosis, cancer; 4) taking glucocorticoids, cytostatics, vitamin D products, phosphate binders; 5) patients with inflammatory diseases affecting kidneys and other organs and systems. Group 1 is represented by clinically healthy individuals matched by age and sex to the index group (n =14): 42.9% males, 57.1% females, average age 30.6 ± 4.2 years, body mass index, systolic and diastolic blood pressure, lipid profile within normal. Group 2 includes patients with T1D showing no signs of CKD (n = 30). Group 3 is represented by patients with T1D showing signs of CKD (n = 129), including stage 1 CKD (group 3.1; n = 60), stage 2 CKD (group 3.2; n = 38), stage 3a CKD (group 3.3; n = 21), stage 3b CKD (group 3.3; n = 10). CKD was staged in accordance with the national clinical guidelines [12]. At admission, the patients had compensated (n = 12; 7.5%), subcompensated, and decompensated T1D; compensation was achieved against the background of therapy in hospital settings; the inflammatory markers were collected before discharge (n = 147; 92.5%). Clinical characteristics of the groups of patients with T1D having and not having CKD are provided in Table 1.

Analysis of the results showed that the group of patients with CKD showed significantly lower eGFR compared to patients with no CKD (p = 0.037). In patients with CKD, the diabetes duration was 13 years, while in the group of patients with no CKD this indicator was significantly lower (p = 0.000). We revealed significant differences in the average glycated hemoglobin levels in patients having and not having CKD (9.8% and 8.1%, respectively). The average systolic and diastolic blood pressure was higher in the group of patients with CKD (p = 0.000); higher total cholesterol levels were reported for the group of patients with CKD (p = 0.035).

Analysis of the results showed that the DM duration was longer in patients with stage 1 CKD compared to patients with no CKD (p < 0.001). The average systolic blood pressure turned out to be significantly higher in the group of patients with stage 1 CKD (p = 0.001). Patients with T1D and stage 2 CKD had lower eGFR compared to patients with no CKD (p = 0.000). The diabetes duration was longer in patients with stage 2 CKD (p = 0.000). Patients with stage 2 CKD had significantly higher average glycated hemoglobin (p = 0.012) and average total cholesterol (p = 0.007) levels. The average systolic and diastolic blood pressure in the group with stage 2 CKD turned out to be significantly higher compared to the group with no CKD (p = 0.001 and p < 0.001). Significant differences were revealed when comparing the groups of patients with stage 3 CKD and no CKD. The average age was higher in the group of patients with stage 3 CKD (p = 0.015). Longer diabetes duration was reported for patients with stage 3 CKD (p = 0.001). The average systolic and diastolic blood pressure turned out to be higher in the group of patients with stage 3 CKD (p < 0.001), the glycated hemoglobin levels were higher in patients with stage 3 CKD (p = 0.010). The results of comparative analysis of the group of patients with stage 2 CKD and the group of patients with stage 3 CKD showed a significant decrease in glomerular filtration rate (p < 0.001).

Albuminuria indicators, as CKD markers, are provided in Table 2.

It was found that patients with stage 1 CKD more often had stage A1 albuminuria (p = 0.031), while patients with stage 3a and 3b stage CKD more often had stage A3 albuminuria (p = 0.022).

Table 1. Clinical characteristics and comparative analysis of the groups of patients with T1D having and not having CKD (*n* = 159)

Indicator		Group with CKD (*n* = 129)	Group without CKD (*n* = 30)	*p*
Sex, abs. (%)	Males	47 (36.4)	12 (40.0)	0.834
	Females	82 (63.6)	18 (60.0)	
Age, years, Me [Q_1; Q_3]		32.0 [25.0; 40.0]	26.0 [22.0; 30.0]	0.001*
Body mass index, kg/m², Me [Q_1; Q_3]		23.7 [21.0; 26.0]	22.7 [20.0; 24.3]	0.163
Systolic blood pressure, mm Hg, Me [Q_1; Q_3]		150.0 [110.0; 160.0]	110.0 [100.0; 110.0]	0.000*
Diastolic blood pressure, mm Hg, Me [Q_1; Q_3]		90.0 [70.0; 90.0]	70.0 [60.0; 70.0]	0.000*
Glomerular filtration rate, mL/min/1.73 m², Me [Q_1; Q_3]		87 [62.0; 111.0]	121.0 [96.0; 124.0]	0.000*
Diabetes duration, years, Me [Q_1; Q_3]		13 [8.0; 20.0]	4.0 [2.0; 8.0]	0.000*
Glycated hemoglobin, %, Me [Q_1; Q_3]		9.8 [8.5; 11.6]	8.1 [7.6; 8.8]	0.000*
Total cholesterol, mmol/L, Me [Q_1; Q_3]		5.2 [4.2-6.3]	4.5 [4.1; 5.5]	0.035*
Triglycerides, mmol/L, Me [Q_1; Q_3]		1.3 [0.8; 1.8]	1.1 [0.8; 1.6]	0.388
LDL cholesterol, mmol/L, Me [Q_1; Q_3]		3.0 [2.2; 4.0]	2.9 [2.1; 3.5]	0.34
LDL cholesterol, mmol/L, Me [Q_1; Q_3]		0.58 [0.35; 0.76]	0.57 [0.40; 0.69]	0.631

Note: * — significant intergroup differences (*p* < 0.05). Categorical indicators were compared using the Pearson's chi-squared test (χ^2), Mann–Whitney *U* test was used in other cases.

To calculate GFR using the formula CKD-EPI (eGFR), we determined serum creatinine concentrations by the kinetic colorimetric method using the Cobas Integra 400 analyzer (Switzerland) [2]. Total white blood cell counts were determined using the CoulterLH 500 hematology analyzer (BeckmanCoulter; USA), while the white blood cell differential was determined by microscopy of the Romanowsky–Giemsa-stained blood smears involving enumeration of 200 cells. The leukocyte intoxication index (LII) was calculated using the following formula:

$$\frac{4 \times \text{myelocytes} + 3 \times \text{immature} + 2 \times \text{band} + \text{segmented neutrophils} \times (\text{plasma cells} + 1)}{\text{lymphocytes} + \text{monocytes} \times (\text{eosinophils} + 1)}$$ [13].

Moreover, we determined the ratio of the quantities of all neutrophil and lymphocyte populations in blood (neutrophils/lymphocytes). Serum IL1β and TNFα concentrations were determined using the Personal LAB automated ELISA testing platform (Adaltis Italia; Italy) and the Vector-Best test systems (Novosibirsk); the results were expressed in pg/mL. Serum concentrations of the highly sensitive CRP were determined using the ChemWell 2910 automated ELISA testing system (Awareness Technology; USA) and the Vector-Best test system (Novosibirsk); the results were expressed in IU/L. Serum concentrations of ceruloplasmin (CP) were determined using the SF-56 spectrophotometer (LOMO-Spectrum; Russia) by the modified method by Revin based on p-phenylenediamine

oxidation; the results were expressed in mg/L [14]. The results obtained were processed using the IBM SPSS Statistics v. 23 software package (SPSS: An IBM Company; USA). The quantitative indicator distribution in the group of patients with stage 1 CKD was tested for normality using the Kolmogorov–Smirnov test, while in the groups with stage 2, 3a and 3b CKD, as well as in healthy individuals and patients with no CKD, the Shapiro–Wilk test was used for this purpose. The data are presented as Me (Q_1; Q_3), where Me is the median, Q_1 and Q_3 are the lower (25) and upper (75) quartiles, respectively. Verification of statistical hypotheses in the groups was performed using the Mann–Whitney *U* test. Spearman's rank correlation coefficient (R) was used to reveal correlations between the studied parameters, and the Chaddock scale was used to estimate the correlation strength.

RESULTS

The eGFR values for the studied groups of patients are provided in Table 3. It has been found that eGFR significantly increases in the group of patients with T1D showing no signs of CKD (group 2) compared to the group of healthy individuals and naturally decreases in the group of patients with CKD (group 3). Furthermore, the increase in group 2 is 17% based on the median relative to the values of the group of healthy individuals, while there is a decrease by 10% in group 3.1 (stage 1 CKD), by 28% in group 3.2 (stage 1 CKD), by 46% in group 3.3 (stage

Table 2. Albuminuria indicators in patients with T1D and CKD, abs. (%)

Albuminuria stage	Group 3				*p*
	Stage 1 CKD (3.1)	Stage 2 CKD (3.2)	Stage 3a CKD (3.3)	Stage 3b CKD (3.4)	
A1	24 (40.0)	13 (34.2)	6 (28.6)	0	0.031*
A2	17 (28.3)	12 (31.6)	4 (19.0)	4 (40.0)	0.649
A3	19 (31.7)	13 (34.2)	11 (52.4)	6 (60.0)	0.022*

Note: * — significant intergroup differences (*p* < 0.05). Categorical indicators were compared using the Pearson's chi-squared test (χ^2).

Table 3. eGFR (mL/min/1.73 m²) in patients with T1D and CKD, Me [Q_1; Q_3]

Healthy (group 1)	No CKD (group 2)	Group 3				p-values with p < 0.05
		Stage 1 CKD (group 3.1)	Stage 2 CKD (group 3.2)	Stage 3a CKD (group 3.3)	Stage 3b CKD (group 3.4)	
105.000 [91.000; 118.000]	123.000 [120.000; 134.000]	94.000 [92.000; 126.000]	76.000 [67.000; 78.000]	56.000 [50.000; 58.000]	37.000 [31.000; 40.000]	$p_{1–2} < 0.001$ $p_{1–3.1} < 0.001$ $p_{1–3.2} < 0.001$ $p_{1–3.3} < 0.001$ $p_{1–3.4} < 0.001$ $p_{2–3.1} = 0.016$ $p_{2–3.2} < 0.001$ $p_{2–3.3} < 0.001$ $p_{2–3.4} < 0.001$ $p_{3.1–3.2} < 0.001$ $p_{3.1–3.3} < 0.001$ $p_{3.1–3.4} < 0.001$ $p_{3.2–3.3} < 0.001$ $p_{3.2–3.4} < 0.001$ $p_{3.3–3.4} < 0.001$

Note: Mann–Whitney U test was used to compare the values.

3a CKD), by 65% in group 3.4 (stage 3b CKD). Moreover, eGFR is significantly decreased in groups 3.1, 3.2, 3.3, 3.4 compared to group 2. The eGFR values of the groups 3.1, 3.2, 3.3, and 3.4 match the criteria of stage 1, stage 2, stage 3a, stage 3b CKD, respectively [12]. The eGFR value of patients with stage 2 CKD is significantly different from the values of the group of patients with stage 1 CKD, the value of patients with stage 3a CKD is significantly different from the values of the group of patients with stage 1 and 2 CKD, the value of patients with stage 3b CKD is significantly different from the values of the groups of patients with stage 1, 2, and 3a CKD.

The results of assessing inflammation severity in patients with T1D and CKD are provided in Table 4. First of all, the changes in serum concentrations of pro-inflammatory cytokines should be noted. Thus, the IL1β concentration in the group of patients with T1D showing no signs of CKD significantly increased (by 31% based on the median) relative to the values of the group of healthy individuals; in the group of patients with T1D and CKD, the IL1β concentration progressively increased from stage 1 to stage 3b: by 40% based on the median relative to the group of healthy individuals in group 3.1, by 91% in group 3.2, 1.8-fold in group 3.3, and 2.4-fold in group 3.4. We revealed significant changes in serum concentrations of IL1β in patients with stage 2, 3a, and 3b CKD compared to the group of patients with T1D showing no signs of CKD and the group of patients with stage 1 CKD, as well as in individuals with stage 3a CKD compared to those with stage 2 CKD, stage 3b CKD compared to those with stage 2 and 3a CKD. Serum concentrations of TNFα were not significantly different from those of the group of healthy individuals, patients with T1D showing no signs of CKD, and patients with T1D and stage 1 and 2 CKD; in patients with T1D and stage 3a and 3b CKD, these increased by 34% based on the median. We revealed changes in serum concentrations of TNFα in patients with stage 2, 3a, and 3b CKD compared to patients with T1D showing no signs of CKD and the group of patients with stage 1 CKD, as well as in patients with stage 3b CKD compared to those with stage 2 CKD.

The severity of the acute phase response associated with T1D, including combined with CKD, was associated with the changes in the content of white blood cell populations in peripheral blood, which, in particular, was reflected in the LII and neutrophil-to-lymphocyte index changes. Thus, LII significantly increased in the groups of patients with T1D and stage 2, 3a, and 3b CKD (2.3-fold, 7.8-fold, and 8.4-fold based on the median, respectively) relative to the values of the group of healthy individuals. Moreover, LII significantly increased in the groups

of patients with T1D and stage 2, 3a, and 3b CKD relative to patients with T1D showing no signs of CKD and stage 1 CKD. In patients with T1D and stage 3a and 3b CKD, LII increased relative to the group with stage 2 CKD. More prominent changes in the population spectrum of white blood cells were reported when assessing the neutrophil-to-lymphocyte index. In patients with T1D and CKD, the index significantly increased relative to the group of healthy individuals: by 22% based on the median in group 3.1, by 81% in group 3.2, 2.3-fold in group 3.3, 5-fold in group 3.4. We noted a significant increase in the neutrophil-to-lymphocyte index in patients with T1D and stage 1, 2, 3a, and 3b CKD relative to the group of patients with T1D showing no signs of CKD, as well as in patients with T1D and stage 3a and 3b CKD relative to the group of patients with T1D and stage 1 and 2 CKD; in patients with T1D and 3b stage relative to patients with 3a stage CKD. We noted the increase in the IL1β and TNFα levels with CKD progression in patients with T1D, but within normal range, which requires continuous monitoring of these indicators.

In the next phase we assessed serum concentrations of the acute phase reactants, CRP and CP (Table 5). Elevated CRP concentrations were found in patients with T1D showing no signs of CKD, as well as in patients with T1D and stage 1, 2, 3a, 3b CKD relative to the group of healthy individuals: 2.7-fold, 3.5-fold, 5.1-fold, 9.9-fold, 33-fold based on the median, respectively. In all groups of patients showing signs of CKD, serum CRP levels were increased relative to the group of patients with T1D showing no signs of CKD; in the groups with T1D and stage 3a and 3b CKD relative to those with T1D and stage 1, 2 CKD, in the group with T1D and stage 3b CKD relative to the group with T1D and stage 3a CKD. We revealed elevated serum concentrations of CP in patients with T1D showing no signs of CKD, as well as in patients with T1D and stage 1, 2, 3a, 3b CKD relative to the group of healthy individuals: by 31%, 16%, 24%, 41%, and 73% based on the median, respectively. Serum CP levels were increased in the groups with T1D and stage 3a and 3b CKD relative to the group of patients with T1D showing no signs of CKD, as well as with T1D and stage 1 CKD; in the group with T1D and stage 3a CKD relative to the group with T1D and stage 2 CKD; in the group with T1D and stage 3b CKD relative to the group with T1D and stage 3a CKD. The increase in CP levels with increasing CKD stage was reported, due to which the dynamic monitoring of this marker is necessary.

We performed analysis of the correlation between eGRF being one of the key kidney function parameters essential for

Table 4. Inflammatory markers in patients with T1D and CKD, Me [Q_1; Q_3]

Indicators	Healthy (group 1)	No CKD (group 2)	Group 3				p-values with p < 0.05
			Stage 1 CKD (3.1)	Stage 2 CKD (3.2)	Stage 3a CKD (3.3)	Stage 3b CKD (3.4)	
IL1β, pg/mL	1.724 [1.553; 2.931]	2.226 [1.410; 2.941]	2.405 [1.930; 3.600]	3.276 [2.590; 6.650]	4.879 [2.241; 7.379]	5.824 [4.793; 8.031]	p_{1-2} = 0.021 $p_{1-3.1}$ = 0.009 $p_{1-3.2}$ = 0.003 $p_{1-3.3}$ = 0.003 $p_{1-3.4}$ = 0.029 $p_{2-3.2}$ = 0.006 $p_{2-3.3}$ = 0.046 $p_{2-3.4}$ = 0.004 $p_{3.1-3.2}$ = 0.044 $p_{3.1-3.3}$ = 0.033 $p_{3.1-3.4}$ = 0.042 $p_{3.2-3.3}$ = 0.001 $p_{3.2-3.4}$ = 0.003 $p_{3.3-3.4}$ = 0.301
TNFα, pg/mL	2.264 [1.981; 2.642]	2.170 [1.415; 3.019]	2.264 [1.604; 2.736]	2.443 [2.358; 3.113]	3.019 [2.547; 3.491]	3.019 [2.311; 3.490]	$p_{1-3.3}$ = 0.001 $p_{1-3.4}$ < 0.000 $p_{2-3.2}$ = 0.005 $p_{2-3.3}$ = 0.047 $p_{2-3.4}$ < 0.000 $p_{3.1-3.2}$ = 0.044 $p_{3.1-3.3}$ = 0.003 $p_{3.1-3.4}$ = 0.005 $p_{3.2-3.4}$ = 0.003
LII, AU	0.320 [0.170; 0.690]	0.560 [0.450; 0.750]	0.485 [0.200; 0.800]	1.050 [0.690; 1.350]	2.800 [1.860; 8.700]	3.000 [1.520; 6.400]	$p_{1-3.2}$ =0.004 $p_{1-3.3}$ < 0.000 $p_{1-3.4}$ < 0.000 $p_{2-3.2}$ = 0.016 $p_{2-3.3}$ < 0.000 $p_{2-3.4}$ < 0.000 $p_{3.1-3.2}$ = 0.027 $p_{3.1-3.3}$ = 0.001 $p_{3.1-3.4}$ < 0.000 $p_{3.2-3.3}$ = 0.002 $p_{3.2-3.4}$ = 0.008
Neutrophils/ lymphocytes, AU	1.720 [1.020; 1.930]	1.680 [1.200; 2.100]	2.100 [1.530; 5.700]	3.160 [2.800; 3.900]	5.600 [3.200; 5.700]	10.295 [2.390; 12.680]	$p_{1-3.1}$ = 0.021 $p_{1-3.2}$ < 0.000 $p_{1-3.3}$ < 0.000 $p_{1-3.4}$ < 0.000 $p_{2-3.1}$ = 0.001 $p_{2-3.2}$ < 0.000 $p_{2-3.3}$ = 0.003 $p_{2-3.4}$ = 0.001 $p_{3.1-3.3}$ = 0.004 $p_{3.1-3.4}$ = 0.013 $p_{3.2-3.3}$ = 0.001 $p_{3.2-3.4}$ = 0.002 $p_{3.3-3.4}$ = 0.020

Note: Mann–Whitney *U* test was used to compare the values.

assessment of CKD progression, CKD staging in accordance with the national and international criteria and the signs of inflammation in patients with T1D and early stage CKD (Table 6). The use of the Chaddock scale in stage 1 CKD revealed a moderate correlation with serum concentrations of TNFα, marked correlation with LII and the neutrophil-to-lymphocyte index, very strong correlation with serum concentrations of IL1β, CRP, and CP; all the correlations were negative. In stage 2 CKD, we revealed a marked correlation with serum concentrations of TNFα, strong correlation with LII and the neutrophil-to-lymphocyte index, very strong correlation with serum concentrations of IL1β, CRP, and CP; all the correlations were negative. In stage 3a CKD, we found a strong correlation with LII and serum CP concentrations, very strong correlation with serum concentrations of IL1β, TNFα, CRP and the neutrophil-to-lymphocyte index. In stage 3b CKD, we revealed a strong correlation with serum concentrations of TNFα, CRP, and CP, very strong correlation with serum concentrations of IL1β, LII and the neutrophil-to-lymphocyte index; the correlation was negative.

DISCUSSION

Assessment of eGFR showed that eGFR was increased in the group of patients with T1D showing no signs of CKD (group 2). Elevated eGFR and hyperfiltration associated with T1D (with the maximum values up to 162 mL/min/1.73 m²) found in 10–67% of patients are considered to result from compensatory renal hypertrophy and hyperfunction in response to hyperglycemia, effects of pro-inflammatory cytokines and growth factors, local angiotensin (II), imbalance of vasoactive factors regulating pre- and postglomerular blood flow, alteration of reabsorption of sodium, glucose, and H⁺ in proximal parts of the nephron [15, 16]. Currently, glomerular hyperfiltration is considered as one of the main mechanisms underlying the emergence and progression of diabetic kidney disease (DKD) [16, 17].

Pathogenesis of the signs of inflammation in the form of increased serum concentrations of IL1β, TNFα, CRP, CP, increased LII and the neutrophil-to-lymphocyte index, found by us in patients with T1D and CKD, is multifactorial [18]. The mechanism underlying formation of phlogogenic potential

Table 5. Markers, acute phase reactants, in patients with T1D and CKD, Me [Q_1; Q_3]

Indicators	Healthy (group 1)	No CKD (group 2)	Group 3				p-values with p < 0.05
			Stage 1 CKD (3.1)	Stage 2 CKD (3.2)	Stage 3a CKD (3.3)	Stage 3b CKD (3.4)	
CP, mg/L	172.050 [132.100; 217.000]	225.800 [183.800; 317.000]	200.150 [181.100; 245.000]	214.400 [198.000; 289.300]	242.300 [152.300; 245.000]	297.550 [268.400; 311.000]	$p_{1-2} = 0.014$ $p_{1-3.1} = 0.001$ $p_{1-3.2} = 0.003$ $p_{1-3.3} = 0.004$ $p_{1-3.4} = 0.029$ $p_{2-3.3} = 0.027$ $p_{2-3.4} = 0.001$ $p_{3.1-3.3} = 0.004$ $p_{3.1-3.4} = 0.008$ $p_{3.2-3.3} = 0.004$ $p_{3.2-3.4} = 0.042$ $p_{3.3-3.4} = 0.008$
CRP, IU/L	0.335 [0.280; 1.820]	1.260 [0.140; 2.300]	1.540 [1.000; 3.050]	2.050 [1.450; 3.170]	3.675 [2.800; 4.150]	11.625 [6.010; 15.395]	$p_{1-2} = 0.003$ $p_{1-3.1} = 0.041$ $p_{1-3.2} = 0.020$ $p_{1-3.3} = 0.001$ $p_{1-3.4} < 0.000$ $p_{2-3.1} = 0.021$ $p_{2-3.2} = 0.002$ $p_{2-3.3} = 0.047$ $p_{2-3.4} < 0.000$ $p_{3.1-3.4} < 0.000$ $p_{3.2-3.3} = 0.001$ $p_{3.2-3.4} = 0.001$ $p_{3.3-3.4} = 0.039$

Note: Mann–Whitney U test was used to compare the values.

in DM includes primarily hyperglycemia resulting in protein glycosylation, formation of advanced glycation end products causing tissue damage and immune cell activation, as well as the release of pro-inflammatory cytokines. Secondly, in DM, excess amounts of glucose result in the increased production of reactive oxygen species, oxidative stress, which causes further damage to the kidney cells and provokes inflammation. Thirdly, in diabetic nephropathy, hyperactivation of the renin-angiotensin system is observed that not only contributes to arterial hypertension, but also increases renal inflammation through production of pro-inflammatory cytokines, such as IL6 and TNFα. Finally, local immune response is activated in response to renal cell damage, when lymphocytes, macrophages and other cells enter the kidney tissue, secrete inflammatory mediators, thereby exacerbating kidney damage.

Activation of myeloid lineage in the bone marrow with the increase in proliferation and differentiation of precursor cells, increase in peripheral blood neutrophil (including myelocyte and metamyelocyte) counts occurs in response to the synthesis, secretion, and increase in blood levels of pro-inflammatory mediators, including the reported IL1β, TNFα. We have reported this fact in the form of the increased LII and neutrophil-to-lymphocyte index. Neutrophils represent a white blood cell population that is most common in humans; their degranulation, phagocytosis, generation of reactive oxygen and nitrogen active species, release of extracellular traps initiate and prolong inflammation, take part in the pathogenesis of myocardial ischemia, heart failure, stroke, and other disorders [19]. It is believed that neutrophil counts and functional activity are associated with chronic inflammation, development of micro- and macroalbuminuria associated with DM, while the increase in neutrophil counts in blood is an early marker of the DM-associated renal damage, DKD progression, along with microalbuminuria and eGFR, as well as shows a nonlinear relationship with the risk of death from DKD [10, 20]. According to the data provided by other researchers, the circulating neutrophil counts positively correlate with DKD-associated proteinuria [21].

The neutrophil-to-lymphocyte ratio of blood indicating systemic inflammation is associated with the prevalence of DKD

Table 6. Correlation between eGFR (mL/min/1.73 m²) and inflammatory markers in patients with T1D and CKD

Indicators	No CKD (group 2)	Group 3			
		Stage 1 CKD (group 3.1)	Stage 2 CKD (group 3.2)	Stage 3a CKD (group 3.3)	Stage 3b CKD (group 3.4)
IL1β, pg/mL	$R = -0.576$ $p = 0.031$	$R = -0.992$ $p < 0.000$	$R = -0.922$ $p < 0.000$	$R = -0.956$ $p = 0.003$	$R = -0.916$ $p = 0.001$
TNFα, pg/mL	$R = 0.559$ $p = 0.038$	$R = -0.448$ $p = 0.002$	$R = -0.616$ $p = 0.019$	$R = -0.986$ $p < 0.000$	$R = -0.842$ $p = 0.009$
LII, AU	$R = -0.018$ $p = 0.951$	$R = -0.566$ $p < 0.000$	$R = -0.801$ $p < 0.000$	$R = -0.750$ $p = 0.003$	$R = -0.955$ $p < 0.000$
Neutrophils/lymphocytes	$R = -0.054$ $p = 0.854$	$R = -0.698$ $p = 0.045$	$R = -0.769$ $p = 0.028$	$R = -0.957$ $p < 0.000$	$R = -0.902$ $p = 0.035$
CRP, IU/L	$R = 0.581$ $p = 0.030$	$R = -0.951$ $p < 0.000$	$R = -0.911$ $p < 0.000$	$R = -0.945$ $p = 0.009$	$R = -0.849$ $p = 0.008$
CP, mg/L	$R = -0.413$ $p = 0.143$	$R = -0.927$ $p < 0.000$	$R = -0.964$ $p < 0.000$	$R = -0.846$ $p = 0.003$	$R = -0.854$ $p = 0.007$

Note: Spearman's rank correlation coefficients (R) are provided.

and cardiovascular disorders, all-cause mortality in DM [22, 23]. The neutrophil-to-lymphocyte index is considered as a reliable measure of the systemic inflammation severity, given the role of neutrophils as nonspecific contributors to inflammation (innate immunity) and lymphocytes as regulators of all inflammatory responses and contributors to adaptive immunity [24]. Positive correlation between the neutrophil-to-lymphocyte index and serum concentrations of IL1β and CRP has been shown [25]. The results of several meta-analyses of clinical trials have shown higher neutrophil-to-lymphocyte index values in patients with diabetic nephropathy compared to patients with DM having no kidney disease, as well as the prospects of using the index for stratification and prediction of the risk of all-cause mortality, cardiovascular mortality [21, 26, 27]. At the same time, CKD also can cause chronic inflammation, worsening damage to organs and tissues and leading to escalation of inflammatory responses [8]. However, all these data are related to the role of neutrophils in patients with T2D. It should be also noted that LII and the neutrophil-to-lymphocyte index have some benefits in terms of affordability, economy and information content compared to other inflammatory markers. According to our data these have shown a strong negative correlation with eGFR in stage 2 CKD and a very strong correlation in stage 3a and 3b CKD.

When blood levels of pro-inflammatory cytokines increase, the synthesis of the inflammation acute phase reactants (APRs) is triggered in hepatocytes, including CRP and CP as members of the first wave (blood levels are increased within the first 6–12 h reaching their maximum after 24 h) and third wave (maximum concentration is achieved within 48–72 h) APRs [28]. APRs are widely used in clinical practice to monitor the course of inflammatory disorders and control treatment. CRP is represented by the native pentameric and monomeric forms showing pleiotropic activity, except for the marker role of inflammation severity and the risk factor of cardiovascular disorders (for highly sensitive CRP fraction) it is directly involved in the pathogenesis of diabetic nephropathy via several mechanisms. The data on the role of CRP in regulation of complement activation via suppression of podocyte autophagy and inhibition of the C3a/C3aR axis signaling are provided, reported in clinical and experimental settings for kidney damage under conditions of DM [29]. Furthermore, in DM, CRP activates the TGFβ/SMAD and κB nuclear factor signaling pathways involved in realization of inflammation in the kidneys and nephrosclerosis associated with diabetic nephropathy via synthesis of IL1β, TNFα, monocyte chemoattractant protein-1, TGFβ1 [27, 30]. The experimental study of streptozotocin-induced DM and the human kidney epithelial cell line has demonstrated CRP involvement in the pathogenesis of diabetic nephropathy via interaction with the FcγRII receptors on the kidney cells, activation of the Wnt/β-catenin, ERK1/2 signaling pathways, and disruption of epithelial-mesenchymal interactions [31]. CRP can cause cell death and progressive renal fibrosis via NF-κB and Smad3-dependent mechanisms [32]. The experimentally induced CRP deficiency inhibits the diabetic nephropathy development [29]. Serum CRP levels are associated with microvascular complications of T2D, including kidney disease [33, 34]. The use of the two-stage regression model in more than 2000 patients with T2D involving assessment of single nucleotide polymorphisms of the CRP gene in the chromosome 1 (1q21–q23) showed a high-level causative relationship between serum CRP levels and the emergence of diabetic nephropathy [35]. Some researchers believe that the serum CRP/albumin index is a more informative independent predictor of the development

of diabetic nephropathy associated with T2D [36]. Furthermore, serum CRP levels are associated with the urinary albumin/creatinine ratio in patients with T2D [37].

Ceruloplasmin not only reflects acute and chronic inflammation in the body, but also represents a metalloprotein possessing antioxidant properties due to its ferroxidase activity, and under conditions of oxidative stress it can function as a pro-oxidant taking part in generation of ROCs and oxidated LDL; it is the latter fact that is considered to be related to its pathogenetic role in the development of DM complications. It has been shown that patients with T2D, microalbuminuria, and diabetic nephropathy show the increased elimination of copper as part of CP with urine, which results in the decreased synthesis of Cu, Zn-superoxide dismutase and the development of oxidative stress [38]. Elevated CP levels are reported for T1D and T2D, including under conditions of diabetic nephropathy [39, 40]. In T2D, CP is considered to be a promising sensitive marker involved in the development of oxidative stress, insulin resistance, lipid metabolism disorders associated with this disease [41]. The role of serum CP as an independent prognostic factor of diabetic nephropathy progression in patients with T2D has been defined. We have clearly shown the increase in serum concentrations of CP in patients with CKD under conditions of T1D, progressing from the 16% increase based on the median in stage 1 CKD of the values of the group of healthy individuals to the 73% increase in stage 3b CKD. A strong negative correlation between CP and the CKD stage based on the eGRF values has been proven. Determination of serum CP concentrations is not widely used in clinical practice, however, it can be useful as a marker of diabetic nephropathy in cases of multiple definitions and growth in dynamics, especially when there is no albuminuria.

It is important to note that chronic inflammation in the kidneys results in damage to small blood vessels and glomeruli, proteinuria and decreased renal filtration capacity. Moreover, chronic inflammation is accompanied by activation of fibroblasts and generation of the extracellular matrix products, which causes interstitial fibrosis and loss of renal function. These mechanisms, as well as the mechanisms underlying inflammation initiation in DM and CKD are intertwined, these enhance one another, creating vicious circles, and lead to progression of diabetic nephropathy, loss of renal function, and the need for substitution therapy. Understanding pathophysiology of inflammation associated with diabetic nephropathy opens up prospects for the development of effective methods for the diagnosis and treatment of this severe condition. The issue of the search for sensitive specific diabetic nephropathy markers is relevant for practical medicine in terms of the DM-associated CKD diagnosis, treatment control, and progression [42]. Of primary importance are the currently used clinical biomarkers, such as eGRF, proteinuria, albuminuria, being the most important predictors of progression of kidney diseases, cardiovascular complications, and mortality in patients with diabetic nephropathy [43]. According to the results of the study, serum levels of IL1β, TNFα, CRP and CP, LII, neutrophil-to-lymphocyte index claim to be promising biomarkers of the kidney damage initiation and progression in patients with T1D and early stage CKD.

CONCLUSIONS

Serum concentrations of IL1β, TNFα, CRP and CP, LII, neutrophil-to-lymphocyte index are increased in patients with T1D and early stage CKD. Serum levels of IL1β, neutrophil-to-lymphocyte index, and CRP and CP concentrations are the

most important indicators of inflammatory activity in patients with T1D and early stage CKD. It is reasonable to measure the dynamics of those, if diabetes is compensated and the patient has no active inflammation, starting from stage 1 CKD. The inflammation and acute phase response severity in patients with T1D and early stage CKD progresses to reach its maximum in stage 3b CKD, when the serum IL1β concentration is increased 2.4-fold, TNFα concentration by 34%, CRP concentration 33-fold, CP concentration by 73%, LII 8.4-fold, neutrophil-to-lymphocyte index 5-fold. It has been found that eGRF, the integral renal function indicator, decreases with increasing serum levels of inflammatory markers in patients with T1D and early stage CKD. The maximum number of

correlations and correlation strength are reported for stage 3a and 3b CKD in patients with T1D, mainly between eGRF and serum concentrations of IL1β and CRP. The results presented expand the knowledge about the role of inflammation and acute phase response in the pathogenesis of CKD in patients with T1D, create prerequisites for further studies, larger-scale in terms of the number of patients and duration, in various regions of the Russian Federation considering age, sex, constitutional features, concomitant disorders, therapy type, and other factor, as well as for modernization of the diagnostic and prognostic criteria, improvement of preventive and therapeutic measures for patients with T1D and early stage CKD.

References

1. Dedov II, Shestakova MV, Vikulova OK, Zheleznjakova AV, Isakov MA, Sazonova DV, i dr. Saharnyj diabet v Rossijskoj Federacii: dinamika jepidemiologicheskih pokazatelej po dannym Federal'nogo registra saharnogo diabeta za period 2010–2022 gg. Saharnyj diabet. 2023; 26 (2): 104–23. DOI: 10.14341/DM13035. Russian.
2. Kidney Disease: Improving Global Outcomes (KDIGO) Diabetes Work Group. KDIGO 2022 Clinical Practice Guideline for Diabetes Management in Chronic Kidney Disease. Kidney Int. 2022; 102 (5S): S1–S127. DOI: 10.1016/j.kint.2022.06.008.
3. Patidar K, Deng JH, Mitchell CS, Ford Versypt AN. Cross-Domain Text Mining of Pathophysiological Processes Associated with Diabetic Kidney Disease. Int J Mol Sci. 2024; 25(8): 4503. DOI: 10.3390/ijms25084503.
4. Eckardt KU, Delgado C, Heerspink HJL, Pecoits-Filho R, Ricardo AC, Stengel B, et al. Trends and perspectives for improving quality of chronic kidney disease care: conclusions from a Kidney Disease: Improving Global Outcomes (KDIGO) Controversies Conference. Kidney Int. 2023; 104 (5): 888–903. DOI: 10.1016/j.kint.2023.05.013.
5. Vyas DA, Eisenstein LG, Jones DS. Hidden in Plain Sight — Reconsidering the Use of Race Correction in Clinical Algorithms. N Engl J Med. 2020; 383 (9): 874–82. DOI: 10.1056/NEJMms2004740.
6. Fan X, Yang M, Lang Y, Lu S, Kong Z, Gao Y, et al. Mitochondrial metabolic reprogramming in diabetic kidney disease. Cell Death Dis. 2024; 15: 442. DOI:10.1038/s41419-024-06833-0.
7. Furman D, Campisi J, Verdin E, Carrera-Bastos P, Targ S, Franceschi C et al. Chronic inflammation in the etiology of disease across the life span. Nat Med. 2019; 25 (12): 1822–32. DOI: 10.1038/s41591-019-0675-0. PubMed PMID: 31806905.
8. Rayego-Mateos S, Rodrigues-Diez RR, Fernandez-Fernandez B, Mora-Fernández C, Marchant V, Donate-Correa J, et al. Targeting inflammation to treat diabetic kidney disease: The road to 2030. Kidney Int. 2023; 103: 282–96. DOI: 10.1016/j.kint.2022.10.030.
9. Varra FN, Varras M, Varra VK, Theodosis-Nobelos P. Molecular and pathophysiological relationship between obesity and chronic inflammation in the manifestation of metabolic dysfunctions and their inflammation-mediating treatment options (Review). Mol Med Rep. 2024; 29: 95. DOI: 10.3892/mmr.2024.13219.
10. Xie R, Bishai DM, Lui DTW, Lee PCH, Yap DYH. Higher circulating neutrophil counts is associated with increased risk of all-cause mortality and cardiovascular disease in patients with diabetic kidney disease. Biomedicines. 2024; 12(8): 1907. DOI: 10.3390/biomedicines12081907. PubMed PMID: 39200371.
11. Saharnyj diabet 1 tipa u vzroslyh: klinicheskie rekomendacii. Rubrikator klinicheskih rekomendacij [Jelektronnyj resurs]. 2022 [data dostupa: 2024 oktjabr' 21]. Available from: https://cr.minzdrav.gov.ru/recomend/286_2. Russian.
12. Hronicheskaja bolezn' pochek (HBP): klinicheskie rekomendacii. Rubrikator klinicheskih rekomendacij [Jelektronnyj resurs]. 2021 [data dostupa: 2024 oktjabr' 21]. Available from: https://cr.minzdrav.gov.ru/schema/469_2. Russian.
13. Ostrovskij VK, Mashhenko AV, Jangolenko DV i dr. Pokazateli krovi i lejkocitarnogo indeksa intoksikacii v ocenke tjazhesti i opredelenii

prognoza pri vospalitel'nyh, gnojnyh i gnojno-destruktivnyh zabolevanijah. Klin. lab. diagnostika. – 2006; 6: 50–3. Russian.
14. Kamyshnikov VS. Kliniko-biohimicheskaja laboratornaja diagnostika. Minsk: Izd-vo «Interpresservis»; 2003. 495 s. Russian.
15. Tonneijck L, Muskiet MH, Smits MM, van Bommel EJ, Heerspink HJ, van Raalte DH, Joles JA. Glomerular Hyperfiltration in Diabetes: Mechanisms, Clinical Significance, and Treatment. J Am Soc Nephrol. 2017; 28 (4): 1023–39. DOI: 10.1681/ASN.2016060666.
16. Kanbay M, Copur S, Guldan M, Ozbek L, Hatipoglu A, Covic A, Mallamaci F, Zoccali C. Proximal tubule hypertrophy and hyperfunction: a novel pathophysiological feature in disease states. Clin Kidney J. 2024; 17 (7): sfae195. DOI: 10.1093/ckj/sfae195.
17. Jin L, Wang X, Liu Y, Xiang Q, Huang R. High levels of blood glycemic indicators are associated with chronic kidney disease prevalence in non-diabetic adults: Cross-sectional data from the national health and nutrition examination survey 2005–2016. J Clin Transl Endocrinol. 2024; 36: 100347. DOI: 10.1016/j.jcte.2024.100347.
18. Rayego-Mateos S, Morgado-Pascual JL, Opazo-Ríos L, Guerrero-Hue M, Garcia-Caballero C, Vazquez-Carballo C, et al. Pathogenic pathways and therapeutic approaches targeting inflammation in diabetic nephropathy. Int J Mol Sci. 2020; 21 (11): 3798. DOI: 10.3390/ijms21113798.
19. Shirakawa K, Sano M. Neutrophils and neutrophil extracellular traps in cardiovascular disease: an overview and potential therapeutic approaches. Biomedicines. 2022; 10: 1850. DOI: 10.3390/biomedicines10081850.
20. Zhang R, Chen J, Xiong Y, Wang L, Huang X, Sun T, et al. Increased neutrophil count Is associated with the development of chronic kidney disease in patients with diabetes. J Diabetes. 2022; 14: 442–54. DOI: 10.1111/1753-0407.13292.
21. Zeng G, Lin Y, Xie P, Lin J, He Y, Wei J. Relationship of the Neutrophil-Lymphocyte Ratio with All-Cause and Cardiovascular Mortality in Patients with Diabetic Kidney Disease: A Prospective Cohort Study of NHANES Study. J Multidiscip Healthc. 2024; 17: 2461–73. DOI: 10.2147/JMDH.S465317. PubMed PMID: 38799017.
22. Wan H, Wang Y, Fang S, Chen Y, Zhang W, Xia F, et al. Associations between the neutrophil-to-lymphocyte ratio and diabetic complications in adults with dabetes: a cross-sectional study. J Diabetes Res. 2020; 2020: 1–9. DOI: 10.1155/2020/6219545
23. Gao JL, Shen J, Yang LP, Liu L, Zhao K, Pan XR, et al. Neutrophil-to-lymphocyte ratio associated with renal function in type 2 diabetic patients. World J Clin Cases. 2024; 12 (14): 2308–15. DOI: 10.12998/wjcc.v12.i14.2308. PubMed PMID: 38765748.
24. Ko HL, Jung J, Lee J, Lim JH, Im DW, Kim YC, et al. Dynamic nature and prognostic value of the neutrophil-to-lymphocyte ratio in critically ill patients with acute kidney injury on continuous renal replacement therapy: A multicenter cohort study. Front Med (Lausanne). 2023; 10: 1162381. DOI: 10.3389/fmed.2023.1162381.
25. Karava V, Kondou A, Dotis J, Taparkou A, Farmaki E, Kollios K, et al. Exploring systemic inflammation in children with chronic kidney disease: correlates of interleukin 6. Pediatr Nephrol. 2024; 39:

1567–76. DOI:10.1007/s00467-023-06234-z.

26. Liu J, Liu X, Li Y, Quan J, Wei S, An S, et al. The association of neutrophil to lymphocyte ratio, mean platelet volume, and platelet distribution width with diabetic retinopathy and nephropathy: a meta-analysis. Biosci Rep. 2018; 38: 2–19. DOI: 10.1042/BSR20180172.

27. Lau LFS, Ng JK, Fung WWS, Chan GCK, Mei-Shan Cheng, Chow KM, et al. Relationship between serial serum neutrophil-lymphocyte ratio, cardiovascular mortality, and all-cause mortality in Chinese peritoneal dialysis patients. Kidney Blood Press Res. 2023; 48 (1): 414–23. DOI: 10.1159/000530554

28. Messias BA, Botelho RV, Saad SS, Mocchetti ER, Turke KC, Waisberg J. Serum C-reactive protein is a useful marker to exclude anastomotic leakage after colorectal surgery. Sci Rep. 2020; 10 (1): 1687. DOI: 10.1038/s41598-020-58780-3.

29. Zhang L, Li W, Gong M, Zhang Z, Xue X, Mao J et al. C-reactive protein inhibits C3a/C3aR-dependent podocyte autophagy in favor of diabetic kidney disease. FASEB J. 2022; 36(6): e22332. DOI: 10.1096/fj.202200198R. PubMed PMID: 35503088.

30. Wang Y, Guo J, Shao B, Chen H, Lan H. The Role of TGF-β1/SMAD in diabetic nephropathy: mechanisms and research development. Sichuan Da Xue Xue Bao Yi Xue Ban. 2023; 54 (6): 1065–73. Chinese. DOI: 10.12182/20231160108. PubMed PMID: 38162063.

31. Zhang L, Shen ZY, Wang K, Li W, Shi JM, Osoro EK, et al. C-reactive protein exacerbates epithelial-mesenchymal transition through Wnt/β-catenin and ERK signaling in streptozocin-induced diabetic nephropathy. FASEB J. 2019; 33 (5): 6551–63. DOI: 10.1096/fj.201801865RR. PubMed PMID: 30794428.

32. Li J, Chen J, Lan HY, Tang Y. Role of C-Reactive protein in Kidney Diseases. Kidney Dis (Basel). 2022; 9 (2): 73–81. DOI: 10.1159/000528693. PubMed PMID: 37065607.

33. Geng T, Zhu K, Lu Q, Wan Z, Chen X, Liu L, et al. Healthy lifestyle behaviors, mediating biomarkers, and risk of microvascular complications among individuals with type 2 diabetes: A cohort study. PLoS Med. 2023; 20 (1): e1004135. DOI: 10.1371/journal.pmed.1004135. PubMed PMID: 36626356.

34. Tang M, Cao H, Wei XH, Zhen Q, Liu F, Wang YF, et al. Association between high-sensitivity C-Reactive protein and Diabetic Kidney Disease in patients with type 2 diabetes mellitus. Front Endocrinol (Lausanne). 2022; 13: 885516. DOI: 10.3389/fendo.2022.885516. PubMed PMID: 35784528.

35. Lin CC, Li CI, Liu CS, Liao LN, Yang CW, Lin CH, et al. Association of high-sensitivity C-reactive protein and diabetic nephropathy in patients with type 2 diabetes: a Mendelian randomization study. BMJ Open Diabetes Res Care. 2023; 11 (1): e003197. DOI: 10.1136/bmjdrc-2022-003197. PubMed PMID: 36828641.

36. Aktas G. Serum C-reactive protein to albumin ratio as a reliable marker of diabetic neuropathy in type 2 diabetes mellitus. Biomol Biomed. 2024; 24 (5): 1380–6. DOI: 10.17305/bb.2024.10426. PubMed PMID: 38635449.

37. Kumari S, Singh B. Assessment of correlation of serum high-sensitive C-Reactive protein, urinary albumin-to-creatinine ratio, and lipid profile in diabetics. J Pharm Bioallied Sci. 2021; 13 (2): S1569–S1572. DOI: 10.4103/jpbs.jpbs_290_21. PubMed PMID: 35018031.

38. Al-Bayati MA, Jamil DA, Al-Aubaidy HA. Cardiovascular effects of copper deficiency on activity of superoxide dismutase in diabetic nephropathy. N Am J Med Sci. 2015; 7(2): 41–6.

39. Lee MJ, Jung CH, Kang YM, Jang JE, Leem J, Park JY, et al. Serum ceruloplasmin level as a predictor for the progression of diabetic nephropathy in korean men with type 2 diabetes mellitus. Diabetes Metab J. 2015; 39 (3): 230–9. DOI: 10.4093/dmj.2015.39.3.230. PubMed PMID: 26124993.

40. de Paula Silva L, de Moraes Rego FG, Picheth G, Müller-Santos M, Alberton D. Prospection of plasma proteins as biomarkers for diabetes mellitus monitoring. J Diabetes Metab Disord. 2021; 20 (1): 611–20. DOI: 10.1007/s40200-021-00788-1. PubMed PMID: 34222081.

41. Wang S, Lu Z, Wang Y, Zhang T, He X. Metalloproteins and apolipoprotein C: candidate plasma biomarkers of T2DM screened by comparative proteomics and lipidomics in ZDF rats. Nutr Metab (Lond). 2020; 17: 66. DOI: 10.1186/s12986-020-00488-2. PubMed PMID: 32817751.

42. Swaminathan SM, Rao IR, Shenoy SV, Prabhu AR, Mohan PB, Rangaswamy D, et al. Novel biomarkers for prognosticating diabetic kidney disease progression. Int Urol Nephrol. 2023; 55 (4): 913–28. DOI: 10.1007/s11255-022-03354-7. PubMed PMID: 36271990.

43. Jung CY, Yoo TH. Pathophysiologic Mechanisms and Potential Biomarkers in Diabetic Kidney Disease. Diabetes Metab J. 2022; 46 (2): 181–97. DOI: 10.4093/dmj.2021.0329.

Литература

1. Дедов И. И., Шестакова М. В., Викулова О. К., Железнякова А. В., Исаков М. А., Сазонова Д. В., и др. Сахарный диабет в Российской Федерации: динамика эпидемиологических показателей по данным Федерального регистра сахарного диабета за период 2010–2022 гг. Сахарный диабет. 2023; 26 (2): 104–23. DOI: 10.14341/DM13035.

2. Kidney Disease: Improving Global Outcomes (KDIGO) Diabetes Work Group. KDIGO 2022 Clinical Practice Guideline for Diabetes Management in Chronic Kidney Disease. Kidney Int. 2022; 102 (5S): S1–S127. DOI: 10.1016/j.kint.2022.06.008.

3. Patidar K, Deng JH, Mitchell CS, Ford Versypt AN. Cross-Domain Text Mining of Pathophysiological Processes Associated with Diabetic Kidney Disease. Int J Mol Sci. 2024; 25(8): 4503. DOI: 10.3390/ijms25084503.

4. Eckardt KU, Delgado C, Heerspink HJL, Pecoits-Filho R, Ricardo AC, Stengel B, et al. Trends and perspectives for improving quality of chronic kidney disease care: conclusions from a Kidney Disease: Improving Global Outcomes (KDIGO) Controversies Conference. Kidney Int. 2023; 104 (5): 888–903. DOI: 10.1016/j.kint.2023.05.013.

5. Vyas DA, Eisenstein LG, Jones DS. Hidden in Plain Sight — Reconsidering the Use of Race Correction in Clinical Algorithms. N Engl J Med. 2020; 383 (9): 874–82. DOI: 10.1056/NEJMms2004740.

6. Fan X, Yang M, Lang Y, Lu S, Kong Z, Gao Y, et al. Mitochondrial metabolic reprogramming in diabetic kidney disease. Cell Death Dis. 2024; 15: 442. DOI:10.1038/s41419-024-06833-0.

7. Furman D, Campisi J, Verdin E, Carrera-Bastos P, Targ S, Franceschi C et al. Chronic inflammation in the etiology of disease across the life span. Nat Med. 2019; 25 (12): 1822–32. DOI: 10.1038/s41591-019-0675-0. PubMed PMID: 31806905.

8. Rayego-Mateos S, Rodrigues-Diez RR, Fernandez-Fernandez B, Mora-Fernández C, Marchant V, Donate-Correa J, et al. Targeting inflammation to treat diabetic kidney disease: The road to 2030. Kidney Int. 2023; 103: 282–96. DOI: 10.1016/j.kint.2022.10.030.

9. Varra FN, Varras M, Varra VK, Theodosis-Nobelos P. Molecular and pathophysiological relationship between obesity and chronic inflammation in the manifestation of metabolic dysfunctions and their inflammation-mediating treatment options (Review). Mol Med Rep. 2024; 29: 95. DOI: 10.3892/mmr.2024.13219.

10. Xie R, Bishai DM, Lui DTW, Lee PCH, Yap DYH. Higher circulating neutrophil counts is associated with increased risk of all-cause mortality and cardiovascular disease in patients with diabetic kidney disease. Biomedicines. 2024; 12(8): 1907. DOI: 10.3390/biomedicines12081907. PubMed PMID: 39200371.

11. Сахарный диабет 1 типа у взрослых: клинические рекомендации. Рубрикатор клинических рекомендаций [Электронный ресурс]. 2022 [дата доступа: 2024 октябрь 21]. Режим доступа: https://cr.minzdrav.gov.ru/recomend/286_2.

12. Хроническая болезнь почек (ХБП): клинические рекомендации. Рубрикатор клинических рекомендаций [Электронный ресурс]. 2021 [дата доступа: 2024 октябрь 21]. Режим доступа: https://cr.minzdrav.gov.ru/schema/469_2.

13. Островский В. К., Мащенко А. В., Янголенко Д. В. и др. Показатели крови и лейкоцитарного индекса интоксикации в оценке тяжести и определении прогноза при воспалительных, гнойных и гнойно-деструктивных заболеваниях. Клин. лаб. диагностика. — 2006; 6: 50–3.

14. Камышников В. С. Клинико-биохимическая лабораторная диагностика. Минск: Изд-во «Интерпрессервис»; 2003. 495 с.

15. Tonneijck L, Muskiet MH, Smits MM, van Bommel EJ, Heerspink HJ, van Raalte DH, Joles JA. Glomerular Hyperfiltration in Diabetes: Mechanisms, Clinical Significance, and Treatment. J Am Soc Nephrol. 2017; 28 (4): 1023–39. DOI: 10.1681/ASN.2016060666.

16. Kanbay M, Copur S, Guldan M, Ozbek L, Hatipoglu A, Covic A, Mallamaci F, Zoccali C. Proximal tubule hypertrophy and hyperfunction: a novel pathophysiological feature in disease states. Clin Kidney J. 2024; 17 (7): sfae195. DOI: 10.1093/ckj/sfae195.

17. Jin L, Wang X, Liu Y, Xiang Q, Huang R. High levels of blood glycemic indicators are associated with chronic kidney disease prevalence in non-diabetic adults: Cross-sectional data from the national health and nutrition examination survey 2005–2016. J Clin Transl Endocrinol. 2024; 36: 100347. DOI: 10.1016/j.jcte.2024.100347.

18. Rayego-Mateos S, Morgado-Pascual JL, Opazo-Ríos L, Guerrero-Hue M, Garcia-Caballero C, Vazquez-Carballo C, et al. Pathogenic pathways and therapeutic approaches targeting inflammation in diabetic nephropathy. Int J Mol Sci. 2020; 21 (11): 3798. DOI: 10.3390/ijms21113798.

19. Shirakawa K, Sano M. Neutrophils and neutrophil extracellular traps in cardiovascular disease: an overview and potential therapeutic approaches. Biomedicines. 2022; 10: 1850. DOI: 10.3390/biomedicines10081850.

20. Zhang R, Chen J, Xiong Y, Wang L, Huang X, Sun T, et al. Increased neutrophil count Is associated with the development of chronic kidney disease in patients with diabetes. J Diabetes. 2022; 14: 442–54. DOI: 10.1111/1753-0407.13292.

21. Zeng G, Lin Y, Xie P, Lin J, He Y, Wei J. Relationship of the Neutrophil-Lymphocyte Ratio with All-Cause and Cardiovascular Mortality in Patients with Diabetic Kidney Disease: A Prospective Cohort Study of NHANES Study. J Multidiscip Healthc. 2024; 17: 2461–73. DOI: 10.2147/JMDH.S465317. PubMed PMID: 38799017.

22. Wan H, Wang Y, Fang S, Chen Y, Zhang W, Xia F, et al. Associations between the neutrophil-to-lymphocyte ratio and diabetic complications in adults with dabetes: a cross-sectional study. J Diabetes Res. 2020; 2020: 1–9. DOI: 10.1155/2020/6219545

23. Gao JL, Shen J, Yang LP, Liu L, Zhao K, Pan XR, et al. Neutrophil-to-lymphocyte ratio associated with renal function in type 2 diabetic patients. World J Clin Cases. 2024; 12 (14): 2308–15. DOI: 10.12998/wjcc.v12.i14.2308. PubMed PMID: 38765748.

24. Ko HL, Jung J, Lee J, Lim JH, Im DW, Kim YC, et al. Dynamic nature and prognostic value of the neutrophil-to-lymphocyte ratio in critically ill patients with acute kidney injury on continuous renal replacement therapy: A multicenter cohort study. Front Med (Lausanne). 2023; 10: 1162381. DOI: 10.3389/fmed.2023.1162381.

25. Karava V, Kondou A, Dotis J, Taparkou A, Farmaki E, Kollios K, et al. Exploring systemic inflammation in children with chronic kidney disease: correlates of interleukin 6. Pediatr Nephrol. 2024; 39: 1567–76. DOI:10.1007/s00467-023-06234-z.

26. Liu J, Liu X, Li Y, Quan J, Wei S, An S, et al. The association of neutrophil to lymphocyte ratio, mean platelet volume, and platelet distribution width with diabetic retinopathy and nephropathy: a meta-analysis. Biosci Rep. 2018; 38: 2–19. DOI: 10.1042/BSR20180172.

27. Lau LFS, Ng JK, Fung WWS, Chan GCK, Mei-Shan Cheng, Chow KM, et al. Relationship between serial serum neutrophil-lymphocyte ratio, cardiovascular mortality, and all-cause mortality in Chinese peritoneal dialysis patients. Kidney Blood Press Res. 2023; 48 (1): 414–23. DOI: 10.1159/000530554

28. Messias BA, Botelho RV, Saad SS, Mocchetti ER, Turke KC, Waisberg J. Serum C-reactive protein is a useful marker to exclude anastomotic leakage after colorectal surgery. Sci Rep. 2020; 10 (1): 1687. DOI: 10.1038/s41598-020-58780-3.

29. Zhang L, Li W, Gong M, Zhang Z, Xue X, Mao J et al. C-reactive protein inhibits C3a/C3aR-dependent podocyte autophagy in favor of diabetic kidney disease. FASEB J. 2022; 36(6): e22332. DOI: 10.1096/fj.202200198R. PubMed PMID: 35503088.

30. Wang Y, Guo J, Shao B, Chen H, Lan H. The Role of TGF-β1/SMAD in diabetic nephropathy: mechanisms and research development. Sichuan Da Xue Xue Bao Yi Xue Ban. 2023; 54 (6): 1065–73. Chinese. DOI: 10.12182/20231160108. PubMed PMID: 38162063.

31. Zhang L, Shen ZY, Wang K, Li W, Shi JM, Osoro EK, et al. C-reactive protein exacerbates epithelial-mesenchymal transition through Wnt/β-catenin and ERK signaling in streptozocin-induced diabetic nephropathy. FASEB J. 2019; 33 (5): 6551–63. DOI: 10.1096/fj.201801865RR. PubMed PMID: 30794428.

32. Li J, Chen J, Lan HY, Tang Y. Role of C-Reactive protein in Kidney Diseases. Kidney Dis (Basel). 2022; 9 (2): 73–81. DOI: 10.1159/000528693. PubMed PMID: 37065607.

33. Geng T, Zhu K, Lu Q, Wan Z, Chen X, Liu L, et al. Healthy lifestyle behaviors, mediating biomarkers, and risk of microvascular complications among individuals with type 2 diabetes: A cohort study. PLoS Med. 2023; 20 (1): e1004135. DOI: 10.1371/journal.pmed.1004135. PubMed PMID: 36626356.

34. Tang M, Cao H, Wei XH, Zhen Q, Liu F, Wang YF, et al. Association between high-sensitivity C-Reactive protein and Diabetic Kidney Disease in patients with type 2 diabetes mellitus. Front Endocrinol (Lausanne). 2022; 13: 885516. DOI: 10.3389/fendo.2022.885516. PubMed PMID: 35784528.

35. Lin CC, Li CI, Liu CS, Liao LN, Yang CW, Lin CH, et al. Association of high-sensitivity C-reactive protein and diabetic nephropathy in patients with type 2 diabetes: a Mendelian randomization study. BMJ Open Diabetes Res Care. 2023; 11 (1): e003197. DOI: 10.1136/bmjdrc-2022-003197. PubMed PMID: 36828641.

36. Aktas G. Serum C-reactive protein to albumin ratio as a reliable marker of diabetic neuropathy in type 2 diabetes mellitus. Biomol Biomed. 2024; 24 (5): 1380–6. DOI: 10.17305/bb.2024.10426. PubMed PMID: 38635449.

37. Kumari S, Singh B. Assessment of correlation of serum high-sensitive C-Reactive protein, urinary albumin-to-creatinine ratio, and lipid profile in diabetics. J Pharm Bioallied Sci. 2021; 13 (2): S1569–S1572. DOI: 10.4103/jpbs.jpbs_290_21. PubMed PMID: 35018031.

38. Al-Bayati MA, Jamil DA, Al-Aubaidy HA. Cardiovascular effects of copper deficiency on activity of superoxide dismutase in diabetic nephropathy. N Am J Med Sci. 2015; 7(2): 41–6.

39. Lee MJ, Jung CH, Kang YM, Jang JE, Leem J, Park JY, et al. Serum ceruloplasmin level as a predictor for the progression of diabetic nephropathy in korean men with type 2 diabetes mellitus. Diabetes Metab J. 2015; 39 (3): 230–9. DOI: 10.4093/dmj.2015.39.3.230. PubMed PMID: 26124993.

40. de Paula Silva L, de Moraes Rego FG, Picheth G, Müller-Santos M, Alberton D. Prospection of plasma proteins as biomarkers for diabetes mellitus monitoring. J Diabetes Metab Disord. 2021; 20 (1): 611–20. DOI: 10.1007/s40200-021-00788-1. PubMed PMID: 34222081.

41. Wang S, Lu Z, Wang Y, Zhang T, He X. Metalloproteins and apolipoprotein C: candidate plasma biomarkers of T2DM screened by comparative proteomics and lipidomics in ZDF rats. Nutr Metab (Lond). 2020; 17: 66. DOI: 10.1186/s12986-020-00488-2. PubMed PMID: 32817751.

42. Swaminathan SM, Rao IR, Shenoy SV, Prabhu AR, Mohan PB, Rangaswamy D, et al. Novel biomarkers for prognosticating diabetic kidney disease progression. Int Urol Nephrol. 2023; 55 (4): 913–28. DOI: 10.1007/s11255-022-03354-7. PubMed PMID: 36271990.

43. Jung CY, Yoo TH. Pathophysiologic Mechanisms and Potential Biomarkers in Diabetic Kidney Disease. Diabetes Metab J. 2022; 46 (2): 181–97. DOI: 10.4093/dmj.2021.0329.

ESTIMATION OF THE IMPACT OF CHRONIC RADIATION EXPOSURE ON TELOMERE LOSS IN WOMEN'S T LYMPHOCYTES

Krivoshchapova IaV ✉

Urals Research Center for Radiation Medicine of the Federal Medical Biological Agency, Chelyabinsk, Russia

Residents of the Techa Riverside villages were chronically exposed to the wide range of doses more than 60 years ago. Telomeric regions of metaphase chromosomes in the cultured peripheral blood T-lymphocytes were the subject of the research. The study aimed to assess the impact of chronic exposure on telomere loss in exposed women of the Southern Urals using a fluorescent staining method. Chromatid and chromosome telomere loss was determined in three dose subgroups: comparison group (0–0.01 Gy), group of exposed individuals with the dose of 0.2–0.9 Gy, and group of exposed individuals with the dose of 1–4.6 Gy. In the sample of female residents of the Southern Urals chronically exposed in the range of absorbed doses to RBM of 0–4.6 Gy, it was shown that there were no differences in telomere loss between the comparison group and the group exposed to the dose exceeding 1 Gy ($p > 0.33$), while the group of individuals exposed to medium doses of 0.2–0.9 Gy was statistically significantly different ($p < 0.05$). Statistically significant differences between all groups were reported for chromosome telomere loss ($p < 0.05$). According to the data obtained, telomere loss was found in 99.85% of donor cells. The loss of telomere region on one of the chromatids occurred statistically significantly more often in all the groups. Thus, in the group exposed to the dose of 0.2–0.9 Gy, the average rate of chromatid telomere loss was higher, it was statistically significantly different from that of the other groups of females of the studied age.

✉ **Correspondence should be addressed:** Yana V. Krivoshchapova
Vorovsky, 68A, Chelyabinsk, 454141, Russia; Yana_ho@mail.ru

ОЦЕНКА ВЛИЯНИЯ ХРОНИЧЕСКОГО РАДИАЦИОННОГО ВОЗДЕЙСТВИЯ НА ПОТЕРЮ ТЕЛОМЕРНЫХ УЧАСТКОВ ХРОМОСОМ В Т-ЛИМФОЦИТАХ У ЖЕНЩИН

Я. В. Кривощапова ✉

Уральский научно-практический центр радиационной медицины, Челябинск, Россия

Более 60 лет назад жители прибрежных сел реки Теча были подвержены хроническому облучению в широком диапазоне доз. Предметом исследования были теломерные районы в метафазных хромосомах культивированных Т-лимфоцитов периферической крови. Целью исследования было оценить влияние хронического облучения на потери теломерных участков хромосом у облученных женщин Южного Урала с применением метода флуоресцентного окрашивания. Определяли хроматидные и хромосомные потери теломерных участков хромосом в трех дозовых подгруппах: группа сравнения (0–0,01 Гр), группа облучения дозой 0,2–0,9 Гр и группа облучения дозой 1–4,6 Гр. В выборке жителей Южного Урала женского пола, подвергшихся хроническому облучению в диапазоне поглощенных доз на ККМ от 0 до 4,6 Гр, было установлено, что хроматидные потери теломер для группы сравнения и группы облученных в дозе более 1 Гр статистически не различимы ($p > 0,33$), в то же время группа облученных средними дозами 0,2–0,9 Гр статистически отличается от них ($p < 0,05$). Для хромосомных потерь установлено статистически значимое различие между всеми группами ($p < 0,05$). Согласно полученным данным, теломерные потери присутствуют в 99,85% клеток доноров. Достоверно чаще во всех группах встречались потери теломерного участка на одной из хроматид. Таким образом, в группе с дозой 0,2–0,9 Гр среднее число потерь хроматид выше и статистически значимо отличается от других групп женского пола в исследуемом возрастном диапазоне.

✉ **Для корреспонденции:** Яна Владимировна Кривощапова
ул. Воровского, д. 68А, г. Челябинск, 454141, Россия; Yana_ho@mail.ru

Ionizing radiation affects human life everywhere: diagnostic medical procedures, travelling by planes, exposure to natural ionizing radiation in the areas with elevated background radiation. In addition to the planned and controlled radiation exposure, there is also accidental radiation exposure due to accidents and incidents involving the ionizing radiation sources. Investigation of mechanisms underlying the effects of radiation on human health is an important and relevant task.

More than 60 years ago more than 100,000 people who lived in the Southern Urals were chronically exposed at a wide

range of cumulative doses. Intake of ^{89,90}Sr radionuclides with food and water caused internal exposure, while external exposure resulted from the proximity to the banks of the Techa River contaminated due to liquid radioactive waste discharges (γ exposure). Changes in the status of multiple body systems were reported after the long-term follow-up of individuals exposed in the Southern Urals [1, 2].

The effects of ionizing radiation on chromosomal rearrangements have been proven by many studies. DNA structure in the cell is altered under exposure to ionizing radiation yielding the compounds capable of damaging DNA. For example, reactive oxygen species, lipid peroxidation products, etc. As a result, interatomic bonds are broken in the sugar-phosphate backbone, which leads to the DNA molecule continuity impairment. When there is no or insufficient repair, such breaks can become an event initiating aging and carcinogenesis [3, 4]. There can be single-strand breaks (when one DNA strand is broken) and double-strand ones (when both strands are broken).

Telomeres, the repeated nucleotide sequences, are responsible for maintaining stability of chromosomes and genome in the nucleus. The study of human chromosome telomeric regions is a pressing scientific issue due to proven involvement of telomeres in such processes, as aging, malignant transformation of cells. A number of genetic disorders are associated with alteration of chromosome telomeric regions.

The earlier studies of chromosome telomeric regions using fluorescence in situ hybridization (FISH) revealed qualitative chromatin changes in exposed individuals. It was reported that telomeric signals were observed in the chromosome arms, which resulted from inversions involving telomeric regions [5]. Significant telomere length reduction in some chromosome arms was also reported in exposed individuals compared with non-exposed ones [6]. When conducting research, the fact was noticed that not all metaphase chromosomes in the cell had four telomeres at the ends; in some chromosomes, telomere regions were not visible at all.

Telomere loss can occur due to gradual telomere shortening during cell division, or as a result of stochastic events, during which the repeated telomere sequences are lost, for example, as a result of terminal deletion or double-strand break within the subtelomeric region [7]. Some studies of tumor cell lines show that such spontaneous telomere deletions are typical of cancer cells [8, 9].

Telomere loss is important for human evolution. Many genetic disorders, such as mental retardation and muscular dystrophy, result from alterations occurring near the ends of chromosomes [10]. Furthermore, women with infertility showed a more pronounced telomere loss, than patients of the control group [11].

Ionizing radiation can also cause loss of chromosome telomeric regions. The underlying mechanism is still a matter of debate for scientists and cannot be clearly defined. Due to the fact that telomeres constitute only 0.02% of the entire human genome, the direct effect of radiation causing chromatid break and telomere loss is unlikely. The literature review suggests that the effects of reactive oxygen species can lead to formation of modified bases and breaks in certain DNA strands, including in telomeric regions [12]. The guanine-rich telomeric DNA sequences (-TTAGGG-) become a target of oxidative damage, since it is guanine that has the lowest oxidation/reduction potential among all nitrogenous bases. Guanine is easily oxidized to 8-oxoguanin considered to be a major oxidative stress biomarker [13]. Single-strand breaks in the G-rich strands regenerate poorly and persist in telomeres for longer

period of time [14]. The double-strand breaks can occur near the telomeres under exposure to ionizing radiation, which can result in chromosomal rearrangements. This represents one of the mechanisms underlying replicative aging of normal human cells caused by ionizing radiation. Cellular alterations affecting the effeciency of the DNA replication mechanism can contribute to replication fork stalling in telomeres and telomere loss [15].

There are also studies showing that chromosome telomeric region losses can result from the effects of different proteins, such as TZAP (telomeric zinc finger-associated protein) with 11 zinc fingers able to bind specifically to telomeres of the chromosomes and truncate them [16].

The use of FISH and locus-specific probes makes it possible to find alterations in telomeric regions of chromosomes. Telomere loss can affect one arm or both arms (chromosome telomere loss in sister chromatids).

The objective of the pilot study was the assessment of the telomere loss in peripheral blood lymphocytes of women exposed on the Techa River using the fluorescent staining method.

METHODS

Characteristics of examined individuals

Since the study of telomere loss was a pilot study conducted in the Urals Research Center for Radiation Medicine of FMBA of Russia for the first time, it was decided to limit the groups based on sex and assess the studied effect in the groups of women only at the initial stage. Inclusion criteria: female residents of the territories contaminated with radionuclides born in 1939–1959, who were chronically exposed at a wide dose range; women of the comparison group, who were not accidentally exposed.

Information about the studied sample and health status of the exposed individuals was provided by the "Database "Man" Department. Individualized cumulative external and internal doses (hereinafter referred to as doses) to RBM were calculated using the TRDS-2016 in the Biophysics laboratory [17]. The data on the history of cancer in the examined individuals were provided by the Epidemiological laboratory of the Urals Research Center for Radiation Medicine. Exclusion criteria: history of autoimmune diseases, cancer, exacerbation of chronic inflammatory diseases; history of taking cytostatics, antibiotics; individuals born in 1961 and later.

A total of 32 women were examined. The comparison group (hereinafter referred to as group 1) consisted of 10 individuals, among them six women had the absorbed doses to RBM within the range of 0.0001–0.01 Gy and four ones were not accidentally exposed. A total of 10 women were chronically exposed to the radiation doses of 0.2–0.9 Gy (hereinafter, group 2); the average dose was 0.64 ± 0.21 Gy. The group of individuals exposed to high doses (hereinafter referred to as group 3) included 12 women with the cumulative doses to RBM exceeding 1 Gy, since cytogenetic effects most often emerge under high-dose exposure [1]. The range was 1.01–4.6 Gy, and the mean dose was 1.7 ± 0.9 Gy (Table 1).

Obtaining the peripheral blood T-lymphocyte metaphase chromosome preparations

The cytogenetic study involved metaphases of the peripheral blood T lymphocytes stimulated with phytohemagglutinin (PHA). The chromosome preparations were obtained in accordance with the protocol accepted in the laboratory: cells were cultured for 54 h. Colcemid was added to a final concentration of 0.1 mg/mL three hours before the end of the cultivation period.

Table 1. Characteristics of examined women

Group	Number of donors, n	Mean age, years (range)	Mean Dose, Gy
Group 1 (comparison) (0–0.01 Gy)	10	65.4 ± 3.3 (62–71)	0.003 ± 0.003
Group 2 (exposed) (0.2–0.9 Gy)	10	74.5 ± 4.6 (69–81)	0.64 ± 0.21
Group 3 (exposed) (1–4.6 Gy)	12	74 ± 2.6 (71–80)	1.7 ± 0.9
All donors (0–4.6 Gy)	32	71.4 ± 5.4 (62–81)	

Hypotonic treatment of metaphase cells was performed 40–50 min before fixation with warm (37 °C) KCl solution (0.55%). Then the mixture was centrifuged. After that the metaphase plate fixation was performed (three parts of 95% ethanol: one part of glacial acetic acid) and chromosome preparations were made [18].

When pipetting the cell suspension on the glass slides, we sought to minimize excess spreading and overlap of chromosomes to achieve the best results, for each metaphase to be suitable for analysis. After the cell suspension was pipetted, the glass slides were heated on the slide dryer at 42 °C and then fluorescent staining was performed.

Method of telomere region staining by fluorescence in situ hybridization (FISH) with locus-specific probes

Probes from the Telomere FISH Kit/Cy3 (Dako; Denmark) were used. Chromosomes were stained in accordance with the probe manufacturer's protocol. The probe stains telomeric regions of chromosomes only, it does not recognize subtelomeric sequences [19]. The manufacturer produces this probe using the Cy3-conjugated peptide nucleic acid being a synthetic DNA analog capable of binding to DNA of chromosomes in accordance with the base pairing rules.

Fluorescently stained preparations were analyzed using the Axio Imager Z2 microscope (Zeiss; Germany) with the DAPI and SpO filters and the Isis software. The Metafer system for metaphase plate search and digitization was configured to automatically acquire images of five frames for the SpO channel, which would differ in height from each other by half a micron. After Metafer took five frames, areas with the highest contrast were automatically selected in each frame in the background mode. This resulted in the final image, where all signals were sharp and high contrast, which improved accuracy of the analysis results. Thus, features of the ISIS software allow one to reliably determine the lack of telomeric signal in any chromatid. For that the digitized image is viewed using the DAPI-SpO filters, along with the black and white inverted image of the chromosome of interest.

When conducting analysis, telomere losses were divided into two types: chromatid and chromosome. Chromatid telomere loss was determined, when there was no telomeric signal in one of sister chromatids, while the other one was intact. Fig. 1 presents the chromosome 5 pair: all four telomeres can be seen in the left chromosome; in the right chromosome it can be seen that one q arm telomeric region is absent. When there were no telomeric signals in both sister chromatids, the telomere loss was considered to be chromosomal (Fig. 2). The lack of two signals in unpaired chromatids or in different arms of the same chromatid were considered as two single chromatid telomere losses.

Metaphases containing 46 chromosomes without overlapping or artifacts were included in the analysis. All the chromosomes were analyzed in each cell. A total of 25–100 cells per donor were counted. The data on telomere loss were entered in the analysis record.

Statistical data processing

Thus, the results of assessing 1,560 cells of 32 individuals aged 62–81 divided into three groups based on the exposure dose were used as baseline data for statistical analysis. All 46 chromosomes were examined in each cell, and the facts of chromatid or chromosome telomere loss were reported for the cell. The results were analyzed using the STATISTICA 10 software package (StatSoft; USA).

RESULTS

Baseline data by dose groups for both telomere loss variants (chromatid and chromosome) are provided in Fig. 3. The studied phenomenon (telomere loss in various dose groups) cannot be represented using normal distribution (Fig. 4), so the nonparametric Mann–Whitney U test was used for intergroup comparison of obtained results.

The lack of differences in the number of telomere losses (chromosome or chromatid) in individual cells between the dose groups was accepted as the null hypothesis. It was found that chromatid losses in the comparison group (group 1) and the group exposed to high radiation doses (group 3) were statistically significantly similar ($p > 0.33$), while the group exposed to medium doses (group 2) was statistically

Fig. 1. Example of finding telomere loss in the red-blue filter and inverted image. All four telomeres are visible in the *left* cnromosome. An example of telomere loss in one q arm chromatid is provided on the *right*
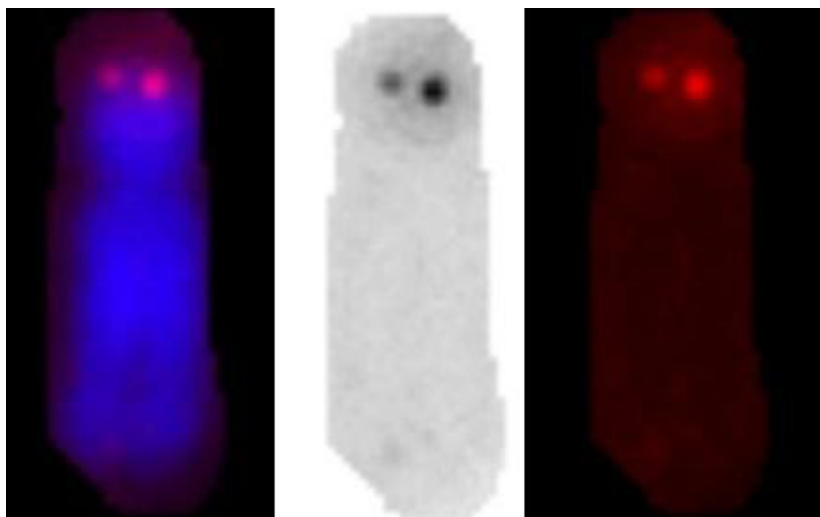
Fig. 2. Example of finding chromosome telomere loss in the red-blue filter and inverted image. No telomeres can be seen in both q arms

significantly different from these two groups ($p < 0.05$). Statistically significant differences between all groups were reported for chromosome telomere loss ($p < 0.05$). Thus, it can be concluded that the average number of chromatid losses in the second group is higher and is statistically significantly different from that in other groups.

Fig. 5 presents box plots of baseline data for each exposure group (rectangles represent the 5th and 95th percentiles, the central point represents the median, and whiskers correspond to minimum and maximum values). Table 2 contains the data of each studied subgroup for the chromatid and chromosome telomere loss: relative content in the cells, median, percentiles 5%–95%, minimum and maximum.

Loss of at least one telomeric region was found in 99.85% of the assessed cells.

Telomere loss in one of the chromatids was significantly more common, than chromosome telomere loss, in all groups ($p < 0.05$).

DISCUSSION

One function of the telomere is ensuring stability of the chromosome. That is why understanding the causes of changes in telomeric regions will shed light on the mechanisms

underlying the development of cancer, human genetic disorders, infertility, and aging of the body [20]. The ionizing radiation effects on human cells can cause alterations at chromatin level, such as DNA strand breaks, improper reunion of which can result in chromosomal rearanngements. These events lead to redistribution of chromatin across the arms of chromosomes and can affect distribution of genes in chromosomes, alter gene expression and, therefore, lead to development of various biomedical effects, which will eventually influence human health [21].

The pilot project presented in this paper is part of the study focused on assessing the telomeric regions of chromosomes conducted at the Laboratory of Radiation Genetics of the Urals Research Center for Radiation Medicine. Such parameters, as the telomere length and rate of inversions involving telomeric regions, were estimated previously in individuals chronically exposed at the Techa River [5, 6]. In this study, telomere loss in metaphase chromosomes of cultured peripheral blood T lymphocytes of the exposed residents of the Southern Urals was the research subject. Fluorescent staining of telomeric chromosome regions was used for this purpose. Analysis of the impact of radiation factor on the loss of chromosome telomeric regions was conducted. According to the data obtained, telomere loss is found in 99.85% of donor cells. It
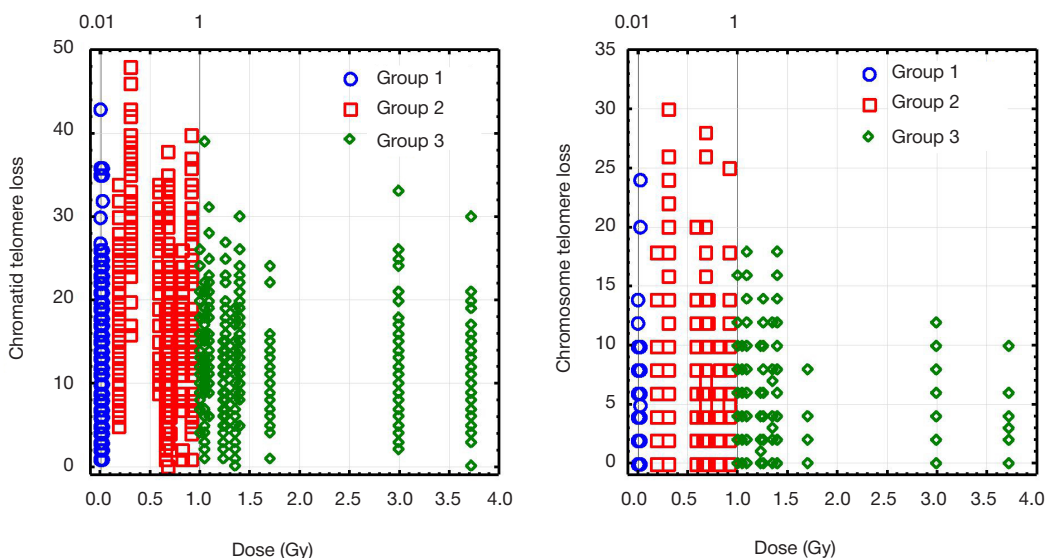
Fig. 3. Baseline data by dose groups
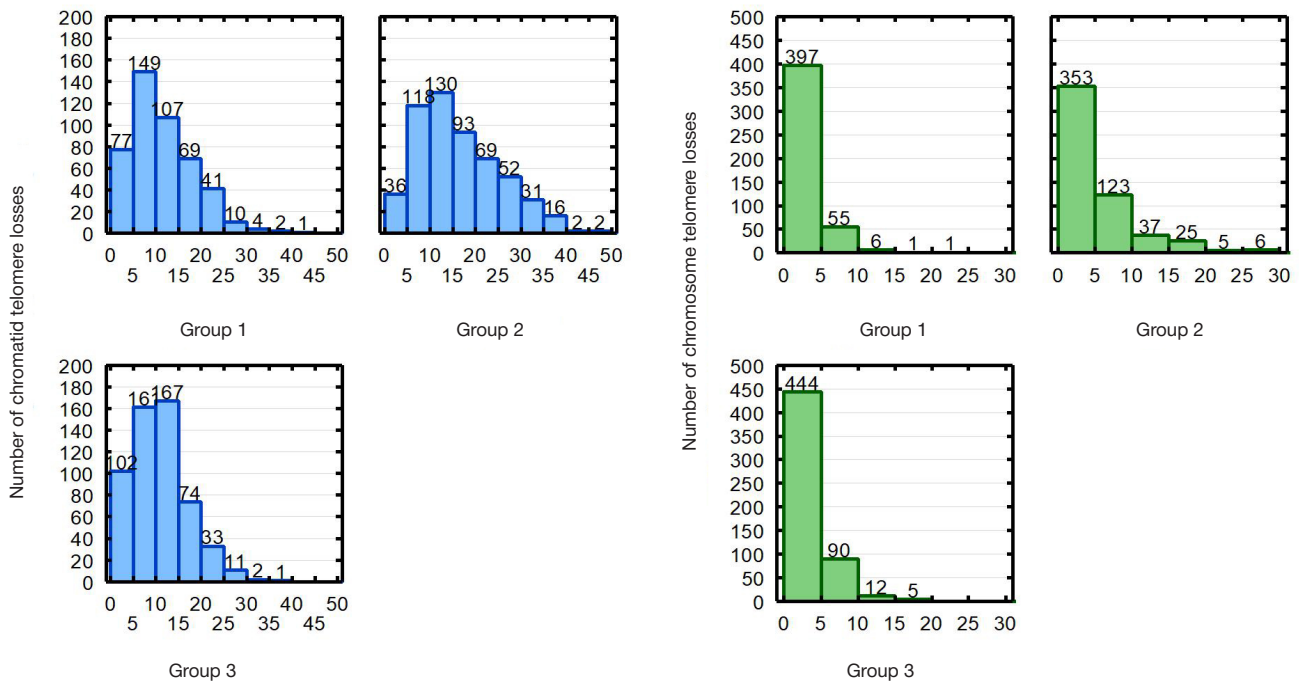
Fig. 4. Rate of chromatid and chromosome telomere loss observations in various exposed groups

has turned out that telomere loss in one of the two chromatids is statistically significantly more common in all groups. The loss of one sister telomere can result from replication defects in the S phase of the cell cycle, while chromosome telomere loss is likely to result from the loss in the pre-synthetic phase, when the chromosome represents one chromatid that is subsequently duplicated in the synthetic phase (consequently, the region with telomere loss is also duplicated yielding chromosome telomere loss) [22, 23]. Furthermore, low rate of chromosome telomere loss compared to chromatid telomere loss can be explained by the fact that these events occur with different probabilities. The chromosome occupies a certain space in the nucleus and normally does not overlap with chromatin of other chromosomes, therefore, the most common alterations are reported within the same chromatid. The ends of arms of sister chromatids lacking telomeric regions can be a marker of cell death. This means that the cell with the large number of telomere losses will be eliminated during cell division in order to preserve genome integrity.

Our study showed that single chromatid losses in the comparison group and the group exposed to high radiation doses were statistically significantly similar ($p > 0.33$), while the group exposed to medium doses was statistically significantly different from these two groups ($p < 0.05$). Statistically significant differences between all dose groups were reported for chromosome telomere loss ($p < 0.05$). Thus, it can be concluded that the average number of chromatid losses in the second group is higher and is statistically significantly different from that in other groups.

Against all expectations, the rate of telomere loss in the group of women exposed to the highest radiation doses showed no statistically significant differences from that in the comparison group. Yet we see that chronic exposure has some effect on the number of telomere losses, based on the results reported for group 2 showing a statistically significantly higher rate of chromosome and chromatid telomere loss compared to women of the comparison group who lived in similar socio-economic conditions but did not have doses of chronic exposure
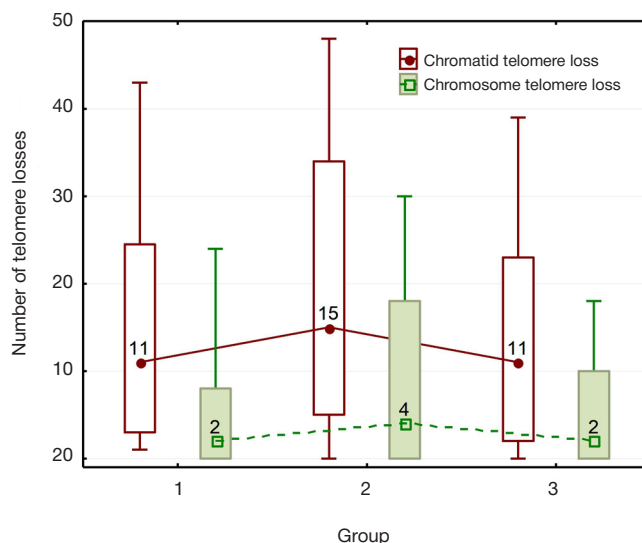
Fig. 5. Median, 5th and 95th percentiles, minima and maxima of baseline data for different exposure groups

Table 2. Median (5% and 95%) telomere loss in T-lymphocytes of exposed women of the Southern Urals

Group	Loss rate, %	Median	Minimum	Maximum	5%	95%
Chromatid telomere loss						
1	7	11	1	43	3	24.5
2	9	15	0	48	5	34
3	6	11	0	39	2	23
Chromosome telomere loss						
1	2	2	0	24	0	8
2	5	4	0	30	0	18
3	3	2	0	18	0	10

exceeding 0.01 Gy. It is likely that damaged chromosomes are eliminated from the cell after certain critical level is reached, As a result, the values of the comparison group and the group of donors exposed to the doses exceeding 1 Gy are at the same level and show no significant differences.

Such paradoxical data actually do not contradict the results of other cytogenetic studies, in which it was assumed that the criteria for selection of donors for cytogenetic testing can contribute to selection of the most radioresistant donors among exposed individuals, who have no autoimmune diseases, cancer or diabetes mellitus in their old age and do not take medicinal drugs that can affect the cytogenetic testing results. This is indirectly confirmed by the studies reporting that the rate of chromosomal aberrations in exposed individuals was equal to that calculated for non-exposed donors [24].

Thus, understanding the mechanisms responsible for the susceptibility of telomeric regions to the effects of external factors will provide new insights into the causes of human genetic disorders, infertility, aging, and cancer. Further investigation of chromosome structure using cytogenetic methods is important to understand the interplay between genes. It is necessary to continue this study and increase the size of the sample in order to confirm the findings, as well as to assess the impact of non-radiation factors.

CONCLUSIONS

In the sample of female residents of the Southern Urals with the combined chronic exposure within the range of absorbed doses to RBM of 0–4.6 Gy, it was shown that chromatid telomere losses reported for the comparison group and the group exposed to high radiation doses exceeding 1 Gy were statistically significantly similar ($p > 0.33$), while the group exposed to medium doses of 0.2–0.9 Gy was statistically significantly different from these two groups ($p < 0.05$). Statistically significant differences between all dose groups were reported for chromosome telomere loss ($p < 0.05$). Thus, the average telomere loss in the second group was higher and was statistically significantly different from that reported for the other groups of females of the same age range.

References

1. Akleev AV, redaktor. Posledstvija radioaktivnogo zagrjaznenija reki Techa. Cheljabinsk: Kniga, 2016; 400 s. Russian.
2. Akhmadullina Y. The Composition of Micronuclei in T-Lymphocytes in Women Affected by Chronic Radiation Exposure. Biology Bulletin. 2023; 50: 2986–96.
3. Shim G, Ricoul M, Hempel WM, et al. Crosstalk between telomere maintenance and radiation effects: A key player in the process of radiation-induced carcinogenesis. Mutation Research/Reviews in Mutation Research. 2014; 760: 1–17.
4. Ljuin B. Geny. M.: BINOM. Laboratorija znanij, 2011; 896 s. Russian.
5. Vozilova AV, Krivoshhapova JaV. Issledovanie chastoty inversij i kompleksnyh translokacij v T-limfocitah u obluchennyh zhitelej Juzhnogo Urala. Radiacionnaja biologija. Radiojekologija. 2022; 62 (4): 408–15. Russian.
6. Krivoshhapova JaV. Vlijanie hronicheskogo obluchenija na telomernye uchastki hromosom T-limfocitov perifericheskoj krovi cheloveka. Medicinskaja genetika. 2022; 21 (11): 40–43. Russian.
7. Muraki K, Nyhan K, Han L, et al. Mechanisms of telomere loss and their consequences for chromosome instability. Front Oncol. 2012; 2: 135.
8. Gisselsson D, Jonson T, Petersen A, et al. Telomere dysfunction triggers extensive DNA fragmentation and evolution of complex chromosome abnormalities in human malignant tumors. Proc Natl Acad Sci USA. 2001; 98: 12683–8.
9. Nakamura AJ, Redon CE, Bonner WM. Telomere-dependent and telomereindependent origins of endogenous DNA damage in tumor cells. Aging. 2009; 1: 212–8.
10. Mefford HC, Trask BJ. The complex structure and dynamic evolution of human subtelomeres. Nat Rev Genet. 2002; 3: 91–102.
11. M'kacher R, Colicchio B, Marquet V. Telomere aberrations, including telomere loss, doublets, and extreme shortening, are increased in patients with infertility. Fertility and Sterility. 2021; 115 (1): 164–73.
12. Coluzzi E, Colamartino M, Cozzi R, et al. Oxidative stress induces persistent telomeric DNA damage responsible for nuclear morphology change in mammalian cells. PLoS One. 2014; 9 (10): e110963. DOI: 10.1371/journal.pone.0110963. PMID: 25354277; PMCID: PMC4212976.
13. Marmij N, Morgunova G, Esipov D, i dr. 8-Okso-2'-dezoksiguanozin: biomarker kletochnogo starenija i okislitel'nogo stressa ili potencial'noe lekarstvo protiv vozrastnyh boleznej? Klinicheskaja gerontologija. 2016; 22 (9–10): 46–47. Russian.
14. Petersen S, Saretzki G, Von Zglinicki T. Preferential accumulation of single-stranded regions in telomeres of human fibroblasts. Exp Cell Res. 1998; 239: 152–60.
15. von Zglinicki T. Oxidative stress shortens telomeres. Trends Biochem. 2002; 27: 339–44.
16. Li JS, Miralles Fusté J, Simavorian T, et al. TZAP: A telomere-associated protein involved in telomere length control. Science. 2017; 10: 355 (6325): 638–41.
17. Shishkina EA, Napier BA, Preston DL, Degteva MO Dose estimates and their uncertainties for use in epidemiological studies of radiation-exposed populations in the Russian Southern Urals. PLoS ONE. 2023; 18 (8): e0288479. Available from: https://doi.org/10.1371/journal.pone.0288479.

18. IAEA. Cytogenetic dosimetry: applications in preparedness for and response to radiation emergencies. Vienna, Austria: IAEA. 2011; 229.

19. Nielsen PE, Egholm M, Berg RH, Buchardt O. Sequence-selective recognition of DNA by strand displacement with a thyminesubstituted polyamide. Sci. 1991; 254 (5037): 1497–500.

20. Akhmadullina YuR, Vozilova AV, Krivoshchapova YaV. The effect of chronic exposure on the parameters of cytogenetic markers of senescence in the residents of the Techa riverside settlements. Extreme medicine. 2024; (2): 53–63. DOI: 10.47183/mes.2024.018.

21. Hoffmann AA, Rieseberg LH. Revisiting the impact of inversions in evolution: from population genetic markers to drivers of adaptive

shifts and speciation. Annu Rev Ecol Evol Syst. 2008; 39: 21–42.

22. Eidelman YA, Salnikov IV, Slanina SV, Andreev SG. Chromosome folding promotes intrachromosomal aberrations under radiation- and nuclease-induced DNA breakage. Int J Mol Sci. 2021; 22 (22): 12186. DOI: 10.3390/ijms222212186.

23. Jullien L, Mestre M, Roux P, Gire V. Eroded human telomeres are more prone to remain uncapped and to trigger a G2 checkpoint response. Nucleic Acids Res. 2013; 41 (2): 900–11.

24. Vozilova AV. Assessment of the effect of chronic exposure on premature aging of human T-lymphocytes based on unstable chromosome aberrations. Extreme medicine. 2023; 2: 79–85. DOI: 10.47183/mes.2023.015.

Литература

1. Аклеев А. В., редактор. Последствия радиоактивного загрязнения реки Теча. Челябинск: Книга, 2016; 400 с.

2. Akhmadullina Y. The Composition of Micronuclei in T-Lymphocytes in Women Affected by Chronic Radiation Exposure. Biology Bulletin. 2023; 50: 2986–96.

3. Shim G, Ricoul M, Hempel WM, et al. Crosstalk between telomere maintenance and radiation effects: A key player in the process of radiation-induced carcinogenesis. Mutation Research/Reviews in Mutation Research. 2014; 760: 1–17.

4. Льюин Б. Гены. М.: БИНОМ. Лаборатория знаний, 2011; 896 с.

5. Возилова А. В., Кривощапова Я. В. Исследование частоты инверсий и комплексных транслокаций в Т-лимфоцитах у облученных жителей Южного Урала. Радиационная биология. Радиоэкология. 2022; 62 (4): 408–15.

6. Кривощапова Я. В. Влияние хронического облучения на теломерные участки хромосом Т-лимфоцитов периферической крови человека. Медицинская генетика. 2022; 21 (11): 40–43.

7. Muraki K, Nyhan K, Han L, et al. Mechanisms of telomere loss and their consequences for chromosome instability. Front Oncol. 2012; 2: 135.

8. Gisselsson D, Jonson T, Petersen A, et al. Telomere dysfunction triggers extensive DNA fragmentation and evolution of complex chromosome abnormalities in human malignant tumors. Proc Natl Acad Sci USA. 2001; 98: 12683–8.

9. Nakamura AJ, Redon CE, Bonner WM. Telomere-dependent and telomereindependent origins of endogenous DNA damage in tumor cells. Aging. 2009; 1: 212–8.

10. Mefford HC, Trask BJ. The complex structure and dynamic evolution of human subtelomeres. Nat Rev Genet. 2002; 3: 91–102.

11. M'kacher R, Colicchio B, Marquet V. Telomere aberrations, including telomere loss, doublets, and extreme shortening, are increased in patients with infertility. Fertility and Sterility. 2021; 115 (1): 164–73.

12. Coluzzi E, Colamartino M, Cozzi R, et al. Oxidative stress induces persistent telomeric DNA damage responsible for nuclear morphology change in mammalian cells. PLoS One. 2014; 9 (10): e110963. DOI: 10.1371/journal.pone.0110963. PMID: 25354277; PMCID: PMC4212976.

13. Мармий Н., Моргунова Г., Есипов Д., и др. 8-Оксо-2'-дезоксигуанозин: биомаркер клеточного старения и окислительного стресса или потенциальное лекарство против

возрастных болезней? Клиническая геронтология. 2016; 22 (9–10): 46–47.

14. Petersen S, Saretzki G, Von Zglinicki T. Preferential accumulation of single-stranded regions in telomeres of human fibroblasts. Exp Cell Res. 1998; 239: 152–60.

15. von Zglinicki T. Oxidative stress shortens telomeres. Trends Biochem. 2002; 27: 339–44.

16. Li JS, Miralles Fusté J, Simavorian T, et al. TZAP: A telomere-associated protein involved in telomere length control. Science. 2017; 10: 355 (6325): 638–41.

17. Shishkina EA, Napier BA, Preston DL, Degteva MO Dose estimates and their uncertainties for use in epidemiological studies of radiation-exposed populations in the Russian Southern Urals. PLoS ONE. 2023; 18 (8): e0288479. Available from: https://doi.org/10.1371/journal.pone.0288479.

18. IAEA. Cytogenetic dosimetry: applications in preparedness for and response to radiation emergencies. Vienna, Austria: IAEA. 2011; 229.

19. Nielsen PE, Egholm M, Berg RH, Buchardt O. Sequence-selective recognition of DNA by strand displacement with a thyminesubstituted polyamide. Sci. 1991; 254 (5037): 1497–500.

20. Ахмадуллина Ю. Р., Возилова А. В., Кривощапова Я. В. Влияние хронического облучения на показатели цитогенетических маркеров старения у жителей прибрежных сел реки Теча. Медицина экстремальных ситуаций. 2024; (2): 56–66. DOI: 10.47183/mes.2024.018.

21. Hoffmann AA, Rieseberg LH. Revisiting the impact of inversions in evolution: from population genetic markers to drivers of adaptive shifts and speciation. Annu Rev Ecol Evol Syst. 2008; 39: 21–42.

22. Eidelman YA, Salnikov IV, Slanina SV, Andreev SG. Chromosome folding promotes intrachromosomal aberrations under radiation- and nuclease-induced DNA breakage. Int J Mol Sci. 2021; 22 (22): 12186. DOI: 10.3390/ijms222212186.

23. Jullien L, Mestre M, Roux P, Gire V. Eroded human telomeres are more prone to remain uncapped and to trigger a G2 checkpoint response. Nucleic Acids Res. 2013; 41 (2): 900–11.

24. Возилова А. В. Оценка влияния хронического облучения на преждевременное старение Т-лимфоцитов человека на основе нестабильных хромосомных аберраций. Медицина экстремальных ситуаций. 2023; 2: 85–90. DOI: 10.47183/mes.2023.015.

ANALYSIS OF THE POSSIBILITIES OF THE FLOW-VOLUME CURVE ASSESSMENT BY THE CHANGES IN ITS SHAPE IN PATIENTS WITH OBSTRUCTIVE AIRWAY DISEASES

Desyatskova EM ✉, Grechenko VV, Soboleva VV

Pirogov Russian National Research Medical University, Moscow, Russia

In case of obstructive disorders, the flow–volume curve has a concave shape, but this feature is not given due attention. The analysis of the velocity indicators of the respiratory function (such as the peak expiratory flow (PEF) and forced expiratory flows (FEFs)) will significantly expand the diagnostic capabilities of the spirometry method. This paper aims to perform a comparative analysis of the diagnostic strength of the methods of the flow-volume curve assessment by the changes in its shape in patients with obstructive airway diseases to determine the most reliable one. The respiratory function of 540 patients was tested (234 are men (57 [36; 67] years) and 306 are women (59 [44; 69] years)), with the ratio of areas under the actual curve and the predicted curve calculated for each one, as well as the angle formed by the curve; the ratio of the actual FEF (henceforth referred to as FEF) to the predicted FEF, cut-off points to differentiate between obstructive diseases and health. On the basis of these results, we concluded whether the patient's bronchi were blocked. The results were then compared to the Knudson reference equations, with the test's operational characteristics calculated compared to the standard. The methods of assessing the angle β and the total concavity of the flow-volume curve have high diagnostic sensitivity (87.8% and 95.6% respectively). The assessment of the area under the curve (AEX-FV) has high diagnostic specificity (88.6%). The results obtained show sufficient diagnostic efficiency of the methods of flow-volume curve estimation by the changes in its shape. However, the use of these methods in isolation from the reference equations does not currently seem reasonable for clinical practice. It appears reasonable to use the reference equations and one of the methods of curve shape assessment together.

Keywords: spirometry, respiratory function, flow-volume curve

АНАЛИЗ ВОЗМОЖНОСТЕЙ МЕТОДА ОЦЕНКИ КРИВОЙ «ПОТОК–ОБЪЕМ» ПО ИЗМЕНЕНИЮ ЕЕ ФОРМЫ ПРИ ОБСТРУКЦИИ БРОНХОВ

Е. М. Десяцкова ✉, В. В. Греченко, В. В. Соболева

Российский национальный исследовательский медицинский университет имени Н. И. Пирогова, Москва, Россия

При обструкции бронхов кривая «поток–объем» имеет характерную вогнутую форму, однако данному признаку не уделяют должного внимания. Анализ скоростных показателей функции внешнего дыхания (ФВД), таких как пиковая объемная скорость выдоха (ПОС) и максимальные объемные скорости выдоха (МОС), позволит расширить диагностические возможности спирометрии. Цель работы — провести сравнительный анализ диагностической эффективности методов оценки кривой «поток–объем» по изменению ее формы на фоне обструктивных нарушений. Оценено 540 проб ФВД пациентов (234 мужчины 57 [36; 67] лет и 306 женщин 59 [44; 69] лет), для каждого определено процентное отношение площадей под фактической кривой и кривой предполагаемой нормы, рассчитан угол, образованный кривой, определено процентное отношение фактических МОС с предположительно нормальными, рассчитаны отрезные точки с целью разграничения обструктивных нарушений и нормы. Сформировано заключение о наличии или отсутствии у пациента обструкции бронхов. Результаты сравнивали с заключениями, полученными с помощью системы Knudson, с расчетом операционных характеристик теста относительно стандарта. Показано, что методы оценки угла β и общей вогнутости кривой обладают высокими значениями чувствительности (87,8% и 95,6% соответственно), а оценка площади под кривой «поток–объем» (AEX-FV) обладает высоким значением специфичности (88,6%). Таким образом, продемонстрирована достаточная диагностическая эффективность методов оценки кривой по изменению ее формы. Однако использование этих методов в отрыве от принятых систем расчета должных не видится целесообразным. Логичным представляется совместное использование системы расчета должных и одного из методов оценки кривой по форме.

Ключевые слова: спирометрия, ФВД, кривая «поток–объем»

In patients with obstructive airway diseases the flow-volume curve is characteristically concave to the X axis, with the level of concavity correlating with the severity of the airway obstruction [1–3]. In practice, however, the changes in the shape of the curve are often ignored when interpreting the results, with only the difference between the patient's respiratory function test results and the approximated values taken into account [1]. Even if the shape is assessed, it is assessed visually, as proper mathematical parameters for assessing concavity have not yet been accepted into clinical practice. Eye estimates are obviously very subjective, because the method requires a certain level of experience and qualifications from the medical professional. Furthermore, it's not rare for the concavity to still be present even when the the patient's respiratory function score falls over 100% of the predicted score, showing a lack of any respiratory dysfunction. If that's the case, even though the patient's life history together with the characteristic shape of the curve might suggest otherwise, these points will not be reflected in the diagnosis, making it impossible to objectively evaluate the patient's condition.

It is also worth noting that diagnosing the patient using only some of the respiratory function scores (including the forced expiratory volume in one second (henceforth referred to as FEV1) decrease rate, the FVC or VC (vital and forced vital capacities) decrease rate and the Tiffno and Gensler indices), on the one hand, decreases the time needed to interpret the results of one test, but, on the other, artificially narrows the clinical possibilities of spirometry. In routine practice, the air flow rate is often not considered, even though it shows the condition of the bronchial tree by levels [3] and could provide a clearer understanding of the patient's condition without resorting to the use of expensive and time-consuming diagnostic procedures (such as chest X-ray or bronchoscopy).

Attempts have been made to make the visual assessment of the curve more objective through analysing additional parameters calculated from the flow-volume curve. For example, one review paper considers several parameters, i.e. evaluation of the angle formed by the curve, evaluation of the area ratio (AEX-FV) and evaluation of the degree of deviation of the actual FEF values from the ones approximated by the authors [4]. However, despite the scientific community's interest in the methods described [5–8], as of today, there is still no definitive understanding of their effectiveness in clinical practice. Therefore, this study aims to conduct a comparative analysis of the diagnostic efficiency of the methods of the flow-volume curve assessment based on changes in its shape in patients with obstructive airway diseases in order to determine the most reliable one.

METHODS

The materials for this study were collected from patients of the Research and Clinical Centre No. 2 of the Petrovsky Russian National Research Center. The following criteria for inclusion in the study were used: seeking medical attention due to conditions included in the J00-J99 ('Diseases of the respiratory system') and Z00-Z99 ('Factors influencing health status and contact with health services') ICD-10 code ranges; the patient's consent to tests; the spirometry test complies with the quality standards required by the European Respiratory Society and the American Thoracic Society (ATS/ERS standards) [9], adopted by the Russian Respiratory Society [1]; the patient is over 18.

540 patients were selected, of whom 234 (43.3%) were male and 306 (56.7%) were female. The mean age was 57 [36; 67]

years in men and 59 [44; 69] years in women. To understand the efficiency of the considered methods in patients of different ages, the sample group was divided into 10-year age intervals. The 18–30 years group included 76 patients, the 31–40 years group included 50 patients, the 41–50 years group included 57 patients, the 51–60 years group included 109 patients, the 61–70 years group included 134 patients, the 71–80 years group included 93 patients, and the 81–90 years group included 21 patients.

For each patient:

1) the presence or absence of bronchial obstruction was determined (by calculating the Tiffno or Gensler index);

2) if obstruction was present, its the degree was determined (by the decrease in the patient's FEV1 relative to the Knudson reference equations);

3) the percentage ratio of areas under the actual flow-volume curve and the assumed normal curve was determined;

4) the angle formed by the curve was calculated;

5) the percentage ratio of the actual and estimated normal FEF was determined.

Respiratory function test results were saved in MS Excel software (USA). The following patient data were recorded: sex and age; height and weight; results of slow vital capacity tests (VC); results of forced vital capacity tests (forced air flow volume and rate, as well as calculated Tiffno and Gensler indices).

Lagrange interpolation was used to calculate the function for the downward part of the flow-volume curve. It was demonstrated that for a curve with interpolation nodes at PEF, FEF_{25}, FEF_{50}, FEF_{75} and FVC, the interpolation function is the following:

$$P_n(x) = ax^4 + bx^3 + cx^2 + dx + e, \qquad (1)$$

where a, b, c, d, e are the coefficients of the interpolation polynomial calculated individually for each patient.

The numerical integration of the above function was used to calculate the AEX-FV. The definite integral of the type

$$\int_{\alpha}^{\beta}(ax^4 + bx^3 + cx^2 + dx + e)dx, \qquad (2)$$

where α, β are the boundaries of the definite integral, was approximately calculated using the left Riemann sum.

The angle β was calculated using the formula for determining the angle between two vectors with the vector dot product
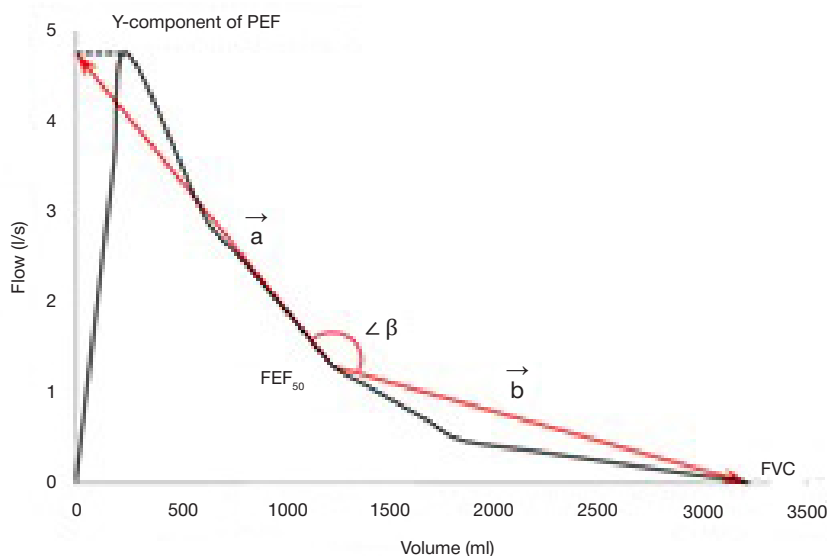

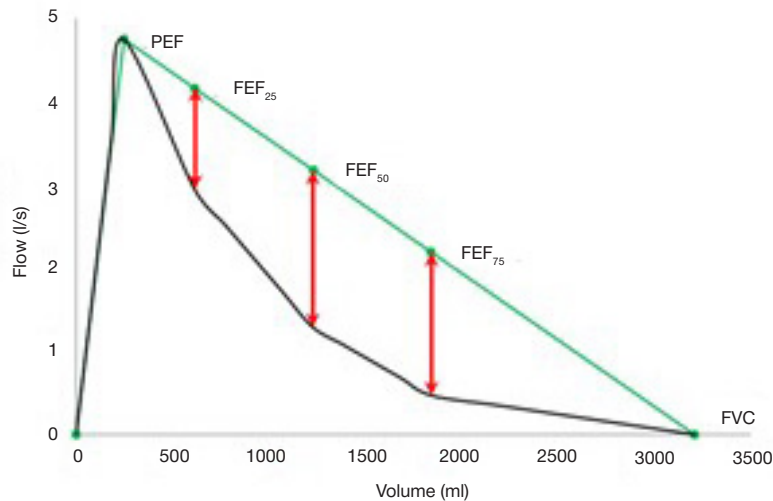**Fig. 1.** Calculating angle β (using FEF_{50} angle as example).

Fig. 2. Determining the degree of deviation of actual FEF values from the predicted values (using a difference of over 200 ml between FVC and VC as example).

and vector length in coordinate form. The two vectors used for calculating the angle were vector a, defined as (FEF_{50}-PEF projection on the Y axis) and vector b, defined as (FEF_{50}-FVC) (Fig.1) [4], with FEF_{50} or FEF_{75} taken as FEFx. For each patient, the FEF_{50} angle was calculated, with the angle centered on FEF_{75} considered to be the angle β, if the actual FEF_{50} exceeded the estimated value of the index.

Therefore, the formula for determining the angle between two vectors is the following:

$$cos(ab) = \frac{-\frac{1}{2}FVC \times (FVC - \frac{1}{2}FVC) - (PEF - FEF_x) \times FEF_x}{\sqrt{(\frac{1}{2}FVC)^2 + (PEF - FEF_x)^2} \times \sqrt{(FVC - \frac{1}{2}FVC)^2 + (FEF_x)^2}}, \quad (3)$$

with FEF_{50} or FEF_{75} taken as FEF_x.

Approximate values of the air flow rate for general concavity assessment were determined using the equation of the straight line connecting the PEF and FVC points. If the difference between FVC and VC is greater than 200 ml, it is more viable to replace FVC with VC and construct a straight line connecting the PEF and VC points. Like in the previous case, the approximate values of the air flow rate will presumably be located on this straight line, but in this case they will be ¼, ½ и ¾ FVC (not VC), because otherwise the logic of the calculations will contradict FEF_{25}, FEF_{50} и FEF_{75} as defined by the Russian Respiratory Society [1], according to which each of these values is equal to the respective fraction of FVC (not VC). This method is visually represented in Fig. 2.

Our assessment of the respiratory function is based on the accepted spirometry results interpreting system, namely, calculating the percentage of the deviation of the actual value from the reference value [1, 2]. This provides for further comparison of the obtained ratio with reference intervals. Because the population size of this study was insufficient to define comparison intervals, it was decided to calculate cut-off points for each method of flow-volume curve assessment by shape

that could unambiguously differentiate between healthy patients and patients with obstructive disorders in the test sample. To determine cut-off points, patients ($n = 81$) were selected from the primary analysis sample who were considered healthy for the purposes of this study, meaning their Tiffno index was greater than 70% [1, 2] and the visual assessment by the functional diagnosis physician did not reveal any abnormalities. The mean values of AEX-FV, angle β, and the percentages of deviation of the actual FEF values from the predicted values were calculated for the obtained test sample. These values were taken as cut-off points. Obstructive disorders were considered confirmed in patients with FEF values smaller than the cut-off points.

The testing of respiratory function by spirometry was performed on a SpiroS-100 spirometer manufactured by the Russian company AltoMedica [10]. Statistical analysis was performed by calculating the absolute and relative frequencies of occurrence of presence and absence of obstruction for each of the described methods of assessing the flow-volume curve shape with further calculation of the operational characteristics of the test relative to the standard (using contingency tables). The Knudson reference equations for respiratory function were chosen as reference in the calculation of operational characteristics because they do not have any restrictions on patients' characteristics (unlike, for example, the Clement [11, 12], GLI [13], and ECCS [14] reference equations). Statistical analysis was performed in IBM SPSS Statistics for Windows v.27.0 (USA), and MedCalc by MedCalc Software Ltd v.23.0.6 (Belguim).

RESULTS

AEX-FV

For each patient in the training sample, the area under the actual flow-volume curve (AEX-FV) was calculated by numerical

Table 1. Cut-off points for AEX-FV evaluation, calculated for the age ranges in question

Age range	Mean area ratio, %	Cut-off point, %
18–30 years	91.7 ± 5.9	86
31–40 years	91.6 ± 5.1	87
41–50 years	91.7 ± 2.7	89
51–60 years	88.9 ± 3.6	85
61–70 years	90.5 ± 4.5	86
71–90 years	82.2 ± 7.8	74

Note: mean area ratios are presented as (mean value ± standard deviation), cut-off point values are rounded to the next integer.

Table 2. Cut-off points for angle β, calculated for the considered age ranges

Age range	$\angle\beta$ at FEF_{50}, °	$\angle\beta$ cut-off point at FEF_{50}, °	$\angle\beta$ at FEF_{75}, °	$\angle\beta$ cut-off point at FEF_{75}, °
18–30 years	166.9 ± 8.9	158	162.3 ± 6.9	155
31–40 years	170.5 ± 8.7	162	157.5 ± 8.5	149
41–50 years	170.0 ± 8.7	161	155.8 ± 7.4	148
51–60 years	169.7 ± 11.5	158	152.7 ± 5.8	147
61–70 years	169.5 ± 6.4	163	148.2 ± 6.8	141
71–90 years	171.6 ± 9.4	162	148.2 ± 6.4	142

Note: mean angle values are presented as (mean value ± standard deviation), cut-off point values are rounded to the next integer.

integration. The area under the predicted values curve was defined as the area of a right-angled triangle equal to half of the product of its cathetes, i.e.

$$S\ (AEX\ Normal) = \tfrac{1}{2} \times PEF \times FVC. \tag{4}$$

In order to come to a conclusion about the reference figure for the percentage ratio of AEX-FV to AEX-Normal, which will allow unambiguous differentiation between healthy patients and patients with obstructive disorders, the mean value for the ratio of AEX-FV to AEX-Normal was calculated (see Table 1). Given the close cut-off point values for all age groups except patients over 70 years of age, an area ratio of 85% was taken as the single cut-off point for these age ranges (calculated as the average between the cut-off point values for the age ranges). Using the AEX-FV evaluation method, 38.1% of patients (206) were found to be healthy and 61.9% of patients (334) were found to have obstructive disorders, whereas with the Knudson reference equations the results were 31.1% of patients (168) and 68.9% of patients (372) respectively.

Angle β

The preliminary calculation of the mean angle showed that in some cases, even though the angle is within normal range and the diagnostic conclusion states the patient is healthy, the concavity of the flow-volume curve towards the X axis is characteristic of obstructive airway diseases. This is caused by a decrease in the FEF_{75} index, which was not previously taken into account in research papers on this issue [4,5]. For this reason, we also calculated the mean angle centred on FEF_{75}, provided that the actual FEF_{50} value exceeds the predicted value. The cut-off points that allow unambiguous differentiation between healthy patients and patients with obstructive disorders are presented in Table 2. Using the angle β evaluation method, 26.9% of patients (145) were found healthy and 73.1% of patients (395) were found to have obstructive disorders, whereas with the Knudson reference equations the results were 31.1% of patients (168) and 68.9% of patients (372) respectively.

Assessment of the general concavity

As per the accepted procedure of generating an assessment report, predicted maximum flow rate values at 25%, 50% and 75% FVC were calculated for each patient, and the percentage deviation of the actual values from the approximate ones was determined. The approximate values were calculated using the following two-point form:

$$\frac{x-x_1}{x_2-x_1} = \frac{y-y_1}{y_2-y_1}. \tag{5}$$

Therefore, FEF was determined at the given levels using the following equation:

$$FEF_y = \frac{(FEF_x - PEF)_x \times (FVC_y - PEF_y)}{FVC_x - PEF_x} + PEF_y, \tag{6}$$

where x and y are the point's positions on the X and Y axis, respectively. It should be noted that in cases where the patient's actual FEF exceeded the predicted value, the actual value was considered normal, and the values' ratios were considered to be 100%. This does not contradict the Russian Spirometry Standards, as the approved algorithm for the evaluation of spirometry indicators allows for a percentage ratio of the actual values to predicted ones greater than 100%, with the value exceeding this mark taken as 100% and considered normal.

We analysed the entire test sample in this manner, determining cut-off points for each considered age range (Table 3). Using the general concavity method, 18.5% of patients (100) were found to be healthy and 81.5% of patients (440) were found to have obstructive disorders, whereas with the Knudson reference equations the results were 31.1% of patients (168) and 68.9% of patients (372) respectively. More obstructive disorders can be detected using the general concavity method compared to the Knudson reference equations (Table 4).

DISCUSSION

The operational characteristics of AEX-FV evaluation are, in general, quite balanced, with the maximum and minimum sensitivity of the test recorded in patients from 61 to 70 years

Table 3. Cut-off points for maximum flow rate at the given FVC percentages calculated for the considered age ranges.

Age range	FEF_{25}	FEF_{50}	FEF_{75}
18–30 years	0.00 [0.00; 1.61]	0.00 [0.00; 1.36]	0.00 [0.00; 2.75]
31–40 years	0.00 [0.00; 4.69]	0.00 [0.00; 11.84]	0.39 [0.00; 13.07]
41–50 years	1.51 [0.00; 7.74]	1.79 [0.00; 5.22]	10.66 [0.00; 21.19]
51–60 years	0.00 [0.00; 6.71]	0.05 [0.00; 12.36]	13.21 [1.98; 20.34]
61–70 years	0.50 [0.00; 5.35]	0.00 [0.00; 5.67]	23.53 [13.96; 36.71]
71–90 years	0.00 [0.00; 3.48]	4.86 [0.00; 14.09]	26.55 [11.08; 32.28]

Note: cut-off point values are presented as Me [Q_1; Q_3].

Table 4. Results of the diagnostic efficiency evaluation of the methods of estimating the flow-volume curve by shape change in the considered age ranges

GS	Diagnosis in the patient's medical history		
RE	AEX-FV	Angle β	General concavity
18–30 years			
n = 76			
S	0.824. 95% CI (0.792; 0.831)	0.880. 95% CI (0.711; 0.967)	1.000. 95% CI (0.857; 1.000)
Sp	0.933. 95% CI (0.682; 0.997)	0.706. 95% CI (0.623; 0.749)	0.529. 95% CI (0.459; 0.529)
31–40 years			
n = 50			
S	0.679. 95% CI (0.544; 0.755)	0.821. 95% CI (0.685; 0.917)	0.929. 95% CI (0.801; 0.987)
Sp	0.864. 95% CI (0.692; 0.961)	0.727. 95% CI (0.554; 0.848)	0.636. 95% CI (0.474; 0.711)
41–50 years			
n = 57			
S	0.694. 95% CI (0.586; 0.754)	0.833. 95% CI (0.725; 0.916)	0.917. 95% CI (0.818; 0.976)
Sp	0.857. 95% CI (0.671; 0.960)	0.619. 95% CI (0.434; 0.761)	0.476. 95% CI (0.307; 0.579)
51–60 years			
n = 109			
S	0.805. 95% CI (0.751; 0.832)	0.854. 95% CI (0.797; 0.899)	0.890. 95% CI (0.836; 0.935)
Sp	0.889. 95% CI (0.726; 0.970)	0.667. 95% CI (0.495; 0.805)	0.556. 95% CI (0.390; 0.693)
61–70 years			
n = 134			
S	0.916. 95% CI (0.884; 0.934)	0.899. 95% CI (0.867; 0.923)	0.975. 95% CI (0.946; 0.992)
Sp	0.800. 95% CI (0.546; 0.944)	0.667. 95% CI (0.412; 0.860)	0.667. 95% CI (0.435; 0.806)
71–80 years			
n = 93			
S	0.674. 95% CI (0.640; 0.685)	0.930. 95% CI (0.899; 0.949)	0.965. 95% CI (0.941; 0.988)
Sp	0.857. 95% CI (0.434; 0.992)	0.714. 95% CI (0.325; 0.946)	0.429. 95% CI (0.128; 0.714)
81–90 years			
n = 21			
S	0.789. 95% CI (0.706; 0.789)	0.947. 95% CI (0.865; 0.947)	1.000. 95% CI (0.950; 1.000)
Sp	1.000. 95% CI (0.209; 1.000)	1.000. 95% CI (0.218; 1.000)	0.500. 95% CI (0.028; 0.500)

Note: GS — gold standard, RE — reference equations, S — diagnostic sensitivity, Sp — diagnostic specificity.

old (0.916) and from 71 to 80 years old (0.674) respectively, and the maximum and minimum specificity recorded in patients from 18 to 30 years old (0.933) and from 61 to 70 years old (0.800) respectively. In elderly patients there is a gradual weakening of respiratory muscles, diagnosed in spirometric examination as a degree of obstruction, while the normal triangular flow-volume curve is almost never found. Thus, in elderly patients there is a characteristic difference between AEX-FV and AEX-Normal, which is natural. Given this age-specific pattern, screening for respiratory pathologies in this age range is somewhat difficult. The results can also be explained by the structure of the test sample used in this study, which included predominantly patients with confirmed respiratory pathologies, whereas to assess the screening power of the test, a large sample of healthy patients is required. In this case, it is reasonable to increase the sample heterogeneity, but due to the limited research capacity of this study, this was not possible.

The method of calculating the angle β formed by the flow-volume curve has a sufficiently high diagnostic sensitivity for all age ranges in question, indicating the significant potential of this method for diagnostics. Additionally, it has the advantage of disorder assessment by levels, unlike, for example, the previously discussed AEX-FV assessment, which evaluates the state of the bronchial tree as a whole. As for specificity, the AEX-FV values were informative in all age groups (except

for the elderly and senile), while the β-angle values were not informative in most age groups. Similarly to the AEX-FV evaluation method, this can be explained by the structure of the analysed data and the higher number of sick patients compared to healthy patients.

As for the assessment of the general flow-volume curve concavity, the sensitivity of this method, similarly to the sensitivity of angle β evaluation, is consistently high for all age groups, indicating a significant quality of diagnostic conclusions based on this method. The specificity, similarly to angle evaluation, is uninformative in all considered age groups.

Therefore, all considered methods of flow-volume curve evaluation by its shape change can be used as clarifying parameters in complicated or ambiguous clinical cases due to their substantial diagnostic capabilities. To improve the quality of spirometric screening for respiratory diseases, the calculation of the ratio of the area under the actual curve to the area under the predicted curve, i.e. AEX-FV, can be used as a clarifying criterion for patients under 70 years of age.

It reasonable to be concerned that the evaluation logic inherent for the methods considered may lead to more frequent false positives compared to the traditional methodology. However, in our opinion, a false positive in the context of this Russian Respiratory Society method [1] will be understood as a hidden obstruction that is not directly detected by reference

equations, Tiffno or Gensler indices, or new parameters for assessing FVC indices (in particular, the lower limit of normality (LLN) [15–17] and z-score [1, 2, 15]). It is our opinion that in this case, heightened obstructive ventilation disorder vigilance of methods of flow-volume curve assessment based on changes in its shape is justified, since hidden obstruction is considered a preclinical stage of COPD and may subsequently lead to respiratory failure [18].

CONCLUSIONS

Today, the percentage of respiratory diseases in the global mortality rate remains significant. For example, COPD, a disease with a pronounced obstructive syndrome, is the third most frequent cause of death in the world. Pathologies of this kind can be diagnosed using various methods, but the simplest and most accessible one is spirometry with the flow-volume curve tracked. Spirometry is based on comparing the obtained values of the patient's respiratory function with the predicted values calculated according to a given system. This approach

has been used in clinical practice for a long time, and has often been criticised. It may be beneficial to consider using new indicators or methods for clarification of the conclusions based on the flow-volume curve. The present study of diagnostic efficiency of flow-curve evaluation based on changes in its shape in patients with obstructive disorders allows us to consider them as highly accurate methods of diagnostics of obstructive processes in bronchi (in particular, the methods of assessing the angle β and the total concavity of the flow-volume curve with the mean diagnostic sensitivity of 87.8% and 95.6%, respectively). In contrast, the AEX-FV assessment has high mean specificity (88.6%), suggesting that it is more oriented towards preventative screening of obstructive type respiratory disorders. However, these methods should not be used in isolation from the accepted reference equations, as, in our opinion, doing so is not reasonable for clinical practice. It appears more logical to use them together to mutually improve diagnostic capabilities. It is this joint use, in our opinion, that can potentially have the greatest efficiency for practical medicine. Thus, the direction of future research in this area is identified.

References

1. Metodicheskie rukovodstva po ispol'zovaniju metoda spirometrii. Rossijskoe respiratornoe obshhestvo, Rossijskaja associacija specialistov funkcional'noj diagnostiki, Rossijskoe nauchnoe medicinskoe obshhestvo terapevtov. M., 2023; 64 s. Russian.
2. Struchkov PV, Drozdov DV, Lukina OF. Spirometrija: rukovodstvo dlja vrachej. M., 2023; 112 s. Russian.
3. Trisvetova EL, Fedorovich SE. Funkcional'nye metody issledovanija vneshnego dyhanija: ucheb.-metod. posobie. Minsk: BGMU, 2016; 28 s. Russian.
4. Maritano Furcada J, Rodríguez CI, Wainstein EJ, Benito HJ. Graphical Analysis Methods in Obstructive Spirometry: Does a Picture Speak More Than a Thousand Words? Arch Bronconeumol (Engl Ed). 2019; 55 (5): 272–4.
5. Ioachimescu OC, Stoller JK. Area under the expiratory flow-volume curve (AEX): actual versus approximated values. J Investig Med. 2020; 68 (2): 403–11.
6. Ioachimescu OC, McCarthy K, Stoller JK. Area under the expiratory flow-volume curve: normative values in the National Health and Nutrition Survey (NHANES) study. J Investig Med. 2022; 70 (5): 1247–57.
7. Kapp MC, Schachter EN, Beck GJ, et al. The shape of the maximum expiratory flow volume curve. Chest. 1988; 94 (4): 799–806.
8. Zhang Y, Xiong X, Dai F, et al. Curvilinearity of a maximum expiratory Flow-Volume curve: a useful indicator for assessing airway obstruction in children with asthma. Respir Care. 2020; 65 (4): 427–36.
9. Stanojevic S, Kaminsky DA, Miller M, et al. ERS/ATS technical

standard on interpretive strategies for routine lung function tests. Eur Respir J. 2021; 60 (1): 2101499.
10. ALTOMEDIKA. Dostupno po ssylke: http://www.altomedika.ru.
11. Klement RF, Zilber NA. Funkcional'no-diagnosticheskie issledovanija v pul'monologii: Metodicheskie rekomendacii. SPb., 1993; 47 s. Russian.
12. Klement RF, Lavrushin AA, Ter-Pogasjan PA, Kotegov Yu. M. Instrukcija po primeneniju formul i tablic dolzhnyh velichin osnovnyh spirograficheskih pokazatelej. L., 1986. Russian.
13. Graham BL, Steenbruggen I, Miller MR, et al. Standardization of spirometry 2019. Update an official American Thoracic Society and European Respiratory Society technical statement. Am J Respir Crit Care Med. 2019; 200 (8): 70–88.
14. Quanjer PH, Tammeling GJ, Cotes JE, et al. Lung volumes and forced ventilatory flows. Report Working Party Standartisation of Lung Function Tests, European Community for Steel and Coal. Official Statement of the European Respiratory Society. Eur Respir J. 1993; 6 (16): 5–40.
15. Kameneva MYu. Spirometrija: kak ocenit' rezul'taty? Bjulleten' fiziologii i patologii dyhanija. 2022; 83: 91–99. Russian.
16. Pellegrino R, Viegri G, Brusasco V, et al. Interpretative strategies for lung function tests. Eur Respir J. 2005; 26 (5): 948–68.
17. Stanojevic S, Wade A, Stocks J, et al. Reference ranges for spirometry across all ages: a new approach. Am J Respir Crit Care Med. 2008; 177: 253–60.
18. Sukhovskiĭ VS, Strelis AK, Grigor'ev EG, Sukhovskaia VV. Probl Tuberk Bolezn Legk. 2008; 7: 39–43.

Литература

1. Методические руководства по использованию метода спирометрии. Российское респираторное общество, Российская ассоциация специалистов функциональной диагностики, Российское научное медицинское общество терапевтов. М., 2023; 64 с.
2. Стручков П. В., Дроздов Д. В., Лукина О. Ф. Спирометрия: руководство для врачей. М., 2023; 112 с.
3. Трисветова Е. Л., Федорович С. Е. Функциональные методы исследования внешнего дыхания: учеб.-метод. пособие. Минск: БГМУ, 2016; 28 с.
4. Maritano Furcada J, Rodríguez CI, Wainstein EJ, Benito HJ. Graphical Analysis Methods in Obstructive Spirometry: Does a Picture Speak More Than a Thousand Words? Arch Bronconeumol

(Engl Ed). 2019; 55 (5): 272–4.
5. Ioachimescu OC, Stoller JK. Area under the expiratory flow-volume curve (AEX): actual versus approximated values. J Investig Med. 2020; 68 (2): 403–11.
6. Ioachimescu OC, McCarthy K, Stoller JK. Area under the expiratory flow-volume curve: normative values in the National Health and Nutrition Survey (NHANES) study. J Investig Med. 2022; 70 (5): 1247–57.
7. Kapp MC, Schachter EN, Beck GJ, et al. The shape of the maximum expiratory flow volume curve. Chest. 1988; 94 (4): 799–806.
8. Zhang Y, Xiong X, Dai F, et al. Curvilinearity of a maximum expiratory Flow-Volume curve: a useful indicator for assessing

airway obstruction in children with asthma. Respir Care. 2020; 65 (4): 427–36.

9. Stanojevic S, Kaminsky DA, Miller M, et al. ERS/ATS technical standard on interpretive strategies for routine lung function tests. Eur Respir J. 2021; 60 (1): 2101499.

10. АЛЬТОМЕДИКА. Доступно по ссылке: http://www.altomedika.ru.

11. Клемент Р. Ф., Зильбер Н. А. Функционально-диагностические исследования в пульмонологии: Методические рекомендации. СПб., 1993; 47 с.

12. Клемент Р. Ф., Лаврушин А. А., Тер-Погасян П. А., Котегов Ю. М. Инструкция по применению формул и таблиц должных величин основных спирографических показателей. Л., 1986.

13. Graham BL, Steenbruggen I, Miller MR, et al. Standardization of spirometry 2019. Update an official American Thoracic Society and European Respiratory Society technical statement. Am J Respir Crit Care Med. 2019; 200 (8): 70–88.

14. Quanjer PH, Tammeling GJ, Cotes JE, et al. Lung volumes and forced ventilatory flows. Report Working Party Standartisation of Lung Function Tests, European Community for Steel and Coal. Official Statement of the European Respiratory Society. Eur Respir J. 1993; 6 (16): 5–40.

15. Каменева М. Ю. Спирометрия: как оценить результаты? Бюллетень физиологии и патологии дыхания. 2022; 83: 91–99.

16. Pellegrino R, Viegri G, Brusasco V, et al. Interpretative strategies for lung function tests. Eur Respir J. 2005; 26 (5): 948–68.

17. Stanojevic S, Wade A, Stocks J, et al. Reference ranges for spirometry across all ages: a new approach. Am J Respir Crit Care Med. 2008; 177: 253–60.

18. Sukhovskiĭ VS, Strelis AK, Grigor'ev EG, Sukhovskaia VV. Probl Tuberk Bolezn Legk. 2008; 7: 39–43.